

The potential drug regulation in arthritic disorders

Edited by

Yan Chang, Shanshan Hu, Heinrich Korner, Kun Lv and Li-Long Pan

Published in

Frontiers in Immunology

Frontiers in Pharmacology



FRONTIERS EBOOK COPYRIGHT STATEMENT

The copyright in the text of individual articles in this ebook is the property of their respective authors or their respective institutions or funders. The copyright in graphics and images within each article may be subject to copyright of other parties. In both cases this is subject to a license granted to Frontiers.

The compilation of articles constituting this ebook is the property of Frontiers.

Each article within this ebook, and the ebook itself, are published under the most recent version of the Creative Commons CC-BY licence. The version current at the date of publication of this ebook is CC-BY 4.0. If the CC-BY licence is updated, the licence granted by Frontiers is automatically updated to the new version.

When exercising any right under the CC-BY licence, Frontiers must be attributed as the original publisher of the article or ebook, as applicable.

Authors have the responsibility of ensuring that any graphics or other materials which are the property of others may be included in the CC-BY licence, but this should be checked before relying on the CC-BY licence to reproduce those materials. Any copyright notices relating to those materials must be complied with.

Copyright and source acknowledgement notices may not be removed and must be displayed in any copy, derivative work or partial copy which includes the elements in question.

All copyright, and all rights therein, are protected by national and international copyright laws. The above represents a summary only. For further information please read Frontiers' Conditions for Website Use and Copyright Statement, and the applicable CC-BY licence.

ISSN 1664-8714
ISBN 978-2-83252-008-6
DOI 10.3389/978-2-83252-008-6

About Frontiers

Frontiers is more than just an open access publisher of scholarly articles: it is a pioneering approach to the world of academia, radically improving the way scholarly research is managed. The grand vision of Frontiers is a world where all people have an equal opportunity to seek, share and generate knowledge. Frontiers provides immediate and permanent online open access to all its publications, but this alone is not enough to realize our grand goals.

Frontiers journal series

The Frontiers journal series is a multi-tier and interdisciplinary set of open-access, online journals, promising a paradigm shift from the current review, selection and dissemination processes in academic publishing. All Frontiers journals are driven by researchers for researchers; therefore, they constitute a service to the scholarly community. At the same time, the *Frontiers journal series* operates on a revolutionary invention, the tiered publishing system, initially addressing specific communities of scholars, and gradually climbing up to broader public understanding, thus serving the interests of the lay society, too.

Dedication to quality

Each Frontiers article is a landmark of the highest quality, thanks to genuinely collaborative interactions between authors and review editors, who include some of the world's best academicians. Research must be certified by peers before entering a stream of knowledge that may eventually reach the public - and shape society; therefore, Frontiers only applies the most rigorous and unbiased reviews. Frontiers revolutionizes research publishing by freely delivering the most outstanding research, evaluated with no bias from both the academic and social point of view. By applying the most advanced information technologies, Frontiers is catapulting scholarly publishing into a new generation.

What are Frontiers Research Topics?

Frontiers Research Topics are very popular trademarks of the *Frontiers journals series*: they are collections of at least ten articles, all centered on a particular subject. With their unique mix of varied contributions from Original Research to Review Articles, Frontiers Research Topics unify the most influential researchers, the latest key findings and historical advances in a hot research area.

Find out more on how to host your own Frontiers Research Topic or contribute to one as an author by contacting the Frontiers editorial office: frontiersin.org/about/contact

The potential drug regulation in arthritic disorders

Topic editors

Yan Chang — Anhui Medical University, China

Shanshan Hu — The First Affiliated Hospital of University of Science and Technology of China Anhui Provincial Hospital, China

Heinrich Korner — University of Tasmania, Australia

Kun Lv — First Affiliated Hospital of Wannan Medical College, China

Li-Long Pan — Jiangnan University, China

Citation

Chang, Y., Hu, S., Korner, H., Lv, K., Pan, L.-L., eds. (2023). *The potential drug regulation in arthritic disorders*. Lausanne: Frontiers Media SA.

doi: 10.3389/978-2-83252-008-6

Table of contents

- 05 **A Novel Drug Combination of Mangiferin and Cinnamic Acid Alleviates Rheumatoid Arthritis by Inhibiting TLR4/NFκB/NLRP3 Activation-Induced Pyroptosis**
Weijie Li, Kexin Wang, Yudong Liu, Hao Wu, Yan He, Congchong Li, Qian Wang, Xiaohui Su, Shikai Yan, Weiwei Su, Yanqiong Zhang and Na Lin
- 24 **Two Main Cellular Components in Rheumatoid Arthritis: Communication Between T Cells and Fibroblast-Like Synoviocytes in the Joint Synovium**
Jiajie Tu, Wei Huang, Weiwei Zhang, Jiawei Mei and Chen Zhu
- 37 **Cuproptosis and cuproptosis-related genes in rheumatoid arthritis: Implication, prospects, and perspectives**
Jianan Zhao, Shicheng Guo, Steven J. Schrodi and Dongyi He
- 48 **Melatonin promotes sirtuin 1 expression and inhibits IRE1α-XBP1S-CHOP to reduce endoplasmic reticulum stress-mediated apoptosis in chondrocytes**
Kunpeng Qin, Hao Tang, Yi Ren, Di Yang, Yetian Li, Wei Huang, Yunfeng Wu and Zongsheng Yin
- 68 **Identification of diagnostic mRNA biomarkers in whole blood for ankylosing spondylitis using WGCNA and machine learning feature selection**
Yaguang Han, Yiqin Zhou, Haobo Li, Zhenyu Gong, Ziyi Liu, Huan Wang, Bo Wang, Xiaojian Ye and Yi Liu
- 79 **Gut microbiota-derived metabolites in inflammatory diseases based on targeted metabolomics**
Hui Xu, Li-Bin Pan, Hang Yu, Pei Han, Jie Fu, Zheng-Wei Zhang, Jia-Chun Hu, Xin-Yu Yang, Adili Keranmu, Hao-Jian Zhang, Meng-Meng Bu, Jian-Dong Jiang and Yan Wang
- 100 **Omaveloxolone inhibits IL-1β-induced chondrocyte apoptosis through the Nrf2/ARE and NF-κB signalling pathways *in vitro* and attenuates osteoarthritis *in vivo***
Zengxin Jiang, Guobin Qi, Wei Lu, Hao Wang, Defang Li, Weibin Chen, Lei Ding, Xiuying Yang, Hengfeng Yuan and Qingmin Zeng
- 116 **miR-210-3p protects against osteoarthritis through inhibiting subchondral angiogenesis by targeting the expression of TGFBR1 and ID4**
Han Tang, Wenrun Zhu, Lu Cao, Jin Zhang, Juncheng Li, Duan Ma and Changan Guo
- 132 **Regulatory role of KCa3.1 in immune cell function and its emerging association with rheumatoid arthritis**
Yi Lin, Ying-Jie Zhao, Hai-Lin Zhang, Wen-Juan Hao, Ren-Di Zhu, Yan Wang, Wei Hu and Ren-Peng Zhou

- 150 **Emerging role of lncRNAs in osteoarthritis: An updated review**
Rongliang Wang, Hoi Ting Shiu and Wayne Yuk Wai Lee
- 170 **3,3'-diindolylmethane inhibits LPS-induced human chondrocytes apoptosis and extracellular matrix degradation by activating PI3K-Akt-mTOR-mediated autophagy**
Hao Tang, Kunpeng Qin, Anquan Wang, Shuang Li, Sheng Fang, Weilu Gao, Ming Lu, Wei Huang, Hui Zhang and Zongsheng Yin



A Novel Drug Combination of Mangiferin and Cinnamic Acid Alleviates Rheumatoid Arthritis by Inhibiting TLR4/NF κ B/NLRP3 Activation-Induced Pyroptosis

Wei jie Li¹, Kexin Wang¹, Yudong Liu¹, Hao Wu², Yan He², Congchong Li¹, Qian Wang³, Xiaohui Su¹, Shikai Yan⁴, Weiwei Su², Yanqiong Zhang^{1*} and Na Lin^{1*}

OPEN ACCESS

Edited by:

Yan Chang,
Anhui Medical University, China

Reviewed by:

Oindrila Rahaman,
Emory University, United States
Qinghua Hu,
China Pharmaceutical University,
China
Zhi Yao,
Tianjin Medical University, China

*Correspondence:

Yanqiong Zhang
yqzhang@icmm.ac.cn
Na Lin
nlin@icmm.ac.cn

Specialty section:

This article was submitted to
Autoimmune and
Autoinflammatory Disorders,
a section of the journal
Frontiers in Immunology

Received: 05 April 2022

Accepted: 13 May 2022

Published: 21 June 2022

Citation:

Li W, Wang K, Liu Y, Wu H, He Y, Li C,
Wang Q, Su X, Yan S, Su W, Zhang Y
and Lin N (2022) A Novel Drug
Combination of Mangiferin and
Cinnamic Acid Alleviates Rheumatoid
Arthritis by Inhibiting TLR4/NF κ B/
NLRP3 Activation-Induced Pyroptosis.
Front. Immunol. 13:912933.
doi: 10.3389/fimmu.2022.912933

¹ Institute of Chinese Materia Medica, China Academy of Chinese Medical Sciences, Beijing, China, ² Guangdong Engineering and Technology Research Center for Quality and Efficacy Reevaluation of Post-Market Traditional Chinese Medicine, Guangdong Provincial Key Laboratory of Plant Resources, School of Life Sciences, Sun Yat-sen University, Guangzhou, China, ³ State Key Laboratory of Natural and Biomimetic Drugs, School of Pharmaceutical Sciences, Peking University, Beijing, China, ⁴ School of Pharmacy, Shanghai Jiao Tong University, Shanghai, China

Growing evidence shows that Baihu-Guizhi decoction (BHGZD), a traditional Chinese medicine (TCM)-originated disease-modifying anti-rheumatic prescription, may exert a satisfying clinical efficacy for rheumatoid arthritis (RA) therapy. In our previous studies, we verified its immunomodulatory and anti-inflammatory activities. However, bioactive compounds (BACs) of BHGZD and the underlying mechanisms remain unclear. Herein, an integrative research strategy combining UFLC-Q-TOF-MS/MS, gene expression profiling, network calculation, pharmacokinetic profiling, surface plasmon resonance, microscale thermophoresis, and pharmacological experiments was carried out to identify the putative targets of BHGZD and underlying BACs. After that, both *in vitro* and *in vivo* experiments were performed to determine the drug effects and pharmacological mechanisms. As a result, the calculation and functional modularization based on the interaction network of the “RA-related gene–BHGZD effective gene” screened the TLR4/PI3K/AKT/NF κ B/NLRP3 signaling-mediated pyroptosis to be one of the candidate effective targets of BHGZD for reversing the imbalance network of “immune-inflammation” during RA progression. In addition, both mangiferin (MG) and cinnamic acid (CA) were identified as representative BACs acting on that target, for the strong binding affinities between compounds and target proteins, good pharmacokinetic features, and similar pharmacological effects to BHGZD. Notably, both BHGZD and the two-BAC combination of MG and CA effectively alleviated the disease severity of the adjuvant-induced arthritis-modified rat model, including elevating pain thresholds, relieving joint inflammation and bone erosion *via* inhibiting NF- κ B *via* TLR4/PI3K/AKT signaling to suppress the activation of the NLRP3 inflammasome, leading to the downregulation of downstream caspase-1, the reduced release of IL-1 β and IL-18, and the modulation of GSDMD-mediated pyroptosis. Consistent data were obtained based on

the *in vitro* pyroptosis cellular models of RAW264.7 and MH7A cells induced by LPS/ATP. In conclusion, these findings offer an evidence that the MG and CA combination identified from BHGZD may interact with TLR4/PI3K/AKT/NF κ B signaling to inhibit NLRP3 inflammasome activation and modulate pyroptosis, which provides the novel representative BACs and pharmacological mechanisms of BHGZD against active RA. Our data may shed new light on the mechanisms of the TCM formulas and promote the modernization development of TCM and drug discovery.

Keywords: rheumatoid arthritis (RA), traditional Chinese medicine-originated disease-modifying anti-rheumatic prescription, pyroptosis, bioactive compound, NLRP3 inflammasome

INTRODUCTION

Rheumatoid arthritis (RA), characterized by hyperplasia and inflammation of the synovial joints, is an intractable and highly prevalent autoimmune disease with unknown pathogenic triggers (1, 2). Currently, the key therapeutic approaches to RA are mainly based on drugs and surgeries (3), including disease-modifying anti-rheumatic drugs (DMARDs), non-steroidal anti-inflammatory drugs (NSAIDs), glucocorticoids, and biological response modifiers, which may reduce synovitis and systemic inflammation (4). However, there are no specific drugs for RA therapy due to its various comorbidities, such as cardiovascular diseases (5–8), osteoporosis (9, 10), interstitial lung disease (9, 11), malignancies (11, 12), and hypertension (13), as well as the heterogeneous and complex clinical manifestations with wide individual differences. Traditional Chinese medicine (TCM), as a complementary and alternative medicine, has its unique advantages in the clinical treatment of RA, especially at the active stage with moist heat arthralgia spasm syndrome (active RA), which is characterized by the hyperactive immune response and excessive inflammatory cytokines, subsequently leading to osteoclast differentiation and active joint inflammation (14, 15). Among TCM-originated DMARDs, Baihu-Guizhi decoction (BHGZD) has been indicated to efficiently reverse the aggressive progression of active RA with moist heat arthralgia spasm syndrome and to reach a remarkable response rate (90%) (16–19). Our previous studies identified the chemical profiling of BHGZD *in vitro* and verified its immunomodulatory and anti-inflammatory activities (20–22). However, the bioactive compounds (BACs) and the underlying mechanisms of BHGZD against active RA have not been fully elucidated.

In the current study, the candidate BACs of BHGZD were identified by the ultra-fast liquid chromatography-quadrupole-time-of-flight tandem mass spectrometry (UFLC-Q-TOF-MS/MS) system *in vivo*. Then, we carried out transcriptomic profiling, target prediction, and network calculation to screen the candidate targets of BHGZD for reversing the imbalance network of “immune-inflammation” during the progression of active RA. After that, the binding affinities between candidate BACs and candidate targets of BHGZD were calculated using the molecular docking simulation, the results of which were subsequently verified by surface plasmon resonance (SPR) assay and microscale thermophoresis (MST) analysis.

Moreover, the *in vivo* biodistribution and pharmacokinetic characteristics of candidate BACs were also determined. Furthermore, the pharmacological effects and the molecular mechanisms of BHGZD, and its representative BACs against active RA were further validated by a series of experiments based on the adjuvant-induced arthritis-modified rat model (AIA-M) as well as LPS/ATP-induced pyroptosis cellular models on both RAW264.7 macrophage and MH7A cells.

MATERIALS AND METHODS

Preparation of BHGZD

Crude drugs of BHGZD formula were purchased from Beijing Tongrentang Co., Ltd. (Beijing, China). BHGZD was prepared according to the original composition of the formula recorded in Chinese pharmacopoeia 2020 edition and our previous study (22) (**Supplementary Materials Section 1**, and **Table S1**).

RA Modeling, Grouping, and Treatment

A total of 49 male Lewis rats (200 ± 20 g in weight, 6–8 weeks old) were obtained from Beijing Vital River Laboratory Animal Technology Co., Ltd. (SCXK 2019-0003, Beijing, China) and randomly divided into two independent clusters: a discovery cluster ($n = 24$) and a validation cluster ($n = 25$). All animals were maintained in specific pathogen-free conditions with a constant temperature of $24 \pm 1^\circ\text{C}$ with a 12-h light/dark cycle, and had free access to standard rodent diet and water. The discovery and validation clusters were respectively used for gene expression profiling and experimental validation. In the discovery cluster, 24 rats were randomly divided into three groups [3 per group for microarray and 5 per group for mRNA sequencing (mRNA-Seq)] (1): the normal control group, (2) the AIA-M model group, and (3) the BHGZD treatment group. In the validation cluster, 25 rats were randomly divided into five groups (5 per group): (1) the normal control group, (2) the AIA-M model group, (3) the BHGZD treatment group, (4) the MG+CA treatment group, and (5) the methotrexate (MTX) treatment group.

The AIA-M rat model was established simulating the pathological changes and characteristics of active RA with moist heat arthralgia spasm syndrome based on our previous studies (20–23). Please see the detailed information on the AIA-

M rat model establishment in **Supplementary Materials Section 2**. The dosage of BHGZD for the corresponding treatment group was 21.4 g/kg, equivalent to two times the clinical dose, which has been proved to exert the most prominent therapeutic efficacy in our previous studies (21, 22). The dosages for the two-BAC combination of MG and CA for the corresponding treatment group were respectively 600.912 mg/kg and 46.652 mg/kg, equivalent to their content in 21.4 g/kg BHGZD. The dosage for MTX was 0.2 mg/kg. All treatments were performed for 30 days *via* oral administration from the day of the primary immunization (20–23).

On the 31st day, all rats were anesthetized by intraperitoneal injection of pentobarbital sodium (50 mg/kg). The blood samples were collected using one-time anticoagulant negative pressure blood collection tubes, and then placed at room temperature for 20 min and centrifuged at 3,000 rpm for 15 min. The sera were collected, vortexed, and centrifuged again at high speed at low temperature (4°C) for 15 min, and stored at –20°C for subsequent assays. Whole blood cells were freshly isolated from blood, then frozen in liquid nitrogen overnight, and stored at –80°C for mRNA-Seq. The synovium tissues were isolated and immediately frozen in liquid nitrogen for microarray analysis. The right joints of rats were removed and preserved in 4% paraformaldehyde (PFA) combined with phosphate-buffered saline (PBS) for 72 h for subsequent assays. The left joints and organs of rats were kept at –80°C for subsequent assays.

Assessment of Arthritis Severity

The severity of arthritis was evaluated by arthritis incidence, hind paw thickness (the diameter of limb), arthritis score, and arthritis surface temperature as in our previous studies (20–24), and is provided in **Supplementary Materials Section 3**. Pain thresholds were evaluated by mechanical-, acetone-, and thermal-induced hyperalgesia as previously described (20–25), and are provided in **Supplementary Materials Section 4**.

Viscera Index and Histology

The viscera indexes were calculated by the weight of the thymus, spleen, liver, and kidney relative to total brain weight. Histological changes were examined using hematoxylin and eosin (H&E), safranin O-fast green (Solarbio, Beijing, China), and Masson trichrome staining (Baso, Wuhan, China) according to routine protocols. Please see detailed information on the protocol in **Supplementary Materials Section 5**.

Micro-Computed Tomography Analysis

To quantitatively evaluate bone formation within the defects, the specimens were scanned using a micro-CT instrument (GE healthcare, USA) at a resolution of 45 µm. The x-ray settings and cylinder region of interest (ROI) are provided in **Supplementary Materials Section 6**.

Gene Expression Profiling

Whole blood cells and the synovium tissues representing the pathological characteristics of systemic disease and target organs during active RA progression were respectively used for whole

rat genome microarray analysis (Agilent Technologies, design ID: 014879, Santa Clara, CA, USA) and mRNA-Seq Illumina NovaSeq 6000 (Illumina, CA, USA) to screen RA-related genes [the significant differentially expressed genes (DEGs) between the AIA-M model group and the normal control group] and BHGZD therapeutic effect-related genes (DEGs between the BHGZD treatment group and the AIA-M model group). The gene expression data have been uploaded and are publicly available in the NCBI GEO database (GEO No. GSE189942, <https://www.ncbi.nlm.nih.gov/geo/query/acc.cgi?acc=GSE189942>, December 3, 2021, and GEO No. GSE190523, <https://www.ncbi.nlm.nih.gov/geo/query/acc.cgi?acc=GSE190523>, December 11, 2021), and the DEGs were identified by referring to the criteria of *t*-test *p*-value < 0.05 and fold change (FC) > 2/<0.5. Please see the detailed information in **Supplementary Materials Section 7**.

Prediction of Putative BHGZD Targets

Drugs with a high similarity score (>0.80) to structures of composite compounds of each ingredient contained in BHGZD were selected based on the TCMIP v2.0 database (Integrative Pharmacology-based Research Platform of Traditional Chinese Medicine, last update in 2021-09-10, <http://www.tcmip.cn/TCMIP/index.php/Home/>) and the Encyclopedia of Traditional Chinese Medicine (ETCM, <http://www.tcmip.cn/ETCM/index.php/Home/>) (26). Therapeutic targets of the similar drugs approved by the Food and Drug Administration (FDA) according to DrugBank Online (Version 5.1.8, released 2021-01-03, <https://go.drugbank.com/>) were identified as putative targets of BHGZD.

Network Construction and Analysis

The RA-related gene interaction network was constructed using the links among the DEGs between the AIA-M model and normal control groups to identify the key RA-related genes. Then, the interaction network of the “key RA-related gene–BHGZD-effective gene” was constructed using the links between the key RA-related genes and BHGZD effective genes. The gene–gene interaction data were collected from the String database (version 10.0, <http://string-db.org/>) (27), and the interaction networks were all visualized by the Cytoscape platform (version 3.9.0, <https://cytoscape.org/>) (28). The network topological properties of nodes, including “Degree”, “Betweenness”, and “Closeness”, were calculated for screening the key network targets according to our previous descriptions (20–25, 29) and **Supplementary Materials Section 8**.

Determining the Chemical Compounds of BHGZD and Absorption Distribution Metabolism Excretion Evaluation

A rapid, sensitive, and reliable method by the UFLC-Q-TOF-MS/MS system was used to identify the chemical profiling of BHGZD as described in **Supplementary Materials Section 9** (30). The reference standards of these compounds (**Supplementary Table S2**) were purchased from Chengdu Must Bio-technology Co., Ltd. (Chengdu, China), the National Institute for the Control of

Pharmaceutical and Biological Products (Beijing, China), and Chengdu DeSiTe Biological Technology Co., Ltd. (Chengdu, China). Then, the ADME information on 19 BACs included in BHGZD was collected from the ETCM database (The Encyclopedia of Traditional Chinese Medicine, <http://www.tcmip.cn/ETCM/>) (26). In addition, *in silico* ADME models were used to identify the candidate BACs of BHGZD by calculating the passive intestinal permeability of the Caco-2 module, the oral bioavailability, and the apparent permeability coefficient (Papp) of each BACs as described in **Supplementary Materials Section 10**.

Molecular Docking Simulation

The molecular docking and virtual screening program was carried out to investigate the direct binding efficiencies of the two BACs contained in BHGZD and the corresponding putative targets. The structures of human TLR4 (PDB ID: 2z65), AKT1 (PDB ID: 3o96), and NFκB (PDB ID: 1nfi) were obtained from the PDB website (The Protein Data Bank, <https://www.rcsb.org/>). For docking analysis, the ligand mangiferin (MG) and cinnamic acid (CA) were downloaded from the ZINC database (last update in 2018-02-14, <http://zinc.docking.org/>) (31) in mol2 format and converted to pdb.files using OpenBabel GUI (last update in 2016-09-21, version 2.4.1, http://openbabel.org/wiki/Main_Page). AutoDock Tools (Version 1.5.6, <https://ccsb.scripps.edu/mgltools/>) was used to convert pdb to pdbqt format. Docking calculations were performed using AutoDock Vina (The Scripps Research Institute, version 1.1.2) and AutoDock (The Scripps Research Institute, version 4.2.6). The visualization and analysis of the results were obtained from AutoDock Vina by PyMOL (Version 2.5, <https://pymol.org/2/>).

SPR Assay

To confirm the binding affinity of recombinant AKT1 protein and MG, SPR assay was performed with Biacore 8K (Biacore, Cytiva), and the K_D value was calculated using the Biacore 8K evaluation software 2.0 (GE Healthcare). Detailed information on SPR assay is provided in **Supplementary Materials Section 11**.

MST Assay

The binding affinity between recombinant TLR4 protein and CA was measured by a NanoTemper Monolith NT.115 instrument (NanoTemper Technologies, Germany). The K_D value was fitted by NanoTemper Monolith affinity software (NanoTemper Technologies, Germany) using 1:1 binding mode. Detailed information on the MST assay is provided in **Supplementary Materials Section 12**.

In Vivo Pharmacokinetic Analysis

To detect the pharmacokinetic parameters of MG and CA *in vivo*, quantification analysis was performed by an ultra-high-performance liquid chromatography (Shimadzu Corp., Japan) tandem ion trap quadrupole QTRAP 6500 plus mass spectrometry (AB Sciex, USA). The quantitative analyses for MG and CA were approved by the Guidance for Bioanalytical Method Validation issued by the Chinese Pharmacopoeia Commission in

2020. The pharmacokinetic parameters were calculated by Drug and Statistic software (Shanghai, China). Detailed information on the collection of blood samples and UHPLC-QTRAP-MS/MS conditions is provided in **Supplementary Materials Section 13**.

Cell Culture, Induction, and Treatment

Mouse macrophage cell line (RAW264.7 cells, Bio-Swamp, Wuhan, China) and fibroblast-like synoviocytes in patients with RA (MH7A cells, Riken cell bank, Ibaraki, Japan) at passage numbers four to eight were used in the current experiment validations. The culture conditions are provided in **Supplementary Materials Section 14**.

The conventional NLRP3 inflammasome activation cellular model was induced by lipopolysaccharide [LPS, *Escherichia coli* (O111:B4), Sigma-Aldrich, St Louis, MO, USA] and adenosine triphosphate (ATP disodium salt hydrate, Sigma-Aldrich, St Louis, MO, USA) as in our previous study (22) (**Supplementary Materials Section 15**).

For the drug treatment, both RAW264.7 and MH7A cells were divided into the following groups: (1) Normal control group: with no stimulation and treatment; (2) LPS/ATP-induced cellular model group: cells were stimulated with the corresponding concentrations of LPS and ATP; (3) BHGZD treatment group: after stimulation, cells were treated with 28.54 μg/ml BHGZD for 24 h, which was determined to be the most effective as in our previous study (22); (4) MG+CA treatment group: after stimulation, cells were treated with the two-BAC combination (1.69 ng/ml MG and 0.13 ng/ml CA, with the same content as that in the 5 μg/ml BHGZD formula) for 24 h; (5) MG treatment group: after stimulation, cells were treated with 1.69 ng/ml MG for 24 h; and (6) CA treatment group: after stimulation, cells were treated with 0.13 ng/ml CA for 24 h. The concentration of DMSO was less than 1‰ of the solution for the *in vitro* experiment.

Cell Viability Assay

Cell viability was analyzed with the cell counting kit-8 (CCK-8) assay kit (Beyotime Biotechnology, Shanghai, China) as described in **Supplementary Materials Section 16**.

Flow Cytometry

To identify and quantify the pyroptosis population of RAW264.7 cells, FITC Apoptosis Detection kit I staining with both the Annexin V-fluorescein isothiocyanate and propidium iodide (PI, BD Biosciences, San Jose, CA, USA) was used according to the manufacturer's guidelines. Flow cytometry was performed using NovoCyte 2040R (ACEA Bioscience, San Diego, CA, USA), and analyzed using the NovoExpress 1.4.1 software (ACEA Bioscience, San Diego, CA, USA). Detailed information of this experiment is provided in **Supplementary Materials Section 17**.

Terminal Deoxynucleotidyl Transferase-Mediated dUTP Biotin Nick End Labeling Staining

The occurrence of pyroptosis in both MH7A cells and synovium tissues in AIA-M rats was determined by *in situ* TUNEL staining

(TUNEL Andy FluorTM 594 Apoptosis Detection Kit, ABP Biosciences, Wuhan, China) in accordance with the manufacturer's protocol. Fluorescence images were visualized and photographed with inverted fluorescence microscopes (MF53, MSHOT, Guangzhou, China; Olympus, BX51, Tokyo, Japan). Detailed information on TUNEL assay is provided in **Supplementary Materials Section 18**.

FAM-FLICA Caspase-1 Assay

Active caspase-1 was visualized by a FAM-FLICA caspase-1 assay kit using a FAM-YVAD-FMK inhibitor probe (ImmunoChemistry Technologies, Bloomington, MN, USA), according to the manufacturer's guidelines. Fluorescence images were visualized and photographed with a confocal microscope (Zeiss LSM 880, Carl Zeiss, Jena, Germany). Detailed information on FAM-FLICA caspase-1 assay is provided in **Supplementary Materials Section 19**.

Immunofluorescence Staining

Double fluorescence staining was performed as described previously (22) (**Supplementary Materials Section 20**). The images were visualized and photographed with a confocal microscope (Zeiss LSM 880, Carl Zeiss, Jena, Germany) or an inverted fluorescence microscope (MF53, MSHOT, Guangzhou, China).

Immunohistochemical Staining

To detect the expression levels of NLRP3/ASC of the knee joints in AIA-M rats and corresponding treatment groups, immunohistochemical staining was carried out using a DAB kit (Cat No. AR1027, Boster Biological Technology Co., Ltd., Wuhan, China) and a rabbit/mouse two-step detection kit (Cat No. SV0002/SV0001, Boster Biological Technology Co., Ltd., Wuhan, China) according to the routine protocols. Immunohistochemistry quantification was performed using ImageJ (Image Progressing and Analysis in Java, version 1.42q, <https://imagej.nih.gov/ij/>), following the ImageJ User Guide.

Western Blotting Analysis

To evaluate the regulation of BHGZD on the candidate targets in arthritic tissue samples, as well as RAW264.7 and MH7A cells, Western blotting analysis was carried out following the protocol as in our previous studies (21, 24, 29). TLR4, phospho-PI3K (p-PI3K), PI3K, p-AKT, p-NFκB-p65, NFκB-p65, NLRP3, ASC, caspase-1, the N-terminal domain of GSDMD (GSDMD-NT), and IL-1β antibodies were used as shown in **Supplementary Table S3**. GAPDH (GAPDH Mouse monoclonal antibody, Abcam, Cambridge, UK) and β-actin (Anti-beta-Actin/β-Actin Antibody, Boster Biological Technology, California, USA) were used as loading controls for arthritic tissue samples and cultured cells, respectively.

Cytokine Analysis and Lactate Dehydrogenase Measurement

To evaluate the therapeutic effects of two BACs from BHGZD on the regulation of the “immune-inflammation” system, the levels of cytokines, proteins, and LDH release in RAW264.7 and MH7A cellular supernatant, as well as the sera of AIA-M rats were determined using enzyme-linked immunosorbent assay

(ELISA) to assess the integrity of membranes in accordance with the manufacturer's guidelines.

Statistical Analyses

Statistical analyses were performed using GraphPad Prism 8.0 Software (San Diego, CA, USA). Data are expressed as the mean ± SD and analyzed by one-way ANOVA with Bonferroni's or Dunnett's post-hoc test for comparison of multiple columns. Differences were considered statistically significant when the *p*-value was less than 0.05.

RESULTS

BHGZD Reverses the Imbalance of the “Immune-Inflammation” System in Active RA Rats

The AIA-M rat model was successfully established (the achievement ratio of this model was 100%) and verified according to its reliable and rapid-onset characteristics, and severe disease progression by external stimulus of wind, dampness, and heat, which may be the major pathological changes and features of active RA with moist heat arthralgia spasm syndrome (22). In contrast, the administration of BHGZD effectively alleviated the disease severity in arthritis of active RA rats. Detailed information on the characterizations of the active RA rat model and the therapeutic effects of BHGZD in active RA severity based on this model was reported in our previous study (22).

To determine the candidate targets of BHGZD against active RA, the gene expression profiles of whole blood cells and synovium tissues were carried out. A total of 473 RA-related genes (275 upregulated and 178 downregulated genes) and 1,802 BHGZD therapeutic effect-related genes (456 upregulated and 1,346 downregulated genes) were identified. The heatmap and volcano plot of DEGs are shown in **Figures 1A–H**, suggesting a distinct separation between the AIA-M model and normal control groups, as well as the BHGZD treatment and AIA-M model groups. Among them, there were 135 RA-related genes reversely regulated by the treatment of BHGZD (**Table 1**). Detailed information on the RA-related genes and BHGZD therapeutic effect-related genes is respectively provided in **Supplementary Tables S4 and S5**.

In addition, 238 putative targets of *Anemarrhena asphodeloides* Bge., *Cinnamomum cassia* Presl, and *Glycyrrhiza uralensis* Fisch., and 197 putative targets of Gypsum, contained in BHGZD with a high similarity score (>0.80), were predicted based on the TCMIP v2.0 platform, such as NAHD, HSD17B1, CFTR, TTGR, MIF, OXYR, CYP1A2, ESRRA, JAK1, ESRRB, CSNK2A1, ANXA5, ARSA, ATSK, C3L, CACNA1C, CACNA1S, CACNA2D1, CACNB1, CACNB2, CACNG1, CCKAR, CCL5, CD1D, CGIA, CRCA, CSLA, CSLB, and EGF. On the basis of the ETCM database, 184 putative targets of 31 bioactive chemical compounds contained in BHGZD, and 53 putative targets of *Oryza sativa* L. were collected, including ACO2, AKR1B1, ANG, APRT, BHMT, C8G, CPB1, CS, CTDSP1, GNMT, HGS,

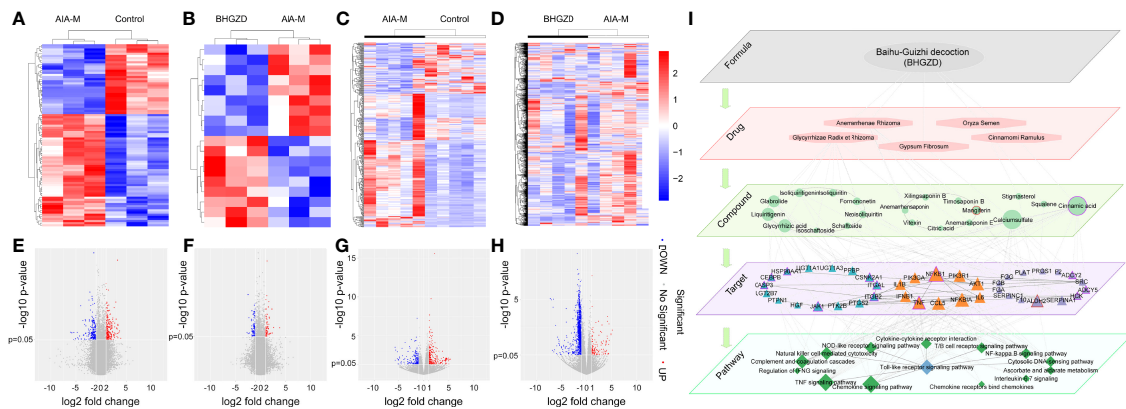


FIGURE 1 | Transcriptomic profiling-based differential data analysis and biomolecular network-based investigation of AIA-M candidate markers and candidate targets of Baihu-Guizhi decoction (BHGDZ) against AIA-M (Control, AIA-M, BHGDZ). **(A)** The heatmap of the significant differentially expressed genes (DEGs) between the AIA-M model group and the normal control group in synovium using microarray analysis ($n = 3$ per group). **(B)** The heatmap of DEGs between the BHGDZ treatment group and the AIA-M model group in synovium using microarray analysis ($n = 3$ per group). **(C)** The heatmap of the DEGs between the AIA-M model group and the normal control group in whole blood cells using RNA sequencing (RNA-Seq) analysis ($n = 5$ per group). **(D)** The heatmap of DEGs between the BHGDZ treatment group and the AIA-M model group in whole blood cells using RNA-Seq analysis ($n = 5$ per group). **(E)** The volcano plot of the DEGs between the AIA-M model group and the normal control group in synovium using microarray analysis ($n = 3$ per group). **(F)** The volcano plot of the DEGs between the BHGDZ treatment group and the AIA-M model group in synovium using microarray analysis ($n = 3$ per group). **(G)** The volcano plot of the DEGs between the AIA-M model group and the normal control group in whole blood cells using RNA sequencing (RNA-Seq) analysis ($n = 5$ per group). **(H)** The volcano plot of the DEGs between the BHGDZ treatment group and the AIA-M model group in whole blood cells using RNA-Seq analysis ($n = 5$ per group). **(I)** The subnetwork of the “formula-drug-compound-target-pathway” network is constructed using the links between key RA-related genes and BHGDZ effective genes. The ellipse refers to BHGDZ. Light orange hexagons refer to drugs contained in BHGDZ. Green circles refer to compounds contained in BHGDZ. Triangles refer to targets. Green diamonds refer to pathways. Triangles with red circles refer to the targets of mangiferin (MG). Triangles with purple circles refer to the targets cinnamic acid (CA).

HS3ST3A1, VDR, CYP27B1, KCND1, KCNA3, PRKAB1, ADH1A, KCNA10, and GAMT. There were a total of 635 genes, including RA-related genes reversely regulated by BHGZD, putative targets of bioactive chemical compounds, and the known therapeutic targets of drug contained in BHGZD, considered as BHGZD effective genes.

Then, the interaction network of the “RA-related gene-BHGZD effective gene” was constructed using the links among RA-related genes and BHGZD effective genes. Following the calculation of the nodes’ topological features in the network (the median values of “Degree”, “Betweenness”, and “Closeness” were 7.0000, 0.0009, and 0.2860, respectively), four BHGZD candidate targets (PI3K, AKT1, NFκB, and IL-1β) against active RA (**Figure 11**, and **Supplementary Table S6**) were identified due to their topological importance. In addition, previous data obtained from our research group and from other research groups indicated that BHGZD may restore the imbalance of the “immune-inflammation” system *via* inhibiting TLR4-induced NLRP3 inflammasome signaling (21, 22), and TLR4/NFκB signaling may play a vital role in the regulation of the inflammatory response (32, 33). Moreover, PI3K/AKT signaling is involved in the process and release of pro-inflammatory cytokines (34, 35), and the activation of this signaling leads to autoimmunity, showing the increased activity in some autoimmune diseases, including RA (36). On this basis, we hypothesize that BHGZD might reverse the main pathological changes of active RA, including synovial inflammation, cartilage damage, and bone erosion, *via* regulating TLR4/PI3K/AKT/NFκB/NLRP3 signaling.

MG and CA May Be the Representative BACs Contained in BHGZD Against Active RA

To screen the potential BACs contained in BHGZD against active RA, herein we identified the chemical profiling of this herbal formula in sera using the UFLC-Q-TOF-MS/MS system. As a result, a total of 31 chemical compounds were identified in the serum samples 2 h after the treatment of BHGZD. Among them, 14, 16, and 1 chemical compound were from *Anemarrhenae Rhizoma*, *Glycyrrhizae Radix et Rhizoma*, and *Cinnamomi Ramulus*, respectively, and belong to glycosides, flavonoids, organic acid, triterpenoids, and saponins. Quantitatively, timosaponin B II, mangiferin, glycyrrhizic acid, neomangiferin, 7-O-methyl mangiferin, anemarrhensaponin I, vitexin, formononetin, liquiritigenin, isoliquiritin, isoliquiritin apioside, isoschaftoside, and isovitexin were all detected at 30 min after the treatment of BHGZD. Detailed information on chemical profiling is provided in **Supplementary Table S7**, and the quantitative detection data are provided in **Supplementary Table S8**. In addition, the drug-like properties of the chemical compounds contained in BHGZD, including the intestinal absorption rate and oral bioavailability, were evaluated using ADME models *in silico*, and a total of 8 candidate BACs with good drug-likeness were identified (**Supplementary Table S9**).

After that, molecular docking was performed to determine the binding affinities of candidate BACs contained in BHGZD to corresponding proteins of TLR4/PI3K/AKT/NFκB/NLRP3 signaling. As a result, a total of 9 chemical compounds were

TABLE 1 | The information on 135 RA-related genes reversely regulated by the treatment of Baihu-Guizhi decoction (BHGZD).

Samples	Gene Symbol	AIA-M vs. Con	p-value	log2 Fold Change	BHGZD vs. AIA-M	p-value	log2 Fold Change
Synovium	ACKR4	Down	0.0389	-1.4327	Up	0.0011	1.1346
Synovium	AQP3	Down	0.0419	-4.6637	Up	0.0003	4.6114
Synovium	ARSI	Up	0.0157	1.1593	Down	0.0043	-1.9063
Synovium	C7	Up	0.0046	1.0014	Down	0.0142	-1.2088
Synovium	CAR13	Up	0.0411	1.3595	Down	0.0136	-1.9177
Synovium	CFB	Up	0.0087	2.3269	Down	0.0100	-1.9143
Synovium	CHL1	Up	0.0266	1.3184	Down	0.0082	-1.7127
Synovium	CUBN	Down	0.0440	-1.5011	Up	0.0272	2.0115
Synovium	CYP26A1	Up	0.0410	1.2507	Down	0.0032	-1.5831
Synovium	CYP2W1	Up	0.0302	1.6286	Down	0.0320	-2.3456
Synovium	EGLN3	Down	0.0224	-1.5984	Up	0.0216	1.4110
Synovium	EXPH5	Down	0.0254	-1.2262	Up	0.0204	1.6917
Synovium	GAS2	Up	0.0374	3.1797	Down	0.0478	-1.2633
Synovium	MARCKS	Up	0.0360	1.1328	Down	0.0142	-1.3571
Synovium	HHIP	Down	0.0135	-1.6433	Up	0.0307	1.4088
Synovium	ID4	Down	0.0244	-1.6145	Up	0.0089	1.3183
Synovium	PKHD1L1	Down	0.0199	-1.6321	Up	0.0298	1.6867
Synovium	TNMD	Up	0.0418	3.3639	Down	0.0245	-5.1964
Synovium	TUBB3	Up	0.0089	1.5756	Down	0.0031	-2.1800
Synovium	UNC5CCL	Down	0.0172	-1.8548	Up	0.0164	1.3891
Synovium	UTS2R	Up	0.0234	3.6773	Down	0.0391	-3.3398
Synovium	VSNL1	Down	0.0251	-1.1707	Up	0.0161	1.0142
Whole Blood Cells	ADCY5	Up	1.5517	0.0011	Down	-1.4196	0.0001
Whole Blood Cells	AGRP	Up	1.4030	0.0234	Down	-2.2359	0.0001
Whole Blood Cells	ALDOC	Up	2.4691	0.0010	Down	-1.3832	0.0036
Whole Blood Cells	ANGPTL2	Up	3.7609	0.0417	Down	-2.6154	0.0384
Whole Blood Cells	ASTN1	Up	1.1875	0.0034	Down	-1.4422	0.0000
Whole Blood Cells	ATF5	Up	1.7382	0.0006	Down	-1.7147	0.0144
Whole Blood Cells	BFSP2	Up	1.3618	0.0039	Down	-1.5460	0.0004
Whole Blood Cells	BGLAP	Up	1.1948	0.0072	Down	-1.3003	0.0003
Whole Blood Cells	BRICD5	Up	4.9630	0.0180	Down	-4.5770	0.0112
Whole Blood Cells	BTLA	Down	-1.0068	0.0352	Up	1.0449	0.0059
Whole Blood Cells	CASP12	Down	-3.1532	0.0011	Up	2.2173	0.0236
Whole Blood Cells	CBLN2	Up	1.1423	0.0021	Down	-1.5381	0.0000
Whole Blood Cells	CCDC92	Up	1.7220	0.0000	Down	-1.7041	0.0001
Whole Blood Cells	CD177	Down	-1.9882	0.0031	Up	2.0804	0.0098
Whole Blood Cells	CD79AL	Down	-1.1535	0.0081	Up	1.1442	0.0045
Whole Blood Cells	CDCA2	Down	-3.2077	0.0117	Up	2.8039	0.0013
Whole Blood Cells	CELA1	Up	1.5977	0.0012	Down	-1.6140	0.0007
Whole Blood Cells	CLU	Up	1.0155	0.0039	Down	-1.4820	0.0000
Whole Blood Cells	CRABP1	Up	1.9562	0.0243	Down	-1.9772	0.0081
Whole Blood Cells	CRABP2	Down	-4.8634	0.0057	Up	3.8683	0.0101
Whole Blood Cells	CTDSPL	Up	1.0889	0.0348	Down	-1.0297	0.0089
Whole Blood Cells	CTTN	Up	1.0143	0.0137	Down	-1.9100	0.0000
Whole Blood Cells	CXCL2	Up	1.9025	0.0012	Down	-1.2825	0.0001
Whole Blood Cells	CXXC4	Up	1.1896	0.0126	Down	-1.5581	0.0000
Whole Blood Cells	DACT1	Up	3.5048	0.0091	Down	-2.7562	0.0059
Whole Blood Cells	DDX25	Down	-3.1180	0.0396	Up	2.9352	0.0077
Whole Blood Cells	DENND2C	Up	1.1059	0.0242	Down	-1.3200	0.0006
Whole Blood Cells	DNAH1	Up	1.1723	0.0186	Down	-1.6980	0.0002
Whole Blood Cells	DOK4	Up	1.2929	0.0109	Down	-1.2531	0.0079
Whole Blood Cells	ECE2	Up	3.5704	0.0297	Down	-7.0144	0.0000
Whole Blood Cells	EHD2	Up	1.0293	0.0323	Down	-1.7746	0.0001
Whole Blood Cells	ELN	Up	4.4083	0.0335	Down	-6.1763	0.0005
Whole Blood Cells	ERFE	Up	3.3489	0.0315	Down	-2.7202	0.0101
Whole Blood Cells	F11R	Up	1.1213	0.0037	Down	-1.5369	0.0000
Whole Blood Cells	F2RL3	Up	1.1166	0.0056	Down	-1.5841	0.0000
Whole Blood Cells	FAM184A	Up	1.6124	0.0416	Down	-1.5781	0.0007
Whole Blood Cells	GADD45G	Up	1.1221	0.0463	Down	-1.1012	0.0309
Whole Blood Cells	GAS2L1	Up	1.1011	0.0021	Down	-1.4515	0.0001
Whole Blood Cells	GNAZ	Up	1.0121	0.0086	Down	-1.4201	0.0000
Whole Blood Cells	GP1BB	Up	1.9090	0.0008	Down	-1.5758	0.0431
Whole Blood Cells	GP9	Up	1.0026	0.0038	Down	-1.4034	0.0002

(Continued)

TABLE 1 | Continued

Samples	Gene Symbol	AIA-M vs. Con	p-value	log2 Fold Change	BHGZD vs. AIA-M	p-value	log2 Fold Change
Whole Blood Cells	GRB10	Up	2.6721	0.0005	Down	-1.3209	0.0028
Whole Blood Cells	GSTA1	Up	1.0067	0.0053	Down	-1.3929	0.0008
Whole Blood Cells	HIVEP3	Down	-1.7890	0.0017	Up	1.0399	0.0267
Whole Blood Cells	KATNAL1	Up	1.5441	0.0248	Down	-1.2866	0.0069
Whole Blood Cells	KCNS3	Up	1.0348	0.0105	Down	-1.4733	0.0003
Whole Blood Cells	KLHL13	Up	2.3729	0.0216	Down	-2.3771	0.0009
Whole Blood Cells	KLRA22	Down	-2.1066	0.0132	Up	1.6770	0.0175
Whole Blood Cells	LARGE1	Up	1.0049	0.0112	Down	-1.4699	0.0001
Whole Blood Cells	LHFPL6	Up	2.1809	0.0305	Down	-1.2276	0.0290
Whole Blood Cells	LIPG	Down	-1.2935	0.0374	Up	1.3060	0.0134
Whole Blood Cells	LOC100912228	Up	1.0055	0.0074	Down	-1.4317	0.0003
Whole Blood Cells	LOC102556092	Up	1.1719	0.0026	Down	-1.5513	0.0000
Whole Blood Cells	LOXL3	Up	1.3740	0.0022	Down	-1.4840	0.0002
Whole Blood Cells	LRRC71	Up	1.4124	0.0178	Down	-1.5799	0.0003
Whole Blood Cells	LY6G6F	Up	1.0222	0.0043	Down	-1.4740	0.0000
Whole Blood Cells	LYVE1	Up	1.0159	0.0023	Down	-1.3934	0.0000
Whole Blood Cells	MAPK8IP1	Up	2.5304	0.0317	Down	-2.4659	0.0016
Whole Blood Cells	MCPT1L1	Up	1.8206	0.0003	Down	-1.7125	0.0000
Whole Blood Cells	MEST	Up	1.5656	0.0296	Down	-1.7263	0.0007
Whole Blood Cells	MMRN1	Up	1.0609	0.0026	Down	-1.5474	0.0000
Whole Blood Cells	MMRN2	Down	-2.8201	0.0275	Up	3.0209	0.0015
Whole Blood Cells	MRV1	Up	1.0361	0.0113	Down	-1.4740	0.0000
Whole Blood Cells	MSRA	Up	1.8396	0.0266	Down	-1.1511	0.0301
Whole Blood Cells	MYCT1	Up	1.1718	0.0058	Down	-1.5488	0.0000
Whole Blood Cells	MYL9	Up	1.2004	0.0009	Down	-1.5114	0.0000
Whole Blood Cells	NRGN	Up	1.1404	0.0008	Down	-1.4248	0.0001
Whole Blood Cells	NRIP3	Up	1.1768	0.0188	Down	-1.0978	0.0016
Whole Blood Cells	OLFM4	Down	-1.0349	0.0065	Up	1.1084	0.0336
Whole Blood Cells	PCDHGB5	Down	-3.9559	0.0262	Up	3.5018	0.0274
Whole Blood Cells	PDE3A	Up	1.0241	0.0116	Down	-1.4264	0.0001
Whole Blood Cells	PF4	Up	1.2675	0.0007	Down	-1.4629	0.0004
Whole Blood Cells	PKIA	Up	1.2370	0.0016	Down	-1.3519	0.0002
Whole Blood Cells	PLA2G2A	Up	1.3067	0.0003	Down	-1.5044	0.0001
Whole Blood Cells	PLOD2	Up	1.3673	0.0338	Down	-1.8337	0.0000
Whole Blood Cells	PLTP	Up	1.4100	0.0003	Down	-1.3760	0.0012
Whole Blood Cells	PPIF	Up	1.0631	0.0030	Down	-1.3334	0.0001
Whole Blood Cells	PROSER2	Up	2.4378	0.0106	Down	-1.4237	0.0073
Whole Blood Cells	PTPN13	Up	4.1086	0.0158	Down	-2.6389	0.0331
Whole Blood Cells	RASL10A	Up	1.1205	0.0028	Down	-1.3945	0.0001
Whole Blood Cells	REEP2	Up	1.0181	0.0048	Down	-1.4944	0.0000
Whole Blood Cells	RPAP1	Up	1.0304	0.0027	Down	-1.4851	0.0000
Whole Blood Cells	RPP25	Up	1.8057	0.0048	Down	-1.5779	0.0320
Whole Blood Cells	RT1-HA	Down	-1.3847	0.0248	Up	1.1581	0.0230
Whole Blood Cells	RTP4	Down	-1.1421	0.0350	Up	1.1822	0.0025
Whole Blood Cells	SCAI	Down	-1.2765	0.0173	Up	1.1195	0.0207
Whole Blood Cells	SCARF1	Up	1.7774	0.0006	Down	-1.5817	0.0020
Whole Blood Cells	SEC14L5	Up	1.3750	0.0134	Down	-1.8066	0.0013
Whole Blood Cells	SEMA5A	Up	2.8501	0.0110	Down	-4.0576	0.0003
Whole Blood Cells	SEPT10	Down	-1.7620	0.0426	Up	1.5958	0.0271
Whole Blood Cells	SERPINE2	Up	2.2082	0.0383	Down	-1.4497	0.0397
Whole Blood Cells	Sh3bgr	Up	2.4272	0.0004	Down	-1.3007	0.0077
Whole Blood Cells	SHPK	Up	1.0305	0.0005	Down	-1.1246	0.0000
Whole Blood Cells	SLC6A4	Up	1.0946	0.0021	Down	-1.5201	0.0000
Whole Blood Cells	SMPDL3B	Up	1.0133	0.0071	Down	-1.0129	0.0042
Whole Blood Cells	STON2	Up	1.8772	0.0063	Down	-1.6397	0.0004
Whole Blood Cells	SYT5	Up	1.1579	0.0003	Down	-1.3477	0.0002
Whole Blood Cells	SYTL4	Up	1.6712	0.0402	Down	-1.6984	0.0001
Whole Blood Cells	TAL1	Up	1.0319	0.0073	Down	-1.5858	0.0000
Whole Blood Cells	THBS1	Up	1.0434	0.0086	Down	-1.5613	0.0000
Whole Blood Cells	TMEM56	Up	1.7935	0.0015	Down	-2.3856	0.0015
Whole Blood Cells	TP53TG5	Up	4.6235	0.0109	Down	-3.3568	0.0168
Whole Blood Cells	TREML1	Up	1.0076	0.0069	Down	-1.4372	0.0002
Whole Blood Cells	TRIM17	Up	1.6098	0.0278	Down	-1.1120	0.0370

(Continued)

TABLE 1 | Continued

Samples	Gene Symbol	AIA-M vs. Con	p-value	log2 Fold Change	BHGZD vs. AIA-M	p-value	log2 Fold Change
Whole Blood Cells	TYRO3	Up	1.0424	0.0372	Down	-1.7972	0.0000
Whole Blood Cells	UNC13B	Up	1.2061	0.0047	Down	-1.4375	0.0000
Whole Blood Cells	VSIG2	Up	1.4849	0.0204	Down	-1.2263	0.0039
Whole Blood Cells	VWF	Up	1.0792	0.0005	Down	-1.4591	0.0000
Whole Blood Cells	WNT2	Up	2.4945	0.0406	Down	-2.3451	0.0055
Whole Blood Cells	XKR8	Up	1.0216	0.0050	Down	-1.4189	0.0002
Whole Blood Cells	YAP1	Up	2.6466	0.0060	Down	-1.9990	0.0002
Whole Blood Cells	ZCCHC12	Up	3.7146	0.0010	Down	-2.1065	0.0024
Whole Blood Cells	ZFP780B-PS1	Down	-1.6098	0.0081	Up	1.3243	0.0131

AIA-M vs. Con: the significant differentially expressed genes (DEGs) between the AIA-M model group and the normal control group. BHGZD vs. BHGZD: the DEGs between the BHGZD treatment group and the AIA-M model group.

found to bind these proteins with binding affinities of more than -4.0 kcal/mol (**Supplementary Table S10**). In particular, MG (**Figure 2A**) from *Anemarrhenae Rhizoma* and CA (**Figure 2B**) from *Cinnamomi Ramulus* docked well into the TLR4, AKT, and NF κ B binding cavity with more robust interactions and stronger binding affinity (MG-TLR4 -6.6 , CA-TLR4 -6.1 , MG-AKT -9.2 , CA-AKT -6.6 , MG-NF κ B -7.7 , and CA-NF κ B -5.3 kcal/mol, **Figures 2C–E**). Experimentally, MST and SPR assays were carried out to verify the direct binding efficiency of CA to TLR4 and MG to AKT, respectively. As shown in **Figures 2F** and **G**, the mean K_D values of 2.11×10^{-4} and 3.83×10^{-5} M for CA-TLR4 and MG-AKT, respectively, indicated strong binding affinities.

Moreover, the content of MG and CA was determined to be 336.96 ng and 26.14 ng in 1 mg of BHGZD lyophilized powder, respectively, with a conversion ratio of 8.33% (calculated by the weight of BHGZD lyophilized powder divided by the weight of crude herbs contained in BHGZD; 1 g of BHGZD lyophilized powder is equivalent to the amount of 12 g of BHGZD).

The UHPLC-QTRAP-MS/MS system was further used to detect the pharmacokinetic properties of MG and CA in sera after the treatment of BHGZD (**Supplementary Figure S1**). A summary of MG and CA pharmacokinetic parameters using a non-compartment model analysis is presented in **Table 2**, and the mean plasma concentration–time profiles from time 0 to 24 h after

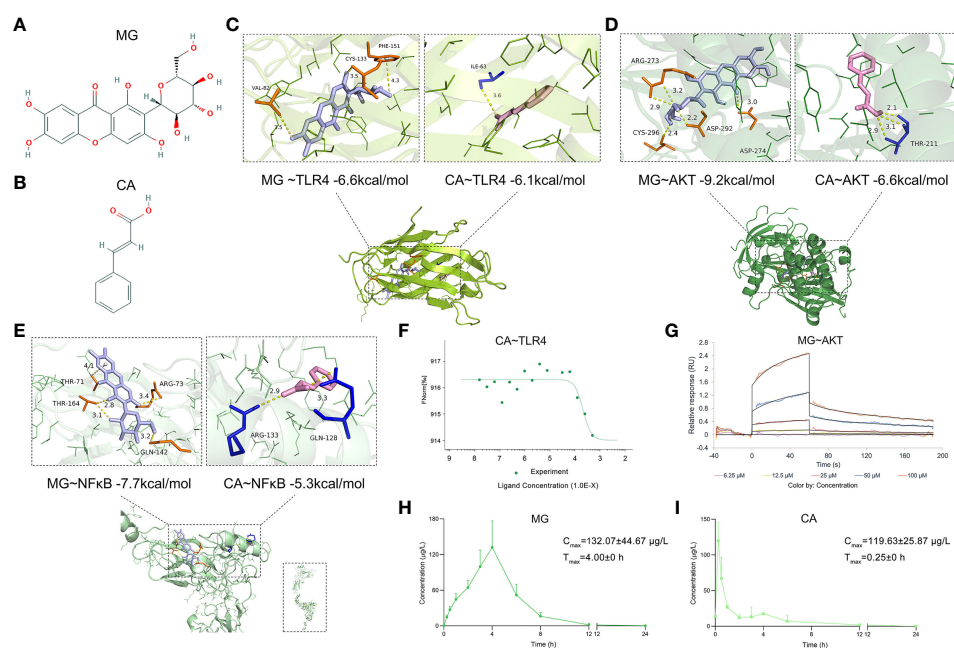


FIGURE 2 | Chemical structures of MG and CA, molecular docking simulation of the binding patterns of them with corresponding proteins, as well as the mean plasma concentration–time curves of MG and CA after the treatment of BHGZD. **(A)** Chemical structure of MG (obtained from PubChem databases, CID 5281647). **(B)** Chemical structure of CA (obtained from PubChem databases, CID 444539). **(C)** Molecular docking simulation of the binding patterns of TLR4 with MG and CA, respectively. **(D)** Molecular docking simulation of the binding pattern of AKT with MG and CA, respectively. **(E)** Molecular docking simulation of the binding pattern of NF κ B with MG and CA, respectively. **(F)** Microscale thermophoresis (MST)-determined binding affinity between CA and TLR4 protein. **(G)** Surface plasmon resonance (SPR) assay of the interaction between MG and AKT1 protein. **(H)** The mean plasma concentration–time curves of MG after the treatment of BHGZD for 12 days at the dosage of 21.4 g/kg each day ($n = 3$ per group). **(I)** The mean plasma concentration–time curves of CA after the treatment of BHGZD for 12 days at the dosage of 21.4 g/kg each day ($n = 3$ per group).

TABLE 2 | Pharmacokinetic parameters analyzed by the UHPLC-QTRAP-MS/MS system.

Pharmacokinetic Parameter	Mangiferin (MG)		Cinnamic acid (CA)	
	Mean \pm SD	RSD/%	Mean \pm SD	RSD/%
C_{max} (μ g/L)	132.07 \pm 44.67	33.80	119.63 \pm 25.87	21.60
T_{max} (h)	4.00 \pm 0.00	0.00	0.25 \pm 0.00	0.00
$AUC_{(0-t)}$ (μ g/L \cdot h)	578.42 \pm 182.51	31.60	102.48 \pm 67.77	66.10
$AUC_{(0-\infty)}$ (μ g/L \cdot h)	579.07 \pm 181.70	31.40	144.23 \pm 30.36	21.00
$t_{1/2Z}$ (h)	1.26 \pm 0.23	17.90	1.65 \pm 1.34	81.10
$MRT_{(0-t)}$ (h)	4.23 \pm 0.30	7.10	1.93 \pm 0.35	18.30
$MRT_{(0-\infty)}$ (h)	4.25 \pm 0.28	6.50	2.26 \pm 0.80	35.20

C_{max} , the maximum plasma concentration. T_{max} , the time to reach the maximum plasma concentration. $AUC_{(0-t)}$, area under the concentration–time curve from zero to the last sampling time. $AUC_{(0-\infty)}$, area under the concentration–time curve from zero to infinity. $T_{1/2Z}$, apparent elimination half-life. $MRT_{(0-t)}$, mean residence time from zero to the last sampling time. $MRT_{(0-\infty)}$, mean residence time from zero to infinity. Data are expressed as the mean \pm SD.

the treatment of BHGZD at a dosage of 21.4 g/kg each day are shown in **Figures 2H** and **I**. Briefly, the maximum plasma concentration (C_{max}) of MG and CA was 132.01 μ g/L and 119.63 μ g/L, respectively. The time to reach the maximum plasma concentration (T_{max}) for MG and CA in rats receiving BHGZD was 4.00 h and 0.25 h, respectively. The plasma concentration–time curve $AUC_{(0-24h)}$ of MG and CA was 578.42 μ g/L \cdot h and 102.48 μ g/L \cdot h, respectively. The apparent elimination half-life ($T_{1/2Z}$) and mean retention time (MRT) of MG (1.26 h and 4.23 h, respectively) and CA (1.65 h and 1.93 h, respectively) in rats after the treatment of BHGZD were measured.

Both BHGZD and the Two-BAC Combination of MG and CA Improve Arthritis Severity in Active RA Rats

To verify the pharmacological effects of the two-BAC combination of MG and CA against active RA, the *in vivo* experiments were performed based on the AIA-M rat model (22, 24). Similar pathological characteristics and changes in AIA-M rats were observed from the validation cluster to the discovery cluster (**Figure 3**). As a result, the ankles and knuckle joints of AIA-M rats with severe redness and swelling were remarkably improved by the treatment of the two-BAC combination (equivalent to BHGZD at a dose of 21.4 g/kg) and BHGZD (dose of 21.4 g/kg, **Figures 3A** and **B**). Importantly, both the treatment of BHGZD and the two-BAC combination significantly alleviated disease severity, including reducing arthritis incidence, the diameter of the limb, and arthritis score (all $p < 0.05$, on the 27th day after immunization), and simultaneously elevated pain thresholds (mechanical-, acetone-, and thermal-induced hyperalgesia), all of which were similar to the pharmacological effects of MTX (positive drug, dose of 0.2 mg/kg, **Figures 3C** and **D**).

In order to investigate the joint destruction and synovial inflammation, both the ankle and knee joints of AIA-M rats in different groups were scanned using Micro-CT analysis on the 31st day after immunization. The quantified data revealed that BMD, TMD, BV/TV ratio, and Tb.Th were dramatically decreased, and BS/BV ratio and Tb.Sp was observably increased in the AIA-M model group (all $p < 0.05$, **Figure 3E** and **Supplementary Figure S2B**) with rough bone surfaces and severe bone erosion (**Figure 3F**, and **Supplementary Figure S2A**). As shown in **Figure 3F**, both BHGZD and the two-BAC

combination treatment groups showed smooth bone surface with a significantly increased BMD, TMD, BV/TV ratio, and Tb.Th, as well as a significantly decreased BS/BV ratio and Tb.Sp (all $p < 0.05$, **Figure 3E** and **Supplementary Figure S2B**), suggesting that the two-BAC combination may efficiently reverse bone erosion, which was similar to the pharmacological effects of MTX.

Moreover, H&E, safranin O fast green, and Masson trichrome staining were carried out to evaluate the degree of joint lesions in AIA-M rats. As shown in **Figures 3G** and **H**, the treatment of the two-BAC combination, BHGZD, and MTX all apparently reversed the histopathological changes of knee joints in AIA-M rats, including the decreased inflammatory cell infiltration, the prevention of cartilage and bone destruction, and synovial hyperplasia (all $p < 0.05$). Consistently, a significant reduction of the safranin O fast green-positive area and an elevation of the Masson-positive area were observed on the cartilage surface of AIA-M rats, reflecting a loss of articular cartilage, but reversed by the two-BAC combination, similar to the pharmacological effects of BHGZD and MTX (all $p < 0.05$, **Figures 3G** and **H**). These findings revealed that BHGZD and the two-BAC combination of MG and CA may effectively alleviate the progression of bone damages, repair bone erosion, and simultaneously improve pathological changes of articular cartilage and synovial inflammation in the arthritic joints of AIA-M rats.

In terms of the response to inflammation, pathological changes of the thymus and spleen and viscera indexes in different groups were examined. As shown in **Figure S2C**, the lower proportion of white pulp in the spleen with decreased cell density lymphatic sheath, lymphoid follicular hyperplasia, marginal zone, red pulp, and germinal center was observed in AIA-M rats, which were significantly improved by the treatment of BHGZD and the two-BAC combination (all $p < 0.05$, **Supplementary Figure S2D**). A thinner thymic cortex, less thymic lobule, an unclear boundary, and more vacuoles in the cytoplasm of epithelial reticular cells were also observed in AIA-M rats, which were remarkably improved by the treatment of BHGZD and the two-BAC combination (**Supplementary Figure S2C**). The treatment with BHGZD and the two-BAC combination protected the morphological structure of the spleen and thymus, and simultaneously decreased spleen and thymus indexes significantly (all $p < 0.05$, **Supplementary Figure S2E**).

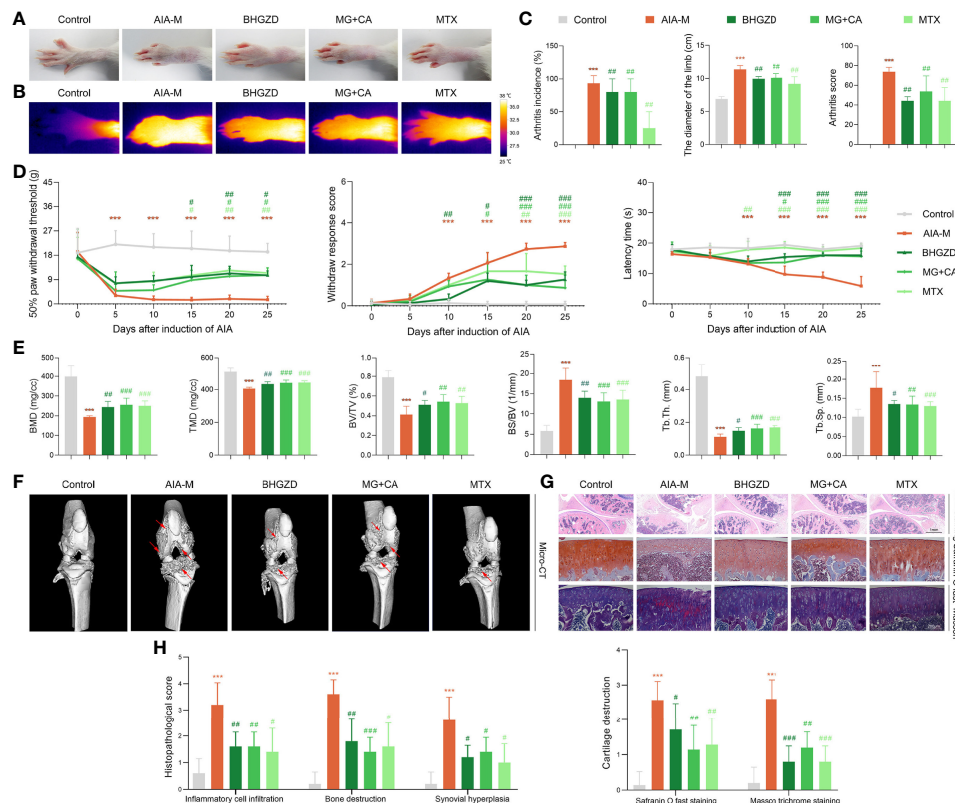


FIGURE 3 | Therapeutic effects of BHGZD, two-BAC combination, and MTX on the severity of arthritis in AIA-M rats (Control, AIA-M, BHGZD, MG+CA, and MTX). **(A)** Representative images of arthritis. **(B)** Infrared thermography. **(C)** Arthritis incidence ($n = 3$ per group), and arthritis score on the 27th day after immunization ($n \geq 4$ per group, all experiments were performed in triplicate). **(D)** The pain thresholds (mechanical-, acetone-, and thermal-induced hyperalgesia, $n \geq 4$ per group, all experiments were performed in triplicate). **(E)** Quantitative micro-computed tomography (micro-CT) analysis of bone mineral density (BMD), tissue mineral density (TMD), bone volume/tissue volume (BV/TV), bone surface/bone volume (BS/BV), trabecular separation (Tb.Sp), and trabecular thickness (Tb.Th) on the 31st day after immunization ($n \geq 5$ per group, all experiments were performed in triplicate). **(F)** Representative micro-CT images of knee joints showing bone erosion levels (the red arrow indicates the position of the bone destruction). **(G)** Pathological changes in the knee joints using hematoxylin and eosin (H&E, scale bar represents 1 mm), safranin O fast green (scale bar represents 200 μ m), and Masson trichrome staining (scale bar represents 200 μ m) in different groups ($n = 5$ per group). **(H)** Quantitative analysis of H&E staining in inflammatory cell infiltration, bone destruction, and synovial hyperplasia. Cartilage destruction of safranin O fast, and Masson trichrome staining ($n = 5$ per group). Data are expressed as the mean \pm SD. ***, $p < 0.001$, comparison with the normal control group; #, ##, ###, $p < 0.05$, $p < 0.01$, $p < 0.001$, respectively, comparison with the AIA-M model group.

Furthermore, H&E-stained tissues of liver and kidney, and the liver and kidney indexes showed no toxic damages (**Supplementary Figures S2C and F**).

Both BHGZD and the Two-BAC Combination of MG and CA Suppress NLRP3 Inflammasome-Induced Pyroptosis Via Regulating TLR4/PI3K/AKT/NF κ B Signaling

The above network-based data imply that BHGZD might reverse the imbalance of the “immune-inflammation” system during active RA progression *via* regulating TLR4/PI3K/AKT/NF κ B/NLRP3 signaling. To the best of our knowledge, pyroptosis is a kind of NLRP3 inflammasome-induced inflammatory cell death, characterized by cell swelling and release of pro-inflammatory cytokines depending on the activation of caspase-1, contributing to inflammation in arthritis (37). The formation of the NLRP3

inflammasome complex requires the interaction of NLRP3 with ASC and caspase-1, which are vital for the assembly and activation of the NLRP3 inflammasome. In our previous study, the immunomodulatory and anti-inflammatory activities of BHGZD were verified, especially in inhibiting pyroptotic death, which may be attributed to the activation of TLR4-NLRP3 inflammasome signaling (22). Currently, our TUNEL data showed a significant proportion of pyroptosis cells in the arthritic joints of AIA-M rats, which was improved by the treatment of BHGZD and the two-BAC combination (**Figure 4A**). Similar to the pharmacological effects of MTX, high expression levels of NLRP3 and ASC, high expression and enhanced activity of caspase-1, and increased expression of IL-1 β and IL-18 (the signature inflammatory cytokines in pyroptosis) in the AIA-M model group (all $p < 0.05$) were all significantly decreased by the treatment of BHGZD and the two-BAC combination (all $p < 0.05$, **Figures 4B–E**). Pyroptosis was assessed by LDH activity, which may be used to verify cell membrane

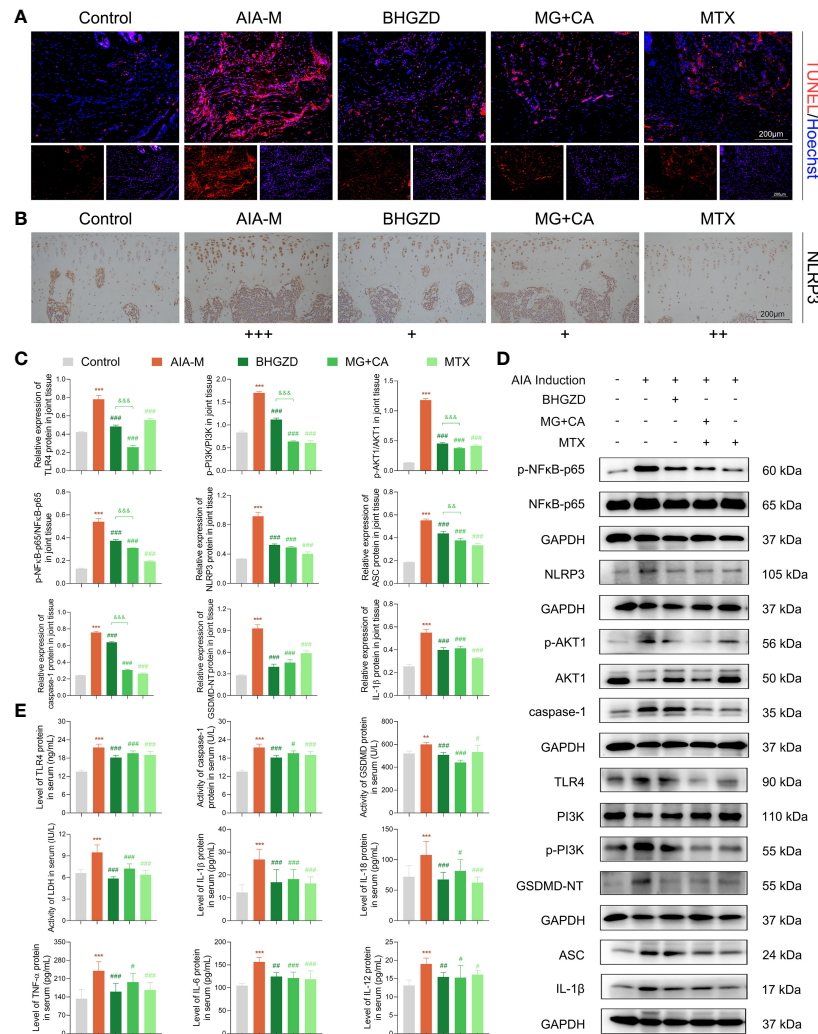


FIGURE 4 | Regulatory effects of BHGZD, the two-BAC combination, and MTX on the expression of TLR4, p-PI3K/PI3K, p-AKT1/AKT1, p-NFκB-p65/NFκB-p65, NLRP3, ASC, caspase-1, GSDMD-NT, IL-1β, IL-18, IL-6, TNF-α, and IL-12 in AIA-M rats of different groups (Control, AIA-M, BHGZD, MG+CA, and MTX). **(A)** Representative images of pyroptosis in the knee joints of AIA-M rats detected by deoxynucleotidyltransferase-mediated UTP end labeling (TUNEL) assay (scale bar represents 200 μm, TUNEL red, Hoechst blue). **(B)** The expression of NLRP3 protein in the knee joints of AIA-M rats (scale bar represents 200 μm). **(C, D)** The protein expression of TLR4, p-PI3K/PI3K, p-AKT1/AKT1, p-NFκB-p65/NFκB-p65, NLRP3, ASC, caspase-1, GSDMD-NT, and IL-1β in the knee joints of AIA-M rats using Western blotting analysis ($n = 3$ per group). **(E)** The expression levels of TLR4, TNF-α, IL-6, IL-1β, IL-18, and IL-12 in the sera of AIA-M rats using enzyme-linked immunosorbent assay (ELISA) analysis, and the activities of caspase-1, GSDMD-NT, and LDH in the sera of AIA-M rats using ELISA analysis ($n \geq 3$ per group, all experiments were performed in triplicate). Data are expressed as the mean \pm SD. **, $p < 0.01$, $p < 0.001$, respectively, comparison with the normal control group; #, ##, ###, $p < 0.05$, $p < 0.01$, $p < 0.001$, respectively, comparison with the AIA-M model group; &&, &&&, $p < 0.01$, $p < 0.001$, comparison with the treatment of BHGZD.

integrity and the release of intracellular soluble component. Consistently, the enhancing activity of LDH in the sera of AIA-M rats was observed, which was significantly decreased by the treatment of BHGZD, the two-BAC combination, and MTX (all $p < 0.05$, **Figure 4E**), suggesting the alleviation of downstream membrane damage.

To verify the *in vivo* findings based on AIA-M rats, an established method (LPS plus ATP) was applied to induce NLRP3 inflammasome activation in both RAW264.7 and MH7A cells. The cell viability on RAW264.7 cells with the

treatment of MG and CA was initially examined using the CCK8 assay, and the results exhibited no cell toxicity under 0.21–6.74 ng/ml MG or 0.02–0.52 ng/ml CA treatment alone, as shown in **Supplementary Figure S2G**. Thus, 1.69 ng/ml MG and 0.13 ng/ml CA treatment were chosen in the following assays (the same content as that in the 5 μg/ml BHGZD formula). Flow cytometry analysis revealed that MG, CA, and the two-BAC combination treatment prominently reduced the PI [a marker of cells that stains necrotic, dead, and membrane-compromised cells (38)] positive cell rate of RAW264.7 cells induced by LPS/ATP,

which was inferior to that in the BHGZD treatment group (all $p < 0.05$, **Figures 5A and B**). As shown in **Figures 5C and 6A**, LPS/ATP induced an increase in the number of both FLICA-positive RAW264.7 cells and TUNEL-positive MH7A cells, which was reduced by the treatment of BHGZD, MG, CA, and the two-BAC combination. Intriguingly, the inhibition of MG or CA alone on cell pyroptosis induced by LPS/ATP was weaker than that in the two-BAC combination treatment group (all $p < 0.05$, **Figures 5A–C and 6A**). In addition, the expression levels of NLRP3, ASC, and caspase-1 were significantly increased in both RAW264.7 and MH7A cells induced by LPS/ATP, the same as the levels of IL-1 β , IL-18, and LDH release in the supernatant of RAW264.7 and MH7A cells, which were all reduced by the treatment of BHGZD, MG, CA, and the two-BAC combination (all $p < 0.05$, **Figures 5D–G and 6B–E**). GSDMD, a crucial mediator of pyroptosis downstream of canonical and non-canonical inflammasomes (39–41), is cleaved by caspase-1 at a specific site (GSDMD-NT) and subsequently causes cell lysis and IL-1 β release (42, 43). In the current study, the activities of GSDMD-NT in sera

and its levels in knee joints were both significantly elevated in AIA-M rats, which was reduced by the treatment of BHGZD, the two-BAC combination, and MTX (all $p < 0.05$, **Figures 4C–E**). Notably, GSDMD-NT occurred in both RAW264.7 and MH7A cells induced by LPS/ATP, which was decreased by the treatment of BHGZD, MG, CA, and the two-BAC combination (**Figures 5E, F and 6C, D**).

After determining the inhibitory effects of BHGZD and the two-BAC combination on NLRP3 inflammasome-induced pyroptosis, we further investigated the changes of its upstream determinant TLR4/PI3K/AKT/NF κ B signaling in different groups. Importantly, the expression levels of TLR4 in both sera and knee joints of AIA-M rats were increased, and subsequently were effectively reversed by the treatment of the two-BAC combination, with similar trends to BHGZD and MTX (all $p < 0.05$, **Figures 4C–E**). The protein expression ratios of p-PI3K/PI3K, p-NF κ B-p65/NF κ B-p65, and p-AKT1/AKT1 were all significantly increased in AIA-M rats, which were distinctively reduced by the treatment of BHGZD and the two-BAC

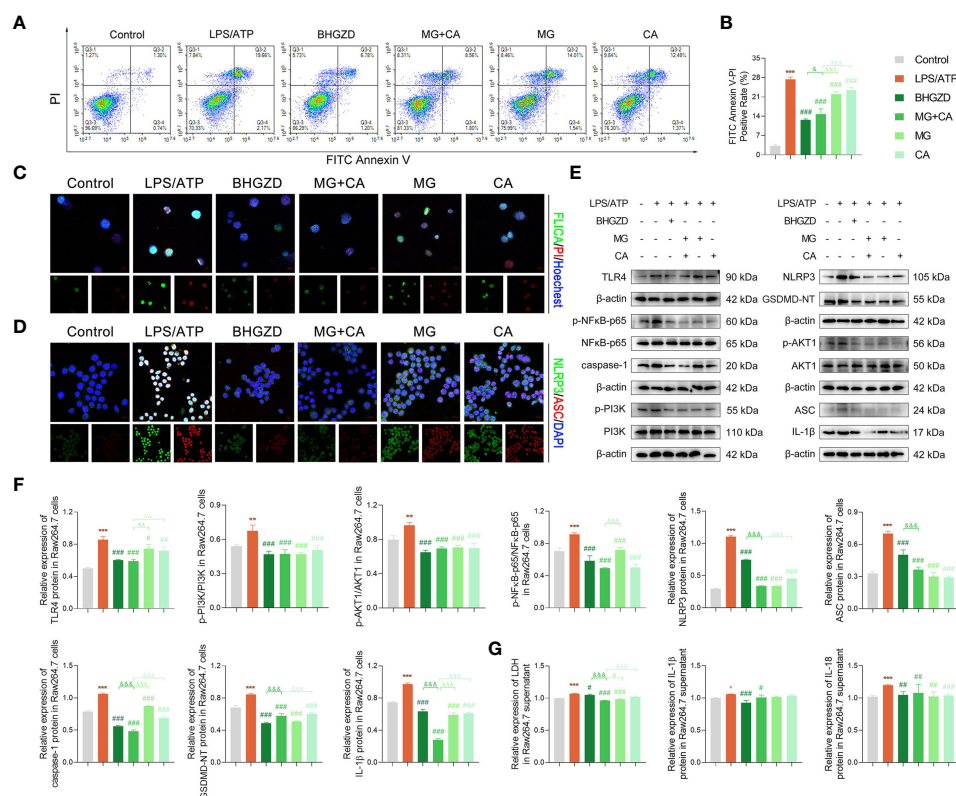


FIGURE 5 | BHGZD inhibits LPS/ATP-induced pyroptosis in RAW264.7 macrophage by downregulating TLR4, p-PI3K/PI3K, p-AKT1/AKT1, p-NF κ B-p65/NF κ B-p65, NLRP3, ASC, caspase-1, GSDMD-NT, IL-1 β , and IL-18 (Control, AIA-M, BHGZD, MG+CA, MG, and CA). **(A, B)** Flow cytometry analysis for Annexin V/PI staining in RAW264.7 cells ($n \geq 3$ per group, all experiments were performed in triplicate). **(C)** Representative images of FAM-FLICA Caspase-1 that binds only to activated caspase-1 (scale bar represents 50 μ m, FAM-FLICA green, PI red, Hoechst blue). **(D)** Expression of NLRP3 and ASC protein measured by immunofluorescent staining and confocal microscopy in RAW264.7 cells (scale bar represents 50 μ m, NLRP3 FITC green, ASC CY3 red, DAPI blue). **(E, F)** Expression levels of TLR4, p-PI3K/PI3K, p-AKT1/AKT1, p-NF κ B-p65/NF κ B-p65, NLRP3, ASC, caspase-1, GSDMD-NT, and IL-1 β in RAW264.7 cells measured by Western blotting ($n = 3$ per group). **(G)** Levels of IL-1 β , IL-18, and LDH release in RAW264.7 cells detected by ELISA ($n \geq 3$ per group, all experiments were performed in triplicate). *, **, ***, $p < 0.05$, $p < 0.01$, $p < 0.001$, respectively, comparison with the normal control group; #, ##, ###, $p < 0.05$, $p < 0.01$, $p < 0.001$, respectively, comparison with LPS/ATP-induced model; &, &&, &&&, $p < 0.05$, $p < 0.01$, $p < 0.001$, respectively, comparison with the treatment of BHGZD; Δ , $\Delta\Delta$, $\Delta\Delta\Delta$, $p < 0.005$, $p < 0.01$, $p < 0.001$, comparison with the treatment of the two-BAC combination.

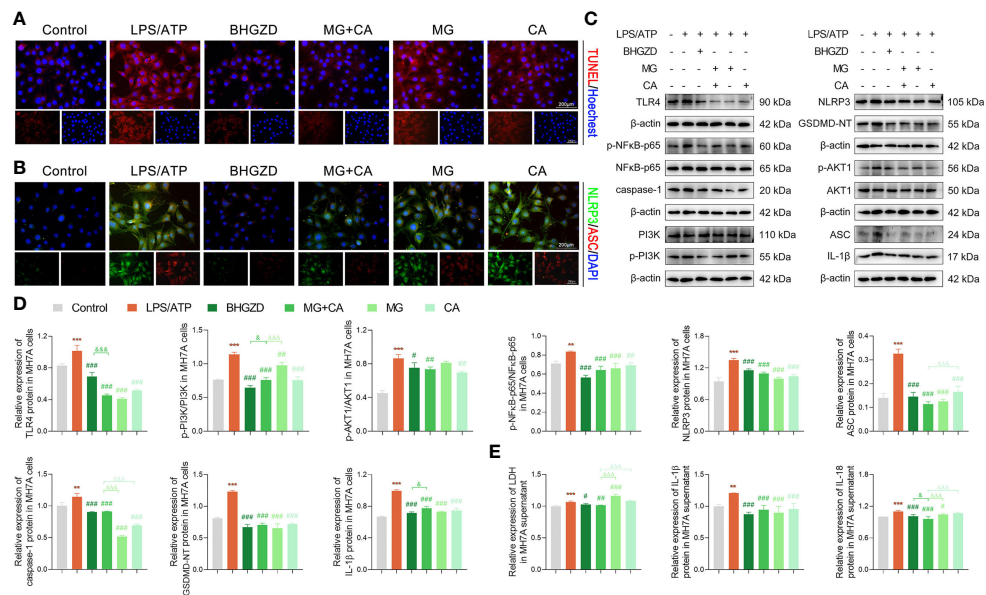


FIGURE 6 | BHGZD inhibits LPS/ATP-induced pyroptosis in MH7A cells by downregulating TLR4, p-PI3K/p13K, p-AKT1/AKT1, p-NFκB-p65/NFκB-p65, NLRP3, ASC, caspase-1, GSDMD-NT, IL-1β, and IL-18 (Control, AIA-M, BHGZD, MG+CA, MG, and CA). **(A)** TUNEL staining of MH7A cells (scale bar represents 200 μm, TUNEL red, Hoechst blue). **(B)** Expression of NLRP3 and ASC protein measured by immunofluorescent staining and confocal microscopy in MH7A cells (scale bar represents 200 μm, NLRP3 FITC green, ASC CY3 red, DAPI blue). **(C, D)** Expression levels of TLR4, p-PI3K/p13K, p-AKT1/AKT1, p-NFκB-p65/NFκB-p65, NLRP3, ASC, caspase-1, GSDMD-NT, and IL-1β in MH7A cells measured by Western blotting ($n = 3$ per group). **(E)** Levels of IL-1β, IL-18, and LDH release in MH7A cells evaluated by ELISA ($n \geq 3$ per group, all experiments were performed in triplicate). **, ***, $p < 0.01$, $p < 0.001$, respectively, comparison with the normal control group; #, ##, ###, $p < 0.05$, $p < 0.01$, $p < 0.001$, respectively, comparison with LPS/ATP-induced model; &, &&, &&&, $p < 0.05$, $p < 0.001$, comparison with the treatment of BHGZD; △△△, $p < 0.001$, comparison with the treatment of two-BAC combination.

combination (all $p < 0.05$, **Figures 4C, D**), indicating their inhibitory effects on TLR4/PI3K/AKT/NFκB signaling activation. In addition to the increased accumulation of inflammatory cells, the expression levels of inflammatory cytokines in AIA-M rats sera, including TNF-α, IL-6, and IL-12, were abnormally elevated in AIA-M rats, and reduced by the treatment of the two-BAC combination, in accordance with the effects of BHGZD and MTX (all $p < 0.05$, **Figure 4E**). Interestingly, we also achieved the same findings in the *in vitro* experiment validations based on both RAW264.7 and MH7A cells induced by LPS/ATP (all $p < 0.05$, **Figures 5E–G and 6C–E**).

These findings demonstrated that both BHGZD and the two-BAC combination of MG and CA may suppress TLR4/PI3K/AKT/NFκB signaling-related protein activation, and subsequently inhibit NLRP3 inflammasome-induced pyroptosis.

DISCUSSION

Growing clinical evidence shows that various immune cells sustainably influx and migrate into the joints *via* secreting different types of immunomodulatory cytokines, leading to pyroptosis-induced persistent synovitis and cartilage degradation (44, 45). Thus, reversing the imbalance of the “immune-inflammation” system, especially alleviating pyroptosis, may be a promising therapeutic strategy for active RA. The current study performed an integrative research combining UFLC-Q-TOF-MS/

MS, gene expression profiling, network calculation, pharmacokinetic profiling, SPR/MST assay, and pharmacological experiment validations, and identified TLR4/PI3K/AKT/NFκB/NLRP3 signaling-induced pyroptosis as one of the candidate effective targets of BHGZD for reversing the imbalance network of “immune-inflammation” during active RA progression. In addition, both MG and CA were identified as representative BACs acting on that target, for the strong binding affinities between compounds and target proteins, good pharmacokinetic features, and similar pharmacological effects to BHGZD. Notably, both BHGZD and the two-BAC combination of MG and CA effectively improved disease severity of active RA rats including elevating pain thresholds, relieving joint inflammation and bone erosion *via* inhibiting TLR4/PI3K/AKT/NFκB signaling to suppress the activation of the NLRP3 inflammasome, leading to the downregulation of downstream caspase-1, the reduced release of IL-1β, and the modulation of GSDMD-mediated pyroptosis. Consistent data were obtained based on the *in vitro* pyroptosis models of RAW264.7 and MH7A cells induced by LPS/ATP. Thus, RAW264.7 macrophages might be the probable immune cells targeted by both BHGZD and the two-BAC combination of MG and CA.

Currently, the AIA-M rat model was established simulating the pathogenetic characteristics of active RA with moist heat arthralgia spasm syndrome on the basis of male Lewis rats according to our previous studies (20–23). The abnormal changes in indicators reflecting the imbalance of the “immune-

inflammation” system, including distinct redness and swelling, an increase in arthritis surface temperature, arthritis incidence, the diameter of the limb, arthritis score, pathologic changes of the thymus and spleen, as well as severe inflammatory cell infiltration, cartilage and bone destruction, synovial hyperplasia, and the high levels of inflammatory mediators, such as TLR4, IL-6, IL-12, IL-1 β , IL-18, and TNF- α , were observed as the distinctive characteristics and biological basis of AIA-M rats, which may be in line with the clinical manifestations in active RA patients. Following the transcriptomic profiling and biomolecular network analyses, a series of active RA-related genes were also identified, and functionally involved in the regulation of the “immune-inflammation” system accordingly.

Considering that TCM contributed to the multi-target interactions of the complex ingredients of its herbal drugs (46–

48), pharmaceutical development has consistently been an urgent challenge. Therefore, a new method that combines BACs contained in herbal formulas has been strongly indicated for new drug discovery. Herein, the two BACs, namely, MG from *Anemarrhenae Rhizoma* and CA from *Cinnamomi Ramulus*, were identified as the representative BACs of BHGZD for the strong binding affinities between compounds and target proteins, good pharmacokinetic properties, the high content and the importance of the formula, and similar pharmacological effects to BHGZD. Interestingly, the treatment of MG or CA alone did not exert prominently therapeutic effects compared to that of the two-BAC combination. Similar to the BHGZD formula, the two-BAC combination treatment of MG and CA may exert satisfying therapeutic efficacy on both *in vivo* and *in vitro* experiments via regulating TLR4/PI3K/AKT/NF κ B signaling, which plays a vital

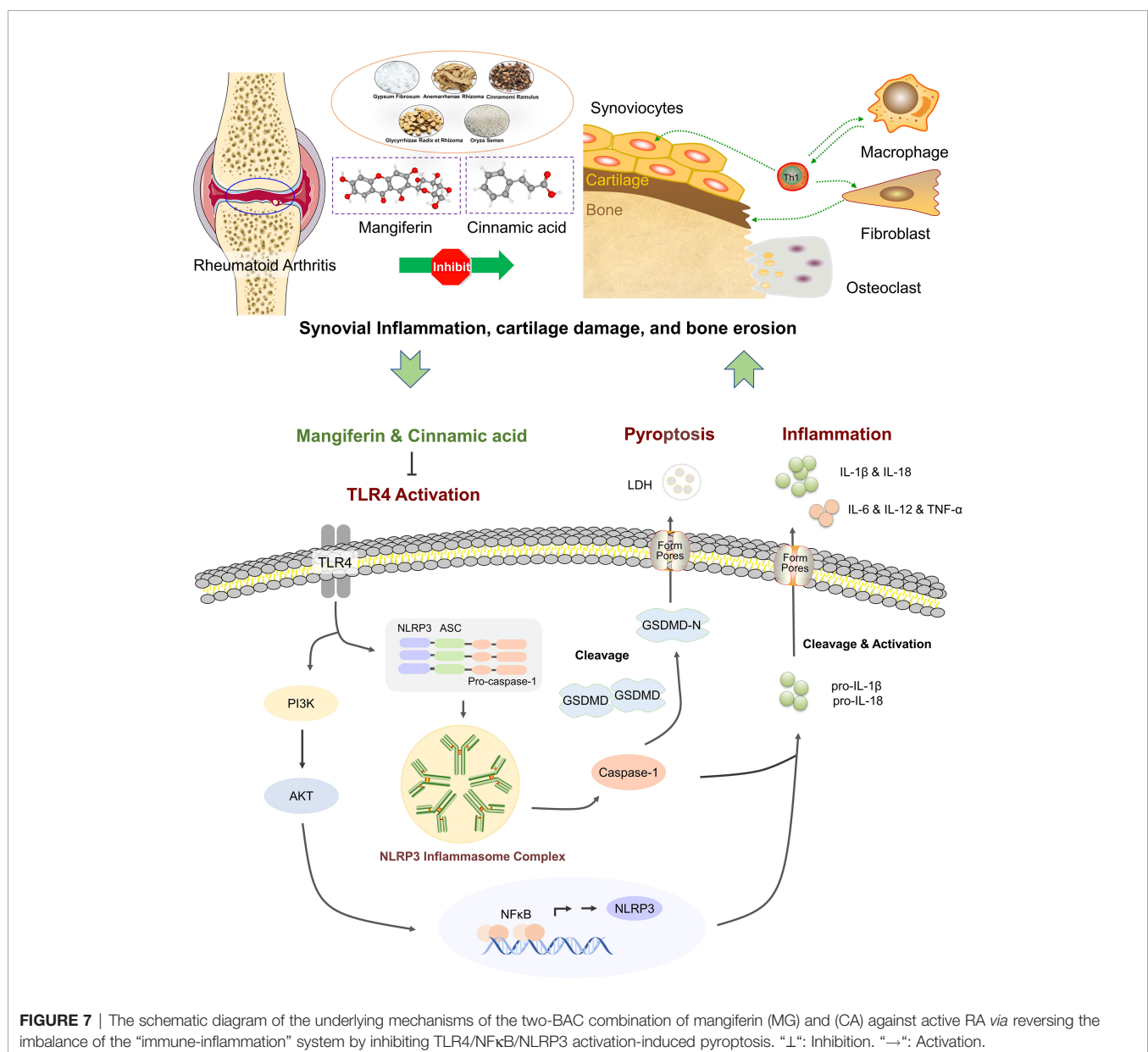


FIGURE 7 | The schematic diagram of the underlying mechanisms of the two-BAC combination of mangiferin (MG) and (CA) against active RA via reversing the imbalance of the “immune-inflammation” system by inhibiting TLR4/NF κ B/NLRP3 activation-induced pyroptosis. “ \perp ”: Inhibition. “ \rightarrow ”: Activation.

role in synovial inflammation, cartilage degradation, and bone erosion by regulating inflammation response, immune disorder cells, and pyroptosis (37, 49–52). More importantly, the two-BAC combination of MG and CA offers key potential advantages over BHGZD for the following points. Firstly, the two-BAC combination may exert similar pharmacological effects in treating AIA-M rats with a definite material basis. Secondly, the two-BAC combination may be flexible in design, easily synthesized on a large scale, easily absorbed, and relatively stable, not dependent on the cultivations of crude herbs. Thirdly, it is better to understand the underlying molecular mechanisms of TCM-based RA therapeutics.

In conclusion, our data offer an evidence that the MG and CA combination from BHGZD may interact with TLR4/PI3K/AKT/NFκB signaling to inhibit NLRP3 inflammasome activation and modulate pyroptosis, which provides the novel representative BACs and pharmacological mechanisms of BHGZD against active RA (Figure 7). The findings may shed new light on the mechanisms of the TCM formula, and promote the modernization development of TCM and drug discovery.

DATA AVAILABILITY STATEMENT

The datasets presented in this study can be found in online repositories. The name of the repository and accession number (s) can be found below: NCBI Gene Expression Omnibus; GSE190523, GSE189942.

ETHICS STATEMENT

The study was approved by the Research Ethics Committee of the Institute of Chinese Materia Medica, China Academy of Chinese Medical Sciences, Beijing, China [Ethics Approval Number: 2019-026 and IBTCMCACMS21-2105-01, certificate number of the facility: SYXK (Beijing) 2021-0017]. All animal studies were treated in accordance with the guidelines and

regulations for the use and care of animals of the Center for Laboratory Animal Care, China Academy of Chinese Medical Sciences. All animal-handling procedures were performed according to the *Guide for the Care and Use of Laboratory Animals* of the National Institutes of Health and followed the guidelines of the Animal Welfare Act.

AUTHOR CONTRIBUTIONS

NL and YZ engaged in study design and coordination, material support for obtained funding, and supervised study. YZ designed the experimental validation and revised the manuscript. WL performed most of the experiments and statistical analysis, as well as wrote the manuscript. SY and WS performed parts of the experiments, reviewed and approved the final manuscript. The other authors performed parts of the experiments. All authors contributed to the article and approved the final manuscript.

FUNDING

This study is funded by the National Natural Science Foundation of China (81630107), the Scientific and Technological Innovation Project of China Academy of Chinese Medical Sciences (CI2021A03808 and CI2021A01508), and the National Key Research and Development Program of China (2018YFC1705201). No study sponsors are involved in the research process of this project.

SUPPLEMENTARY MATERIAL

The Supplementary Material for this article can be found online at: <https://www.frontiersin.org/articles/10.3389/fimmu.2022.912933/full#supplementary-material>

REFERENCES

- Firestein GS, McInnes IB. Immunopathogenesis of Rheumatoid Arthritis. *Immunity* (2017) 46(2):183–96. doi: 10.1016/j.immuni.2017.02.006
- Catrina AI, Svensson CI, Malmstrom V, Schett G, Klareskog L. Mechanisms Leading From Systemic Autoimmunity to Joint-Specific Disease in Rheumatoid Arthritis. *Nat Rev Rheumatol* (2017) 13(2):79–86. doi: 10.1038/nrrheum.2016.200
- Tak PP, Kalden JR. Advances in Rheumatology: New Targeted Therapeutics. *Arthritis Res Ther* (2011) 13 Suppl 1:S5. doi: 10.1186/1478-6354-13-S1-S5
- Burmester GR, Pope JE. Novel Treatment Strategies in Rheumatoid Arthritis. *Lancet* (2017) 389(10086):2338–48. doi: 10.1016/S0140-6736(17)31491-5
- England BR, Thiele GM, Anderson DR, Mikuls TR. Increased Cardiovascular Risk in Rheumatoid Arthritis: Mechanisms and Implications. *BMJ* (2018) 361:k1036. doi: 10.1136/bmj.k1036
- Semb AG, Kvien TK, Aastveit AH, Jungner I, Pedersen TR, Walldius G, et al. Lipids, Myocardial Infarction and Ischaemic Stroke in Patients With Rheumatoid Arthritis in the Apolipoprotein-Related Mortality Risk (Amoris) Study. *Ann Rheum Dis* (2010) 69(11):1996–2001. doi: 10.1136/ard.2009.126128
- Solomon DH, Karlson EW, Rimm EB, Cannuscio CC, Mandl LA, Manson JE, et al. Cardiovascular Morbidity and Mortality in Women Diagnosed With Rheumatoid Arthritis. *Circulation* (2003) 107(9):1303–7. doi: 10.1161/01.cir.0000054612.26458.b2
- Bordy R, Totson P, Prati C, Marie C, Wendling D, Demougeot C. Microvascular Endothelial Dysfunction in Rheumatoid Arthritis. *Nat Rev Rheumatol* (2018) 14(7):404–20. doi: 10.1038/s41584-018-0022-8
- Sapir-Koren R, Livshits G. Postmenopausal Osteoporosis in Rheumatoid Arthritis: The Estrogen Deficiency-Immune Mechanisms Link. *Bone* (2017) 103:102–15. doi: 10.1016/j.bone.2017.06.020
- Adami G, Saag KG. Osteoporosis Pathophysiology, Epidemiology, and Screening in Rheumatoid Arthritis. *Curr Rheumatol Rep* (2019) 21(7):34. doi: 10.1007/s11926-019-0836-7
- Simon TA, Thompson A, Gandhi KK, Hochberg MC, Suissa S. Incidence of Malignancy in Adult Patients With Rheumatoid Arthritis: A Meta-Analysis. *Arthritis Res Ther* (2015) 17:212. doi: 10.1186/s13075-015-0728-9
- England BR, Hershberger D. Management Issues in Rheumatoid Arthritis-Associated Interstitial Lung Disease. *Curr Opin Rheumatol* (2020) 32(3):255–63. doi: 10.1097/bor.0000000000000703

13. Qindeel M, Ullah MH, Fakhar Ud D, Ahmed N, Rehman AU. Recent Trends, Challenges and Future Outlook of Transdermal Drug Delivery Systems for Rheumatoid Arthritis Therapy. *J Control Release* (2020) 327:595–615. doi: 10.1016/j.jconrel.2020.09.016
14. Guo D, Lv J, Chen X, Yan X, Ma F, Liu Y, et al. Study of Mirna Interactome in Active Rheumatoid Arthritis Patients Reveals Key Pathogenic Roles of Dysbiosis in the Infection-Immune Network. *Rheumatol (Oxford)* (2021) 60 (3):1512–22. doi: 10.1093/rheumatology/keaa369
15. Zhang P, Li J, Han Y, Yu XW, Qin L. Traditional Chinese Medicine in the Treatment of Rheumatoid Arthritis: A General Review. *Rheumatol Int* (2010) 30(6):713–8. doi: 10.1007/s00296-010-1370-0
16. Fang L. The Clinical Effect of Baihu Plus Guizhi Decoction in Treating Rheumatoid Arthritis With Damp-Heat Arthralgia Syndrome and its Influence on the Expression of RF, IL-22, IL-35 and GPI. *Global Tradit Chin Med* (2018) 11(06):964–7. doi: 10.14164/j.cnki.cn11-5581/r.2022.02.078
17. Yuan L, Wu J, Tang J, Chen Y, Zhang Z. Clinical Observation on Baihu Plus Guizhi Decoction Combined With Western Medicine in Treating Rheumatoid Arthritis of Rheumatic Fever Arthralgia Syndrome. *J Liaoning Univ Tradit Chin Med* (2019) 21(12):168–71. doi: 10.13194/j.issn.1673-842x.2019.12.044
18. Yuan L. Clinical Observation on Baihu Plus Guizhi Decoction Combined With Western Medicine in Treating Rheumatoid Arthritis of Rheumatic Fever Arthralgia Syndrome. *Guangzhou Chin Med* (2020). doi: 10.27879/d.cnki.ggzxy.2020.000306
19. Wu D. Efficacy of Baihu-Guizhi Decoction Combined With Western Medicine in Treating Rheumatoid Arthritis. *Chin J Urban Rural Enterp Hyg* (2021) 36(01):158–60. doi: 10.16286/j.1003-5052.2021.01.067
20. Li W, Lu J, Mao X, Guo Q, Wang X, Guo M, et al. A Comparative Study on the Mechanisms of Two Classical Herbal Formulae for Rheumatoid Arthritis Applying Cold and Heat Patterns Based on Target Network. *Acta Pharm Sin A* (2018) 53(09):1387–97. doi: 10.16438/j.0513-4870.2018-0519
21. Li W, Mao X, Wu H, Guo M, Su X, Lu J, et al. Deciphering the Chemical Profile and Pharmacological Mechanisms of Baihu-Guizhi Decoction Using Ultra-Fast Liquid Chromatography-Quadrupole-Time-Of-Flight Tandem Mass Spectrometry Coupled With Network Pharmacology-Based Investigation. *Phytomed Int J phytother phytopharmacol* (2020) 67:153156. doi: 10.1016/j.phymed.2019.153156
22. Li W, Mao X, Wang X, Liu Y, Wang K, Li C, et al. Disease-Modifying Anti-Rheumatic Drug Prescription Baihu-Guizhi Decoction Attenuates Rheumatoid Arthritis Via Suppressing Toll-Like Receptor 4-Mediated Nlrp3 Inflammasome Activation. *Front Pharmacol* (2021) 12:743086. doi: 10.3389/fphar.2021.743086
23. Mao X. The Key Material Basis Identification and Pharmacological Mechanism Investigation of Chinese Herbal Formula Wutou Decoction Against Rheumatoid Arthritis With Cold Syndrome. *Chin Acad Chin Med Sci* (2020). doi: 10.27658/d.cnki.gzzxy.2020.000124
24. Mao X, Li W, Chen W, Li Y, Wang Q, Wang X, et al. Exploring and Characterizing a Novel Combination of Paeoniflorin and Talatizidine for the Treatment of Rheumatoid Arthritis. *Pharmacol Res* (2020) 153:104658. doi: 10.1016/j.phrs.2020.104658
25. Guo Q, Mao X, Zhang Y, Meng S, Xi Y, Ding Y, et al. Guizhi-Shaoyao-Zhimu Decoction Attenuates Rheumatoid Arthritis Partially by Reversing Inflammation-Immune System Imbalance. *J Trans Med* (2016) 14(1):165. doi: 10.1186/s12967-016-0921-x
26. Xu HY, Zhang YQ, Liu ZM, Chen T, Lv CY, Tang SH, et al. EtcM: An Encyclopaedia of Traditional Chinese Medicine. *Nucleic Acids Res* (2019) 47 (D1):D976–D82. doi: 10.1093/nar/gky987
27. Szklarczyk D, Franceschini A, Wyder S, Forslund K, Heller D, Huerta-Cepas J, et al. String V10: Protein-Protein Interaction Networks, Integrated Over the Tree of Life. *Nucleic Acids Res* (2015) 43(Database issue):D447–52. doi: 10.1093/nar/gku1003
28. Shannon P, Markiel A, Ozier O, Baliga NS, Wang JT, Ramage D, et al. Cytoscape: A Software Environment for Integrated Models of Biomolecular Interaction Networks. *Genome Res* (2003) 13(11):2498–504. doi: 10.1101/gr.1239303
29. Zhang Y, Mao X, Guo Q, Bai M, Zhang B, Liu C, et al. Pathway of Ppar-Gamma Coactivators in Thermogenesis: A Pivotal Traditional Chinese Medicine-Associated Target for Individualized Treatment of Rheumatoid Arthritis. *Oncotarget* (2016) 7(13):15885–900. doi: 10.18632/oncotarget.7419
30. He Y, Su W, Chen T, Zeng X, Yan Z, Guo J, et al. Identification of Prototype Compounds and Derived Metabolites of Naixintong Capsule in Beagle Dog Urine and Feces by Uflc-Q-ToF-Ms/Ms. *J Pharm Biomed Anal* (2019) 176:112806. doi: 10.1016/j.jpba.2019.112806
31. Sterling T, Irwin JJ. Zinc 15-Ligand Discovery for Everyone. *J Chem Inf Model* (2015) 55(11):2324–37. doi: 10.1021/acs.jcim.5b00559
32. Pandey MK, Sung B, Ahn KS, Kunnumakkara AB, Chaturvedi MM, Aggarwal BB. Gambogic Acid, a Novel Ligand for Transferrin Receptor, Potentiates Tnf-Induced Apoptosis Through Modulation of the Nuclear Factor-KappaB Signaling Pathway. *Blood* (2007) 110(10):3517–25. doi: 10.1182/blood-2013-03-494385
33. Wang Y, Cui Y, Cao F, Qin Y, Li W, Zhang J. Ganglioside Gd1a Suppresses Lps-Induced Pro-Inflammatory Cytokines in Raw264.7 Macrophages by Reducing Mapks and Nf-Kappab Signaling Pathways Through Tlr4. *Int Immunopharmacol* (2015) 28(1):136–45. doi: 10.1016/j.intimp.2015.05.044
34. Villegas SN, Gombos R, Garcia-Lopez L, Gutierrez-Perez I, Garcia-Castillo J, Vallejo DM, et al. P13k/Akt Cooperates With Oncogenic Notch by Inducing Nitric Oxide-Dependent Inflammation. *Cell Rep* (2018) 22(10):2541–9. doi: 10.1016/j.celrep.2018.02.049
35. Khan H, Sureda A, Belwal T, Cetinkaya S, Sunter I, Tejada S, et al. Polyphenols in the Treatment of Autoimmune Diseases. *Autoimmun Rev* (2019) 18 (7):647–57. doi: 10.1016/j.autrev.2019.05.001
36. Ma Z, Yu R, Zhu Q, Sun L, Jian L, Wang X, et al. Cxcl16/Cxcr6 Axis Promotes Bleomycin-Induced Fibrotic Process in Mrc-5 Cells Via the P13k/Akt/Foxo3a Pathway. *Int Immunopharmacol* (2020) 81:106035. doi: 10.1016/j.intimp.2019.106035
37. Spel L, Martinon F. Inflammasomes Contributing to Inflammation in Arthritis. *Immunol Rev* (2020) 294(1):48–62. doi: 10.1111/imr.12839
38. Yang J, Zhao Y, Zhang P, Li Y, Yang Y, Yang Y, et al. Hemorrhagic Shock Primes for Lung Vascular Endothelial Cell Pyroptosis: Role in Pulmonary Inflammation Following Lps. *Cell Death Dis* (2016) 7(9):e2363. doi: 10.1038/cddis.2016.274
39. Shi J, Zhao Y, Wang K, Shi X, Wang Y, Huang H, et al. Cleavage of Gsdmd by Inflammatory Caspases Determines Pyroptotic Cell Death. *Nature* (2015) 526 (7575):660–5. doi: 10.1038/nature15514
40. Micaroni M, Stanley AC, Khromykh T, Venturato J, Wong CX, Lim JP, et al. Rab6a/a' Are Important Golgi Regulators of Pro-Inflammatory Tnf Secretion in Macrophages. *PLoS One* (2013) 8(2):e57034. doi: 10.1371/journal.pone.0057034
41. Kayagaki N, Stowe IB, Lee BL, O'Rourke K, Anderson K, Warming S, et al. Caspase-11 Cleaves Gasdermin D for Non-Canonical Inflammasome Signalling. *Nature* (2015) 526(7575):666–71. doi: 10.1038/nature15541
42. Evavold CL, Ruan J, Tan Y, Xia S, Wu H, Kagan JC. The Pore-Forming Protein Gasdermin D Regulates Interleukin-1 Secretion From Living Macrophages. *Immunity* (2018) 48(1):35–44.e6. doi: 10.1016/j.immuni.2017.11.013
43. DiPeso L, Ji DX, Vance RE, Price JV. Cell Death and Cell Lysis Are Separable Events During Pyroptosis. *Cell Death Discovery* (2017) 3:17070. doi: 10.1038/cddiscovery.2017.70
44. Yap HY, Tee SZ, Wong MM, Chow SK, Peh SC, Teow SY. Pathogenic Role of Immune Cells in Rheumatoid Arthritis: Implications in Clinical Treatment and Biomarker Development. *Cells* (2018) 7(10):161. doi: 10.3390/cells7100161
45. Alenzi FQ. The Significance and Occurrence of Tnf Receptor Polymorphisms in the Saudi Population. *Saudi J Biol Sci* (2016) 23(6):767–72. doi: 10.1016/j.sjbs.2016.04.015
46. Wang X, Morris-Natschke SL, Lee KH. New Developments in the Chemistry and Biology of the Bioactive Constituents of Tanshen. *Med Res Rev* (2007) 27 (1):133–48. doi: 10.1002/med.20077
47. Jiang M, Lu C, Chen G, Xiao C, Zha Q, Niu X, et al. Understanding the Molecular Mechanism of Interventions in Treating Rheumatoid Arthritis Patients With Corresponding Traditional Chinese Medicine Patterns Based on Bioinformatics Approach. *Evid Based Complement Alternat Med* (2012) 2012:129452. doi: 10.1155/2012/129452
48. Fan W, Fan L, Peng C, Zhang Q, Wang L, Li L, et al. Traditional Uses, Botany, Phytochemistry, Pharmacology, Pharmacokinetics and Toxicology of Xanthium Strumarium L.: A Review. *Molecules* (2019) 24(2):359. doi: 10.3390/molecules24020359
49. Hennessy EJ, Parker AE, O'Neill LA. Targeting Toll-Like Receptors: Emerging Therapeutics? *Nat Rev Drug Discovery* (2010) 9(4):293–307. doi: 10.1038/nrd3203

50. Feng FB, Qiu HY. Effects of Artesunate on Chondrocyte Proliferation, Apoptosis and Autophagy Through the Pi3k/Akt/Mtor Signaling Pathway in Rat Models With Rheumatoid Arthritis. *Biomed pharmacother = Biomed pharmacotherapie* (2018) 102:1209–20. doi: 10.1016/j.biopha.2018.03.142
51. AnticaM, KusicB, HranilovicD, DietzAB, Vuk-PavlovicS. Cloning the Cdn for Murine U2 Snmp-A' Gene and Its Differential Expression in Lymphocyte Development. *Immunol Lett* (2002) 82(3):217–23. doi: 10.1016/s0165-2478(02)00064-0
52. Behl T, Chadha S, Sachdeva M, Kumar A, Hafeez A, Mehta V, et al. Ubiquitination in Rheumatoid Arthritis. *Life Sci* (2020) 261:118459. doi: 10.1016/j.lfs.2020.118459

Conflict of Interest: The authors declare that the research was conducted in the absence of any commercial or financial relationships that could be construed as a potential conflict of interest.

Publisher's Note: All claims expressed in this article are solely those of the authors and do not necessarily represent those of their affiliated organizations, or those of the publisher, the editors and the reviewers. Any product that may be evaluated in this article, or claim that may be made by its manufacturer, is not guaranteed or endorsed by the publisher.

Copyright © 2022 Li, Wang, Liu, Wu, He, Li, Wang, Su, Yan, Su, Zhang and Lin. This is an open-access article distributed under the terms of the Creative Commons Attribution License (CC BY). The use, distribution or reproduction in other forums is permitted, provided the original author(s) and the copyright owner(s) are credited and that the original publication in this journal is cited, in accordance with accepted academic practice. No use, distribution or reproduction is permitted which does not comply with these terms.

GLOSSARY

ADME	absorption distribution metabolism excretion
AIA	adjuvant-induced arthritis
AKT1: RAC	alpha serine/threonine-protein kinase
ANOVA	analysis of variance
ASC	apoptosis-associated speck-like protein containing a CARD
ATP	adenosine triphosphate
BAC	bovine serum albumin
BACs	bioactive compounds
BHGZD	Baihu-Guizhi decoction
BMD	bone mineral density
BS/BV	bone surface/bone volume
BV/TV	bone volume/tissue volume
CA	cinnamic acid
CASP1	caspase-1
CCK-8	cell counting kit-8
Cmax	the maximum plasma concentration
DAPI	4', 6-diamidino-2-phenylindole
DMARDs	disease-modifying anti-rheumatic drugs
ELISA	enzyme-linked immunosorbent assay
FBS	fetal bovine serum
FDA	Food and Drug Administration
GSDMD	gasdermin
H&E staining	hematoxylin and eosin staining
IL-12	interleukin-12
IL-18	interleukin-18
IL-1 β	interleukin-1 beta
IL-6	interleukin-6
LDH	lactate dehydrogenase
LPS	lipopolysaccharide
MG	mangiferin
Micro-CT	micro-computed tomography
MST	Microscale thermophoresis
MTX	methotrexate
NF κ B-P65	NF-kappa B transcription factor p65 subunit
NLRP3	NOD-like receptor pyrin domain containing 3
NSAIDs	non-steroidal anti-inflammatory drugs
PBS	phosphate-buffered saline
PFA	paraformaldehyde
PI3K	phosphatidylinositol 3 kinase
PIK3CG	phosphatidylinositol 4, 5-bisphosphate 3-kinase catalytic subunit gamma isoform
PK	pharmacokinetic
RA	rheumatoid arthritis
RNA-Seq	RNA sequencing
ROI	region of interest
SPR	surface plasmon resonance
Tb.Sp	trabecular separation
Tb.Th	trabecular thickness
TCM	traditional Chinese medicine
TLR4	toll-like receptor 4
Tmax	the time to reach the maximum plasma concentration
TMD	tissue mineral density
TNF	tumor necrosis factor
TUNEL assay	deoxynucleotidyltransferase-mediated UTP end labeling
TwHF	Tripterygium wilfordii Hook F
UFLC-Q-TOF-	the ultra-fast liquid chromatography-quadrupole-time-of-flight
MS/MS	tandem mass spectrometry
WTD	Wu-Tou decoction



Two Main Cellular Components in Rheumatoid Arthritis: Communication Between T Cells and Fibroblast-Like Synoviocytes in the Joint Synovium

Jiajie Tu^{1,2†}, Wei Huang^{3†}, Weiwei Zhang⁴, Jiawei Mei³ and Chen Zhu^{3*}

¹ Institute of Clinical Pharmacology, Anhui Medical University, Key Laboratory of Anti-Inflammatory and Immune Medicine, Ministry of Education, Anhui Collaborative Innovation Center of Anti-Inflammatory and Immune Medicine, Hefei, China, ² Department of Gynecology, The First Affiliated Hospital of Shenzhen University, Health Science Center, Shenzhen Second People's Hospital, Shenzhen, China, ³ Department of Orthopaedics, The First Affiliated Hospital of USTC, Division of Life Sciences and Medicine, University of Science and Technology of China, Hefei, China, ⁴ Departments of Geriatrics, The First Affiliated Hospital of USTC, Division of Life Sciences and Medicine, University of Science and Technology of China, Hefei, China

OPEN ACCESS

Edited by:

Heinrich Kerner,
University of Tasmania, Australia

Reviewed by:

Yujie Deng,
Guangzhou Regenerative Medicine
and Health Guangdong Laboratory,
China
Ha-Reum Lee,
Chungnam National University, South
Korea

*Correspondence:

Chen Zhu
zhuchena@ustc.edu.cn

[†]These authors have contributed
equally to this work

Specialty section:

This article was submitted to
Autoimmune and Autoinflammatory
Disorders,
a section of the journal
Frontiers in Immunology

Received: 17 April 2022

Accepted: 25 May 2022

Published: 01 July 2022

Citation:

Tu J, Huang W, Zhang W, Mei J and
Zhu C (2022) Two Main Cellular
Components in Rheumatoid Arthritis:
Communication Between T Cells
and Fibroblast-Like Synoviocytes
in the Joint Synovium.
Front. Immunol. 13:922111.
doi: 10.3389/fimmu.2022.922111

Rheumatoid arthritis (RA) is a chronic autoimmune disease that endangers the health of approximately 1% of the global population. Current RA medications on the market mainly include non-steroidal anti-inflammatory drugs, biological agents, and disease-modifying drugs. These drugs aim to inhibit the overactivated immune response or inflammation of RA, but they cannot cure RA. A better understanding of the pathogenesis of RA will provide a new understanding to search for RA targets and for drug development. The infiltration of T cells and hyper-proliferation of fibroblast-like synoviocytes (FLS) in the synovium of patients with RA are significantly upregulated. Furthermore, the abnormal activation of these two types of cells has been confirmed to promote development of the course of A by many studies. This article systematically summarizes the interactions between T cells and FLS in RA synovial tissues, including one-way/mutual regulation and direct/indirect regulation between the two. It further aims to investigate the pathogenesis of RA from the perspective of mutual regulation between T cells and FLS and to provide new insights into RA research.

Keywords: RA, T cells, FLS, cellular interaction, therapy

1 INTRODUCTION

In the past few decades, extensive research has been conducted to illustrate the important role of T lymphocytes (T cell) in rheumatoid arthritis (RA) (1). In RA, T cell can interact with antigen-presenting cells, including dendritic cell, macrophage, B lymphocyte (B cell), and even non-professional antigen-presenting cell, such as fibroblast-like synoviocyte (FLS). During T cell activation, CD4⁺ T cells initially form contacts with human leukocyte antigen (HLA) or major histocompatibility class II (MHC-II) molecules and co-stimulatory molecules (e.g., CD28) of other

cells, leading to the maturation of CD4⁺ cells (2). Subsequently, antigens presented by other cells promote the activation of CD8⁺ T cells, further exacerbating inflammation in RA (3). The interaction between T cells and other cellular components is a key factor in RA pathogenesis.

Apart from immune cells, non-immune cells of target organs also play a vital role in various autoimmune diseases, forming the foundation of the pathogenesis of these diseases (4). FLS are a special type of non-immune cells present in synovial tissue around joints. FLS play an important destructive role in the pathogenesis of RA; specifically, the numbers of FLS significantly increase and become an important part of the destructive pannus that characterizes the synovial membrane of patients with RA. In addition, FLS in RA exhibit an aggressive phenotype and mediate inflammation and joint destruction. Therefore, cellular crosstalk between FLS and other cellular components might also play an important role in RA, especially in the pathology of the joint synovium.

In this review, we summarize the pathophysiological features of T cells and FLS, which are two important cellular types in the joint synovium of patients with RA, at the functional and molecular level. Further, we outline the interactions between T cells and FLS in RA. Finally, we summarize the potential therapeutic options by explaining the roles of these cells in RA.

2 INDIRECT REGULATION OF T CELLS IN RA BY FLS

2.1 Indirect Promotion of T Cell Survival and Chemotaxis by FLS in RA

RA is an autoimmune disease associated with severe synovitis and the destruction of bone and cartilage. In the synovial tissues of patients with RA, T cells can interact with other immune cells, such as macrophages and B cells, and other non-immune cells,

including FLS, leading to T cell recruitment, activation, and cytokine production (5). This section focuses on these functions of T cells mediated by FLS-secreted chemokines (**Figure 1**).

CD13 released from FLS induces chemotaxis and T cell activation through a pertussis toxin-sensitive G protein-coupled receptor in RA (6). FLS-derived stromal cell-derived factor (SDF)-1 and vascular cell adhesion molecule (VCAM)-1 recruit T cells *via* their corresponding receptors, CXCR4 and integrins alpha (VLA)-4, respectively, in RA (7). FLS can produce an abundance of proinflammatory cytokines in RA joints. For example, interleukin (IL)-15 is mainly responsible for local T cell activation and proliferation (8). The action of FLS-derived IL-7 is essential for lymphoid neogenesis in the RA synovium (9). The Janus kinase (JAK)/signal transducer and activator of transcription (STAT) pathway in FLS is indirectly activated by the tumor necrosis factor (TNF) through the autocrine expression of type I interferon (IFN), resulting in IFN- α/β receptor engagement and the production of chemokines by T cells, which play a role in the effects of the JAK inhibitor CP-690550 (tofacitinib) in the treatment of RA. The reduction of chemokine synthesis mediated by FLS limits the recruitment of T cells and other infiltrating leucocytes (10).

2.2 Indirect Regulation of CD4⁺ T Cell Differentiation in RA by FLS

In addition to recruiting and activating T cells, FLS can also promote the differentiation of proinflammatory subtypes and inhibit the differentiation of anti-inflammatory subtypes of T cells in the synovial joints of patients with RA (11) (**Figure 2**). FLS co-cultured with peripheral blood mononuclear cells (PBMCs) increase peripheral T follicular helper (Tfh) cell (CD4⁺CXCR5⁺ICOS⁺) count in patients with RA (12). Adiponectin-stimulated FLS can also promote Tfh generation, predominantly *via* IL-6 production in RA (13). P53 abrogates

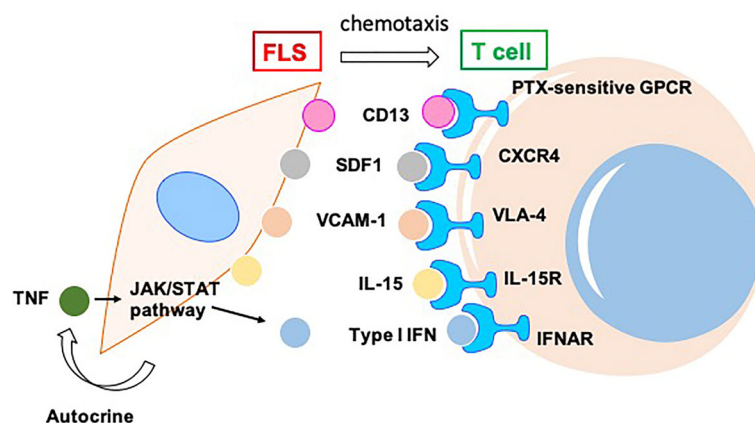


FIGURE 1 | RA-FLS indirectly promotes survival and chemotaxis of T cells in joint synovium of patients with RA *via* by producing various chemokines, including CD13, SDF1, VCAM1, IL15, TNF, and type I IFN. SDF, Stromal cell-derived factor; VCAM, Vascular cell adhesion molecule; VLA, Integrins alpha; CXCR, CXC motif chemokine receptor; IL, interleukin; JAK, Janus kinase; STAT, signal transducer and activator of transcription; TNF, tumor necrosis factor; IFN, interferon.

FLS-induced Th1 and Th17 cell differentiation in RA (14). Upregulated KAT7, an H4-specific histone acetylase in FLS, promotes Th17 cell differentiation in RA by inducing C-C motif chemokine ligand (CCL) 20 expression and the p44/42 mitogen-activated protein kinase pathway (15). Further, myeloid-related protein (MRP)8/MRP14 is an endogenous Toll-like receptor 4 (TLR4) ligand. MRP8 produced by FLS can promote Th17 differentiation by enhancing the expression of IL-6 in RA. MRP8 induces IL-6 secretion in FLS *via* TLR4/phosphoinositide 3-kinase (PI3K)/nuclear factor kappa B (NF- κ B) and mitogen-activated protein kinase signaling pathways in RA (16). Moreover, IL-34/colony stimulating factor 1 receptor (CSF-1R) axis-induced FLS upregulate Th17 production through increased IL-6 in RA (17). In addition, cysteine-rich protein 61 (Cyr61) induces IL-6 production by FLS, promoting Th17 differentiation *via* the Avb5/Akt/NF- κ B signaling pathway in RA (18). Co-cultured FLS enhance PBMC-secreted IL-17-A, IL-6, IFN γ , and IL-1 β production in RA (19). FLS and macrophages are the main sources of IL-26 in RA joints. IL-26 induces production of the proinflammatory cytokines IL-1 β , IL-6, and TNF- α in monocytes. IL-26-stimulated monocytes selectively promote the generation of ROR γ ⁺ Th17 cells through IL-1 β secretion by monocytes. Therefore, IL-26 is constitutively

produced by FLS, induces proinflammatory cytokines in myeloid cells, and promotes Th17 cell differentiation in RA (20). Synovial fluid and FLS from patients with RA suppress enhancer of zeste homolog 2 (EZH2) expression in CD4⁺ T cells. EZH2 deficiency attenuates regulatory T cells (Treg) differentiation in RA (21). Overall, IL-6 seems to be a key inflammatory factor released by FLS in RA. Thus, FLS indirectly affect the differentiation of T cells in the synovial joints of patients with RA through IL-6, promoting the differentiation of Th17 and Tfh cells.

3 INDIRECT REGULATION OF FLS IN RA BY T CELLS

3.1 Promotion of FLS Inflammatory Phenotypes in RA *via* Cytokines From T Cells

3.1.1 Indirect Effects of Th17 Cells on FLS in RA

Different subtypes of CD4⁺ T cells can be detected in the synovial joints of patients with RA (22). Th17 promotes the development of RA and is an important aspect of the proinflammatory

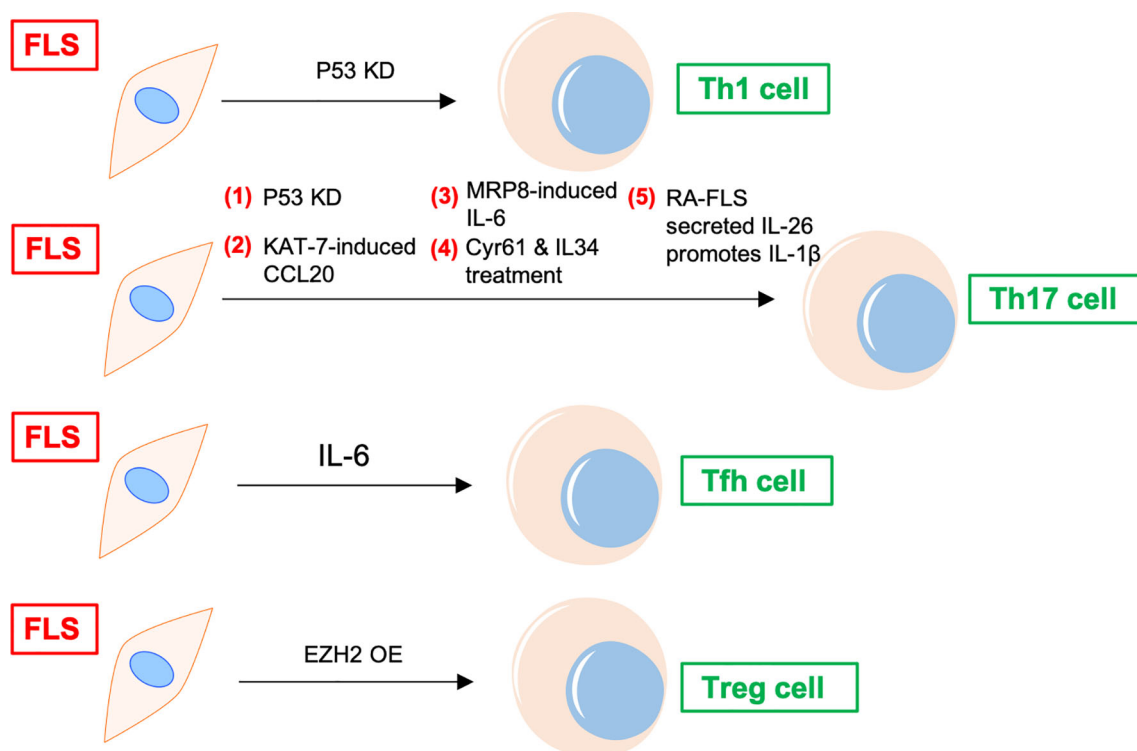


FIGURE 2 | FLS regulates differentiation of CD4⁺ T cells in RA. P53 KD and EZH2 OE promote Th1 and Treg differentiation of T cells in RA synovium, respectively. FLS promotes Tfh differentiation of T cells *via* IL-6. FLS directly induces Th17 differentiation through cytokines, including CCL20, MRP8, IL-6, and IL-26, etc. KD, knockdown; OE, overexpression; Tfh, T follicular helper; CCL, C-C motif chemokine ligand; MRP, myeloid-related protein; TLR, Toll-like receptor; Cyr61, cysteine-rich protein 61; EZH, enhancer of zeste homolog; Treg, regulatory T cells.

function of FLS. Transcripts of *IL-17R*, as well as those of *IL-17RB*, *C*, and *D*, have been previously detected in the FLS of patients with RA (23) (**Figure 3A**).

Th17 cells induce secretion of the cytokine granulocyte-macrophage colony-stimulating factor (GM-CSF) in synovial stroma and innate lymphoid cells to initiate and augment autoimmune arthritis (24). Th17 cells and IL-17 increase autophagy of FLS by causing mitochondrial dysfunction in RA (25). The blockade of IL-17 alleviates inflammation in rat arthritis and matrix metalloproteinase (MMP)-13 expression from FLS (26). In addition, IL-17-induced receptor activator of NF- κ B ligand (RANKL) expression is decreased by the inhibition of Act1, TNF receptor-associated factor 6 (TRAF6), and activator protein (AP)-1. In the absence of RANKL, IL-17-prestimulated FLS induce osteoclastogenesis from monocytes, which is repressed by the inhibition of TNF- α (27). FLS express two types of phospholipase D, namely PLD1 and PLD2. PLD regulates the Th17-promoted production of proinflammatory cytokines by FLS (28). The dihydroartemisinin derivative DC32 inhibits the Th17-induced invasion and migration of FLS by decreasing the secretion of MMPs (MMP-2, MMP-3) *in vitro* (29).

Th17-cell-secreted IL-17A and TNF- α have synergistic effects on promoting the production of inflammatory cytokines in FLS from patients with RA, the human leukemia cell line THP-1, and the rheumatoid synovial fibroblast cell line MH7A. IL-17A and TNF- α also promote the proliferation and migration of MH7A cells. However, a novel dual targeting fusion protein (targeting TNF- α and IL-17A) was found to be more efficient in inhibiting these synergistic effects when compared to the effects of etanercept (30). Stromal cell-derived factor 1 (SDF-1) is overproduced in RA FLS, and IL-17 upregulates the expression of SDF-1 in RA FLS *via* pathways mediated by PI3K, NF- κ B, and AP-1 (31).

3.1.2 Indirect Effects of Th1/Th2 Cells on FLS in RA

Apart from Th17, Th1 and CXCR3⁺ Th2 phenotypes are the main subtypes of T helper cells in the synovium of patients with RA; IL-4 and IL-13 induce FLS to produce a series of inflammatory cytokines, such as IL-6, CCL2, CXCL1, and CXCL8, whereas IFN γ promotes the expression of CXCL10 (32). Both Th1 and Th17 cells produce IL-17 and IFN γ . The expression of CD40, intercellular adhesion molecule 1 (ICAM-1), and MHC-II in FLS is upregulated upon co-culture with Th1 cells, whereas Th17 cells induce only ICAM-1 in FLS. Both T cell subsets promote the production of IL-6 and IL-8 by FLS from patients with RA (33). T cell-derived IL-2 might activate FLS (via IL-2 receptor (CD122) and (CD132) chains) to produce MCP-1, thus recruiting macrophages into the rheumatoid synovium and promoting inflammation (34). Both Th1 and Th2 cells express macrophage migration inhibitory factor (MIF). MMPs are induced by FLS after co-culture with Th1 and Th2 cells, and activated T helper cells are more effective than resting cells. The neutralization of MIF by an anti-MIF antibody leads to the downregulation of MMP in both Th1- and Th2-stimulated FLS (35) (**Figure 3B**).

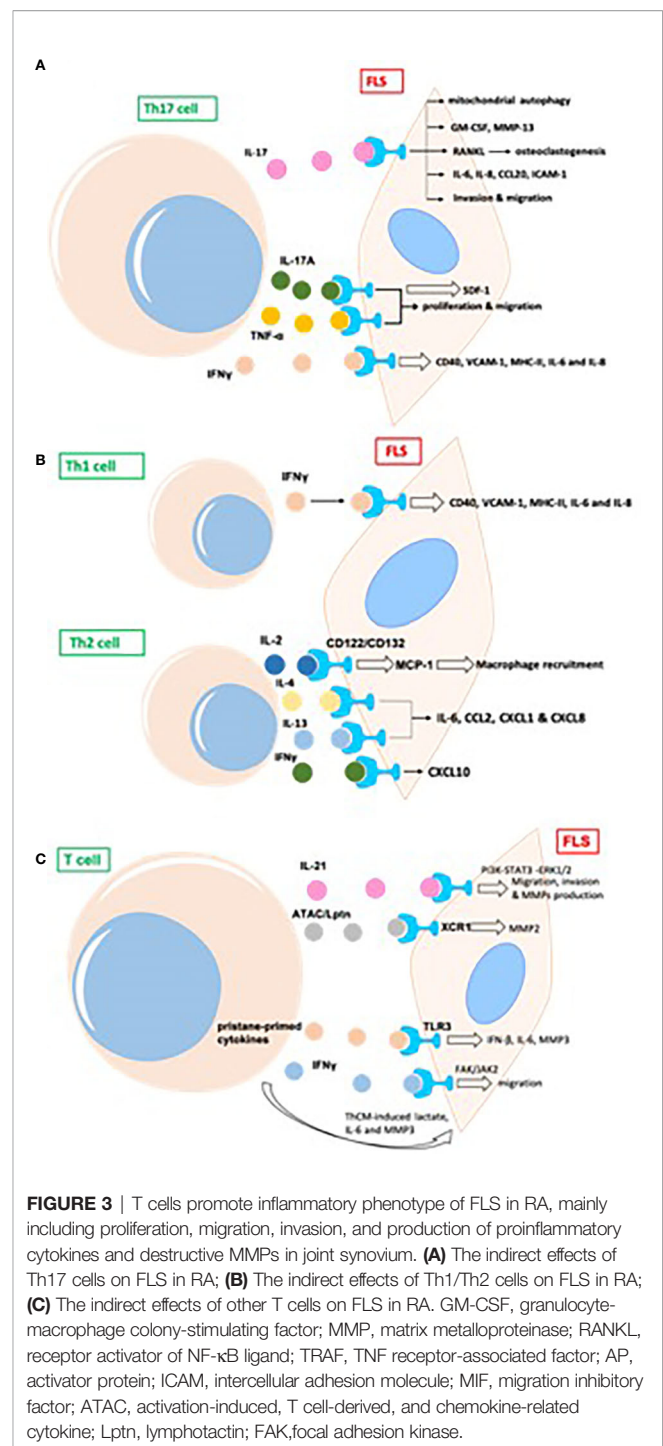


FIGURE 3 | T cells promote inflammatory phenotype of FLS in RA, mainly including proliferation, migration, invasion, and production of proinflammatory cytokines and destructive MMPs in joint synovium. **(A)** The indirect effects of Th17 cells on FLS in RA; **(B)** The indirect effects of Th1/Th2 cells on FLS in RA; **(C)** The indirect effects of other T cells on FLS in RA. GM-CSF, granulocyte-macrophage colony-stimulating factor; MMP, matrix metalloproteinase; RANKL, receptor activator of NF- κ B ligand; TRAF, TNF receptor-associated factor; AP, activator protein; ICAM, intercellular adhesion molecule; MIF, migration inhibitory factor; ATAC, activation-induced, T cell-derived, and chemokine-related cytokine; Lptn, lymphotactin; FAK, focal adhesion kinase.

3.1.3 Indirect Effects of Other T Cells on FLS in RA

IL-21 is produced primarily by CD4⁺ T cells and natural killer T cells. IL-21 induces the migration, invasion, and production of MMPs (MMP-2, MMP-3, MMP-9, MMP-13) in FLS from patients with RA (36). IL-21 promotes activation of the PI3K, STAT3, and ERK1/2 pathways in FLS, and the inhibition of these

pathways attenuates IL-21-mediated migration and the production of MMPs (36). The percentage of T cells from the synovial fluid in patients with RA is upregulated relative to that in patients with psoriatic arthritis (37). The proportion of IL-21⁺CD4⁺ T cells from peripheral blood in patients with RA is positively associated with IgM-rheumatoid factor, serum anticyclic citrullinated peptide antibodies, and disease activity score 28 (DAS28). IL-21 expression in synovial fluid is correlated with MMPs; IL-21 significantly induces the production of MMPs in synovial biopsies from patients with RA (37). CD4⁺IL-21⁺ T cells sorted from synovial fluid promote the secretion of MMPs by FLS to a greater extent than medium or CD4⁺IL-21⁻ T cells in an *in vitro* co-culture system. The blockage of IL-21 and TNF leads to the downregulation of MMPs from FLS (37).

In phorbol myristate acetate/ionomycin-stimulated PBMCs, activation-induced, T cell-derived, and chemokine-related cytokine (ATAC)/lymphotactin (Lptn) is detected in CD8⁺ T cells and is upregulated in CD4⁺CD28⁻ T cells from patients with RA as compared with their levels in healthy controls (38). FLS express the ATAC/Lptn receptor XCR1 in the RA synovium. ATAC/Lptn leads to the marked downregulation of MMP2 production in FLS (38). TLR3 is induced in the synovium of rats with pristane-induced arthritis (39). In addition, activation of the TLR3 signaling pathway promotes the development of this arthritis model. Interestingly, pristane-primed T cell-derived cytokines further promote FLS activation (39).

IFN γ produced by T cell stimulation promotes the phosphorylation of focal adhesion kinase (FAK)-Y925, which is important for cell migration (40). SiRNA-mediated knockdown of JAK2, but not JAK1, substantially suppresses FAK activation *via* IFN γ . IFN γ -induced FAK activation and invasion of FLS are also blocked by baricitinib (JAK inhibitor) (40). Soluble mediators released by Th cells drive synovial fluid towards a glycolytic and proinflammatory phenotype. Targeting JAKs or glycolytic enzymes modulates synovial fluid glucose metabolism and decreases the secretion of IL-6 and MMP3 (41). Therefore, targeting glycolytic pathways represents a potential therapeutic strategy to treat inflammation in synovial fluid (41) (Figure 3C).

4 DIRECT INTERACTION BETWEEN FLS AND T CELLS IN RA

4.1 Direct Regulation of T cells by FLS in RA

In addition to indirect regulation through cytokines and chemokines, there is a direct interaction between T cells and FLS in the synovium of patients with RA. Different antigen-presenting cells, including B cells, macrophages, and dendritic cells, interact directly with T cells. FLS, as non-immune cells, also have antigen-presenting capabilities. This section summarizes the direct communication between T cells and FLS in the synovium of patients with RA (Figure 4).

Despite not being professional antigen-presenting cells, FLS can also present peptides, such as human cartilage gp-39 and human type II collagen (CII), derived from autoantigens discovered in the joint tissues of patients with RA, to activated T cells *in vitro* in an IFN-dependent and MHC-restricted manner (42). Cell-cell contact between T cells and FLS induce the lymphocytic expression of aminopeptidase N/CD13 and results in lymphocytic activation (43). Both FLS (production of SDF-1) and CD8/CD4⁺ T cells (expression of CXCR4) play a positive role in the recruitment of T cells in the joint synovium (44). CD4⁺ T cells abnormally express CX3CR1 in the synovium of patients with RA. Fractalkine (FKN) induces the adhesion of CD4⁺ T cells and survival signals and co-stimulates the secretion of inflammatory cytokines and granules. CD4⁺ T cells accept primary stimulatory and co-stimulatory signals from non-professional antigen-presenting cells, such as FLS, in the RA synovial microenvironment (45).

A previous study showed the effects of FLS on the recruitment, activation, and expansion of T cells in RA in a CD47-TSP1 (thrombospondin-1)-dependent manner (46). TSP1-mediated co-stimulation is achieved through its independent interaction with CD36 on antigen-presenting cells and with CD47 on T cells. A CD47-TSP1-CD36 trimolecular complex is a new co-stimulatory pathway that represses the activation of T cells. Because the lesions in rheumatoid synovitis are sites of antigenic recognition, the identification of TSP1 on

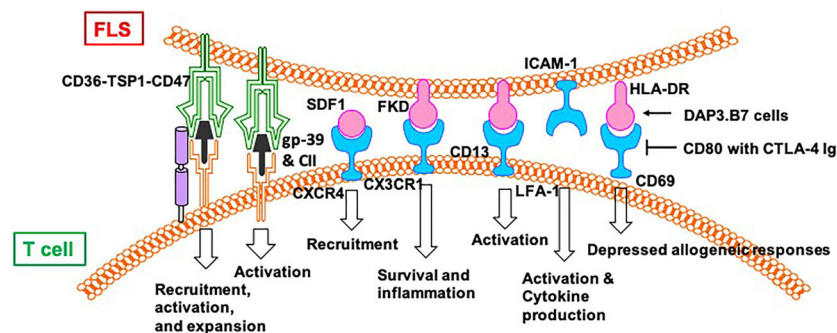


FIGURE 4 | FLS directly regulate functions of T cells in RA.

antigen-presenting cells such as FLS suggests the central role of TSP1 in the expansion of T cells in RA (47). Direct contact between T cells and FLS induces the expression of HLA-DR on FLS and CD69 on T cells in an allogeneic and autologous manner. The addition of DAP3.B7 cells to co-cultures of T cells and FLS alleviates the repressed allogeneic activation of T cells (48). The allogeneic response by T cells to FLS in the presence of DAP3.B7 cells can be blocked by inhibiting CD80 with CTLA-4 Ig (48). Strong expression of B7-H3 was detected on FLS in synovial tissue of a patient with RA (49). Cells expressing B7-H3 are distinct from but very close to cells expressing CD45, CD3, and CD20. In addition, FLS and T cell co-cultures show localization of B7-H3 in the contact section between them but this is distinct from CD11a/CD18 (LFA-1)⁺ T cells and ICAM-1⁺ FLS. Blocking B7-H3 on FLS affects the interactions between FLS and T cells. Resting T cells have upregulated IL-2, TNF- α , and IFN- γ , whereas cytokine-activated T cells exhibit downregulated cytokine production. However, cytokine production by T cells activated *via* TCR is not affected by B7-H3 (49).

4.2 Direct Regulation of FLS by T Cells in RA

Direct contact between activated CD4⁺ T cells and an FLS-facilitated hGITR–GITRL interaction lead to the upregulation of MMP-13 (50). CII-reactive T cells induce the secretion of chemokines (IL-8, MCP-1, and MIP-1 α) through interactions with FLS in RA joints, which is mediated by CD40L–CD40 communication (51). FKN–CX3CR1 receptor–ligand interactions affect FLS growth and T cell functions. FLS promote autocrine growth by releasing FKN and triggering the activity of CX3CR1. This growth-promotion loop is amplified by CX3CR1⁺ T cell-produced TNF- α upon stimulation by FKN⁺ FLS (52).

Mutual activation of T cells and FLS results in increased proliferation and expression of ICAM-1 and VCAM-1 by both CD4⁺ T cells and FLS (53). The interaction between CD4⁺ T cells and FLS results in the upregulation of TNF- α , IFN- γ , and IL-17A from CD4⁺ T cells and the secretion of other cytokines, including IL-6, IL-8, and vascular endothelial growth factor (VEGF). Moreover, CD4⁺ T cells cultured in conditional medium promote invasiveness and glycolysis in FLS while repressing oxidative phosphorylation, with the effects paralleled by induced glucose transporters GLUT1 and GLUT3, key glycolytic enzymes GSK3A, HK2, LDHA, and PFKFB3, VEGF, and MMPs, which is alleviated by the glycolytic inhibitor 2-DG and adenosine monophosphate analogue 5-aminoimidazole-4-carboxamide ribonucleotide (53).

Co-culture with T cells induces the phosphorylation of protein kinase Akt (Ser473) and downstream mediators, including GSK-3 α/β , FoxO1/3a, and mouse double minute (MDM)-2, in FLS from patients with RA (54). Co-cultured T cells also promote the proliferation of FLS and the production of IL-6, which is repressed by blocking antibodies to CD11a and ICAM-2. T cell-mediated phospho-Akt upregulation is unique to

FLS because no such effect is observed in B cells and dendritic cells. Selective involvement of the LFA-1–ICAM-2 pathway has been confirmed based on increased ezrin phosphorylation at Tyr353 downstream of ICAM-2, which supports cell survival through Akt activation (54).

The rapid and robust adhesion of cytokine-activated T cells (Tck) and super antigen-activated T cells to FLS leads to flattening and a crawling movement in T cells on the cellular surface of FLS (55). Tck activates FLS to secrete IL-6 and IL-8 in a cell contact-dependent manner, which is further activated by IL-17. Antibody blocking of membrane TNF- α on the Tck surface inhibits cytokine production by FLS, demonstrating a novel mechanism of TNF- α during T cells–FLS interactions in the RA synovium (55) (**Figure 5**).

4.3 Direct Mutual Regulation of T Cells and FLS in RA

In addition to the one-way direct regulation, there is a direct and mutual crosstalk between T cells and FLS in the synovium of patients with RA. This two-way communication further leads to the development of RA (56) (**Figure 6**). The T cells from patients with RA with a stronger response to CII show higher expression of inflammatory mediators, including IL-15, TNF- α , IFN, and IL-17. When co-incubated with RA FLS, T cells can stimulate the secretion of TNF- α , IL-15, and IL-18 from FLS during CII stimulation. In contrast, T cells also produce higher amounts of IL-17 and IFN- γ during co-culture with RA FLS. The crosstalk between T cells and FLS requires direct cell–cell contact and occurs in a CD40L–CD40 dependent manner (57).

IL-17 induces the expression of IL-32 in FLS from patients with RA, which activates the secretion of IL-17 from CD4⁺ T cells (58). IL-17 and IL-32 are co-localized near tartrate resistant acid phosphatase-positive areas in joints from patients with RA. IL-32 and IL-17 promote osteoclast differentiation in a synergistic manner, and both promote osteoclast resorption *via* RANKL (58).

The interactions between FLS from rats with collagen-induced arthritis (CIA) and rat CCR7[−] effector memory T (T_{em}) cells is regulated by KCa1.1 and Kv1.3 (59). Blocking KCa1.1 on FLS reduces the promoting effects of FLS on the proliferation and migration of T_{em} cells, and blocking Kv1.3 on T_{em} cells reduces the effects of T_{em} cells on the expression of KCa1.1 and MHCII and the invasion of FLS. Furthermore, combination therapies comprising selective KCa1.1 and Kv1.3 inhibitors are more efficacious than monotherapies in alleviating disease features of rat arthritis models (59).

Macrophage-produced PGE2 is a response to IL-17 of T cells, which negatively regulates the expression of TNF- α and IL-17, as well as the TNF- α /IL-1-mediated activation of FLS *via* EP2 and EP4 receptors, resulting in the modulation of proinflammatory cascades in RA (60). A CTLA4–FasL fusion protein suppresses FLS proliferation and the development of adjuvant-induced arthritis (AIA) in rats. However, CTLA4–FasL also acts as an effective inhibitor for T cells; it not only inhibits the activation of T cells but also promotes activated T cell death (61).

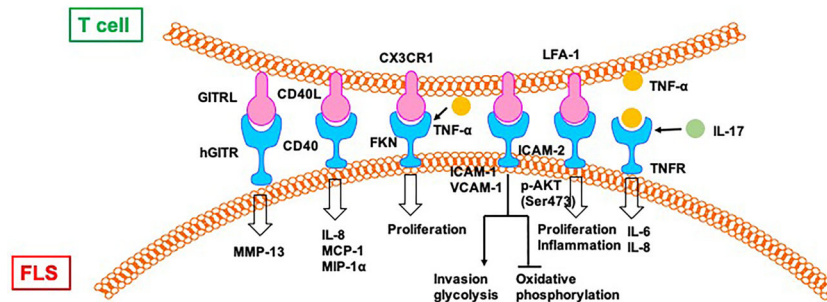


FIGURE 5 | T cells directly regulate FLS in RA. CII, type II collagen; FKN, Fractalkine; TSP, thrombospondin.

5 CORRELATION BETWEEN T CELLS AND FLS IN RA

The numbers of FLS and T cells in the synovial tissue of patients with RA are closely associated with joint damage (62). RA naïve T cells share hypermethylation sites with FLS. FLS-representative DNA methylation signatures derived from blood might serve as biomarkers of RA risk or disease status (63). In the following section, we summarize some recent studies reporting that some treatments for RA (**Table 1**) or the regulation of a specific gene/protein (**Table 2**) can affect the function of both T cells and FLS in RA.

5.1 Simultaneous Effect of an RA Drug on T Cells and FLS

IL-21 induces the expression of Beclin-1, autophagy-related 5 (Atg5), and LC3-phosphatidylethanolamine conjugate 3-II (LC3-II) through the inhibition of C/EBP homologous protein

(CHOP) in FLS from rats with adjuvant-induced arthritis. Berberine (BBR), an alkaloid derivative predominantly present in Oregon grapes and shoots of barberry, represses FLS autophagy *via* PI3K/Akt signaling by inhibiting autophagic elements, p62 sequestration, and the induction of CHOP. In addition, IL-21 induces the hyper-proliferation of FLS by upregulating the B-cell lymphoma-2 (Bcl-2)/Bcl-2 associated X protein (BAX) ratio, which can be reversed by BBR. IL-21 also promotes CD4⁺ CD196⁺ Th17 cell expansion *via* the PI3K/Akt pathway, and BBR can repress the expansion of Th17 cells by repressing the specific transcriptional factor RORγt in Th17 cells in a PI3K/AKT-dependent manner. Furthermore, BBR promotes the expansion of CD4⁺CD25⁺ Treg cells, which exerts an effect opposite to that of Th17 cells, through induction of a specific Treg transcriptional factor, forkhead box P3 (Foxp3), *via* aryl hydrocarbon receptor (AhR) and the upregulation of cytochrome P450 family 1, subfamily A, polypeptide 1 (CYP1A1) (64).

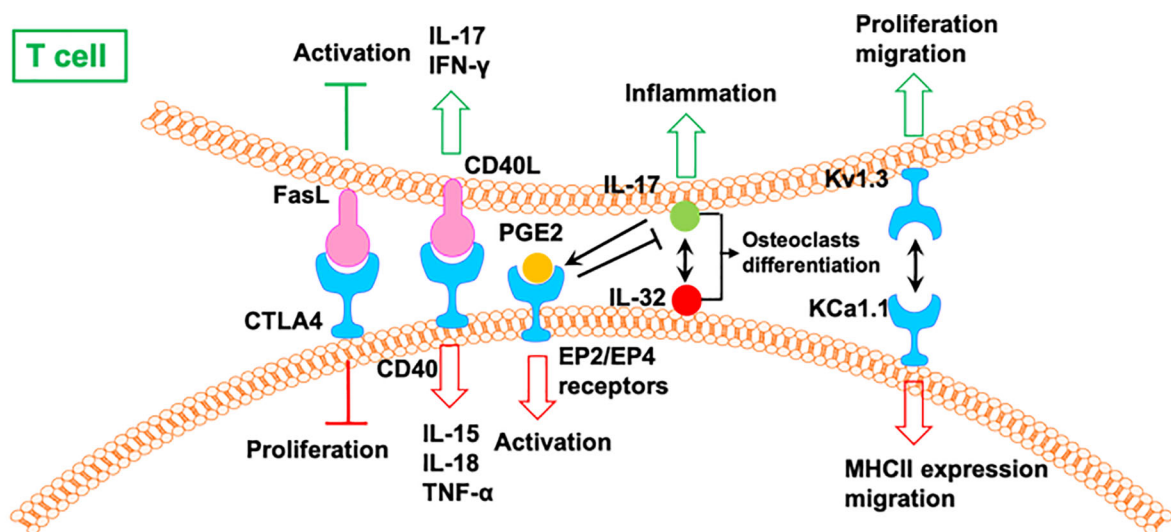


FIGURE 6 | The mutual regulation of T cells and FLS in RA. CIA, collagen-induced arthritis; T_{em}, effector memory T; AIA, adjuvant-induced arthritis.

TABLE 1 | The medicinal treatment regimens that can affect the functions of both T cells and FLS in RA.

Treatment	T cells	FLS	Other	Ref
BBR	BBR inhibits the proliferation of Th17 cells through downregulation of ROR γ t and promotes the differentiation of Treg cells through induction of Foxp3 activation via up-regulation of AhR and CYP1A1.	BBR inhibited autophagy in AA-FLS mediated through PI3K/Akt signaling via suppression of autophagic elements, p62 sequestration and induction of CHOP. BBR inhibited the proliferation of AA-FLS via promotion of apoptosis.		(64)
Silibinin	Silibinin inhibits Th17 cell differentiation.	Silibinin suppresses cell viability and increases apoptosis of RA-FLS. The production of inflammatory cytokines in RA-FLS and a CIA rat model is inhibited by silibinin.		(65)
Single use or combination treatment with LMT-28 and metformin	Single use or combination treatment with LMT-28 and metformin suppress Th17 differentiation.	Single use or combination treatment with LMT-28 and metformin and IL-6 signaling in FLS.		(66, 67)
LMT-28 and THP combination	LMT-28 and THP combination inhibits Th17 differentiation.	LMT-28 and THP combination suppresses of IL-6 or TNF-induced signaling pathways in RA-FLS.	LMT-28 and THP combination inhibits osteoclastogenesis.	(68)
Diallyl Trisulfide	Diallyl Trisulfide represses Th17 differentiation and has a therapeutic effect of CIA mice.	Diallyl Trisulfide induces FLS apoptosis of CIA mice.		(69)
Oroxylin A	Oroxylin A-treated mice shows an increase in Treg and reduction in Th17 cells in the ILN.	Oroxylin A decreases the secretion of IL-1 β and IL-6 from TNF α -stimulated RA FLS <i>in vitro</i> .		(70)
Formyl peptide receptor agonist Cpd43	Cpd43 inhibits the expansion, activation and differentiation of arthritogenic effector CD4 T cells.	Cpd43 inhibits proliferation of FLS.		(71)
MTX	In T cell lines, MTX inhibits activation of NF- κ B via depletion of BH4 and up-regulation of JNK-dependent p53 activity.	Inhibition of NF- κ B activation by MTX is prevented by adenosine receptor antagonists in FLS.		(72)
CP-25	CP-25 decreases the expression of BAFF-R in CD4+ T cells.	CP-25 inhibits the proliferation and cytokine secretion of FLS co-cultured with BAFF-activated CD4+ T cells.		(73)
Bortezomib plus MSC combination	Bortezomib plus MSC combination restores TLR expression and Treg frequency in blood.	Bortezomib plus MSC combination normalizes FLS proliferation, apoptosis and cytokine secretion.	Human UC-MSCs suppress the inflammatory effects of FLSs and T cells of RA.	(74, 75)
monoclonal BsAb (TNF- α and CXCL10)	The BsAb inhibited CXCL10-mediated CD8+ T cell migration.	The BsAb inhibited TNF- α induced ICAM-1 and VCAM-1 in FLS. The BsAb decreased the expression of TNFSF11 and the production of IL-6 in FLS stimulated with TNF- α and CXCL10.		(76)
FL-BsAb1/17	FL-BsAb1/17 could repress the production of IL-1 and IL-17 in T cells.	FL-BsAb1/17 could significantly decrease the production of IL-6 in FLS.		(73)
Huayu Tongbi Fang	Huayu Tongbi Fang decreased GM-CSF production by T cells.	Huayu Tongbi Fang could inhibit FLS activation.		(77)
Clarithromycin	As clarithromycin suppressed HLA-DR and costimulatory molecule expression was enhanced by IFN, autologous T cell proliferation was inhibited by clarithromycin.	Clarithromycin suppressed the production of these cytokines including IL-1, IL-6, IL-8, G-CSF and GM-CSF but did not enhance IL-10 production of FLS.		(78)

Atg5, autophagy-related 5; *CHOP*, C/EBP homologous protein; *BBR*, Berberine; *BCL*, B-cell lymphoma; *BAX*, Bcl-2 associated X protein; *FOXp3*, forkhead box P3; *AhR*, aryl hydrocarbon receptor; *CYP1A1*, cytochrome P450 family 1, subfamily A, polypeptide 1; *SIRT*, Sirtuin1; *THP*, tetrahydropapaverine; *MTX*, methotrexate; *BH4*, tetrahydrobiopterin; *JNK*, Jun-N-terminal kinase; *BsAb*, bispecific antibody; *CP-25*, Paeoniflorin-6'-O-benzene sulfonate; *BAFF-R*, B cell-activating factor, belonging to the TNF family-receptor; *UC-MSCs*, umbilical cord-derived mesenchymal stem/stromal cells.

Silibinin, a natural polyphenolic flavonoid, represses cell proliferation and induces the apoptosis of FLS from patients with RA in an NF- κ B pathway-dependent manner. Silibinin also represses Sirtuin1 (SIRT1), and SIRT1 knockdown enhances silibinin-induced apoptosis in FLS. Silibinin also inhibits arthritis development in a CIA rat model and the secretion of inflammatory cytokines in FLS from patients with RA. In addition, it inhibits the differentiation of Th17 cells *in vitro* (65).

Single-use or combination treatment with LMT-28 (a derivative of oxazolidinone) and metformin significantly

ameliorates arthritic signs in rats with CIA by suppressing Th17 differentiation and IL-6 signaling in FLS (66, 67). A combination of LMT-28 and tetrahydropapaverine (THP, benzylisoquinoline alkaloid) could attenuate RA through the suppression of Th17 differentiation in T cells and proinflammatory cytokine-induced inflammation in FLS (68). Diallyl trisulfide induces FLS apoptosis, represses Th17 differentiation, and has a therapeutic effect on mice with CIA by blocking NF- κ B and Wnt pathways (69). Oroxylin A-treated CIA mice demonstrate an upregulation of Treg cells and

TABLE 2 | Specific gene/protein that can affect the functions of both T cells and FLS in RA.

Molecule	T cells	FLS	Other	Ref
CCL3	CCL3 could up-regulate CD4 ⁺ T cells to mediate the inflammatory response.	CCL3 enhanced the expression level of pro-inflammatory cytokines in RA-FLS via activation of the PI3K/AKT signaling pathway.		(79)
IL-21	IL-21 induced RANKL expression in CD4 ⁺ T cells from RA patients.	IL-21 induced RANKL expression in RA-FLS.	IL-21 enhanced osteoclastogenesis <i>in vitro</i> .	(80, 81)
CTX	CTX suppressed the abnormal increasing of CD4 ⁺ T cells/CD8 ⁺ T cells ratio, and inhibited T cell proliferation.	CTX inhibited the proliferation of the RA-FLS via suppression of NF- κ B signaling pathway.		(79)
rhIL23R-CHR	rhIL23R-CHR decreased secretions of IL-17 and IL-9, whereas FoxP3 was activated in the process in the CIA rats.	rhIL23R-CHR repressed proinflammatory effects on FLS.	synergetic effects with TNF- α	(82)
cDHPS	cDHPS restored the balance of Th17 and Treg cells of CIA mice.	cDHPS reduced the secretion of pro-inflammatory mediators related to FLS activation,	cDHPS repressed angiogenesis, articular cartilage degradation and osteoclast differentiation, inhibited HIF-1 α expression and promoted anti-inflammatory mediator release in the joint tissues and serum of CIA mice .	(83)
DP	DP suppressed lipopolysaccharide-induced pro-inflammatory cytokine expression in Jurkat T lymphocytes.	DP inhibited p65 acetylation in MH7A cells, a human RA-FLS line.	DP specifically inhibited the HAT activities of p300/CBP. DP-induced hypoacetylation was accompanied by cytosolic accumulation of p65 and nuclear localization of I κ B α . Accordingly, DP treatment inhibited TNF α -stimulated increases in NF- κ B function and expression of NF- κ B target genes in these cells.	(84)

CTX, Cobrotoxin; cDHPS, *Dendrobium huoshanense* stem polysaccharide; DP, Delphinidin.

downregulation of Th17 cells in the inguinal lymph nodes. Oroxylin A also represses the production of IL-1 β and IL-6 from TNF α -stimulated FLS *in vitro* (70). The formyl peptide receptor agonist Cpd43 inhibits the expansion of arthritogenic effector CD4 T cells and FLS and reduces joint damage in CIA and AIA mice (71).

Previous results also showed that methotrexate (MTX) represses the NF- κ B pathway in T cells and FLS. In T cell lines, MTX blocks the NF- κ B pathway by repressing tetrahydrobiopterin (BH4) and inducing p53 in a Jun-N-terminal kinase (JNK)-dependent manner (72). Levels of phosphorylated RelA are decreased in low-dose MTX-treated patients with RA. However, the MTX-mediated inhibition of the NF- κ B pathway is completely prevented by adenosine receptor antagonists in FLS from patients with RA but not *via* BH4 and JNK (72). Clarithromycin represses the secretion of cytokines such as IL-1, IL-6, IL-8, G-CSF, and GM-CSF but does not enhance the production of IL-10 by FLS. As clarithromycin suppresses HLA-DR and co-stimulatory molecule expression is enhanced by IFN, the proliferation of autologous T cells is markedly inhibited by clarithromycin. Clarithromycin exerts a considerable immunosuppressive effect on FLS by inhibiting co-stimulatory molecule expression, cytokine production, and antigen-specific T cell proliferation induced by FLS (78).

The effects of a monoclonal bispecific antibody (BsAb) targeting TNF- α and CXCL10 was also evaluated in RA (76). BsAb repressed the CXCL10-mediated migration of CD8⁺ T cells. Further, the effect of binding of the BsAb to TNF- α was comparable to that of adalimumab; BsAb also repressed TNF- α -mediated cell death and the expression of VCAM-1 and ICAM-1 in FLS. BsAb was also found to inhibit TNFSF11 and IL-6 in

TNF- α - and CXCL10-stimulated FLS (76). Another recombinant IgG-like bispecific antibody (FL-BsAb1/17) targeting IL-1 β and IL-17A also showed considerable effects for RA treatment, which could repress the secretion of IL-6 in FLS from patients with RA (73). Paeoniflorin-6'-O-benzene sulfonate (CP-25) decreases the expression of B cell-activating factor, belonging to the TNF family-receptor (BAFF-R), in CD4⁺ T cells and represses cell proliferation and cytokine production in FLS co-cultured with BAFF-activated CD4⁺ T cells (85). A Chinese herbal formula, Huayu Tongbi Fang, also represses FL-mediated inflammation in rats by suppressing T cells and FLS-producing GM-CSF (77). Human umbilical cord-derived mesenchymal stem/stromal cells (UC-MSCs) inhibit the inflammatory features of FLS and T cells from patients with RA and alleviate the progression of CIA, implying that UC-MSCs can be used as a potential therapeutic strategy for RA (74). The combination of bortezomib and MSCs rescues TLR expression and the ratio of Treg cells in peripheral blood and normalizes FLS proliferation, apoptosis, and cytokine secretion (75).

5.2 Regulation of T cells and FLS by a Common Factor in RA

CCL3 enhances the expression of proinflammatory cytokines (including IL-6, IL-1 β , TNF- α , and RANKL) in RA-FLS by activating the PI3K/AKT signaling pathway. Moreover, CCL3 can upregulate CD4⁺ T cells to mediate the inflammatory response in RA (86). Cobrotoxin (CTX) suppresses the abnormal increase in CD4⁺/CD8⁺ T cells and inhibits T cell proliferation. CTX also inhibits the proliferation of cultured FLS by inhibiting the NF- κ B signaling pathway (79).

rhIL23R-CHR can be used to inhibit the IL-23-related pathway to explore the role of IL-23 in the dysfunction of Th17/Th9/Treg cells in rats with CIA. CIA rats demonstrate downregulation of the production of IL-9 and IL-17 and upregulation of FoxP3 upon rhIL23R-CHR treatment, implying that IL-23 could alleviate the dysfunctions of Th17/Th9/Treg cells. Furthermore, IL-23 also promotes the proinflammatory features of FLS *in vitro*, showing synergetic outcomes with TNF- α (82).

RANKL is expressed by both FLS and sub-lining T lymphocytes (87). IL-21 promotes RANKL in CD4⁺ T cells from CIA and in CD4⁺ T cells and FLS from patients with RA. IL-21 also induces osteoclastogenesis by inducing RANKL expression in CD4⁺ T cells and FLS *in vitro* (80). Another study detected RANKL⁺ cells in FLS and infiltrating mononuclear cells of synovial tissue of patients with RA (81). Double immunostaining detected RANKL⁺ cells in CD3⁺ and CD4⁺ T cells. RANKL is elevated and osteoprotegerin is lowered in the synovial fluid of patients with RA. The ratio of the concentration of RANKL to that of osteoprotegerin is also upregulated in the synovial fluid of patients with RA compared to that in the synovial fluid of patients administered oroxylin A or with gout. In addition, RANKL⁺ T cells promote osteoclastogenesis from peripheral monocytes. The promoting function of RANKL osteoclastogenesis was confirmed by osteoprotegerin-mediated inhibition in a dose-dependent manner (81).

Dendrobium huoshanense stem polysaccharide (cDHPS) alleviates the imbalance in Th17/Treg cells; represses the production of FLS activation-associated proinflammatory cytokines, damage to articular cartilage, the formation of osteoclasts, and angiogenesis; reduces HIF-1 α ; and induces anti-inflammatory cytokines in joint synovium and serum of CIA mice (83). Delphinidin represses the histone acetyltransferase activities of p300/CBP and p65 acetylation in MH7A cells, which are a human RA FLS cell line (84). Delphinidin-mediated hypoacetylation is characterized by the cytosolic accumulation of NF- κ B activator p65 and nuclear localization of the NF- κ B inhibitor IKB α . Delphinidin suppresses the TNF- α -induced upregulation of the NF- κ B pathway in MH7A cells. It also represses LPS-induced proinflammatory cytokine production in Jurkat T lymphocytes, implying that a histone acetyltransferase inhibitor can efficiently suppress cytokine-mediated immune responses (84).

6 CONCLUSION AND PERSPECTIVE

T cells and FLS play an important role in the pathogenesis of RA. T cells show a systematic disorder in patients with RA, and FLS promote inflammation and damage the joints locally in the joint synovium of patients with RA. However, since T cells can be recruited to the joint synovium through blood and lymphatic circulation, there is a possibility of interactions between the two cellular components in the joint synovium. Recent publications have confirmed many means of communication between T cells

and FLS in the joint synovium in RA, including direct or indirect interactions and one-way or two-way interactions, further amplifying the severity of synovitis. Therefore, blocking this key interaction has the potential to relieve the symptoms of RA or even completely treat RA.

Many agents can directly affect both FLS and T cells in RA. The dual effect of those potential drugs on FLS and T cells presents a promising solution for the treatment of RA and thus, should be further studied in the future. For example, blocking the proinflammatory cytokine (CCL3, IL-21, and IL-23) pathways will block the activation of T cells and FLS-mediated proinflammatory effects because their receptors are commonly expressed on T cells and FLS (88). In addition, for some pathways that can act mutually between T cells and FLS, such as PGE2/EP receptors and Kv1.3/KCa1.1, inhibitors that stop these bidirectional effects should be designed and tested to prevent the cascading proinflammatory effects and relieve the symptoms of RA (89).

But there are still some unsolved issues with the current research, which leads to obstacles to potential application in the future. For example, FLS is not professional APC, and it is not clear whether the molecular mechanism of the signals that activate T cells is exactly the same as that of APCs, and the interaction between FLS and different subtypes of CD4⁺ T cells is also not entirely clear. Secondly, in the joint synovial tissue of RA patients, in addition to FLS and T cells, there are many other important cell types, including B cells, macrophages, etc., and the interaction network between these cells also needs to be further clarified. Finally, the interaction between T cells and FLS in most of the literature mentioned in this review was confirmed by *in vitro* experiments, and whether the same regulatory patterns still exist in the *in vivo* environment require better *in vivo* models to confirm. All of these issues need further in-depth study before clinic application.

AUTHOR CONTRIBUTIONS

JT and WH drafted the manuscript. JT, TL, WZ, and CZ revised the manuscript. All authors contributed to the article and approved the submitted version.

FUNDING

This work was supported by the National Natural Science Foundation of China (Grant No. 81871788 and 31900616), the Project for Science and Technology leader of Anhui Province (Grant No. 2018H177), the Scientific Research Fund of Anhui Education (Grant No. 2017jyxm1097), the Anhui Provincial Postdoctoral Science Foundation (Grant No. 2019B302), Youth Program of the Provincial Natural Science Foundation of Anhui (2008085MH247), The project of improvement of scientific ability of Anhui Medical University(2020xkjT009) and the Sanming Project of Medicine in Shenzhen (SZSM201812041).

REFERENCES

- Tu J, Huang W, Zhang W, Mei J, Zhu C. A Tale of Two Immune Cells in Rheumatoid Arthritis: The Crosstalk Between Macrophages and T Cells in the Synovium. *Front Immunol* (2021) 12:655477. doi: 10.3389/fimmu.2021.655477
- Morch AM, Bálint S, Santos AM, Davis SJ, Dustin ML. Coreceptors and TCR Signaling – the Strong and the Weak of it. *Front Cell Dev Biol* (2020) 8:597627. doi: 10.3389/fcell.2020.597627
- Malmström V, Trollmo C, Klareskog L. Modulating Co-Stimulation: A Rational Strategy in the Treatment of Rheumatoid Arthritis? *Arthritis Res Ther* (2005) 7 (Suppl 2):S15–20. doi: 10.1186/ar1505
- Tu J, Hong W, Zhang P, Wang X, Körner H, Wei W. Ontology and Function of Fibroblast-Like and Macrophage-Like Synoviocytes: How do They Talk to Each Other and Can They Be Targeted for Rheumatoid Arthritis Therapy? *Front Immunol* (2018) 9:1467. doi: 10.3389/fimmu.2018.01467
- Schonfeldova B, Zec K, Udalova IA. Synovial Single-Cell Heterogeneity, Zonation and Interactions: A Patchwork of Effectors in Arthritis. *Rheumatol (United Kingdom)* (2022) 61:913–25. doi: 10.1093/rheumatology/keab721
- Morgan R, Endres J, Behbahani-Nejad N, Phillips K, Ruth JH, Friday SC, et al. Expression and Function of Amino-peptidase N/CD13 Produced by Fibroblast-Like Synoviocytes in Rheumatoid Arthritis: Role of CD13 in Chemotaxis of Cytokine-Activated T Cells Independent of Enzymatic Activity. *Arthritis Rheumatol* (2015) 67:74–85. doi: 10.1002/art.38878
- Bryant J, Ahern DJ, Brennan FM. CXCR4 and Vascular Cell Adhesion Molecule 1 are Key Chemokine/Adhesion Receptors in the Migration of Cytokine-Activated T Cells. *Arthritis Rheum* (2012) 64:2137–46. doi: 10.1002/art.34394
- Harada S, Yamamura M, Okamoto H, Morita Y, Kawashima M, Aita T, et al. Production of Interleukin-7 and Interleukin-15 by Fibroblast-Like Synoviocytes From Patients With Rheumatoid Arthritis. *Arthritis Rheum* (1999) 42:1508–16. doi: 10.1002/1529-0131(199907)42:7<1508::AID-ANR26>3.0.CO;2-L
- Timmer TCG, Baltus B, Vondenhoff M, Huizinga TWJ, Tak PP, Verweij CL, et al. Inflammation and Ectopic Lymphoid Structures in Rheumatoid Arthritis Synovial Tissues Dissected by Genomics Technology: Identification of the Interleukin-7 Signaling Pathway in Tissues With Lymphoid Neogenesis. *Arthritis Rheum* (2007) 56:2492–502. doi: 10.1002/art.22748
- Rosengren S, Corr M, Firestein GS, Boyle DL. The JAK Inhibitor CP-690,550 (Tofacitinib) Inhibits TNF-Induced Chemokine Expression in Fibroblast-Like Synoviocytes: Autocrine Role of Type I Interferon. *Ann Rheum Dis* (2012) 71:440–7. doi: 10.1136/ard.2011.150284
- Bustamante MF, Garcia-Carbonell R, Whisenant KD, Guma M. Fibroblast-Like Synovocyte Metabolism in the Pathogenesis of Rheumatoid Arthritis. *Arthritis Res Ther* (2017) 19:1–12. doi: 10.1186/s13075-017-1303-3
- Tang Y, Wang B, Sun X, Li H, Ouyang X, Wei J, et al. Rheumatoid Arthritis Fibroblast-Like Synoviocytes Co-Cultured With PBMC Increased Peripheral CD4+CXCR5+ICOS+ T Cell Numbers. *Clin Exp Immunol* (2017) 190:384–93. doi: 10.1111/cei.13025
- Liu R, Zhao P, Zhang Q, Che N, Xu L, Qian J, et al. Adiponectin Promotes Fibroblast-Like Synoviocytes Producing IL-6 to Enhance T Follicular Helper Cells Response in Rheumatoid Arthritis. *Clin Exp Rheumatol* (2020) 38:11–8. doi: 10.1002/art.22439
- Tang BX, You X, Zhao LD, Li Y, Zhang X, Tang FL, et al. P53 in Fibroblast-Like Synoviocytes can Regulate T Helper Cell Functions in Patients With Active Rheumatoid Arthritis. *Chin Med J (Engl)* (2011) 124:364–8. doi: 10.3760/cma.j.issn.0366-6999.2011.03.008
- Gao S, Qi X, Li J, Sang L. Upregulated KAT7 in Synovial Fibroblasts Promotes Th17 Cell Differentiation and Infiltration in Rheumatoid Arthritis. *Biochem Biophys Res Commun* (2017) 489:235–41. doi: 10.1016/j.bbrc.2017.05.143
- Lee DG, Woo JW, Kwok SK, La CM, Park SH. MRP8 Promotes Th17 Differentiation via Upregulation of IL-6 Production by Fibroblast-Like Synoviocytes in Rheumatoid Arthritis. *Exp Mol Med* (2013) 45:1–9. doi: 10.1038/emmm.2013.39
- Wang B, Ma Z, Wang M, Sun X, Tang Y, Li M, et al. IL-34 Upregulated Th17 Production Through Increased IL-6 Expression by Rheumatoid Fibroblast-Like Synoviocytes. *Mediators Inflammation* (2017) 2017:1567120. doi: 10.1155/2017/1567120
- Lin J, Zhou Z, Huo R, Xiao L, Ouyang G, Wang L, et al. Cyr61 Induces IL-6 Production by Fibroblast-Like Synoviocytes Promoting Th17 Differentiation in Rheumatoid Arthritis. *J Immunol* (2012) 188:5776–84. doi: 10.4049/jimmunol.1103201
- Eljaafari A, Tartelin M-L, Aissaoui H, Chevrel G, Osta B, Lavocat F, et al. Bone Marrow- and Synovium-Derived Mesenchymal Cells Promote Th-17 Cells Through Caspase-1 Activation: Contribution to Rheumatoid Arthritis Chronicity. *Arthritis Rheum* (2012) 64(7):2147–57. doi: 10.1002/art
- Corvaisier M, Delneste Y, Jeanvoine H, Preisser L, Blanchard S, Garo E, et al. IL-26 Is Overexpressed in Rheumatoid Arthritis and Induces Proinflammatory Cytokine Production and Th17 Cell Generation. *PLoS Biol* (2012) 10(9):e1001395. doi: 10.1371/journal.pbio.1001395
- Xiao X, Li Y, Jiang X, Ji X, Lu X, Yang B, et al. EZH2 Deficiency Attenuates Treg Differentiation in Rheumatoid Arthritis. *J Autoimmun* (2019) 108:102404. doi: 10.1016/j.jaut.2020.102404
- Wu X, Liu Y, Jin S, Wang M, Jiao Y, Yang B, et al. Single-Cell Sequencing of Immune Cells From Anticitrullinated Peptide Antibody Positive and Negative Rheumatoid Arthritis. *Nat Commun* (2021) 12(1):4977. doi: 10.1038/s41467-021-25246-7
- Hwang SY, Kim HY. Expression of IL-17 Homologs and Their Receptors in the Synovial Cells of Rheumatoid Arthritis Patients. *Mol Cells* (2005) 19:180–4.
- Hirota K, Hashimoto M, Ito Y, Matsuura M, Ito H, Tanaka M, et al. Autoimmune Th17 Cells Induced Synovial Stromal and Innate Lymphoid Cell Secretion of the Cytokine GM-CSF to Initiate and Augment Autoimmune Arthritis. *Immunity* (2018) 48:1220–32.e5. doi: 10.1016/j.immuni.2018.04.009
- Kim EK, Kwon JE, Lee SY, Lee EJ, Kim DS, Moon SJ, et al. IL-17-Mediated Mitochondrial Dysfunction Impairs Apoptosis in Rheumatoid Arthritis Synovial Fibroblasts Through Activation of Autophagy. *Cell Death Dis* (2017) 8(1):e2565. doi: 10.1038/cddis.2016.490
- Shui XL, Lin W, Mao CW, Feng YZ, Kong JZ, Chen SM. Blockade of IL-17 Alleviated Inflammation in Rat Arthritis and MMP-13 Expression. *Eur Rev Med Pharmacol Sci* (2017) 21:2329–37.
- Kim KW, Kim HR, Kim BM, La CM, Lee SH. Th17 Cytokines Regulate Osteoclastogenesis in Rheumatoid Arthritis. *Am J Pathol* (2015) 185:3011–24. doi: 10.1016/j.ajpath.2015.07.017
- Friday SC, Fox DA. Phospholipase D Enzymes Facilitate IL-17- and Tnf α -Induced Expression of Proinflammatory Genes in Rheumatoid Arthritis Synovial Fibroblasts (RASf). *Immunol Lett* (2016) 174:9–18. doi: 10.1016/j.imlet.2016.04.001
- Fan M, Li Y, Yao C, Liu X, Liu J. Dihydroartemisinin Derivative DC32 Attenuates Collagen-Induced Arthritis in Mice by Restoring the Treg/Th17 Balance and Inhibiting Synovitis Through Down-Regulation of IL-6. *Int Immunopharmacol* (2018) 65:233–43. doi: 10.1016/j.intimp.2018.10.015
- Liu Z, Song L, Wang Y, Xu P, Guo X, Yang J, et al. A Novel Fusion Protein Attenuates Collagen-Induced Arthritis by Targeting Interleukin 17A and Tumor Necrosis Factor α . *Int J Pharm* (2018) 547:72–82. doi: 10.1016/j.jipharm.2018.05.058
- Kim KW, La CM, HR K, JH Ju, MK P, HJ Oh, et al. Up-Regulation of Stromal Cell-Derived Factor 1 (CXCL12) Production in Rheumatoid Synovial Fibroblasts Through Interactions With T Lymphocytes: Role of Interleukin-17 and CD40L-CD40 Interaction. *Arthritis Rheum* (2007) 56:1076–86. doi: 10.1002/art.22439
- Aldridge J, Ekwall AKH, Mark L, Bergström B, Andersson K, Gertsson I, et al. T Helper Cells in Synovial Fluid of Patients With Rheumatoid Arthritis Primarily Have a Th1 and a CXCR3+Th2 Phenotype. *Arthritis Res Ther* (2020) 22:1–11. doi: 10.1186/s13075-020-02349-y
- Kato H, Endres J, Fox DA. The Roles of IFN- γ Versus IL-17 in Pathogenic Effects of Human Th17 Cells on Synovial Fibroblasts. *Mod Rheumatol* (2013) 23:1140–50. doi: 10.1007/s10165-012-0811-x
- Corrigall VM, Arastu M, Khan S, Shah C, Fife M, Tak PP, et al. Functional IL-2 Receptor β (CD122) and γ (CD132) Chains Are Expressed by Fibroblast-Like Synoviocytes: Activation by IL-2 Stimulates Monocyte Chemoattractant Protein-1 Production. *J Immunol* (2001) 166:4141–7. doi: 10.4049/jimmunol.1201455
- Schurigt U, Pfirschke C, Irmeler IM, Hükel M, Gajda M, Janik T, et al. Interactions of T Helper Cells With Fibroblast-Like Synoviocytes: Up-Regulation of Matrix Metalloproteinases by Macrophage Migration

- Inhibitory Factor From Both Th1 and Th2 Cells. *Arthritis Rheum* (2008) 58:3030–40. doi: 10.1002/art.23904
36. Saadatmand S, Vos JR, Hoening MJ, Oosterwijk JC, Koppert LB, De BGH, et al. Interleukin-21 Induces Migration and Invasion of Fibroblast-Like Synoviocytes From Patients With Rheumatoid Arthritis. *Clin Exp Immunol* (2016) 184:2–31. doi: 10.1111/cei.12751
 37. Lebre MC, Vieira PL, Tang MW, Aarrass S, Helder B, Newsom-Davis T, et al. Synovial IL-21/TNF-Producing CD4+ T Cells Induce Joint Destruction in Rheumatoid Arthritis by Inducing Matrix Metalloproteinase Production by Fibroblast-Like Synoviocytes. *J Leukoc Biol* (2017) 101:775–83. doi: 10.1189/jlb.5a0516-217r
 38. Blaschke S, Middel P, Dorner BG, Blaschke V, Hummel KM, Kroczeck RA, et al. Expression of Activation-Induced, T Cell-Derived, and Chemokine-Related Cytokine/Lymphotactin and Its Functional Role in Rheumatoid Arthritis. *Arthritis Rheum* (2003) 48:1858–72. doi: 10.1002/art.11171
 39. Zhu W, Meng L, Jiang C, He X, Hou W, Xu P, et al. Arthritis is Associated With T-Cell-Induced Upregulation of Toll-Like Receptor 3 on Synovial Fibroblasts. *Arthritis Res Ther* (2011) 13(3):R103. doi: 10.1186/ar3384
 40. Karonitsch T, Beckmann D, Dalwigk K, Niederreiter B, Studenic P, Byrne RA, et al. Targeted Inhibition of Janus Kinases Abates Interferon Gamma-Induced Invasive Behaviour of Fibroblast-Like Synoviocytes. *Rheumatol (United Kingdom)* (2018) 57:572–7. doi: 10.1093/rheumatology/kex426
 41. Kvackay P, Yao N, Schnotz JH, Scarpone R, Carvalho R de A, Klika KD, et al. Increase of Aerobic Glycolysis Mediated by Activated T Helper Cells Drives Synovial Fibroblasts Towards an Inflammatory Phenotype: New Targets for Therapy? *Arthritis Res Ther* (2021) 23:1–15. doi: 10.1186/s13075-021-02437-7
 42. Tran CN, Davis MJ, Tesmer LA, Endres JL, Motyl CD, Smuda C, et al. Presentation of Arthritogenic Peptide to Antigen-Specific T Cells by Fibroblast-Like Synoviocytes. *Arthritis Rheum* (2007) 56:1497–506. doi: 10.1002/art.22573
 43. Riemann D, Röntsch J, Hause B, Langner J, Kehlen A. Cell-Cell Contact Between Lymphocytes and Fibroblast-Like Synoviocytes Induces Lymphocytic Expression of Aminopeptidase N/CD13 and Results in Lymphocytic Activation. *Adv Exp Med Biol* (2000) 477:57–66. doi: 10.1007/0-306-46826-3_6
 44. Bradfield PF, Amft N, Vernon-Wilson E, Exley AE, Parsonage G, Rainer GE, et al. Rheumatoid Fibroblast-Like Synoviocytes Overexpress the Chemokine Stromal Cell-Derived Factor 1 (CXCL12), Which Supports Distinct Patterns and Rates of CD4+ and CD8+ T Cell Migration Within Synovial Tissue. *Arthritis Rheum* (2003) 48:2472–82. doi: 10.1002/art.11219
 45. Sawai H, Park YW, Roberson J, Imai T, Goronzy JJ, Weyand CM. T Cell Costimulation by Fractalkine-Expressing Synoviocytes in Rheumatoid Arthritis. *Arthritis Rheum* (2005) 52:1392–401. doi: 10.1002/art.21140
 46. Vallejo AN, Yang H, Klimiuk PA, Weyand CM, Goronzy JJ. Synovial-Mediated Expansion of Inflammatory T Cells in Rheumatoid Synovitis Is Dependent on CD47-Thrombospondin 1 Interaction. *J Immunol* (2003) 171:1732–40. doi: 10.4049/jimmunol.171.4.1732
 47. Vallejo AN, Mücke LO, Klimiuk PA, Weyand CM, Goronzy JJ. Central Role of Thrombospondin-1 in the Activation and Clonal Expansion of Inflammatory T Cells. *J Immunol* (2000) 164:2947–54. doi: 10.4049/jimmunol.164.6.2947
 48. Corrigan VM, Solau-Gervais E, Panayi GS. Lack of CD80 Expression by Fibroblast-Like Synoviocytes Leading to Anergy in T Lymphocytes. *Arthritis Rheum* (2000) 43:1606–15. doi: 10.1002/1529-0131(200007)43:7<1606::AID-ANR26>3.0.CO;2-O
 49. Tran CN, Thacker SG, Louie DM, Oliver J, White PT, Endres JL, et al. Interactions of T Cells With Fibroblast-Like Synoviocytes: Role of the B7 Family Costimulatory Ligand B7-H3. *J Immunol* (2008) 180:2989–98. doi: 10.4049/jimmunol.180.5.2989
 50. Kim SJ, Shin HH, Park SY, Lee DS, Lee EA, Cho SD, et al. Induction of MMP-13 Expression by Soluble Human Glucocorticoid-Induced Tumor Necrosis Factor Receptor in Fibroblast-Like Synovial Cells. *Osteoarthritis Cartil* (2006) 14:146–53. doi: 10.1016/j.joca.2005.08.012
 51. Min DJ, Cho ML, SH L, SY M, WU K, JK M, et al. Augmented Production of Chemokines by the Interaction of Type II Collagen-Reactive T Cells With Rheumatoid Synovial Fibroblasts. *Arthritis Rheum* (2004) 50:1146–55. doi: 10.1002/art.20133
 52. Sawai H, Park YW, He X, Goronzy JJ, Weyand CM. Fractalkine Mediates T Cell-Dependent Proliferation of Synovial Fibroblasts in Rheumatoid Arthritis. *Arthritis Rheum* (2007) 56:3215–25. doi: 10.1002/art.22919
 53. Petrasca A, Phelan JJ, Ansboro S, Veale DJ, Fearon U, Fletcher JM. Targeting Bioenergetics Prevents CD4 T Cell-Mediated Activation of Synovial Fibroblasts in Rheumatoid Arthritis. *Rheumatol (United Kingdom)* (2020) 59:2816–28. doi: 10.1093/rheumatology/kez682
 54. Singh K, Colmegna I, He X, Weyand CM, Goronzy JJ. Synovialocyte Stimulation by the LFA-1–Intercellular Adhesion Molecule-2–Ezrin–Akt Pathway in Rheumatoid Arthritis. *J Immunol* (2008) 180:1971–8. doi: 10.4049/jimmunol.180.3.1971
 55. Tran CN, Lundy SK, White PT, Endres JL, Motyl CD, Gupta R, et al. Molecular Interactions Between T Cells and Fibroblast-Like Synoviocytes: Role of Membrane Tumor Necrosis Factor- α on Cytokine-Activated T Cells. *Am J Pathol* (2007) 171:1588–98. doi: 10.2353/ajpath.2007.070004
 56. Bombardieri MP, Webb DL, Conrad P, Marlor CW, Sarr T, Ranges GE, et al. Cell Contact Between T Cells and Synovial Fibroblasts Causes Induction of Adhesion Molecules and Cytokines. *J Leukoc Biol* (1993) 54:399–406. doi: 10.1002/jlb.54.5.399
 57. Cho ML, Yoon CH, Hwang SY, Park MK, Min SY, Lee SH, et al. Effector Function of Type II Collagen-Stimulated T Cells From Rheumatoid Arthritis Patients: Cross-Talk Between T Cells and Synovial Fibroblasts. *Arthritis Rheum* (2004) 50:776–84. doi: 10.1002/art.20106
 58. Moon YM, Yoon BY, Her YM, Oh HJ, Lee JS, Kim KW, et al. IL-32 and IL-17 Interact and Have the Potential to Aggravate Osteoclastogenesis in Rheumatoid Arthritis. *Arthritis Res Ther* (2012) 14(6):R246. doi: 10.1186/ar4089
 59. Tanner MR, Pennington MW, Chauhan SS, Laragione T, Gulko PS, Beeton C. KCa1.1 and Kv1.3 Channels Regulate the Interactions Between Fibroblast-Like Synoviocytes and T Lymphocytes During Rheumatoid Arthritis. *Arthritis Res Ther* (2019) 21:1–21. doi: 10.1186/s13075-018-1783-9
 60. Akaogi J, Nozaki T, Satoh M, Yamada H. Role of PGE2 and EP Receptors in the Pathogenesis of Rheumatoid Arthritis and as a Novel Therapeutic Strategy. *Endocrine Metab Immune Disord - Drug Targets* (2012) 6:383–94. doi: 10.2174/187153006779025711
 61. Zhang W, Wang B, Wang F, Zhang J, Yu J. CTLA4-FasL Fusion Product Suppresses Proliferation of Fibroblast-Like Synoviocytes and Progression of Adjuvant-Induced Arthritis in Rats. *Mol Immunol* (2012) 50:150–9. doi: 10.1016/j.molimm.2012.01.007
 62. Kraan MC, Haringman JJ, Weeden H, Barg EC, Smith MD, Ahern MJ, et al. T Cells, Fibroblast-Like Synoviocytes, and Granzyme B+ Cytotoxic Cells are Associated With Joint Damage in Patients With Recent Onset Rheumatoid Arthritis. *Ann Rheum Dis* (2004) 63:483–8. doi: 10.1136/ard.2003.009225
 63. Brooke A, Bs R, Mph CH, Ma MC, Shao X, Ba HLQ, et al. Rheumatoid Arthritis Naïve T Cells Share Hypermethylation Sites With Synoviocytes. *Arthritis Rheumatol* (2017) 69:550–9. doi: 10.1002/art
 64. Dinesh P, Rasool MK. Berberine Mitigates IL-21/IL-21R Mediated Autophagic Influx in Fibroblast-Like Synoviocytes and Regulates Th17/Treg Imbalance in Rheumatoid Arthritis. *Apoptosis* (2019) 24:644–61. doi: 10.1007/s10495-019-01548-6
 65. Tong WW, Zhang C, Hong T, Liu DH, Wang C, Li J, et al. Silibinin Alleviates Inflammation and Induces Apoptosis in Human Rheumatoid Arthritis Fibroblast-Like Synoviocytes and has a Therapeutic Effect on Arthritis in Rats. *Sci Rep* (2018) 8:1–12. doi: 10.1038/s41598-018-21674-6
 66. Park YH, Jang YJ, Choi Y, Lee K, Kim HJ, Cho O, et al. Combination of LMT-28 and Metformin Improves Beneficial Anti-Inflammatory Effect in Collagen-Induced Arthritis. *Pharmacology* (2021) 106:53–9. doi: 10.1159/000507451
 67. Park YH, Kim HJ, Heo TH. A Directly GP130-Targeting Small Molecule Ameliorates Collagen-Induced Arthritis (CIA) by Inhibiting IL-6/GP130 Signaling and Th17 Differentiation. *Clin Exp Pharmacol Physiol* (2020) 47:628–39. doi: 10.1111/1440-1681.13215
 68. Park Y, Jung H, Lee K, Choi Y, Heo T. Combination of Gp130-Targeting and TNF-Targeting Small Molecules in Alleviating Arthritis Through the Down-Regulation of Th17 Differentiation and Osteoclastogenesis. *Biochem Biophys Res Commun* (2019) 522(4):1030–36. doi: 10.1016/j.bbrc.2019.11.183
 69. Liang JJ, Li HR, Chen Y, Zhang C, Chen DG, Liang ZC, et al. Diallyl Trisulfide can Induce Fibroblast-Like Synovial Apoptosis and has a Therapeutic Effect on Collagen-Induced Arthritis in Mice via Blocking NF- κ B and Wnt Pathways. *Int Immunopharmacol* (2019) 71:132–8. doi: 10.1016/j.intimp.2019.03.024
 70. Wang YL, Gao JM, Xing LZ. Therapeutic Potential of Oroxylin A in Rheumatoid Arthritis. *Int Immunopharmacol* (2016) 40:294–9. doi: 10.1016/j.intimp.2016.09.006

71. Odobasic D, Jia Y, Kao W, Fan H, Wei X, Gu R, et al. Formyl Peptide Receptor Activation Inhibits the Expansion of Effector T Cells and Synovial Fibroblasts and Attenuates Joint Injury in Models of Rheumatoid Arthritis. *Int Immunopharmacol* (2018) 61:140–9. doi: 10.1016/j.intimp.2018.05.028
72. Spurlock CF, Gass HM, Bryant CJ, Wells BC, Olsen NJ, Aune TM. Methotrexate-Mediated Inhibition of Nuclear Factor κ B Activation by Distinct Pathways in T Cells and Fibroblast-Like Synoviocytes. *Rheumatol (United Kingdom)* (2014) 54:178–87. doi: 10.1093/rheumatology/keu279
73. Wang Y, Wu Q, Liu Z, Guo X, Zhou L, Wang Y, et al. A Recombinant IgG-Like Bispecific Antibody Acting as Interleukin-1 β and Interleukin-17A Inhibitor Exhibits a Promising Efficacy for Rheumatoid Arthritis. *BioMed Pharmacother* (2017) 89:426–37. doi: 10.1016/j.biopha.2017.02.045
74. Liu Y, Mu R, Wang S, Long L, Liu X, Li R, et al. Therapeutic Potential of Human Umbilical Cord Mesenchymal Stem Cells in the Treatment of Rheumatoid Arthritis. *Arthritis Res Ther* (2010) 12:1–13. doi: 10.1186/ar3187
75. Papadopoulou A, Yiangou M, Athanasiou E, Zogas N, Kaloyannidis P, Batsis I, et al. Mesenchymal Stem Cells are Conditionally Therapeutic in Preclinical Models of Rheumatoid Arthritis. *Ann Rheum Dis* (2012) 71:1733–40. doi: 10.1136/annrheumdis-2011-200985
76. Kang SE, Park JK, Yoo HJ, Kang HS, Park YW, Park BC, et al. Efficacy of Novel Bispecific Antibody Targeting TNF- α /CXCL10 in the Treatment of Experimental Arthritis. *Transl Res* (2021) 232:75–87. doi: 10.1016/j.trsl.2021.01.004
77. Chen H, Wang C, Li J, Huandike M, Liu J, Huang Q, et al. Chinese Herbal Formula, Huayu Tongbi Fang, Attenuates Inflammatory Proliferation of Rat Synoviocytes Induced by IL-1 β by Regulating Proliferation and Differentiation of T Lymphocytes. *Evidence-Based Complement Altern Med* (2020) 2020:1706837. doi: 10.1155/2020/1706837
78. Matsuoka N, Eguchi K, Kawakami A, Tsuboi M, Kawabe Y, Aoyagi T, et al. Inhibitory Effect of Clarithromycin on Costimulatory Molecule Expression and Cytokine Production by Synovial Fibroblast-Like Cells. *Clin Exp Immunol* (1996) 104:501–8. doi: 10.1046/j.1365-2249.1996.46752.x
79. Zhu Q, Huang J, Wang SZ, Qin ZH, Lin F. Cobrotoxin Extracted From Naja Atr Venom Relieves Arthritis Symptoms Through Anti-Inflammation and Immunosuppression Effects in Rat Arthritis Model. *J Ethnopharmacol* (2016) 194:1087–95. doi: 10.1016/j.jep.2016.11.009
80. Kwok SK, Cho ML, Park MK, Oh HJ, Park JS, Her YM, et al. Interleukin-21 Promotes Osteoclastogenesis in Humans With Rheumatoid Arthritis and in Mice With Collagen-Induced Arthritis. *Arthritis Rheum* (2012) 64:740–51. doi: 10.1002/art.33390
81. Kotake S, Udagawa N, Hakoda M, Mogi M, Yano K, Tsuda E, et al. Activated Human T Cells Directly Induce Osteoclastogenesis From Human Monocytes: Possible Role of T Cells in Bone Destruction in Rheumatoid Arthritis Patients. *Arthritis Rheum* (2001) 44:1003–12. doi: 10.1002/1529-0131(200105)44:5<1003::aid-anr179>3.0.co;2-%23
82. Guo W, Yu D, Wang X, Luo C, Chen Y, Lei W, et al. Anti-Inflammatory Effects of Interleukin-23 Receptor Cytokinebinding Homology Region Rebalance T Cell Distribution in Rodent Collagen-Induced Arthritis. *Oncotarget* (2016) 7:31800–13. doi: 10.18632/oncotarget.9309
83. Shang ZZ, Qin DY, Li QM, Zha XQ, Pan LH, Peng DY, et al. Dendrobium Huoshanense Stem Polysaccharide Ameliorates Rheumatoid Arthritis in Mice via Inhibition of Inflammatory Signaling Pathways. *Carbohydr Polym* (2021) 58(3):718–29. doi: 10.1016/j.carbpol.2021.117657
84. Seong AR, Yoo JY, Choi KC, Lee MH, Lee YH, Lee J, et al. Delphinidin, a Specific Inhibitor of Histone Acetyltransferase, Suppresses Inflammatory Signaling via Prevention of NF- κ B Acetylation in Fibroblast-Like Synoviocyte MH7A Cells. *Biochem Biophys Res Commun* (2011) 410:581–6. doi: 10.1016/j.bbrc.2011.06.029
85. Jia X, Wei F, Sun X, Chang Y, Xu S, Yang X, et al. CP-25 Attenuates the Inflammatory Response of Fibroblast-Like Synoviocytes Co-Cultured With BAFF-Activated CD4+ T Cells. *J Ethnopharmacol J* (2016) 189:194–201. doi: 10.1016/j.jep.2016.05.034
86. Zhang G, Liu HB, Zhou L, Cui XQ, Fan XH. CCL3 Participates in the Development of Rheumatoid Arthritis by Activating AKT. *Eur Rev Med Pharmacol Sci* (2018) 22:6625–32. doi: 10.26355/eurrev_201810_16137
87. Vandooren B, Cantaert T, Noordenbos T, Tak PP, Baeten D. The Abundant Synovial Expression of the RANK/RANKL/osteoprotegerin System in Peripheral Spondylarthritis is Partially Disconnected From Inflammation. *Arthritis Rheum* (2008) 58:718–29. doi: 10.1002/art.23290
88. Fitch E, Harper E, Skorcheva I, Kurtz SE, Blauvelt A. Pathophysiology of Psoriasis: Recent Advances on IL-23 and Th17 Cytokines. *Curr Rheumatol R* (2007) 9:461–7. doi: 10.1007/s11926-007-0075-1
89. Mathieu MC, Lord-Dufour S, Bernier V, Boie Y, Burch JD, Clark P, et al. Mutual Antagonistic Relationship Between Prostaglandin E2 and IFN- γ : Implications for Rheumatoid Arthritis. *Eur J Immunol* (2008) 38:1900–12. doi: 10.1002/eji.200838170

Conflict of Interest: The authors declare that the research was conducted in the absence of any commercial or financial relationships that could be construed as a potential conflict of interest.

Publisher's Note: All claims expressed in this article are solely those of the authors and do not necessarily represent those of their affiliated organizations, or those of the publisher, the editors and the reviewers. Any product that may be evaluated in this article, or claim that may be made by its manufacturer, is not guaranteed or endorsed by the publisher.

Copyright © 2022 Tu, Huang, Zhang, Mei and Zhu. This is an open-access article distributed under the terms of the Creative Commons Attribution License (CC BY). The use, distribution or reproduction in other forums is permitted, provided the original author(s) and the copyright owner(s) are credited and that the original publication in this journal is cited, in accordance with accepted academic practice. No use, distribution or reproduction is permitted which does not comply with these terms.



OPEN ACCESS

EDITED BY

Shanshan Hu,
Anhui Medical University, China

REVIEWED BY

Weinan Zhou,
University of Illinois at Urbana-
Champaign, United States
Xin Yin,
Penn State Milton S. Hershey Medical
Center, United States

*CORRESPONDENCE

Shicheng Guo
Shicheng.Guo@wisc.edu
Steven J. Schrodi
Schrodi@wisc.edu
Dongyi He
dongyihe@medmail.com.cn

SPECIALTY SECTION

This article was submitted to
Autoimmune and Autoinflammatory
Disorders,
a section of the journal
Frontiers in Immunology

RECEIVED 27 April 2022

ACCEPTED 18 July 2022

PUBLISHED 04 August 2022

CITATION

Zhao J, Guo S, Schrodi SJ and He D
(2022) Cuproptosis and cuproptosis-
related genes in rheumatoid
arthritis: Implication,
prospects, and perspectives.
Front. Immunol. 13:930278.
doi: 10.3389/fimmu.2022.930278

COPYRIGHT

© 2022 Zhao, Guo, Schrodi and He.
This is an open-access article
distributed under the terms of the
Creative Commons Attribution License
(CC BY). The use, distribution or
reproduction in other forums is
permitted, provided the original
author(s) and the copyright owner(s)
are credited and that the original
publication in this journal is cited, in
accordance with accepted academic
practice. No use, distribution or
reproduction is permitted which
does not comply with these terms.

Cuproptosis and cuproptosis- related genes in rheumatoid arthritis: Implication, prospects, and perspectives

Jianan Zhao^{1,2,3}, Shicheng Guo^{4,5*}, Steven J. Schrodi^{4,5*}
and Dongyi He^{1,2,3,6*}

¹Department of Rheumatology, Shanghai Guanghua Hospital, Shanghai University of Traditional Chinese Medicine, Shanghai, China, ²Guanghua Clinical Medical College, Shanghai University of Traditional Chinese Medicine, Shanghai, China, ³Institute of Arthritis Research in Integrative Medicine, Shanghai Academy of Traditional Chinese Medicine, Shanghai, China, ⁴Computation and Informatics in Biology and Medicine, University of Wisconsin-Madison, Madison, WI, United States, ⁵Department of Medical Genetics, School of Medicine and Public Health, University of Wisconsin-Madison, Madison, WI, United States, ⁶Arthritis Institute of Integrated Traditional and Western Medicine, Shanghai Chinese Medicine Research Institute, Shanghai, China

Rheumatoid arthritis (RA) is an autoimmune disease that severely affects patients' physical and mental health, leading to chronic synovitis and destruction of bone joints. Although various available clinical treatment options exist, patients respond with varying efficacies due to multiple factors, and there is an urgent need to discover new treatment options to improve clinical outcomes. Cuproptosis is a newly characterized form of cell death. Copper causes cuproptosis by binding to lipid-acylated components of the tricarboxylic acid cycle, leading to protein aggregation, loss of iron-sulfur cluster proteins, and eventually proteotoxic stress. Targeting copper cytotoxicity and cuproptosis are considered potential options for treating oncological diseases. The synovial hypoxic environment and the presence of excessive glycolysis in multiple cells appear to act as inhibitors of cuproptosis, which can lead to excessive survival and proliferation of multiple immune cells, such as fibroblast-like synoviocytes, effector T cells, and macrophages, further mediating inflammation and bone destruction in RA. Therefore, in this study, we attempted to elaborate and summarize the linkage of cuproptosis and key genes regulating cuproptosis to the pathological mechanisms of RA and their effects on a variety of immune cells. This study aimed to provide a theoretical basis and support for translating preclinical and experimental results of RA to clinical protocols.

KEYWORDS

rheumatoid arthritis, autoimmune disease, inflammation, cuproptosis, cuproptosis-related genes

Introduction

Rheumatoid arthritis (RA) is an autoimmune disease characterized by chronic synovitis, presence of multiple autoantibodies, and bone and joint destruction (1). Genetic factors (common risk variants), environmental factors (smoking), genetic and environmental interactions (epigenetic mechanisms), and metabolic abnormalities are risk factors for RA (2). RA affects 1% of the global population and is more prevalent in women than in men (3). Current clinical treatment options for RA include disease-modifying anti-rheumatic drugs, non-steroidal anti-inflammatory drugs (NSAIDs), and biological and non-biological agents. Painkillers and NSAIDs reduce pain and stiffness, but NSAIDs have limited effectiveness and may cause stomach irritation, heart problems, and kidney damage (1). Disease-modifying antirheumatic drugs (DMARDs) are the primary treatment, and when used in combination, these drugs can slow the progression of RA and protect joints and other tissues from permanent damage. However, some DMARDs have multiple adverse effects, such as nausea, liver damage, bone marrow suppression, and development of lung infections (1). Biological agents, including anti-TNF- α antibodies, are also effective, but there are still adverse events, such as infection at the injection site and variation in the efficacy (1). In addition, proper lifestyle management, exercise, and food supplementation are prescribed as complementary therapies. However, due to multiple heterogeneous factors and a complex network of immune-inflammatory pathological mechanisms in RA, available therapies have shown limited clinical efficacy in some patients (2). Therefore, innovative discovery of new drug targets and elucidation of new mechanisms are of great importance for the clinical management of RA.

Cell death is closely associated with RA. Reduced apoptosis in fibroblast-like synoviocytes (FLS) leads to harmful and excessive proliferation, and other pro-inflammatory cell death mechanisms (e.g., pyroptosis and necroptosis) promote inflammation in RA (4). Tsvetkov et al. have characterized a novel form of cell death called “cuproptosis” (5). Cuproptosis in human cells occurs when mitochondrial respiration is disrupted, primarily by the direct binding of excess copper to the lipid-acylated components of the tricarboxylic acid (TCA) cycle. This leads to aggregation of lipid-acylated-related proteins, loss of iron-sulfur cluster proteins, and ultimately, cell death due to intracellular proteotoxic stress (5). In addition, Tsvetkov et al. identified 10 key genes for cuproptosis, including positive regulation factors (ferredoxin 1 (*FDX1*), lipoic acid synthetase (*LIAS*), lipoyltransferase 1 (*LIPT1*), dihydrolipoamide dehydrogenase (*DLD*), drolipoamide S-acetyltransferase (*DLAT*), pyruvate dehydrogenase E1 subunit alpha 1 (*PDHA1*), and pyruvate dehydrogenase E1 subunit beta (*PDHB*)) and negative regulatory factors (metal-regulatory transcription

factor-1 (*MTF1*), glutaminase (*GLS*), and cyclin-dependent kinase inhibitor 2A (*CDKN2A*)) (5). A meta-analysis of 1444 patients with RA showed that their serum copper levels were significantly higher when compared to that of healthy controls (6). Similarly, Ma et al. found elevated serum copper and decreased zinc and selenium levels in RA patients by systematic evaluation and meta-analysis of common trace metals in them, with possible geographical differences in all three, and that serum selenium levels positively correlated with steroid treatment (7). In addition, serum copper levels were higher in patients with active RA, positively correlated with erythrocyte sedimentation rate (ESR) and morning stiffness, and negatively correlated with hemoglobin levels, which are auxiliary markers for disease assessment (8). Therefore, given the excess copper levels in RA, we sought to elucidate its potential association with RA by searching for cuproptosis and cuproptosis-related genes in *PubMed* to provide theoretical references and guidance for the discovery and innovative development of clinical treatment options for RA.

Relationship between cuproptosis and RA

Tsvetkov et al. characterized an extensive and detailed characterization of cuproptosis (5). First, the factors necessary for cuproptosis include the presence of glutathione, and the mitochondrial metabolism of galactose and pyruvate (5). Second, cuproptosis appears to be more dependent on mitochondrial respiration, which is inhibited under various conditions such as hypoxia, and presence of mitochondrial antioxidants, inhibitors of mitochondrial function and fatty acids (5). Finally, the knockdown of seven genes that positively regulate cuproptosis may inhibit cuproptosis. For example, knockdown of *FDX1* results in the loss of protein-lipid acylation, decreased mitochondrial respiration, accumulation of pyruvate and α -glutarate, and loss of iron-sulfur cluster proteins (5). In addition, accumulation of regulatory gene oligomers is important for the occurrence of cuproptosis (5). Synovial tissue of patients with RA presents a hypoxic environment due to chronic inflammation, vascular proliferation, and excessive cell proliferation (9). Under hypoxic conditions, multiple mediators of bone destruction (matrix metalloproteinases (MMPs)), pro-inflammatory factors (interleukin 8 (*IL-8*) and *IL-6*), and chemokines (chemokine (C-C motif) ligand 20 (*CCL20*)) are involved in bone destruction and inflammatory processes in RA (10, 11). Multiple cells in RA are characterized by an imbalance between cell survival and cell death. The metabolic mechanisms associated with cuproptosis may be linked to these cells. For example, the overall glucose and glutamine levels were reduced in RA FLS, showing enhanced depletion, and indicating that glutamine plays an essential role in

FLS proliferation. Glutamine is a critical factor in cuproptosis and its reduced levels, which lead to significant inhibition of cuproptosis, may contribute to the abnormal proliferation of FLS. RA FLS have multiple tumor-like features and survive and over proliferate in a tumor-like microenvironment. The aberrant proliferation of RA FLS is partially attributed to the inhibition of apoptosis (12, 13). The hypoxic environment may also inhibit cuproptosis and thus may contribute to abnormal cell survival and proliferation. The link between copper and hypoxia is complex. Hypoxic conditions promote copper cytotoxicity by inhibiting antioxidant defense mechanisms by increasing reactive oxygen species (ROS), copper transport, and mitotic phagocytosis, with specific molecular mechanisms possibly involving MTF1 and the forkhead box O-3 (FoxO3) signaling pathway (14). Additionally, similar to the inhibition of cuproptosis by the glycolytic effect of FLS, effector T cells exert their effect through the mTOR-dependent pathway, using glycolysis to take in large amounts of glutamine and glucose to provide energy, which may also inhibit cuproptosis, thereby exerting a pro-inflammatory effect. Overactivation of the glycolytic pathway may also inhibit Treg cell function (15). Activated M1 pro-inflammatory macrophages are glycolytic and release pro-inflammatory mediators through multiple mechanisms to destroy tissues (15). These factors may promote inflammatory effects by inhibiting the cuproptosis process in pro-inflammatory cell populations (Table 1). Next, we describe the potential association between critical genes associated with cuproptosis and RA development.

PDHA1

Lactate levels are significantly increased and glucose concentrations are significantly decreased in RA synovial membranes, suggesting excessive activation of glycolytic pathways (16). Glycolysis converts glucose to pyruvate, and the downstream pathways of glycolysis include lactate fermentation and oxidation of pyruvate (17). *PDHA* has been extensively studied in tumor cells. Tumor cells promote their growth primarily by enhancing the glycolytic pathway and attenuating oxidative phosphorylation, which appears to also like the excessive glycolysis in RA FLS. During oxidative phosphorylation, the pyruvate dehydrogenase complex (PDHC) converts pyruvate to acetyl coenzyme A. *PDHA1*, a subunit of PDHC, is a key component linking glycolysis and the TCA cycle (18). *PDHA1* inhibition affects PDHC activity, leading to tumor cell glycolysis, enhanced consumption of glucose and glutamine, and inhibition of oxidative phosphorylation (19). Gut microbial-derived butyrate inhibits sirtuin 3 and mitochondrial complex I in tumor cells to prevent the conversion of TCA cycle intermediates to adenosine triphosphate (ATP). Butyrate induces hyperacetylation of *PDHA1* to relieve the inhibition of *PDHA1* phosphorylation at serine 293 to promote tumor cell apoptosis (20). The transcription factor RUNX family transcription factor 2 (*RUNX2*) promotes the expression of several glycolytic proteins (phosphorylated protein kinase B (*PKB*), hexokinase 2 (*HK2*), and PDH kinase 1 (*PDHK1*)), inhibits the expression of

TABLE 1 The potential function of cuproptosis-related genes in RA.

Gene	May affect cells in RA	Function
<i>PDHA1</i>	FLS, Macrophages	<i>PDHA1</i> inhibition may contribute to the FLS hyperproliferative state. <i>PDHA1</i> may synergize with STAT3 to regulate the macrophage inflammatory response.
<i>PDHB</i>	Treg cell, FLS,	<i>PDHB</i> may co-regulate Treg cells and maintain functional integrity with DJ-1. Downregulation of <i>PDHB</i> may contribute to the abnormal proliferative state of RA FLS
<i>GLS</i>	FLS, CD4+T cell (Th1, Th2, Th17), B cell	<i>GLS1</i> may promote aberrant proliferation of RA FLS, and <i>GLS1</i> inhibition has different effects on different CD4+ T cell subpopulations. <i>GLS</i> is involved in regulating B cell activation and antibody production.
<i>LIAS</i>	Treg cell	<i>LIAS</i> is mainly involved through the regulation of oxidative stress and inflammation and has potential links to RA.
<i>DLAT</i>	FLS	<i>DLAT</i> may influence the development of RA mainly by affecting pyruvate oxidation in the PDHC, TCA cycle, and mitochondrial function
<i>FDX1</i>	Dendritic cells, monocytes-macrophages, Treg cells	<i>FDX1</i> mainly affects fatty acid oxidation and steroid regulation, affecting different cells.
<i>MTF1</i>	FLS, T cells	<i>MTF1</i> stimulates FLS recruitment and inflammatory factor production, promotes angiogenesis, and facilitates pro-inflammatory T cell arrest in the joints.
<i>CDKN2A</i>	Macrophages, T cells, B cells, FLS	<i>CDKN2A</i> is a marker of cellular senescence and may be involved in the aberrant proliferation of FLS and regulation of inflammatory factor release, promoting pro-inflammatory responses in monocytes and macrophages, and may be involved in the functional regulation of abnormal T and B cells.
<i>LIPT1</i>	FLS	<i>LIPT1</i> is mainly responsible for regulating glutamine metabolism aiming to support mitochondrial respiration, TGA cycling, and fatty acid production, which may promote the abnormal proliferative process of FLS.

PDHA1 and sirtuin 6 (*SIRT6*), and suppresses the rate of mitochondrial oxygen consumption (a marker of mitochondrial oxidative phosphorylation), thereby promoting tumor cell proliferation (21). Therefore, it can be speculated that *PDHA1* may be involved in RA FLS by regulating the glycolytic process. *PDHA1* in RA FLS may be in an inhibited state, thus contributing to the excessive glycolytic and hyperproliferative state of FLS.

In addition to what has been described above, *PDHA1* can also be potentially linked to RA through the regulation of inflammation. The release of the NLRP3 inflammasome and related pro-inflammatory mediators plays an important role in the inflammation in RA (4). Activation of the nucleotide-binding oligomerization domain (NOD)-like receptor pyrin domain containing 3 (*NLRP3*) inflammasome requires lactate fermentation and inhibition of *PDHA1* leads to impaired pyruvate oxidation. NLRP3 inflammasome activation leads to release of *IL-1 β* pro-inflammatory mediators (17). Macrophages are important effector cells that are involved in the inflammatory response to RA. Macrophage *SIRT-3* is deacetylated at lysine 83, which activates *PDHA1*, and inhibits NLRP3 inflammasome activation and *IL-1 β* release (22). In addition, the LPS-induced *in vitro* cell model is an important model for RA inflammation (23). Melatonin receptor 1 (*MT1*) inhibits LPS-induced aerobic glycolysis and impairs oxidative phosphorylation by promoting *PDHA1* expression to suppress inflammation (24). The role of *MT1* has been extensively studied in RA. *MT1* plays critical roles such as altering the *Th1/Th17* balance to suppress inflammation (25) and reducing inflammation and cartilage degradation through the phosphatidylinositol 3-kinase (*PI3K*)/protein kinase B (*AKT*), extracellular signal-regulated kinase (*ERK*), and nuclear factor- κ B (*NF- κ B*) signaling pathways, as well as tumor necrosis factor α (*TNF α*) and *IL-1 β* (26). In summary, *PDHA1* appears to be a potent regulator of excessive glycolysis and inflammation and is regulated by different transcriptional mechanisms. Further studies specific to RA are still needed.

PDHB

PDHB is a subunit of pyruvate dehydrogenase, which is similar in function to *PDHA1* in that they both catalyze pyruvate to acetyl coenzyme A (27). *PDHB* has been identified as a susceptibility gene for RA and its expression is downregulated in various tissues and cells (28). Deglycase DJ-1 was found to bind *PDHB* in Tregs, inhibit *PDHA* phosphorylation, and promote *PDH* activity and oxidative phosphorylation to maintain Treg cell differentiation and the functional integrity of T cells (29). In addition, *PDHB* has also been studied in various tumor cells. As previously mentioned, it may be linked to abnormalities in RA FLS. Maternally expressed gene 3 (*MEG3*) inhibits miRNA (miR)-103a-3p, upregulates *PDHB*-induced endoplasmic reticulum stress proteins' expressions (glucose-

regulated protein 78 (GRP78), activating transcription factor 6 (ATF6), C/EBP homologous protein (CHOP), caspase-3, and caspase-9), inhibits cell viability, colony formation ability and invasion, blocks the cell cycle, and induces apoptosis in tumor cells (30). MiR-203, miR-146b-5p, and miR-363-3p promote pro-tumor cell growth, invasion, inhibition of apoptosis, and enhancement of glycolysis by targeting *PDHB* (31–33). *PDHB* also inhibits *RasV12*-driven *ERK* signaling and tumor cell proliferation (34). The interaction between *PDHB* and NIMA-related kinase 10 (*NEK10*) may be necessary for maintaining mitochondrial homeostasis, and *NEK10* knockdown leads to increased mitochondrial damage and dysfunction (35). Thus, *PDHB* appears to be regulated by multiple miRNAs, while abnormalities in multiple miRNAs contribute to the pathological progression of RA, and the interconnection between the two deserves further exploration (36). In conclusion, downregulation of *PDHB* may contribute to the abnormal proliferative state of FLS in RA and may lead to defective Treg function through reduced binding to DJ-1.

GLS

GLS primarily includes two isoforms, *GLS1* and *GLS2*, which are the key enzymes for glutamine metabolism. *GLS1* exists in two splice variants: *KGA* and *GAC* (37). *GLS1* may promote abnormal proliferative processes in RA FLS. In response to the inflammatory factor *IL-17*, the mRNA expression of *GLS1* was upregulated, whereas the expression of *GLS2* was extremely low, implying that *GLS1* is primarily responsible for glutamine metabolism. Furthermore, the inhibition of *GLS1* suppresses the proliferation of RA FLS and improves joint inflammation in arthritic mice (38).

GLS1 inhibition has multiple effects on CD4⁺ T cells and their subpopulations. First, it leads to α -CD3/CD28-induced suppression of CD4⁺ T cell proliferation and decreased expression of T cell activation markers CD25 and CD226 (39). Second, it inhibits cytokine secretion from multiple CD4⁺ T cell-differentiated T cell subsets, e.g., *IL-2* and interferon gamma (*IFN- γ*) (Th1 cytokines), *TNF- α* , *IL-6*, *IL-4* (Th2 cytokines), and *IL-17a* (Th17 cytokines) (39). Finally, the percentage of CD4⁺ T cells expressing chemokine (C-C motif) receptor 6 (*CCR6*) and C-X-C chemokine receptor 3 (*CXCR3*) is reduced (39), both of which have essential roles in inflammatory chemotaxis in RA (40, 41). Th17 is a critical pro-inflammatory mediator in RA that releases *IL-17* pro-inflammatory factors to promote inflammation, which preferentially uses glycolysis and glutamine catabolism to provide energy (42). Peroxisome proliferator-activated receptor gamma (*PPAR- γ*) expression is significantly reduced in the synovial membranes of RA patients (43). *PPAR- γ* activation inhibits Th17 differentiation by suppressing glutamine catabolism. On one hand, the specific mechanism may involve *PPAR- γ* -inhibiting *GLS1* and decreasing

2-hydroxyglutarate (2-HG) levels, thereby regulating lysine demethylase 5 (*KDM5*)-specific trimethylation of Histone H3 at Lysine 4 (H3K4me3) modifications in the promoter and *CNS2* binding regions of the *IL-17* locus. In contrast, *PPAR-γ* inhibits *GLS1* and reduces GSH levels, increases ROS levels, and downregulates retinoic acid-related orphan receptor gamma (*RORγt*) expression (44). In conclusion, *GLS1* may primarily affect FLS, B cell and CD4⁺ T cell subsets in RA by promoting FLS cell proliferation, inflammatory cell differentiation, and pro-inflammatory cytokine release.

LIAS

LIAS is an iron-sulfur cluster mitochondrial enzyme that replicates the final step of the *ab initio* pathway that catalyzes lipoic acid biosynthesis, in which lipoic acid is a powerful antioxidant (45). Lipoic acid can be synthesized in the mitochondria by an enzymatic reaction involving octanoic acid. Lipoic acid is essential for mitochondrial α -keto acid dehydrogenase activity and plays an important role in mitochondrial energy metabolism (46). Mitochondria are important organelles in organisms and play several roles, including providing energy to the cell through oxidative phosphorylation and ATP synthesis. When mitochondria produce energy, they store the electrochemical potential energy in the inner mitochondrial membrane. On both sides of the inner membrane, an asymmetric distribution of protons and other ion concentrations results in the mitochondrial membrane potential. Glycolysis oxidizes pyruvate and combines it with coenzyme A, a reaction coupled with the reduction of NAD⁺, to produce CO₂ and acetyl coenzyme A. Acetyl coenzyme A can enter the tricarboxylic acid cycle, which produces ATP (or GTP), more CO₂, FADH₂, and NADH (47). NADH is then involved in the electron transport chain and oxidative phosphorylation. Oxidative stress is an important factor in mitochondrial dysfunction that leads to RA injury and RA-related atherosclerosis (48). *LIAS* is primarily associated with oxidative stress, inflammation, and RA. Significantly lower *LIAS* expression in mice after LPS induction is accompanied by enhanced inflammatory response and tissue damage (49). *LIAS* overexpression in experimental atherosclerotic mice significantly increases the number of Tregs and reduces T-cell infiltration (50). Similarly, reduced liver *LIAS* in mice with hepatic fibrosis is accompanied by mitochondrial dysfunction and morphological abnormalities, including mitochondrial edema, reduced density or vacuolization of mitochondrial cristae and matrix, reduced activity of mitochondrial complexes I, II, IV, and V, increased mitochondrial fission activity, and reduced mitochondrial fusion activity (51). Overexpression of *LIAS* reduced hepatic oxidative stress in non-alcoholic fatty liver disease in mice and protected mitochondrial function by upregulating the nuclear factor

erythroid 2-related factor 2 to reduce ROS production (52), attenuated the chronic inflammatory response, inhibited NF- κ B activity in lung fibrosis in mice (53), significantly increased Treg cell numbers, and reduced T cell infiltration (50). Mutations in *LIAS* stabilize *HIF-1 α* in its non-hydroxylated form and promote *HIF-1* activation by inhibiting the activity of prolyl hydroxylases (PHDs), which potentially leads to enhanced glycolytic effects in cells (54). Therefore, *LIAS* and *HIF-1* may be involved in RA progression.

DLAT

E4 transcription factor 1 (*E4F1*) is a crucial gene involved in controlling mitochondrial function and cell cycle checkpoints that can interact with RA via *P53* (55, 56). *E4F1* regulates *DLAT*. These two factors may synergistically regulate the pathogenesis of RA (57). Mitochondrial PDHC is primarily involved in pyruvate oxidation and the TCA cycle, and provides energy to the body (57). Sirtuin 4 (*SIRT4*) has enzymatic hydrolytic activity and it was significantly downregulated and markedly correlated positively with anti-cyclic citrullinated peptide (anti-CCP) antibody, ESR, and C-reactive protein (CRP) levels in patients with RA (58, 59). *SIRT4* can hydrolyze the lipoamide cofactors of *DLAT*, thereby inhibiting PDH activity (59). In addition, component 1 Q subcomponent-binding protein (C1QBP) in the mitochondria is associated with histological inflammation scores in RA. It can regulate mitochondrial metabolism by affecting PDGH activity through binding to *DLAT* (60, 61). Therefore, *DLAT* may influence the development of RA primarily by affecting pyruvate oxidation in PDHC, the TCA cycle, and mitochondrial function.

FDX1

FDX1 is a member of the ferredoxin family, which comprises iron-sulfur (Fe/S) proteins (62). The transcription factors *c-Jun* and *SF1* can synergistically promote the transcription and expression of *FDX1* (63). *FDX1* influences immune cells (dendritic cells, monocytes, macrophages, and iTreg cells) (64). Monocytes in RA prefer to use fatty acid oxidation to provide energy and drive receptor activator of nuclear factor kappa-B ligand (RANKL)-induced osteoclast survival and the associated bone destruction (65). *FDX1* was found to significantly promote ATP production in these cells. *FDX1* knockdown significantly promotes production of fructose 6-phosphate, thus affecting downstream glycolysis, and decreases the levels of many long-chain fatty acids, indicating that it promotes fatty acid oxidation (64).

Abnormalities in and regulation of steroid production play an important role in RA. For example, there are multiple

abnormal steroid-related metabolites in patients with RA (66). Increased pro-inflammatory factors in RA may be associated with the reduced renal clearance of steroids (67). *FDX1* may be involved in RA development, by potentially influencing this process. Ferredoxin reductase transfers electrons from nicotinamide adenine dinucleotide phosphate (NADPH) to *FDX1*, reducing members of the mitochondrial cytochrome P450 protein family such as cytochrome P450 11A1 (*CYP11A1*) and *CYP11B* (62). *CYP11A1* catalyzes the conversion of cholesterol to pregnenolone *via* side-chain cleavage in the mitochondria, which is the rate-limiting step in adrenal steroid biosynthesis (63). *CYP11B* promotes the conversion of cortisol to corticosterone, or aldosterone (62). *CYP11A1* also converts vitamin D3 to the non-calcemic analog 20S-hydroxyvitamin, which significantly reduces the release of pro-inflammatory T cell subsets and pro-inflammatory cytokines, increases the proportion of Treg cells, and improves symptoms in a mouse model of arthritis (68).

MTF1

MTF1 is a classical metal-binding transcription factor closely associated with copper homeostasis in eukaryotic organisms (69). Copper loading induces transcriptional activation of metallothionein (*MT*) through *MTF1* and metal responsive element (MRE)-dependent pathways and promotes the nuclear expression of *MTF1*, which promotes metallothionein expression (70). When copper is depleted, *MTF1* also binds to the MRE of *CTR1B* to promote its transcription and expression of *CTR1B*, facilitating the introduction of copper to maintain copper homeostasis (71). In addition to *MTF1* to maintain copper homeostasis, mammalian cells express a variety of copper transporter proteins or enzymes, such as copper transporter 1 (*CTR1*), cytochrome c-oxidase 1 (*Cox1*), *Cox2*, *Cox11*, *Cox17*, synthesis of cytochrome c oxidase 1 (*Sco1*), *Sco2*, superoxide dismutase 1 (*SOD1*), antioxidant-1 (*Atox1*), ATPase copper transporting alpha (*ATP7A*), ATPase copper transporting beta (*ATP7B*), extracellular superoxide dismutase (*ecSOD*, *SOD3*), and lysyl oxidase (*LOX*). Copper homeostasis can be divided into several stages. Firstly, *CTR1* uptake of copper, where the copper is transported *via* protein interactions to three different sites for further processing. For example, ligand-bound copper ions and copper transport proteins, such as *Cox1*, *Cox2*, *Cox11*, and *Cox17*, are subsequently transported to *Sco1* and *Sco2* in mitochondria (72) whereas in the cytoplasmic lysates and mitochondrial gap copper is transported to *SOD1* (72). Copper is transported *via* *ATP7A* or *ATP7B* to the secreted enzymes *EcSOD*, *SOD3*, and *LOX* (72). Other copper transporter proteins and their specific roles have been clearly described, and here we focus only on cuproptosis-related genes (72).

MTF1 can directly or indirectly regulate a variety of cellular functions, and is mainly associated with hypoxic conditions in patients with RA. The RA risk SNP (*rs28411362*) forms a 3D contact with the *MTF1* promoter during inflammatory factor-stimulated chromatin remodeling of RA FLS, whose binding motif stimulates FLS recruitment, and *MTF1* inhibition significantly suppresses FLS cytokine and chemokine production and improves the mouse arthritis model (73). Under hypoxic conditions, *MTF1* expression promotes the transcriptional activation of phosphatidylinositol glycan anchor biosynthesis class F (*PIGF*) to promote angiogenesis and enhance endothelial growth and permeability *via* the vascular endothelial growth factor (*VEGF*) (74). *MTF1* also promotes the activity of hypoxia-inducible factor-1 (*HIF-1*) (75). *HIF-1 α* is a major regulator of cells under hypoxic conditions and is highly expressed in the RA synovium (10, 76, 77). *HIF-1 α* can also induce MMP-3 production to promote bone destruction (10). *HIF-1 α* promotes pro-inflammatory T cell arrest in joints and Th17 differentiation through transcriptional activation of *ROR γ T* and tertiary complex formation with *ROR γ T* and p300 recruitment to the *IL-17* promoter. *HIF-1* inhibits Treg development by targeting forkhead box P3 (*FOXP3*) for proteasomal degradation (77). *HIF-1 α* promotes the conversion of pyruvate to lactate by increasing *LDHA* activity. High concentrations of lactate promote cell proliferation of FLS (10, 76, 77). Furthermore, in addition to its effects on RA FLS, high lactate concentrations can promote pro-inflammatory T-cell arrest in the joints. It is worth noting that *MTF1* responds to copper stimulation through different binding genes (78), and phosphorylation of *MTF1* is essential for the functional activation of MTF (79). For example, *MTF1* promotes *ATP7B* expression by binding to the MRE in the promoter region of *ATP7B* to promote Wilson's disease caused by copper overload (80). Phosphorylation of the kinase *LATS* of the Hippo pathway and inhibition of *MTF1* protects cells from heavy metal-induced cytotoxicity (81). Thus, *MTF1* primarily responds to excess copper levels in RA, and the hypoxic environment affects multiple pathological aspects of RA.

CDKN2A

The fraction of cells expressing p16 (*CDKN2A*) is a typical marker of cellular senescence (82). Cellular senescence has been associated with RA in various cell types. For example, senescent T cells are highly inflammatory, secrete cytotoxic mediators, and express natural killer receptors (NKR), bypassing their antigenic specificity (83, 84). Histone deacetylase1 (*HDAC1*) is overexpressed in RA FLS and promotes cell proliferation in FLS (85). The deacetylase (*HDA*) inhibitor FK228 inhibits joint swelling, synovial inflammation, and bone destruction in mice with experimentally induced arthritis. It also inhibits the proliferation of RA FLS *in vitro* by a mechanism that involves

FK228, thereby inducing high histone acetylation and CDKN2A expression in synovial cells, upregulating p21, and decreasing the release of TNF and IL-1 β (86). However, it is noteworthy that the senescent phenotype of RA FLS highly expresses CDKN2A and releases more pro-inflammatory mediators in response to TNF or oxidative stress stimuli to promote inflammation (87). The histone methyltransferase EZH2 is strongly induced in chronic inflammation of RA FLS, which may suppress CDKN2A expression and thus contribute to the abnormal response to FLS (88). In addition to its potential effects on RA FLS, CDKN2A may affect RA by influencing the function of macrophages, T cells, and leukocytes. Oxidized low-density lipoprotein (*ox-LDL*) activates multiple immune cells in RA to promote the secretion of pro-inflammatory mediators and assemble Abs to promote the production of immune complexes to mediate RA pathological progression (89). *Ox-LDL* promotes the secretion of TNF- α and IL-1 β by macrophages and functions via the MEG3/miR-204/CDKN2A axis (90). CDKN2A expression in macrophages inhibits LPS-induced IL-6 production by a specific mechanism involving CDKN2A, promoting ubiquitin-dependent degradation of IRAK1 and impairing the activation of AP-1 (91). Reduced expression of CDKN2A in leukocytes appears to be associated with increased CD14++CD16++ monocyte subsets, increased immune complex responses, and overproduction of pro-inflammatory factors in RA (2, 92). EZH2 is also thought to be essential for B and T cell development, and IL-17 in RA patients with RA synovial fluid may inhibit EZH2 expression downregulation in CD4+ T cells and suppress Treg

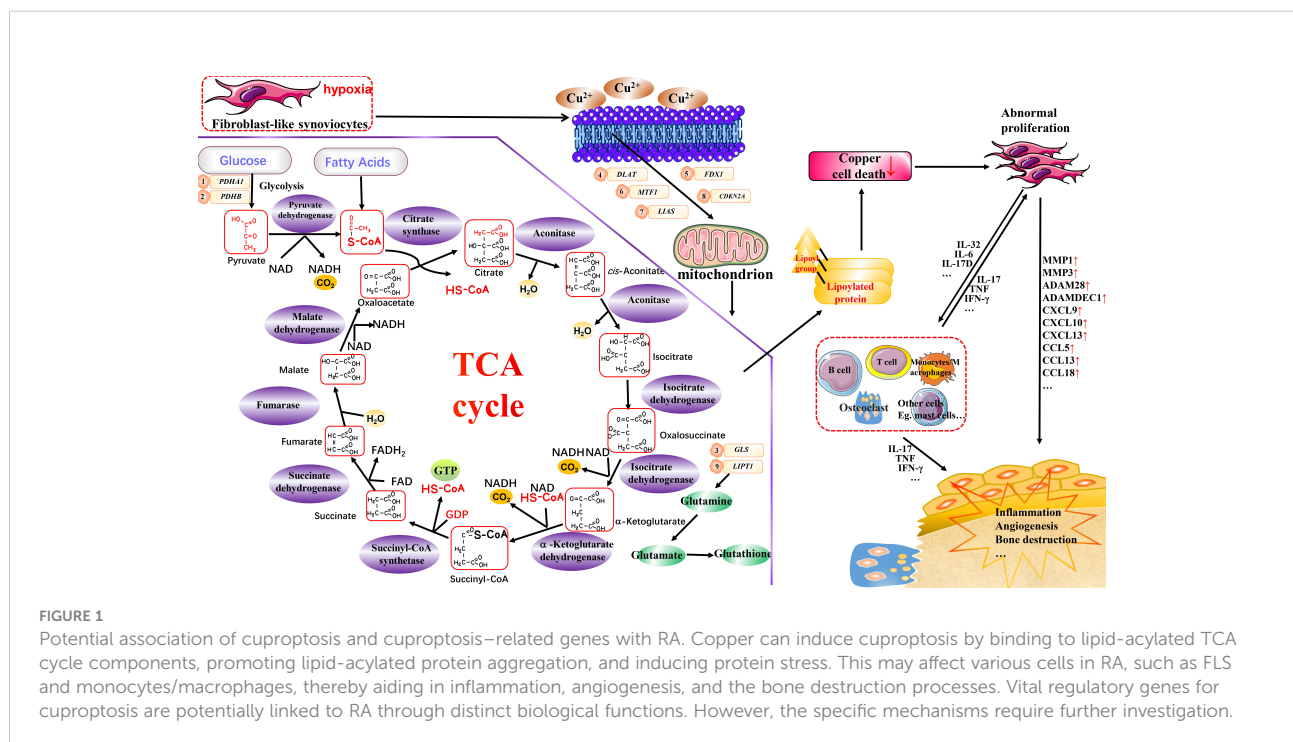
differentiation (93). EZH2 also suppresses CDKN2A expression in naive CD8+ T cells by reducing H3K27me3 levels at two loci (50) and by controlling B-cell maturation (94). Therefore, EZH2 may work in combination with CDKN2A to regulate abnormal T and B cell responses in RA.

LIPT1

LIPT1 primarily encodes LIPT1, which catalyzes the transfer of lipoic acid from the H protein of the glycine cleavage system to the E2 subunit of 2-ketoacid dehydrogenase, an essential step in lipid acylation (95, 96). LIPT1 is primarily responsible for regulating glutamine metabolism to support mitochondrial respiration, the TGA cycle, and fatty acid production (95). Mutations in *LIPT1* impair mitochondrial proteolipid acylation and TGA cycling, and promote the accumulation of lactate and pyruvate (95). Among them, lactate and pyruvate can stimulate synovial cell proliferation, angiogenesis, and vascular opacification in patients with RA (97). Little research has been conducted on *LIPT1* in diseases, and further studies are still needed.

Conclusion

A specific concentration of copper in an organism contributes to organismal homeostasis. However, the imbalance in copper homeostasis may affect the organism by



triggering cuproptosis, leading to disease development. Cuproptosis is considered a potential therapeutic option for oncological diseases, and its possible association with RA is multifaceted (Figure 1). First, cuproptosis in multiple immune cells may be suppressed, and this suppression contributes to their over-proliferation in RA. Secondly, several essential regulatory genes of cuproptosis have been identified to be associated with multiple RA processes, such as aberrant FLS proliferation and inflammatory processes in various immune cells. *PDHA1* regulates glycolysis and inflammation; miRNAs primarily regulate *PDHB*, *GLS1*, and *LIPT1* regulate glutamine metabolism; *DLAT* regulates mitochondrial function and the TCA cycle metabolism; and *FDX1* regulates fatty acid oxidation and steroidogenesis; *MTF1* and *LIAS* regulate copper homeostasis; and *HIF-1* and *CDKN2A* regulate cellular senescence. Finally, it is worth noting that cuproptosis is a newly characterized form of cell death, and its specific mechanisms and effects on disease are not as well studied as other forms of cell death, such as apoptosis and ferroptosis. Well-designed preclinical experiments and clinical trials are still required for in-depth studies of cuproptosis and its associated genes in the context of RA, which still present a significant challenge. However, it is undeniably a research direction with great potential.

Author contributions

JZ is responsible for the collection, collation, and writing of the original manuscript. SG, SS, and DH are responsible for the concept development, revision, and manuscript review. All authors reviewed and accepted the final version.

References

1. Scott DL, Wolfe F, Huizinga TW. Rheumatoid arthritis. *Lancet* (2010) 376 (9746):1094–108. doi: 10.1016/s0140-6736(10)60826-4
2. Zhao J, Guo S, Schrodi SJ, He D. Molecular and cellular heterogeneity in rheumatoid arthritis: Mechanisms and clinical implications. *Front Immunol* (2021) 12:790122. doi: 10.3389/fimmu.2021.790122
3. McInnes IB, Schett G. Pathogenetic insights from the treatment of rheumatoid arthritis. *Lancet* (2017) 389(10086):2328–37. doi: 10.1016/s0140-6736(17)31472-1
4. Zhao J, Jiang P, Guo S, Schrodi SJ, He D. Apoptosis, autophagy, NETosis, necroptosis, and pyroptosis mediated programmed cell death as targets for innovative therapy in rheumatoid arthritis. *Front Immunol* (2021) 12:809806. doi: 10.3389/fimmu.2021.809806
5. Tsvetkov P, Coy S, Petrova B, Dreishpoon M, Verma A, Abdusamad M, et al. Copper induces cell death by targeting lipoylated TCA cycle proteins. *Science* (2022) 375(6586):1254–61. doi: 10.1126/science.abf0529
6. Xin L, Yang X, Cai G, Fan D, Xia Q, Liu L, et al. Serum levels of copper and zinc in patients with rheumatoid arthritis: a meta-analysis. *Biol Trace Elem Res* (2015) 168(1):1–10. doi: 10.1007/s12011-015-0325-4
7. Ma Y, Zhang X, Fan D, Xia Q, Wang M, Pan F. Common trace metals in rheumatoid arthritis: A systematic review and meta-analysis. *J Trace Elem Med Biol* (2019) 56:81–9. doi: 10.1016/j.jtemb.2019.07.007
8. Chakraborty M, Chutia H, Changkakati R. Serum copper as a marker of disease activity in rheumatoid arthritis. *J Clin Diagn Res* (2015) 9(12):Bc09–11. doi: 10.7860/jcdr/2015/14851.7001
9. Hitchon CA, El-Gabalawy HS, Bezabeh T. Characterization of synovial tissue from arthritis patients: a proton magnetic resonance spectroscopic investigation. *Rheumatol Int* (2009) 29(10):1205–11. doi: 10.1007/s00296-009-0865-z
10. Ahn JK, Koh EM, Cha HS, Lee YS, Kim J, Bae EK, et al. Role of hypoxia-inducible factor-1alpha in hypoxia-induced expressions of IL-8, MMP-1 and MMP-3 in rheumatoid fibroblast-like synoviocytes. *Rheumatol (Oxford)* (2008) 47(6):834–9. doi: 10.1093/rheumatology/ken086
11. Bosco MC, Delfino S, Ferlito F, Battaglia F, Puppo M, Gregorio A, et al. Hypoxic synovial environment and expression of macrophage inflammatory protein 3gamma/CCL20 in juvenile idiopathic arthritis. *Arthritis Rheumatol* (2008) 58(6):1833–8. doi: 10.1002/art.23516
12. Bartok B, Firestein GS. Fibroblast-like synoviocytes: key effector cells in rheumatoid arthritis. *Immunol Rev* (2010) 233(1):233–55. doi: 10.1111/j.0105-2896.2009.00859.x
13. Bottini N, Firestein GS. Duality of fibroblast-like synoviocytes in RA: passive responders and imprinted aggressors. *Nat Rev Rheumatol* (2013) 9(1):24–33. doi: 10.1038/nrrheum.2012.190

Funding

This work was funded by the National Natural Science Funds of China (82074234 and 82071756), National Key Research and Development Project (2018YFC1705200 and 2018YFC1705203), Shanghai Chinese Medicine Development Office, National Administration of Traditional Chinese Medicine, Regional Chinese Medicine (Specialist) Diagnosis and Treatment Center Construction Project-Rheumatology, State Administration of Traditional Chinese Medicine, National TCM Evidence-Based Medicine Research and Construction Project, Basic TCM Evidence-Based Capacity Development Program, Shanghai Municipal Health Commission, and East China Region-based Chinese and Western Medicine Joint Disease Specialist Alliance.

Conflict of interest

The authors declare that the research was conducted in the absence of any commercial or financial relationships that could be construed as a potential conflict of interest.

Publisher's note

All claims expressed in this article are solely those of the authors and do not necessarily represent those of their affiliated organizations, or those of the publisher, the editors and the reviewers. Any product that may be evaluated in this article, or claim that may be made by its manufacturer, is not guaranteed or endorsed by the publisher.

14. Pan Y, Ai CX, Zeng L, Liu C, Li WC. Modulation of copper-induced antioxidant defense, Cu transport, and mitophagy by hypoxia in the large yellow croaker (*Larimichthys crocea*). *Fish Physiol Biochem* (2020) 46(3):997–1010. doi: 10.1007/s10695-020-00765-0
15. Murray PJ, Rathmell J, Pearce E. SnapShot: Immunometabolism. *Cell Metab* (2015) 22(1):190–e1. doi: 10.1016/j.cmet.2015.06.014
16. Ciurtin C, Cojocaru VM, Miron IM, Preda F, Milicescu M, Bojinca M, et al. Correlation between different components of synovial fluid and pathogenesis of rheumatic diseases. *Rom J Intern Med* (2006) 44(2):171–81.
17. Lin HC, Chen YJ, Wei YH, Lin HA, Chen CC, Liu TF, et al. Lactic acid fermentation is required for NLRP3 inflammasome activation. *Front Immunol* (2021) 12:630380. doi: 10.3389/fimmu.2021.630380
18. Liu Z, Yu M, Fei B, Fang X, Ma T, Wang D. miR-21–5p targets PDHA1 to regulate glycolysis and cancer progression in gastric cancer. *Oncol Rep* (2018) 40(5):2955–63. doi: 10.3892/or.2018.6695
19. Liu L, Cao J, Zhao J, Li X, Suo Z, Li H. PDHA1 gene knockout in human esophageal squamous cancer cells resulted in greater warburg effect and aggressive features *In vitro* and *in vivo*. *Onco Targets Ther* (2019) 12:9899–913. doi: 10.2147/ott.S226851
20. Xu S, Liu CX, Xu W, Huang L, Zhao JY, Zhao SM. Butyrate induces apoptosis by activating PDC and inhibiting complex I through SIRT3 inactivation. *Signal Transduct Target Ther* (2017) 2:16035. doi: 10.1038/sigtrans.2016.35
21. Choe M, Brusgard JL, Chumsri S, Bhandary L, Zhao XF, Lu S, et al. The RUNX2 transcription factor negatively regulates SIRT6 expression to alter glucose metabolism in breast cancer cells. *J Cell Biochem* (2015) 116(10):2210–26. doi: 10.1002/jcb.25171
22. Wei T, Gao J, Huang C, Song B, Sun M, Shen W. SIRT3 (Sirtuin-3) prevents ang II (Angiotensin II)-induced macrophage metabolic switch improving perivascular adipose tissue function. *Arterioscler Thromb Vasc Biol* (2021) 41(2):714–30. doi: 10.1161/atvbaha.120.315337
23. Kitamura K, Sasaki M, Matsumoto M, Shionoya H, Iida K. Protective effect of bacteroides fragilis LPS on escherichia coli LPS-induced inflammatory changes in human monocytic cells and in a rheumatoid arthritis mouse model. *Immunol Lett* (2021) 233:48–56. doi: 10.1016/j.imlet.2021.03.008
24. Gu C, Wang F, Zhang YF, Wei SZ, Liu JY, Sun HY, et al. Microglial MT1 activation inhibits LPS-induced neuroinflammation via regulation of metabolic reprogramming. *Aging Cell* (2021) 20(6):e13375. doi: 10.1111/accel.13375
25. Sun J, Li L, Li L, Ding L, Liu X, Chen X, et al. Metallothionein-1 suppresses rheumatoid arthritis pathogenesis by shifting the Th17/Treg balance. *Eur J Immunol* (2018) 48(9):1550–62. doi: 10.1002/eji.201747151
26. Huang CC, Chiou CH, Liu SC, Hu SL, Su CM, Tsai CH, et al. Melatonin attenuates TNF- α and IL-1 β expression in synovial fibroblasts and diminishes cartilage degradation: Implications for the treatment of rheumatoid arthritis. *J Pineal Res* (2019) 66(3):e12560. doi: 10.1111/jpi.12560
27. Li A, Zhang Y, Zhao Z, Wang M, Zan L. Molecular characterization and transcriptional regulation analysis of the bovine PDHB gene. *PloS One* (2016) 11(7):e0157445. doi: 10.1371/journal.pone.0157445
28. Wu C, Tan S, Liu L, Cheng S, Li P, Li W, et al. Transcriptome-wide association study identifies susceptibility genes for rheumatoid arthritis. *Arthritis Res Ther* (2021) 23(1):38. doi: 10.1186/s13075-021-02419-9
29. Danileviciute E, Zeng N, Capelle CM, Paczia N, Gillespie MA, Kurniawan H, et al. PARK7/DJ-1 promotes pyruvate dehydrogenase activity and maintains t (reg) homeostasis during ageing. *Nat Metab* (2022) 4(5):589–607. doi: 10.1038/s42255-022-00576-y
30. Wang G, Ye Q, Ning S, Yang Z, Chen Y, Zhang L, et al. LncRNA MEG3 promotes endoplasmic reticulum stress and suppresses proliferation and invasion of colorectal carcinoma cells through the MEG3/miR-103a-3p/PDHB ceRNA pathway. *Neoplasia* (2021) 68(2):362–74. doi: 10.4149/neo_2020_200813N858
31. Zhu Y, Wu G, Yan W, Zhan H, Sun P. miR-146b-5p regulates cell growth, invasion, and metabolism by targeting PDHB in colorectal cancer. *Am J Cancer Res* (2017) 7(5):1136–50.
32. Xu DX, Guo JJ, Zhu GY, Wu HJ, Zhang QS, Cui T. MiR-363-3p modulates cell growth and invasion in glioma by directly targeting pyruvate dehydrogenase b. *Eur Rev Med Pharmacol Sci* (2018) 22(16):5230–9. doi: 10.26355/eurrev_201808_15721
33. Xiaohong Z, Lichun F, Na X, Kejian Z, Xiaolan X, Shaosheng W. MiR-203 promotes the growth and migration of ovarian cancer cells by enhancing glycolytic pathway. *Tumour Biol* (2016) 37(11):14989–97. doi: 10.1007/s13277-016-5415-1
34. Tang H, Luo X, Li J, Zhou Y, Li Y, Song L, et al. Pyruvate dehydrogenase b promoted the growth and migration of the nasopharyngeal carcinoma cells. *Tumour Biol* (2016) 37(8):10563–9. doi: 10.1007/s13277-016-4922-4
35. Peres de Oliveira A, Basei FL, Slepicka PF, de Castro Ferezin C, Melo-Hanchuk TD, de Souza EE, et al. NEK10 interactome and depletion reveal new roles in mitochondria. *Proteome Sci* (2020) 18:4. doi: 10.1186/s12953-020-00160-w
36. Chang C, Xu L, Zhang R, Jin Y, Jiang P, Wei K, et al. MicroRNA-mediated epigenetic regulation of rheumatoid arthritis susceptibility and pathogenesis. *Front Immunol* (2022) 13:838884. doi: 10.3389/fimmu.2022.838884
37. Taylor L, Curthoys NP. Glutamine metabolism: Role in acid-base balance*. *Biochem Mol Biol Educ* (2004) 32(5):291–304. doi: 10.1002/bmb.2004.494032050388
38. Takahashi S, Saegusa J, Sendo S, Okano T, Akashi K, Irino Y, et al. Glutaminase 1 plays a key role in the cell growth of fibroblast-like synoviocytes in rheumatoid arthritis. *Arthritis Res Ther* (2017) 19(1):76. doi: 10.1186/s13075-017-1283-3
39. Sener Z, Cedervik FH, Volchenkov R, Holen HL, Skålhegg BS. T Helper cell activation and expansion is sensitive to glutaminase inhibition under both hypoxic and normoxic conditions. *PloS One* (2016) 11(7):e0160291. doi: 10.1371/journal.pone.0160291
40. Meitei HT, Jadhav N, Lal G. CCR6–CCL20 axis as a therapeutic target for autoimmune diseases. *Autoimmun Rev* (2021) 20(7):102846. doi: 10.1016/j.autrev.2021.102846
41. Lacotte S, Brun S, Muller S, Dumortier H. CXCR3, inflammation, and autoimmune diseases. *Ann N Y Acad Sci* (2009) 1173:310–7. doi: 10.1111/j.1749-6632.2009.04813.x
42. Sun L, Fu J, Zhou Y. Metabolism controls the balance of Th17/T-regulatory cells. *Front Immunol* (2017) 8:1632. doi: 10.3389/fimmu.2017.01632
43. Li XF, Sun YY, Bao J, Chen X, Li YH, Yang Y, et al. Functional role of PPAR- γ on the proliferation and migration of fibroblast-like synoviocytes in rheumatoid arthritis. *Sci Rep* (2017) 7(1):12671. doi: 10.1038/s41598-017-12570-6
44. Miao Y, Zheng Y, Geng Y, Yang L, Cao N, Dai Y, et al. The role of GLS1-mediated glutaminolysis/2-HG/H3K4me3 and GSH/ROS signals in Th17 responses counteracted by PPAR γ agonists. *Theranostics* (2021) 11(9):4531–48. doi: 10.7150/thno.54803
45. Krishnamoorthy E, Hassan S, Hanna LE, Padmalayam I, Rajaram R, Viswanathan V. Homology modeling of homo sapiens lipoic acid synthase: Substrate docking and insights on its binding mode. *J Theor Biol* (2017) 420:259–66. doi: 10.1016/j.jtbi.2016.09.005
46. Shay KP, Moreau RF, Smith EJ, Smith AR, Hagen TM. Alpha-lipoic acid as a dietary supplement: molecular mechanisms and therapeutic potential. *Biochim Biophys Acta* (2009) 1790(10):1149–60. doi: 10.1016/j.bbagen.2009.07.026
47. King A, Selak MA, Gottlieb E. Succinate dehydrogenase and fumarate hydratase: linking mitochondrial dysfunction and cancer. *Oncogene* (2006) 25(34):4675–82. doi: 10.1038/sj.onc.1209594
48. Wójcik P, Gęgotek A, Źarković N, Skrzydlewska E. Oxidative stress and lipid mediators modulate immune cell functions in autoimmune diseases. *Int J Mol Sci* (2021) 22(2):723. doi: 10.3390/ijms22020723
49. Yi X, Kim K, Yuan W, Xu L, Kim HS, Homeister JW, et al. Mice with heterozygous deficiency of lipoic acid synthase have an increased sensitivity to lipopolysaccharide-induced tissue injury. *J Leukoc Biol* (2009) 85(1):146–53. doi: 10.1189/jlb.0308161
50. Tian S, Nakamura J, Hiller S, Simington S, Holley DW, Mota R, et al. New insights into immunomodulation via overexpressing lipoic acid synthase as a therapeutic potential to reduce atherosclerosis. *Vasc Pharmacol* (2020) 133–134:106777. doi: 10.1016/j.vph.2020.106777
51. Luo J, Shen S. Lipoic acid alleviates schistosomiasis-induced liver fibrosis by upregulating Drp1 phosphorylation. *Acta Trop* (2020) 206:105449. doi: 10.1016/j.actatropica.2020.105449
52. Xu G, Yan T, Peng Q, Li H, Wu W, Yi X, et al. Overexpression of the lias gene attenuates hepatic steatosis in leprdb/db mice. *J Endocrinol* (2021) 248(2):119–31. doi: 10.1530/joe-19-0606
53. Zhao Y, Xu G, Li H, Chang M, Guan Y, Li Y, et al. Overexpression of endogenous lipoic acid synthase attenuates pulmonary fibrosis induced by crystalline silica in mice. *Toxicol Lett* (2020) 323:57–66. doi: 10.1016/j.toxlet.2020.01.023
54. Burr SP, Costa AS, Grice GL, Timms RT, Lobb IT, Freisinger P, et al. Mitochondrial protein lipoylation and the 2-oxoglutarate dehydrogenase complex controls HIF1 α stability in aerobic conditions. *Cell Metab* (2016) 24(5):740–52. doi: 10.1016/j.cmet.2016.09.015
55. Rodier G, Kirsh O, Baraibar M, Houllès T, Lacroix M, Delpech H, et al. The transcription factor E4F1 coordinates CHK1-dependent checkpoint and mitochondrial functions. *Cell Rep* (2015) 11(2):220–33. doi: 10.1016/j.celrep.2015.03.024
56. Taghadossi M, Adib M, Jamshidi A, Mahmoudi M, Farhadi E. The p53 status in rheumatoid arthritis with focus on fibroblast-like synoviocytes. *Immunol Res* (2021) 69(3):225–38. doi: 10.1007/s12026-021-09202-7
57. Lacroix M, Rodier G, Kirsh O, Houles T, Delpech H, Seyran B, et al. E4F1 controls a transcriptional program essential for pyruvate dehydrogenase activity. *Proc Natl Acad Sci USA* (2016) 113(39):10998–1003. doi: 10.1073/pnas.1602754113

58. Hussain MZ, Haris MS, Khan MS, Mahjabeen I. Role of mitochondrial sirtuins in rheumatoid arthritis. *Biochem Biophys Res Commun* (2021) 584:60–5. doi: 10.1016/j.bbrc.2021.11.016
59. Mathias RA, Greco TM, Oberstein A, Budayeva HG, Chakrabarti R, Rowland EA, et al. Sirtuin 4 is a lipamidase regulating pyruvate dehydrogenase complex activity. *Cell* (2014) 159(7):1615–25. doi: 10.1016/j.cell.2014.11.046
60. Chen R, Xiao M, Gao H, Chen Y, Li Y, Liu Y, et al. Identification of a novel mitochondrial interacting protein of C1QBP using subcellular fractionation coupled with CoIP-MS. *Anal Bioanal Chem* (2016) 408(6):1557–64. doi: 10.1007/s00216-015-9228-7
61. de Seny D, Bianchi E, Baiwir D, Cobraiville G, Collin C, Deliege M, et al. Proteins involved in the endoplasmic reticulum stress are modulated in synovitis of osteoarthritis, chronic pyrophosphate arthropathy and rheumatoid arthritis, and correlate with the histological inflammatory score. *Sci Rep* (2020) 10(1):14159. doi: 10.1038/s41598-020-70803-7
62. Sheftel AD, Stehling O, Pierik AJ, Elsässer HP, Mühlenhoff U, Webert H, et al. Humans possess two mitochondrial ferredoxins, Fdx1 and Fdx2, with distinct roles in steroidogenesis, heme, and Fe/S cluster biosynthesis. *Proc Natl Acad Sci U S A* (2010) 107(26):11775–80. doi: 10.1073/pnas.1004250107
63. Roumaud P, Rwigemera A, Martin LJ. Transcription factors SF1 and cJUN cooperate to activate the Fdx1 promoter in MA-10 leydig cells. *J Steroid Biochem Mol Biol* (2017) 171:121–32. doi: 10.1016/j.jsbmb.2017.03.003
64. Zhang Z, Ma Y, Guo X, Du Y, Zhu Q, Wang X, et al. FDX1 can impact the prognosis and mediate the metabolism of lung adenocarcinoma. *Front Pharmacol* (2021) 12:749134. doi: 10.3389/fphar.2021.749134
65. Yoon N, Jang AK, Seo Y, Jung BH. Metabolomics in autoimmune diseases: Focus on rheumatoid arthritis, systemic lupus erythematosus, and multiple sclerosis. *Metabolites* (2021) 11(12):812. doi: 10.3390/metabo11120812
66. Yousri NA, Bayoumy K, Elhaq WG, Mohney RP, Emadi SA, Hammoudeh M, et al. Large Scale metabolic profiling identifies novel steroids linked to rheumatoid arthritis. *Sci Rep* (2017) 7(1):9137. doi: 10.1038/s41598-017-05439-1
67. Straub RH, Weidner C, Demmel B, Herrmann M, Kees F, Schmidt M, et al. Renal clearance and daily excretion of cortisol and adrenal androgens in patients with rheumatoid arthritis and systemic lupus erythematosus. *Ann Rheum Dis* (2004) 63(8):961–8. doi: 10.1136/ard.2003.014274
68. Postlethwaite AE, Tuckey RC, Kim TK, Li W, Bhattacharya SK, Myers LK, et al. 20S-hydroxyvitamin D₃, a secosteroid produced in humans, is anti-inflammatory and inhibits murine autoimmune arthritis. *Front Immunol* (2021) 12:678487. doi: 10.3389/fimmu.2021.678487
69. Balamurugan K, Schaffner W. Copper homeostasis in eukaryotes: teetering on a tightrope. *Biochim Biophys Acta* (2006) 1763(7):737–46. doi: 10.1016/j.bbamcr.2006.05.001
70. Chen GH, Lv W, Xu YH, Wei XL, Xu YC, Luo Z. Functional analysis of MTF-1 and MT promoters and their transcriptional response to zinc (Zn) and copper (Cu) in yellow catfish *pelteobagrus fulvidraco*. *Chemosphere* (2020) 246:125792. doi: 10.1016/j.chemosphere.2019.125792
71. Selvaraj A, Balamurugan K, Yepiskoposyan H, Zhou H, Egli D, Georgiev O, et al. Metal-responsive transcription factor (MTF-1) handles both extremes, copper load and copper starvation, by activating different genes. *Genes Dev* (2005) 19(8):891–6. doi: 10.1101/gad.1301805
72. Fukai T, Ushio-Fukai M, Kaplan JH. Copper transporters and copper chaperones: roles in cardiovascular physiology and disease. *Am J Physiol Cell Physiol* (2018) 315(2):C186–c201. doi: 10.1152/ajpcell.00132.2018
73. Tsuchiya H, Ota M, Sumitomo S, Ishigaki K, Suzuki A, Sakata T, et al. Parsing multiomics landscape of activated synovial fibroblasts highlights drug targets linked to genetic risk of rheumatoid arthritis. *Ann Rheum Dis* (2020) 80(4):440–50. doi: 10.1136/annrheumdis-2020-218189
74. Green CJ, Lichtlen P, Huynh NT, Yanovsky M, Laderoute KR, Schaffner W, et al. Placenta growth factor gene expression is induced by hypoxia in fibroblasts: a central role for metal transcription factor-1. *Cancer Res* (2001) 61(6):2696–703.
75. Murphy BJ, Sato BG, Dalton TP, Laderoute KR. The metal-responsive transcription factor-1 contributes to HIF-1 activation during hypoxic stress. *Biochem Biophys Res Commun* (2005) 337(3):860–7. doi: 10.1016/j.bbrc.2005.09.124
76. Gaber T, Häupl T, Sandig G, Tykwincka K, Fangradt M, Tschirschmann M, et al. Adaptation of human CD4+ T cells to pathophysiological hypoxia: a transcriptome analysis. *J Rheumatol* (2009) 36(12):2655–69. doi: 10.3899/jrheum.090255
77. Dang EV, Barbi J, Yang HY, Jinasena D, Yu H, Zheng Y, et al. Control of T (H)17/T(reg) balance by hypoxia-inducible factor 1. *Cell* (2011) 146(5):772–84. doi: 10.1016/j.cell.2011.07.033
78. Tavera-Montañez C, Hainer SJ, Cangussu D, Gordon SJV, Xiao Y, Reyes-Gutierrez P, et al. The classic metal-sensing transcription factor MTF1 promotes myogenesis in response to copper. *FASEB J* (2019) 33(12):14556–74. doi: 10.1096/fj.201901606R
79. LaRochelle O, Gagné V, Charron J, Soh JW, Séguin C. Phosphorylation is involved in the activation of metal-regulatory transcription factor 1 in response to metal ions. *J Biol Chem* (2001) 276(45):41879–88. doi: 10.1074/jbc.M108313200
80. Stalke A, Pfister ED, Baumann U, Illig T, Reischl E, Sandbothe M, et al. MTF1 binds to metal-responsive element e within the ATP7B promoter and is a strong candidate in regulating the ATP7B expression. *Ann Hum Genet* (2020) 84(2):195–200. doi: 10.1111/ahg.12355
81. Han H, Nakaoka HJ, Hofmann L, Zhou JJ, Yu C, Zeng L, et al. The hippo pathway kinases LATS1 and LATS2 attenuate cellular responses to heavy metals through phosphorylating MTF1. *Nat Cell Biol* (2022) 24(1):74–87. doi: 10.1038/s41556-021-00813-8
82. Uyar B, Palmer D, Kowald A, Murua Escobar H, Barrantes I, Möller S, et al. Single-cell analyses of aging, inflammation and senescence. *Ageing Res Rev* (2020) 64:101156. doi: 10.1016/j.arr.2020.101156
83. Goronzy JJ, Henel G, Sawai H, Singh K, Lee EB, Pryshchep S, et al. Costimulatory pathways in rheumatoid synovitis and T-cell senescence. *Ann N Y Acad Sci* (2005) 1062:182–94. doi: 10.1196/annals.1358.022
84. Cove LP, De Maeyer RPH, Gomes DCO, Akbar AN. The role of senescent T cells in immunopathology. *Ageing Cell* (2020) 19(12):e13272. doi: 10.1111/acel.13272
85. Horiuchi M, Morinobu A, Chin T, Sakai Y, Kurosaka M, Kumagai S. Expression and function of histone deacetylases in rheumatoid arthritis synovial fibroblasts. *J Rheumatol* (2009) 36(8):1580–9. doi: 10.3899/jrheum.081115
86. Nishida K, Komiyama T, Miyazawa S, Shen ZN, Furumatsu T, Doi H, et al. Histone deacetylase inhibitor suppression of autoantibody-mediated arthritis in mice via regulation of p16INK4a and p21(WAF1/Cip1) expression. *Arthritis Rheumatol* (2004) 50(10):3365–76. doi: 10.1002/art.20709
87. Del Rey MJ, Valín Á, Usategui A, Ergueta S, Martín E, Municio C, et al. Senescent synovial fibroblasts accumulate prematurely in rheumatoid arthritis tissues and display an enhanced inflammatory phenotype. *Immun Ageing* (2019) 16:29. doi: 10.1186/s12979-019-0169-4
88. Trenkmann M, Brock M, Gay RE, Kolling C, Speich R, Michel BA, et al. Expression and function of EZH2 in synovial fibroblasts: epigenetic repression of the wnt inhibitor SFRP1 in rheumatoid arthritis. *Ann Rheum Dis* (2011) 70(8):1482–8. doi: 10.1136/ard.2010.143040
89. Rhoads JP, Lukens JR, Wilhelm AJ, Moore JL, Mendez-Fernandez Y, Kanneganti TD, et al. Oxidized low-density lipoprotein immune complex priming of the Nlrp3 inflammasome involves TLR and FcγR cooperation and is dependent on CARD9. *J Immunol* (2017) 198(5):2105–14. doi: 10.4049/jimmunol.1601563
90. Yan L, Liu Z, Yin H, Guo Z, Luo Q. Silencing of MEG3 inhibited ox-LDL-induced inflammation and apoptosis in macrophages via modulation of the MEG3/miR-204/CDKN2A regulatory axis. *Cell Biol Int* (2019) 43(4):409–20. doi: 10.1002/cbin.11105
91. Murakami Y, Mizoguchi F, Saito T, Miyasaka N, Kohsaka H. p16 (INK4a) exerts an anti-inflammatory effect through accelerated IRAK1 degradation in macrophages. *J Immunol* (2012) 189(10):5066–72. doi: 10.4049/jimmunol.1103156
92. Martínez-Hervás S, Sánchez-García V, Herrero-Cervera A, Vinué Á, Real JT, Ascaso JF, et al. Type 1 diabetic mellitus patients with increased atherosclerosis risk display decreased CDKN2A/2B/2BAS gene expression in leukocytes. *J Transl Med* (2019) 17(1):222. doi: 10.1186/s12967-019-1977-1
93. Xiao XY, Li YT, Jiang X, Ji X, Lu X, Yang B, et al. EZH2 deficiency attenuates treg differentiation in rheumatoid arthritis. *J Autoimmun* (2020) 108:102404. doi: 10.1016/j.jaut.2020.102404
94. Jacobsen JA, Woodard J, Mandal M, Clark MR, Bartom ET, Sigvardsson M, et al. EZH2 regulates the developmental timing of effectors of the pre-antigen receptor checkpoints. *J Immunol* (2017) 198(12):4682–91. doi: 10.4049/jimmunol.1700319
95. Ni M, Solmonson A, Pan C, Yang C, Li D, Notzon A, et al. Functional assessment of lipoyltransferase-1 deficiency in cells, mice, and humans. *Cell Rep* (2019) 27(5):1376–86.e6. doi: 10.1016/j.celrep.2019.04.005
96. Mayr JA, Feichtinger RG, Tort F, Ribes A, Sperl W. Lipoid acid biosynthesis defects. *J Inher Metab Dis* (2014) 37(4):553–63. doi: 10.1007/s10545-014-9705-8
97. Chang X, Wei C. Glycolysis and rheumatoid arthritis. *Int J Rheum Dis* (2011) 14(3):217–22. doi: 10.1111/j.1756-185X.2011.01598.x

Glossary

RA	rheumatoid arthritis
TCA cycle	tricarboxylic acid cycle
NSAIDs	non-steroidal anti-inflammatory drugs
FLS	fibroblast-like synoviocytes
FDX1	ferredoxin 1
LIAS	lipoic acid synthetase
LIPT1	lipoyltransferase 1
DLD	dihydrolipoamide dehydrogenase
DLAT	dihydrolipoamide S-acetyltransferase
PDHA1	pyruvate dehydrogenase E1 subunit alpha 1
PDHB	pyruvate dehydrogenase E1 subunit beta
MTF1	metal-regulatory transcription factor-1
GLS	glutaminase
CDKN2A	cyclin-dependent kinase inhibitor 2A
MMPs	matrix metalloproteinases
IL	interleukin
CCL20	chemokine (C-C motif) ligand 20
FoxO3	forkhead box O-3
PDHC	the pyruvate dehydrogenase (PDH) complex
ATP	adenosine triphosphate
RUNX2	RUNX family transcription factor 2
PKB	phosphorylated protein kinase B
HK2	hexokinase 2
PDHK1	PDH kinases 1
SIRT6	sirtuin 6
PI3K	phosphatidylinositol 3-kinase
AKT	protein kinase B
ERK	the extracellular signal-regulated kinase
NF- κ B	nuclear factor- κ B
TNF α	tumor necrosis factor α
NLRP3	the nucleotide-binding oligomerization domain (NOD)-like receptor pyrin domain containing 3
MEG3	maternally expressed gene 3
miR	miRNA
GRP78	glucose-regulated protein 78
ATF6	activating transcription factor 6
CHOP	C/EBP homologous protein
NEK10	NIMA-related kinase 10
IFN- γ	interferon γ
CCR6	chemokine (C-C motif) receptor 6
CXCR3	C-X-C chemokine receptor 3
PPAR- γ	peroxisome proliferator-activated receptor γ
2-HG	2-hydroxyglutarate
KDM5	lysine demethylase 5
H3K4me3	trimethylation of Histone H3 at Lysine 4
ROS	reactive oxygen species
ROR γ t	retinoic acid-related orphan receptor γ t
E4F1	E4 transcription factor 1

Continued

SIRT4	sirtuin 4
anti-CCP	the antibodies cyclic citrullinated peptides
ESR	erythrocyte sedimentation rate
CRP	C-reactive protein
C1QBP	component 1 q subcomponent-binding protein
Fe/S	iron-sulfur
RANKL	receptor activator of nuclear factor κ -B ligand
NADPH	nicotinamide adenine dinucleotide phosphate
CYP11A1	cytochrome P450 11A1
MRE	metal responsive element
PIGF	phosphatidylinositol glycan anchor biosynthesis class F
HIF-1	hypoxia-inducible factor-1
FOXP3	forkhead box P3
PHDs	prolyl hydroxylases
ox-LDL	oxidized low-density lipoprotein
NKR	natural killer receptors

(Continued)



OPEN ACCESS

EDITED BY
Shanshan Hu,
Anhui Medical University, China

REVIEWED BY
Pietro Di Fazio,
Philipps University of Marburg, Germany
Xu Teng,
Hebei Medical University, China

*CORRESPONDENCE
Yunfeng Wu,
wuyunfengaydl@sina.com
Zongsheng Yin,
yinzongsheng@ahmu.edu.cn

[†]These authors contributed equally to
this work

SPECIALTY SECTION
This article was submitted to
Inflammation Pharmacology,
a section of the journal
Frontiers in Pharmacology

RECEIVED 10 May 2022
ACCEPTED 15 July 2022
PUBLISHED 11 August 2022

CITATION
Qin K, Tang H, Ren Y, Yang D, Li Y,
Huang W, Wu Y and Yin Z (2022),
Melatonin promotes sirtuin 1 expression
and inhibits IRE1 α –XBP1S–CHOP to
reduce endoplasmic reticulum
stress–mediated apoptosis
in chondrocytes.
Front. Pharmacol. 13:940629.
doi: 10.3389/fphar.2022.940629

COPYRIGHT
© 2022 Qin, Tang, Ren, Yang, Li, Huang,
Wu and Yin. This is an open-access
article distributed under the terms of the
[Creative Commons Attribution License](https://creativecommons.org/licenses/by/4.0/)
(CC BY). The use, distribution or
reproduction in other forums is
permitted, provided the original
author(s) and the copyright owner(s) are
credited and that the original
publication in this journal is cited, in
accordance with accepted academic
practice. No use, distribution or
reproduction is permitted which does
not comply with these terms.

Melatonin promotes sirtuin 1 expression and inhibits IRE1 α –XBP1S–CHOP to reduce endoplasmic reticulum stress–mediated apoptosis in chondrocytes

Kunpeng Qin^{1†}, Hao Tang^{1†}, Yi Ren¹, Di Yang², Yetian Li¹,
Wei Huang³, Yunfeng Wu^{4*} and Zongsheng Yin^{1*}

¹Department of Orthopaedics, The First Affiliated Hospital of Anhui Medical University, Hefei, China, ²The Key Laboratory of Microbiology and Parasitology of Anhui Province, The Key Laboratory of Zoonoses of High Institutions in Anhui, Anhui Medical University, Hefei, China, ³Department of Orthopaedics, The First Affiliated Hospital of USTC, Division of Life Sciences and Medicine, University of Science and Technology of China, Hefei, China, ⁴Department of Orthopaedics, The First Affiliated Hospital of Anhui Medical University, Anhui China. Anhui Public Health Clinical Center, Hefei, China

Osteoarthritis (OA) is the most common chronic disease characterized by a loss of chondrocytes and the degeneration of cartilage. Inflammation plays an important role in the pathogenesis and progression of OA via the activation of the endoplasmic reticulum (ER) stress signaling pathway. In this study, we stimulated human primary chondrocytes with lipopolysaccharide (LPS) to reduce cell viability and induce chondrocyte apoptosis. LPS-stimulated human primary chondrocytes induced ER stress and significantly upregulated the ER chaperone glucose–regulated protein 78 (GRP78) and increased the expression level of C/EBP–homologous protein (CHOP), a key mediator of ER stress–induced apoptosis. Interestingly, melatonin treatment attenuated ER stress–mediated chondrocyte apoptosis. Melatonin inhibited the expression of cleaved caspase-3, cleaved caspase-10, Bax, CHOP, GRP78, cleaved caspase-4, phospho–inositol–requiring enzyme 1 α (P-IRE1 α), and spliced X-box-binding protein 1 (XBP1S). In an anterior cruciate ligament transection mouse model of OA, melatonin (50 and 150 mg/kg) dose–dependently relieved joint cartilage degeneration and inhibited of chondrocyte apoptosis. Immunohistochemical analysis indicated that melatonin could promote SIRT1 the expression and inhibit CHOP and cleaved caspase-3 expression in OA mice. In conclusion, our findings demonstrate for the first time that melatonin inhibits the IRE1 α –XBP1S–CHOP signaling pathway by promoting the expression of SIRT1 in LPS-treated human chondrocytes and delaying OA progression *in vivo*.

KEYWORDS

melatonin, osteoarthritis, endoplasmic reticulum stress, apoptosis, IRE1 α –XBP1S–CHOP

Introduction

Osteoarthritis (OA) is a common degenerative condition that affects many people worldwide. Its primary causes include obesity, aging, genetics, and trauma, and it is characterized by a loss of cartilage cells and the gradual degradation of cartilage (Li et al., 2014; Uehara et al., 2014; Chen et al., 2017; Shi et al., 2017). Chondrocytes, the only cells in articular cartilage, are primarily responsible for maintaining the dynamic balance of articular cartilage by regulating anabolism and catabolism of the extracellular matrix (Thomas et al., 2007). Persistent inflammation and apoptosis of chondrocytes are important processes involved in the development of OA (Kaczanowski, 2016; Moon et al., 2016; Robinson et al., 2016; Dai et al., 2018). Apoptosis is a process that is regulated by genes and ultimately leads to cell death (D'arcy, 2019). Currently there are three known triggers of apoptosis, the exogenous apoptosis pathway, the mitochondrial-mediated endogenous apoptosis pathway, and the endoplasmic reticulum (ER) stress (ERS)-mediated apoptosis pathway. Of these, the ERS-mediated apoptosis pathway has attracted the most attention (Kaczanowski, 2016; Moon et al., 2016).

Accumulation of misfolded proteins within the ER lumen leads to ER stress. Stressed cells then activate a downstream adaptive mechanism to alleviate the stress and restore ER homeostasis (Hetz et al., 2020). This adaptive mechanism is known as the unfolded protein response (UPR) (Tavernier et al., 2017). Mild ERS helps misfolded and unfolded proteins to fold correctly, and supports the degradation of misfolded proteins, thereby promoting cell survival and maintaining balance in the intracellular environment. If stress factors persist however, ERS will exceed the UPR threshold and cell apoptosis will be induced (Xin et al., 2014; Sepulveda et al., 2018). UPR occurs mainly through the activation of resident ER, activating transcription factor 6 (ATF6), protein kinase R (PRK)-like ER kinase (PERK), and inositol-requiring protein 1- α (IRE1- α)-sensor transmembrane proteins by activating the corresponding signaling pathways (Abdullah and Ravanani, 2018). PERK-eukaryotic initiation factor 2 α (eIF2 α)-C/EBP homologous protein (CHOP), IRE1 α -X-box-binding protein 1 (XBP1)-CHOP, and ATF6-XBP1-CHOP have been described as the three pathways key to inducing apoptosis (Komoike and Matsuoka, 2016). As the most conservative signaling pathway in the UPR, the IRE1 α -XBP1-CHOP pathway plays a significant role in ERS and is considered a promising target for drug therapy. The IRE1 α signaling pathway and its relationship with chondrocyte apoptosis have been extensively studied (Wu et al., 2018). Inhibition of apoptosis and the promotion of cartilage regeneration are both of clinical significance with respect to delaying the development of OA by directly blocking the IRE1 α pathway. To date however, no relevant *in vivo* or *in vitro* studies have been published (Huang et al., 2021). A sustained inflammatory response during OA results in chronic

ER stress (Zhang et al., 2019a); thus, in the current study lipopolysaccharide (LPS) was used to induce ERS and apoptosis to investigate OA treatment mechanisms.

Accumulation of misfolded proteins within the ER lumen leads to ER stress. Stressed cells then activate a downstream adaptive mechanism to alleviate the stress and restore ER homeostasis (Hetz et al., 2020). This adaptive mechanism is known as the unfolded protein response (UPR) (Tavernier et al., 2017). Mild ERS helps misfolded and unfolded proteins to fold correctly, and supports the degradation of misfolded proteins, thereby promoting cell survival and maintaining balance in the intracellular environment. If stress factors persist however, ERS will exceed the UPR threshold and cell apoptosis will be induced (Xin et al., 2014; Sepulveda et al., 2018). UPR occurs mainly through the activation of resident ER, activating transcription factor 6 (ATF6), protein kinase R (PRK)-like ER kinase (PERK), and inositol-requiring protein 1- α (IRE1- α)-sensor transmembrane proteins by activating the corresponding signaling pathways (Abdullah and Ravanani, 2018). PERK-eukaryotic initiation factor 2 α (eIF2 α)-C/EBP homologous protein (CHOP), IRE1 α -X-box-binding protein 1 (XBP1)-CHOP, and ATF6-XBP1-CHOP have been described as the three pathways key to inducing apoptosis (Komoike and Matsuoka, 2016). As the most conservative signaling pathway in the UPR, the IRE1 α -XBP1-CHOP pathway plays a significant role in ERS and is considered a promising target for drug therapy. The IRE1 α signaling pathway and its relationship with chondrocyte apoptosis have been extensively studied (Wu et al., 2018). Inhibition of apoptosis and the promotion of cartilage regeneration are both of clinical significance with respect to delaying the development of OA by directly blocking the IRE1 α pathway. To date however, no relevant *in vivo* or *in vitro* studies have been published (Huang et al., 2021). A sustained inflammatory response during OA results in chronic ER stress (Zhang et al., 2019a); thus, in the current study lipopolysaccharide (LPS) was used to induce ERS and apoptosis to investigate OA treatment mechanisms.

Silent information regulator 2 type 1 (SIRT1) has been implicated in several age-related conditions such as cancer, obesity, cardiovascular disease, dementia, type 2 diabetes, arthritis, osteoporosis, and OA (Morris, 2013). It is a histone deacetylase that relies on nicotinamide adenine dinucleotide, which has a protective effect in human chondrocytes and can prevent OA progression (Lim et al., 2012; Terauchi et al., 2016). It can reportedly promote cell survival while suppressing cell apoptosis by modulating multiple transcription factors, including nuclear factor- κ B, p53, forkhead box O protein, DNA repair factor Ku70, and transcription co-activator p300 (Vaziri et al., 2001; Brunet et al., 2004; Cohen et al., 2004; Yeung et al., 2004; Bouras et al., 2005). The protective role of SIRT1 in ERS-induced cells has been demonstrated in previous investigations (Feng et al., 2019; Luo et al., 2019; Hu et al., 2020). Previous studies have also shown that SIRT1 levels in

normal cartilage samples taken from elderly individuals are lower than those in samples taken from younger people, and that SIRT1 levels in samples from OA patients are lower than those in samples from healthy people. SIRT1 is a potential therapeutic option for the treatment of OA because it plays a crucial role in articular cartilage protection (Sacitharan et al., 2020). Luo et al. (Luo et al., 2019) reported that SIRT1 reduces hypoxia-induced apoptosis through the IRE1 α pathway, thereby protecting cardiomyocytes from hypoxic stress. It was recently shown that Sirt1 inhibition induces hyperacetylation and phosphorylation of eIF2 α and PERK to regulate PERK-ATF4 signaling of ER stress (Prola et al., 2017; Kang et al., 2018). Additionally, SIRT1 deacetylates PERK physically through physical interactions (Zhang et al., 2021). It has been shown that SIRT1 deacetylates XBP1s and inhibits the transcriptional activity of XBP1s to regulate UPR signaling (Wang et al., 2011). Luo and collaborators reported that reported that SIRT1 reduces hypoxia-induced apoptosis through the IRE1 α pathway, thereby protecting cardiomyocytes from hypoxic stress. (Luo et al., 2019). However, whether SIRT1 can regulate ERS and slow the progression of OA in human chondrocytes via the IRE1 α -XBP1S-CHOP pathway is unclear.

N-acetyl-5-methoxy tryptamine (melatonin) is a hormone produced by the pineal gland in mammals, including humans. It has a variety of biological functions including anti-oxidative, anti-inflammatory, and anti-apoptotic effects (Mazzon et al., 2006; García et al., 2014). It is evidently effective for the treatment of several pathological conditions including cancer, neurotoxicity, OA, and liver and metabolic diseases, but the specific mechanisms by which melatonin exerts its effects remain unclear (Pei et al., 2009; Liu et al., 2014). Many *in vivo* and *in vitro* studies have shown that melatonin inhibits ERS-mediated apoptosis in some cells (Chen Y. et al., 2016; Zhou et al., 2020; Qin et al., 2021). In a recent study melatonin prevented chronic obstructive pulmonary disease by inhibiting ERS and apoptosis via the upregulation of SIRT1 expression in mice (He et al., 2019).

However, whether melatonin inhibits ERS-induced apoptosis in human chondrocytes by activating SIRT1 protein levels remains unclear. In the current study the effects of melatonin on LPS-induced chondrocyte apoptosis were investigated, as were the potential mechanisms involved. The therapeutic effects of melatonin were also investigated in a murine model of arthritis of the knee.

Materials and methods

Patients and tissue samples

The study was approved by the Research Ethics Committee of the First Affiliated Hospital of Anhui Medical University, china written informed consent was obtained from all individuals before their operations. International Cartilage Repair Society

grade 4 human OA cartilage was obtained from the knee joints of 26 OA patients (mean age 62.73 ± 5.5 years) at the First Affiliated Hospital of Anhui Medical University. The cartilage was stored at 4°C for 2–3 h to extract primary cartilage cells.

Reagents and antibodies

Fetal bovine serum, Dulbecco's modified Eagle medium (DMEM)/F12 medium, and phosphate-buffered saline (PBS) were purchased from HyClone (Logan, UT, United States). Melatonin (73314) was purchased from Med Chem Express (Princeton, NJ, United States). LPS (ST1470), tunicamycin (TM) (SC0393), 4',6-diamidino-2-phenylindole (DAPI) (P0131), 0.25% trypsin (C0205), and EX527 were purchased from Beyotime (Shanghai, China). Primary antibodies against SIRT1 (13161-1-AP), Bax (50599-2-Ig), glucose-regulated protein 78 (GRP78) (11587-1-AP), CHOP (15204-1-AP), IRE1 α (27528-1-AP), and β -actin (15204-1-p) were purchased from Proteintech (Wuhan, Hubei), as were horseradish peroxidase (HRP)-conjugated secondary antibodies. Phospho-IRE1 α (P-IRE1 α) (ab124945), Bcl-2 antibodies (ab32124), cleaved caspase-4 (ab22687), and cleaved caspase-10 (ab11475) were purchased from Abcam (Cambridge, United Kingdom), and XBP1S (#40435) and cleaved caspase-3 (Asp175) were purchased from Cell Signaling Technology (Danvers, MA, United States). Cell-counting kit 8 (CCK-8) was purchased from Beyotime.

Chondrocyte isolation and culture identification and treatment

Primary human knee chondrocytes were isolated from OA cartilage tissue using a previously described protocol (Tardif et al., 2009). Briefly, OA cartilage tissue was collected from the proximal tibia and distal femur and washed three times with sterile PBS. The samples were then sliced into pieces measuring 1 mm³, trypsinized in sequential digestion (ethylenediaminetetraacetic acid [EDTA]-free trypsin) for 30 min, and treated with 0.2% type II collagenase dissolved in DMEM/F12 at 37°C for 10 h. Tissues and cells were then passed through a 50-ml filter to remove undigested contents, then cells were transferred into a 15-ml tube and centrifuged. Chondrocytes were then obtained via centrifugation. The supernatant was discarded and cell pellets were resuspended in a 25 cm² cell culture flask with 3 ml of DMEM containing 10% fetal bovine serum and 1% penicillin/streptomycin. Cells were cultured at 37°C in a 5% CO₂ humidified atmosphere. The culture medium was replaced every 2–3 days. After two or three passages, chondrocytes were used in assays. For LPS treatment different concentrations were added to the culture medium (0, 1, 5, 10, 20, or 50 μ g/ml), and 10 μ g/ml was ultimately chosen for further experimentation. When the cells reached 70–80% confluence the medium was replaced, and the cells were divided into different treatment groups. Melatonin was

dissolved in absolute ethyl alcohol to obtain an initial stock concentration of 250 mM, which was then diluted with basic medium to create stocks of 5, 10, 50, and 100 μ M for use. There were no concerns of potential absolute ethyl alcohol-mediated toxicity. Chondrocyte identification was performed via Alcian blue staining as previously described (Schofield et al., 1975). In short, chondrocytes were fixed with 4% paraformaldehyde for 20 min, followed by staining with 0.5% Alcian blue for 30 min. They were then washed with distilled water, and assessed via microscopy (LEICA, Wetzlar, Germany).

Cell viability assay

The viability of articular chondrocytes was assessed using the CCK-8. Chondrocytes were seeded at 5×10^4 cells per well in a 96-well plate well overnight. A drug-inoculation assay was performed when the cells reached 60–70% confluence. Chondrocytes were treated with increasing concentrations of melatonin (0, 5, 10, 50, and 100 μ M) or LPS (10 μ g/ml) for 24 h, then 100 μ l of CCK-8 solution (10 μ L CCK-8 + 90 μ l basal medium) was added to each well followed by incubation at 37°C in the dark for 2 h. Lastly, the absorbance of each sample was determined via a Thermomax microplate reader (Bio-Tek Instruments, Winooski, VT, United States) at a wavelength of 450 nm. Each sample was plated in triplicate, and data are representative of three independent experiments.

Flow cytometry

Briefly, chondrocytes in 6-well plates were exposed to LPS, TM (1 μ M), a classic ERS inducer, or melatonin + LPS for 24 h. Each group was prepared separately. At the end of the experiment chondrocytes were digested with EDTA-free trypsin and centrifuged to obtain cell pellets. The cell pellets were gently resuspended in 500 μ l of 1 \times annexin V binding buffer (Beyotime), then stained with annexin V-fluorescein isothiocyanate and propidium iodide for 10 min at room temperature in the dark. The stained chondrocytes were assessed via flow cytometry (BD, Franklin Lakes, NJ, United States), and the rate of apoptosis was expressed as the percentage of cells with annexin V-fluorescein isothiocyanate positivity and propidium iodide positivity/negativity. Each sample was assessed in triplicate, and data are representative of three independent experiments.

Quantitative real-time polymerase chain reaction

Total RNA was obtained from chondrocytes using TRIzol (Invitrogen, Carlsbad, CA, United States), then 1 μ g of RNA was reverse-transcribed into complementary DNA using a specific

reverse-transcription kit (Accurate Biotechnology, Changsha, China) in accordance with the manufacturer's instructions. qPCR Master Mix (Accurate Biotechnology) was then used to perform quantitative real-time polymerase chain reaction (qRT-PCR) assays using corresponding primers. Gene expression levels were normalized to glyceraldehyde 3-phosphate dehydrogenase (GAPDH) levels, and data were quantified via the $-\Delta\Delta C_t$ method. Each sample was assessed in triplicate, and data are representative of three independent experiments. The primer sequences used are shown in Table 1.

Western blot assay

Melatonin-pretreated chondrocytes were incubated with LPS in a 6-well plate. After 24 h chondrocytes were washed with cold PBS and lysed in RIPA lysis buffer containing a protease inhibitor mixture and a phosphatase inhibitor cocktail (Roche Diagnostics, Basel, Switzerland) for 30 min to extract total intracellular proteins. A BCA protein assay kit (Beyotime) was used to measure total protein concentrations. Equal concentrations of total protein were separated on 10% SDS-PAGE gels and transferred to polyvinylidene difluoride membranes (Millipore, Burlington, MA, United States), which were activated by methyl alcohol and incubated overnight at 4°C with primary antibodies against Bcl-2 (1:1,000), cleaved caspase-3 (1:500), Bax (1:2000), SIRT1 (1:500), CHOP (1:500), GRP78 (1:1,000), XBP1S (1:500), IRE1 α (1:2000), and P-IRE1 α (1:1,000). The membranes were then washed for 10 min three times with tris-buffered saline containing 0.1% Tween-20, then incubated with HRP-conjugated secondary antibody for 1 h at room temperature. Images of blots were obtained via the Chemo Dox XRS system (Bio-Rad Laboratories, Hercules, CA, United States). ImageJ version 6.0 (U.S. National Institutes of Health, Bethesda, MD, United States) was used to calculate the optical density of each band. Each sample was assessed in triplicate, and data are representative of three independent experiments.

Immunofluorescence assays

Chondrocytes were seeded on a slide in a 6-well plate (1×10^6 cells/well) and fixed with freshly prepared 4% paraformaldehyde for 15 min. The cells were then treated with 0.5% (v/v) Triton X-100 for 10 min after being washed three times with PBS and blocked with 5% (w/v) bovine serum albumin for 1 h at room temperature. They were then incubated with primary antibodies against cleaved caspase-3 (1:200), SIRT1 (1:200), CHOP (1:200), and XBP1S (1:500) overnight at 4°C, followed by incubation with fluorescent secondary antibodies (1:300) (Thermo Fisher Scientific, Waltham, MA, United States) in a dark room. DAPI (Beyotime) was subsequently added for 2 min. An inverted fluorescence microscope (LEICA) was used to

TABLE 1 Primer sequences of target genes.

Gene	Forward primer (5–3')	Reverse primer (5–3')
GRP78	AGGGCAACCGCATCACG	ATCGCCAATCAGACG
CHOP	GAACAGTGGGCATCACCTC	CAGTCCCTCCTCAGCAT
XPB1S	AGCAGCAAGTGGTGGATT	CTCTGGAACCTCGTCA
BCL2	ACGGTGGTGGAGGAATCTTCAG	GGTGTGCAGATGCCGGTTCAG
SIRT1	GACGACGAGGGCGAGGAG	ACAGGAGGTTGTCTCGGTAGC
COLII	ACGCTCAAGTCGCTGAACAACC	ATCCAGTAGTCTCCGCTCTTCCAC
GAPDH	TGGCCTTCCGTGTTCTCTAC	GAGTTGCTGTTGAAGTCGCA

examine and photograph the samples. Each sample was assessed in triplicate, and data are representative of three independent experiments.

Transmission electron microscopy

Human chondrocytes were cultured in 25 cm² culture flasks. We washed them with PBS and collected cells with 0.05% trypsin-free EDTA treatment. The cell aggregates were fixed with 2.5% glutaraldehyde, and the samples were dehydrated by a series of incubations in 50, 70, 90, and 100% ethanol, then dehydrated with 100% acetone and embedded in epoxy resin. An ultramicrotome was used to cut the fixed cell aggregates into ultrathin sections, stained them, and inspected their ultrastructure using a transmission electron microscope (Talos L120C G2; Thermo Fisher Scientific, Waltham, MA, United States).

Mouse OA model

All mouse experiments were approved by the Ethics Committee for Animal Research, Anhui Medical University, Anhui, China. Forty 10–12 week-old male C57/BL mice weighing 25–30 g were provided by the Laboratory Animal Center of Anhui Medical University (He Fei, China). OA was induced in the mice via anterior cruciate ligament (ACL) transection (ACLT) of the right knee. Arthrotomy without transection of the ACL in the right knee joint was also performed in 10 C57/BL mice, which were used as a control group. The mice were randomly divided into four groups: a sham group, an ACLT group, an ACLT + low-dose melatonin treatment group, and an ACLT + high-dose melatonin treatment group. After the ACLT surgery, melatonin was injected intraperitoneally once a day for 8 weeks. Briefly, anesthesia was induced via intraperitoneal injection of 50 mg/L chloral hydrate, hair was shaved at the operation site, and the left posterior region was fixed in the supine position. The knee joint was exposed after a medial capsular

incision and gentle lateral displacement of the extensor mechanism without transection of the patellar ligament, the ACL was transected, and the joints were flushed with sterile saline prior to closure of the joint capsule. The articular cavity was then sutured with 7–0 surgical sutures, and the skin wound was closed. Topical amoxicillin was applied to prevent wound infection. Anesthesia recovery and wound healing were monitored.

Intraperitoneal injection of melatonin

Melatonin (100 mg) was dissolved in 1 ml of absolute ethanol then diluted to a final concentration of 10 mg/ml in normal saline. Mice were intraperitoneally injected with either low-dose melatonin (50 mg/kg) or high-dose melatonin (150 mg/kg) once a day for 8 weeks (Zhang et al., 2019b). They were then euthanized, and knee joint samples were collected.

Micro-computed tomography

Knee joints were evaluated via micro-computed tomography (CT) (Sky Scan 1,176; Bruker, Billerica, MA, United States), conducted for 120 min at 800 μ A and 50 kV with a resolution of 12 μ m. Micro-CT data were analyzed by CTAn (SkyScan, United States) and mimics medical 21 (Materialise, Belgium). The 3D structural parameters analyzed included the BMD and region of interest of the subchondral region of the tibial plateau, selected for analysis with the following morphological parameters: 1) Bone volume/total tissue volume (BV/TV) (%); 2) trabecular thickness (Tb.Th) (mm); 3) trabecular number (Tb.N) (1/mm); 4) trabecular separation (Tb.Sp) (mm); and 5) trabecular mesh factor (Tb.Pf) (1/mm).

Histology

Mice were killed 8 weeks after the surgery. Knee joints were dissected, fixed in 4% paraformaldehyde for 24 h, decalcified in

10% EDTA for 2–3 weeks, paraffin-embedded, sectioned coronally at a thickness of 5 μ m, stained with safranin O and fast-green, then stained with hematoxylin-eosin in accordance with the manufacturer's instructions. OA severity was determined using the Osteoarthritis Research Society International (OARSI) scoring system (Glasson et al., 2010).

Immunohistochemical analysis

Expression levels of CHOP, cleaved caspase-3, and SIRT1 were detected via immunohistochemical staining. Cartilage tissue was fixed with paraformaldehyde, embedded in paraffin, then cut into 5-mm-thick sections. The sections were then deparaffinized, treated with 3% hydrogen peroxide for 15 min, sealed with 5% normal serum, and blocked for 30 min. After incubation with primary antibodies against CHOP (1:300), cleaved caspase-3 (1:400), and SIRT1 (1:300) the sections were incubated with the secondary antibody. Images of the sections in each group were acquired via light microscopy. ImageJ version 6.0 was used to analyze each image. Levels of CHOP, cleaved caspase-3, and SIRT1 were determined via integral absorbance values.

Statistical analysis

All data are representative of three independent experiments. All results are presented as mean \pm standard deviation. All statistical analysis was performed using the unpaired Student's *t*-test for two groups, or one-way analysis of variance for more than two groups, via GraphPad Prism version 9 (GraphPad Software, San Diego, CA, United States). $P < 0.05$ was considered statistically significant.

Results

Effects of melatonin on human primary chondrocyte viability with or without LPS

CCK-8 assay was used to assess the effects of melatonin on chondrocyte viability at different time periods (24, 48, and 72 h) following treatment with or without LPS at different concentrations. An LPS concentration of 10 μ g/ml obviously reduced chondrocyte viability (Figure 1B). Treatment with melatonin at a concentration of ≤ 100 μ M had no cytotoxic effect on chondrocytes (Figure 1C), and 10–100 μ M of melatonin markedly alleviated LPS-induced cytotoxicity in a concentration-dependent manner (Figure 1D). Previous studies showed that a dose range of 10 nM–100 μ M is ideal for studying the effects of melatonin (Liu et al., 2011; Quan et al., 2015; Xiong et al., 2015). Therefore, a dose of 10 μ M

melatonin was used as the therapeutic concentration. In addition, OA is a chronic degenerative joint disease characterized by persistent aseptic inflammation. Hence a relatively moderate amount of LPS (10 μ g/ml) was used to stimulate human primary chondrocytes for 24 h to mimic aseptic inflammation in OA *in vitro*. Therefore 10 μ M of melatonin and 10 μ g/ml of LPS were used in the subsequent experiments.

Melatonin protected human primary chondrocytes from LPS-induced apoptosis

To investigate the effects of melatonin on LPS-induced apoptosis in chondrocytes, we treated chondrocytes with 10 μ g/ml of LPS with or without melatonin. First, primary human chondrocytes were pretreated with 10 μ g/ml LPS for 2 h, and then with or without 10 μ M melatonin for 24 h. Western blotting showed that melatonin suppressed pro-apoptotic proteins (cleaved caspase-3, cleaved caspase-10, Bax) and promoted a greater level of anti-apoptotic protein (bcl-2) compared to that in the LPS group (Figures 2A,B). The results revealed that the apoptosis of chondrocytes induced by LPS was significantly reduced after melatonin treatment. qRT-PCR results showed that melatonin-treated chondrocytes markedly elevated the expression levels of COLII and Bcl-2 compared to LPS-treated chondrocytes (Figure 2C), Flow cytometry and fluorescence analysis were used to assess the degree of apoptosis of chondrocytes (Figures 2D,E), and the results showed that LPS stimulation caused a significant increase in the apoptosis of human primary chondrocytes; however, the effect of LPS on apoptosis was significantly inhibited by melatonin. In addition, immunofluorescence staining for cleaved caspase-3 was consistent with the western blot results (Figures 2F,G). Therefore, the findings indicated that melatonin could inhibit LPS-induced chondrocyte apoptosis.

Melatonin inhibits ERS in human chondrocytes induced by LPS

First, we evaluated whether the anti-apoptotic effect of melatonin inhibited ERS. The ERS-related biomarkers GRP78, CHOP and cleaved caspase-4 were analyzed by western blotting (Figures 3A,B). The messenger RNA expression levels of GRP78 and CHOP were analyzed by qRT-PCR (Figure 3C). The results showed that CHOP, GRP78 and cleaved caspase-4 were significantly increased in LPS-stimulated human primary chondrocytes. Moreover, treatment with melatonin could reverse the upregulation of

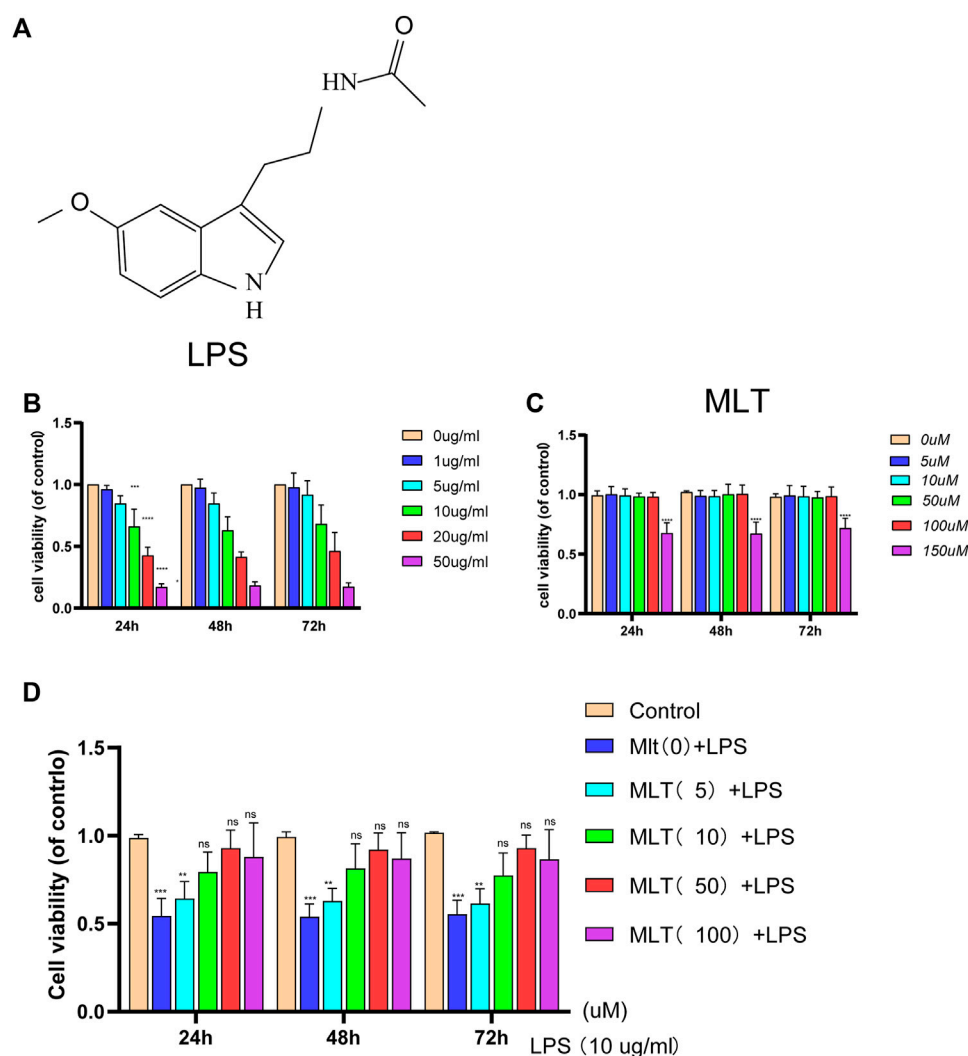


FIGURE 1

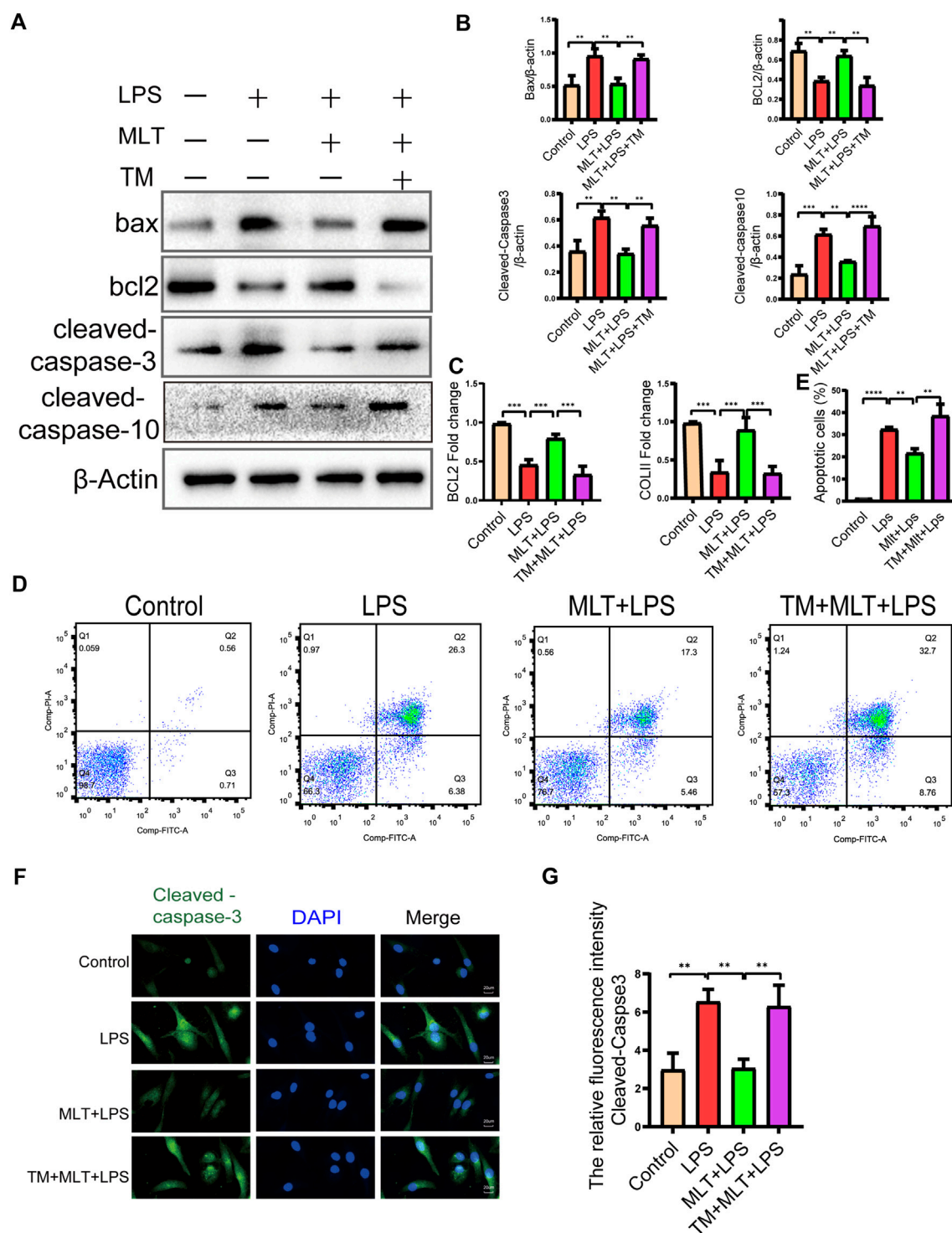
The effect of melatonin on the viability of human chondrocytes with or without lipopolysaccharide (LPS). **(A)** The chemical structure of melatonin. **(B,C)** The cytotoxicity effects of LPS and melatonin on human chondrocytes at different concentrations were tested at 24, 48, and 72 h using a cell-counting kit 8. **(D)** The viability of human chondrocytes treated with LPS (10 µg/ml) after different concentrations melatonin treatment. The experiment was repeated three times independently. All values are shown as mean \pm standard deviation. ** $p < 0.01$, *** $p < 0.001$, **** $p < 0.0001$. ns: not significant. Abbreviations: LPS, lipopolysaccharide; ns, not significant; MLT, melatonin.

ERS induced by LPS. Melatonin added to the human primary chondrocytes without LPS did not change the levels of CHOP, GRP78 and cleaved caspase-4 compared to those in the control group, indicating that Melatonin alone did not influence ER state of chondrocyte (figures no showed). The immunofluorescence staining for CHOP were consistent with the western blot and qRT-PCR results (Figures 3D,E). The results of transmission electron microscopy showed that the ER of the human chondrocytes treated with LPS was in an expanded state, and the expansion of the ER was reduced following treatment with melatonin (Figure 3F). ERS markers

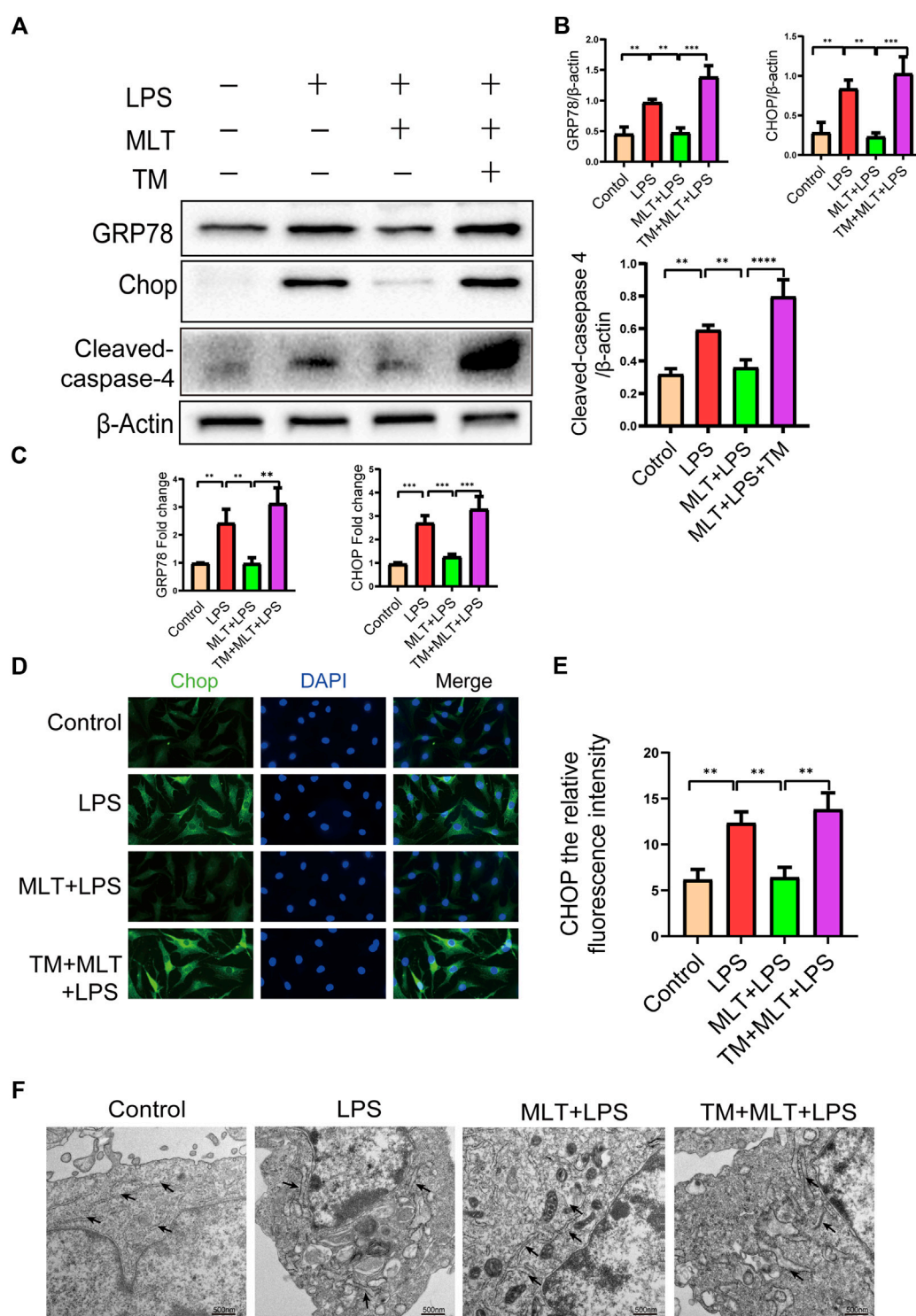
were also detected in human chondrocytes treated with TM, and TM attenuated the downregulation of ERS by melatonin.

Melatonin attenuates LPS-Induced apoptosis of human primary chondrocytes by inhibiting ERS

To further explore whether melatonin inhibited ERS in human primary chondrocytes treated with LPS, we used TM, to activate ERS in human primary chondrocytes. Western blot results (Figures

**FIGURE 2**

Melatonin inhibited apoptosis in human chondrocytes stimulated by lipopolysaccharide (LPS). **(A,B)** We detected the protein levels of Bcl-2, Bax, cleaved caspase-10 and cleaved caspase-3 in each group. **(C)** mRNA expression levels of collagen II and Bcl-2 in each group were measured using qRT-PCR **(D–E)** Apoptosis of human chondrocytes were determined by flow cytometry following annexin V-PE and propidium iodide staining. **(F,G)** Quantification of the intensity of cleaved caspase-3 in human chondrocytes in each group was performed with immunofluorescence staining. The experiment was repeated three times independently. All values are shown as mean \pm standard deviation. $^{**}p < 0.01$, $^{***}p < 0.001$, $^{****}p < 0.0001$. **Abbreviations:** DAPI, 4',6-diamidino-2-phenylindole; ns, not significant; PI, propidium iodide; LPS, lipopolysaccharide; MLT, melatonin; TM, tunicamycin.

**FIGURE 3**

Melatonin inhibited inflammation-induced endoplasmic reticulum stress in human chondrocytes. **(A,B)** Western blot analysis Protein expression levels of GRP78, CHOP and cleaved caspas-4 were determined by western blotting. **(C)** The messenger RNA expression levels of glucose-regulated protein 78 (GRP78) and C/EBP homologous protein (CHOP) were checked by real-time polymerase chain reaction analysis in each group. **(D,E)** CHOP immunofluorescence staining. Obvious increasingly bright green spots indicate elevated CHOP expression (bar, 20 μ m). **(F)** The effect of altered endoplasmic reticulum morphology after treatment was observed with transmission electron microscopy (bar, 500 nm) (black arrows refer to the endoplasmic reticulum). The experiment was repeated three times independently. All values are shown as mean \pm standard deviation. ** p < 0.01, *** p < 0.001, **** p < 0.0001. Abbreviations: LPS, lipopolysaccharide; ns, not significant; MLT, melatonin; TM, tunicamycin.

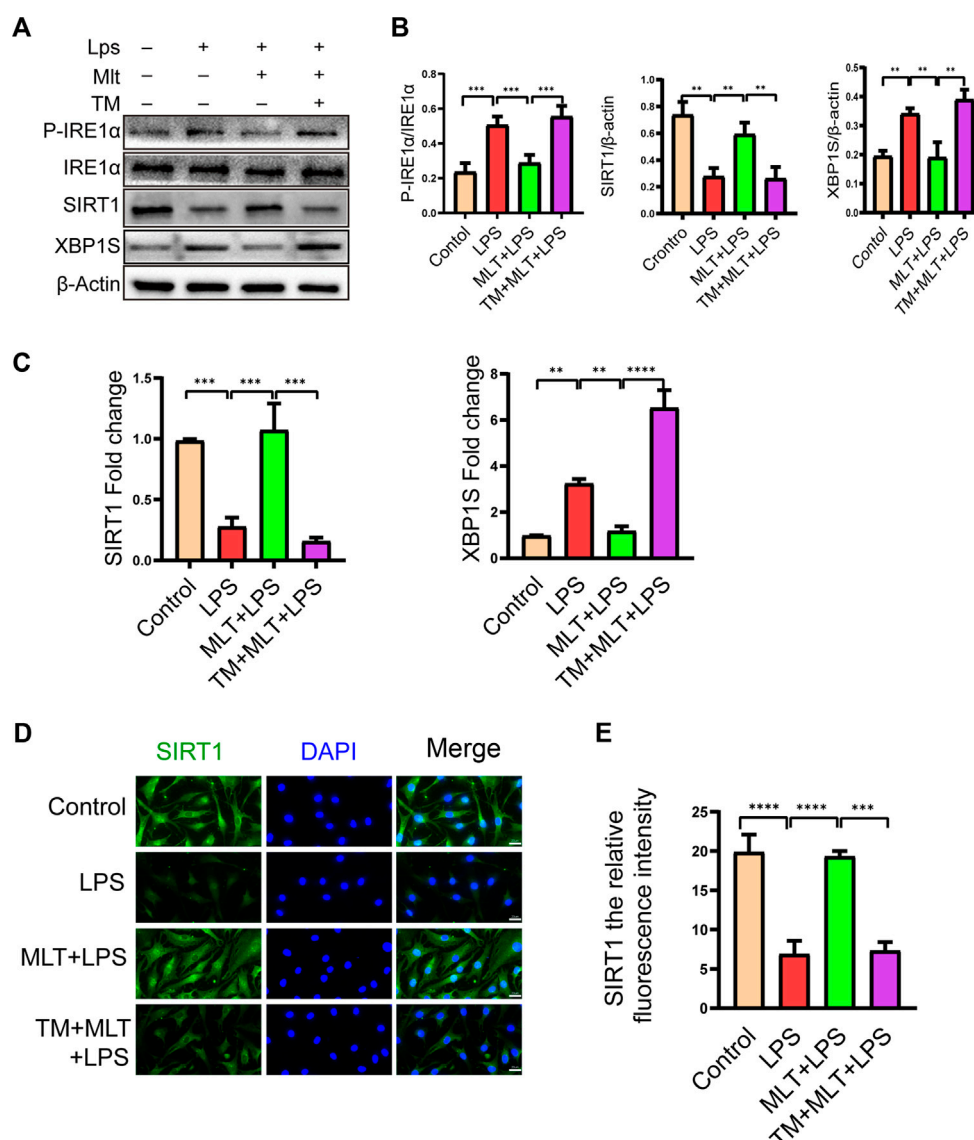


FIGURE 4

Melatonin upregulated the expression of sirtuin 1 (SIRT1) and attenuated the activation of the inositol-requiring enzyme 1α-X-box-binding protein 1 (IRE1α-XBP1S) pathway. (A,B) The protein expression levels of SIRT1 and P-IRE1α, P-IRE1α and XBP1S proteins were determined by western blot analysis. (C) We evaluated the messenger RNA expression level of SIRT1 and XBP1S by real-time polymerase chain reaction analysis. (D,E) SIRT1 immunofluorescence staining and quantification of the number of SIRT1-positive human chondrocytes in different groups. The experiment was repeated three times independently. Significantly increased green spots indicate that SIRT1 protein expression is upregulated (bar, 20 μm). All values are shown as the mean ± standard deviation. ***p* < 0.01, ****p* < 0.001, *****p* < 0.0001. Abbreviation: ns, not significant.

3A,B) and qRT-PCR (Figure 3C) showed that the expression levels of CHOP, GRP78 and cleaved caspase-4 in human primary chondrocytes treated with TM were significantly increased compared to those in the melatonin + LPS group. In addition, the fluorescence staining of CHOP showed that TM increased the expression of ERS (Figures 3D,E). Transmission electron microscopy revealed the inhibitory effect of melatonin on ERS, while TM reverses the protective effect of melatonin on ERS (Figure 3F). We confirmed that melatonin protects chondrocytes

from inflammation-induced apoptosis. To verify whether melatonin inhibited LPS-Induced chondrocyte apoptosis by inhibiting the ERS of human primary chondrocytes, we activated ERS using TM and measured the expression levels of pro-apoptotic biomarker, including cleaved caspase-3, cleaved caspase-10 and Bax and anti-apoptotic biomarkers: Bcl-2, (Figures 2A,B). Flow cytometry (Figures 2D,E) and immunofluorescence assays (Figures 2F,G) were also used to detect the level of apoptosis of human primary chondrocytes treated with TM. In summary, these

results revealed that TM can reduce the anti-apoptotic activity of melatonin and melatonin attenuates apoptosis by inhibiting ER stress.

Melatonin enhanced SIRT1 expression and inhibited the IRE1 α -XBP1S-CHOP pathway in LPS-Treated human primary chondrocytes

According to our results, melatonin increased the expression of SIRT1 and inhibited the IRE1 α -XBP1S-CHOP pathway in chondrocytes treated with LPS. Previous research has shown that the expression of SIRT1 in OA chondrocytes is significantly lower than that in normal cells (Sacitharan et al., 2020). Therefore, we measured the expression levels of SIRT1 and IRE1 α -XBP1S-CHOP pathway-associated proteins. As shown in Figure 4, LPS reduced SIRT1 expression in human primary chondrocytes, and melatonin treatment eliminated the inducing effect of LPS. We also observed that the SIRT1 protein expression level in chondrocytes treated with melatonin alone did not change compared to that in the control group. In addition, our results revealed that melatonin attenuated p-IRE1 α and XBP1S protein levels in LPS-stimulated human primary chondrocytes (Figures 4A,B). The results of qRT-PCR (Figure 4C) and SIRT1 immunofluorescence staining (Figures 4D,E) were consistent with the western blotting. Immunofluorescence results showed that SIRT1 can co-localize with IRE1 α (Supplementary Figure S1), which provides a basis for the study of the interrelationship between SIRT1 and IRE1.

Melatonin inhibits ERS-Related human primary chondrocyte apoptosis by promoting SIRT1 activation and inhibiting the IRE1 α -XBP1S-CHOP signaling pathway in chondrocytes

To assess the roles of SIRT1 and IRE1 α -XBP1S activation in ERS-Induced chondrocyte apoptosis, cells were treated with TM to activate ER stress. Our results revealed that TM downregulated SIRT1 expression and upregulated P-IRE1 α and XBP1S expression (Figures 4A,B). In addition, we used EX527, a known SIRT1 inhibitor, to treat human chondrocytes. Our results showed that the protein levels of GRP78, CHOP and cleaved caspase-4 were elevated in the EX527 (10 μ M) + melatonin + LPS group (Figures 5A,B). CHOP immunofluorescence result was similar to the western blot results (Figures 5C,D). In addition, transmission electron microscopy observed the extent of ER expansion of chondrocytes, and melatonin inhibited ERS (Figure 5E). These results demonstrated that inhibition of SIRT1 and activation of IRE1 α are related to chondrocyte apoptosis induced by ERS.

Melatonin inhibits the ERS of human primary chondrocytes induced by LPS by promoting SIRT1 expression and inhibiting the IRE1 α -XBP1S-CHOP signaling axis

Melatonin inhibited LPS-induced apoptosis in human primary chondrocytes by promoting SIRT1 expression while suppressing the IRE1 α -XBP1S-CHOP pathway. However, the interaction between SIRT1 and the IRE1 α -XBP1S-CHOP pathway remains uncharacterized. To further investigate the connections between SIRT1 and IRE1 α -XBP1S-CHOP, EX527 was used to downregulate SIRT1 expression in human primary chondrocytes. EX527 treatment reduced the levels of SIRT1 protein. P-IRE1 α , XBP1S, and CHOP protein levels were reduced by melatonin, and P-IRE1 α and XBP1S protein levels in chondrocytes treated with LPS were increased (Figures 6A,B). SIRT1 and XBP1S immunofluorescence results were consistent with the western blotting (Figures 6C-F). Collectively the data indicate that SIRT1 inhibits ERS in human primary chondrocytes by inhibiting the IRE1 α -XBP1S-CHOP pathway.

Melatonin attenuates mouse chondrocyte apoptosis, inhibits ERS, and delays OA progression in a mouse model

Changes in bone mineral density and bone morphology were observed via micro-CT. The subchondral region of the tibia was used as the region of interest to determine the percentage of bone, bone volume/total tissue volume (BV/TV), trabecular number (Tb.N), trabecular thickness (Tb.Th), trabecular pattern factor (Tb.Pf), and trabecular separation (Tb.Sp). In the treatment groups BMD, BV/TV, Tb.N, and Tb.Th were increased compared with the OA group, whereas Tb. Sp and Tb. Pf were decreased. These results indicated that melatonin attenuated OA in a dose-dependent manner (Figures 7A,B). Melatonin reversed this situation in a concentration-dependent manner. Hematoxylin and eosin staining and safranin O of tissue from the knee joints of sham group mice revealed that the articular cartilage was smooth and red (Figure 8A). In the OA group severe damage, erosion, and destruction of articular cartilage were evident, but melatonin attenuated the apoptosis of chondrocytes and slowed the progression of OA in OA mice in a concentration-dependent manner. OARSI scores were highly consistent with the histology results (Figure 8C). OARSI scores in the OA group were markedly greater than those in the sham group, but melatonin reduced the OARSI scores in the OA group in a concentration-dependent manner. Immunohistochemical staining of mouse cartilage showed that melatonin attenuated the expression levels of cleaved caspase-3 and

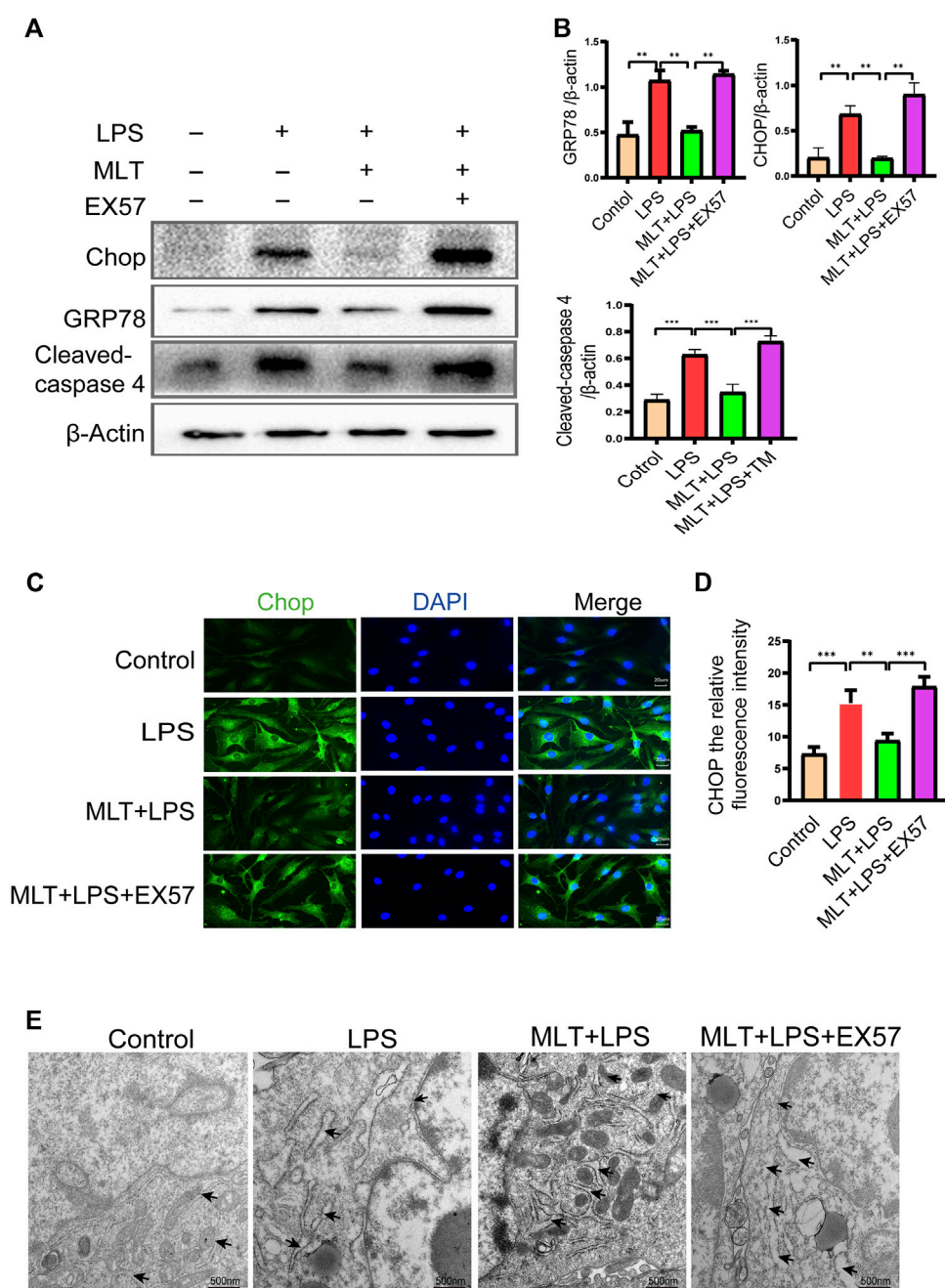


FIGURE 5

EX527 attenuated the inhibitory effect of melatonin on the endoplasmic reticulum stress of human chondrocytes induced by inflammation. (A,B) Expression levels of GRP78, C/EBP homologous protein (CHOP) and cleaved caspase-4 was determined by western blotting. (C,D) A representative CHOP level was detected by immunofluorescence staining to the endoplasmic reticulum. ImageJ was used to detect the fluorescence intensity of CHOP (bar, 20 μ m). (E) The effect of altered endoplasmic reticulum morphology was observed with transmission electron microscopy (bar, 500 nm (black arrows refer to the endoplasmic reticulum); TM, tunicamycin; EX527, a classic sirtuin 1 inhibitor. The experiment was repeated three times independently. All values are shown as mean \pm standard deviation. * p < 0.05, ** p < 0.01, *** p < 0.001, **** p < 0.0001. Abbreviations: MLT, melatonin; ns, not significant.

CHOP in OA cartilage, and increased SIRT1 expression compared to the OA group, and these results were similar to those of the *in vitro* studies (Figures 8B,D). Collectively

these results indicate that melatonin inhibited ERS and had obvious anti-apoptotic effects in the *in vitro* and *in vivo* experiments.

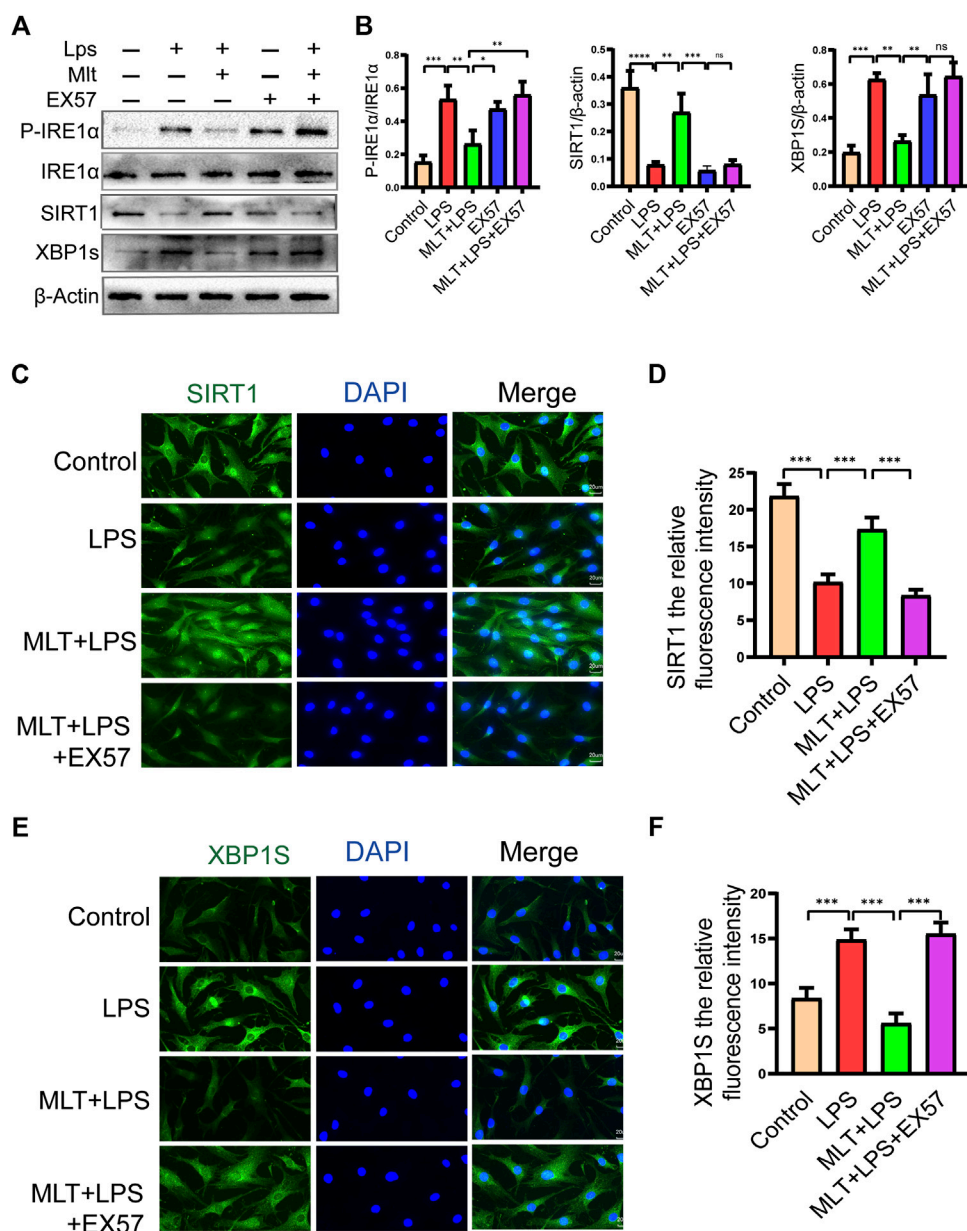


FIGURE 6

EX527 eliminated the protective effect of melatonin on human chondrocytes stimulated by lipopolysaccharide by inhibiting the inositol-requiring enzyme 1α-X-box-binding protein 1s (IRE1α-XBP1S) pathway. (A,B) Western blot analysis was performed to detect the protein expression level of SIRT1 and P-IRE1α, IRE1α and XBP1S after EX527 treatment. (C–F) Immunofluorescence staining of sirtuin 1 (SIRT1) and XBP1S (bar, 20 μm). ImageJ was used to detect the fluorescence intensity of SIRT1 and XBP1S. The experiment was repeated three times independently. All values are shown as the mean ± standard deviation. * $p < 0.05$, ** $p < 0.01$, *** $p < 0.001$, **** $p < 0.0001$. Abbreviations: LPS: lipopolysaccharide; MLT, melatonin; ns, not significant; TM, tunicamycin; EX527, a classic SIRT1 inhibitor.

Discussion

OA is a multifactorial disease (Koyama et al., 2014). Despite numerous recent studies the pathogenesis of OA is not fully understood. Increasing evidence indicates that the onset of OA is related to the death of chondrocytes (Thomas

et al., 2007; Ryu et al., 2012), and apoptosis of chondrocytes plays a crucial role in the onset and progression of OA (Dai et al., 2018; Park et al., 2020). The occurrence and development of OA are due to the loss of cartilage cells, resulting in the degradation of cartilage and thickening of subchondral bone. Mild inflammation and ERS are adaptive

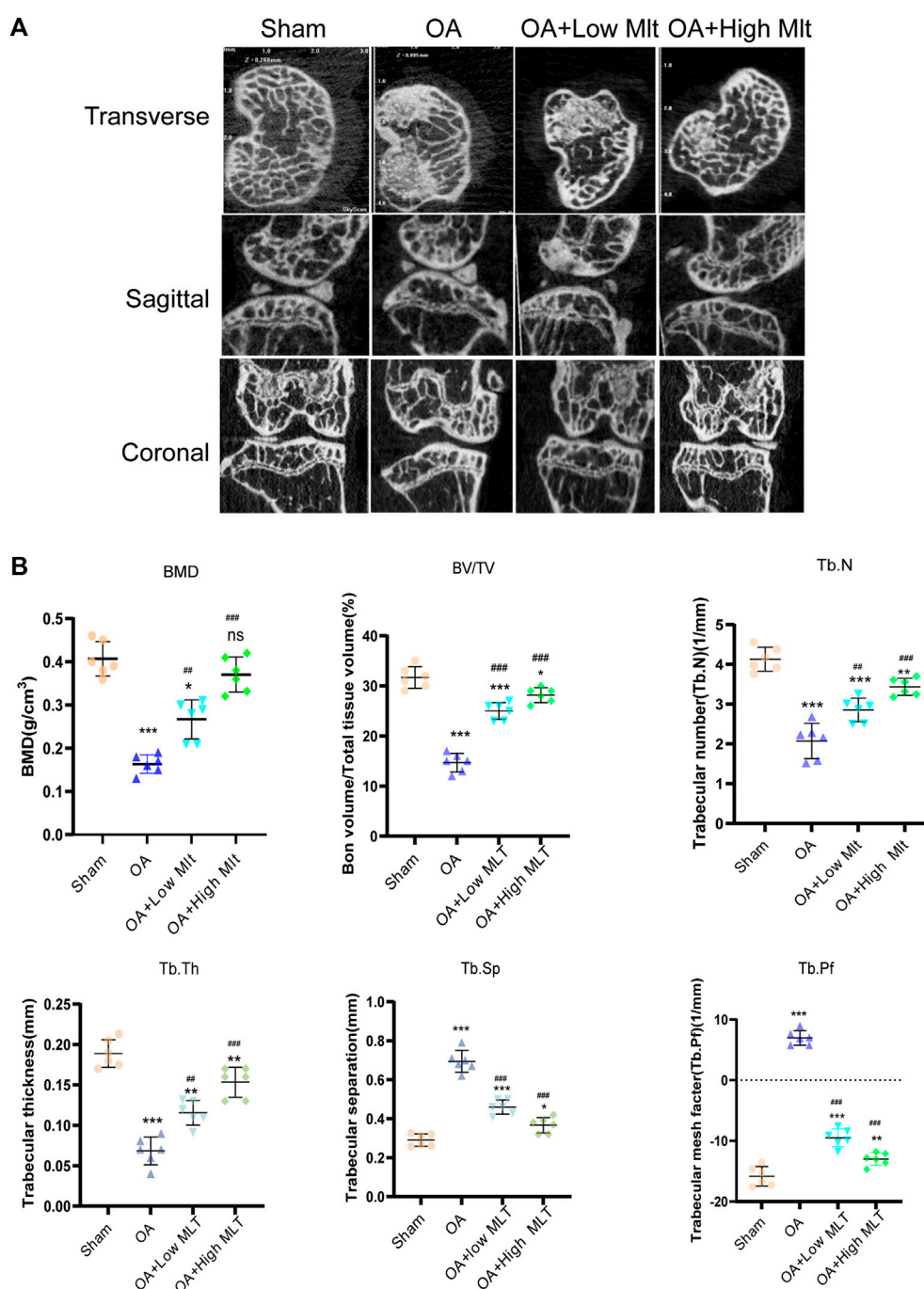


FIGURE 7

Preventive effect of melatonin on OA development in mice. (A,B) Analysis of bone destruction and knee joint bone histomorphometric parameters using micro-CT data. Data were shown as mean \pm standard deviation and analyzed using one-way ANOVA (each group $n = 6$). * $p < 0.05$, ** $p < 0.01$, *** $p < 0.001$, ns: not significant versus the normal group, # $p < 0.05$, ## $p < 0.01$, ### $p < 0.001$, #### $p < 0.0001$, ns: not significant versus the OA group.

self-protection mechanisms of chondrocytes. Under prolonged or severe ERS conditions however, the dynamic balance of the ER cannot be restored, and the excessive

activation of the UPR cannot be ameliorated (Xin et al., 2014). During unremitting ER stress chondrocytes activate the UPR, ultimately leading to apoptosis of cells (Tabas and

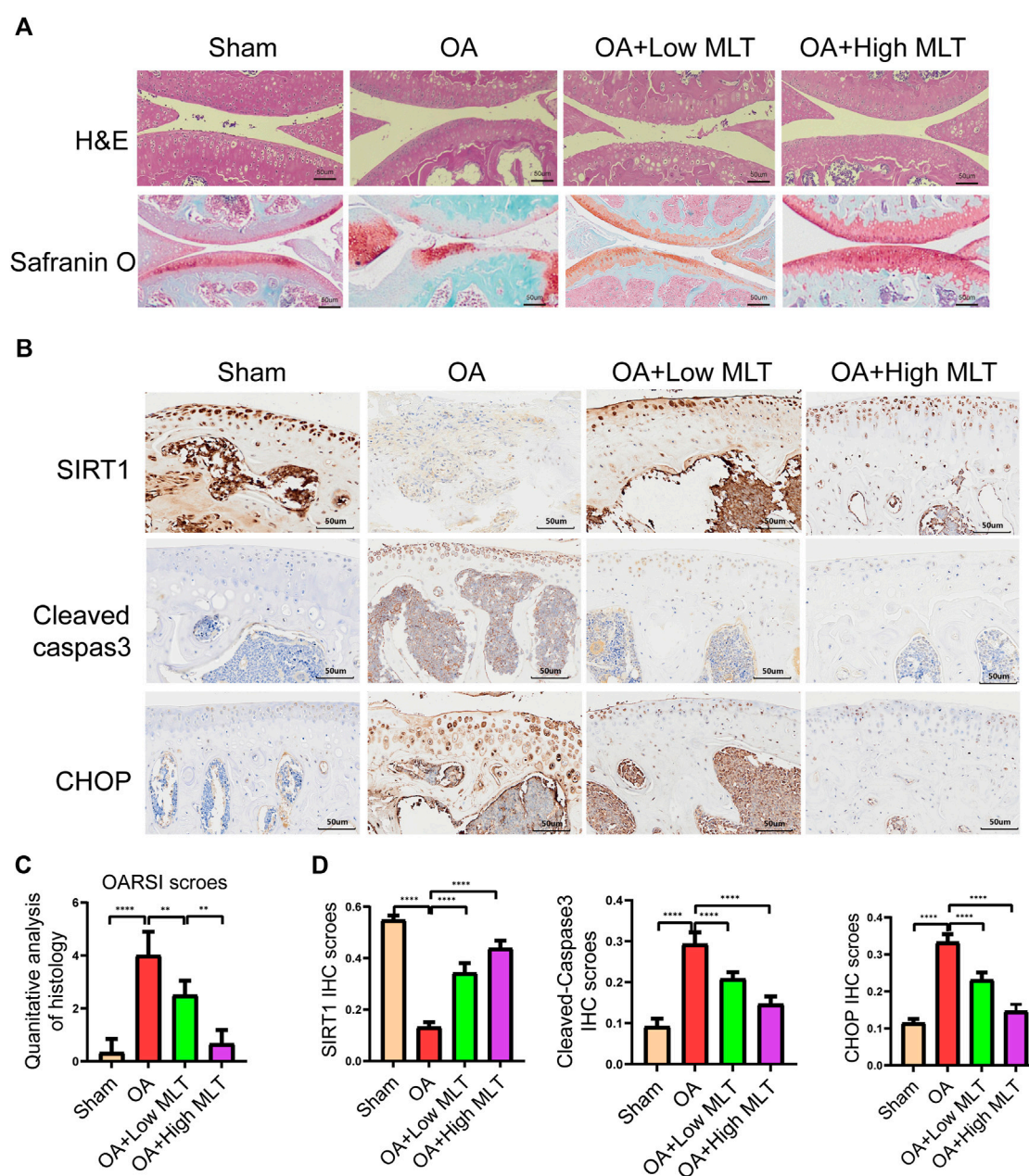


FIGURE 8

Melatonin inhibited apoptosis of chondrocytes and endoplasmic reticulum stress in the mouse ACLT model. (A) Hematoxylin and eosin staining safranin O staining and (bar, 50 μ m) were performed to complete histological analysis and microscopic observation of cartilage destruction in each group at 8 weeks after surgery. The pathological manifestations of osteoarthritis were cartilage destruction and defects. (B,D) Immunohistochemical staining and quantification of immunohistochemical staining of cleaved caspase-3, chop, and sirtuin1 expression in each group (bar, 50 μ m). (C) The scores for the four groups of articular cartilage were based on the International Association for Osteoarthritis Research system, as shown in the figure. All values are shown as the mean \pm standard deviation (each group $n = 6$). * $p < 0.05$ ** $p < 0.01$, *** $p < 0.001$ **** $p < 0.0001$, ns: not significant versus the normal group. Abbreviations; IHC, immunohistochemical; high melatonin, 150 mg/ml; low melatonin, 50 mg/ml.

Ron, 2011). Recent studies have shown that continuous inflammatory stimulation can lead to ERS (Zhang et al., 2019a), and the occurrence of ERS can initiate apoptotic signals through the IRE1 α signaling pathway.

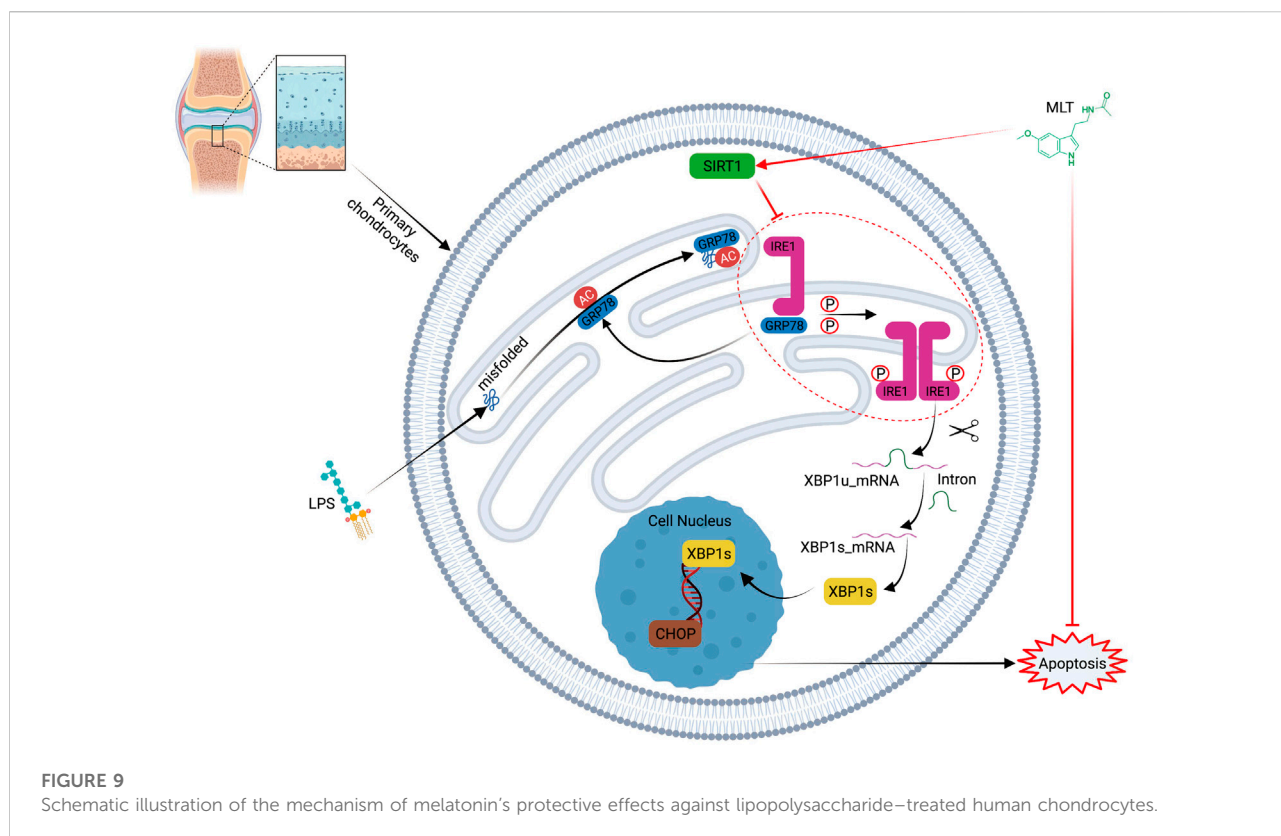
IRE1 α is an ER transmembrane protein that plays a key role in regulating the UPR clock after ER stress activation. UPRs caused by long-term chronic inflammation can cause IRE1 α to be phosphorylated, causing the splicing of XBP1, which results in

the activation of downstream pro-apoptotic proteins including CHOP (Uehara et al., 2014). Notably IRE1 α is involved in cell differentiation and extracellular matrix formation in chondrocytes, and regulates the expression of chondrocyte survival proteins including Bcl-2 and XBP1S (Han et al., 2013; Wu et al., 2018). In the current study the apoptosis biomarkers cleaved caspase-3 and Bax were upregulated in LPS-stimulated chondrocytes, whereas the anti-apoptotic protein Bcl-2 was downregulated. We proved during this study for the first time that melatonin significantly reduces the apoptosis of chondrocytes.

Typical biomarkers of ERS include CHOP and GRP78 (Malhotra and Kaufman, 2007; Uehara et al., 2014). In the present study the protein levels of CHOP, GRP78, and caspase-4 were significantly reduced by treatment with melatonin (10 μ M). Moreover, melatonin inhibited ERS caused by inflammation. In mammalian cells, ER stress activates the three main ER-localized transmembrane signaling proteins IRE1 α , PERK, and ATF6, which in turn activate UPR (Hotamisligil, 2010). Previous studies have shown that ERS promotes IRE1 α phosphorylation, which leads to increased XBP1 cutting and promotes the degradation of OA cartilage (Walter et al., 2015). A delay in the development of OA was achieved by inhibiting ERS, thus, the excessive activation of IRE1 α induced a terminal UPR that led to apoptotic signals via XBP1 messenger RNA splicing (Chen and Cubillos-Ruiz, 2021). We first found that melatonin relieved the ERS of chondrocytes by inhibiting the IRE1 α -XBP1S-CHOP signaling pathway. The classic ERS inducer TM was used to further investigate the relationship between ERS and apoptosis in human primary chondrocytes. TM attenuated the anti-apoptotic effect of melatonin in chondrocytes. The above experimental results indicate that melatonin inhibited the ERS-mediated apoptosis of chondrocytes by inhibiting the IRE1 α -XBP1S-CHOP signaling pathway, especially by directly inhibiting CHOP. However, whether the protective effect of melatonin on OA chondrocytes is achieved through the other two ERS-related pathways requires further experimental research. With the progression of OA, SIRT1 continues to decrease in the cartilage of OA patients. SIRT1 regulates expression of the extracellular matrix, and has anti-catabolic, anti-inflammatory, anti-oxidant, and anti-apoptotic effects (Deng et al., 2019). In chondrocytes SIRT1 can protect cartilage by regulating mitochondrial biogenesis, oxidative stress, autophagy, and ERS, and it can also inhibit chondrocyte hypertrophy and degeneration (Fujita et al., 2011; Wang et al., 2015). Therefore, SIRT1 has emerged as a promising therapeutic target for the treatment of OA.

Based on previous research results, the current study investigated whether melatonin inhibits inflammation mediated ERS and the apoptosis of chondrocytes through SIRT1. In this study, the experimental results indicated that LPS decreased the expression of SIRT1. Then, after treatment

with melatonin, SIRT1 expression was significantly increased. To confirm that melatonin regulated ERS through SIRT1, we used an exclusive SIRT1 inhibitor, EX57, and we observed that EX57 significantly elevated the protein levels of CHOP, GRP78 and caspase-4, reversing the inhibitory effect of melatonin on the ER. These results indicate that SIRT1 inhibits the apoptosis of inflammation-induced chondrocytes by alleviating ERS. Previous study showed that SIRT1 plays a crucial role in regulating ERS-related apoptosis (Prola et al., 2017; Huang et al., 2018; Li et al., 2018). SIRT1 regulates the IRE1 α -XBP1S-CHOP signaling pathway and promote the formation of growth cartilage plates (Chou et al., 2019). Previous research also demonstrated that SIRT1 activation can inhibit cadmium-induced ERS by inhibiting the IRE1 α -XBP1S pathway (Romeo-Guitart et al., 2018). However, the relationship between SIRT1 and the IRE1 α -XBP1S-CHOP signaling pathway in chondrocytes needs to be further explored. Human chondrocytes treated with the classic SIRT1 inhibitor EX57 showed markedly elevated expression levels of P-IRE1 α , XBP1S, and CHOP. For the first time, our experiment has confirmed the importance of SIRT1 for ERS-mediated apoptosis and revealed that its mechanism of action is through the inhibition of the IRE1 α -XBP1S-CHOP signaling pathway. Based on the above experimental results, we found for the first time that melatonin inhibits the IRE1 α -XBP1S-CHOP signaling pathway by promoting SIRT1 expression in human primary chondrocytes induced by inflammation *in vitro*. However, whether the protective effect of melatonin and the expression of SIRT1 in OA are related to the other two pathways of ERS needs to be further verified. The typical features of OA progression are obvious destruction of articular surfaces and lesions and apoptosis of chondrocytes. The ACLT mouse model is a the widely used OA model in several studies (Zhou et al., 2019). Here, the mouse ACLT model was used to imitate the progression of OA. The concentration of melatonin varies greatly in animal models of different diseases. Zhang et al. (Zhang et al., 2019b) used a melatonin solution at a dose of 10 mg/ml in the treatment of ACLT models of OA, where intra-articular injection of the same amount (10 μ L) of melatonin achieved a good curative effect. Meanwhile, other research has studied the effects of prenatal use of melatonin on the regulation of neonatal brain inflammation. In a study, intraperitoneal injection of melatonin (5 mg/kg) effectively reduced neonatal inflammation and related brain damage caused by maternal LPS (Carlioni et al., 2016). According to another study, melatonin at a concentration of 10 mg/kg/day had a protective effect on COPD by reducing lung tissue cell apoptosis and ERS in COPD rats (He et al., 2019). Chen et al. (Chen S. J. et al., 2016) demonstrated that a melatonin dose of 200 mg/kg delivered through subcutaneous injection had a good effect on immune encephalomyelitis. In summary, melatonin at a dosage of up to 200 mg/kg is safe. In our experiments and related reports, the therapeutic effect of



melatonin is dose-dependent, so we tested whether melatonin delayed the progression of OA at a low concentration of 50 mg/kg and a high concentration of 150 mg/kg. We assessed the effect of the drug on body weight in mice, these results show that melatonin attenuates weight gain with age in male mice (Supplementary Figure S2), similar to what has been reported in the literature (Tamura et al., 2021).

In the current study micro-CT indicated that melatonin could delay the progression of OA. We also found that in a mouse model of OA melatonin delayed joint degeneration and reduced chondrocyte apoptosis in a concentration-dependent manner. Our study revealed for the first time that melatonin inhibits the protein expression levels of CHOP and cleaved caspase-3 by promoting the expression of SIRT1. These results indicate that the potential mechanism of melatonin-based resistance to apoptosis is activation of SIRT1 expression, and inhibition of ERS.

We conclude from our experiments that melatonin can delay the progression of OA by inhibiting ERS-induced apoptosis of chondrocytes *in vivo* and *in vitro*. Furthermore, melatonin protects articular cartilage by promoting SIRT1 expression and inhibiting ERS and apoptosis by blocking the IRE1 α -XBP1S-CHOP signaling pathway (Figure 9). The protective effect of melatonin on cartilage was similarly verified *in vivo* experiments. Based on

the above experimental results, melatonin may be a treatment option for OA. We also verified that melatonin reduces ERS of arthritic chondrocytes through the perk pathway (Supplementary Figure S3). Therefore, these results suggest that melatonin may alleviate chondrocyte apoptosis through the IRE1 pathway, but the IRE1 pathway is not the only pathway and further experimental exploration is needed regarding the effect of melatonin on ERS in chondrocytes.

Data availability statement

The original contributions presented in the study are included in the article/Supplementary Materials, further inquiries can be directed to the corresponding authors.

Ethics statement

This study was approved by the Research Ethics Committee of the First Affiliated Hospital of Anhui Medical University (Number: PJ2022-02-25) and all animal experiments were approved by the Ethics Committee for Animal Research, Anhui Medical University (Number: LLSC20190547).

Author contributions

YW and ZY: conceived and designed experiments. KQ: carried out experiments, methodology, formal analysis, and writing—review and editing. HT and WH, methodology, formal analysis. YR and DY: performed sample collection and formal analysis. WH and YT: formal analysis. and ZY approved the manuscript. All authors have read and approved the final manuscript.

Funding

This study was supported by the Provincial Natural Science Foundation of Anhui (2008085MH247).

Acknowledgments

The author would like to thank Li Yu, Jilong Shen, and Qinglin Luo. (the Key Laboratory of Microbiology and Parasitology of Anhui Province, the Key Laboratory of Zoonoses of High Institutions in Anhui, Anhui Medical University, Hefei, China) for providing the experimental platform and technical support.

Conflict of interest

The authors declare that the research was conducted in the absence of any commercial or financial relationships that could be construed as a potential conflict of interest.

References

- Abdullah, A., and Ravanani, P. (2018). The unknown face of Irf1 - beyond Er stress. *Eur. J. Cell Biol.* 97, 359–368. doi:10.1016/j.ejcb.2018.05.002
- Bouras, T., Fu, M., Sauve, A. A., Wang, F., Quong, A. A., Perkins, N. D., et al. (2005). Sirt1 deacetylation and repression of P300 involves lysine residues 1020/1024 within the cell cycle regulatory domain 1. *J. Biol. Chem.* 280, 10264–10276. doi:10.1074/jbc.M408748200
- Brunet, A., Sweeney, L. B., Sturgill, J. F., Chua, K. F., Greer, P. L., Lin, Y., et al. (2004). Stress-dependent regulation of foxo transcription factors by the Sirt1 deacetylase. *Science* 303, 2011–2015. doi:10.1126/science.1094637
- Carlson, S., Favrais, G., Saliba, E., Albertini, M. C., Chalon, S., Longini, M., et al. (2016). Melatonin modulates neonatal brain inflammation through endoplasmic reticulum stress, autophagy, and mir-34a/silent information regulator 1 pathway. *J. Pineal Res.* 61, 370–380. doi:10.1111/jpi.12354
- Chen, C., Zhang, C., Cai, L., Xie, H., Hu, W., Wang, T., et al. (2017). Baicalin suppresses il-1 β -induced expression of inflammatory cytokines via blocking nf- κ b in human osteoarthritis chondrocytes and shows protective effect in mice osteoarthritis models. *Int. Immunopharmacol.* 52, 218–226. doi:10.1016/j.intimp.2017.09.017
- Chen, S. J., Huang, S. H., Chen, J. W., Wang, K. C., Yang, Y. R., Liu, P. F., et al. (2016a). Melatonin enhances interleukin-10 expression and suppresses chemotaxis to inhibit inflammation *in situ* and reduce the severity of experimental autoimmune encephalomyelitis. *Int. Immunopharmacol.* 31, 169–177. doi:10.1016/j.intimp.2015.12.020
- Chen, X., and Cubillos-Ruiz, J. R. (2021). Endoplasmic reticulum stress signals in the tumour and its microenvironment. *Nat. Rev. Cancer* 21, 71–88. doi:10.1038/s41568-020-00312-2
- Chen, Y., Zhang, J., Zhao, Q., Chen, Q., Sun, Y., Jin, Y., et al. (2016b). Melatonin induces anti-inflammatory effects to play a protective role via endoplasmic reticulum stress in acute pancreatitis. *Cell. Physiol. Biochem.* 40, 1094–1104. doi:10.1159/000453164
- Chou, X., Ding, F., Zhang, X., Ding, X., Gao, H., and Wu, Q. (2019). Sirtuin-1 ameliorates cadmium-induced endoplasmic reticulum stress and pyroptosis through xbp-1s deacetylation in human renal tubular epithelial cells. *Arch. Toxicol.* 93, 965–986. doi:10.1007/s00204-019-02415-8
- Cohen, H. Y., Miller, C., Bitterman, K. J., Wall, N. R., Hekking, B., Kessler, B., et al. (2004). Calorie restriction promotes mammalian cell survival by inducing the Sirt1 deacetylase. *Science* 305, 390–392. doi:10.1126/science.1099196
- D'arcy, M. S. (2019). Cell death: A review of the major forms of apoptosis, necrosis and autophagy. *Cell Biol. Int.* 43, 582–592. doi:10.1002/cbin.11137
- Dai, M., Sui, B., Xue, Y., Liu, X., and Sun, J. (2018). Cartilage repair in degenerative osteoarthritis mediated by squid type ii collagen via immunomodulating activation of M2 macrophages, inhibiting apoptosis and hypertrophy of chondrocytes. *Biomaterials* 180, 91–103. doi:10.1016/j.biomaterials.2018.07.011

The handling editor SH declared a shared parent affiliation with the authors at the time of review.

Publisher's note

All claims expressed in this article are solely those of the authors and do not necessarily represent those of their affiliated organizations, or those of the publisher, the editors and the reviewers. Any product that may be evaluated in this article, or claim that may be made by its manufacturer, is not guaranteed or endorsed by the publisher.

Supplementary material

The Supplementary Material for this article can be found online at: <https://www.frontiersin.org/articles/10.3389/fphar.2022.940629/full#supplementary-material>

SUPPLEMENTARY FIGURE S1

The colocalization of SIRT1 with IRE1 by Immunofluorescence (bar, 20 μ m).

SUPPLEMENTARY FIGURE S2

Effects of long-term melatonin treatment on body weight with aging. 10-weeks mice were divided into sham group, OA group, low-dose melatonin (50 mg/kg) and high-dose melatonin (150 mg/kg). Body weights were measured at 0, 2, 4, 6, 8, 10, 12 weeks after operation, (each group n = 6).

SUPPLEMENTARY FIGURE S3

Melatonin attenuates the activation of PERK pathway

(A) Melatonin attenuated the phosphorylation of PERK. (B) EX527 eliminated the protective effect of melatonin on human chondrocytes stimulated by lipopolysaccharide by inhibiting the phosphorylation of PERK.

- Deng, Z., Li, Y., Liu, H., Xiao, S., Li, L., Tian, J., et al. (2019). The role of sirtuin 1 and its activator, resveratrol in osteoarthritis. *Biosci. Rep.* 39, BSR20190189. doi:10.1042/BSR20190189
- Feng, K., Ge, Y., Chen, Z., Li, X., Liu, Z., Li, X., et al. (2019). *Curcumin inhibits the perk-eif2 α -chop pathway through promoting Sirt1 expression in oxidative stress-induced rat chondrocytes and ameliorates osteoarthritis progression in a rat model.* *Oxid Med Cell Longev.* 8574386. doi:10.1155/2019/8574386.2019
- Fujita, N., Matsushita, T., Ishida, K., Kubo, S., Matsumoto, T., Takayama, K., et al. (2011). Potential involvement of Sirt1 in the pathogenesis of osteoarthritis through the modulation of chondrocyte gene expressions. *J. Orthop. Res.* 29, 511–515. doi:10.1002/jor.21284
- García, J. J., López-Pingarrón, L., Almeida-Souza, P., Tres, A., Escudero, P., García-Gil, F. A., et al. (2014). Protective effects of melatonin in reducing oxidative stress and in preserving the fluidity of biological membranes: A review. *J. Pineal Res.* 56, 225–237. doi:10.1111/jpi.12128
- Glasson, S. S., Chambers, M. G., Van Den Berg, W. B., and Little, C. B. (2010). The oarsi histopathology initiative - recommendations for histological assessments of osteoarthritis in the mouse. *Osteoarthritis Cartil.* 18 (3), S17–S23. doi:10.1016/j.joca.2010.05.025
- Han, X., Zhou, J., Zhang, P., Song, F., Jiang, R., Li, M., et al. (2013). Ire1 α dissociates with bip and inhibits Er stress-mediated apoptosis in cartilage development. *Cell. Signal.* 25, 2136–2146. doi:10.1016/j.cellsig.2013.06.011
- He, B., Zhang, W., Qiao, J., Peng, Z., and Chai, X. (2019). Melatonin protects against copd by attenuating apoptosis and endoplasmic reticulum stress via upregulating Sirt1 expression in rats. *Can. J. Physiol. Pharmacol.* 97, 386–391. doi:10.1139/cjpp-2018-0529
- Hetz, C., Zhang, K., and Kaufman, R. J. (2020). Mechanisms, regulation and functions of the unfolded protein response. *Nat. Rev. Mol. Cell Biol.* 21, 421–438. doi:10.1038/s41580-020-0250-z
- Hotamisligil, G. S. (2010). Endoplasmic reticulum stress and the inflammatory basis of metabolic disease. *Cell* 140, 900–917. doi:10.1016/j.cell.2010.02.034
- Hu, T., Shi, J. J., Fang, J., Wang, Q., Chen, Y. B., and Zhang, S. J. (2020). Quercetin ameliorates diabetic encephalopathy through Sirt1/Er stress pathway in Db/Db mice. *Aging (Albany Ny)* 12, 7015–7029. doi:10.18632/aging.103059
- Huang, D., Yan, M. L., Chen, K. K., Sun, R., Dong, Z. F., Wu, P. L., et al. (2018). Cardiac-specific overexpression of silent information regulator 1 protects against heart and kidney deterioration in cardiorenal syndrome via inhibition of endoplasmic reticulum stress. *Cell. Physiol. Biochem.* 46, 9–22. doi:10.1159/000488404
- Huang, R., Hui, Z., Wei, S., Li, D., Li, W., Daping, W., et al. (2021). Ire1 signaling regulates chondrocyte apoptosis and death fate in the osteoarthritis. *J. Cell. Physiol.* 237, 118–127. doi:10.1002/jcp.30537
- Kaczanowski, S. (2016). Apoptosis: Its origin, history, maintenance and the medical implications for cancer and aging. *Phys. Biol.* 13, 031001. doi:10.1088/1478-3975/13/3/031001
- Kang, X., Yang, W., Wang, R., Xie, T., Li, H., Feng, D., et al. (2018). Sirtuin-1 (Sirt1) stimulates growth-plate chondrogenesis by attenuating the perk-eif-2 α -chop pathway in the unfolded protein response. *J. Biol. Chem.* 293, 8614–8625. doi:10.1074/jbc.M117.809822
- Komoike, Y., and Matsuoka, M. (2016). Endoplasmic reticulum stress-mediated neuronal apoptosis by acrylamide exposure. *Toxicol. Appl. Pharmacol.* 310, 68–77. doi:10.1016/j.taap.2016.09.005
- Koyama, M., Furuhashi, M., Ishimura, S., Mita, T., Fuseya, T., Okazaki, Y., et al. (2014). Reduction of endoplasmic reticulum stress by 4-phenylbutyric acid prevents the development of hypoxia-induced pulmonary arterial hypertension. *Am. J. Physiol. Heart Circ. Physiol.* 306, H1314–H1323. doi:10.1152/ajpheart.00869.2013
- Li, N., Zhou, H., Ma, Z. G., Zhu, J. X., Liu, C., Song, P., et al. (2018). Geniposide alleviates isoproterenol-induced cardiac fibrosis partially via Sirt1 activation *in vivo* and *in vitro*. *Front. Pharmacol.* 9, 854. doi:10.3389/fphar.2018.00854
- Liu, L., Zhu, Y., Xu, Y., and Reiter, R. J. (2011). Melatonin delays cell proliferation by inducing G1 and G2/M phase Arrest in A human osteoblastic cell line hFOB 1.19. *J. Pineal Res.* 50, 222–231. doi:10.1111/j.1600-079X.2010.00832.x
- Li, Z. C., Xiao, J., Peng, J. L., Chen, J. W., Ma, T., Cheng, G. Q., et al. (2014). Functional annotation of rheumatoid arthritis and osteoarthritis associated genes by integrative genome-wide gene expression profiling analysis. *Plos One* 9, E85784. doi:10.1371/journal.pone.0085784
- Lim, H. D., Kim, Y. S., Ko, S. H., Yoon, I. J., Cho, S. G., Chun, Y. H., et al. (2012). Cytoprotective and anti-inflammatory effects of melatonin in hydrogen peroxide-stimulated chon-001 human chondrocyte cell line and rabbit model of osteoarthritis via the Sirt1 pathway. *J. Pineal Res.* 53, 225–237. doi:10.1111/j.1600-079X.2012.00991.x
- Liu, X., Xu, Y., Chen, S., Tan, Z., Xiong, K., Li, Y., et al. (2014). Rescue of proinflammatory cytokine-inhibited chondrogenesis by the antiarthritic effect of melatonin in synovium mesenchymal stem cells via suppression of reactive oxygen species and matrix metalloproteinases. *Free Radic. Biol. Med.* 68, 234–246. doi:10.1016/j.freeradbiomed.2013.12.012
- Luo, G., Jian, Z., Zhu, Y., Zhu, Y., Chen, B., Ma, R., et al. (2019). Sirt1 promotes autophagy and inhibits apoptosis to protect cardiomyocytes from hypoxic stress. *Int. J. Mol. Med.* 43, 2033–2043. doi:10.3892/ijmm.2019.4125
- Malhotra, J. D., and Kaufman, R. J. (2007). Endoplasmic reticulum stress and oxidative stress: A vicious cycle or A double-edged sword? *Antioxid. Redox Signal.* 9, 2277–2293. doi:10.1089/ars.2007.1782
- Mazzon, E., Esposito, E., Crisafulli, C., Riccardi, L., Muià, C., Di Bella, P., et al. (2006). Melatonin modulates signal transduction pathways and apoptosis in experimental colitis. *J. Pineal Res.* 41, 363–373. doi:10.1111/j.1600-079X.2006.00378.x
- Moon, H. S., Kim, B., Gwak, H., Suh, D. H., and Song, Y. S. (2016). Autophagy and protein kinase rna-like endoplasmic reticulum kinase (Perk)/Eukaryotic initiation factor 2 α kinase (Eif2 α) pathway protect ovarian cancer cells from metformin-induced apoptosis. *Mol. Carcinog.* 55, 346–356. doi:10.1002/mc.22284
- Morris, B. J. (2013). Seven sirtuins for seven deadly diseases of aging. *Free Radic. Biol. Med.* 56, 133–171. doi:10.1016/j.freeradbiomed.2012.10.525
- Park, D. R., Kim, J., Kim, G. M., Lee, H., Kim, M., Hwang, D., et al. (2020). Osteoclast-associated receptor blockade prevents articular cartilage destruction via chondrocyte apoptosis regulation. *Nat. Commun.* 11, 4343. doi:10.1038/s41467-020-18208-y
- Pei, M., He, F., Wei, L., and Rawson, A. (2009). Melatonin enhances cartilage matrix synthesis by porcine articular chondrocytes. *J. Pineal Res.* 46, 181–187. doi:10.1111/j.1600-079X.2008.00646.x
- Prola, A., Pires Da Silva, J., Guilbert, A., Lecru, L., Piquereau, J., Ribeiro, M., et al. (2017). Sirt1 protects the heart from Er stress-induced cell death through Eif2 α deacetylation. *Cell Death Differ.* 24, 343–356. doi:10.1038/cdd.2016.138
- Qin, D. Z., Cai, H., He, C., Yang, D. H., Sun, J., He, W. L., et al. (2021). Melatonin relieves heat-induced spermatocyte apoptosis in mouse testes by inhibition of Atf6 and perk signaling pathways. *Zool. Res.* 42, 514–524. doi:10.24272/j.issn.2095-8137.2021.041
- Quan, X., Wang, J., Liang, C., Zheng, H., and Zhang, L. (2015). Melatonin inhibits tunicamycin-induced endoplasmic reticulum stress and insulin resistance in skeletal muscle cells. *Biochem. Biophys. Res. Commun.* 463, 1102–1107. doi:10.1016/j.bbrc.2015.06.065
- Robinson, W. H., Lepus, C. M., Wang, Q., Raghu, H., Mao, R., Lindstrom, T. M., et al. (2016). Low-grade inflammation as A key mediator of the pathogenesis of osteoarthritis. *Nat. Rev. Rheumatol.* 12, 580–592. doi:10.1038/nrrheum.2016.136
- Romeo-Guitart, D., Leiva-Rodríguez, T., Espinosa-Alcantud, M., Sima, N., Vaquero, A., Domínguez-Martín, H., et al. (2018). Sirt1 activation with neuroheal is neuroprotective but Sirt2 inhibition with Ak7 is detrimental for disconnected motoneurons. *Cell Death Dis.* 9, 531. doi:10.1038/s41419-018-0553-6
- Ryu, J. H., Shin, Y., Huh, Y. H., Yang, S., Chun, C. H., and Chun, J. S. (2012). Hypoxia-inducible factor-2 α regulates fas-mediated chondrocyte apoptosis during osteoarthritic cartilage destruction. *Cell Death Differ.* 19, 440–450. doi:10.1038/cdd.2011.111
- Sacitharan, P. K., Bou-Gharios, G., and Edwards, J. R. (2020). Sirt1 directly activates autophagy in human chondrocytes. *Cell Death Discov.* 6, 41. doi:10.1038/s41420-020-0277-0
- Schofield, B. H., Williams, B. R., and Doty, S. B. (1975). Alcian blue staining of cartilage for electron microscopy. Application of the critical electrolyte concentration principle. *Histochem. J.* 7, 139–149. doi:10.1007/BF01004558
- Sepulveda, D., Rojas-Rivera, D., Rodríguez, D. A., Groenendyk, J., Köhler, A., Lebeaupin, C., et al. (2018). Interactome screening identifies the Er luminal chaperone Hsp47 as A regulator of the unfolded protein response transducer Ire1 α . *Mol. Cell* 69, 238–252. E7. doi:10.1016/j.molcel.2017.12.028
- Shi, X., Ye, H., Yao, X., and Gao, Y. (2017). The involvement and possible mechanism of Nr4a1 in chondrocyte apoptosis during osteoarthritis. *Am. J. Transl. Res.* 9, 746–754.
- Tabas, I., and Ron, D. (2011). Integrating the mechanisms of apoptosis induced by endoplasmic reticulum stress. *Nat. Cell Biol.* 13, 184–190. doi:10.1038/ncb0311-184
- Tamura, I., Tamura, H., Kawamoto-Jozaki, M., Doi-Tanaka, Y., Takagi, H., Shirafuta, Y., et al. (2021). Long-term melatonin treatment attenuates body weight gain with aging in female mice. *J. Endocrinol.* 251, 15–25. doi:10.1530/JOE-20-0462

- Tardif, G., Pelletier, J. P., Boileau, C., and Martel-Pelletier, J. (2009). The bmp antagonists follistatin and gremlin in normal and early osteoarthritic cartilage: An immunohistochemical study. *Osteoarthr. Cartil.* 17, 263–270. doi:10.1016/j.joca.2008.06.022
- Tavernier, S. J., Osorio, F., Vandersarren, L., Vetter, J., Vanlangenakker, N., Van Isterdael, G., et al. (2017). Regulated ire1-dependent mrna decay sets the threshold for dendritic cell survival. *Nat. Cell Biol.* 19, 698–710. doi:10.1038/ncb3518
- Terauchi, K., Kobayashi, H., Yatabe, K., Yui, N., Fujiya, H., Niki, H., et al. (2016). The nad-dependent deacetylase sirtuin-1 regulates the expression of osteogenic transcriptional activator runt-related transcription factor 2 (Runx2) and production of matrix metalloproteinase (Mmp)-13 in chondrocytes in osteoarthritis. *Int. J. Mol. Sci.* 17, E1019. doi:10.3390/ijms17071019
- Thomas, C. M., Fuller, C. J., Whittles, C. E., and Sharif, M. (2007). Chondrocyte death by apoptosis is associated with cartilage matrix degradation. *Osteoarthr. Cartil.* 15, 27–34. doi:10.1016/j.joca.2006.06.012
- Uehara, Y., Hirose, J., Yamabe, S., Okamoto, N., Okada, T., Oyadomari, S., et al. (2014). Endoplasmic reticulum stress-induced apoptosis contributes to articular cartilage degeneration via C/ebp homologous protein. *Osteoarthr. Cartil.* 22, 1007–1017. doi:10.1016/j.joca.2014.04.025
- Vaziri, H., Dessain, S. K., Ng Eaton, E., Imai, S. I., Frye, R. A., Pandita, T. K., et al. (2001). Hsr2(Sirt1) functions as an nad-dependent P53 deacetylase. *Cell* 107, 149–159. doi:10.1016/s0092-8674(01)00527-x
- Walter, F., Schmid, J., Düssmann, H., Concannon, C. G., and Prehn, J. H. (2015). Imaging of single cell responses to Er stress indicates that the relative dynamics of ire1/xbp1 and perk/atf4 signalling rather than A switch between signalling branches determine cell survival. *Cell Death Differ.* 22, 1502–1516. doi:10.1038/cdd.2014.241
- Wang, F. M., Chen, Y. J., and Ouyang, H. J. (2011). Regulation of unfolded protein response modulator Xbp1s by acetylation and deacetylation. *Biochem. J.* 433, 245–252. doi:10.1042/BJ20101293
- Wang, Y., Zhao, X., Lotz, M., Terkeltaub, R., and Liu-Bryan, R. (2015). Mitochondrial biogenesis is impaired in osteoarthritis chondrocytes but reversible via peroxisome proliferator-activated receptor Γ coactivator 1 α . *Arthritis Rheumatol.* 67, 2141–2153. doi:10.1002/art.39182
- Wu, L., Liu, H., Li, L., Xu, D., Gao, Y., Guan, Y., et al. (2018). 5, 7, 3', 4'-tetramethoxyflavone protects chondrocytes from Er stress-induced apoptosis through regulation of the Ire1a pathway. *Connect. Tissue Res.* 59, 157–166. doi:10.1080/03008207.2017.1321639
- Xin, Q., Ji, B., Cheng, B., Wang, C., Liu, H., Chen, X., et al. (2014). Endoplasmic reticulum stress in cerebral ischemia. *Neurochem. Int.* 68, 18–27. doi:10.1016/j.neuint.2014.02.001
- Xiong, X. C., Zhu, Y., Ge, R., Liu, L. F., and Yuan, W. (2015). Effect of melatonin on the extracellular-regulated kinase signal pathway activation and human osteoblastic cell line hfob 1.19 proliferation. *Int. J. Mol. Sci.* 16, 10337–10353. doi:10.3390/ijms160510337
- Yeung, F., Hoberg, J. E., Ramsey, C. S., Keller, M. D., Jones, D. R., Frye, R. A., et al. (2004). Modulation of nf-kappab-dependent transcription and cell survival by the Sirt1 deacetylase. *Embo J.* 23, 2369–2380. doi:10.1038/sj.emboj.7600244
- Zhang, L., Xing, R., Huang, Z., Zhang, N., Zhang, L., Li, X., et al. (2019a). Inhibition of synovial macrophage pyroptosis alleviates synovitis and fibrosis in knee osteoarthritis. *Mediators Inflamm.* 2019, 2165918. doi:10.1155/2019/2165918.2019
- Zhang, Y., He, L., Tu, M., Huang, M., Chen, Y., Pan, D., et al. (2021). The ameliorative effect of terpinen-4-ol on Er stress-induced vascular calcification depends on sirt1-mediated regulation of perk acetylation. *Pharmacol. Res.* 170, 105629. doi:10.1016/j.phrs.2021.105629
- Zhang, Y., Lin, J., Zhou, X., Chen, X., Chen, A. C., Pi, B., et al. (2019b2019). Melatonin prevents osteoarthritis-induced cartilage degradation via targeting microRNA-140. *Oxid. Med. Cell. Longev.*, 9705929. doi:10.1155/2019/9705929
- Zhou, F., Mei, J., Han, X., Li, H., Yang, S., Wang, M., et al. (2019). Kinsenoside attenuates osteoarthritis by repolarizing macrophages through inactivating nf- κ b/mapk signaling and protecting chondrocytes. *Acta Pharm. Sin. B* 9, 973–985. doi:10.1016/j.apsb.2019.01.015
- Zhou, R., Ma, Y., Tao, Z., Qiu, S., Gong, Z., Tao, L., et al. (2020). Melatonin inhibits glucose-induced apoptosis in osteoblastic cell line through perk-eif2 α -atf4 pathway. *Front. Pharmacol.* 11, 602307. doi:10.3389/fphar.2020.602307



OPEN ACCESS

EDITED BY

Kun Lv,
First Affiliated Hospital of Wannan
Medical College, China

REVIEWED BY

Zhirui Zeng,
Guizhou Medical University, China
James Cheng-Chung Wei,
Chung Shan Medical University
Hospital, Taiwan

*CORRESPONDENCE

Bo Wang
dr.wangbo@vip.163.com
Xiaojuan Ye
yexj2002@163.com
Yi Liu
ley582196589@163.com

[†]These authors have contributed
equally to this work

SPECIALTY SECTION

This article was submitted to
Autoimmune and Autoinflammatory
Disorders,
a section of the journal
Frontiers in Immunology

RECEIVED 29 May 2022

ACCEPTED 24 August 2022

PUBLISHED 13 September 2022

CITATION

Han Y, Zhou Y, Li H, Gong Z,
Liu Z, Wang H, Wang B, Ye X and
Liu Y (2022) Identification of
diagnostic mRNA biomarkers in
whole blood for ankylosing spondylitis
using WGCNA and machine learning
feature selection.
Front. Immunol. 13:956027.
doi: 10.3389/fimmu.2022.956027

COPYRIGHT

© 2022 Han, Zhou, Li, Gong, Liu, Wang,
Wang, Ye and Liu. This is an open-
access article distributed under the
terms of the [Creative Commons
Attribution License \(CC BY\)](#). The use,
distribution or reproduction in other
forums is permitted, provided the
original author(s) and the copyright
owner(s) are credited and that the
original publication in this journal is
cited, in accordance with accepted
academic practice. No use,
distribution or reproduction is
permitted which does not comply with
these terms.

Identification of diagnostic mRNA biomarkers in whole blood for ankylosing spondylitis using WGCNA and machine learning feature selection

Yaguang Han^{1†}, Yiqin Zhou^{1,2†}, Haobo Li^{1†}, Zhenyu Gong³,
Ziye Liu¹, Huan Wang¹, Bo Wang^{1*}, Xiaojuan Ye^{4*} and Yi Liu^{1,4*}

¹Department of Orthopaedics, Shanghai Changzheng Hospital, Naval Medical University, Shanghai, China, ²Department of Radiology, Longhua Hospital, Shanghai University of Traditional Chinese Medicine, Shanghai, China, ³Department of Neurosurgery, Klinikum rechts der Isar, Technische Universität München, Munich, Germany, ⁴Department of Orthopaedics, Tongren Hospital, Shanghai Jiao Tong University School of Medicine, Shanghai, China

Ankylosing spondylitis (AS) is a common inflammatory spondyloarthritis affecting the spine and sacroiliac joint that finally results in sclerosis of the axial skeleton. Aside from human leukocyte antigen B27, transcriptomic biomarkers in blood for AS diagnosis still remain unknown. Hence, this study aimed to investigate credible AS-specific mRNA biomarkers from the whole blood of AS patients by analyzing an mRNA expression profile (GSE73754) downloaded Gene Expression Omnibus, which includes AS and healthy control blood samples. Weighted gene co-expression network analysis was performed and revealed three mRNA modules associated with AS. By performing gene set enrichment analysis, the functional annotations of these modules revealed immune biological processes that occur in AS. Several feature mRNAs were identified by analyzing the hubs of the protein-protein interaction network, which was based on the intersection between differentially expressed mRNAs and mRNA modules. A machine learning-based feature selection method, SVM-RFE, was used to further screen out 13 key feature mRNAs. After verifying by qPCR, IL17RA, Sqstm1, Picalm, Eif4e, Srrt, Lrrfip1, Synj1 and Cxcr6 were found to be significant for AS diagnosis. Among them, Cxcr6, IL17RA and Lrrfip1 were correlated with severity of AS symptoms. In conclusion, our findings provide a framework for identifying the key mRNAs in whole blood of AS that is conducive for the development of novel diagnostic markers for AS.

KEYWORDS

weighted gene co-expression network analysis (WGCEA), recursive feature elimination (RFE), ankylosing spondylitis (AS), mRNAs biomarkers, support vector machine

Introduction

As a kind of chronic axial spondyloarthritis, ankylosing spondylitis (AS) is characterized by aseptic sacroiliitis, spinal stiffness and deformity, ultimately leading to severe disability in patients. Due to the undefined etiology and paucity of early effective detecting methods, the diagnosis of AS is delayed for an average of 8 years (1–3). To date, human leukocyte antigen B27 (HLA-B27), C-reactive protein (CRP) and matrix metalloproteinase 3 (MMP-3), have been found to be associated with AS and positive in 85–95% of patients with AS (4, 5). However, they are also significantly positive in most patients with other immunologic disorders (6–10), indicating their insufficient diagnostic value for assessing AS activity and predicting therapeutic effectiveness. Therefore, to facilitate early diagnosis and assess AS activity, finding novel biomarkers with satisfactory sensitivity and specificity by exploring the molecular mechanisms of AS is crucial.

With the rise of high-throughput transcriptomic techniques such as microarray and sequencing, multiple bioinformatic methods have subsequently been developed and applied in the construction of gene correlation networks on a large scale to shed new light on screening key RNAs in terms of molecular interactions and the exploration of candidate biomarkers for diseases (11). Compared with other developed network analytical methods, weighted gene co-expression network analysis (WGCNA) is a novel systematic biological method that describes the correlation between the expression levels of genes with a weighted value rather than with the all-or-none dichotomy (12). Compared with analyzing single differentially expressed genes, WGCNA can cluster mRNAs into different modules that are more stable and comprehensive in reflecting the underlying pathological mechanism of transcriptomic alterations by calculating the topological parameters of gene correlations. Moreover, WGCNA reveals the correlation of each mRNA module with different clinical traits of interest, which provides more clues for identifying specific biomarkers or therapeutic targets (13).

Abbreviations: AS, ankylosing spondylitis; HLA-B27, human leukocyte antigen B27; GEO, Gene Expression Omnibus; GO, Gene Ontology; HC, healthy control; WGCNA, weighted gene co-expression network analysis; GSEA, gene set enrichment analysis; PPI, protein-protein interaction; STRING, Search Tool for the Retrieval of Interacting Genes/Proteins; MMP-3, matrix metalloproteinase 3; SVM, support vector machine; RFE, recursive feature elimination; ROC, receiver operating characteristic; APCs, antigen presenting cells; TNF, tumor necrosis factor; CXCR6, C-X-C Motif Chemokine Receptor 6; eIF4E, eukaryotic translation initiation factor 4E; LRRFIP1, LRR Binding FLII Interacting Protein 1; MAPK8IP3, mitogen-activated protein kinase 8 interacting protein 3; ESR, erythrocyte sedimentation rate; CRP, C-reactive protein; BASDAI, Bath Ankylosing Spondylitis Disease Activity Index; VAS, visual analog scale.

Generally, the use of traditional experimental methods to validate the function of genes filtered by microarray and sequencing is a long process because of the large amount of data (14). Furthermore, the redundancy and collinearity of high-throughput data severely disrupt the accuracy of bioinformatic analyses. To solve this problem, many gene selection algorithms based on machine learning have been proposed to remove irrelevant or redundant information or features. Among these algorithms, recursive feature elimination based on support vector machine (SVM-RFE) is an effective tool for gene selection (15). As a backward elimination method, SVM-RFE can rank the different genes or features based on the squared sum of the feature coefficients and select the top-ranked genes that significantly influence the classification or identification of different clinical traits (16). Hence, applying SVM-RFE in identifying key mRNAs or biomarkers from transcriptomic data is promising.

To identify novel biomarkers for AS from whole blood, we utilized a microarray dataset to perform WGCNA. After generating the modules of mRNAs specific to AS, we performed gene set enrichment analysis (GSEA) with Gene Ontology (GO) on the mRNAs of these modules and then overlapped them with differentially expressed mRNAs to screen out more specific feature mRNAs to construct a protein-protein interaction (PPI) network. Based on this network, we found hub mRNAs by Cytoscape calculation. Then, we utilized SVM-RFE analysis on these hub mRNAs and screened out 13 feature mRNAs. After verification through qRT-PCR and correlation analysis, 8 key mRNAs were finally identified as the key biomarkers for AS diagnosis.

Patients and methods

AS patients and control group

The Ethics Committee of Shanghai Changzheng Hospital has approved this study. All included AS patients and control donors provided the informed consent including details of present study. According to the modified New York criteria (17), 40 AS patients were included in this study. In addition, 40 healthy donors were recruited in control group. The general information (age and gender), symptoms, erythrocyte sedimentation rate (ESR), C-reactive protein (CRP) and Bath Ankylosing Spondylitis Disease Activity Index (BASDAI) of patients were recorded (Table 1).

Acquisition of microarray data and processing

The microarray dataset GSE73754 by Eric Gracey et al (18) was downloaded from the Gene Expression Omnibus (GEO)

database for analysis. This dataset comprises whole blood mRNA expression data from 72 subjects (52 AS patients and 20 healthy controls). The raw data of GSE73754 were preprocessed using the “affy” and “limma” packages available from Bioconductor in R. The missing values were replenished using the k-nearest neighbor algorithm (19). The normalization of raw data was performed using the robust multiarray average algorithm (20). The batch effect was eliminated using the “sva” package of R based on the COMBAT method. Due to the public availability of relevant data, approval from a local ethics committee was not required.

WGCNA

The “WGCNA” package of R was used for clustering modules and constructing a co-expression network. To eliminate noise and speed up the computation, the mRNAs whose variance in expression was in the top 25% of all the expression profiles were selected. The power parameter β was determined based on the function of the scale-free topology fit index. Based on the weighted Pearson correlation coefficients, an adjacency matrix was constructed to reveal unsupervised co-expression relationships between each mRNA. To simplify this step, the function “blockwiseConsensusModules” was performed with a minimum module size of 30 to construct a network and detect a consensus module. The conservation of each module was assessed using the “modulePreservation” function, which predicts the Z-score. Module-trait correlations were calculated using “modTraitCor” to detect the modules correlated with AS.

GSEA

GSEA of GO is an effective computational method that assesses an a priori-defined set of genes enriched in specific biological states (21). GSEA was performed on the modules selected from WGCNA with the GO gene sets database

(c5.all.v6.2.symbols.gmt). The cutoff criterion of the P-value was set as < 0.05 .

Identification of differentially expressed mRNAs

The screening of differentially expressed mRNAs was performed using the “limma” package of R software (version 3.6.2), and Benjamini-Hochberg adjusted P-values < 0.01 and $|\text{fold change}| > 1$ were set as the cutoff criteria. The heatmap was visualized using the “pheatmap” package of R.

PPI network construction and hub gene identification

The online analysis tool, Search Tool for the Retrieval of Interacting Genes/Proteins (STRING), was used to evaluate the interactions between each of the selected mRNAs. Afterwards, a PPI network was constructed using Cytoscape. The nodes' scores of each mRNA in the PPI network were obtained by the cytoHubba plugin of Cytoscape and were defined as the criterion for further mRNA selection.

Support vector machine based recursive feature elimination

As a powerful machine learning model, SVM has been widely applied in the functional prediction of biological molecules (22). In this study, SVM modeling was performed by using the “e1071” package of R, in which the radial basis function was the selected kernel function.

SVM-RFE is a backward feature deletion method that loops around SVM²². First, all of the original features are used to build the SVM learning model to obtain the absolute coefficient $|w|$ of each input feature. Second, the features are ranked based on the square of $|w|$, and the bottom-ranked features are discarded.

TABLE 1 General information of the AS patients and control donors.

	AS group (n=40)	Control group (n=40)
Age (years)	41.2±11.4	42.9±12.3
Gender(male/female)	15/6	15/5
Positive rate of HLA-B27	85.71%	N/A
Duration of back pain (months)	3.52±2.51	N/A
ESR, mm/hour	49.95±25.63	N/A
CRP, mg/L	33.27±14.86	N/A
BASDAI (10-mm VAS)	5.29±1.44	N/A

ESR, erythrocyte sedimentation rate; CRP, C-reactive protein; BASDAI, Bath Ankylosing Spondylitis Disease Activity Index; VAS, visual analog scale.

Then, the rest of the features are subject to a new loop of SVM model building and ranking with the same procedures as before. These procedures are repeated until all features are removed. The order of removed features represents the level of feature importance (23). The top-ranked features that are discarded later are deemed to be more informative than those that are discarded earlier. In this study, the features correspond to mRNAs. To determine how many top-ranked mRNAs should be selected, 5-fold cross-validation was performed on the dataset. This method randomly divides the dataset into 5 sections, of which 4 sections are selected as the training set, with the last section as the testing set. Depending on these sets, SVM is built with different numbers of top mRNAs for calculating the generalized prediction error. These procedures are repeated 5 times. Finally, the number of top-ranked mRNAs corresponding to the minimum error is the optimal number of selected mRNAs. Using the “pROC” package of R, receiver operating characteristic (ROC) curve analysis was performed to calculate the area under the curve (AUC) value for each selected feature mRNA to evaluate its predictive capability for the diagnosis of AS.

Validation of mRNA expression

5 ml of whole blood was drawn into an EDTA tube from AS patients before medical interventions. Ficoll was used to separate mononuclear cells from whole blood. The total RNA was isolated from mononuclear cells by using TRIzol LS reagent (Ambion). The extracted RNA was used to synthesize cDNA with a Reverse Transcription kit (Takara). The expression of RNAs was firstly determined by 1.5% agarose gel electrophoresis. Electrophoresis was performed at a constant voltage of 100 V for 30 min in TBE running buffer, and the retardation of RNA mobility was visualized under UV light. Quantitative real-time PCR (qRT-PCR) was performed using SYBR Green qPCR Master Mix (Takara) in qPCR CFX 96 Thermocycler system (Bio-Rad). The primers for each selected mRNAs were listed in [Supplementary Table S1](#). The reactions were run according to the following conditions: initial hold at 95°C for 10 min, followed by 40 cycles of amplification at 95°C for 15 s, and annealing for 60s at 60°C and drawing the melting curves by increasing from 60°C to 95°C (0.3°C per second). All expression values were normalized to the expression of GAPDH. Relative expression levels are obtained by calculating $2^{-\Delta\Delta CT}$.

Statistical analysis

The statistical analysis was performed with R software (version 3.6.2). The continuous variables were presented with Mean \pm SD, while the categorical variables were presented with quartile. The expression values of mRNAs were compared by

using one-way analysis of variance (ANOVA) between AS group and control group. Correlation between expression of mRNAs and BASDAI was evaluated by using Pearson’s correlation coefficient test. The $P < 0.05$ was selected as the cut-off for statistical significance.

Results

Generation of key modules associated with AS by WGCNA

The initial step was to generate consensus modules of mRNA expression by constructing a weighted gene co-expression network. We made hclust analysis, with height 45 as cutoff. There was no outlier in included samples ([Supplementary Figure S1](#)). The determination of the soft thresholding power β is entailed in raising Pearson correlation matrices to obtain the network (24). According to the criterion of approximate scale-free topology, in which the scale-free topology model fit index was more than 0.9 and the mean connectivity degree was close to 0, the optimal power β was chosen to be 14 ([Figure 1A](#)). Afterwards, the weighted co-expression networks were constructed, and consensus modules with similar expression trends were clustered and labeled with different colors, as shown in a dendrogram ([Figure 1B](#)). Then, the correlation matrices between consensus modules and clinical traits (AS and HC) were calculated ([Figure 1C](#)). Based on the cutoff of 0.3 to correlation, the Blue, Yellow and Gray modules with specific relation to AS were selected for further investigation. There were 463 mRNAs in the Blue module, 318 mRNAs in the Yellow module, and 404 mRNAs in the Gray module, of which information about the network is presented in [Supplementary Table S2](#). In addition, we performed correlation analysis of Module Membership vs. Gene Significance, and found significant correlation coefficients were 0.28 in Blue module, 0.44 in Grey module, and 0.38 in Yellow module, respectively ([Supplementary Figure S2](#)).

GSEA with GO on selected modules

To further investigate the role of the selected mRNA modules and pathological processes in white blood cells, we performed GSEA with GO terms on mRNAs of the Blue, Yellow and Gray modules. As shown in [Figure 2](#), mRNAs in the Blue module were enriched in the top 10 GO terms with the lowest normalized P-value, including “leukocyte chemotaxis”, “leukocyte migration”, “cell chemotaxis” and “regulation of inflammatory response”, which implicated active inflammatory and immune responses in AS patients’ blood. However, in contrast to the Blue module, most GO terms enriched by the mRNAs in the Yellow and Gray modules are unspecific to AS activity, except for “leukocyte cell

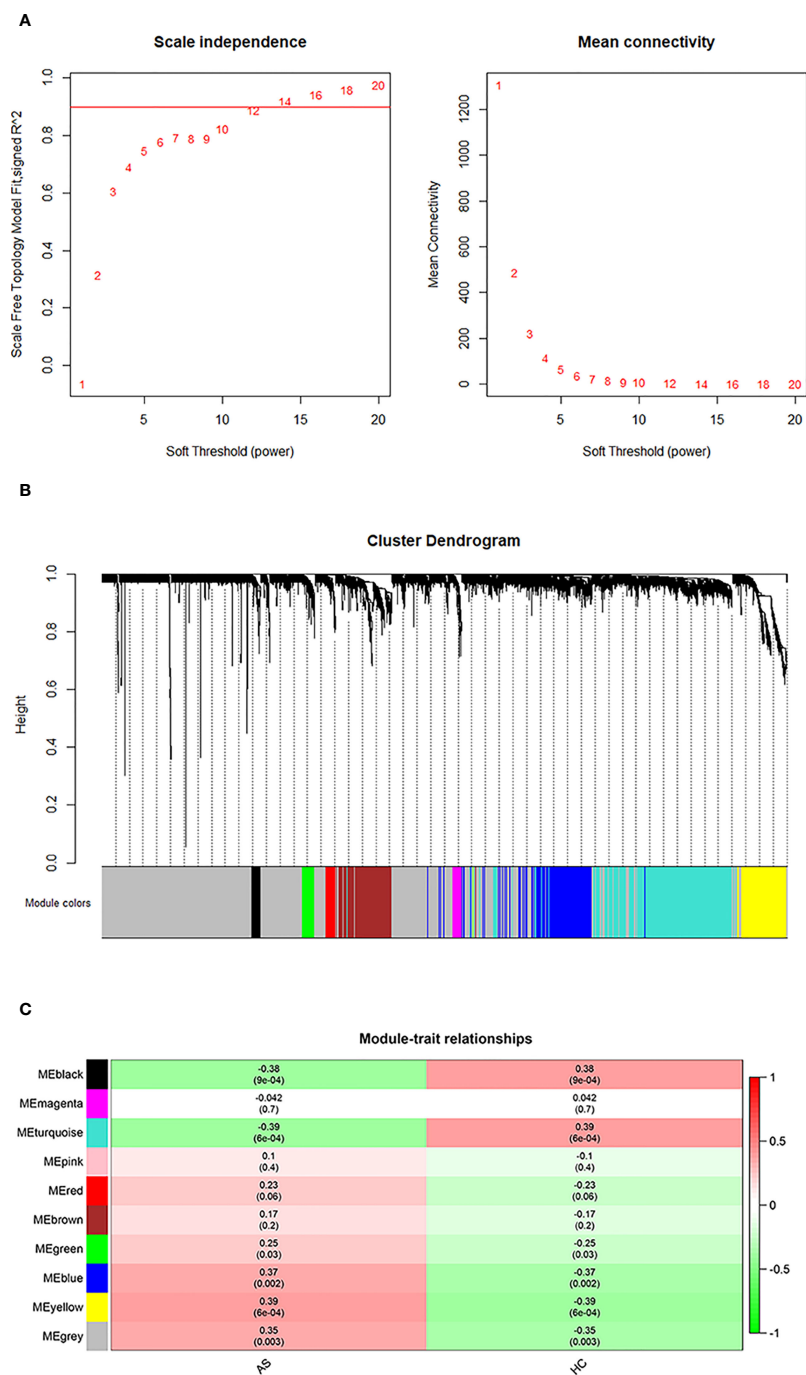


FIGURE 1 WGCNA analysis. **(A)** Determination of an optimal soft-thresholding power β by calculating the scale-free topology mode fit and mean connectivity. **(B)** The cluster dendrogram of mRNAs in GSE73754, revealing different mRNA co-expression modules marked with colors. **(C)** The heatmap for module-traits relationships, in which the correlation of different modules with AS or HC, P-values are presented in each cell.



adhesion”, suggesting that these two modules may represent secondary pathological processes of AS. Therefore, it can be inferred that mRNAs in the Blue module exert more imperative effects than those in the Yellow and Gray modules and are immune dysregulated by AS activity.

Screening of differential expressed mRNAs

To further investigate the discrepancy in whole blood between AS and HC, we filtered differentially expressed mRNAs. A total of 1116 mRNAs were differentially expressed, among which 491 mRNAs were upregulated and 625 mRNAs were downregulated ([Supplementary Table S3](#)). Next, we constructed a heatmap for the top 100 most differentially expressed mRNAs to show the consistencies and discrepancies in mRNA expression among the samples. As shown in [Supplementary Figure S3](#), most AS blood samples are clustered together with similar expression tendencies, which means that their expression patterns differ from the patterns of HC samples.

Selection of feature mRNAs from modules and differential expressed mRNAs

To obtain comprehensive information from the whole blood mRNA expression of AS, finding a balance between WGCNA modules and differentially expressed mRNAs is critical. Accordingly, we overlapped 1185 mRNAs from the Blue module, Yellow module and Gray module with 1116 differentially expressed mRNAs and screened out 296 feature mRNAs for AS. The intersection of each module with

differentially expressed mRNAs is shown in [Supplementary Table S4](#).

Construction of PPI network based on feature mRNAs

Given the interaction between key genes in various pathological processes, performing interaction network analysis on mRNA groups is effective for identifying candidate biomarkers. To this end, we constructed a PPI network on the 296 feature mRNAs by STRING ([Supplementary Figure S4](#)). A total of 427 protein interactions and 280 gene nodes were identified in this network with an enrichment P-value of 5.26×10^{-7} .

In the expression network, hub genes are a series of key genes that have great topological connectiveness with their neighboring genes. To distinguish the hub genes in a network, Closeness Centrality (CC) and Betweenness Centrality (BC), which are based on a concept of moving along the most optimal and shortest paths throughout a network, are widely used in network analysis (25). Because of the vague principles of the usage of these 12 parameters, we simultaneously applied all of them to measure the connectiveness of mRNAs in the PPI network. After inputting the data of the PPI network into Cytoscape and calculating each nodes' scores through cytoHubba, we sorted feature mRNAs by 12 nodes' scores in descending order and generated 12 sequences of mRNAs. Then, we selected the top 25% mRNAs from these 12 sequences and converted these selected mRNAs together. Finally, according to the occurrence of mRNAs in each sequence, 63 mRNAs appearing more than 4 times were obtained as the hub genes ([Supplementary Table S5](#)). The interaction network of these feature mRNAs is shown in [Supplementary Figure S5](#).

Identification of key mRNAs by SVM-RFE

Although the 63 selected feature mRNAs can serve as biomarkers for AS, there is still much redundant information in them, resulting in poor feasibility in practical applications. To solve this problem, we applied SVM-RFE according to the feature ranking of the correlation coefficients to eliminate relatively unspecific feature mRNAs and preserve the key mRNAs. To determine the optimal number of feature mRNAs with the greatest accuracy in the SVM model, 5-fold cross-validation was introduced into the SVM classifier step, and the error rates of different numbers of mRNAs were captured. We plotted the change in the 5-fold cross-validation error rate at each recursive step (Supplementary Figure S6). The error rate fluctuated with increasing numbers of mRNAs until it reached a minimum with 14 feature mRNAs, suggesting that discrimination between AS and HC reached almost 90% accuracy. ROC curve analysis was further carried out, and the AUC values of the 14 key mRNAs were calculated to reveal their predictive power (Figure 3). Accordingly, MAP3K11 was discarded because of its nonsignificant predictive power in distinguishing between AS and HC. Among the 13 remaining selected feature mRNAs, Sqstm1, Srrt, Cxcr6, Eif4e, Ppid, H2afy, Card11, IL17ra, Picalm, Lrrfip1, Polr2a, Mapk8ip3 and Synj1 were screened out as the key mRNAs of AS for further analysis.

Validation of key mRNAs expression

To verify the prediction of bioinformatic and SVM analysis, we performed qRT-PCR and agarose gel electrophoresis to test the expression levels of these 12 key mRNAs in whole blood of AS group and control group. As shown in Figure 4, the expression of Sqstm1, Srrt, Cxcr6, and Eif4e were significantly down-regulated in AS patients, while the expression of IL17ra, Picalm, Lrrfip1 and Synj1 were significantly up-regulated compared with control group. In addition, there were no significant differences on the expression of Ppid, H2afy, Card11, Mapk8ip3 and Polr2a between

two groups. These results indicated the expression patterns of 8 significant key mRNAs in included patients were consistent with bioinformatic analysis and SVM prediction.

Correlating analysis between BASDAI and expression of key mRNAs

To further examine the predictive strength of 8 significant key mRNAs, we analyzed the correlation between their expression levels and BASDAI of AS patients. In a total of 40 blood samples from AS group, a significant correlation between BASDAI and expression level was revealed in three key mRNAs (Cxcr6, IL17ra, Lrrfip1), while the remaining 5 mRNAs showed no significant correlation with BASDAI (Figure 5). There, Cxcr6, IL17ra, Lrrfip1 were proposed to serve as the potential biomarkers for AS.

Discussion

While HLA-B27 has been demonstrated to mainly account for the genetic effects of AS, the other undefined markers may be associated with this immunologic disease (4, 26, 27). People with positive HLA-B27 have a significantly higher risk of developing AS than those with negative HLA-B27. However, most of the former remain healthy, implying that in addition to HLA-B27, other potential factors may contribute to the onset of AS (28, 29). Hence, elucidating AS pathogenesis from the perspective of immune regulation, especially associated with blood karyocytes, can be regarded as a promising direction for finding diagnostic biomarkers with reliable specificity and sensitivity beyond HLA-B27. In present study, we explored the microarray dataset of GSE73754 by WGCNA and PPI network construction, and then identified 3 modules (Blue, Yellow and Gray) and 63 hub mRNAs.

Several studies have demonstrated the pivotal role of adaptive immune responses in AS pathogenesis (30). The interaction between CD4⁺ T cells and HLA-B27 triggers the cascade reaction of various chemokines and cytokines, contributing to

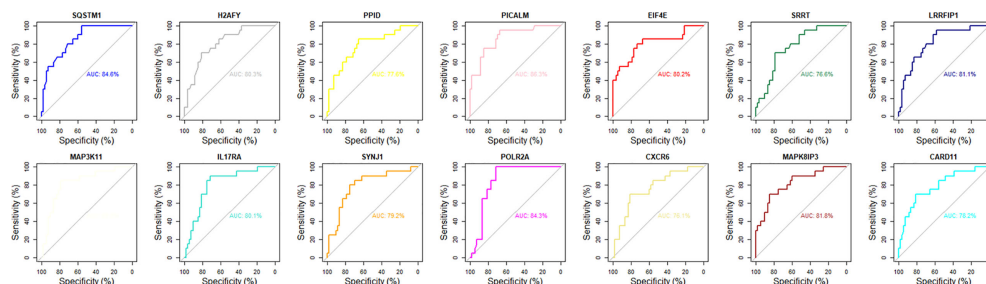


FIGURE 3
The ROC curve analysis of 14 key mRNAs in diagnostic specificity for AS.

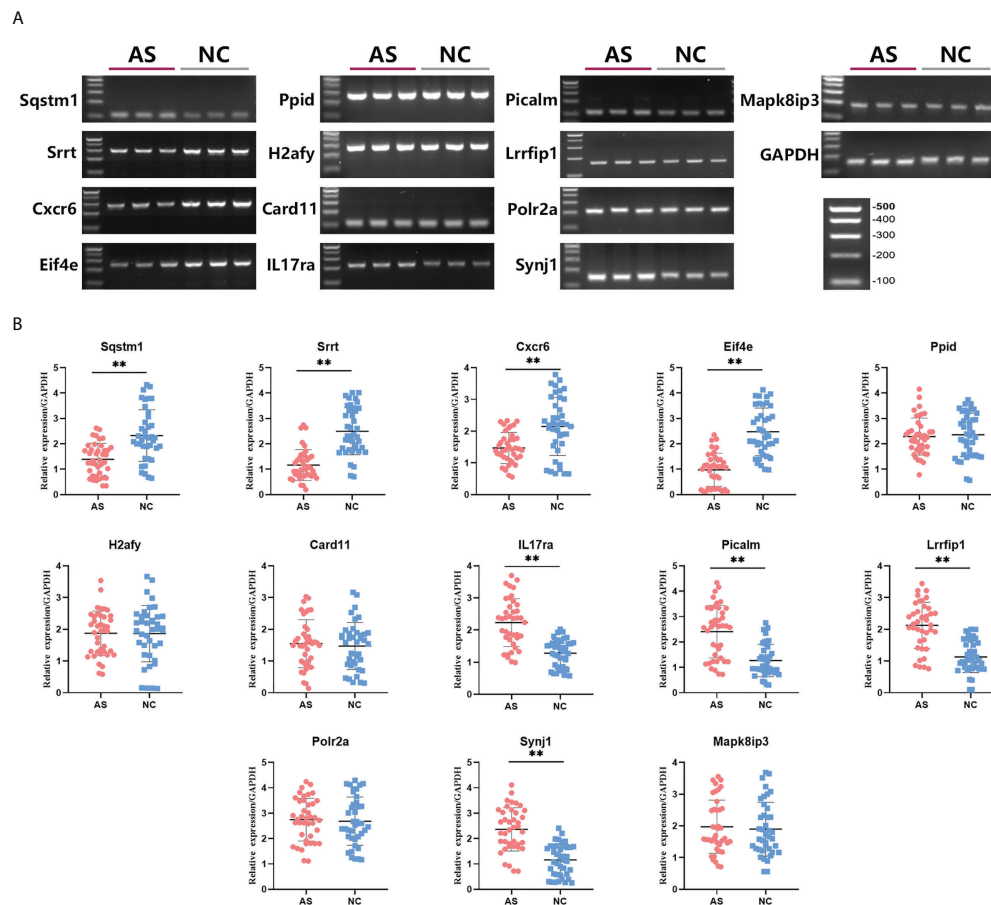


FIGURE 4

Differences in relative expression level of 13 key mRNAs between AS group and control group. Agarose electrophoresis (A) and qRT-PCR quantification (B) for *Sqstm1*, *Srrt*, *Cxcr6*, *Eif4e*, *Ppid*, *H2afy*, *Card11*, *IL17ra*, *Picalm*, *Lrrfip1*, *Polr2a*, *Synj1* and *Mapk8ip3*. ** means P-value < 0.01.

inflammatory damage and bone erosion in AS (31). In addition to the adaptive immune response, innate immune abnormalities also contribute to the initiation of AS (32). In AS, Tumor necrosis factor (TNF) mediates the destabilization of bone morphogenetic signaling proteins in osteoblasts and inhibits the expression of insulin-like growth factor-1, osterix and Runx2, resulting in poor osteoblastogenesis (33–35). Consistent with the preceding findings, the GSEA results of this study regarding GO terms in the Blue module showed the involvement of inflammatory and immune responses in AS, further verifying the imperative role of immune dysregulation in AS progression. However, the results of GO enrichment in Yellow and Gray modules revealed a negative relationship with immune response. Although the mRNAs in the Yellow and Gray modules seem to reflect uncorrelated effects with immune responses, the possibility of their synergism with the immune response cannot be ruled out and needs to be further explored.

In analyzing thousands of gene expression data through bioinformatic method, the “curse of dimensionality” cannot be

denied which severely impairs the accuracy of classification and prediction. To reduce the dimensionality, wrapper methods have been developed to be incorporated into a machine learning algorithm, which evaluate the values of different features according to the pre-estimated errors (36). SVM-RFE, as a novel established wrapper method for feature selection, can refine the optimum feature by ranking the coefficients of different features obtained by SVM (23). This is because the rank of each coefficient indirectly reflects the orthogonal degree between the feature and hyperplane generated by SVM. The orthogonality of a feature to the hyperplane signifies that this feature is more informative than others (23). In this study, we used a PPI network to identify 63 hub mRNAs that are already highly correlated with AS. However, to some extent, using these 63 mRNAs as biomarkers for further prediction is also a kind of high-dimensional modeling, which likewise encounters overfitting or other high-dimensional challenges. Therefore, to address these problems, we utilized SVM-RFE and optimally selected 13 out of the 63 feature mRNAs based on a 5-fold cross-

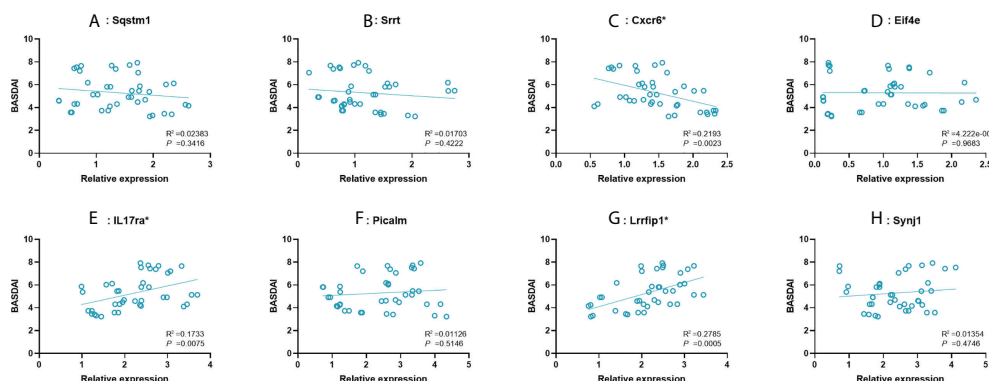


FIGURE 5

Correlation between expression value of 8 significant mRNAs and BASDAI. (A–H): Sqstm1, Srtr, Cxcr6, Eif4e, IL17ra, Picalm, Lrrfp1, Synj1. R², correlation coefficient. BASDAI, Bath Ankylosing Spondylitis Disease Activity Index; VAS, visual analog scale.

validation error rate. Moreover, ROC curves were subsequently plotted and reflected the significant specificities of these 13 key mRNAs for recognizing AS. Then, 8 of 13 key mRNAs (Sqstm1, Srtr, Cxcr6, Eif4e, IL17ra, Picalm, Synj1 and Lrrfp1) in AS blood sample showed significant consistence with microarray data in qRT-PCR validation, and 3 of them (Cxcr6, IL17ra, Lrrfp1) were correlated with symptomatic severity of AS, indicating the efficacy of SVM screening combined with bioinformatics.

IL-17ra is one of five well-known receptor subtypes for IL-17 ligands. When bound by IL-17, this receptor upregulates the expression of various cytokines and chemokines to exert a proinflammatory role in host defense. In whole blood, IL-17 and its receptors are mainly expressed in Th17 cells and neutrophils and were demonstrated to play a pivotal role in AS patients (37–39). Evidence suggests that the binding of IL17 to its receptor triggers several feedback-loop mechanisms in spondyloarthritis, resulting in the proliferation of Th17 cells, thereby causing increased production of IL-17 (40). This was further highlighted by the significant remission of AS symptoms after the application of inhibitory medication targeting IL-17 pathways (41, 42). In addition to IL-17RA, the downregulation of Sqstm1 in whole blood may be related to AS. As a kind of ubiquitin binding protein, Sqstm1 is reduced when autophagy is activated, which subsequently increases the level of IL23 in the intestinal mucosal surfaces of AS patients (43). Intriguingly, thus far, there is no robust proof to verify the direct involvement of the other significant feature mRNAs (Cxcr6, eIF4E, Lrrfp1, Srtr, Synj1 and Picalm) in AS pathogenesis. Cxcr6, eIF4E, and Lrrfp1, were found to be related to innate or adaptive immune processes. C-X-C Motif Chemokine Receptor 6 (CXCR6), a kind of chemokine receptor, is mainly expressed on the CD4⁺ T cell surface and mediates a series of immune cellular activation and chemotaxis events (44). Eukaryotic translation initiation factor 4E (eIF4E) is mainly expressed in macrophages and activated following the stimulation of LPS, leading to the upregulation of IκBα, which

inhibits the expression of inflammatory cytokines and genes (45). LRR Binding FLII Interacting Protein 1 (LRRFIP1) was found to be involved in the innate defense against pathogenic organisms and in the regulation of autoimmune disorders (46). In our study, upregulated IL-17RA and Cxcr6 were found to be positively correlated with BASDAI, while downregulated Lrrfp1 was negatively correlated, implying the potential of IL-17RA, Cxcr6 and Lrrfp1 in predicting AS symptom. In addition, the biological function of Srtr, Synj1 and Picalm has not been shown to be specific to AS, even though they are significant differential expressed in AS patients. But this does not mean that they are unqualified to serve as biomarkers. Their correlations with AS need further investigation to be elucidated in the future.

Undeniably, there was an inevitable limitation in our study. Because of the shortage of a proper microarray dataset for the whole blood of AS patients, there were not sufficient samples for randomly selecting and establishing a training set and testing set for machine learning, so we were incapable of further verifying the efficacy of the SVM classifier made of feature mRNAs. Further studies are expected to include more available datasets and verify the accuracy of prediction.

In summary, this study reveals that IL17RA, Sqstm1, Picalm, Eif4e, Srtr, Lrrfp1, Synj1, Cxcr6 can be seen as potential predictors for AS. These mRNAs may function *via* involvement in various pathways of AS, especially in immune-related pathways. Exploration of their function in AS pathology may be beneficial for the diagnosis of AS.

Data availability statement

The datasets presented in this study can be found in online repositories. The names of the repository/repositories and accession number(s) can be found in the article/Supplementary Material.

Ethics statement

The studies involving human participants were reviewed and approved by The Ethics Committee of Shanghai Changzheng Hospital. The patients/participants provided their written informed consent to participate in this study. Written informed consent was obtained from the individual(s) for the publication of any potentially identifiable images or data included in this article.

Author contributions

YL, YH, ZG, and XY were involved in the concept and design of the study. YL, YH, and YZ drafted the manuscript. YL, YH, YZ, HL, ZG, ZL, HW, BW and XY were involved in analysis and interpretation of the data and revision of the manuscript.

Funding

This study was supported by the National Key R&D Program of China (2020YFC2008404).

Conflict of interest

The authors declare that the research was conducted in the absence of any commercial or financial relationships that could be construed as a potential conflict of interest.

Publisher's note

All claims expressed in this article are solely those of the authors and do not necessarily represent those of their affiliated organizations, or those of the publisher, the editors and the reviewers. Any product that may be evaluated in this article, or claim that may be made by its manufacturer, is not guaranteed or endorsed by the publisher.

Supplementary material

The Supplementary Material for this article can be found online at: <https://www.frontiersin.org/articles/10.3389/fimmu.2022.956027/full#supplementary-material>

References

- Rudwaleit M, Khan MA, Sieper J. The challenge of diagnosis and classification in early ankylosing spondylitis: do we need new criteria? *Arthritis Rheum* (2005) 52:1000–8. doi: 10.1002/art.20990
- Feldtkeller E, Khan MA, van der Heijde D, van der Linden S, Braun J. Age at disease onset and diagnosis delay in HLA-B27 negative vs Positive patients ankylosing spondylitis. *Rheum Int* (2003) 23:61–6. doi: 10.3390/cells8020108
- Yang H, Chen Y, Xu W, Shao M, Deng J, Xu S, et al. Epigenetics of ankylosing spondylitis: Recent developments. *Int J Rheum Dis* (2021) 24:487–93. doi: 10.1111/1756-185X.14080
- Danve A, O'Dell J. The ongoing quest for biomarkers in ankylosing spondylitis. *Int J Rheum Dis* (2015) 18:826–34. doi: 10.1111/1756-185X.12779
- Reveille JD. Genetics of spondyloarthritis-beyond. *Nat Rev Rheum* (2012) 8:296–304. doi: 10.1038/nrrheum.2012.41
- Toivanen P, Toivanen A. Two forms of reactive arthritis? *Ann Rheum Dis* (1999) 58:737–41. doi: 10.1136/ard.58.12.737
- Eder L, Chandran V, Pellet F, Shanmugarajah S, Rosen CF, Bull SB, et al. Human leucocyte antigen risk alleles for psoriatic arthritis among patients with psoriasis. *Ann Rheum Dis* (2012) 71:50–5. doi: 10.1136/ard.2011.155044
- Visvanathan S, Wagner C, Marini JC, Baker D, Gathany T, Han J, et al. Inflammatory biomarkers, disease activity and spinal disease measures in patients with ankylosing spondylitis after treatment with infliximab. *Ann Rheum Dis* (2008) 67:511–7. doi: 10.1136/ard.2007.071605
- Maksymowich WP, Landewé R, Conner-Spady B, Dougados M, Mielants H, van der Tempel H, et al. Serum matrix metalloproteinase 3 is an independent predictor of structural damage progression in patients with ankylosing spondylitis. *Arthritis Rheum* (2007) 56:1846–53. doi: 10.1002/art.22589
- Arends S, van der Veer E, Groen H, Houtman PM, Jansen TLTA, Leijnsma MK, et al. Serum MMP-3 level as a biomarker for monitoring and predicting response to etanercept treatment in ankylosing spondylitis. *J Rheum* (2011) 38:1644–50. doi: 10.3899/jrheum.101128
- Kanwal A, Fazal S. Construction and analysis of protein-protein interaction network correlated with ankylosing spondylitis. *Gene* (2018) 638:41–51. doi: 10.1016/j.gene.2017.09.049
- Langfelder P, Horvath S. WGCNA: an R package for weighted correlation network analysis. *BMC Bioinf* (2008) 9:559. doi: 10.1186/1471-2105-9-559
- Chen L, Yuan L, Qian K, Qian G, Zhu Y, Wu C-L, et al. Identification of biomarkers associated with pathological stage and prognosis of clear cell renal cell carcinoma by Co-expression network analysis. *Front Physiol* (2018) 9:399. doi: 10.3389/fphys.2018.00399
- Cebeci O, Budak H. Global expression patterns of three festuca species exposed to different doses of glyphosate using the affymetrix GeneChip wheat genome array. *Comp Funct Genomics* (2009) 2009:505701. doi: 10.1155/2009/505701
- Duan K-B, Rajapakse JC, Wang H, Azuaje F. Multiple SVM-RFE for gene selection in cancer classification with expression data. *IEEE Trans Nanobioscience* (2005) 4:228–34. doi: 10.1109/TNB.2005.853657
- Zhou X, Tuck DP. MSVM-RFE: extensions of SVM-RFE for multiclass gene selection on DNA microarray data. *Bioinformatics* (2007) 23:1106–14. doi: 10.1093/bioinformatics/btm036
- van der Linden S, Valkenburg HA, Cats A. Evaluation of diagnostic criteria for ankylosing spondylitis. a proposal for modification of the new York criteria. *Arthritis Rheum* (1984) 27:361–8. doi: 10.1002/art.1780270401
- Gracey E, Yao Y, Green B, Qiayum Z, Baglaenko Y, Lin A, et al. Sexual dimorphism in the Th17 signature of ankylosing spondylitis. *Arthritis Rheum* (2016) 68:679–89. doi: 10.1002/art.39464
- Lakshminarayanan K, Harp SA, Samad T. Imputation of missing data in industrial databases. *Appl Intell* (1999) 11:259–75. doi: 10.1023/A:1008334909089
- Gautier L, Cope L, Bolstad BM, Irizarry RA. Affy-analysis of affymetrix GeneChip data at the probe level. *Bioinformatics* (2004) 20:307–15. doi: 10.1093/bioinformatics/btg405
- Yang Y, Lu Q, Shao X, Mo B, Nie X, Liu W, et al. Development of a three-gene prognostic signature for hepatitis b virus associated hepatocellular carcinoma based on integrated transcriptomic analysis. *J Cancer* (2018) 9:1989–2002. doi: 10.7150/jca.23762
- Yang Y, Zheng H, Wang C, Xiao W, Liu T. Predicting apoptosis protein subcellular locations based on the protein overlapping property matrix and tri-gram encoding. *Int J Mol Sci* (2019) 20(9):2344. doi: 10.3390/ijms20092344

23. Guyon I, Weston J, Barnhill S, Vapnik V. Gene selection for cancer classification using support vector machines. *Machine Learning* (2002) 46(1–3):389–422.
24. Zhang B, Horvath S. A general framework for weighted gene co-expression network analysis. *Stat Appl Genet Mol Biol* (2005) 4(1). doi: 10.2202/1544-6115.1128
25. Zhao B, Wang J, Li M, Wu F-X, Pan Y. Prediction of essential proteins based on overlapping essential modules. *IEEE Trans Nanobioscience* (2014) 13:415–24. doi: 10.1109/TNB.2014.2337912
26. Brown MA, Kennedy LG, MacGregor AJ, Darke C, Duncan E, Shatford JL, et al. Susceptibility to ankylosing spondylitis in twins: the role of genes. *HLA Environ. Arthritis Rheum* (1997) 40:1823–8. doi: 10.1002/art.1780401015
27. Huang C-H, Wei JC-C, Chang W-C, Chiou S-Y, Chou C-H, Lin Y-J, et al. Higher expression of whole blood microRNA-21 in patients with ankylosing spondylitis associated with programmed cell death 4 mRNA expression and collagen cross-linked c-telopeptide concentration. *J Rheum* (2014) 41:1104–11. doi: 10.3899/jrheum.130515
28. McVeigh CM, Cairns AP. Diagnosis and management of ankylosing spondylitis. *BMJ* (2006) 333:581–5. doi: 10.1136/bmj.38954.689583.DE
29. Wei JC-C, Leong P-Y, Liu G-Y. Chaperone/scaffolding/adaptor protein 14-3-3 η (eta): A diagnostic marker of rheumatoid arthritis. *Int J Rheum Dis* (2020) 23:1439–42. doi: 10.1111/1756-185X.14004
30. Mauro D, Thomas R, Guggino G, Lories R, Brown MA, Ciccia F. Ankylosing spondylitis: an autoimmune or autoinflammatory disease? *Nat Rev Rheum* (2021) 17:387–404. doi: 10.1038/s41584-021-00625-y
31. Lata M, Hettinghouse AS, Liu C-J. Targeting tumor necrosis factor receptors in ankylosing spondylitis. *Ann N Y Acad Sci* (2019) 1442(1):5–16. doi: 10.1111/nyas.13933
32. Vanaki N, Aslani S, Jamshidi A, Mahmoudi M. Role of innate immune system in the pathogenesis of ankylosing spondylitis. *BioMed Pharmacother* (2018) 105:130–43. doi: 10.1016/j.biopha.2018.05.097
33. Gilbert L, He X, Farmer P, Rubin J, Drissi H, van Wijnen AJ, et al. Expression of the osteoblast differentiation factor RUNX2 (Cbfa1/AML3/Peap2alpha a) is inhibited by tumor necrosis factor-alpha. *J Biol Chem* (2002) 277:2695–701. doi: 10.1074/jbc.M106339200
34. Gilbert LC, Rubin J, Nanes MS. The p55 TNF receptor mediates TNF inhibition of osteoblast differentiation independently of apoptosis. *Am J Physiol Endocrinol Metab* (2005) 288:E1011–8. doi: 10.1152/ajpendo.00534.2004
35. Abbas S, Zhang Y-H, Clohisy JC, Abu-Amer Y. Tumor necrosis factor-alpha inhibits pre-osteoblast differentiation through its type-1 receptor. *Cytokine* (2003) 22:33–41. doi: 10.1016/S1043-4666(03)00106-6
36. Inza I, Sierra B, Blanco R, Larrañaga P. Gene selection by sequential search wrapper approaches in microarray cancer class prediction. *J Intell Fuzzy Syst Appl Eng Technol* (2002) 12:25–33.
37. Miossec P, Kolls JK. Targeting IL-17 and TH17 cells in chronic inflammation. *Nat Rev Drug Discovery* (2012) 11:763–76. doi: 10.1038/nrd3794
38. McGonagle DG, McInnes IB, Kirkham BW, Sherlock J, Moots R. The role of IL-17A in axial spondyloarthritis and psoriatic arthritis: recent advances and controversies. *Ann Rheum Dis* (2019) 78:1167–78. doi: 10.1136/annrheumdis-2019-215356
39. Gu J, Wei Y-L, Wei JCC, Huang F, Jan M-S, Centola M, et al. Identification of RGS1 as a candidate biomarker for undifferentiated spondylarthritis by genome-wide expression profiling and real-time polymerase chain reaction. *Arthritis Rheum* (2009) 60:3269–79. doi: 10.1002/art.24968
40. Benedetti G, Miossec P. Interleukin 17 contributes to the chronicity of inflammatory diseases such as rheumatoid arthritis. *Eur J Immunol* (2014) 44:339–47. doi: 10.1002/eji.201344184
41. van der Heijde D, Cheng-Chung Wei J, Dougados M, Mease P, Deodhar A, Maksymowych WP, et al. Ixekizumab, an interleukin-17A antagonist in the treatment of ankylosing spondylitis or radiographic axial spondyloarthritis in patients previously untreated with biological disease-modifying anti-rheumatic drugs (COAST-v): 16 week results of a phase 3 randomised, double-blind, active-controlled and placebo-controlled trial. *Lancet* (2018) 392:2441–51. doi: 10.1016/S0140-6736(18)31946-9
42. Deodhar A, Poddubnyy D, Pacheco-Tena C, Salvarani C, Lespessailles E, Rahman P, et al. Efficacy and safety of ixekizumab in the treatment of radiographic axial spondyloarthritis: Sixteen-week results from a phase III randomized, double-blind, placebo-controlled trial in patients with prior inadequate response to or intolerance of tumor necrosis factor inhibitors. *Arthritis Rheum* (2019) 71:599–611. doi: 10.1002/art.40753
43. Ciccia F, Accardo-Palumbo A, Rizzo A, Guggino G, Raimondo S, Giardina A, et al. Evidence that autophagy, but not the unfolded protein response, regulates the expression of IL-23 in the gut of patients with ankylosing spondylitis and subclinical gut inflammation. *Ann Rheum Dis* (2014) 73:1566. doi: 10.1136/annrheumdis-2012-202925
44. Heesch K, Raczkowski F, Schumacher V, Hünemörder S, Panzer U, Mittrücker H-W. The function of the chemokine receptor CXCR6 in the T cell response of mice against listeria monocytogenes. *PLoS One* (2014) 9:e97701. doi: 10.1371/journal.pone.0097701
45. Bao Y, Wu X, Chen J, Hu X, Zeng F, Cheng J, et al. Brd4 modulates the innate immune response through Mnk2-eIF4E pathway-dependent translational control of IkB α . *Proc Natl Acad Sci USA* (2017) 114:E3993–4001. doi: 10.1073/pnas.1700109114
46. Takimoto M. Multidisciplinary roles of LRRFIP1/GCF2 in human biological systems and diseases. *Cells* (2019) 8(2):108. doi: 10.3390/cells8020108



OPEN ACCESS

EDITED BY

Heinrich Korner,
University of Tasmania, Australia

REVIEWED BY

Saartjie Roux,
Nelson Mandela University, South Africa
Fulvio Mattivi,
University of Trento, Italy

*CORRESPONDENCE

Yan Wang,
wangyan@imm.ac.cn
Jian-Dong Jiang,
jjiang.jdong@163.com

SPECIALTY SECTION

This article was submitted to
Inflammation Pharmacology,
a section of the journal
Frontiers in Pharmacology

RECEIVED 13 April 2022

ACCEPTED 26 August 2022

PUBLISHED 27 September 2022

CITATION

Xu H, Pan L-B, Yu H, Han P, Fu J,
Zhang Z-W, Hu J-C, Yang X-Y,
Keranmu A, Zhang H-J, Bu M-M,
Jiang J-D and Wang Y (2022), Gut
microbiota-derived metabolites in
inflammatory diseases based on
targeted metabolomics.
Front. Pharmacol. 13:919181.
doi: 10.3389/fphar.2022.919181

COPYRIGHT

© 2022 Xu, Pan, Yu, Han, Fu, Zhang, Hu,
Yang, Keranmu, Zhang, Bu, Jiang and
Wang. This is an open-access article
distributed under the terms of the
[Creative Commons Attribution License](#)
(CC BY). The use, distribution or
reproduction in other forums is
permitted, provided the original
author(s) and the copyright owner(s) are
credited and that the original
publication in this journal is cited, in
accordance with accepted academic
practice. No use, distribution or
reproduction is permitted which does
not comply with these terms.

Gut microbiota-derived metabolites in inflammatory diseases based on targeted metabolomics

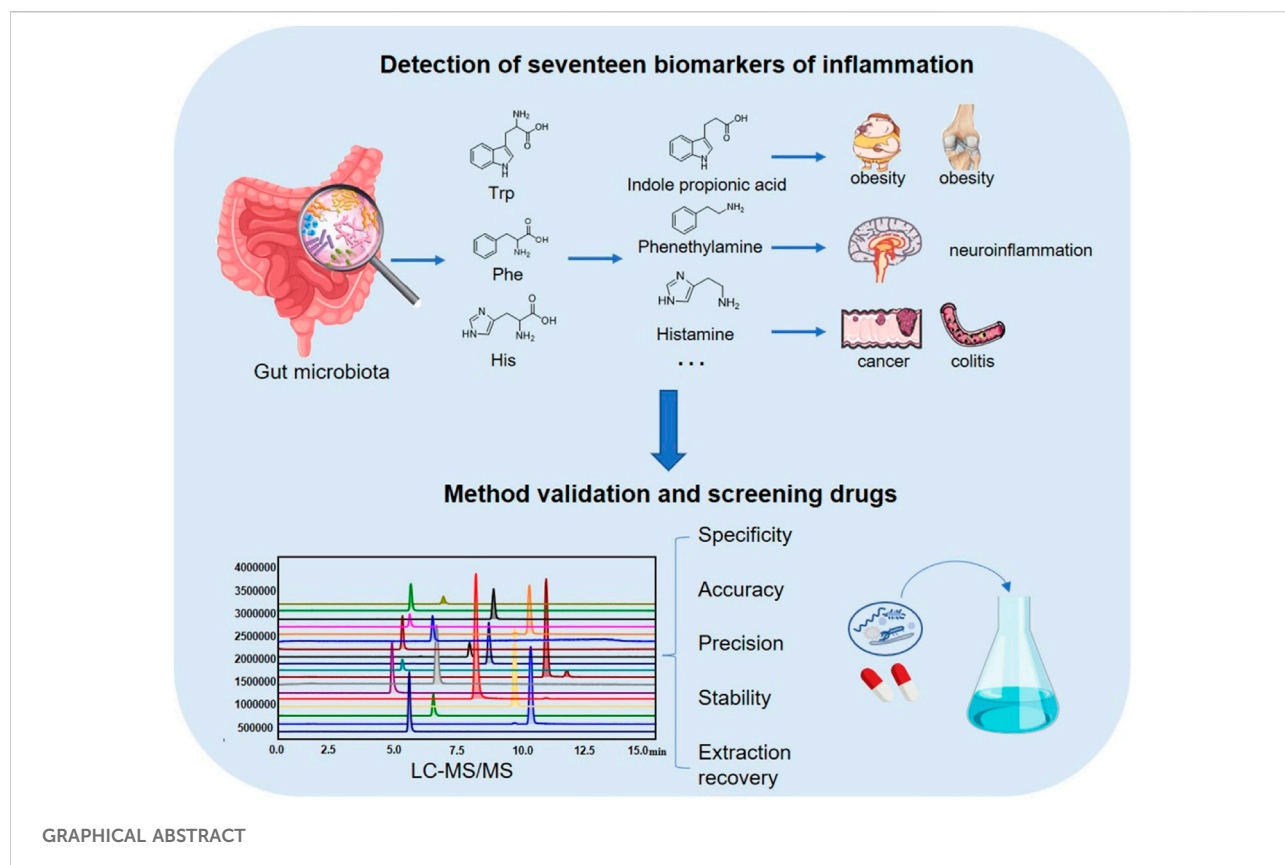
Hui Xu, Li-Bin Pan, Hang Yu, Pei Han, Jie Fu, Zheng-Wei Zhang,
Jia-Chun Hu, Xin-Yu Yang, Adili Keranmu, Hao-Jian Zhang,
Meng-Meng Bu, Jian-Dong Jiang* and Yan Wang*

State Key Laboratory of Bioactive Substance and Function of Natural Medicines, Institute of Materia Medica, Chinese Academy of Medical Sciences/Peking Union Medical College, Beijing, China

The gut microbiota plays an important role in inflammatory diseases. Metabolites in the three metabolic pathways of tryptophan (Trp), histidine (His), and phenylalanine (Phe) can affect various inflammatory conditions, such as obesity, diabetes, arthritis, colitis, atherosclerosis, and neuroinflammation. We established an LC-MS/MS method to measure 17 metabolites—Trp, 3-indole-acetic acid (Iaa), 3-indole-lactate (Ila), 3-indole-propionic acid (Ipa), 3-indole formaldehyde (Iald), kynurenine (Kn), kynurenic acid (Kyna), 3-Hydroxyanthranilic acid (3-Haa), His, 3-methylhistidine (3-Mhis), histamine (Hist), imidazole propionic acid (Imp), 4-imidazoacetic acid (Imaa), urocanic acid (Ua), Phe, phenylethylamine (Pea), and hippuric acid (Ha)—in the three metabolic pathways. The method exhibited high sensitivity and good selectivity, linearity, accuracy, precision, stability; and recovery rate; all met the requirements of biological sample analysis. By establishing a rheumatoid arthritis (RA) model of Sprague-Dawley rats and performing 16S rRNA sequencing on their feces, it was found that there was dysbiosis, including changes in phylum level, genus level, and α biodiversity of gut bacteria. The contents of the microbiota metabolites Iaa and Ipa in the model group were significantly decreased, and those of Iald, Kn, Kyna, Ha, and Imp were significantly increased. The common therapeutic drugs *Tripterygium* glycosides, total glucosides of peony, and their main active ingredients were screened by *in vitro* incubation with gut bacteria: it was found that *Tripterygium* glycosides and their active ingredients could lead to a variation in metabolites in the Trp and Phe pathways. Total glucosides and active components of peony could lead to a variation in metabolites in the Phe pathway of the gut microbiota.

KEYWORDS

inflammatory diseases, amino acid metabolites, tryptophan, phenylalanine, histidine, gut microbiota, LC-MS/MS



Introduction

Inflammation is the body's defense response to stimuli such as infection and tissue damage, including acute and chronic inflammation. Acute inflammation is of short duration, while chronic inflammation is associated with the immune system and underlies the progression of diseases such as obesity (Truax et al., 2018), diabetes (Kanazawa et al., 2021), arthritis (Vadell et al., 2020), inflammatory bowel disease (Silverberg et al., 2005), cardiovascular diseases (Ridker et al., 2019), neurological disease (Jensen et al., 2019), cancer (Singh N. et al., 2019), and autoimmune disease (Cai et al., 2019). These inflammatory diseases seriously affect human health and quality of life. Although they are also influenced by important factors other than inflammation, inhibition of inflammation often improves the clinical symptoms of these diseases (Ridker et al., 2017; Jensen et al., 2019; Vadell et al., 2020; Chicco et al., 2021). However, the mode of action of inflammation is very complex and has not yet been fully elucidated.

There are more than 100 trillion microorganisms in the human intestine, collectively referred to as the "gut microbiota", which play a very important role in maintaining human health and are considered the "invisible organ" of the human body (Collins and Patterson, 2020; Pan et al., 2020; Wang et al., 2021). In recent years,

the pathogenesis of inflammation-related diseases has been shown to be closely related to the gut microbiota, including intestinal inflammation, inflammation of organs other than the gut, and systemic inflammation (Yang et al., 2020b; Zhang X. et al., 2021; He et al., 2021; Shang et al., 2021). Targeting the gut microbiota for the treatment of inflammatory diseases has great potential. The mechanism of gut microbiota involvement in the occurrence and development of inflammatory diseases is very complex, and research on how intestinal metabolites and the host interact to affect diseases is a hot topic. The influence of gut metabolites on the inflammation of organs other than the gut and on systemic inflammation is mainly because the metabolites can be absorbed into the blood by intestinal epithelial cells to enter systemic circulation.

We selected the metabolic pathways of three essential amino acids—tryptophan (Trp), phenylalanine (Phe), and histidine (His)—which are closely related to inflammation. The metabolism of Trp by bacteria is mainly divided into two pathways: indole and kynurenine. A portion of Trp is metabolized into Iaa, Ipa, Ila, and Iald, which are released into the systemic circulation. Trp is metabolized by *Lactobacilli* in the gut through aromatic amino acid aminotransferase (ArAT) and indole lactate dehydrogenase (ILDH) to the intermediate product indolepyruvate, which further generates Iald. *Peptostreptococcus* bacteria such as *P. anaerobius* and *P. stomatis* that contain the

TABLE 1 Optimized multiple reaction monitoring (MRM, positive) and mass spectrometry (MS) conditions.

Analyte	Formula	MW	Precursor Ion (m/z)	Quantification (m/z)	Quantifier (m/z)	Q1 CE (volt)	Q2 CE (volt)	Q3 CE (volt)
Hippuric acid (Ha)	C ₉ H ₉ NO ₃	179.17	179.75	105.05	77.00	-21.0	-13.0	-10.0
Imidazole-4-acetic acid (Imaa)	C ₅ H ₆ N ₂ O ₂	126.11	127.00	54.00	81.10	-13.0	-30.0	-19.0
Phenylethylamine (Pea)	C ₈ H ₁₁ N	121.18	122.05	77.05	105.05	-12.0	-28.0	-13.0
3-Methylhistidine (3-Mhis)	C ₇ H ₁₁ N ₃ O ₂	169.18	170.00	94.95	109.10	-10.0	-30.0	-29.0
Urocanic acid (Ua)	C ₆ H ₆ N ₂ O ₂	138.12	139.00	93.00	121.10	-15.0	-22.0	-15.0
Imidazole propionic acid (Imp)	C ₆ H ₈ N ₂ O ₂	140.14	140.95	81.10	123.05	-10.0	-22.0	-30.0
Tryptophan (Trp)	C ₁₁ H ₁₂ N ₂ O ₂	204.23	205.00	189.20	146.10	-16.0	-10.0	-17.0
Phenylalanine (Phe)	C ₉ H ₁₁ NO ₂	165.19	166.00	120.10	103.00	-12.0	-13.0	-11.0
Histidine (His)	C ₆ H ₉ N ₃ O ₂	155.15	156.00	110.05	93.00	-10.0	-15.0	-10.0
Histamine (Hist)	C ₅ H ₉ N ₃	111.15	112.05	95.10	83.04	-10.0	-15.0	-18.0
Indole formaldehyde Iald)	C ₉ H ₇ NO	145.16	145.95	91.05	118.00	-16.0	-26.0	-13.0
Kynurenic acid (Kyna)	C ₁₀ H ₇ NO ₃	189.17	189.90	144.00	171.96	-13.0	-19.0	-13.0
Indole lactic acid (Ila)	C ₁₁ H ₁₁ NO ₃	205.21	205.90	130.00	117.89	-15.0	-33.0	-20.0
Indole acetic acid (Iaa)	C ₁₀ H ₉ NO ₂	175.18	176.00	130.00	77.03	-12.0	-14.0	-20.0
Indole propionic acid (Ipa)	C ₁₁ H ₁₁ NO ₂	189.20	189.95	130.15	55.01	-10.0	-17.0	-19.0
Kynurenine (Kn)	C ₁₀ H ₁₂ N ₂ O ₃	208.22	209.10	192.00	146.00	-15.0	-11.0	-18.0
3-Hydroxyanthranilic acid (3-Haa)	C ₇ H ₇ NO ₃	153.14	153.90	136.00	108.00	-18.0	-14.0	-22.0

phenyllactate dehydratase gene cluster (fldAIBC) in the gut can metabolize Trp into Iaa, Ipa, and Ila (Włodarska et al., 2017; Roager and Licht, 2018). The other portion of Trp is metabolized into Kn by indoleamine 2,3-dioxygenase 1 (IDO1) and Kyna; Kn is further converted into 3-Haa through hydroxylation (Agus et al., 2018). Phe is produced in the gut microbiota by *Morganella morganii* decarboxylase to phenylethylamine. It is first metabolized into trans-cinnamic acid, which is further metabolized to hippuric acid. His is produced by histidine decarboxylase (HDC) to generate histamine, which is further oxidized to imidazole-4-acetic acid. Histamine is a well-known proinflammatory factor that induces different immune cells to produce inflammatory mediators and cytokines (Branco et al., 2018). His is degraded by histidine ammonia lyase (HAL) or histidase to urocanic acid, which is reduced to imidazole propionic acid by urocanic acid reductase (Acuña et al., 2021). These amino acid metabolites are closely related to inflammatory diseases. The Trp metabolite Iald can activate aromatic hydrocarbon receptor (AHR) and induce the expression of interleukin-22 (IL-22) to improve the intestinal barrier and alleviate colitis in mice (Teng et al., 2018). The His metabolite histamine can modulate NLRP6 inflammasome signaling and downstream antimicrobial peptide secretion, promote interleukin-18 (IL-18) secretion from intestinal epithelial cells, and shape the gut microenvironment through the metabolite-inflammasome-antimicrobial peptide axis (Levy et al., 2015). Phe metabolites are related to neuritis. Therefore, the search for inflammation-related amino acid

microbiota metabolites is of great significance for elucidating the mechanisms of various inflammatory diseases and screening drugs.

Although many LC-MS/MS analytical methods for determining Trp metabolites have been reported in the literature, there are few analytical methods for His and Phe metabolites, and there is still no simultaneous analytical method for the determination of the 17 metabolites on three metabolic pathways of Trp, His, and Phe (Fuertig et al., 2016; Wang et al., 2019). We constructed a simple and rapid LC-MS/MS analytical method with sufficient sensitivity to detect intestinal content; this method can be applied to various inflammatory diseases as targeted metabolomics.

Materials and methods

Reagents and materials

Trp, indole acetic acid (Iaa), indole propionic acid (Ipa), indole lactic acid (Ila), kynurenine (Kn), kynurenic acid (Kyna), His, histamine (Hist), urocanic acid (Ua), Phe, hippuric acid (Ha), acetaminophen (IS), triptolide (TL), celastrol (CSL), wilforine (WR), wilforide A, and triptonide (TN), paeoniflorin, albiflorin std, and benzoylpaeoniflorin were purchased from Solarbio Scientific Ltd. (Beijing, China). 3-hydroxyanthranilic acid (3-Haa) and indole formaldehyde (Iald) were purchased from Yuanye Biotechnology Co., Ltd.

(Shanghai, Beijing). Imidazole propionic acid (Imp), imidazole-4-acetic acid (Imaa), 3-methyl-L-histidine (3-Mhis), and phenethylamine (Pea) were purchased from Aladdin Biochemical Technology Co., Ltd. (Shanghai, China). The purities of all the reference standards were greater than 98%. *Tripterygium wilfordii* polyglycoside tablets (henceforth referred to as “*Tripterygium* glycosides”) were purchased from Zhejiang Deen Pharmaceutical Co., Ltd. (Hangzhou, China). Total glucosides of white peony capsules (henceforth referred to as “total glucosides of peony”) were purchased from Ningbo Lihua Pharmaceutical Co., Ltd. Formic acid (100%), complete Freund’s adjuvant, and isoflurane were purchased from Merck (Darmstadt, Germany). Acetonitrile and methanol were purchased from Fisher Scientific (HPLC grade, Fairlawn, United States). Deionized distilled water was purchased from Hangzhou Wahaha Group Co., Ltd. (Hangzhou, China). TNF- α , IL-1 β , and IL-6 kits were purchased from Nanjing Jiancheng Bioengineering Institute (Nanjing, China). Anaerobic culture medium was purchased from Qingdao Hope Bio-Technology Co., Ltd. (Qingdao, China).

Instruments

A high-performance liquid chromatography–mass spectrometry (LC–MS/MS 8060, Shimadzu, Japan) instrument was utilized. A vortex mixer (VortexGenie2, United States), a small benchtop high-speed centrifuge (Eppendorf 5418, Germany), a 1–14 small benchtop high-speed centrifuge (D-37520, Sigma, Germany), an analytical balance (XS1050U, Mettler - Toledo, Switzerland), an incubator shaker (LYZ-100, Shanghai Longyue Co., Ltd., China), and a nitrogen vaporizer (MD 200-2, Hangzhou Diansheng Instrument Co., Ltd., China) were utilized.

Animals

Sprague–Dawley rats (180–220 g, 6–8 weeks, male) were provided by Beijing Huafukang Biotechnology Co., Ltd. (Beijing, China). All animals had free access to food and water. The temperature was maintained at 22–24°C with a light/dark cycle of 12 h and a relative humidity of 40–60%. Fresh stool samples were collected in sterile nitrogen-filled zip-lock bags and kept at –70°C.

LC–MS/MS conditions

Analysis was performed using a liquid chromatography–tandem mass spectrometer LC–MS/MS 8060 (Shimadzu, Japan) equipped with an ESI source. Separation was performed using a C18 column (250 mm \times 4.6 mm \times 5 μ m, SVEA, Sweden). The flow rate was 0.4 ml/min, and the column temperature was maintained

at 25°C. The mobile phases were formic acid: water (0.1:100, v/v) as mobile phase A, and methanol:acetonitrile (1:1) and 0.1% formic acid as mobile phase B. The binary gradient elution conditions were: (A:B): 0.01 min–5 min, 70:30→5:95; 5–8 min, 5:95; 8.01 min–16 min, 70:30. Detection was performed using multiple reaction monitoring (MRM) in positive mode, and the optimized MRM parameters for each compound are shown in [Table 1](#). The mass condition parameters were set as: nebulizer gas, 3 L/min; drying gas, 10.0 L/min; heating gas, 10.0 L/min; interface temperature, 300°C; collision-induced dissociation (CID) gas, 230 kPa; DL temperature, 250°C; thermal block temperature, 400°C; interface voltage, –4.5 kV. The autosampler was kept at 4°C.

Standard solutions and sample preparation

Trp, Kn, Phe, His, Hist, 3-Mhis, Ua, and Pea were dissolved in 2% aqueous formic acid, and Iaa, Ila, Ipa, Iald, Kyna, 3-Haa, Imp, Ha, and Imaa were dissolved in methanol containing 2% formic acid, all prepared to 1 mg/ml, for use. The IS was dissolved in methanol containing 2% formic acid to prepare 1 mg/ml. The lower limits of quantitation and detection were determined by serial dilutions of the non-matrix stock solution in methanol containing 2% formic acid. After mixing the intestinal contents of 20 normal rats, anaerobic culture medium at a 1:20 (weight: volume) ratio as matrix was added. Calibration standards were prepared by spiking the mixed stocking solutions at a volume ratio of 1:9, then adding at a volume ratio of 1:3 of methanol containing IS (1 μ g/ml) and 2% formic acid (100, 200, 500, 1000, 2000, 8000, 10,000, and 12500 ng/ml for Trp, Phe, His, and Imp; 20, 40, 100, 200, 400, 1000, 2000, and 2500 ng/ml for other compounds); 5 μ L of the supernatant was taken for injection after centrifugation at 12,000 rpm for 10 min at 4°C. Low concentration QC, medium concentration QC, and high concentration QC were prepared by spiking the mixed stocking solutions in matrix at a volume ratio of 1:9 (200, 2000, and 10,000 ng/ml for Trp, Phe, His, and Imp; 40, 400, and 2000 ng/ml for other compounds). The specific steps are shown in [Supplementary Figure S1](#). For sample preparation, added methanol solution containing IS (1 μ g/ml) and 2% formic acid at a volume ratio of 1:3.5 μ L of the supernatant was taken for injection after centrifugation at 12,000 rpm for 10 min at 4°C.

Method validation

Specificity and residue

Specificity was obtained by comparing the chromatogram of the standard added to the matrix to the chromatogram of the matrix. After five consecutive injections of high concentration quality control (HQC), the residue was judged by the response of the injection blank solvent.

Accuracy and precision

Accuracy was assessed on samples of known analytes, using three batches of quality control samples with high, medium, and low concentrations, five samples per concentration, and expressed as measured value/true value*100%.

Precision was repeated for three consecutive days using three batches of high, medium, and low concentrations of quality control samples, with five samples per concentration; the precision was expressed as the relative standard deviation.

Linear range and lower limit of quantitation

A non-zero calibration curve was established by plotting the peak area ratio of analyte to internal standard (Y) versus the nominal concentration of compound added to the matrix sample (X). The correlation coefficient (R^2) was used to assess linearity and was fitted with a weighting factor of $1/X$. The linear range was accepted when the relative error of the calibrator was within $\pm 15\%$ of the theoretical concentration.

The lower limit of quantification was determined by continuous dilution of the standard solution. A signal-to-noise (S/N) ratio greater than 3 for each compound is the LLOD, and an S/N greater than 10 is the instrument's LLOQ.

Stability

Stability was assessed using spiked samples (LQC, MQC, and HQC), five samples of each concentration, placed at 4°C for 12 h before or after sample treatment, or by repeated freeze–thaw cycles at -20°C before treatment three times. Stability was calculated by the ratio of the concentration of each compound before treatment to the concentration of the corresponding sample after treatment. Data in the 85–115% range are considered stable.

Extraction recovery

Extraction recovery is the ratio of sample concentration after extraction/before extraction; data in the 85–115% range are considered acceptable.

Matrix effect

Matrix effect = (concentration of standard-spiked samples – concentration of matrix)/standards free from matrix.

Establishment of a rat model of rheumatoid arthritis

Ten Sprague-Dawley rats (male, 6–8 weeks) were randomly divided into two groups—a blank control group and a model group—with five animals in each group. After isoflurane anesthesia, 100 μL of normal saline was injected into the soles of the right feet of the blank group, and 100 μL of complete Freund's adjuvant was injected into the soles of the right feet of the model group. After 21 days, the exact same procedure was

repeated. After 25 days, the rats were weighed, fresh feces and blood were collected, and the rats were sacrificed by removing their cervical vertebrae. The contents of intestinal bacteria were collected, and the spleen was weighed.

16S rRNA sequencing of feces

The DNA extraction

DNA was extracted using PowerSoil DNA Isolation Kit (MoBio Laboratories, Carlsbad, CA) following the manual. Purity and quality of the genomic DNA were checked on 1% agarose gels and a NanoDrop spectrophotometer (Thermo Scientific).

PCR amplification

The V3-4 hypervariable region of bacterial 16S rRNA gene were amplified with the primers 338F (ACTCCTACGGGAGGC AGCAG) and 806R (GGACTACHVGGGTWTCTAAT). For each fecal sample, a ten-digit barcode sequence was added to the 5' end of the forward and reverse primers (provided by Allwegene Company, Beijing). The PCR was carried out on a Mastercycler Gradient (Eppendorf, Germany) using 25 μL reaction volumes, containing 12.5 μL KAPA 2G Robust Hot Start Ready Mix, 1 μL Forward Primer (5 μM), 1 μL Reverse Primer (5 μM), 5 μL DNA (total template quantity is 30 ng), and 5.5 μL H_2O . Cycling parameters were 95°C for 5 min, followed by 28 cycles of 95°C for 45 s, 55°C for 50 s, and 72°C for 45 s, with a final extension at 72°C for 10 min. The PCR products were purified using a Agencourt AMPure XP Kit.

High throughput sequencing

Deep sequencing was performed on the Miseq platform at Allwegene Company (Beijing). After the run, image analysis, base calling, and error estimation were performed using Illumina Analysis Pipeline Version 2.6.

Data analyses

The raw data were first screened: sequences were removed from consideration if they were shorter than 230 bp, had a low-quality score (≤ 20), contained ambiguous bases, or did not exactly match the primer sequences and barcode tags. Qualified reads were separated using the sample-specific barcode sequences and trimmed with Illumina Analysis Pipeline Version 2.6. The dataset was then analyzed using QIIME. The sequences were clustered into operational taxonomic units (OTUs) at a similarity level of 97%, to generate rarefaction curves and calculate the richness and diversity indices (including Chao 1, Observed_ species, PD_ whole_ trees, and Shannon indices). Histogram analysis of α biodiversity was performed using GraphPad Prism 8. The Ribosomal Database

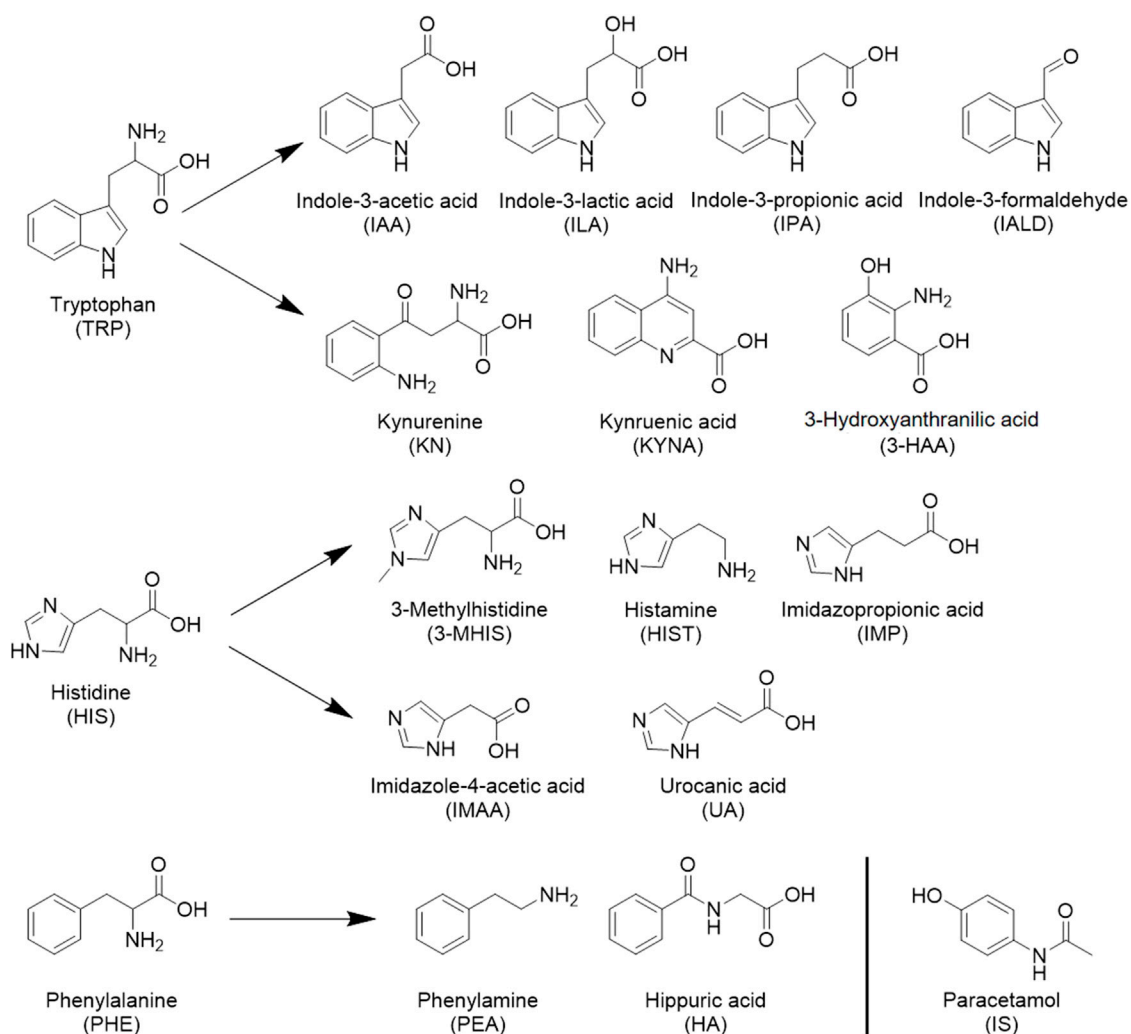


FIGURE 1
Seventeen metabolites and internal standard structural formulas measured.

Project (RDP) Classifier tool was used to classify all sequences into different taxonomic groups. To examine the similarity between different samples, clustering analyses and PCA were used based on the OTU information from each sample using R. The evolution distances between microbial communities from each sample were calculated using the Bray Curtis algorithms and represented as an unweighted pair group method with an arithmetic mean (UPGMA) clustering tree describing the dissimilarity (1-similarity) between multiple samples. A Newick-formatted tree file was generated using this analysis. To compare the membership and structure of communities in different samples, histogram analysis of changes in phylum level relative abundance was performed using GraphPad Prism 8. Changes in relative abundance at genus level were shown as a heatmap, which was processed in R.

Screening of drugs for RA *in vitro*

The intestinal contents of normal Sprague-Dawley rats were obtained, weighed, added to anaerobic culture medium at a 1:20 (w/v) ratio, preincubated for half an hour at 37°C and 200 rpm, and 10 μ L of the target drugs or compounds solutions (1 mg/ml and 10 mg/ml) was added to 990 μ L of anaerobic culture medium containing gut microbiome to achieve final concentrations of 10 μ g/ml (low dose) and 100 μ g/ml (high dose). The drug or compound solutions were added in advance, and anaerobic culture medium containing gut microbiome was added during nitrogen purging. Chosen drugs and compounds includes *Tripterygium* glycosides, triptolide, celastrol, wilforine, wilforlide A, triptonide, total glucosides of peony, paeoniflorin, albiflorin std, and benzoylpaeoniflorin. For

total glucosides of peony, the contents of the capsule were weighed and dissolved with methanol. For *Tripterygium* glycosides, we first crushed the tablets with a mortar, then weighed them, added methanol, and dissolved them by ultrasound. All dissolved drug or compound solutions should be filtered by microporous membranes (0.22 μm). We first added the solution filtered by the microporous membrane to the EP tube, then added intestinal bacterial incubation solution. For the control group, exactly the same procedure was repeated, except that the compound and drug solutions were replaced with methanol solution. After incubating for 12 h at 37°C and 200 rpm, the samples were immediately analyzed according to “Standard Solutions and Sample Preparation”.

Data sets were obtained from LC-MS. Modules for quantitative analysis were selected by SIMCA (MKS Umetrics, Sweden). Automatic construction simulation was then performed on adjusted parameters and number groups. Finally, data from all groups were scored and a principal component analysis (PCA) score graph was acquired.

Imported data sets were obtained from LC-MS into R software. We read the data set, defined the colors of the heatmap, modified the legend size and scope, and performed normalization of datasets which controlled ranges from -1 to 1 . Finally, the heatmap was acquired.

Statistical analysis

Data analysis was performed using GraphPad Prism 8. A two-sided t test was used; $p < 0.05$ was considered statistically significant. Heatmaps were processed in R, with blue representing lower levels and red representing higher levels. The PCA graph was processed using SIMCA (MKS Umetrics, Sweden), and the data were normalized before plotting.

Results

Method development

To establish targeted metabolomics methods, we optimized mass spectrometry, chromatographic conditions, and sample preparation in order to obtain optimal sensitivity, separation, and quantitative accuracy.

Mass spectrometric conditions

Mass spectrometric detection was performed using multiple reaction monitoring (MRM) with electrospray ionization (ESI). The structural formulas of the 17 metabolites and the internal standard determined in this paper are shown in Figure 1; all contain nitrogen groups, and the response is higher in positive ion mode. The optimized mass spectrometry parameters of the

17 metabolites—such as molecular weight, transition, and collision energy—are shown in Table 1.

Chromatographic conditions

In terms of column selection, the target compounds had almost no retention on Bridge C18 column (2.1 mm \times 100 mm, 2.7 μm), while all compounds eluted within 0.5 min. On the Acquity UPLC HSS T3 column, the peak shape of the indole derivative exhibited severe tailing. Finally, a SVEA C18 opal column (250 mm \times 4.6 mm \times 5 μm) was selected, exhibiting good resolution and a symmetrical peak shape. The flow rate was 0.4 ml/min. Water with 0.1% formic acid (FA) was used as the aqueous mobile phase, and 0.1% FA in methanol: acetonitrile (1:1) was used as the organic mobile phase. When the organic phase is pure methanol or pure acetonitrile, the analyte exhibited a front or split peak phenomenon. When the organic phase was adjusted to methanol: acetonitrile (1:1), the peak shape of the analyte was more symmetrical. Considering that the mass spectrometry conditions were in positive ion mode and that most metabolites contain carboxyl groups, a certain concentration of acid was chosen for addition to the mobile phase to improve the mass spectral response and peak shape; 0.1% acetic acid, 0.2% acetic acid, 0.5% acetic acid, and 0.1 and 0.5% FA were successively tested. The addition of acetic acid delayed the metabolite peak and prolonged the time of the whole chromatographic method. The best response was obtained with 0.1% FA, so this was chosen for addition to the aqueous and organic phases. The gradient elution conditions were: 0–5 min, 30–95% B; 5–8 min, 95%; 8.01–16 min, 30% B. Considering the structural formulas of the 17 metabolites, it was difficult to obtain the isotopic internal standard related to each substance, so acetaminophen with a similar structure was selected.

Sample preparation

In the extraction of intestinal content, the extraction solvent and extraction method were mainly investigated. Water, methanol, and acetonitrile were considered when choosing the extraction solvent, with water extracting the best peak shape. The extraction methods considered the following: direct treatment after mixing, posttreatment with ice bath ultrasound for 1 h, and shaking at 150 rpm and 20°C for 1 h. There will be a small number of interference peaks with the same MRM after shaking or sonication. There was no significant difference in the response of the target compound compared with the direct treatment by mixing. Therefore, the samples were processed directly after mixing. In addition, the Trp metabolites measured in the literature are unstable under conventional processing conditions, and methanol containing 2% FA (Ma et al., 2021) or methanol containing 10 mg/ml ascorbic acid (Fuertig et al., 2016) is generally chosen as the precipitant. In this experiment, it was found that adding methanol containing 2% FA to the precipitating agent resulted in a better peak shape.

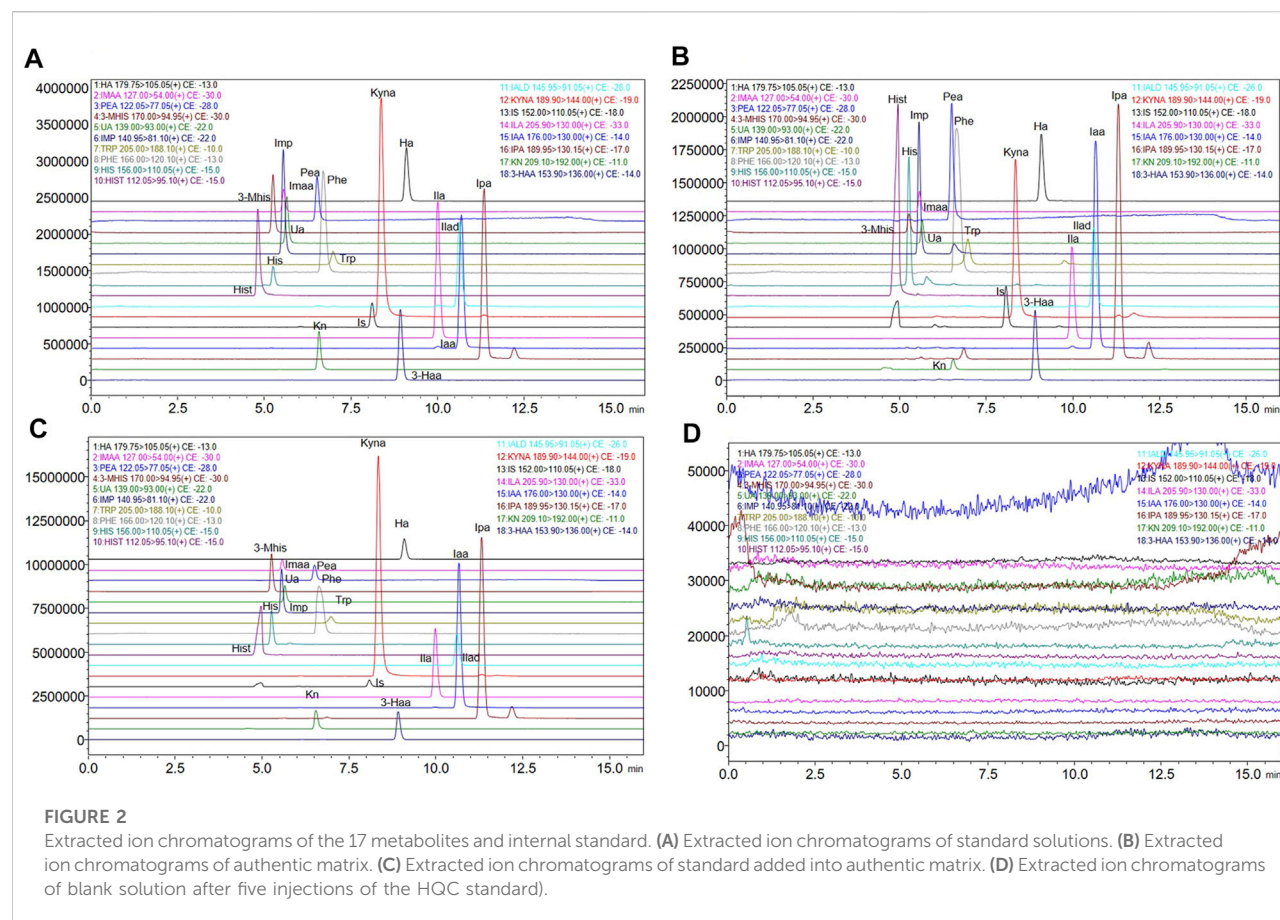


TABLE 2 Retention time, linearity, quantitative range, and lower limit of quantitation of 17 metabolites.

Analyte	Rt (min)	Linear range(ng/ml)	R ²	LLODng/ml	LLOQng/ml
Ha	9.1	20–2500	0.996	1	2
Imaa	5.5	20–2500	0.999	0.5	2
Pea	6.5	20–2500	0.996	0.5	1
3-Mhis	5.2	20–2500	0.994	1	2
Ua	5.6	20–2500	0.991	1	2
Imp	5.5	100–12500	0.998	0.05	0.1
Trp	7.1	100–12500	0.997	0.5	1
Phe	8.7	100–12500	0.997	0.5	1
His	5.2	100–12500	0.999	0.1	1
Hist	4.8	20–2500	0.993	1	5
Iald	10.6	20–2500	0.999	0.5	2
Kyna	8.5	20–2500	0.997	1	2
Ila	10.1	20–2500	0.997	1	5
Iaa	10.7	20–2500	0.999	0.5	1
Ipa	11.3	20–2500	0.993	0.5	1
Kn	6.5	20–2500	0.993	0.5	1
3-Haa	8.9	20–2500	0.992	0.5	1

TABLE 3 Precision and accuracy of 17 metabolites.

Analyte	Concentrationng/ml	Intraday(<i>n</i> = 5)		Interday (<i>n</i> = 15)	
	LQC	Accuracy (%)	RSD (%)	Accuracy (%)	RSD (%)
	MQC				
	HQC				
Ha	40	94.97	11.53	96.27	7.01
	400	100.06	5.37	105.82	5.06
	2000	92.03	5.40	97.37	5.22
Imaa	40	100.88	4.99	101.32	5.33
	400	104.59	4.57	106.80	3.55
	2000	95.00	2.11	97.74	4.30
Pea	40	92.98	3.50	97.79	5.85
	400	101.14	4.86	106.14	4.57
	2000	102.98	5.88	99.03	6.70
3-Mhis	40	95.05	10.21	97.35	6.57
	400	102.40	3.99	104.51	3.80
	2000	92.33	3.23	96.71	5.16
Ua	40	100.84	5.44	100.80	5.32
	400	104.19	3.96	106.81	3.35
	2000	91.99	2.28	95.68	4.39
Imp	200	92.16	8.25	94.94	6.70
	2000	107.50	3.79	114.01	7.28
	10000	92.07	2.92	95.01	6.42
Hist	40	95.69	6.15	98.64	5.13
	400	103.14	5.80	103.32	5.42
	2000	92.20	2.84	93.53	3.05
Iald	40	94.02	3.95	95.51	3.74
	400	102.19	4.56	104.95	3.41
	2000	92.34	2.03	97.13	4.65
Kyna	40	96.11	8.39	97.60	5.94
	400	102.98	3.61	103.89	3.09
	2000	93.18	3.95	98.90	5.78
Ila	40	98.64	4.78	100.32	3.49
	400	95.52	4.53	102.78	6.56
	2000	92.92	3.79	96.03	5.50
Iaa	40	99.68	5.11	97.45	4.09
	400	98.38	3.60	103.71	5.03
	2000	101.64	3.18	99.38	3.15
Ipa	40	97.71	5.80	98.63	4.28
	400	100.82	3.34	104.81	3.96
	2000	90.69	1.72	96.09	5.14
Kn	40	100.11	1.98	99.32	3.38
	400	98.31	4.41	103.59	4.90
	2000	89.45	2.66	95.88	8.37
3-Haa	40	98.88	3.12	100.65	3.24
	400	98.15	2.42	103.25	5.64
	2000	94.51	2.15	98.32	5.15

(Continued on following page)

TABLE 3 (Continued) Precision and accuracy of 17 metabolites.

Analyte	Concentrationng/ml	Intraday(<i>n</i> = 5)		Interday (<i>n</i> = 15)	
	LQC	Accuracy (%)	RSD (%)	Accuracy (%)	RSD (%)
	MQC				
	HQC				
Trp	200	89.30	5.98	95.23	7.51
	2000	98.02	1.74	106.22	6.79
	10000	96.71	5.16	99.75	4.47
Phe	200	88.80	7.14	93.79	8.41
	2000	99.01	3.08	107.58	6.86
	10000	91.40	3.13	96.52	5.90
His	200	98.54	7.76	90.38	10.78
	2000	104.81	4.10	107.71	5.37
	10000	94.44	3.19	96.20	2.96

Method validation

Method validation was performed to obtain repeatable, stable targeted metabolomics. To validate the endogenous compound analysis methods, the following three methods are mainly adopted: 1) use of an isotope-labeled internal standard; 2) adding a standard to a surrogate matrix (Virág et al., 2020); and 3) adding standards to an authentic matrix (Fuertig et al., 2016). In this experiment, the corresponding isotope-labeled internal standards of the 17 substances were difficult to obtain, and the endogenous substances in the matrix could not be completely removed by various treatment methods. Therefore, the standards were added to the authentic matrix for method validation.

Specificity and carryover

Figures 2A–C shows the chromatograms of the standard substance, authentic matrix, and authentic matrix with standards. In the chromatogram of the authentic samples, all 17 metabolites corresponded to the retention time of the standard chromatogram. In authentic samples, multiple chromatographic peaks appear under the same MRM conditions, such as Imp, Trp, the IS and Ipa, but such compounds have proper chromatographic resolution. The peak shape of the chromatographic peaks after adding the standard to the authentic samples was good, and the retention time was consistent with that of the standard. After five consecutive high concentration QC (HQC) injections, the blank solvent chromatogram is shown in Figure 2D, indicating that there is no residue.

Linearity and lower limit of quantitation

Considering the concentration levels of these metabolites in intestinal bacterial samples, Trp, Phe, His, and imidazole propionic acid were basically at the microgram level, and the

quantitative range was set as 100 ng/ml–12500 ng/ml. The quantitative range of other substances was set as 20 ng/ml–2500 ng/ml. A calibration curve for the analytes was built using the peak area ratio of each analyte to internal standard versus analyte concentration, plotted using 1/*x* weighted least squares linear regression. The correlation coefficient R^2 was used to represent the linearity, and the R^2 values of the 17 substances were all greater than 0.99. Since the metabolites in the matrix cannot be removed, we used the standard solution to calculate the lower limit of quantitation (LLOQ) and lower limit of detection (LLOD), as shown in Table 2.

Accuracy and precision

According to the verification principle of the biological sample analysis method in the *Chinese Pharmacopoeia*, the low concentration QC (LQC), middle concentration QC (MQC), and high concentration QC (HQC) concentrations of Trp, Phe, His, and Imp were set as 200 ng/ml, 2000 ng/ml, and 10000 ng/ml, respectively. The LQC, MQC, and HQC concentrations of the other 13 metabolites were set to 40 ng/ml, 400 ng/ml, and 2000 ng/ml, respectively. The precision and accuracy of the 17 metabolites are shown in Table 3. The intraday accuracy was 88.80–107.50%, and the RSD was 1.72–11.53%. The inter-day accuracy was 90.38–114.01%, and the RSD was 2.96–10.78%, which were within the acceptable range, as shown in Table 3.

Stability

Taking the needs of practical experiments into account, the spiked samples were placed at 4°C for 12 h before or after treatment or freeze-thawed at –20°C thrice before treatment. The stability under the three conditions is shown in Table 4, and

TABLE 4 Stability of 17 metabolites under three conditions.

Analyte	Concentration (ng/ml)	Stability before treatment (4°C 12 h)		Stability after treatment (4°C 12 h)		Repeated freezing and thawing 3 times (-20°C)	
	LQC	Mean (%)	SD (%)	Mean (%)	SD (%)	Mean (%)	SD (%)
	MQC						
	HQC						
Ha	40	103.12	7.11	95.10	6.29	91.00	5.77
	400	103.14	6.28	92.98	5.01	100.42	3.87
	2000	105.99	6.12	93.86	3.11	99.08	2.36
Imaa	40	98.58	4.16	90.81	6.18	98.56	5.89
	400	97.64	5.05	94.79	2.81	104.90	3.96
	2000	101.76	3.59	92.29	4.26	96.13	1.67
Pea	40	107.75	2.88	92.29	4.36	91.77	6.07
	400	101.63	4.12	95.94	4.84	109.92	4.50
	2000	92.65	7.57	99.67	4.27	97.11	2.01
3-Mhis	40	107.05	11.84	94.43	5.73	96.83	5.95
	400	97.94	2.29	93.84	3.36	104.44	4.20
	2000	102.41	3.75	92.62	4.18	92.59	3.41
Ua	40	100.10	5.50	98.73	3.05	91.14	6.18
	400	102.25	3.80	95.06	4.22	106.14	2.29
	2000	102.59	3.16	97.82	2.65	96.98	3.38
Imp	200	110.04	10.35	103.03	6.33	92.72	8.68
	2000	99.69	4.17	85.06	5.66	98.00	1.83
	10000	99.94	3.52	96.56	4.75	93.18	2.03
Hist	40	102.12	7.19	97.87	9.26	90.21	2.32
	400	103.69	4.84	101.13	6.69	88.34	8.83
	2000	97.30	4.72	100.27	6.47	93.78	1.91
Iald	40	107.84	3.48	105.49	4.76	91.34	4.35
	400	104.79	2.72	88.89	3.73	107.27	3.37
	2000	106.78	2.02	92.16	3.96	98.43	1.69
Kyna	40	103.97	7.14	98.91	6.38	99.91	5.57
	400	104.08	2.52	98.12	4.24	107.81	3.96
	2000	109.31	4.15	94.71	2.74	91.24	3.02
Ila	40	102.94	4.12	98.54	1.34	92.41	7.63
	400	108.75	5.87	95.84	2.93	99.43	5.21
	2000	101.77	3.98	93.89	3.67	93.59	1.99
Iaa	40	100.49	5.05	102.97	4.99	90.68	2.77
	400	109.14	1.61	102.67	6.02	102.22	4.59
	2000	96.13	3.62	100.45	2.33	97.10	3.37
Ipa	40	102.44	9.15	95.92	3.95	91.87	4.24
	400	98.62	4.78	89.72	3.19	110.39	1.76
	2000	106.94	3.78	94.39	2.90	95.49	1.23
Kn	40	98.20	3.18	98.79	8.43	89.68	3.87
	400	96.98	5.06	88.73	2.85	104.88	4.98
	2000	100.10	4.67	95.39	3.95	90.56	1.87
3-Haa	40	100.25	6.17	95.97	3.96	88.63	9.39
	400	101.65	3.82	96.55	5.20	100.50	3.51

(Continued on following page)

TABLE 4 (Continued) Stability of 17 metabolites under three conditions.

Analyte	Concentration (ng/ml)	Stability before treatment (4°C 12 h)		Stability after treatment (4°C 12 h)		Repeated freezing and thawing 3 times (-20°C)	
	LQC	Mean (%)	SD (%)	Mean (%)	SD (%)	Mean (%)	SD (%)
	MQC						
	HQC						
Trp	2000	101.87	2.51	88.61	2.45	95.02	3.30
	200	101.89	4.95	89.90	6.94	89.65	7.47
	2000	106.21	2.75	106.35	3.10	99.13	3.44
	10000	98.02	6.60	105.63	4.43	95.38	1.29
Phe	200	102.35	6.75	91.91	7.36	88.96	3.32
	2000	109.05	3.78	101.04	3.16	97.09	3.89
	10000	106.54	3.50	102.75	2.49	96.36	1.86
	His	94.62	9.56	107.88	8.31	95.42	4.21
His	2000	101.91	4.50	105.82	4.53	98.44	5.37
	10000	104.70	3.23	100.81	4.44	100.94	1.49

all metabolites are in the range of 85–115%, which meets the requirements of biological sample analysis.

Extraction recovery

The extraction recovery rate = the concentration of the sample after extraction/the concentration of the sample before extraction * 100%; the extraction recovery rate of 17 substances was 88.34–114.26%, which met the requirements of biological sample analysis (see Table 5).

Matrix effect

The results showed that the matrix effect was consistent at different levels and in the range of 86.38–112.64%, as shown in Table 6.

Establishment of the rheumatoid arthritis rat model

We applied the previously established targeted omics approach to the model of rheumatoid arthritis, a classic inflammation-related disease. We first demonstrated the successful establishment of rheumatoid arthritis. The model group was initiated by intradermal injection of complete Freund's adjuvant (CFA) at the base of the hind paw region (Choudhary et al., 2018) and recorded as Day 0. On the second day, the injected soles of the rats were observed to be red and swollen. On the 21st day, when the rats were injected again, the toe and ankle joints were observed to be swollen. The other soles that were not injected also showed redness and swelling of the

soles and joints. On the 25th day, the rats were weighed, blood and feces were collected, and the gut microbiota, feces, and spleen were collected after sacrifice. The process is shown in Figure 3A. Using a kit to measure inflammatory factors in plasma, it was found that, compared with the control group, the inflammatory factors IL-6, IL-1 β , and TNF- α were significantly increased in the model group, as shown in Figures 3B–D. The spleen and rats were weighed, and the spleen weight/body weight was recorded as the immune index. The immune index in the model group was significantly increased, as shown in Figure 3E, which proved that the model was successfully constructed.

16S RNA sequencing of feces of rheumatoid arthritis rats and determination of the intestinal contents

Since all the metabolites we measured were microbiota metabolites, we also examined the changes of intestinal microbiota in rats with rheumatoid arthritis. We hoped to determine whether there is a correlation between changes in intestinal microbiota and changes in these metabolites in rats with rheumatoid arthritis. The feces of model and control rats were analyzed by 16S sequencing. Compared with the control group, the α -biodiversity of the model group decreased, as shown in Figures 4A–D. Analysis of the gut microbiota in the feces revealed dysbiosis. As shown in Figures 4E,F, the phylum level is mainly composed of Firmicutes and Bacteroidetes, accounting for more than 95% of the total bacteria—similar to the

TABLE 5 Extraction recoveries of 17 metabolites.

Analyte	Concentration (ng/ml)	Extraction recovery	
	LQC	Mean (%)	SD (%)
	MQC		
	HQC		
Ha	40	97.68	6.80
	400	104.24	3.30
	2000	99.76	3.83
Imaa	40	101.16	5.58
	400	105.07	2.11
	2000	107.34	1.70
Pea	40	104.89	4.08
	400	104.50	1.43
	2000	103.99	1.68
3-Mhis	40	100.22	6.69
	400	101.41	3.44
	2000	105.77	3.43
Ua	40	99.39	5.30
	400	102.54	4.99
	2000	107.48	2.77
Imp	200	104.15	2.48
	2000	104.36	2.05
	10000	113.49	3.19
Hist	40	99.99	5.10
	400	101.02	3.24
	2000	103.76	5.89
Iald	40	109.19	6.13
	400	102.36	1.32
	2000	111.08	5.23
Kyna	40	98.77	3.18
	400	102.92	3.96
	2000	104.35	3.80
Ila	40	101.59	6.16
	400	105.04	2.42
	2000	105.62	1.95
Iaa	40	101.73	3.31
	400	100.37	2.26
	2000	91.47	3.10
Ipa	40	99.57	2.66
	400	103.04	1.14
	2000	114.26	5.34
Kn	40	105.06	4.72
	400	101.19	1.95
	2000	110.80	2.85
3-Haa	40	98.28	5.04
	400	99.73	4.21
	2000	106.02	2.86

(Continued in next column)

TABLE 5 (Continued) Extraction recoveries of 17 metabolites.

Analyte	Concentration (ng/ml)	Extraction recovery	
	LQC	Mean (%)	SD (%)
	MQC		
	HQC		
Trp	200	96.81	4.03
	2000	96.05	3.32
	10000	96.61	1.64
Phe	200	108.99	7.94
	2000	103.38	1.51
	10000	101.32	2.83
His	200	98.65	8.08
	2000	91.23	1.88
	10000	88.34	3.54

composition of the human gut microbiota (Turnbaugh et al., 2006). The abundance of Bacteroidetes in the model group increased while the abundance of Firmicutes was decreased. In other phyla with relatively low contents, the abundance of Proteobacteria and Verrucomicrobiota was elevated and the abundance of Cyanobacteria decreased. As shown in Figure 5A, at the genus level, the relative abundances of *g__undentified*, *g__Turicibacter*, and *g__Lachnoclostridium* increased and the relative abundances of *g__Ruminococcus_gnavus_group*, *g__UCG-005*, *g__Ruminococcus*, *g__Jeotgalicoccus*, *g__Sellimonas*, *g__Erysipelotrichaceae_UCG-003*, and *g__Eubacterium_oxidoreducens_group* decreased compared to the control group. The intestinal contents samples were analyzed, as shown in Figure 5B. Compared with the control group, the three amino acids in the model group changed significantly: Phe was significantly decreased ($p < 0.05$), and His and Trp were significantly increased ($p < 0.001$). In the Trp pathway, Iaa and Ipa were significantly decreased ($p < 0.001$ and $p < 0.001$), and Iald, Kn, and Kyna were significantly increased ($p < 0.001$, $p < 0.001$, and $p < 0.001$). In the Phe pathway, Ha was significantly elevated ($p < 0.001$). In the His pathway, Imp was significantly elevated ($p < 0.001$).

Screening of drugs for RA in vitro

The field of gut bacteria is a new direction in studying the mechanism of drug action. Here, we selected several Chinese patent drugs and their effective components commonly used in the clinical treatment of arthritis and used the targeted omics method established by us to provide new ideas for the study of

TABLE 6 Matrix effects of 17 metabolites.

Analyte	Concentration (ng/ml)	Matrix effect	
	LQC	Mean (%)	SD (%)
	MQC		
	HQC		
Ha	40	95.08	9.82
	400	91.14	4.82
	2000	91.54	3.46
Imaa	40	98.59	7.81
	400	98.17	3.19
	2000	99.36	3.72
Pea	40	93.12	2.19
	400	93.67	4.13
	2000	112.64	9.19
3-Mhis	40	96.16	12.38
	400	97.58	1.77
	2000	96.64	1.94
Ua	40	102.04	4.19
	400	96.28	2.13
	2000	97.23	2.32
Imp	200	97.18	12.70
	2000	87.59	3.91
	10000	101.66	5.05
Hist	40	96.69	4.60
	400	104.55	3.60
	2000	99.66	2.66
Iald	40	95.95	5.28
	400	96.28	2.95
	2000	93.89	2.83
Kyna	40	95.90	9.42
	400	97.77	2.80
	2000	94.84	3.66
Ila	40	97.98	5.59
	400	91.93	4.89
	2000	99.88	3.27
Iaa	40	104.74	5.92
	400	93.62	4.70
	2000	103.61	2.70
Ipa	40	99.15	7.27
	400	93.05	3.20
	2000	94.62	1.51
Kn	40	101.29	3.92
	400	91.96	3.52
	2000	97.16	1.09
3-Haa	40	96.66	5.33
	400	96.06	5.90
	2000	98.09	3.36

(Continued in next column)

TABLE 6 (Continued) Matrix effects of 17 metabolites.

Analyte	Concentration (ng/ml)	Matrix effect	
	LQC	Mean (%)	SD (%)
	MQC		
	HQC		
Trp	200	89.21	5.15
	2000	92.39	3.32
	10000	97.68	4.79
Phe	200	86.38	6.97
	2000	90.47	2.36
	10000	96.06	2.53
His	200	106.30	10.33
	2000	98.39	3.04
	10000	98.16	1.87

their mechanism of action from the perspective of intestinal bacteria. *Tripterygium wilfordii* and *Paeonia lactiflora* are both commonly used Chinese herbal medicines for the treatment of rheumatoid arthritis (Zhang and Wei, 2020; Zhang Y. et al., 2021). We chose total glucosides of paeony (the extract composition of white paeony capsules is shown in Supplementary Table S1). Their active ingredients are paeoniflorin, albiflorin std, and benzoylpaeoniflorin. *Tripterygium wilfordii* polyglycoside tablets (the extract composition of which is shown in Supplementary Table S2) has as active ingredients triptolide, celastrol, wilforine, wilforlide A, and triptonide. We incubated these drugs *in vitro* with the gut bacteria of SD rats and then measured them with established targeted metabolomics for a preliminarily exploration of whether they can change the concentration of these metabolites.

As shown in Figure 6A, principal component analysis (PCA) was performed on 11 high-dose groups and a control group. It was found that, except for the triptolide group, the other groups were separated from the control group. These results showed that the addition of drugs changed metabolites in the *in vitro* incubation system compared to the control group. As shown in Figure 6B, *Tripterygium* glycoside and its active ingredient groups, the high-dose triptolide group, the low-dose wilforine group, and the high-dose wilforine group showed a significant increase of indole propionic acid in gut bacteria ($p < 0.01$, $p < 0.05$, $p < 0.05$). The high-dose celastrol group showed a significant increase of indoleacetic acid ($p < 0.001$). The high-dose celastrol group, high-dose wilforine group, low-dose wilforlide A group, and high-dose *Tripterygium* glycoside group showed significant increase of Pea ($p < 0.05$, $p < 0.05$, $p < 0.05$, and $p < 0.05$). The low-dose celastrol group, the low-dose and high-dose wilforine groups, the high-dose wilforlide A

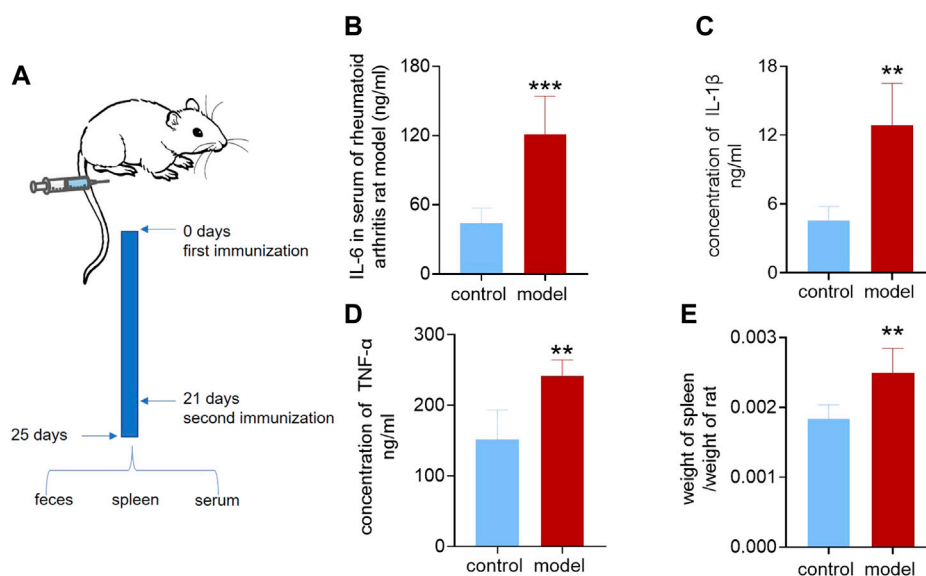


FIGURE 3

Inflammatory factors and immunization index of the rheumatoid arthritis rat model. (A) Establishment of the rheumatoid arthritis rat model. (B) Interleukin-6 in serum of the rheumatoid arthritis rat model and control group. (C) Interleukin-1 β in serum of rheumatoid arthritis rat model and control group. (D) Tumor necrosis factor- α in serum of the rheumatoid arthritis rat model and control group. (E) Ratio of spleen weight to body weight of rheumatoid arthritis rat model and control group. A two-sided t test was used, and $p < 0.05$ was considered statistically significant. ** $p < 0.01$, *** $p < 0.001$.

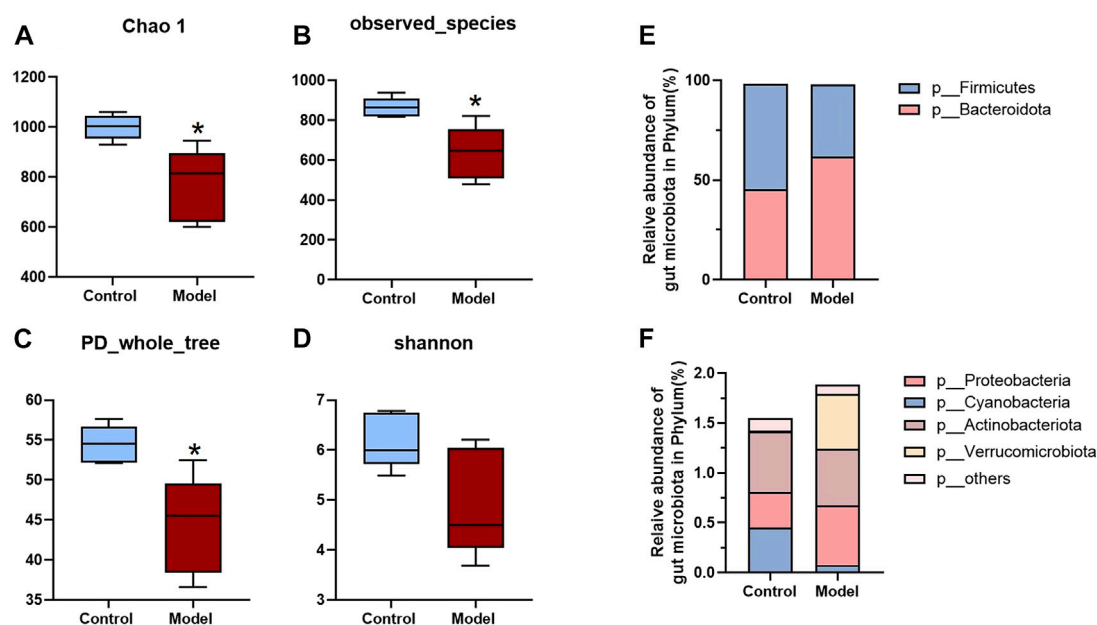


FIGURE 4

Analysis of fecal diversity and phylum level of RA rats. (A–D) Chao 1, Observed_species, PD_whole_trees and Shannon indices of model and control groups. (E,F) The relative abundance of bacteria at the phylum level. A two-sided t test was used, and $p < 0.05$ was considered statistically significant. * $p < 0.05$, ** $p < 0.01$.

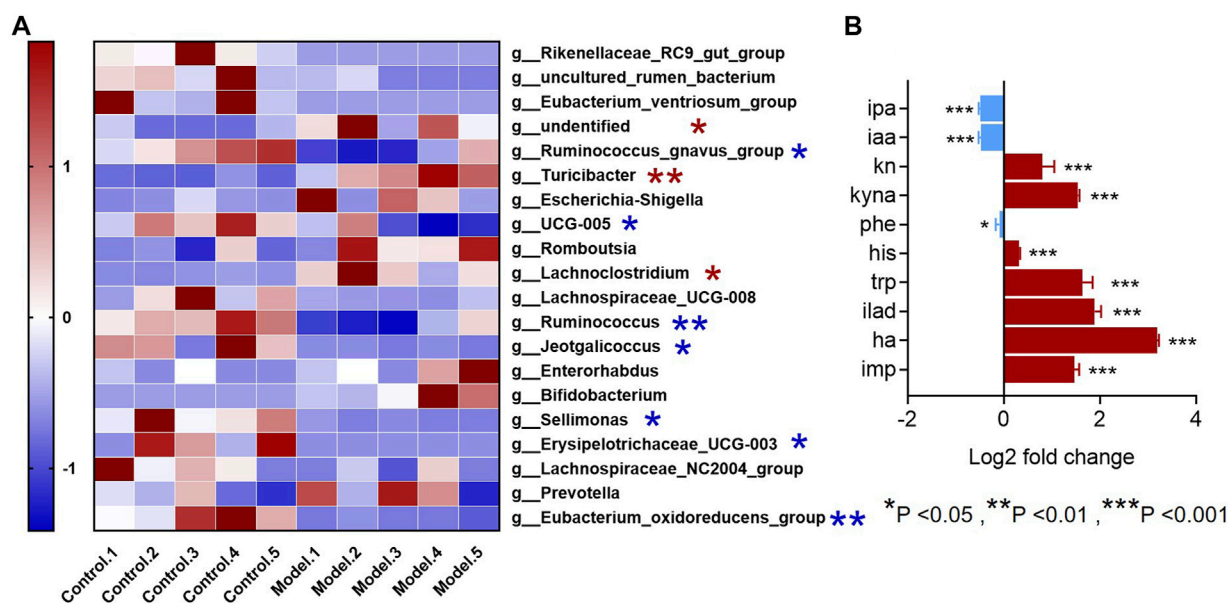


FIGURE 5

Genus-level differences in fecal microbiota and metabolite differences in intestinal microbiota samples in the RA model. (A) The top-20 bacterial genera with the most substantial change in abundance after the establishment of rheumatoid arthritis rat model. (*The red pentagram represents bacteria with abundance increased after the establishment of rheumatoid arthritis model. *The blue pentagram represents bacteria with decreased abundance after the establishment of rheumatoid arthritis model.) (B) Differences in metabolites in the gut microbiota of model rats and the control group. A two-sided *t* test was used and *p* < 0.05 was considered statistically significant. **p* < 0.05, ***p* < 0.01, ****p* < 0.001.

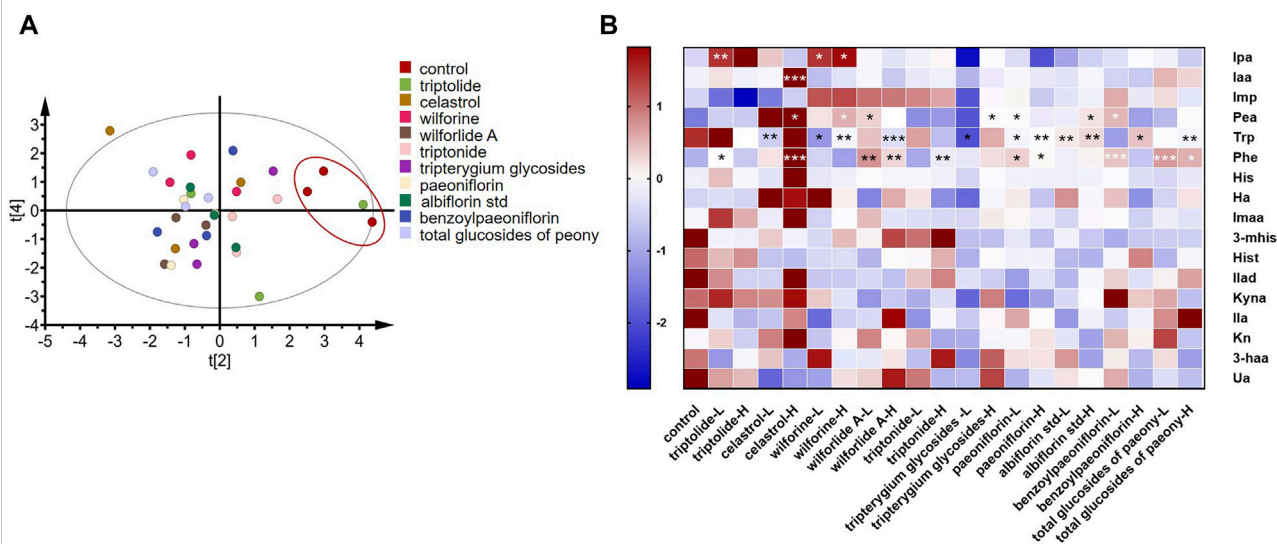


FIGURE 6

Screening of drugs for rheumatoid arthritis *in vitro*. (A) Principal component analysis plots of *in vitro* high-dose group samples. (B) Changes in metabolites after drug treatment *in vitro*. A two-sided *t* test was used and *p* < 0.05 was considered statistically significant. **p* < 0.05, ***p* < 0.01, ****p* < 0.001. (L means low dose 10 ug/ml, H means high dose 100 ug/ml, "Tripterygium glycoside" represents *Tripterygium wilfordii* polyglycoside tablets, "total glucosides of peony" represents total glucosides of white peony capsules.)

group, and the low-dose *Tripterygium* glycoside group showed a significant decrease of Trp ($p < 0.01$, $p < 0.05$, $p < 0.01$, $p < 0.001$, $p < 0.05$). The low-dose triptolide group, the high-dose celastrol group, the low-dose and high-dose wilforlide A groups, and the high-dose triptonide group significantly elevated Phe ($p < 0.05$, $p < 0.001$, $p < 0.01$, $p < 0.01$, and $p < 0.01$). In the total glucosides of paeony and its active components, the low-dose paeoniflorin group, the high-dose albiflorin std group, and the low-dose benzoyl paeoniflorin group significantly elevated Pea ($p < 0.05$, $p < 0.05$, $p < 0.05$). The low-dose and high-dose paeoniflorin groups, the low-dose and high-dose albiflorin std groups, the high-dose benzoyl paeoniflorin group, and the high-dose total glucosides of paeony group can significantly decrease Trp ($p < 0.05$, $p < 0.01$, $p < 0.01$, $p < 0.01$, $p < 0.05$, and $p < 0.01$). The low-dose and high-dose paeoniflorin group, low-dose benzoyl paeoniflorin group, and low-dose and high-dose total glucosides of paeony group can significantly elevate Phe ($p < 0.05$, $p < 0.05$, $p < 0.001$, $p < 0.001$, and $p < 0.05$) (p values of differential metabolites compared with the control group after incubation with drugs or compounds are shown in [Supplementary Table S3](#)). Therefore, gut microbiota derived metabolites in Trp and Phe pathways occurred in variations after incubation with *Tripterygium* glycosides and their active components, including two increasing beneficial Trp metabolites: indole propionic acid and indole acetic acid. Concentrations of phenylethylamine in the gut microbiota increased after incubation with total glucosides and active components of peony.

Discussion

We successfully developed a simple, rapid, and derivatization-free LC-MS/MS method for the simultaneous determination of 17 metabolites targeting Phe, Trp, and His in intestinal content, targeting three metabolic pathways. The method has good specificity, and high sensitivity, accuracy, precision, and recovery rate, meets the requirements of biological sample analysis, and can be successfully applied to bacterial samples.

In this experiment, a rat model of rheumatoid arthritis was selected, and dysbiosis was found in the feces of the model group. In our experiments, increased abundances of *g__Turicibacter* and *g__Lachnoclostridium* and decreased abundances of *g__Erysipelotrichaceae_UCG-003* were observed in the model group. *g__Turicibacter* belongs to the phylum Firmicutes ([Maki and Looft, 2022](#)) and is a strictly anaerobic Gram-positive rod-shaped bacterium ([Bossard et al., 2002](#)), the specific function of which is still unclear. However, studies have shown that it is positively correlated with a variety of inflammatory diseases and its abundance is increased in hepatitis mice ([Yang et al., 2020a; Somm et al., 2021](#)). One study showed that the use of icariin significantly reduced the abundance of the genus *g__Turicibacter* in colitis

mice ([Zhang H. et al., 2021](#)). Similarly, the same phenomenon occurred during the treatment of colitis mice with caffeic acid ([Wan et al., 2021](#)). Its abundance was significantly increased in a chronic inflammation-based mouse model of atherosclerosis and was significantly positively correlated with plaque area in the mouse aorta ([Huang K. et al., 2021](#)). *g__Lachnoclostridium* produces short-chain fatty acids mainly through the 4-aminobutyrate/succinate pathway ([Zhao E. et al., 2021](#)) and is a proinflammatory bacterium. Its relative abundance is significantly increased in mice with ulcerative colitis ([Wang et al., 2018](#)), patients with eosinophilic inflammation ([Kim et al., 2020](#)), and mice with atherosclerosis ([Sun et al., 2021](#)). *g__Erysipelotrichaceae_UCG-003* is a butyric acid-producing bacterium that can be induced by helper T-cell 17 (Th17 cells) ([Cheng et al., 2021](#)); a clinical experiment showed that the bacterium was more abundant in healthy aging volunteers than in the diseased aging group ([Singh H. et al., 2019](#)). Another clinical study showed that the abundance of this bacterium was significantly decreased in lung cancer patients compared to healthy patients ([Zhao F. et al., 2021](#)). Therefore, it is speculated that *g__Erysipelotrichaceae_UCG-003* is a beneficial bacterium, although the specific mechanism is still unclear. Less consistent with the literature is the decreased abundance of *g__Ruminococcus_gnavus_group* in the model group. This is a mucin-degrading gut bacterium ([Ahn et al., 2022](#)) belonging to the phylum Firmicutes ([Graziani et al., 2016](#)) and is enriched in patients with inflammatory bowel disease. *g__Ruminococcus_gnavus_group* can produce an inflammatory polysaccharide, which can induce dendritic cells to produce inflammatory cytokines such as TNF- α , further leading to the progression of Crohn's disease. Although not the same as our research results, a study based on genomic analysis of *g__Ruminococcus_gnavus_group* mainly secreted glycoside hydrolase and polysaccharide lyase, suggesting that these bacteria may be closer to the intestinal mucosa or adhere to the position of the intestinal mucosa ([Graziani et al., 2016](#)). Therefore, this bacterium has a greater effect on inflammatory bowel disease, but the mechanism may be different from that of rheumatoid arthritis. The functions of *g__undidentified*, *g__Eubacterium_oxidoreducens_group*, *g__Jeotgalicoccus*, and *g__Sellimonas* are not very well studied, this being the first time they have been found to be significantly reduced in rheumatoid arthritis rats. Unfortunately, in the rat model of rheumatoid arthritis, the different genera we found were not related to the metabolism of the three amino acids we measured. Therefore, we did not find a correlation between changes in gut bacteria and changes in these metabolites in rats with rheumatoid arthritis—one of the limitations of our study. However, many of these different bacteria were related to butyric acid metabolism, so our results suggest that butyric acid can also be a direction for research on rheumatoid arthritis and intestinal bacteria which is worthy of further exploration.

Furthermore, we used the established targeted metabolomics method to measure the concentration of the metabolites in intestinal content of the model mice; differential metabolites were found. Iaa and Ipa were significantly decreased, but Iald, Kn, Kyna, Ha, and Imp were significantly increased. Among them, Iaa and Ipa were negatively correlated with inflammation. These indole derivatives can act on pregnane X receptors (PXR) and AhR and have a certain inhibitory effect on inflammatory diseases such as colitis (Huang W. et al., 2021), arthritis (Rosser et al., 2020), steatohepatitis (Ji et al., 2019; Zhao et al., 2019), ankylosing spondylitis (Shen et al., 2022), and obesity (Su et al., 2022)—consistent with our experimental results. Trp is metabolized by bacteria into two pathways, indole derivatives and kynurenine, which antagonize each other. Therefore, the change trend of Kn and Kyna is opposite to that of indole derivatives. Studies have shown that Iald induces IL-22 by activating the AHR pathway and has an inhibitory effect on inflammation (Teng et al., 2018). However, another study showed that, although Iald has anti-inflammatory activity *in vitro*, it has pro-osteoclastogenesis and pro-angiogenic effects (Langan et al., 2021), which may be the reason for the significantly higher concentration of Iald in the model group. Hippuric acid, a biomarker identified from the urine of rheumatoid arthritis rats, inhibits osteoclast production *in vitro* to prevent osteoclasts from increasing bone resorption; this may be related to the underlying mechanism of rheumatoid arthritis (Jiang et al., 2016; Zhao et al., 2020). Ha has been identified as a biomarker of rheumatoid arthritis, and a study has revealed that hippuric acid inhibits osteoclast production *in vitro* to prevent osteoclasts from increasing bone resorption; this may be related to rheumatoid arthritis. Imidazole propionic acid is a newly discovered product of His metabolism by intestinal bacteria that positively correlates with systemic inflammation and is a biomarker related to diabetes (Koh et al., 2018). One study showed that it was negatively correlated with anti-inflammatory bacteria (Molinaro et al., 2020), which is consistent with our experimental results. In conclusion, these metabolites of intestinal content in rheumatoid arthritis model rats appeared varied. We then screened *Tripterygium* glycosides, total peony glucosides, and their active ingredients *in vitro*. The results showed that *Tripterygium* glycosides could modulate Trp and Phe pathways, especially Ipa, Iaa, and Pea. Total peony glucosides can modulate the Phe pathway, especially phenylethylamine. It has been documented in the literature that phenethylamine has an effect on the progression of chronic inflammation in humans (Maráková et al., 2020), especially neuroinflammation (Chen et al., 2022). However, phenethylamine has been less studied in nonbrain inflammatory diseases.

There is currently no targeted metabolomic method of simultaneously targeting the inflammatory markers of these three amino acid pathways. Due to the close connection between inflammatory diseases and intestinal microbiota, it

is very important to establish our method. However, our experiment still has certain limitations. Some different genera were identified in the analysis of the fecal samples of the model rats but the functional analysis did not find that these genera had metabolic effects on the three amino acid pathways. Therefore, further *in vivo* experiments may be required for confirmation. In conclusion, it was found that the pathogenesis of RA was related to dysbacteriosis, that Iaa and Ipa in the bacterial microbiota were significantly decreased, and that Iald, Kn, Kyna, Ha, and Imp were significantly increased. Using the method of *in vitro* incubation, the commonly used drugs for the treatment of RA—*Tripterygium* glycosides, total peony glucosides, and their corresponding monomers—were screened, and metabolites in Trp and Phe pathways occurred. Their variations of Ipa, Iaa, and Pea deserve special attention, which may be related to the mechanism of the treatment of rheumatoid arthritis. Our method can identify targets for the interaction of inflammatory diseases and microbiota and can be applied to the mechanistic study and drug screening of other inflammatory diseases. However, our research existed some limitations in the *in vitro* screening of drugs. We selected the gut microbiome of healthy rats to incubate with drugs, which were more related to the drugs' preventive effects. Further studies are needed to more widely apply our approach to drug screening for the treatment of RA and mechanism elucidation, including whether drugs can reverse gut microbiota-derived metabolites of RA model rats *in vitro*, whether drugs can reverse metabolites of gut microbiome in RA model rats after dosing of drugs, and whether drugs can reverse these metabolites in patients with rheumatoid arthritis. These are all worthy of further exploration.

Conclusion

In summary, we established targeted metabolomics of bacterial inflammatory markers and completed method validation. A typical inflammatory disease model of rheumatoid arthritis was then established, and we successfully applied targeted metabolomics of inflammatory markers to this model of inflammatory disease. In addition, we screened rheumatoid arthritis drugs *in vitro* and found that their treatment of rheumatoid arthritis may be related to microbial metabolites. In conclusion, our study may provide new insights into the mechanisms of inflammatory diseases and drug screening.

Data availability statement

The data presented in the study are deposited in the NCBI database, accession number PRJNA877047.

Ethics statement

The animal study was reviewed and approved by Ethics of the Chinese Academy of Medical Sciences and Peking Union Medical College and the Committee on the Care and Use of Laboratory Institutional Animals.

Author contributions

HX conducted the experiment and wrote the article; L-BP, HY, and PH analyzed the data; JF, Z-WZ, J-CH, X-YY, AK, H-JZ, and M-MB gave some suggestions and revised the article. J-DJ and YW provided resources and guidance for the paper. All the authors reviewed the results and approved the final version of the manuscript.

Funding

This project was supported by the CAMS Innovation Fund for Medical Sciences (CIFMS; Nos. 2022-I2M-JB-011, 2021-1-I2M-007, 2021-I2M-1-027, 2021-I2M-1-028, China, National Natural Science Foundation of China) (Nos. 81973290 and 82173888), and Beijing Key Laboratory of Non-Clinical Drug Metabolism and PK/PD study (Z141102004414062, China).

References

- Acuña, I., Ruiz, A., Cerdó, T., Cantarero, S., López-Moreno, A., Aguilera, M., et al. (2021). Rapid and simultaneous determination of histidine metabolism intermediates in human and mouse microbiota and biomatrices. *Biofactors* 48, 315–328. doi:10.1002/biof.1766
- Agus, A., Planchais, J., and Sokol, H. (2018). Gut microbiota regulation of tryptophan metabolism in health and disease. *Cell Host Microbe* 23 (6), 716–724. doi:10.1016/j.chom.2018.05.003
- Ahn, J. R., Lee, S. H., Kim, B., Nam, M. H., Ahn, Y. K., Park, Y. M., et al. (2022). *Ruminococcus gnavus* ameliorates atopic dermatitis by enhancing Treg cell and metabolites in BALB/c mice. *Pediatr. Allergy Immunol.* 33 (1), e13678. doi:10.1111/pai.13678
- Bosshard, P. P., Zbinden, R., and Altwegg, M. (2002). *Turicibacter sanguinis* gen. nov., sp. nov., a novel anaerobic, Gram-positive bacterium. *Int. J. Syst. Evol. Microbiol.* 52 (4), 1263–1266. doi:10.1099/00207713-52-4-1263
- Branco, A., Yoshikawa, F. S. Y., Pietrobon, A. J., and Sato, M. N. (2018). Role of histamine in modulating the immune response and inflammation. *Mediat. Inflamm.* 2018, 9524075. doi:10.1155/2018/9524075
- Cai, Y., Xue, F., Quan, C., Qu, M., Liu, N., Zhang, Y., et al. (2019). A critical role of the IL-1 β -IL-1R signaling pathway in skin inflammation and psoriasis pathogenesis. *J. Invest. Dermatol.* 139 (1), 146–156. doi:10.1016/j.jid.2018.07.025
- Chen, K., Palagashvili, T., Hsu, W., Chen, Y., Tabakoff, B., Hong, F., et al. (2022). Brain injury and inflammation genes common to a number of neurological diseases and the genes involved in the Genesis of GABAergic neurons are altered in monoamine oxidase B knockout mice. *Brain Res.* 1774, 147724. doi:10.1016/j.brainres.2021.147724
- Cheng, S., Hu, J., Wu, X., Pan, J. A., Jiao, N., Li, Y., et al. (2021). Altered gut microbiome in FUT2 loss-of-function mutants in support of personalized medicine for inflammatory bowel diseases. *J. Genet. Genomics* 48 (9), 771–780. doi:10.1016/j.jgg.2021.08.003
- Chicco, F., Magrì, S., Cingolani, A., Paduano, D., Pesenti, M., Zara, F., et al. (2021). Multidimensional impact of mediterranean diet on IBD patients. *Inflamm. Bowel Dis.* 27 (1), 1–9. doi:10.1093/ibd/izaa097
- Choudhary, N., Bhatt, L. K., and Prabhavalkar, K. S. (2018). Experimental animal models for rheumatoid arthritis. *Immunopharmacol. Immunotoxicol.* 40 (3), 193–200. doi:10.1080/08923973.2018.1434793
- Collins, S. L., and Patterson, A. D. (2020). The gut microbiome: An orchestrator of xenobiotic metabolism. *Acta Pharm. Sin. B* 10 (1), 19–32. doi:10.1016/j.apsb.2019.12.001
- Fuertig, R., Ceci, A., Camus, S. M., Bezard, E., Luippold, A. H., and Hengerer, B. (2016). LC-MS/MS-based quantification of kynurenine metabolites, tryptophan, monoamines and neopterin in plasma, cerebrospinal fluid and brain. *Bioanalysis* 8 (18), 1903–1917. doi:10.4155/bio-2016-0111
- Graziani, F., Pujol, A., Nicoletti, C., Dou, S., Maresca, M., Giardina, T., et al. (2016). *Ruminococcus gnavus* E1 modulates mucin expression and intestinal glycosylation. *J. Appl. Microbiol.* 120 (5), 1403–1417. doi:10.1111/jam.13095
- He, Y., Ma, J., Fan, X., Ding, L., Ding, X., Zhang, Q. Y., et al. (2021). The key role of gut-liver axis in pyrrolizidine alkaloid-induced hepatotoxicity and enterotoxicity. *Acta Pharm. Sin. B* 11 (12), 3820–3835. doi:10.1016/j.apsb.2021.07.013
- Huang K, K., Liu, C., Peng, M., Su, Q., Liu, R., Guo, Z., et al. (2021). Glycoursodeoxycholic acid ameliorates atherosclerosis and alters gut microbiota in apolipoprotein E-deficient mice. *J. Am. Heart Assoc.* 10 (7), e019820. doi:10.1161/jaha.120.019820
- Huang W, W., Cho, K. Y., Meng, D., and Walker, W. A. (2021). The impact of indole-3-lactic acid on immature intestinal innate immunity and development: A transcriptomic analysis. *Sci. Rep.* 11 (1), 8088. doi:10.1038/s41598-021-87353-1

Acknowledgments

We would like to thank Shimadzu (China) Co., Ltd., for technological support.

Conflict of interest

The authors declare that the research was conducted in the absence of any commercial or financial relationships that could be construed as a potential conflict of interest.

Publisher's note

All claims expressed in this article are solely those of the authors and do not necessarily represent those of their affiliated organizations, or those of the publisher, the editors and the reviewers. Any product that may be evaluated in this article, or claim that may be made by its manufacturer, is not guaranteed or endorsed by the publisher.

Supplementary material

The Supplementary Material for this article can be found online at: <https://www.frontiersin.org/articles/10.3389/fphar.2022.919181/full#supplementary-material>

- Jensen, C. S., Bahl, J. M., Østergaard, L. B., Høgh, P., Wermuth, L., Heslegrave, A., et al. (2019). Exercise as a potential modulator of inflammation in patients with Alzheimer's disease measured in cerebrospinal fluid and plasma. *Exp. Gerontol.* 121, 91–98. doi:10.1016/j.exger.2019.04.003
- Ji, Y., Gao, Y., Chen, H., Yin, Y., and Zhang, W. (2019). Indole-3-Acetic acid alleviates nonalcoholic fatty liver disease in mice via attenuation of hepatic lipogenesis, and oxidative and inflammatory stress. *Nutrients* 11 (9), E2062. doi:10.3390/nu11092062
- Jiang, H., Liu, J., Wang, T., Gao, J. R., Sun, Y., Huang, C. B., et al. (2016). Urinary metabolite profiling provides potential differentiation to explore the mechanisms of adjuvant-induced arthritis in rats. *Biomed. Chromatogr.* 30 (9), 1397–1405. doi:10.1002/bmc.3697
- Kanazawa, A., Aida, M., Yoshida, Y., Kaga, H., Katahira, T., Suzuki, L., et al. (2021). Effects of synbiotic supplementation on chronic inflammation and the gut microbiota in obese patients with type 2 diabetes mellitus: A randomized controlled study. *Nutrients* 13 (2), 558. doi:10.3390/nu13020558
- Kim, J. H., Kim, S. H., Lim, J. Y., Kim, D., Jeong, I. S., Lee, D. K., et al. (2020). Association between the sinus microbiota with eosinophilic inflammation and prognosis in chronic rhinosinusitis with nasal polyps. *Exp. Mol. Med.* 52 (6), 978–987. doi:10.1038/s12276-020-0458-1
- Koh, A., Molinaro, A., Ståhlman, M., Khan, M. T., Schmidt, C., Mannerås-Holm, L., et al. (2018). Microbially produced imidazole propionate impairs insulin signaling through mTORC1. *Cell* 175 (4), 947–961. doi:10.1016/j.cell.2018.09.055
- Langan, D., Perkins, D. J., Vogel, S. N., and Moudgil, K. D. (2021). Microbiota-derived metabolites, indole-3-aldehyde and indole-3-acetic acid, differentially modulate innate cytokines and stromal remodeling processes associated with autoimmune arthritis. *Int. J. Mol. Sci.* 22 (4), 2017. doi:10.3390/jms22042017
- Levy, M., Thaiss, C. A., Zeevi, D., Dohnalová, L., Zilberman-Schapira, G., Mahdi, J. A., et al. (2015). Microbiota-modulated metabolites shape the intestinal microenvironment by regulating NLRP6 inflammasome signaling. *Cell* 163 (6), 1428–1443. doi:10.1016/j.cell.2015.10.048
- Ma, S. R., Yu, J. B., Fu, J., Pan, L. B., Yu, H., Han, P., et al. (2021). Determination and application of nineteen monoamines in the gut microbiota targeting phenylalanine, tryptophan, and glutamic acid metabolic pathways. *Molecules* 26 (5), 1377. doi:10.3390/molecules26051377
- Maki, J. J., and Looft, T. (2022). *Turicibacter bilis* sp. nov., a novel bacterium isolated from the chicken eggshell and swine ileum. *Int. J. Syst. Evol. Microbiol.* 72 (1), 005153. doi:10.1099/ijsem.0.005153
- Maráková, K., Piešťanský, J., Zelinková, Z., and Mikuš, P. (2020). Simultaneous determination of twelve biogenic amines in human urine as potential biomarkers of inflammatory bowel diseases by capillary electrophoresis - tandem mass spectrometry. *J. Pharm. Biomed. Anal.* 186, 113294. doi:10.1016/j.jpba.2020.113294
- Molinaro, A., Bel Lassen, P., Henricsson, M., Wu, H., Adriouch, S., Belda, E., et al. (2020). Imidazole propionate is increased in diabetes and associated with dietary patterns and altered microbial ecology. *Nat. Commun.* 11 (1), 5881. doi:10.1038/s41467-020-19589-w
- Pan, L., Han, P., Ma, S., Peng, R., Wang, C., Kong, W., et al. (2020). Abnormal metabolism of gut microbiota reveals the possible molecular mechanism of nephropathy induced by hyperuricemia. *Acta Pharm. Sin. B* 10 (2), 249–261. doi:10.1016/j.apsb.2019.10.007
- Ridker, P. M., Everett, B. M., Pradhan, A., MacFadyen, J. G., Solomon, D. H., Zaharris, E., et al. (2019). Low-dose methotrexate for the prevention of atherosclerotic events. *N. Engl. J. Med.* 380 (8), 752–762. doi:10.1056/NEJMoa1809798
- Ridker, P. M., Everett, B. M., Thuren, T., MacFadyen, J. G., Chang, W. H., Ballantyne, C., et al. (2017). Antiinflammatory therapy with canakinumab for atherosclerotic disease. *N. Engl. J. Med.* 377 (12), 1119–1131. doi:10.1056/NEJMoa1707914
- Roager, H. M., and Licht, T. R. (2018). Microbial tryptophan catabolites in health and disease. *Nat. Commun.* 9 (1), 3294. doi:10.1038/s41467-018-05470-4
- Rosser, E. C., Piper, C. J. M., Matei, D. E., Blair, P. A., Rendeiro, A. F., Orford, M., et al. (2020). Microbiota-derived metabolites suppress arthritis by amplifying aryl-hydrocarbon receptor activation in regulatory B cells. *Cell Metab.* 31 (4), 837–851. doi:10.1016/j.cmet.2020.03.003
- Shang, J., Ma, S., Zang, C., Bao, X., Wang, Y., and Zhang, D. (2021). Gut microbiota mediates the absorption of FLZ, a new drug for Parkinson's disease treatment. *Acta Pharm. Sin. B* 11 (5), 1213–1226. doi:10.1016/j.apsb.2021.01.009
- Shen, J., Yang, L., You, K., Chen, T., Su, Z., Cui, Z., et al. (2022). Indole-3-Acetic acid alters intestinal microbiota and alleviates ankylosing spondylitis in mice. *Front. Immunol.* 13, 762580. doi:10.3389/fimmu.2022.762580
- Silverberg, M. S., Satsangi, J., Ahmad, T., Arnott, I. D., Bernstein, C. N., Brant, S. R., et al. (2005). Toward an integrated clinical, molecular and serological classification of inflammatory bowel disease: Report of a working party of the 2005 montreal world congress of gastroenterology. *Can. J. Gastroenterol.* 19, 5A–36A. doi:10.1155/2005/269076
- Singh H, H., Torralba, M. G., Moncera, K. J., DiLello, L., Petrini, J., Nelson, K. E., et al. (2019). Gastro-intestinal and oral microbiome signatures associated with healthy aging. *Geroscience* 41 (6), 907–921. doi:10.1007/s11357-019-00098-8
- Singh N, N., Baby, D., Rajguru, J. P., Patil, P. B., Thakkannavar, S. S., and Pujari, V. B. (2019). Inflammation and cancer. *Ann. Afr. Med.* 18 (3), 121–126. doi:10.4103/aam.aam_56_18
- Somm, E., Montandon, S. A., Loizides-Mangold, U., Gañá, N., Lazarevic, V., De Vito, C., et al. (2021). The GLP-1R agonist liraglutide limits hepatic lipotoxicity and inflammatory response in mice fed a methionine-choline deficient diet. *Transl. Res.* 227, 75–88. doi:10.1016/j.trsl.2020.07.008
- Su, X., Zhang, M., Qi, H., Gao, Y., Yang, Y., Yun, H., et al. (2022). Gut microbiota-derived metabolite 3-indoleacetic acid together with LPS induces IL-35(+) B cell generation. *Microbiome* 10 (1), 13. doi:10.1186/s40168-021-01205-8
- Sun, Y., Wu, D., Zeng, W., Chen, Y., Guo, M., Lu, B., et al. (2021). The role of intestinal dysbacteriosis induced arachidonic acid metabolism disorder in inflaming in atherosclerosis. *Front. Cell. Infect. Microbiol.* 11, 618265. doi:10.3389/fcimb.2021.618265
- Teng, Y., Ren, Y., Sayed, M., Hu, X., Lei, C., Kumar, A., et al. (2018). Plant-derived exosomal MicroRNAs shape the gut microbiota. *Cell Host Microbe* 24 (5), 637–652. doi:10.1016/j.chom.2018.10.001
- Truax, A. D., Chen, L., Tam, J. W., Cheng, N., Guo, H., Koblansky, A. A., et al. (2018). The inhibitory innate immune sensor NLRP12 maintains a threshold against obesity by regulating gut microbiota homeostasis. *Cell Host Microbe* 24 (3), 364–378. doi:10.1016/j.chom.2018.08.009
- Turnbaugh, P. J., Ley, R. E., Mahowald, M. A., Magrini, V., Mardis, E. R., and Gordon, J. I. (2006). An obesity-associated gut microbiome with increased capacity for energy harvest. *Nature* 444 (7122), 1027–1031. doi:10.1038/nature05414
- Vadell, A. K. E., Bärebring, L., Hulander, E., Gertsson, I., Lindqvist, H. M., and Winkvist, A. (2020). Anti-inflammatory Diet in Rheumatoid Arthritis (ADIRA)-a randomized, controlled crossover trial indicating effects on disease activity. *Am. J. Clin. Nutr.* 111 (6), 1203–1213. doi:10.1093/ajcn/nqaa019
- Virág, D., Király, M., Drahos, L., Édes, A. E., Gecse, K., Bagdy, G., et al. (2020). Development, validation and application of LC-MS/MS method for quantification of amino acids, kynurenine and serotonin in human plasma. *J. Pharm. Biomed. Anal.* 180, 113018. doi:10.1016/j.jpba.2019.113018
- Wan, F., Zhong, R., Wang, M., Zhou, Y., Chen, Y., Yi, B., et al. (2021). Caffeic acid supplement alleviates colonic inflammation and oxidative stress potentially through improved gut microbiota community in mice. *Front. Microbiol.* 12, 784211. doi:10.3389/fmicb.2021.784211
- Wang, C. S., Li, W. B., Wang, H. Y., Ma, Y. M., Zhao, X. H., Yang, H., et al. (2018). VSL#3 can prevent ulcerative colitis-associated carcinogenesis in mice. *World J. Gastroenterol.* 24 (37), 4254–4262. doi:10.3748/wjg.v24.i37.4254
- Wang, L. S., Zhang, M. D., Tao, X., Zhou, Y. F., Liu, X. M., Pan, R. L., et al. (2019). LC-MS/MS-based quantification of tryptophan metabolites and neurotransmitters in the serum and brain of mice. *J. Chromatogr. B Anal. Technol. Biomed. Life Sci.* 1112, 24–32. doi:10.1016/j.jchromb.2019.02.021
- Wang, Y., Tong, Q., Ma, S. R., Zhao, Z. X., Pan, L. B., Cong, L., et al. (2021). Oral berberine improves brain dopa/dopamine levels to ameliorate Parkinson's disease by regulating gut microbiota. *Signal Transduct. Target. Ther.* 6 (1), 77. doi:10.1038/s41392-020-00456-5
- Włodarska, M., Luo, C., Kolde, R., d'Hennezel, E., Annand, J. W., Heim, C. E., et al. (2017). Indoleacrylic acid produced by commensal *Peptostreptococcus* species suppresses inflammation. *Cell Host Microbe* 22 (1), 25–37. doi:10.1016/j.chom.2017.06.007
- Yang, X., Mo, W., Zheng, C., Li, W., Tang, J., and Wu, X. (2020a). Alleviating effects of noni fruit polysaccharide on hepatic oxidative stress and inflammation in rats under a high-fat diet and its possible mechanisms. *Food Funct.* 11 (4), 2953–2968. doi:10.1039/d0fo00178c
- Yang, X., Yu, D., Xue, L., Li, H., and Du, J. (2020b). Probiotics modulate the microbiota-gut-brain axis and improve memory deficits in aged SAMP8 mice. *Acta Pharm. Sin. B* 10 (3), 475–487. doi:10.1016/j.apsb.2019.07.001

Zhang H, H., Zhuo, S., Song, D., Wang, L., Gu, J., Ma, J., et al. (2021). Icariin inhibits intestinal inflammation of DSS-induced colitis mice through modulating intestinal flora abundance and modulating p-p65/p65 molecule. *Turk. J. Gastroenterol.* 32 (4), 382–392. doi:10.5152/tjg.2021.20282

Zhang, L., and Wei, W. (2020). Anti-inflammatory and immunoregulatory effects of paeoniflorin and total glucosides of paeony. *Pharmacol. Ther.* 207, 107452. doi:10.1016/j.pharmthera.2019.107452

Zhang X, X., Han, Y., Huang, W., Jin, M., and Gao, Z. (2021). The influence of the gut microbiota on the bioavailability of oral drugs. *Acta Pharm. Sin. B* 11 (7), 1789–1812. doi:10.1016/j.apsb.2020.09.013

Zhang Y, Y., Mao, X., Li, W., Chen, W., Wang, X., Ma, Z., et al. (2021). *Tripterygium wilfordii*: An inspiring resource for rheumatoid arthritis treatment. *Med. Res. Rev.* 41 (3), 1337–1374. doi:10.1002/med.21762

Zhao E, E., Zhang, W., Geng, B., You, B., Wang, W., and Li, X. (2021). Intestinal dysbacteriosis leads to kidney stone disease. *Mol. Med. Rep.* 23 (3), 180. doi:10.3892/mmr.2020.11819

Zhao F, F., An, R., Wang, L., Shan, J., and Wang, X. (2021). Specific gut microbiome and serum metabolome changes in lung cancer patients. *Front. Cell. Infect. Microbiol.* 11, 725284. doi:10.3389/fcimb.2021.725284

Zhao, H., Lazarenko, O. P., and Chen, J. R. (2020). Hippuric acid and 3-(3-hydroxyphenyl) propionic acid inhibit murine osteoclastogenesis through RANKL-RANK independent pathway. *J. Cell. Physiol.* 235 (1), 599–610. doi:10.1002/jcp.28998

Zhao, Z. H., Xin, F. Z., Xue, Y., Hu, Z., Han, Y., Ma, F., et al. (2019). Indole-3-propionic acid inhibits gut dysbiosis and endotoxin leakage to attenuate steatohepatitis in rats. *Exp. Mol. Med.* 51 (9), 1–14. doi:10.1038/s12276-019-0304-5



OPEN ACCESS

EDITED BY

Yan Chang,
Anhui Medical University, China

REVIEWED BY

Xiuguo Han,
Shanghai Jiao Tong University, China
Chao Zhuang,
The Affiliated Changzhou No.2 People's
Hospital of Nanjing Medical University,
China

*CORRESPONDENCE

Qingmin Zeng,
qingminzeng1703@163.com
Hengfeng Yuan,
yuanhf@shsmu.edu.cn
Xiuying Yang,
dryangyingzi@163.com

[†]These authors have contributed equally
to this work

SPECIALTY SECTION

This article was submitted to
Inflammation Pharmacology,
a section of the journal
Frontiers in Pharmacology

RECEIVED 25 May 2022

ACCEPTED 10 August 2022

PUBLISHED 27 September 2022

CITATION

Jiang Z, Qi G, Lu W, Wang H, Li D,
Chen W, Ding L, Yang X, Yuan H and
Zeng Q (2022), Omaveloxolone inhibits
IL-1 β -induced chondrocyte apoptosis
through the Nrf2/ARE and NF- κ B
signalling pathways *in vitro* and
attenuates osteoarthritis *in vivo*.
Front. Pharmacol. 13:952950.
doi: 10.3389/fphar.2022.952950

COPYRIGHT

© 2022 Jiang, Qi, Lu, Wang, Li, Chen,
Ding, Yang, Yuan and Zeng. This is an
open-access article distributed under
the terms of the [Creative Commons
Attribution License \(CC BY\)](https://creativecommons.org/licenses/by/4.0/). The use,
distribution or reproduction in other
forums is permitted, provided the
original author(s) and the copyright
owner(s) are credited and that the
original publication in this journal is
cited, in accordance with accepted
academic practice. No use, distribution
or reproduction is permitted which does
not comply with these terms.

Omaveloxolone inhibits IL-1 β -induced chondrocyte apoptosis through the Nrf2/ARE and NF- κ B signalling pathways *in vitro* and attenuates osteoarthritis *in vivo*

Zengxin Jiang^{1,2†}, Guobin Qi^{3†}, Wei Lu^{4†}, Hao Wang⁵, Defang Li²,
Weibin Chen², Lei Ding², Xiuying Yang^{6*}, Hengfeng Yuan^{1*} and
Qingmin Zeng^{2*}

¹Department of Orthopaedics, Shanghai Jiaotong University Affiliated Sixth People's Hospital, Shanghai, China, ²Department of Orthopedic Surgery, Fudan University Jinshan Hospital, Shanghai, China, ³Department of Orthopedic Surgery, Zhongshan Hospital, Fudan University, Shanghai, China, ⁴Department of Orthopedic Surgery, Shanghai TCM-Integrated Hospital Shanghai University of TCM, Shanghai, China, ⁵Department of Orthopaedics, The Second Affiliated Hospital of Chongqing Medical University, Chongqing, China, ⁶Department of Radiology, Fudan University Jinshan Hospital, Shanghai, China

Osteoarthritis (OA) is a common degenerative joint disease. Effective drugs that can halt or decelerate osteoarthritis progression are still lacking. Omaveloxolone is a semisynthetic oleanane triterpenoid exerting antioxidative and anti-inflammatory effects. The present study aims to determine whether omaveloxolone has a therapeutic effect on OA. Chondrocytes were treated with interleukin (IL)-1 β to establish an OA cell model *in vitro*. Indicators of cell viability, oxidative stress, inflammation, cell apoptosis and extracellular matrix (ECM) degradation were investigated. Proteins related to the Nuclear factor erythroid derived-2-related factor 2 (Nrf2)/antioxidant response element (ARE) and nuclear factor kappa-light-chain-enhancer of activated B cells (NF- κ B) signalling pathways were assessed using Western blotting. A destabilized medial meniscus surgery-induced OA rat model was used *in vivo*. Gait analysis, microcomputed tomography analysis, and histopathological and immunohistochemical analyses were performed to determine the therapeutic effect of omaveloxolone on attenuating osteoarthritis *in vivo*. The results showed that omaveloxolone exerts antioxidative, anti-inflammatory, antiapoptotic and anti-ECM degradation effects via activation of the Nrf2/ARE signalling pathway and inhibition of the NF- κ B signalling pathway in chondrocytes *in vitro* and attenuates OA progression *in vivo*, suggesting that omaveloxolone may be a potential therapeutic agent for OA.

KEYWORDS

osteoarthritis, omaveloxolone, Nrf2, NF- κ B, apoptosis

Introduction

Osteoarthritis (OA) is a chronic degenerative disease characterized by the degeneration of articular cartilage. The prevalence of OA has been rapidly increasing owing to an ageing population as well as an obesity epidemic. Approximately 300 million people suffer from OA worldwide (Vitaloni et al., 2020). OA is a leading cause of disability (Hunter et al., 2020). Nonsteroidal anti-inflammatory drugs (NSAIDs), selective cyclooxygenase-2 inhibitors and acetaminophen are used clinically for symptomatic relief. However, they cannot effectively prevent the progression of OA (Abdel-Aziz et al., 2021; Zhang et al., 2021b). Patients with severe OA eventually require arthroplasty. OA constitutes a considerable burden on society worldwide (Hawker and King, 2022).

Chondrocytes, the only cell population of articular cartilage, play a crucial role in maintaining articular cartilage homeostasis (Chen et al., 2021). Hence, the survival of chondrocytes is critical and essential for the structural preservation, functional regulation and extracellular matrix (ECM) turnover of articular cartilage (Hall, 2019). Growing evidence demonstrates an association between chondrocyte death and OA (Yang et al., 2021). Increased reactive oxygen species (ROS) generation and inflammation can initiate chondrocyte apoptosis, which contributes to the occurrence and development of OA. Inhibiting chondrocyte apoptosis is a potential therapeutic intervention for OA (Blanco et al., 1998; Hashimoto et al., 1998; Hwang and Kim, 2015; Chow and Chin, 2020).

Omaveloxolone (also known as RTA408) is a semisynthetic oleanane triterpenoid and a novel compound in the antioxidant inflammation modulator class (Probst et al., 2015). Omaveloxolone is one of the most potent activators of the nuclear factor erythroid derived-2-related factor 2 (Nrf2)/Nrf2 activates antioxidant response element (ARE) pathway (active at nanomolar concentrations) (Cuadrado et al., 2018). Increasing evidence indicates that targeting the Nrf2/ARE signalling pathway is of pharmacological interest in the treatment of OA. Nrf2 is a critical regulatory factor in the system of oxidative stress defence. Nrf2 binds to the inhibitory protein Kelch-like ECH-associated protein 1 (Keap1) in the cytoplasm under physiological conditions. Nrf2 dissociates from Keap1 and translocates into the nucleus under stress or pathological conditions. ARE-regulated antioxidant proteins, including haem oxygenase-1 (HO-1) and NADPH quinone oxidoreductase 1 (NQO-1), to exert antioxidant effects (Ulasov et al., 2021; Panda et al., 2022). Several previous studies have confirmed that the Nrf2/ARE signalling pathway plays a protective role in articular cartilage (Marchev et al., 2017; Song et al., 2021; Chen et al., 2022). Consequently, agents, including omaveloxolone, may have therapeutic potential for the treatment of OA for their ability to activate Nrf2/ARE signalling pathway.

In addition, omaveloxolone is also an effective inhibitor of the Nuclear factor kappa-light-chain-enhancer of activated

B cells (NF- κ B) signalling pathway (Sun et al., 2020; Zhang et al., 2021). NF- κ B is also an important regulator of oxidative stress and inflammation. NF- κ B dimers interact with inhibitory I κ B proteins in the cytoplasm under physiological conditions. NF- κ B dimers translocate from the cytoplasm into the nucleus to activate NF- κ B-dependent genes following injury or stress. The canonical and noncanonical pathways are the two major signalling pathways involved in the activation of the NF- κ B signalling pathway. The canonical pathway is dependent on IKK β and NEMO, while the non-canonical pathway is dependent on IKK α (Rigoglou and Papavassiliou, 2013; Jimi et al., 2019). The NF- κ B signalling pathway has been identified as a key contributing factor that is abnormally activated in OA. Inhibition of the NF- κ B signalling pathway shows therapeutic potential in the treatment of OA (Marcu et al., 2010; Choi et al., 2019; Lepetos et al., 2019). It is conceivable that omaveloxolone with a suppressive role in NF- κ B signaling would have therapeutic potential for OA.

Omaveloxolone has been shown to have strong antioxidant and anti-inflammatory effects by activating the Nrf2 pathway and/or suppressing the NF- κ B signalling pathway *in vitro* or *in vivo* in studies of some diseases, such as acute asthma exacerbation, nonalcoholic steatohepatitis, acute kidney injury and neurodegenerative diseases (Han et al., 2017; Yang et al., 2019; Zhang et al., 2019; Reisman et al., 2020). In addition, the safety of omaveloxolone was preliminarily confirmed in a phase I clinical trial in patients with metastatic non-small-cell lung cancer or melanoma and a phase II clinical trial in Friedreich ataxia (Creelan et al., 2017; Lynch et al., 2019; Madsen et al., 2020).

Given the effects of omaveloxolone on the regulation of the Nrf2/ARE and NF- κ B signalling pathways and the critical role of the NF- κ B pathways in OA, omaveloxolone may have potential as a therapy for OA. However, supporting evidence is still lacking. We thus conducted the current study to explore the roles and mechanism of omaveloxolone in protecting chondrocytes against IL-1 β -induced cell apoptosis *in vitro* and to determine the potential therapeutic effects of omaveloxolone on preventing OA *in vivo*.

Materials and methods

Cell isolation and culture

All animal experiments in the present study were approved by the Committee on Ethics of Animal Experiments of Fudan University Jinshan Hospital (Shanghai, China). Four, 4-week-old male Sprague-Dawley (SD) rats (Shanghai SLAC Laboratory Animal Co. LTD) were euthanized by an overdose of carbon dioxide. The cartilage of the hip joints was harvested, cut into small pieces and digested with 0.1% collagenase II (Gibco; Grand Island, NY, United States) at 37°C overnight. The chondrocytes were collected and cultured in Dulbecco's modified Eagle's medium (DMEM, Gibco) with 10% foetal bovine serum (FBS, Gibco) in a 5% CO₂ atmosphere at 37°C.

Cell viability assay

The cell viability of chondrocytes was measured using a Cell Counting Kit-8 (CCK-8, Beyotime Institute of Biotechnology, Shanghai, China). Cells were treated with different concentrations of omaveloxolone (5, 10, 25, 50, 100, 250, 500, 1000 and 2000 nM) for 24, 48 and 72 h. IL-1 β (10 ng/ml, PeproTech EC, London, United Kingdom) was used to mimic inflammatory conditions (Jin et al., 2021). DMEM containing 10% CCK-8 solution was added to each well for 2 h. Absorption was detected at 450 nm using a microplate reader (Epoch; BioTek Instruments Inc., Vermont, United States).

ROS level evaluation

2',7'-dichlorofluorescein diacetate (DCFH-DA, Sigma-Aldrich, Missouri, United States) staining was used to evaluate ROS levels in chondrocytes 24 h after treatment. Briefly, chondrocytes were washed with PBS twice, stained with 10 μ M DCFH-DA for 30 min, washed with serum-free DMEM three times to remove the DCFH-DA solution and observed under an Olympus FV3000 confocal laser scanning microscope. In addition, cells were collected and stained with DCFH-DA for flow cytometry analysis using a BD Accuri C6 plus flow cytometer (BD Biosciences, Vianen, Netherlands) to quantify ROS levels.

Malondialdehyde (MDA) and superoxide dismutase (SOD) evaluation

MDA content in chondrocytes was detected using an MDA assay kit (Beyotime). SOD levels in chondrocytes were determined using a SOD assay kit (Nanjing Jiancheng Bioengineering Institute, Jiangsu, China). In brief, cell lysates were cultured with working buffer for 30 min at 37°C according to the manufacturer's instructions 24 h after treatment. Absorbance was detected at a wavelength of 523 nm (MDA) or 450 nm (SOD) using a microplate reader. A bicinchoninic acid (BCA) protein assay kit (Beyotime) was used to determine the total protein concentration to normalize the MDA and SOD levels.

Mitochondrial membrane potential determination

The mitochondrial membrane potential of chondrocytes was detected using a JC-1 mitochondrial membrane potential assay kit (Abcam, Cambridge, United Kingdom) 24 h after treatment. Chondrocytes were stained with JC-1 (5 μ g/ml) for 25 min followed by Hoechst 33,342 (Thermo Fisher, Waltham, MA, United States) staining for 5 min at 37°C. The cells were then observed under an Olympus FV3000 confocal laser scanning microscope. In addition, cells were collected and stained with JC-

1 for flow cytometry analysis using a BD Accuri C6 plus flow cytometer to quantify mitochondrial membrane potential levels.

Annexin V-fluorescein isothiocyanate (FITC)/propidium iodide (PI) staining

Chondrocyte apoptosis was measured using an Annexin V-FITC kit (BD Bioscience, CA, United States) 24 h after treatment. Then, 5 μ L Annexin V was added to the chondrocytes for 30 min, and 5 μ L PI was added for 5 min at 37°C in the dark. Flow cytometry analysis was performed using a BD Accuri C6 plus flow cytometer. Chondrocytes were observed under an Olympus FV3000 confocal laser scanning microscope.

Western blotting

Chondrocytes were lysed in radioimmunoprecipitation assay buffer to extract total protein. In addition, a nuclear protein extraction kit (Beyotime) was used to extract nuclear protein from chondrocytes. Proteins were separated by sodium dodecyl sulfate-polyacrylamide gel electrophoresis and transferred to polyvinylidene fluoride membranes (Beyotime). Membranes were incubated overnight at 4°C with the following primary antibodies: inducible nitric oxide synthase (iNOS, 1:2,000, ab178945, Abcam), cyclooxygenase-2 (COX-2, 1:2,000, ab188183, Abcam), B cell lymphoma 2 (Bcl2, 1:2,000, ab196495, Abcam), Bcl2-Associated X (Bax, 1:2,000, ab32503, Abcam), metalloproteinase with matrix metalloproteinase (MMP) 3 (1:2,000, ab52915, Abcam), MMP13 (1:2,000, 18165-1-AP, Proteintech, Wuhan, China), collagen type II (1:2,000, ab188570, Abcam), aggrecan (1:2,000, 13880-1-AP, Proteintech), phosphorylated P65 (p-P65) (1:1,000; ab76302, Abcam), P65 (1:1,000; ab19870, Abcam), p-IkB α (1:1,000; ab133462, Abcam), IkB α (1:1,000; ab32518, Abcam), Nrf2 (1:1,000, 16396-1-AP, Proteintech), HO-1 (1:2,000, ab13243, Abcam), NQO-1 (1:2,000, 11451-1-AP, Proteintech), Lamin B1 (1:2,000, 12987-1-AP, Proteintech) and β -actin (1:5,000; #4970, Cell Signaling Technology Inc., Danvers, MA, United States). Membranes were subsequently cultured with the corresponding secondary antibodies (horseradish peroxidase-labelled goat anti-rabbit IgG and anti-mouse IgG, Proteintech). Signals of target proteins were visualized using enhanced chemiluminescence on an imaging system (Tanon, Shanghai, China). Relative protein levels were quantified using ImageJ software (version 1.8.0; National Institutes of Health, Bethesda, MA, United States) normalized to β -actin or Lamin B1.

Immunofluorescence assay

Immunofluorescence was performed to explore the changes in the expression of aggrecan, collagen type II, MMP3 and MMP13. Chondrocytes were incubated in blocking solution

and stained with primary antibodies against aggrecan, collagen type II, MMP3 and MMP13 overnight at 4°C. Chondrocytes were then stained with the FITC- or phycoerythrin (PE)-conjugated secondary antibody (Thermo Fisher). The nucleus was labelled with Hoechst 33,342. Cells were observed under an Olympus FV3000 confocal laser scanning microscope.

Animal model

Twenty-four 4-week-old SD rats were used for *in vivo* experiments. Animal experiments were performed after 1week adaptive feeding. Destabilized medial meniscus (DMM) surgery was performed to induce OA in the right knee of rats as described previously (Lin et al., 2022; Teng et al., 2022). The rats were randomized to four groups (sham group, DMM group, DMM +200 µg/kg omaveloxolone group and DMM +500 µg/kg omaveloxolone group), with six rats in each group. Omaveloxolone was dissolved in normal saline. Rats received intraperitoneal injections of omaveloxolone every 3 days. Intraperitoneal injections of omaveloxolone were performed 2 weeks after modeling. The omaveloxolone dosages were based on our pre-experiment results and previous study (Sun et al., 2020).

CatWalk XT gait analysis

The Catwalk-gait test was performed using the Catwalk automated gait analysis system (Noldus Information Technology, Wageningen, Netherlands). Rats walked freely on a glass floor lit by green light, and the position of the rat footprints was recorded by a high-speed video camera. The recorded data were analysed using catwalk program software (Noldus, CatWalk XT version 10.6.608).

Radiographic analysis

Increasing evidence indicates that subchondral bone changes are crucial pathological changes in OA (Li et al., 2013; Aizah et al., 2021; Hu et al., 2021). Hence, structural alterations of subchondral bone architecture were evaluated in this study. Rats were euthanized by carbon dioxide 8 weeks after the omaveloxolone treatment. The right knee joints were harvested. Microcomputed tomography (micro-CT) images of the knee joints were obtained using a SCANCO 50 (Switzerland). Three-dimensional (3D) images of the knee joints were reconstructed. Bone morphometric parameters of tibial subchondral bone, including bone mineral density (BMD), bone volume (BV)/total volume (TV), trabecular number (Tb. N), trabecular separation (Tb. Sp) and trabecular thickness (Tb.th) were analysed.

Histopathology and immunohistochemistry analysis

Knee joints of rats were fixed with 4% paraformaldehyde and decalcified in 10% ethylenediamine tetraacetic acid (EDTA). Tissues were processed and embedded in paraffin for histopathological examination. The sections were stained with haematoxylin-eosin (HE), safranin O/fast green (SO/FG) and toluidine blue (TB). For IHC analysis, antigen retrieval was performed using microwave treatment. Endogenous peroxidases were blocked using 3% hydrogen peroxide. Goat serum (10%) was used to block nonspecific staining. Sections were incubated with the primary antibody against collagen type II and aggrecan at 4°C overnight, followed by the secondary biotinylated antibody (Proteintech) for 30 min at 37°C. Sections were stained with 3,3'-diaminobenzidine tetrahydrochloride for 25 s and then stained with haematoxylin for 5 min at room temperature. Sections were digitally scanned using a BX51 Olympus fluorescence microscope. Collagen type II levels were quantified using ImageJ software.

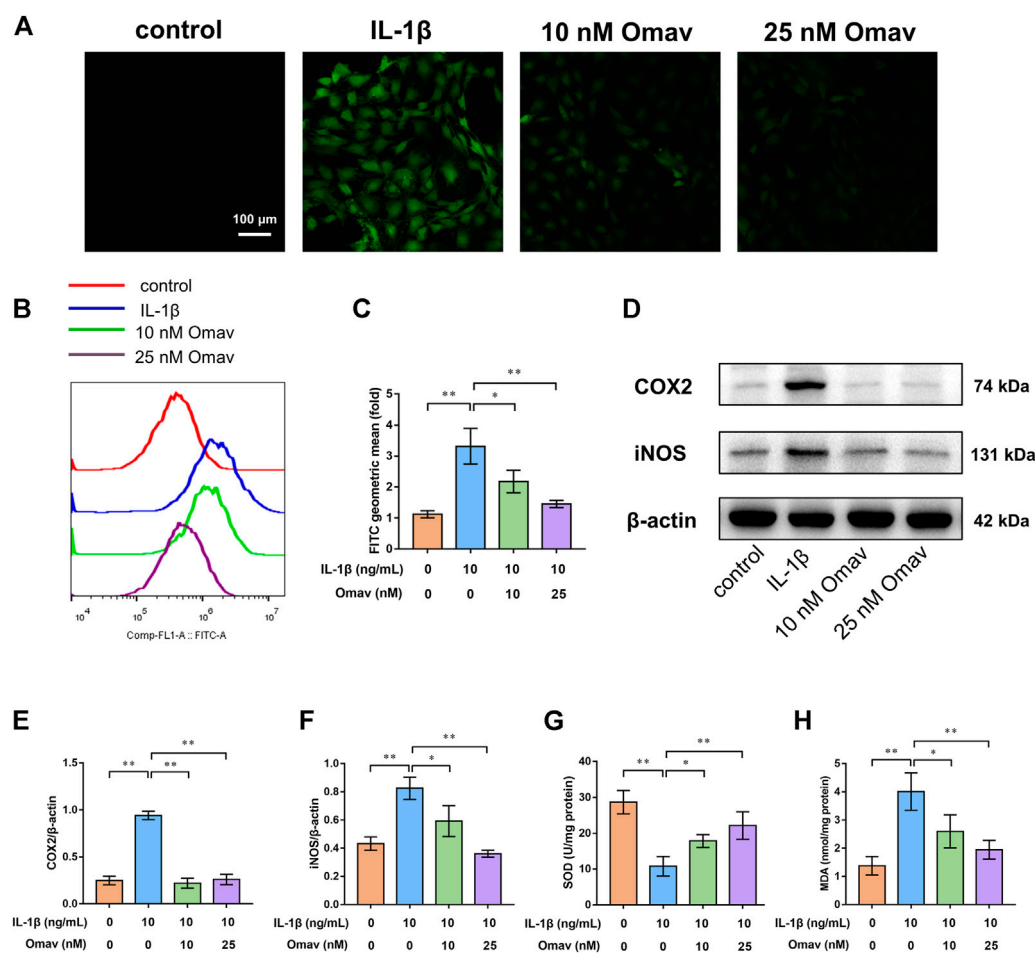
Statistical analysis

All experiments were replicated independently three times. Data are presented as the mean ± standard deviation. A two-tailed Student's *t* test was applied for two-group comparisons. The Mann-Whitney test was used for nonparametric data (OARSI scoring and Mankin scoring). *p* values <0.05 were considered statistically significant. Statistical analyses were performed using SPSS software (version 22.0; IBM Corp.).

Results

Omaveloxolone improved the viability of chondrocytes exposed to IL-1 β

The structural formula of omaveloxolone is presented in Figure 1G. The cell cytotoxicity of different concentrations of omaveloxolone (5, 10, 25, 50, 100, 250, 500, 1000 and 2000 nM) was assessed using a CCK8 assay. No significant cytotoxicity of omaveloxolone on chondrocytes was observed at concentrations below or equal to 500 nM at 24, 48 and 72 h (Figures 1A–C). Therefore, omaveloxolone at concentrations below or equal to 500 nM was used to evaluate the effects on the viability of chondrocytes exposed to IL-1 β . The results showed that 10, 25, 50, 100, 250 and 500 nM significantly improved the viability of chondrocytes exposed to IL-1 β at 24, 48, and 72 h (Figures 1D–F). 10 nM was the lowest effective concentration able to effectively improve the cell viability and thus was selected for subsequent treatments. At concentration of 25 and 50 nM, omaveloxolone had the best effects on improving the viability of

**FIGURE 2**

Omaveloxolone exerted antioxidant and anti-inflammatory effects on chondrocytes exposed to IL-1β. **(A)** Representative fluorescence confocal microscopic images of chondrocytes stained with DCFH-DA (scale bar, 100 μm). **(B and C)** Chondrocytes stained with DCFH-DA were assessed by flow cytometry to quantify the ROS level. **(D)** Representative Western blots. Quantitative analysis of COX2 **(E)** and iNOS **(F)** was performed. **(G)** The SOD levels in chondrocytes among the four groups. **(H)** MDA levels in chondrocytes among the four groups. * $p < 0.05$ and ** $p < 0.01$.

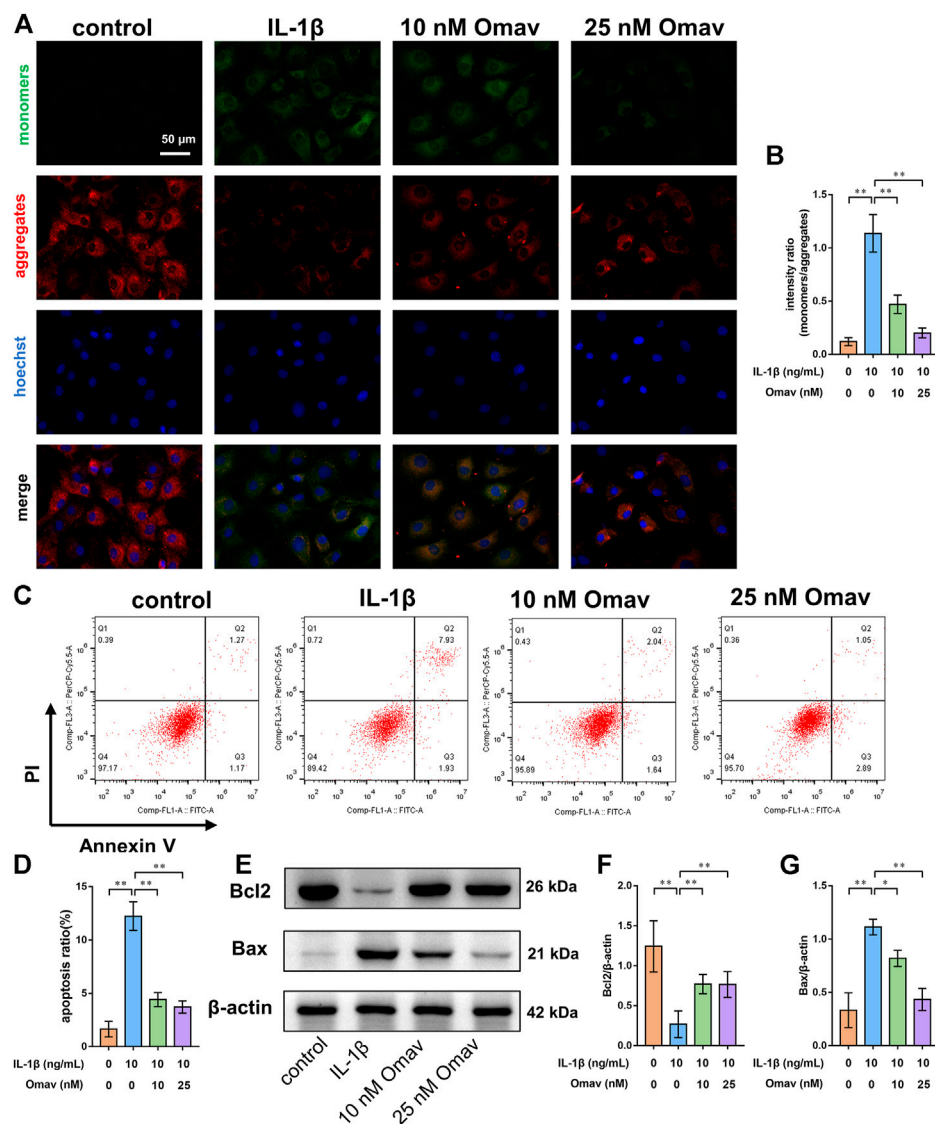
reversed by administration of 10 and 25 nM omaveloxolone (Figures 2E,F). The results suggested that omaveloxolone could suppress inflammation in chondrocytes exposed to IL-1β.

Omaveloxolone prevented the apoptosis of chondrocytes exposed to IL-1β

Mitochondrial membrane potential was assessed using JC-1 staining. Representative fluorescence confocal microscopic images are shown in Figure 3A. Green fluorescence indicates decreased mitochondrial membrane potential, while red fluorescence indicates normal mitochondrial membrane potential. The results showed that IL-1β exposure led to decreased mitochondrial membrane potential in chondrocytes,

which is a landmark event in early apoptosis. Omaveloxolone (10 and 25 nM) significantly improved the mitochondrial membrane potential in chondrocytes exposed to IL-1β (Figures 3A,B).

Chondrocyte apoptosis was then detected using Annexin V/PI staining. The results of flow cytometry showed that IL-1β increased the apoptosis ratio of chondrocytes, while 10 and 25 nM of omaveloxolone significantly reduced the apoptosis ratio of chondrocytes exposed to IL-1β (Figures 3C,D). In addition, the apoptosis markers Bax and Bcl2 were measured using Western blotting. IL-1β decreased Bcl2 protein levels but increased Bax protein levels in chondrocytes. Omaveloxolone (10 and 25 nM) promoted Bcl2 protein expression and inhibited Bax protein expression in chondrocytes exposed to IL-1β (Figures 3E-G). The results above indicated that omaveloxolone effectively prevented IL-1β-induced apoptosis of chondrocytes.

**FIGURE 3**

Omaveloxolone prevented IL-1 β -induced chondrocyte apoptosis. (A) Representative fluorescence confocal microscopic images of chondrocytes stained with JC-1 (scale bar, 50 μ m). (B) Mitochondrial membrane potential quantitative analysis. (C) Chondrocytes were stained with Annexin V/PI and measured by flow cytometry. (D) Quantitative analysis of the apoptosis ratio of chondrocytes. (E) Representative Western blots. Quantitative analysis of Bcl2 (F) and Bax (G) was performed. * $p < 0.05$ and ** $p < 0.01$.

Omaveloxolone inhibited ECM degradation of chondrocytes exposed to IL-1 β

To assess the degree of ECM degeneration, ECM proteins and ECM degrading enzymes, including collagen type II, aggrecan, MMP3 and MMP13, were evaluated using immunofluorescence and Western blotting assays. Representative fluorescence confocal microscopic images are shown in Figures 4A–D. The results of quantitative analysis of the fluorescence intensity showed that IL-1 β

decreased the expression levels of collagen type II and aggrecan while increasing the expression levels of MMP 3 and MMP 13. Omaveloxolone (10 and 25 nM) increased the expression levels of collagen type II and aggrecan but reduced the expression levels of collagen type II and aggrecan (Figures 4E–H). The results of the Western blotting assay showed that 10 and 25 nM of omaveloxolone significantly promoted collagen type II and aggrecan protein expression while inhibiting MMP 3 and MMP 13 protein expression (Figures 5A–E), which is consistent with the immunofluorescence results. The results indicated that

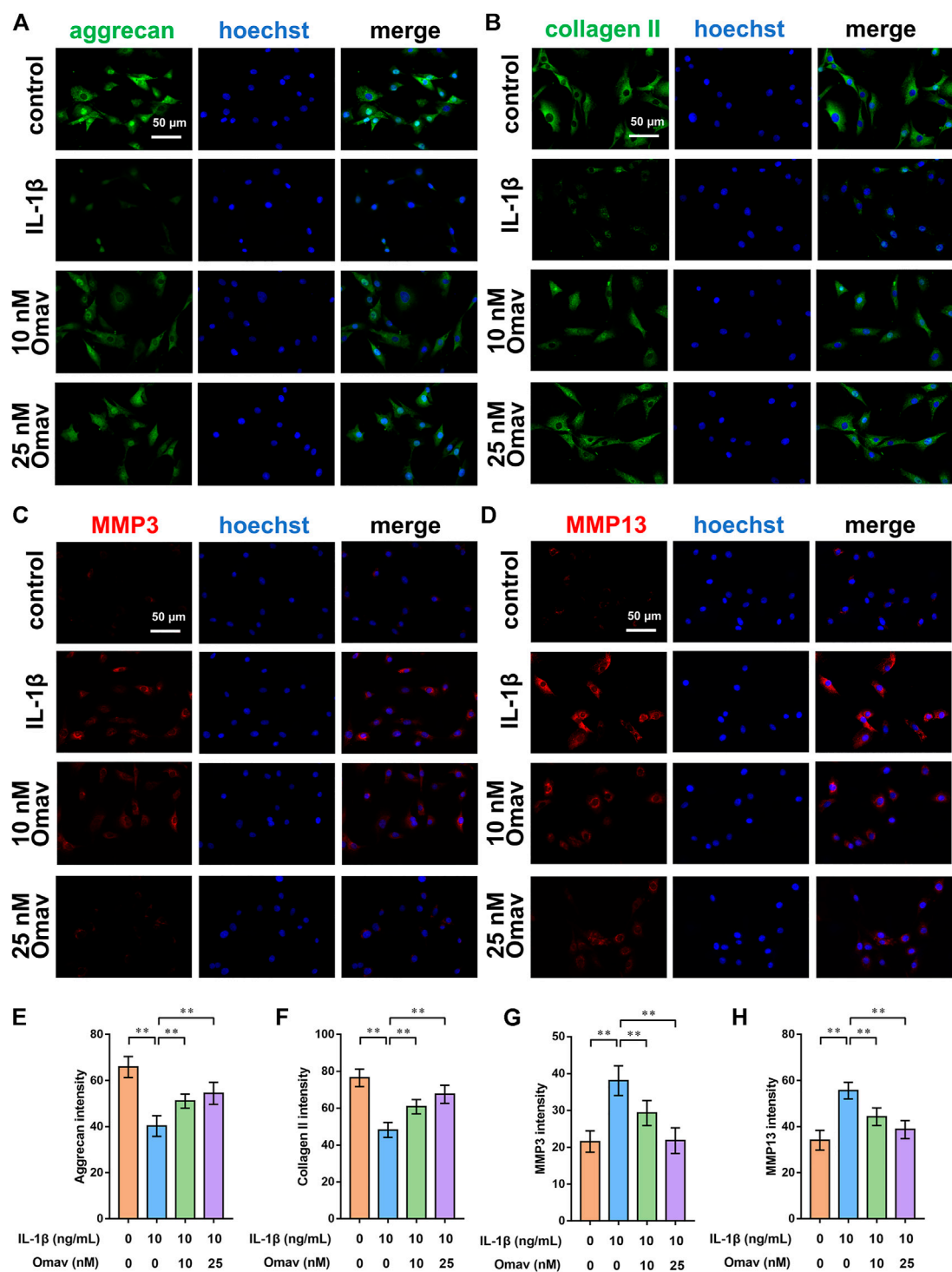


FIGURE 4
Omaveloxolone suppressed IL-1 β -induced ECM degradation *in vitro*. Representative immunofluorescence images of aggrecan (A), collagen type II (B), MMP3 (C) and MMP13 (D) (scale bar, 50 μ m). The results of the quantitative analysis showed that omaveloxolone enhanced aggrecan (E) and collagen type II (F) protein expression while inhibiting MMP3 (G) and MMP13 (H) protein expression in chondrocytes exposed to IL-1 β . ** p < 0.01.

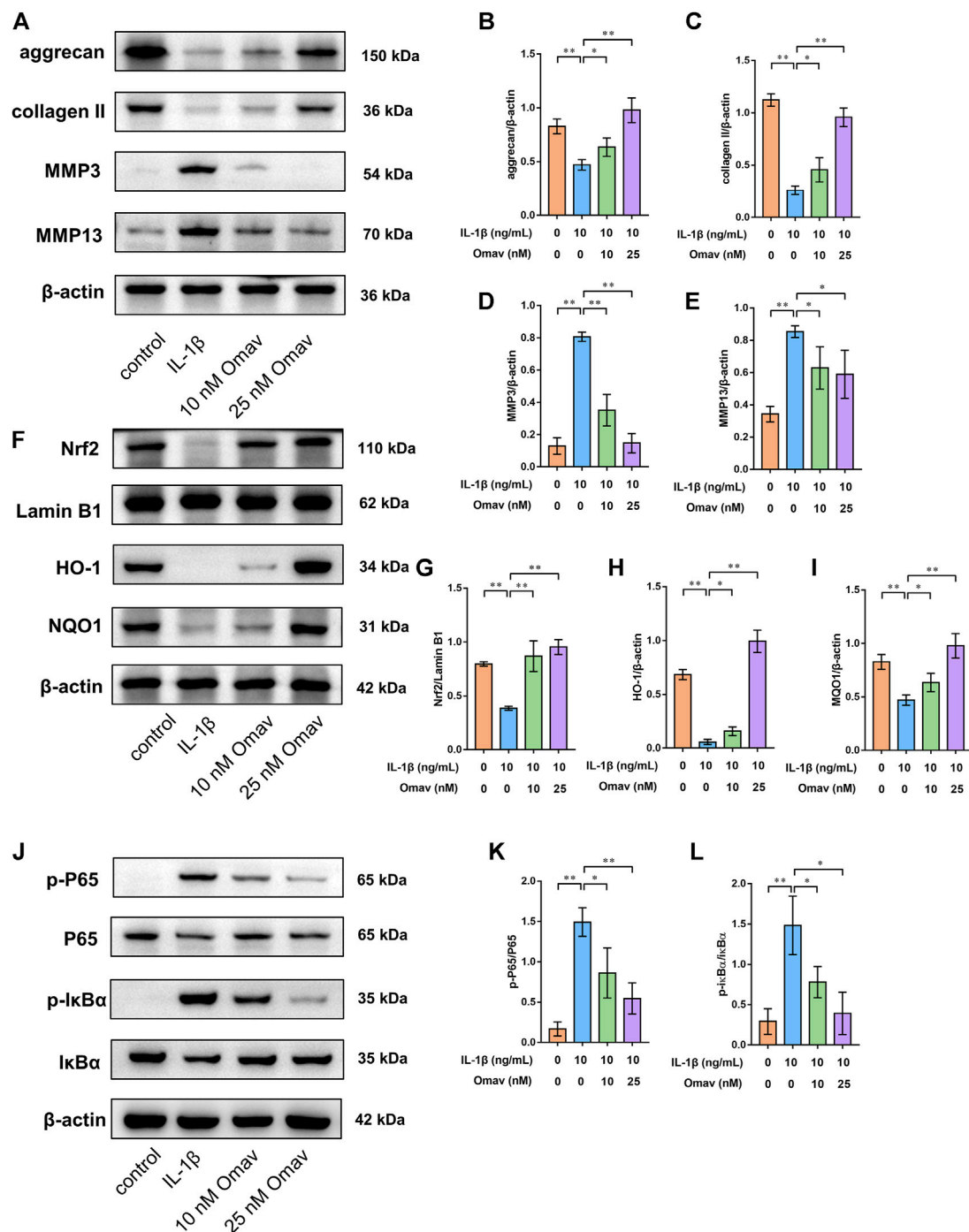


FIGURE 5

Omaveloxolone activated the Nrf2/ARE signalling pathway while suppressing the NF- κ B signalling pathway in chondrocytes exposed to IL-1 β . (A) Representative Western blots of proteins involved in ECM degradation. Quantitative analysis of aggrecan (B), collagen type II (C), MMP3 (D) and MMP13 (E) was performed. (F) Representative Western blots of proteins involved in the Nrf2/ARE signalling pathway. Quantitative analysis of Nrf2 (G), HO-1 (H) and NQO1 (I) was performed. (J) Representative Western blots of proteins involved in the NF- κ B signalling pathway. Omaveloxolone (10 and 25 nM) reduced the p-P65/P65 ratio (K) and p-I κ B α /I κ B α ratio (L). * p < 0.05 and ** p < 0.01.

omaveloxolone could inhibit ECM degradation in chondrocytes exposed to IL-1 β .

Omaveloxolone activated the Nrf2/ARE signalling pathway while suppressing the NF- κ B signalling pathway in chondrocytes exposed to IL-1 β

To explore the underlying mechanism by which omaveloxolone prevents IL-1 β -induced apoptosis of chondrocytes, the expression of proteins involved in the Nrf2/ARE and NF- κ B signalling pathways was assessed by Western blotting.

To assess the Nrf2/ARE signalling pathway, chondrocytes were pretreated with 10 nM or 25 nM of omaveloxolone for 2 h and then incubated with 10 ng/ml IL-1 β for another 24 h. The results showed that 10 and 25 nM of omaveloxolone promoted Nrf2 translocation into the cell nucleus and thus enhanced HO-1 and NQO1 protein expression in chondrocytes exposed to IL-1 β , suggesting that the Nrf2/ARE signalling pathway, an important antioxidant signalling pathway, was activated by omaveloxolone (Figures 5F–I).

In addition, for assessment of the NF- κ B signalling pathway, chondrocytes were pretreated with 10 nM or 25 nM of omaveloxolone for 2 h and then incubated with 10 ng/ml IL-1 β for another 1 h (Xian et al., 2022; Yao et al., 2022). The results of Western blotting analysis showed that 10 and 25 nM of omaveloxolone reduced the p-P65/P65 and p-I κ B α /I κ B α ratio, indicating that omaveloxolone could suppress the NF- κ B signalling pathway in chondrocytes exposed to IL-1 β (Figure 5J–L).

Omaveloxolone alleviated osteoarthritis in rats

Gait analysis is commonly used to assess pain-related behaviours in a rat OA model. CatWalk data were obtained as the right hind (RH)/left hind (LH) limb ratio of light intensity, print area, duty cycle, stance phrase, swing phrase and swing speed. The results of CatWalk analysis showed that the RH/LH ratios of light intensity, print area, duty cycle, stance phrase and swing speed were decreased, while the RH/LH ratio of swing phrase was increased in rats with OA compared with those in control rats. Low dose of omaveloxolone (200 μ g/kg) and high dose of omaveloxolone (500 μ g/kg) significantly improved the RH/LH ratios of light intensity, print area and swing speed in rats with OA. In addition, high dose of omaveloxolone effectively improved the RH/LH ratios of the stance phase (Figure 6G). These results suggest that omaveloxolone is beneficial for relieving pain in OA rats.

Histopathology and immunohistochemistry analyses were performed to evaluate the protective effects of omaveloxolone on

OA in rats. Representative images of HE, SO/FG and TB staining are shown in Figure 7A. Severe cartilage erosion, massive proteoglycan loss, and decreased number and disordered arrangement of chondrocytes were observed in the OA group. These pathological changes could be ameliorated by low and high doses of omaveloxolone. Histological evaluation was performed using the Osteoarthritis Research Society International (OARSI) scoring system and the modified Mankin scoring system. The results showed that the OARSI scores and Mankin scores of the low-dose and high-dose of omaveloxolone groups were higher than those of the OA groups (Figures 7B,C). Representative immunohistochemistry images of collagen type II and aggrecan are also shown in Figure 7A. The quantitative analysis results showed that.

The expression level of collagen type II in the OA group was lower than that in the control group. Low-dose and high-dose omaveloxolone both increased collagen type II and aggrecan levels *in vivo* (Figures 7D,E).

Furthermore, microCT analysis was performed to assess the changes in the microarchitecture of the subchondral bone. Representative 3D images are shown in Figure 6A. Quantitative analysis of bone microarchitecture parameters showed that both the low dose and high dose of omaveloxolone increased BMD, BV/TV, Tb. th and Tb.N in rats with OA. No significant difference was observed in Tb. Sp among the four groups (Figures 6B–F). The results of behavioural, radiographic, histopathology and immunohistochemistry assays indicate that omaveloxolone effectively alleviated osteoarthritis in rats.

Omaveloxolone toxicity assessment *in vivo*

Major organs (lungs, heart, liver, spleen and kidneys) of rats were harvested and stained with H&E to evaluate the potential toxicity of omaveloxolone. No obvious pathological changes were observed among the four groups, suggesting that 200 and 500 μ g/kg omaveloxolone did not cause significant organ toxicity after 8 weeks of treatment. (Figure 8).

Discussion

Omaveloxolone is a semisynthetic oleanane triterpenoid. Mounting studies have shown that omaveloxolone can exert antioxidative and anti-inflammatory effects via activation of the Nrf2/ARE signalling pathway and inhibition of the NF- κ B signalling pathway (Probst et al., 2015; Han et al., 2017; Sun et al., 2020). Therefore, we conducted the current study to explore the effects of omaveloxolone on attenuating OA.

We first explored the effect of omaveloxolone on the viability of chondrocytes exposed to IL-1 β *in vitro*. Omaveloxolone at

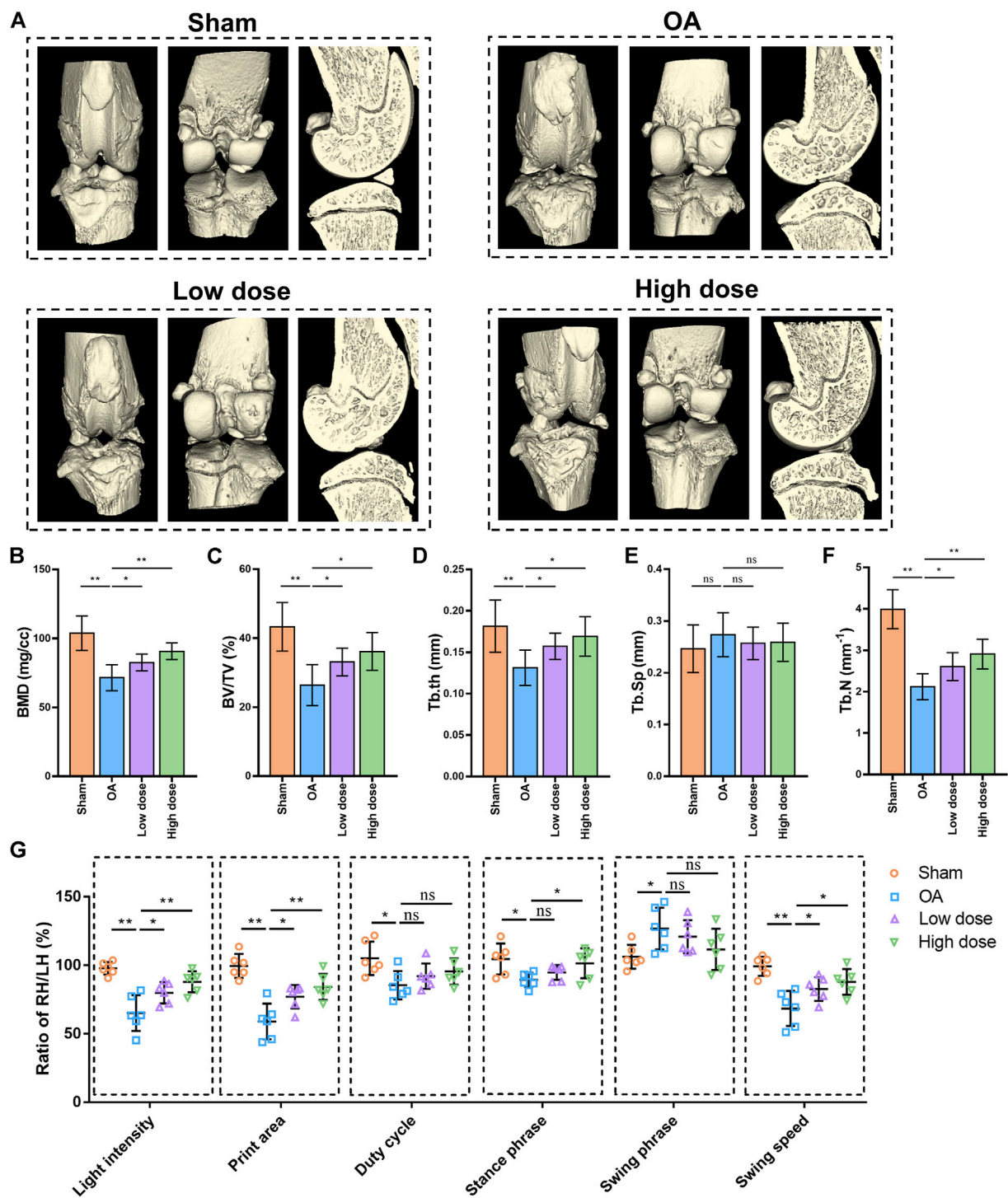


FIGURE 6

Omaveloxolone relieved pain and suppressed subchondral bone loss and microarchitecture deterioration in OA rats. (A) Representative 3D reconstructed images of right knee joints. Quantitative analysis of bone morphometric parameters of tibial subchondral bone, including BMD (B), BV/TV (C), Tb.th (D), Tb.Sp (E) and Tb.N (F). (G) Gait analysis of light intensity, print area, duty cycle, stance phase, swing phase and swing speed. * $p < 0.05$ and ** $p < 0.01$. n. s., not significant.

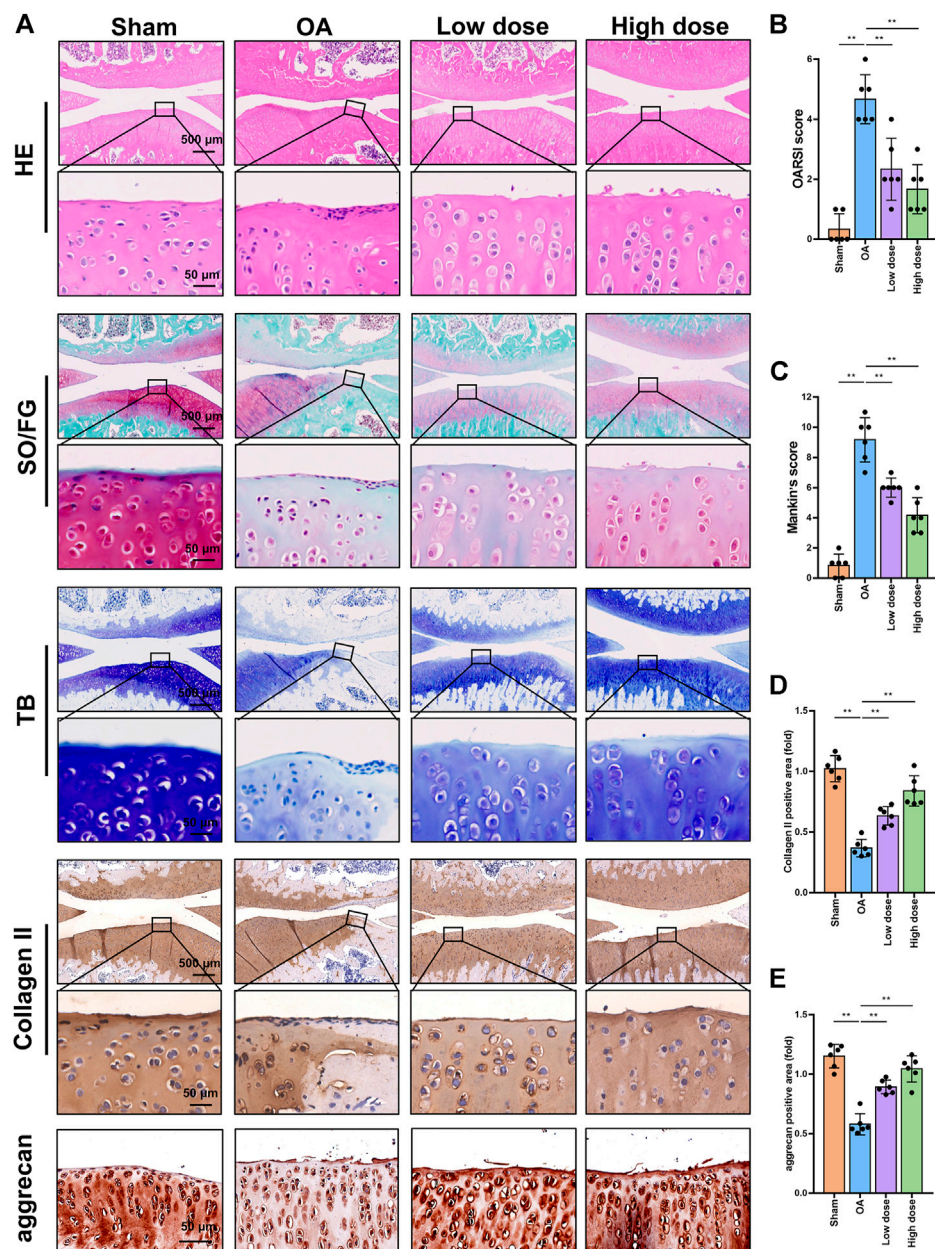


FIGURE 7

Histopathology and immunohistochemistry analysis of rat knee joints. (A) Representative images of HE, SO/FG, TB, collagen type II and aggrecan staining. Images are presented at low magnification (×4 magnification, scale bar, 500 μm) and high magnification (×40 magnification, scale bar, 50 μm). Omaveloxolone (200 and 500 μg/kg) significantly reduced OARSI scores (B) and Mankin scores (C). Omaveloxolone (200 and 500 μg/kg) significantly increased collagen type II (D) and aggrecan levels (E) in OA rats. ***p* < 0.01.

concentrations lower than or equal to 500 nM improved the viability of chondrocytes exposed to IL-1β without significant cytotoxicity. Classic indices correlated with inflammation and oxidative stress were then detected. Omaveloxolone (10 and 25 nM) significantly prevented ROS production, reduced SDO levels and increased MDA levels in chondrocytes treated with IL-1β, suggesting that omaveloxolone could prevent IL-1β-mediated

oxidative stress in chondrocytes. In addition, 10 and 25 nM of omaveloxolone effectively suppressed COX2 and iNOS protein expression, indicating that omaveloxolone could inhibit inflammation in chondrocytes. Inflammation and redox imbalance are important pathogenic factors of OA (Henrotin et al., 2003; Lepetsos and Papavassiliou, 2016; Rahmati et al., 2016). Excessive ROS generation and inflammation contribute to

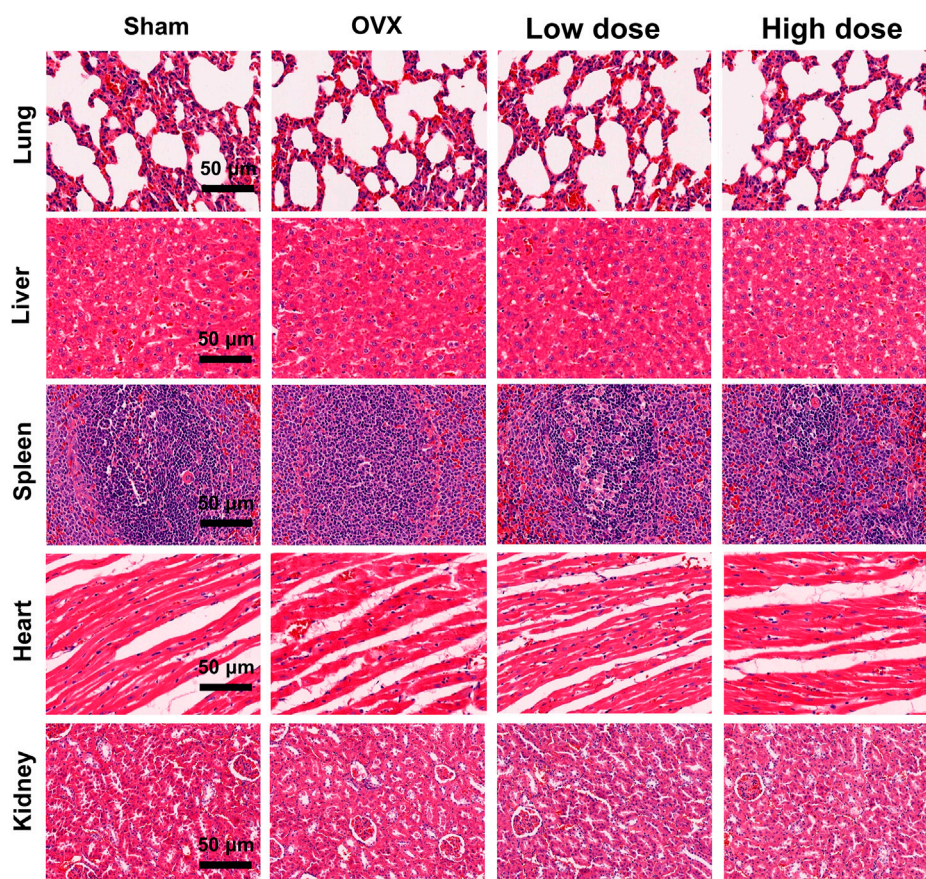


FIGURE 8

H&E staining of major organs. No obvious pathological changes were observed in the lungs, liver, spleen, heart or kidneys between the four groups, which indicates that 200 and 500 ug/kg omaveloxolone did not cause significant organ toxicity in rats after 8 weeks of treatment. (scale bar, 50 μ m).

the acceleration of chondrocyte apoptosis and cartilage degradation. Therapeutic agents based on antioxidative and anti-inflammatory effects may be readily available and effective (Ziskoven et al., 2010; Zhuo et al., 2012; Tudorachi et al., 2021). This study demonstrated that omaveloxolone protects cells against oxidative injury and inflammation.

Apoptosis is strongly correlated with excessive inflammation and oxidative stress. Excessive chondrocyte apoptosis is considered a key factor for OA progression (Blanco et al., 1998). Therefore, we explored the effects of omaveloxolone on chondrocyte apoptosis. The results showed that omaveloxolone significantly improved mitochondrial membrane potential, enhanced Bcl2 protein expression and inhibited Bax protein expression in chondrocytes exposed to IL-1 β . The decrease in mitochondrial membrane potential provided significant evidence of early apoptosis of chondrocytes. Omaveloxolone upregulated the anti-apoptotic protein Bcl2 and downregulated the pro-apoptosis protein Bax, which led to a reduced susceptibility of cells to apoptotic stimuli, such as IL-1 β (Dadsena et al., 2021; Lalier et al., 2022; Spitz and

Gavathiotis, 2022). The results of the Annexin V/PI staining assay also confirmed that omaveloxolone effectively reduced the apoptosis ratio of chondrocytes treated with IL-1 β .

ECM degradation is also a key event in OA progression. The imbalance of synthesis and decomposition of the cartilage matrix caused by various factors results in cartilage degeneration. The results of immunofluorescence and Western blotting assays showed that omaveloxolone significantly promoted collagen type II and aggrecan protein expression while inhibiting MMP 3 and MMP 13 protein expression. Collagen type II and aggrecan are the predominant components in articular cartilage. MMP3 is remarkably active against aggrecan (Vo et al., 2013). The main role of MMP13 is to degrade collagen type II (Akhtar et al., 2017). Cartilage degradation occurs once the homeostasis of these ECM proteins and ECM degrading enzymes is disrupted. Hence, the results demonstrated that omaveloxolone could inhibit ECM degradation in chondrocytes exposed to IL-1 β .

To explore the underlying mechanism by which omaveloxolone prevents IL-1 β -induced cell damage, the

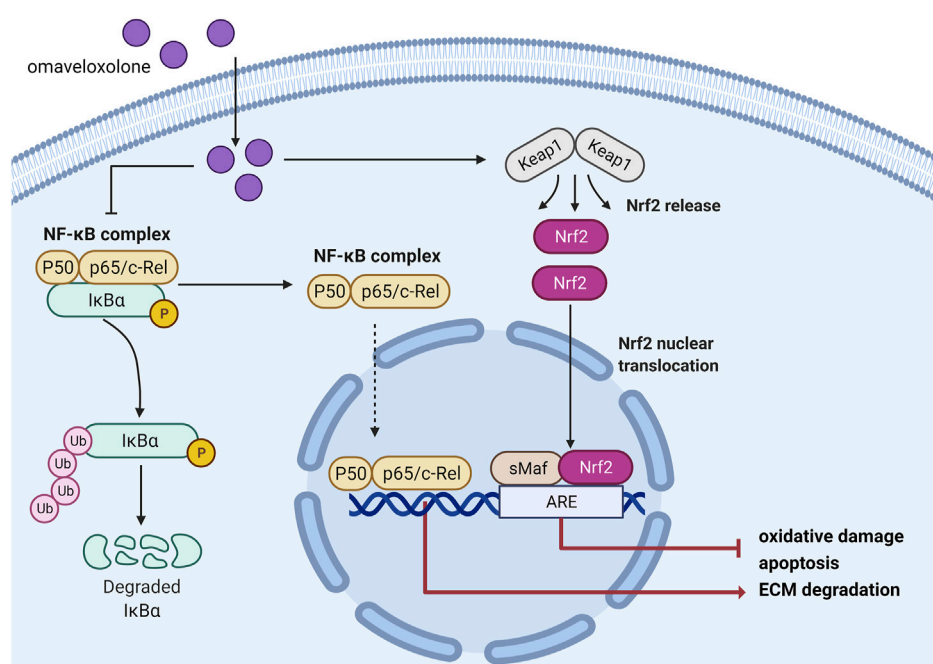


FIGURE 9

Schematic diagram of the mechanisms by which omaveloxolone affects chondrocytes.

expression levels of proteins involved in the Nrf2/ARE and NF-κB signalling pathways were assessed. The results showed that omaveloxolone promoted Nrf2 translocation into the cell nucleus, enhanced HO-1 and NQO1 protein expression and reduced the p-P65/P65 and p-IκBα/IκBα ratios in chondrocytes exposed to IL-1β. Nrf2 is a master regulator of antioxidant gene activation. After Nrf2 is translocated into the nucleus it can promote the expression of downstream genes, including HO-1 and NQO1, thereby exerting an antioxidant effect (Khan et al., 2018). Cartilage destruction in Nrf2 knockout OA model mice becomes more obvious and severe, suggesting that Nrf2 activation has chondroprotective potential (Cai et al., 2015). Many drugs have also been shown to protect chondrocytes by activating the Nrf2 signalling pathway. Targeting the Nrf2/ARE signalling pathway might be an effective approach for treating OA (Marchev et al., 2017; Chen et al., 2022). Additionally, the NF-κB signalling pathway is activated in OA joints. The activation of the NF-κB signalling pathway is critical for the expression of inflammation-related proteins in chondrocytes, including COX2, iNOS, MMP3 and MMP13 (Marcu et al., 2010). Targeted NF-κB inhibitors have therapeutic potential for the treatment of OA. Therefore, omaveloxolone may exert chondroprotective effects by activating the Nrf2/ARE signalling pathway and suppressing the NF-κB signalling pathway (Figure 9).

A DMM-induced OA rat model was established to examine the effects of omaveloxolone on OA *in vivo*. The results of gait

analysis showed that omaveloxolone was beneficial for relieving pain in OA rats. Histopathology and immunohistochemistry analyses provided evidence that omaveloxolone could inhibit chondrocyte loss, improve chondrocyte cell morphology, and increase the levels of proteoglycans, collagen type II and aggrecan in articular cartilage of OA rats. The results of the OARSI scores and Mankin scores also verified the chondroprotective effect of omaveloxolone *in vivo*.

The results of the microCT analysis suggest that omaveloxolone can effectively suppress subchondral bone loss and microarchitecture deterioration in OA rats. These findings support the therapeutic potential of omaveloxolone for OA treatment. Considering that the systemic administration of omaveloxolone may cause potential organ toxicity, H&E staining of the lungs, heart, liver, spleen and kidneys was performed, and the results suggest an absence of major organ toxicity, which provides preliminary evidence of the safety of omaveloxolone in rats.

In conclusion, the present study indicates that omaveloxolone can exert antioxidative, anti-inflammatory, antiapoptotic and anti-ECM degradation effects via activation of the Nrf2/ARE signalling pathway and inhibition of the NF-κB signalling pathway in chondrocytes *in vitro*. Moreover, omaveloxolone attenuates OA progression *in vivo*. However, our study does have some limitations. First, only one time point was investigated in our *in vivo* study. Therefore, data on the long-term effects of omaveloxolone in the treatment of OA and assessments of the potential toxicity of long-term administration of omaveloxolone are

lacking. In addition, further studies are needed to explore other possible underlying molecular mechanisms of omaveloxolone in chondrocyte protection.

Data availability statement

The original contributions presented in the study are included in the article/supplementary materials, further inquiries can be directed to the corresponding authors.

Ethics statement

The Shanghai Public Health Clinical Center Laboratory Animal Welfare & Ethics Committee approved the animal study (No.2022-A018-01).

Author contributions

QZ, XY and LD contributed to conception and design of the study. ZJ, GQ and WL performed the research. HW and DL analyzed the data. ZJ, GQ, WC and HY performed the manuscript editing. All authors contributed to editorial changes in the manuscript. All authors read and approved the final manuscript.

References

- Abdel-Aziz, M. A., Ahmed, H. M. S., El-Nekeety, A. A., and Abdel-Wahhab, M. A. (2021). Osteoarthritis complications and the recent therapeutic approaches. *Inflammopharmacology* 29, 1653–1667. doi:10.1007/s10787-021-00888-7
- Aizah, N., Chong, P. P., and Kamarul, T. (2021). Early alterations of subchondral bone in the rat anterior cruciate ligament transection model of osteoarthritis. *Cartilage* 13 (2), 1322S–1333S. doi:10.1177/1947603519878479
- Akhtar, N., Khan, N. M., Ashruf, O. S., and Haqqi, T. M. (2017). Inhibition of cartilage degradation and suppression of PGE(2) and MMPs expression by pomegranate fruit extract in a model of posttraumatic osteoarthritis. *Nutrition* 33, 1–13. doi:10.1016/j.nut.2016.08.004
- Blanco, F. J., Guitian, R., Vázquez-Martul, E., de Toro, F. J., and Galdo, F. (1998). Osteoarthritis chondrocytes die by apoptosis. A possible pathway for osteoarthritis pathology. *Arthritis Rheum.* 41 (2), 284–289. doi:10.1002/1529-0131(199802)41:2<284::Aid-art12>3.0.Co;2-t
- Cai, D., Yin, S., Yang, J., Jiang, Q., and Cao, W. (2015). Histone deacetylase inhibition activates Nrf2 and protects against osteoarthritis. *Arthritis Res. Ther.* 17, 269. doi:10.1186/s13075-015-0774-3
- Chen, H., Qin, J., Shi, H., Li, Q., Zhou, S., and Chen, L. (2022). Rhoifolin ameliorates osteoarthritis via the Nrf2/NF- κ B axis: *In vitro* and *in vivo* experiments. *Osteoarthr. Cartil.* 30 (5), 735–745. doi:10.1016/j.joca.2022.01.009
- Chen, H., Tan, X. N., Hu, S., Liu, R. Q., Peng, L. H., Li, Y. M., et al. (2021). Molecular mechanisms of chondrocyte proliferation and differentiation. *Front. Cell Dev. Biol.* 9, 664168. doi:10.3389/fcell.2021.664168
- Choi, M. C., Jo, J., Park, J., Kang, H. K., and Park, Y. (2019). NF- κ B signaling pathways in osteoarthritic cartilage destruction. *Cells* 8 (7), 734. doi:10.3390/cells8070734
- Chow, Y. Y., and Chin, K. Y. (2020). The role of inflammation in the pathogenesis of osteoarthritis. *Mediat. Inflamm.* 2020, 8293921. doi:10.1155/2020/8293921
- Creelan, B. C., Gabrilovich, D. I., Gray, J. E., Williams, C. C., Tanvetyanon, T., Haura, E. B., et al. (2017). Safety, pharmacokinetics, and pharmacodynamics of oral omaveloxolone (RTA 408), a synthetic triterpenoid, in a first-in-human trial of patients with advanced solid tumors. *Onco. Targets. Ther.* 10, 4239–4250. doi:10.2147/OTT.S136992
- Cuadrado, A., Manda, G., Hassan, A., Alcaraz, M. J., Barbas, C., Daiber, A., et al. (2018). Transcription factor NRF2 as a therapeutic target for chronic diseases: A systems medicine approach. *Pharmacol. Rev.* 70 (2), 348–383. doi:10.1124/pr.117.014753
- Dadsena, S., King, L. E., and García-Sáez, A. J. (2021). Apoptosis regulation at the mitochondria membrane level. *Biochim. Biophys. Acta. Biomembr.* 1863 (12), 183716. doi:10.1016/j.bbmem.2021.183716
- Hall, A. C. (2019). The role of chondrocyte morphology and volume in controlling phenotype-implications for osteoarthritis, cartilage repair, and cartilage engineering. *Curr. Rheumatol. Rep.* 21 (8), 38. doi:10.1007/s11926-019-0837-6
- Han, P., Qin, Z., Tang, J., Xu, Z., Li, R., Jiang, X., et al. (2017). RTA-408 protects kidney from ischemia-reperfusion injury in mice via activating Nrf2 and downstream GSH biosynthesis gene. *Oxid. Med. Cell. Longev.* 2017, 7612182. doi:10.1155/2017/7612182
- Hashimoto, S., Takahashi, K., Amiel, D., Coutts, R. D., and Lotz, M. (1998). Chondrocyte apoptosis and nitric oxide production during experimentally induced osteoarthritis. *Arthritis Rheum.* 41 (7), 1266–1274. doi:10.1002/1529-0131(199807)41:7<1266::Aid-art18>3.0.Co;2-y
- Hawker, G. A., and King, L. K. (2022). The burden of osteoarthritis in older adults. *Clin. Geriatr. Med.* 38 (2), 181–192. doi:10.1016/j.cger.2021.11.005
- Henrotin, Y. E., Bruckner, P., and Pujol, J. P. (2003). The role of reactive oxygen species in homeostasis and degradation of cartilage. *Osteoarthr. Cartil.* 11 (10), 747–755. doi:10.1016/s1063-4584(03)00150-x
- Hu, W., Chen, Y., Dou, C., and Dong, S. (2021). Microenvironment in subchondral bone: Predominant regulator for the treatment of osteoarthritis. *Ann. Rheum. Dis.* 80 (4), 413–422. doi:10.1136/annrheumdis-2020-218089

Funding

The work was supported by the sixth key specialty construction project of Shanghai Jinshan Health Commission (grant numbers: JSZK 2019B01).

Acknowledgments

Schematics were created with BioRender.com.

Conflict of interest

The authors declare that the research was conducted in the absence of any commercial or financial relationships that could be construed as a potential conflict of interest.

Publisher's note

All claims expressed in this article are solely those of the authors and do not necessarily represent those of their affiliated organizations, or those of the publisher, the editors and the reviewers. Any product that may be evaluated in this article, or claim that may be made by its manufacturer, is not guaranteed or endorsed by the publisher.

- Hunter, D. J., March, L., and Chew, M. (2020). Osteoarthritis in 2020 and beyond: A lancet commission. *Lancet* 396 (10264), 1711–1712. doi:10.1016/s0140-6736(20)32230-3
- Hwang, H. S., and Kim, H. A. (2015). Chondrocyte apoptosis in the pathogenesis of osteoarthritis. *Int. J. Mol. Sci.* 16 (11), 26035–26054. doi:10.3390/ijms161125943
- Jimi, E., Fei, H., and Nakatomi, C. (2019). NF- κ B signaling regulates physiological and pathological chondrogenesis. *Int. J. Mol. Sci.* 20 (24), 6275. doi:10.3390/ijms20246275
- Jin, J., Lv, X., Wang, B., Ren, C., Jiang, J., Chen, H., et al. (2021). Limonin inhibits IL-1 β -induced inflammation and catabolism in chondrocytes and ameliorates osteoarthritis by activating Nrf2. *Oxid. Med. Cell. Longev.* 2021, 7292512. doi:10.1155/2021/7292512
- Khan, N. M., Ahmad, I., and Haqqi, T. M. (2018). Nrf2/ARE pathway attenuates oxidative and apoptotic response in human osteoarthritis chondrocytes by activating ERK1/2/ELK1-P70S6K-P90RSK signaling axis. *Free Radic. Biol. Med.* 116, 159–171. doi:10.1016/j.freeradbiomed.2018.01.013
- Lalier, L., Vallette, F., and Manon, S. (2022). Bcl-2 family members and the mitochondrial import machineries: The roads to death. *Biomolecules* 12 (2), 162. doi:10.3390/biom12020162
- Lepetso, P., and Papavassiliou, A. G. (2016). ROS/oxidative stress signaling in osteoarthritis. *Biochim. Biophys. Acta* 1862 (4), 576–591. doi:10.1016/j.bbdis.2016.01.003
- Lepetso, P., Papavassiliou, K. A., and Papavassiliou, A. G. (2019). Redox and NF- κ B signaling in osteoarthritis. *Free Radic. Biol. Med.* 132, 90–100. doi:10.1016/j.freeradbiomed.2018.09.025
- Li, G., Yin, J., Gao, J., Cheng, T. S., Pavlos, N. J., Zhang, C., et al. (2013). Subchondral bone in osteoarthritis: Insight into risk factors and microstructural changes. *Arthritis Res. Ther.* 15 (6), 223. doi:10.1186/ar4405
- Lin, T., Zhao, Y., Chen, J., Wu, C., Li, Z., Cao, Y., et al. (2022). Carboxymethyl chitosan-assisted MnO(x) nanoparticles: Synthesis, characterization, detection and cartilage repair in early osteoarthritis. *Carbohydr. Polym.* 294, 119821. doi:10.1016/j.carbpol.2022.119821
- Lynch, D. R., Farmer, J., Hauser, L., Blair, I. A., Wang, Q. Q., Mesaros, C., et al. (2019). Safety, pharmacodynamics, and potential benefit of omaveloxolone in Friedreich ataxia. *Ann. Clin. Transl. Neurol.* 6 (1), 15–26. doi:10.1002/actn.3.660
- Madsen, K. L., Buch, A. E., Cohen, B. H., Falk, M. J., Goldsberry, A., Goldstein, A., et al. (2020). Safety and efficacy of omaveloxolone in patients with mitochondrial myopathy: MOTOR trial. *Neurology* 94 (7), e687–e698. doi:10.1212/WNL.0000000000008861
- Marchev, A. S., Dimitrova, P. A., Burns, A. J., Kostov, R. V., Dinkova-Kostova, A. T., and Georgiev, M. I. (2017). Oxidative stress and chronic inflammation in osteoarthritis: Can NRF2 counteract these partners in crime? *Ann. N. Y. Acad. Sci.* 1401 (1), 114–135. doi:10.1111/nyas.13407
- Marcu, K. B., Otero, M., Olivetto, E., Borzi, R. M., and Goldring, M. B. (2010). NF- κ B signaling: Multiple angles to target OA. *Curr. Drug Targets* 11 (5), 599–613. doi:10.2174/138945010791011938
- Panda, H., Wen, H., Suzuki, M., and Yamamoto, M. (2022). Multifaceted roles of the KEAP1-NRF2 system in cancer and inflammatory disease milieu. *Antioxidants (Basel)* 11 (3), 538. doi:10.3390/antiox11030538
- Probst, B. L., Trevino, I., McCauley, L., Bumeister, R., Dulubova, I., Wigley, W. C., et al. (2015). RTA 408, A novel synthetic triterpenoid with broad anticancer and anti-inflammatory activity. *PLoS One* 10 (4), e0122942. doi:10.1371/journal.pone.0122942
- Rahmati, M., Mobasheri, A., and Mozafari, M. (2016). Inflammatory mediators in osteoarthritis: A critical review of the state-of-the-art, current prospects, and future challenges. *Bone* 85, 81–90. doi:10.1016/j.bone.2016.01.019
- Reisman, S. A., Ferguson, D. A., Lee, C. I., and Proksch, J. W. (2020). Omaveloxolone and TX63682 are hepatoprotective in the STAM mouse model of nonalcoholic steatohepatitis. *J. Biochem. Mol. Toxicol.* 34, e22526. doi:10.1002/jbt.22526
- Rigoglou, S., and Papavassiliou, A. G. (2013). The NF- κ B signalling pathway in osteoarthritis. *Int. J. Biochem. Cell Biol.* 45 (11), 2580–2584. doi:10.1016/j.biocel.2013.08.018
- Song, Y., Hao, D., Jiang, H., Huang, M., Du, Q., Lin, Y., et al. (2021). Nrf2 regulates CHI3L1 to suppress inflammation and improve post-traumatic osteoarthritis. *J. Inflamm. Res.* 14, 4079–4088. doi:10.2147/jir.S310831
- Spitz, A. Z., and Gavathiotis, E. (2022). Physiological and pharmacological modulation of BAX. *Trends Pharmacol. Sci.* 43 (3), 206–220. doi:10.1016/j.tips.2021.11.001
- Sun, X., Xie, Z., Hu, B., Zhang, B., Ma, Y., Pan, X., et al. (2020). The Nrf2 activator RTA-408 attenuates osteoclastogenesis by inhibiting STING dependent NF- κ B signaling. *Redox Biol.* 28, 101309. doi:10.1016/j.redox.2019.101309
- Teng, Y., Jin, Z., Ren, W., Lu, M., Hou, M., Zhou, Q., et al. (2022). Theaflavin-3, 3'-digallate protects cartilage from degradation by modulating inflammation and antioxidant pathways. *Oxid. Med. Cell. Longev.* 2022, 3047425. doi:10.1155/2022/3047425
- Tudorachi, N. B., Totu, E. E., Fifer, A., Ardeleanu, V., Mocanu, V., Mircea, C., et al. (2021). The implication of reactive oxygen species and antioxidants in knee osteoarthritis. *Antioxidants (Basel)* 10 (6), 985. doi:10.3390/antiox10060985
- Ulasov, A. V., Rosenkranz, A. A., Georgiev, G. P., and Sobolev, A. S. (2021). Nrf2/Keap1/ARE signaling: Towards specific regulation. *Life Sci.* 291, 120111. doi:10.1016/j.lfs.2021.120111
- Vitaloni, M., Botto-van Bemden, A., Sciortino, R., Carné, X., Quintero, M., Santos-Moreno, P., et al. (2020). A patients' view of OA: The global osteoarthritis patient perception survey (GOAPPS), a pilot study. *BMC Musculoskelet. Disord.* 21 (1), 727. doi:10.1186/s12891-020-03741-0
- Vo, N. V., Hartman, R. A., Yurube, T., Jacobs, L. J., Sowa, G. A., and Kang, J. D. (2013). Expression and regulation of metalloproteinases and their inhibitors in intervertebral disc aging and degeneration. *Spine J.* 13 (3), 331–341. doi:10.1016/j.spinee.2012.02.027
- Xian, S., Lin, Z., Zhou, C., and Wu, X. (2022). The protective effect of evodiamine in osteoarthritis: An *in vitro* and *in vivo* study in mice model. *Front. Pharmacol.* 13, 899108. doi:10.3389/fphar.2022.899108
- Yang, C. C., Lin, C. C., Jou, M. J., Hsiao, L. D., and Yang, C. M. (2019). RTA 408 inhibits interleukin-1 β -induced MMP-9 expression via suppressing protein kinase-dependent NF- κ B and AP-1 activation in rat brain astrocytes. *Int. J. Mol. Sci.* 20 (11), 2826. doi:10.3390/ijms20112826
- Yang, J., Hu, S., Bian, Y., Yao, J., Wang, D., Liu, X., et al. (2021). Targeting cell death: Pyroptosis, ferroptosis, apoptosis and necroptosis in osteoarthritis. *Front. Cell Dev. Biol.* 9, 789948. doi:10.3389/fcell.2021.789948
- Yao, M., Zhang, C., Ni, L., Ji, X., Hong, J., Chen, Y., et al. (2022). Cepharanthine ameliorates chondrocytic inflammation and osteoarthritis via regulating the MAPK/NF- κ B-Autophagy pathway. *Front. Pharmacol.* 13, 854239. doi:10.3389/fphar.2022.854239
- Zhang, J. H., Yang, X., Chen, Y. P., Zhang, J. F., and Li, C. Q. (2019). Nrf2 activator RTA-408 protects against ozone-induced acute asthma exacerbation by suppressing ROS and γ DT17 cells. *Inflammation* 42 (5), 1843–1856. doi:10.1007/s10753-019-01046-6
- Zhang, L., Zhou, Q., and Zhou, C. L. (2021). RTA-408 protects against propofol-induced cognitive impairment in neonatal mice via the activation of Nrf2 and the inhibition of NF- κ B p65 nuclear translocation. *Brain Behav.* 11 (1), e01918. doi:10.1002/brb3.1918
- Zhang, X. X., He, S. H., Liang, X., Li, W., Li, T. F., and Li, D. F. (2021b). Aging, cell senescence, the pathogenesis and targeted therapies of osteoarthritis. *Front. Pharmacol.* 12, 728100. doi:10.3389/fphar.2021.728100
- Zhuo, Q., Yang, W., Chen, J., and Wang, Y. (2012). Metabolic syndrome meets osteoarthritis. *Nat. Rev. Rheumatol.* 8 (12), 729–737. doi:10.1038/nrrheum.2012.135
- Ziskoven, C., Jäger, M., Zilkens, C., Bloch, W., Brixius, K., and Krauspe, R. (2010). Oxidative stress in secondary osteoarthritis: From cartilage destruction to clinical presentation? *Orthop. Rev.* 2 (2), e23. doi:10.4081/or.2010.e23



OPEN ACCESS

EDITED BY

Shanshan Hu,
Anhui Medical University, China

REVIEWED BY

Chengwen Li,
University of North Carolina at Chapel
Hill, United States
Koichi Matsuo,
Keio University School of Medicine,
Japan

*CORRESPONDENCE

Changan Guo
changanguo@hotmail.com
Duan Ma
duanma@fudan.edu.cn

[†]These authors have contributed
equally to this work

SPECIALTY SECTION

This article was submitted to
Autoimmune and Autoinflammatory
Disorders,
a section of the journal
Frontiers in Immunology

RECEIVED 30 June 2022

ACCEPTED 15 September 2022

PUBLISHED 29 September 2022

CITATION

Tang H, Zhu W, Cao L, Zhang J, Li J,
Ma D and Guo C (2022) miR-210-3p
protects against osteoarthritis through
inhibiting subchondral angiogenesis by
targeting the expression of TGFBR1
and ID4.
Front. Immunol. 13:982278.
doi: 10.3389/fimmu.2022.982278

COPYRIGHT

© 2022 Tang, Zhu, Cao, Zhang, Li, Ma
and Guo. This is an open-access article
distributed under the terms of the
Creative Commons Attribution License
(CC BY). The use, distribution or
reproduction in other forums is
permitted, provided the original author
(s) and the copyright owner(s) are
credited and that the original
publication in this journal is cited, in
accordance with accepted academic
practice. No use, distribution or
reproduction is permitted which does
not comply with these terms.

miR-210-3p protects against osteoarthritis through inhibiting subchondral angiogenesis by targeting the expression of TGFBR1 and ID4

Han Tang^{1†}, Wenrun Zhu^{1†}, Lu Cao^{1†}, Jin Zhang²,
Juncheng Li¹, Duan Ma^{2*} and Changan Guo^{1*}

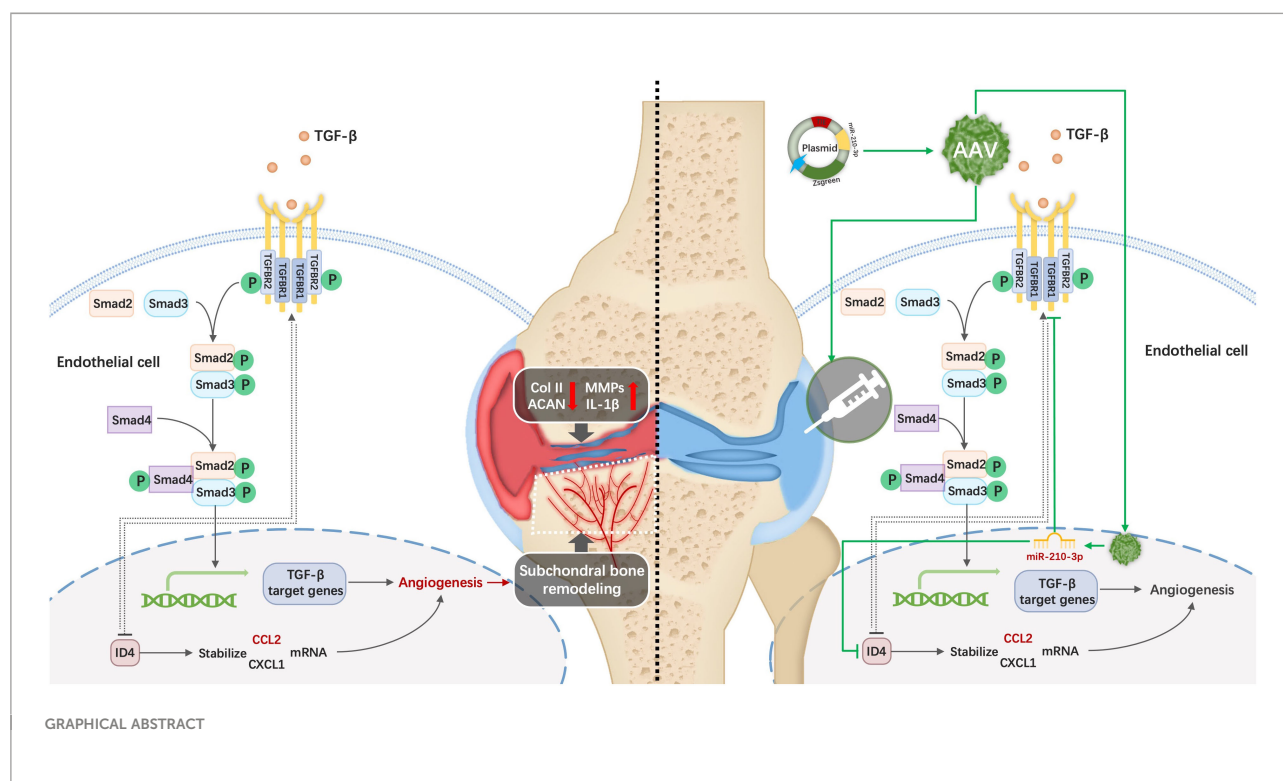
¹Department of Orthopedic Surgery, Zhongshan Hospital, Fudan University, Shanghai, China,

²Key Laboratory of Metabolism and Molecular Medicine, Ministry of Education, Department of Biochemistry and Molecular Biology, School of Basic Medical Sciences, Fudan University, Shanghai, China

Excessive subchondral angiogenesis is a key pathological feature of osteoarthritis (OA), as it alters the balance of subchondral bone remodeling and causes progressive cartilage degradation. We previously found that miR-210-3p correlates negatively with angiogenesis, though the specific mechanism of miR-210-3p-related angiogenesis in subchondral bone during OA progression remains unclear. This study was conducted to identify the miR-210-3p-modulating subchondral angiogenesis mechanism in OA and investigate its therapeutic effect. We found that miR-210-3p expression correlated negatively with subchondral endomucin positive (Emcn⁺) vasculature in the knee joints of OA mice. miR-210-3p overexpression regulated the angiogenic ability of endothelial cells (ECs) under hypoxic conditions *in vitro*. Mechanistically, miR-210-3p inhibited ECs angiogenesis by suppressing transforming growth factor beta receptor 1 (TGFBR1) mRNA translation and degrading DNA-binding inhibitor 4 (ID4) mRNA. In addition, TGFBR1 downregulated the expression of ID4. Reduced ID4 levels led to a negative feedback regulation of TGFBR1, enhancing the inhibitory effect of miR-210-3p on angiogenesis. In OA mice, miR-210-3p overexpression in ECs *via* adeno-associated virus (AAV) alleviated cartilage degradation, suppressed the type 17 immune response and relieved symptoms by attenuating subchondral Emcn⁺ vasculature and subchondral bone remodeling. In conclusion, we identified a miR-210-3p/TGFBR1/ID4 axis in subchondral ECs that modulates OA progression *via* subchondral angiogenesis, representing a potential OA therapy target.

KEYWORDS

osteoarthritis, miR-210-3p, angiogenesis, subchondral bone, adeno-associated virus



Introduction

Osteoarthritis (OA) is a chronic degenerative disease that causes high morbidity and disability rates, endangers the health and quality of life of patients and increases medical care system burden and socioeconomic costs (1, 2). The pathogenic factors of OA include aging (3), mechanical alteration (4), dysfunction of synthesis and metabolism (5), inflammation (6) and immune

Abbreviations: OA, osteoarthritis; ECs, endothelial cells; TGFBR1, transforming growth factor beta receptor 1; ID4, DNA-binding inhibitor 4; AAV, adeno-associated virus; TIE2, tyrosine kinase with immunoglobulin-like and EGF-like domains 2; ACLT, anterior cruciate ligament transection; IGF2, insulin-like growth factor 2; ECs, endothelial cells; OARS, Osteoarthritis Research Society International; MMP13, metalloproteinase 13; Emcn, endomucin; ISH, *in situ* hybridization; HUVECs, human umbilical vein endothelial cells; RT-qPCR, real-time quantitative polymerase chain reaction; FDR, false discovery rate; GO, gene ontology; KEGG, Kyoto Encyclopedia of Genes and Genomes; VEGF, vascular endothelial growth factor; CXCL1, C-X-C motif chemokine ligand 1; CCL2, C-C motif chemokine ligand 2; IL-17, interleukin 17; BMD, bone mineral density; RUNX2, runt-related transcription factor 2; OBs, osteoblasts; OC, osteoclasts; RANKL, receptor activator of nuclear factor κ B ligand; OPG, osteoprotegerin; PGE2, prostaglandin E2; ssDNA, single-stranded DNA; PDGF-BB, platelet-derived growth factor-BB; EP4, prostaglandin E receptor 4.

abnormalities (7). All these complex factors result in joint tissue lesions mainly characterized by cartilage damage, subchondral bone remodeling and osteophyte formation (8–13). In recent years, substantial progress has been achieved in understanding the role of subchondral bone remodeling in the pathogenesis of OA (14–16). As subchondral bone provides mechanical stress support and is the main source of nutrients for cartilage, microenvironmental and structural changes in subchondral bone might affect cartilage metabolism directly or indirectly and are presumed to be one of the factors initiating OA (14). Specifically, aberrant angiogenesis in subchondral bone alters the balance of bone remodeling and results in sclerosis of subchondral bone in pre-OA lesions, which changes the mechanical stress characteristics of the subchondral bone and the nutrition supply pattern of cartilage and increases cartilage vulnerability (14, 17). In advanced OA, increased neurovascular coupling causes the most significant clinical symptom of OA, pain (18). Meanwhile, the subchondral vasculature gradually invades the cartilage through the tidemark and causes more serious degradation of the cartilage matrix (19). Thus, inhibition of subchondral angiogenesis is proposed to be crucial in preventing the pathological progression of OA, allowing cartilage to maintain a “healthy” state.

Bone is a particularly hypoxic tissue with pO_2 levels ranging from less than 1% to 6% (20, 21), and the pO_2 levels in the deep

zone of articular cartilage are also less than 1% (22). Thus, vascular invasion from subchondral bone to cartilage occurs under hypoxic conditions *in vivo*. Notably, miR-210-3p, called the “master miRNA of hypoxia”, exerts multiple and complex effects on different diseases and tissues (23–25). We previously reported significantly increased expression of miR-210-3p in tissues with avascular necrosis of the femoral head (26), indicating that miR-210-3p may be negatively correlated with angiogenesis in subchondral bone. In particular, miR-210-3p manifests antiangiogenic properties in diseases with aberrant vascular formation. For example, miR-210-3p significantly inhibits the angiogenic ability of human retinal vascular endothelial cells by directly targeting insulin-like growth factor 2 (IGF2) in the retina (27). In preeclampsia, overexpression of miR-210-3p impairs extravillous trophoblast formation of endothelial-like networks (28). Therefore, we assume that the decrease in miR-210-3p expression may be attributed to angiogenesis in subchondral bone during the development of OA.

Here, we aimed to study the mechanism by which miR-210-3p affects subchondral angiogenesis and its therapeutic effect on OA. As a method to achieve our goal, we first overexpressed and inhibited miR-210-3p expression in endothelial cells (ECs) to determine its effect on the angiogenic ability of ECs *in vitro*. RNA sequencing and subsequent molecular experiments were implemented to determine the targets and downstream pathways of miR-210-3p. *In vivo*, we selectively overexpressed miR-210-3p in ECs of mice with anterior cruciate ligament transection (ACLT) induced OA to verify its role in the progression of OA using an adeno-associated virus (AAV) containing the tyrosine kinase with immunoglobulin like and EGF like domains 2 (TIE2) promoter (miR-210-3p/TIE2/AAV). We then performed CatWalk, microCT, histological staining, flow cytometry and immunochemistry experiments to evaluate the progression of OA. The regulatory mechanisms employed by miR-210-3p were also investigated in our study. We highlight a novel role of the miR-210-3p/transforming growth factor beta receptor 1 (TGFBRI)/DNA-binding inhibitor 4 (ID4) axis in subchondral ECs that modulates the progression of OA *via* subchondral angiogenesis, thereby suggesting a potential target for OA therapy.

Materials and methods

Cell culture and transduction

Human umbilical vein endothelial cells (HUVECs) were obtained from the Cell Bank of the Chinese Academy of Sciences (Shanghai, China). HUVECs were cultured in Dulbecco's modified Eagle's medium (BI, Israel) supplemented with 10% fetal bovine serum (Gibco, Grand Island, NY, USA), 50 U/ml penicillin and 50 µg/ml streptomycin in the presence of 5% CO₂ and 1% O₂ at 37°C in a humidified incubator. All culture

media were renewed every 3 days. The miR-210-3p mimic, inhibitor and each negative control were synthesized by Ribobio (Guangzhou, China) and transfected into HUVECs using Lipo3000 (Invitrogen, Carlsbad, CA, USA) according to the manufacturer's protocol. In addition, we constructed shRNAs to knock down the expression of TGFBRI and ID4 using the pLKO.1-puro vector. Scrambled shRNA was used as shRNA negative control. Then, we packaged lentiviral particles in HEK293T cells using a packaging system including GAG, TAT, Rev, and VSVG vectors and constructed plasmids. We collected culture medium containing lentiviral particles at 48 and 72 hours and filtered it with a 0.45 µm filter. HUVECs at a 60–80% density were infected for 24 hours and selected with blasticidin, puromycin or neomycin for 7 days to establish overexpression or KD cell lines. The shRNA sequences are listed in Table S1.

Transwell assay

HUVECs cultured under different intervention conditions were digested with 0.25% trypsin and adjusted to a density of 2×10^5 cells/ml with serum-free DMEM. Then, 100 µL of the resuspended cells were added to the upper chamber of transwell plates (8 µm pore size) (Corning, NY, USA). Then, 600 µL of DMEM containing 10% FBS were added to the lower chamber. After 18 h of incubation at 37°C in a 5% CO₂ incubator, the cells were fixed with methanol for 10 min and stained with a 0.1% crystal violet staining solution for 5 min. Next, cotton swabs were used to gently remove cells remaining on the top of the filter. Images of migrated cells were captured using an inverted microscope. Five visual fields were randomly chosen, and stained cells were counted by ImageJ software.

EdU staining

An EdU staining kit was purchased from Ribobio (Guangzhou, China). According to the manual, we diluted the EdU solution at a ratio of 1000:1 with complete culture medium to reach a concentration of 50 µM. Then, we added 100 µL of the diluted EdU solution to each well and incubated the samples for 2 hours. After the incubation, we fixed the cells in each well with 4% paraformaldehyde for 30 min at room temperature, added 50 µL of 2 mg/mL glycine to each well, and incubated the samples for 5 minutes. Next, 100 µL of penetrant (0.5% Triton X-100 in PBS) were added to each well, and the samples were incubated for 10 minutes. Then, we applied Apollo[®] 567 staining solution and Hoechst for EdU and nuclear staining, respectively. The reaction solution was incubated in the dark at room temperature for 30 minutes. Finally, each well was washed with 100 µL of PBS 1–3 times. Images were captured immediately using a fluorescence microscope after the staining was completed.

Tube formation

Ninety-six-well plates were precoated with 50 μ L of Matrigel (Corning, NY, USA) and incubated at 37°C for 30–60 minutes. A total of 50 μ L of the HUVEC suspension (4×10^5 cells/ml) was seeded in Matrigel-coated 96-well plates and incubated with 5% CO₂ at 37°C in a humidified incubator for 6 hours. After the incubation, the formation of tube-like structures was assessed using a phase contrast microscope and ImageJ software.

Western blotting

Adherent cells were digested with RIPA buffer (Biotime, Shanghai, China) containing PMSF (Yeast, Shanghai, China) after two washes with ice-cold PBS. Twenty micrograms of total protein from each sample were separated on SDS-PAGE gels and transferred onto NC membranes (Millipore, Bedford, MA, USA). Then, we used 8% nonfat milk to block nonspecific sites for 1 hour at room temperature. The membranes were then incubated with primary antibodies against vascular endothelial growth factor (VEGF; Servicebio, Wuhan, China), TGFBR1 (Abcam, Cambridge, UK), ID4 (Santa Cruz, Dallas, Texas, USA), C-C motif chemokine ligand 2 (CCL2; Huabio, Hangzhou, China), Smad2 (Santa Cruz, Dallas, Texas, USA), pSmad2 (CST, Danvers, Massachusetts, USA), Smad3 (CST, Danvers, Massachusetts, USA), pSmad3 (CST, Danvers, Massachusetts, USA) and GAPDH (CST, Danvers, Massachusetts, USA) at 4°C overnight. The membranes were washed with TBST 3 times for 10 minutes each and then incubated with a horseradish peroxidase-conjugated goat anti-rabbit or goat anti-mouse IgG secondary antibody (CST, Danvers, Massachusetts, USA) at room temperature for 2 hours according to the species of primary antibody. Finally, the ECL Detection Kit (NCM Biotech, Suzhou, China) was used for detection and photography. Images of protein bands were analyzed using ImageJ software.

Dual-luciferase reporter gene assay

The 500 bp UTRs of TGFBR1 and ID4 containing the predicted binding sites or mutant predicted binding sites of miR-210-3p were subcloned downstream in the pmirGLO miReport vector. We cotransfected the vector and miR-210-3p mimic or scrambled negative control with Lipofectamine 3000 reagent (Invitrogen, Carlsbad, CA, USA) according to the manufacturer's instructions. Forty-eight hours after transfection, we lysed the cells and measured firefly and Renilla luciferase activity with the Dual-Luciferase Reporter Assay System (Solarbio, Peking, China).

Real-time quantitative polymerase chain reaction (RT-qPCR)

Total RNA was extracted from each sample using TRIzol reagent (Thermo, Waltham, Massachusetts, USA), separated using chloroform and precipitated with isopropanol according to the manufacturer's instructions. Then, reverse transcription was performed using the PrimeScript RT Master Mix Kit (Takara, Tokyo, Japan) to acquire cDNAs. RT-qPCR was performed in a 20 μ L reaction system using TB Green Premix Ex Taq (Takara, Tokyo, Japan) according to the manufacturer's instructions. miR-210-3p and U6 were reverse-transcribed using Bulge-Loop miRNA qRT-PCR Primers (Ribobio, Guangzhou, China). GAPDH and U6 were used as internal references for mRNA and miRNA quantification, respectively. The primer sequences are listed in Table S2. Relative gene expression was quantified using the $2^{-\Delta\Delta CT}$ method.

Animal experiments

Animal experiments were performed according to the protocol approved by the Department Laboratory Animal Science of Fudan University. We used 6-week-old C57BL/6 mice and assigned 6 mice to each group. All C57BL/6 mice other than those in the control and sham groups received intra-articular (i.a.) or intravenous (i.v.) injection of AAV-control or miR-210-3p/TIE2/AAV 3 weeks before ACLT. For the i.a. injection, the mice were immobilized in the supine position, the left hindlimb was straightened, and the knee joint and surrounding hair were shaved. We used an insulin syringe and vertically injected 10 μ L of AAV (1.5×10^{12} v.g./mL) into the knee joint. In addition, 100 μ L of AAV (1.5×10^{12} v.g./mL) were used for the i.v. injection. For ACLT, C57BL/6 mice were anesthetized with 0.3% sodium pentobarbital. A 0.5 cm longitudinal incision was made along the left knee joint of the mice. The fascia above the patellar ligament was bluntly separated. A longitudinal incision was made at the medial side of the patellar ligament to open the joint cavity. Then, we pulled the patellar ligament laterally to expose the joint cavity. After blunt separation of the infrapatellar fat pad, we transected the anterior cruciate ligament. Notably, we did not transect the anterior cruciate ligament of the sham group at this step. Then, the joint cavity was washed with saline, and the patellar ligament, fascia and skin were stitched with absorbable sutures after repositioning the ligament.

In situ hybridization (ISH)

ISH staining for miR-210-3p in subchondral bone of normal mice and mice was performed 4 weeks after ACLT. The miR-210-3p probes and ISH kits were purchased from Servicebio (Wuhan, China) and used according to the manufacturer's instructions. Briefly, paraffin sections of mouse knees were

subjected to dewaxing, repair and prehybridization. For hybridization, 50 μ L of the probe-containing hybridization solution were added to cover the tissue, and samples were incubated in a humid chamber at 37°C overnight. After the incubation, sections were washed with 37°C prewarmed 2 \times SSC solution once for 10 minutes and 37°C prewarmed 1 \times SSC solution twice for 5 minutes each. DAPI was used for nuclear staining. Images were captured using a fluorescence microscope.

Histology and immunohistochemical analysis

We harvested the left hind knees of mice after euthanasia at 2 or 4 weeks after ACLT and fixed them with 4% formaldehyde for 48 hours. Then, the knees were immersed in 1.5 M EDTA for 1–1.5 weeks for decalcification. Following dehydration in a gradient of alcohol solutions, the knees were embedded in OCT compound for sectioning (6 μ m). For safranin-O & fast green staining, sections were dewaxed in water and immersed in fast green staining solution for 6 minutes. After washing with distilled water for 1 minute, the sections were immersed in safranin O solution for 4 minutes, rinsed with distilled water for 1 minute and differentiated in glacial acetic acid for 1 minute. The sections were sealed with neutral resin after dehydration. For immunohistochemical staining, sections were dewaxed in water and repaired in boiled antigen retrieval solution for 8 minutes. After blocking with a 3% BSA/PBS solution for 1 hour at room temperature, sections were incubated with anti-endomucin (Emcn; Santa Cruz, Dallas, Texas, USA), anti-matrix metalloproteinase 13 (MMP13; Abcam, Cambridge, UK) and anti-Runx2-related transcription factor 2 (RUNX2; Servicebio, Wuhan, China) antibodies, followed by fluorescent dye-conjugated secondary antibodies (Abcam, Cambridge, UK) for fluorescence imaging and HRP-conjugated secondary antibodies (Servicebio, Wuhan, China) for DAB staining.

Flow cytometry

We harvested inguinal lymph nodes at 2 weeks after ACLT and digested the lymph nodes with a mixture of type II collagenase (Yeesen, Shanghai, China) and DNase I (Yeesen, Shanghai, China) for 20 min at room temperature. The digest was filtered through a 70 μ m cell strainer (Miltenyi, Germany) and then washed with 1 \times PBS. For staining of cytokine interleukin 17a (IL-17a), cells were stimulated with the leucocyte activation cocktail BD Pharmingen (BD Biosciences, Franklin Lakes, New Jersey, U.S.) for 4 hours at 37°C. Then, the cells were incubated with antibodies against surface markers on ice for 30 minutes in the dark. After fixation and permeabilization with a BD CytoFix/CytoPerm Kit (BD Biosciences, Franklin Lakes, New Jersey, U.S.), cells were stained with IL-17a fluorescent antibodies on ice for an additional 30 minutes in the dark. The T cell panel included the following

antibodies: Zombie NTR Fixable Viability APC-Cy7 (Biolegend, San Diego, California, U.S.), CD25 PE-Cy7 (Biolegend), CD3 FITC (Biolegend) and IL-17a PE (Biolegend). Analyses were performed using FlowJo software.

MicroCT analysis

The isolated knee joints were fixed overnight with 4% formaldehyde and analyzed using microCT (Sky-scan 1174, Bruker MicroCT) (voltage, 65 kVp; current, 153 μ A; and resolution, 9 μ m/pixel). We used image reconstruction software (NRecon v1.6, Bruker), data analysis software (CTAn v1.9, Bruker), and 3-dimensional model visualization software (μ CTVol v2.0, Bruker) to analyze the parameters of the tibia subchondral bone. The whole subchondral bone medial compartment was the region of interest, and 100 consecutive images from the medial tibial plateau were used for 3-dimensional reconstruction and analysis. The bone mineral density BMD and bone volume/tissue volume (BV/TV) were measured in three-dimensional structures.

CatWalk analysis

The CatWalk gait analysis system (Noldus Information Technology) was used to measure the disability of mice in this study. Mice were placed individually in the walkway and allowed to walk freely. When the mouse traversed from one side of the walkway to the other, a high-speed color video camera recorded mouse movements and footprints simultaneously. The software automatically identified all contacted areas and assigned them to the respective paws. The durations and left hind limb duty cycle were analyzed.

Statistical analysis

We performed statistical analyses using GraphPad Prism 9 software. Numerical data are presented as the mean \pm SD. Unpaired two-tailed Student's *t* test was used to compare the results from two groups, and one-way ANOVA was used to compare variables between more than two groups. Statistical significance was defined as **P* < 0.05 and ***P* < 0.01.

Results

miR-210-3p expression is negatively related to aberrant subchondral angiogenesis in OA

We applied ACLT to induce OA in mice as a method to verify the potential correlation between miR-210-3p expression and aberrant vascularization of subchondral bone. At 4 weeks after ACLT, the cartilage was significantly degenerated in ACLT mice,

as shown by safranin-O & fast green staining (Figure 1A), and the Osteoarthritis Research Society International (OARSI) scores were also significantly increased compared with those of control mice (Figure 1E). Meanwhile, the expression of MMP13, a molecule directly involved in cartilage degradation, was significantly increased in the cartilage of ACLT mice compared with control mice (Figures 1B, F). Next, we stained for Emcn, a specific marker of capillaries and sinusoids in the metaphysis and diaphysis (29–31), to assess the vasculature in the subchondral bone of mouse knees using immunohistochemical staining. We observed abnormally proliferating Emcn⁺ blood vessels in subchondral bone, and some vessels even invaded the cartilage through the tidemark in ACLT mice (Figures 1C, G). We next validated the expression of miR-210-3p in subchondral bone by performing an ISH assay. The expression of miR-210-3p was significantly decreased in subchondral bone of

ACLT mice compared with control mice (Figures 1D, H). Based on these findings, we speculated that miR-210-3p may be involved in the abnormal vascularization of subchondral bone during the development of OA.

miR-210-3p regulates the angiogenic ability of HUVECs *in vitro* under hypoxia

We transfected the miR-210-3p mimic or inhibitor into HUVECs *in vitro* to investigate the role of miR-210-3p in aberrant angiogenesis of subchondral bone in OA. The miR-210-3p level was substantially increased after the miR-210-3p mimic transfection, as evidenced by the qPCR results (Figure 2D). Briefly, proliferation, migration and tube

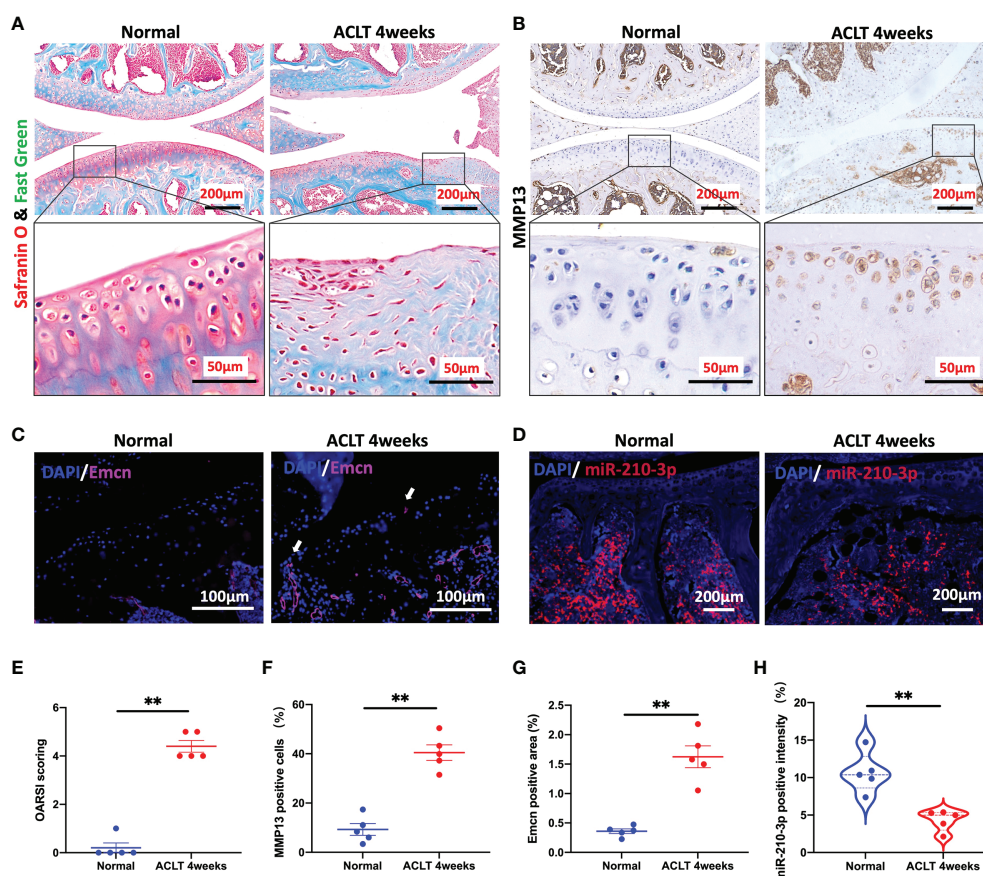


FIGURE 1

miR-210-3p expression is negatively related to aberrant subchondral angiogenesis in OA. Ten-week-old C57BL/6 mice underwent ACLT. Knee joints were harvested at 4 weeks after surgery. $n = 5$ mice per group. (A) Safranin O–fast green staining for the knee joint (sagittal view). Scale bar: 200 μ m (top), 50 μ m (bottom). (B) Immunohistochemical staining for MMP13 in the joint (top) and cartilage (bottom) of normal mice and ACLT for 4 weeks mice. Scale bar: 200 μ m (top), 50 μ m (bottom). (C) Immunofluorescence staining for Emcn (red) and DAPI (blue) in the subchondral bone of tibia. Vessels invading the cartilage are indicated by white arrows. Scale bars: 100 μ m. (D) ISH staining for miR-210-3p (red) and DAPI (blue) in the subchondral bone of tibia. Scale bars: 200 μ m. (E) Calculation of OARSI scores. (F) Quantification of the number of MMP13-positive cells in cartilage. (G) Quantification of the positive area of Emcn staining. (H) Quantification of the intensity of miR-210-3p staining in subchondral bone. ** $P < 0.01$. All data are presented as the means \pm standard deviations. Statistical significance was determined using unpaired, 2-tailed Student's t test.

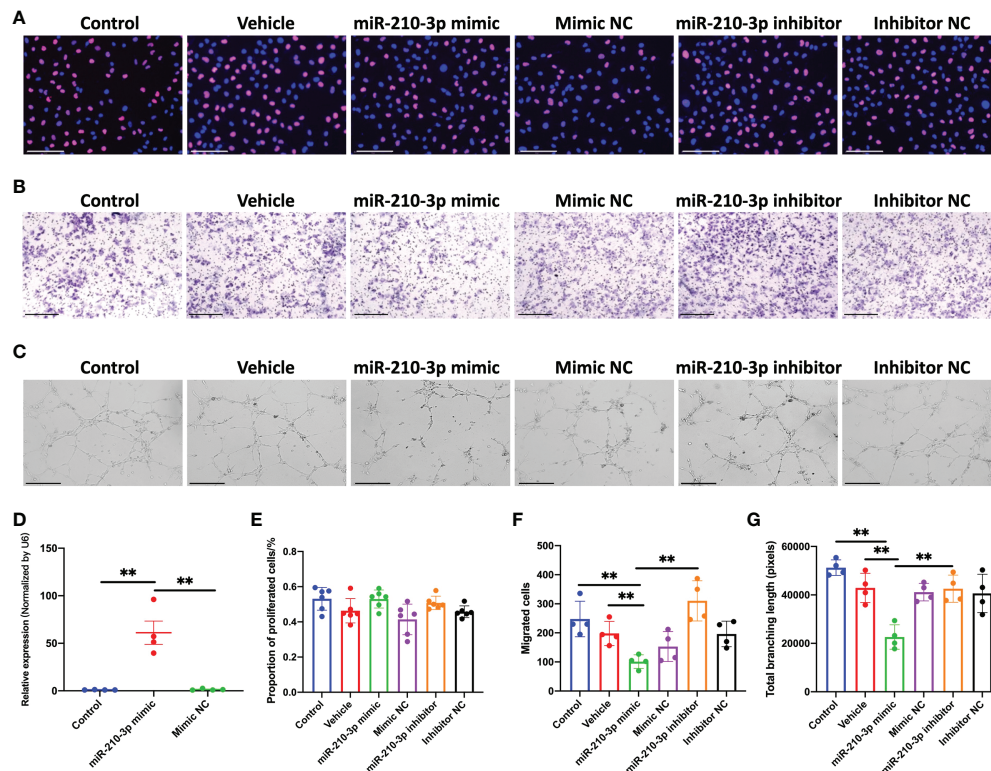


FIGURE 2

miR-210-3p affects the angiogenic ability of HUVECs in vitro under hypoxia. (A) EdU staining for control HUVECs and HUVECs transfected with vehicle, miR-210-3p mimic, mimic NC, miR-210-3p inhibitor or inhibitor NC and cultured under hypoxia (1% O₂). Scale bars: 150 μ m. (B) Transwell assay of control HUVECs and HUVECs transfected with vehicle, miR-210-3p mimic, mimic NC, miR-210-3p inhibitor or inhibitor NC and cultured under hypoxia (1% O₂). Scale bars: 300 μ m. (C) Representative images of tube formation by control HUVECs and HUVECs transfected with vehicle, miR-210-3p mimic, mimic NC, miR-210-3p inhibitor or inhibitor NC. Scale bars: 275 μ m. (D) Quantification of miR-210-3p expression levels in control HUVECs and HUVECs transfected with miR-210-3p mimic or mimic NC using RT-qPCR. (E) Quantification of proportion of proliferated cells. (F) Quantification of the number of migrated cells. (G) Quantification of the total branching length of each group. ** $P < 0.01$. NC, negative control. All data are presented as the means \pm standard deviations. Statistical significance was determined using unpaired, 2-tailed Student's *t* test.

formation were assessed as measures of the angiogenic ability of ECs. Notably, we found that miR-210-3p had no effect on the angiogenesis ability of HUVECs under normoxic conditions (Figure S1). Then, we evaluated the effect of miR-210-3p on the angiogenic ability of HUVECs grown in the presence of 1% oxygen. Our results revealed that miR-210-3p did not affect the proliferation of HUVECs (Figures 2A, F) but significantly repressed the migration (Figures 2B, E) and tube formation (Figures 2C, G) of HUVECs under hypoxic conditions, implying that miR-210-3p may play an important role in EC migration from normoxic to hypoxic regions *in vivo*.

RNA sequencing of miR-210-3p-overexpressing HUVECs and miR-210-3p target prediction

We performed RNA sequencing of miR-210-3p mimic-transfected and control HUVECs under hypoxic conditions to

evaluate the transcriptional changes in the miR-210-3p-overexpressing (OE) HUVECs. The Benjamini-Hochberg false discovery rate (FDR) method was applied to obtain FDR-adjusted p-values (q-values). Based on our results, forced miR-210-3p OE downregulated 43 genes and upregulated 36 genes ($FC > 2$, $q < 0.05$) (Figure 3A). These differentially expressed genes were also displayed in a heatmap (Figure 3B). The Gene Ontology (GO) enrichment results showed that miR-210-3p mainly affected the process of cellular responses to external stimulation such as cytokines and peptides, which are critical in the angiogenic behavior of ECs (Figure 3C). Furthermore, The Kyoto Encyclopedia of Genes and Genomes (KEGG) enrichment analysis showed that VEGF-independent angiogenic signaling pathways, such as the TGF- β signaling pathway and pathways related to cytokine-cytokine receptor interactions, were significantly enriched in miR-210-3p-OE HUVECs (Figure 3D). Subsequently, we used the miWalk database to predict the target genes of miR-210-3p and

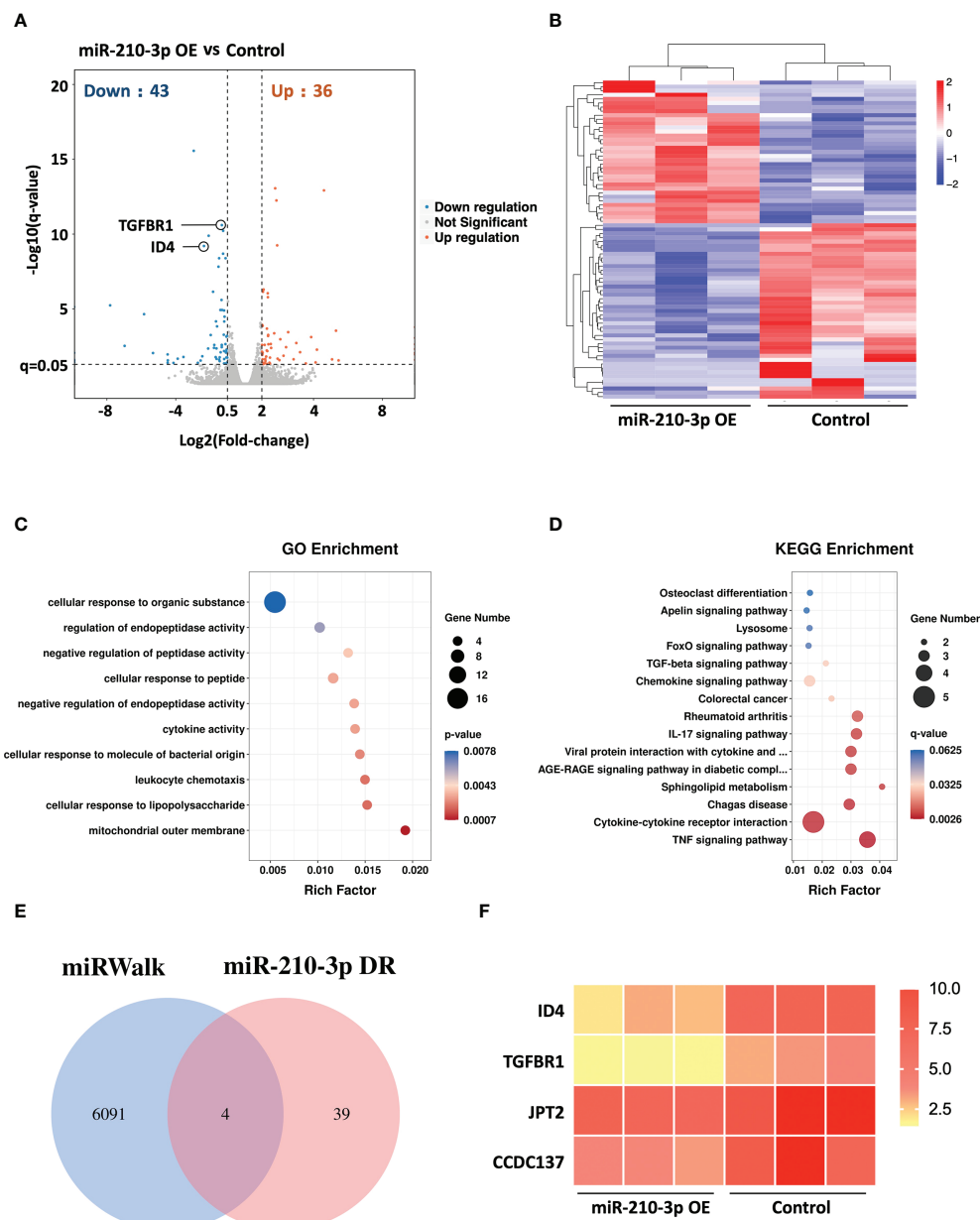


FIGURE 3

RNA sequencing of miR-210-3p-OE HUVECs and miR-210-3p target prediction. RNA sequencing of miR-210-3p-OE HUVECs compared to the control group under hypoxia ($n = 3$). (A) The differential gene expression analysis showed that miR-210-3p overexpression downregulated 43 genes and upregulated 36 genes ($FC > 2$, $q < 0.05$). (B) Heatmap of the differentially expressed genes. (C, D) KEGG and GO enrichment analyses of genes that were differentially expressed in miR-210-3p-OE cells. (E) Venn diagram of miR-210-3p target genes predicted by the miRWalk database intersected with genes downregulated upon miR-210-3p overexpression ($FC > 2$, $q < 0.05$). (F) Heatmap of the 4 intersecting genes.

intersected them with the genes downregulated in miR-210-3p-OE cells identified by RNA sequencing (Figures 3E, F). The results showed 4 overlapping genes. Among these genes, ID4 and TGFBR1 were of particular interest because of their proangiogenic properties. ID4 ranked the highest, and ID4 has

been reported to promote EC-related angiogenesis by affecting the stability of chemokine mRNAs. TGFBR1 is an important membrane receptor in the TGF- β signaling pathway that is closely related to the angiogenesis of ECs. Therefore, we sought to verify ID4 and TGFBR1 as target genes of miR-210-3p.

miR-210-3p directly targets TGFBR1 and ID4

According to our results, the ID4 mRNA and protein levels were significantly decreased in the miR-210-3p mimic group but were significantly increased in the miR-210-3p inhibitor group compared with the control group (Figure 4A), which provided indirect evidence that ID4 is a target gene of miR-210-3p. Consistent with the ID4

expression level, the levels of the proangiogenic chemokines C-X-C motif chemokine ligand 1 (CXCL1) and CCL2 showed similar trends (Figures 4C, D), indicating that CXCL1 and CCL2 may be downstream molecules of ID4. Although TGFBR1 mRNA expression level showed no differences among the groups (Figure 4B), TGFBR1 protein expression was significantly inhibited by the miR-210-3p mimic and was significantly increased in the miR-210-3p inhibitor group (Figures 4D, F). Thus, miR-210-3p

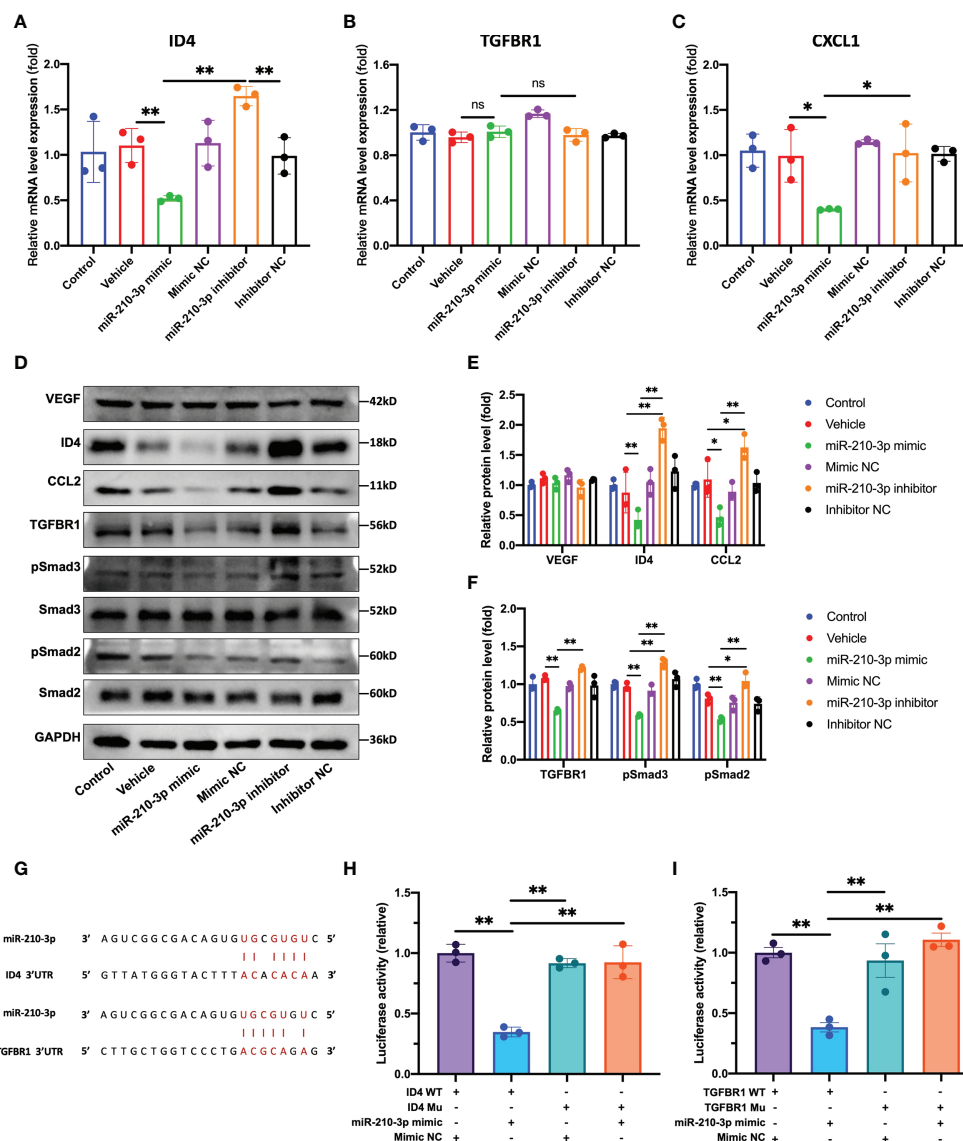


FIGURE 4

miR-210-3p directly targets TGFBR1 and ID4. (A–C) ID4, TGFBR1 and CXCL1 mRNA expression levels quantified by RT–qPCR. (D–F) Representative bands showing the levels of the VEGF, ID4, CCL2, TGFBR1, Smad2, pSmad2, Smad3, pSmad3 and GAPDH proteins (D). The relative VEGF, ID4, CCL2 and TGFBR1 protein levels were normalized to the GAPDH level. The relative pSmad2 and pSmad3 protein levels were normalized to those of Smad2 and Smad3, respectively (E, F). (G) Predicted binding sites for miR-210-3p in the ID4 and TGFBR1 sequences. (H, I) A dual-luciferase reporter assay showed that luciferase activity was significantly inhibited in groups cotransfected with ID4 or TGFBR1 WT vectors and miR-210-3p mimic. ** $P < 0.01$. * $P < 0.05$. WT, wild-type. Mu, mutant. ns, not significance. All data are presented as the means \pm standard deviations. Statistical significance was determined using unpaired, 2-tailed Student's t test.

mainly inhibits the translation of TGFBR1 instead of degrading the TGFBR1 mRNA. Regarding the activation of downstream molecules in the TGF- β signaling pathway, levels of the phosphorylated forms of Smad2/3 showed a similar trend to TGFBR1 (Figures 4D, F), suggesting that miR-210-3p inhibits the activation of the TGF- β signaling pathway by inhibiting TGFBR1 expression. Importantly, the VEGF protein level did not differ among the groups (Figures 4D, E), which further illustrated that miR-210-3p regulates the angiogenic ability of ECs through VEGF-independent signaling pathways. We then validated the predicted sites by which miR-210-3p binds to ID4 and TGFBR1 using a dual-luciferase reporter assay (Figures 4G–I), providing direct evidence that ID4 and TGFBR1 are target genes of miR-210-3p.

Knock down of TGFBR1 and ID4 regulates the angiogenic ability of ECs

Without interfering with the expression of miR-210-3p, we used shRNAs to knock down the expression of TGFBR1 and ID4 to observe whether this approach was sufficient to inhibit the angiogenesis of ECs. We constructed three shRNA plasmids each for TGFBR1 and ID4 (Table S1) and selected one shRNA plasmid each for TGFBR1 and ID4 with satisfactory knockdown (KD) efficiency and no effect on the survival of ECs. Unexpectedly, our results showed that TGFBR1 KD significantly suppressed the expression of ID4 (Figures 5A, C), while ID4 KD increased the expression of TGFBR1 (Figures 5B, D), suggesting that ID4 is also downstream of TGFBR1 and regulates the expression of TGFBR1 expression through negative feedback. Regarding the angiogenesis of ECs, the proliferation, migration and tube formation ability of the TGFBR1 KD group were significantly decreased. Although the proliferation of the ID4 KD group was increased, the migration and tube formation ability were significantly reduced (Figures 5E–J). The effects of TGFBR1 and ID4 KD largely explain the regulation of the angiogenic ability of ECs by miR-210-3p.

miR-210-3p overexpression induced by AAV attenuates OA progression

Based on the results described above, we used miR-210-3p/TIE2/AAV to selectively overexpress miR-210-3p in ECs and observed whether miR-210-3p/TIE2/AAV exerted a therapeutic effect on the OA model. Briefly, we i.a. or i.v. injected miR-210-3p/TIE2/AAV, and ACLT was applied to induce posttraumatic OA 3 weeks after AAV administration. Biological and behavioral tests were performed at 2 and 4 weeks after ACLT (Figure 6A). Before ACLT, we assessed Zsreen fluorescence to determine the efficiency of miR-210-3p/TIE2/AAV infection in each group. Our results illustrated that i.a. administration alone was sufficient to infect the entire knee joint tissue, and i.v. administration induced more obvious infection of blood vessels

in subchondral bone, while the i.a.+i.v. administration showed the most pronounced infection intensity (Figure 6B). In further therapeutic efficacy assessments, we found that the ACLT+miR-210-3p i.a. group, the ACLT+miR-210-3p i.v. group and the ACLT+miR-210-3p i.a.+i.v. group exhibited alleviated cartilage degradation at 2 and 4 weeks compared with the ACLT group, as evidenced by safranin-O & fast green staining and OARSI scores (Figures 6C, F). In addition, the expression of MMP13 in cartilage was also significantly reduced in the three treatment groups compared with the ACLT group (Figure 6D). The proportion of IL-17⁺ cells among T lymphocytes (CD3⁺) in inguinal lymph nodes was doubled at 2 weeks after ACLT and significantly decreased in ACLT+miR-210-3p i.a.+i.v. group (Figures 6E, G). Regarding behavioral testing, the CatWalk analysis results showed that the time it took for mice to pass through the test channel was significantly prolonged in the ACLT group and significantly decreased in the three treatment groups, especially in the ACLT +miR-210-3p i.v. group and ACLT+miR-210-3p i.a.+i.v. group (Figure 6H), while the duty cycle of the left hind limb of mice was significantly reduced in the ACLT group and returned to normal levels in all treatment groups (Figure 6I). Based on these results, miR-210-3p/TIE2/AAV had surprising therapeutic efficacy in attenuating OA progression with respect to cartilage protection, immune change as well as symptom relief.

OA alleviation by miR-210-3p overexpression is attributable to the inhibition of subchondral angiogenesis

We next assessed subchondral bone remodeling and angiogenesis in each group. The microCT results showed that subchondral bone sclerosis occurred in the ACLT group at 2 weeks and was more severe at 4 weeks, which was manifested as higher intensities in the reconstructed 3D images (Figure 7A), increased bone mineral density (BMD) (Figure 7D) and increased relative bone volume fractions (Figure 7E). However, subchondral bone sclerosis was significantly relieved in the treatment groups, especially in the ACLT+miR-210-3p i.a.+i.v. group. Meanwhile, the expression of RUNX2, a key transcription factor associated with osteoblast differentiation, was significantly increased in subchondral bone of the ACLT group, with a positive zone adjacent to the tidemark (dotted lines), and was significantly decreased in the treatment groups (Figure 7B). Notably, Emcn⁺ blood vessels in subchondral bone were abundant and invaded the cartilage layer at 4 weeks after ACLT, as evident from Emcn staining (Figures 7C, F). Impressively, the growth of abnormal Emcn⁺ blood vessels in subchondral bone was effectively inhibited in ACLT+miR-210-3p i.a. group and ACLT+miR-210-3p i.v. group and was particularly reduced in the ACLT+miR-210-3p i.a.+i.v. group. In conclusion, gene therapy with miR-210-3p/TIE2/AAV significantly alleviated the process of OA by inhibiting angiogenesis in subchondral bone.

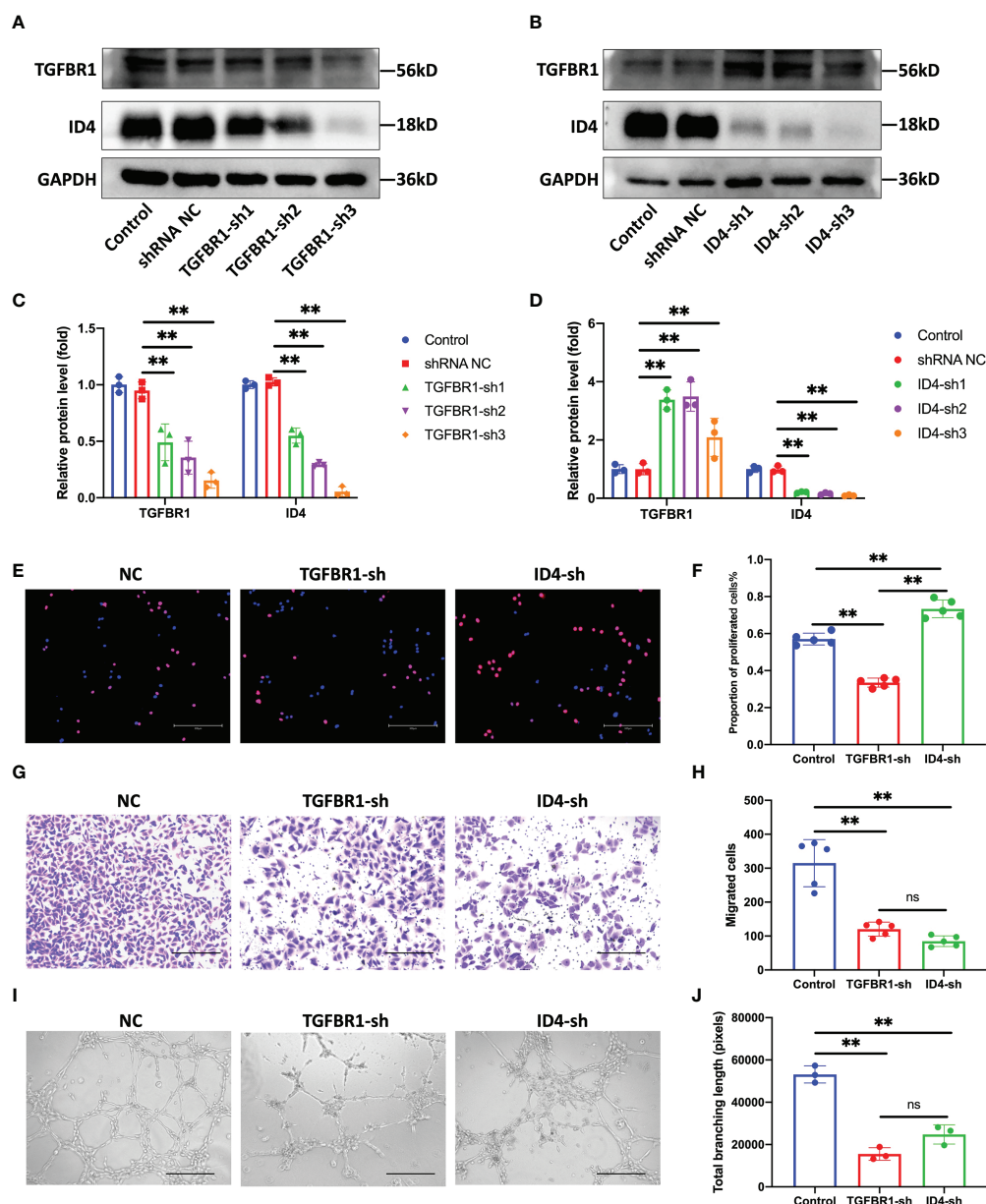


FIGURE 5

Knock down of TGFBR1 and ID4 regulates the angiogenic ability of ECs. (A, C) Representative bands showing the levels of the TGFBR1 and ID4 protein in control, shRNA NC and TGFBR1-sh1-3 HUVECs (A). The relative TGFBR1 and ID4 protein levels were normalized to those of GAPDH (C). (B, D) Representative bands showing the levels of the TGFBR1 and ID4 proteins in control, shRNA NC and ID4-sh1-3 HUVECs (B). The relative TGFBR1 and ID4 protein levels were normalized to those of GAPDH (D). (E, F) Representative images of EdU staining and the proportions of proliferating cells in NC, TGFBR1-sh and ID4-sh HUVECs. Scale bar: 300 μ m. (G, H) Representative images of the transwell assay and the proportions of migrating cells in control, TGFBR1-sh and ID4-sh HUVECs. Scale bar: 300 μ m. (I, J) Representative images of the tube formation assay and the total branching length of control, TGFBR1-sh and ID4-sh HUVECs. Scale bar: 300 μ m. **P < 0.01. ns, not significance. All data are presented as the means \pm standard deviation. Statistical significance was determined using unpaired, 2-tailed Student's t test.

Discussion

As subchondral bone serves as mechanical support and a dominant source of nutrition for cartilage, alterations in the subchondral bone microenvironment are intimately involved in

the progression of OA. These alterations are caused by biological uncoupling and coupling interactions among osteocytes, osteoblasts (OBs), osteoclasts (OCs), ECs and sensory neurons in subchondral bone (15, 32). In the early stage of OA, the balance of subchondral bone remodeling is skewed toward bone

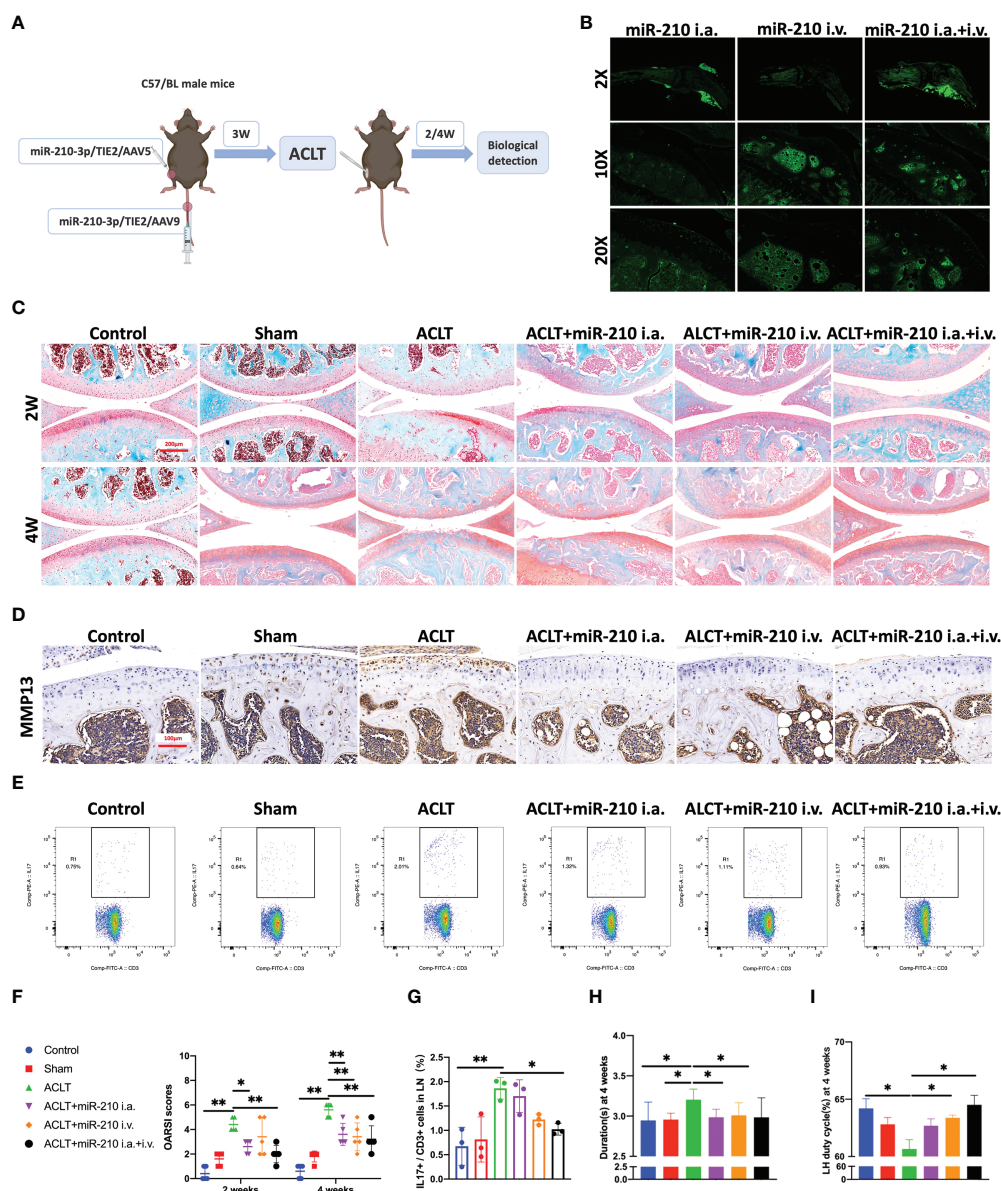


FIGURE 6

miR-210-3p overexpression induced by AAV attenuates OA progression. (A) Design of animal experiments. C57BL/6 mice were i.a. or i.v. injected with miR-210-3p/TIE2/AAV. ACLT was performed to induce posttraumatic OA 3 weeks after AAV administration. Biological and behavioral tests were performed at 2 and 4 weeks after ACLT. (B) Representative photos of Zsreen fluorescence in the affected knees of mice from miR-210-3p/TIE2/AAV i.a., i.v. and i.a.+i.v. injected group. (C) Representative images of safranin-O & fast green staining of LH knee joints in each group at 2 weeks and 4 weeks. Scale bar: 200 μ m. (D) Representative images of immunohistochemical staining for MMP13 in cartilage and subchondral bone of the tibial plateau in each group at 4 weeks. Scale bar: 100 μ m. (E, G) Flow cytometry images and quantified results for IL-17⁺/CD3⁺ cells in inguinal lymph nodes at 2 weeks after ACLT. (F) OARSI scores of LH knees from each group. (H, I) Durations and LH duty cycle of each group at 4 weeks after ACLT. ** P < 0.01. * P < 0.05. LN, lymph nodes. LH, left hindlimb. All data are presented as the means \pm standard deviations. Statistical significance was determined using unpaired, 2-tailed Student's t test.

resorption in response to altered mechanical stress and inflammation. An increased ratio of receptor activator of nuclear factor κ B ligand (RANKL)/osteoprotegerin (OPG) in osteocytes and excessive levels of interleukin (IL)-6, prostaglandin E2 (PGE2) and MMPs produced by OBs promote osteoclastogenesis (33–36). Subsequently, OCs

produce proangiogenic cytokines, such as platelet-derived growth factor-BB (PDGF-BB), VEGF and TGF- β , and promote excessive subchondral neurovascularization and bone formation, causing worsening of joint pain and progressive OA (37, 38). We found that miR-210-3p deficiency is responsible for angiogenesis in subchondral bone in an OA model, and selective

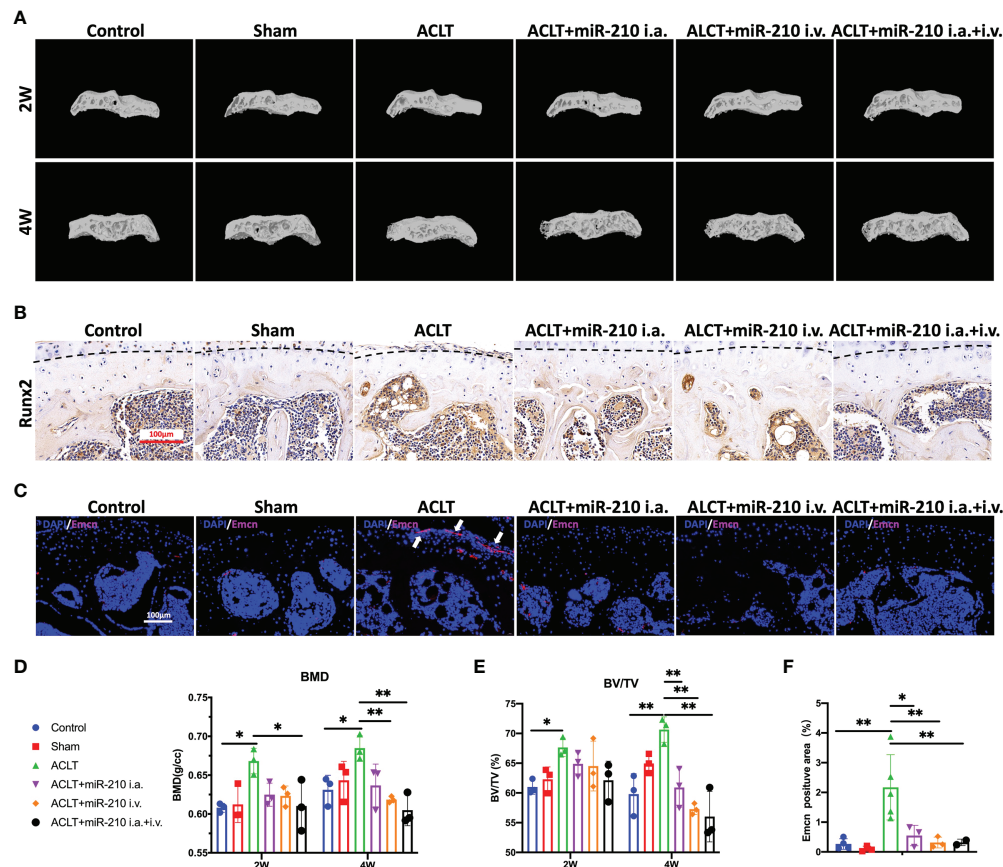


FIGURE 7

OA alleviation by miR-210-3p overexpression is attributable to the inhibition of subchondral angiogenesis. (A) Representative microCT reconstruction images of the tibial plateau of LH knees in each group at 2 weeks and 4 weeks. (B) Representative images of immunohistochemical staining for RUNX2 in subchondral bone of the tibial plateau in each group at 4 weeks. Dotted lines: tidemark. Scale bar: 100 μ m. (C) Representative images of immunofluorescence staining for Emcn (red) and DAPI (blue) in the tibial plateau of LH knees in each group at 4 weeks. Vessels invading the cartilage are indicated by white arrows. Scale bars: 100 μ m. (D, E) Quantification of the BMD and BV/TV of subchondral bone of the tibial plateau in each group at 2 weeks and 4 weeks. (F) Quantification of Emcn positive staining area in each group. ** P < 0.01. * P < 0.05. BMD, bone mineral density. BV/TV, bone volume/tissue volume. All data are presented as the means \pm standard deviations. Statistical significance was determined using unpaired, 2-tailed Student's t test.

overexpression of miR-210-3p in ECs effectively attenuated OA progression, as evidenced by cartilage protection, immune changes and improved mobility. In our opinion, the improvement in mobility is a direct reflection of the treatment effect on OA. We found that the mobility of the treatment groups was almost indistinguishable from that of normal mice, which is fairly rare in previous studies (16, 37), providing evidence that miR-210-3p is an effective treatment target for OA.

A substantial number of epigenetic variations and the expression of noncoding RNAs, such as miRNAs, circular RNAs and long noncoding RNAs, are known to dynamically regulate changes in gene expression in normal and OA articular joints (5, 39–43). However, recent studies have mainly focused on functional noncoding RNAs in cartilage and assessed the efficacy of treatments targeting chondrocytes (44–47), and few reports of noncoding RNAs associated with pathological

changes in subchondral bone, including subchondral angiogenesis, in OA are available. We found that miR-210-3p expression is significantly downregulated in subchondral bone in an OA model in parallel with aberrant subchondral angiogenesis. Indeed, miR-210-3p is widely considered a proangiogenic miRNA involved in ischemia–reperfusion diseases and cancer (48–50). However, we found that selective miR-210-3p overexpression in ECs induced antiangiogenic effects *in vitro* and *in vivo*. This discrepancy may be due to the differences in the biological effects of different miR-210-3p levels on tissues and ECs. Germana Zaccagnini et al. reported that macrophages with elevated miR-210-3p levels in samples with mismatched miR-210-3p levels in ischemic tissue display dysfunctional angiogenesis, leading to impaired tissue repair (51). This finding further illustrates the heterogeneity of miR-210-3p function in cells and tissues. Consistent with our study,

some reports indicate that miR-210-3p inhibits EC function and regulates vascular remodeling in pulmonary hypertension (52, 53) and preeclampsia (28). In summary, we provide the first evidence that miR-210-3p may be exploited as an effective target to inhibit aberrant subchondral angiogenesis in OA. However, we still must explore the molecular mechanism underlying miR-210-3p deficiency in subchondral bone in OA and its effects on processes other than angiogenesis in the subchondral microenvironment in future studies.

AAVs are small (≈ 25 nm in diameter), nonenveloped, single-stranded DNA (ssDNA) viruses that serve as promising vectors for gene therapy in animal experiments and clinical trials (54–59). In this study, we applied AAV vectors to overexpress miR-210-3p in subchondral bone vascular ECs. However, more than ten AAV serotypes have been isolated from human and nonhuman primate tissues, and different serotypes have preferences for distinct cells and tissues (60). For i.a. injection, we selected AAV5 for its cartilage permeability and affinity for blood vessels (61–64). For i.v. injection, we chose AAV9 for its extensive ability to invade the circulatory system and affinity for bone tissue (65). In particular, we added TIE2, an endothelial cell-specific promoter, upstream of the miR-210-3p sequence to specifically overexpress miR-210-3p in vascular ECs. Finally, our study showed that miR-210-3p/TIE2/AAV effectively infected subchondral vascular and inhibited aberrant subchondral bone angiogenesis *in vivo*. Apart from its cartilage-protecting effect, miR-210-3p also showed strong inhibition of subchondral bone sclerosis, similar to therapies targeting PDGF-BB (37) or prostaglandin E receptor 4 (EP4) (34) in OCs. However, the group that received i.a. and i.v. injection of miR-210-3p/TIE2/AAV exhibited a reduced BMD of subchondral bone compared with that of the control group, indicating that high levels of miR-210-3p might impair the subchondral vasculature and result in decreased bone formation.

During the development of OA, the inflammatory environment together with complex multicellular interactions affects subchondral angiogenesis, and the molecular mechanisms remain to be elucidated. In the cartilage layer, hypertrophic chondrocytes express high levels of VEGF (66), and cartilage with high mechanical stress secretes excess TGF- β (67). These molecules further promote vascular invasion of cartilage and disrupt cartilage homeostasis during OA development. In OA subchondral bone, TGF- β 1 produced by OBs is mainly responsible for subchondral angiogenesis in early OA (11). Our study showed that miR-210-3p inhibits the angiogenic ability of ECs by directly inhibiting the translation of the TGFBR1 mRNA and subsequently affecting Smad2/Smad3 phosphorylation under hypoxia. In addition, we also found that miR-210-3p degrades the ID4 mRNA in ECs. ID4 is a member of a protein family that functions as a negative regulator of helix-loop-helix transcription factors. Giulia Fontemaggi et al. reported that ID4 binds and stabilizes mRNAs encoding the proangiogenic factors IL8 and CXCL1 to promote neuroangiogenesis (68). In our study, we

found that ID4 may promote angiogenesis by stabilizing the CXCL1 and CCL2 mRNAs. Interestingly, we identified ID4 as a possible downstream molecule of TGFBR1 that regulates TGFBR1 through negative feedback, producing a strong inhibitory effect on cells overexpressing miR-210-3p. In summary, we verified that miR-210-3p modulates TGFBR1 and ID4 expression and attenuates OA progression by inhibiting subchondral angiogenesis, providing a new therapeutic target for OA treatment.

Nonetheless, this study still has some limitations. First, we did not assess changes in the expression of miR-210-3p in normal and OA human knee joints. Furthermore, the therapeutic effect of miR-210-3p on human OA remains to be further validated. Second, we tested the treatment efficacy of miR-210-3p at 2 weeks and 4 weeks after ACLT in mice, but its long-term therapeutic effects and side effects related to the cardiovascular system and vital organs still require further investigation. Finally, this study only preliminarily suggested that ID4 is downstream of TGFBR1, and we are working to elucidate the specific underlying molecular mechanism.

Conclusion

In conclusion, our study provides the first evidence that miR-210-3p inhibits the angiogenic ability of ECs by directly targeting TGFBR1 and ID4, and the miR-210-3p/TGFBR1/ID4 axis in subchondral ECs modulates the progression of OA *via* subchondral angiogenesis, which might represent a potential target for OA therapy.

Data availability statement

The RNA-seq data of effect of overexpression of miR-210-3p on gene expression of human umbilical vein endothelial cells in hypoxic conditions is available in the GEO database with accession number GSE214170.

Ethics statement

The animal study was reviewed and approved by The Department Laboratory Animal Science Fudan University.

Author contributions

HT, WZ, LC, CG, and DM developed the concept for the study. HT and LC designed the research plan. HT and WZ performed the experiments and analyzed data. HT and WZ wrote and edited the manuscript. LC, JZ, and JL revised the manuscript. All authors read and approved the final version of the manuscript.

Funding

This study was supported by the National Key Research and Development Program of China (Grant. No. 2021YFC270101), the Science and Technology Commission of Shanghai Municipality (Grant. No. 22ZR1410800) and the National Natural Science Foundation of China (Grant. No.8167090095).

Conflict of interest

The authors declare that the research was conducted in the absence of any commercial or financial relationships that could be construed as a potential conflict of interest.

References

- Hunter DJ, Bierma-Zeinstra S. Osteoarthritis. *Lancet* (2019) 393 (10182):1745–59. doi: 10.1016/S0140-6736(19)30417-9
- Safiri S, Kolahi AA, Smith E, Hill C, Bettampadi D, Mansournia MA, et al. Global, regional and national burden of osteoarthritis 1990–2017: A systematic analysis of the global burden of disease study 2017. *Ann Rheum Dis* (2020) 79 (6):819–28. doi: 10.1136/annrheumdis-2019-216515
- Jeon OH, Kim C, Laberge RM, Demaria M, Rathod S, Vasserot AP, et al. Local clearance of senescent cells attenuates the development of post-traumatic osteoarthritis and creates a pro-regenerative environment. *Nat Med* (2017) 23 (6):775–81. doi: 10.1038/nm.4324
- Zhang H, Shao Y, Yao Z, Liu L, Zhang H, Yin J, et al. Mechanical overloading promotes chondrocyte senescence and osteoarthritis development through downregulating Fbxw7. *Ann Rheum Dis* (2022) 81(5):676–86. doi: 10.1136/annrheumdis-2021-221513
- Ito Y, Matsuzaki T, Ayabe F, Mokuda S, Kurimoto R, Matsushima T, et al. Both microRNA-455-5p and -3p repress hypoxia-inducible factor-2alpha expression and coordinately regulate cartilage homeostasis. *Nat Commun* (2021) 12(1):4148. doi: 10.1038/s41467-021-24460-7
- Sanchez-Lopez E, Coras R, Torres A, Lane NE, Guma M. Synovial inflammation in osteoarthritis progression. *Nat Rev Rheumatol* (2022) 18 (5):258–75. doi: 10.1038/s41584-022-00749-9
- Faust HJ, Zhang H, Han J, Wolf MT, Jeon OH, Sadtler K, et al. IL-17 and immunologically induced senescence regulate response to injury in osteoarthritis. *J Clin Invest* (2020) 130(10):5493–507. doi: 10.1172/JCI134091
- Lin W, Klein J. Recent progress in cartilage lubrication. *Adv Mater* (2021) 33 (18):e2005513. doi: 10.1002/adma.202005513
- Wang Z, Jones G, Winzenberg T, Cai G, Laslett LL, Aitken D, et al. Effectiveness of curcuma longa extract for the treatment of symptoms and effusion-synovitis of knee osteoarthritis: A randomized trial. *Ann Intern Med* (2020) 173(11):861–9. doi: 10.7326/M20-0990
- Zhang H, Lin C, Zeng C, Wang Z, Wang H, Lu J, et al. Synovial macrophage M1 polarisation exacerbates experimental osteoarthritis partially through r-Spondin-2. *Ann Rheum Dis* (2018) 77(10):1524–34. doi: 10.1136/annrheumdis-2018-213450
- Zhen G, Wen C, Jia X, Li Y, Crane JL, Mears SC, et al. Inhibition of tgfbeta signaling in mesenchymal stem cells of subchondral bone attenuates osteoarthritis. *Nat Med* (2013) 19(6):704–12. doi: 10.1038/nm.3143
- Yusup A, Kaneko H, Liu L, Ning L, Sadatsuki R, Hada S, et al. Bone marrow lesions, subchondral bone cysts and subchondral bone attrition are associated with histological synovitis in patients with end-stage knee osteoarthritis: A cross-sectional study. *Osteoarthr Cartil* (2015) 23(11):1858–64. doi: 10.1016/j.joca.2015.05.017
- Martel-Pelletier J, Barr AJ, Cicuttini FM, Conaghan PG, Cooper C, Goldring MB, et al. Osteoarthritis. *Nat Rev Dis Primers* (2016) 2:16072. doi: 10.1038/nrdp.2016.72
- Hu Y, Chen X, Wang S, Jing Y, Su J. Subchondral bone microenvironment in osteoarthritis and pain. *Bone Res* (2021) 9(1):20. doi: 10.1038/s41413-021-00147-z
- Hu W, Chen Y, Dou C, Dong S. Microenvironment in subchondral bone: Predominant regulator for the treatment of osteoarthritis. *Ann Rheum Dis* (2020) 80(4):413–22. doi: 10.1136/annrheumdis-2020-218089
- Zhu S, Zhu J, Zhen G, Hu Y, An S, Li Y, et al. Subchondral bone osteoclasts induce sensory innervation and osteoarthritis pain. *J Clin Invest* (2019) 129 (3):1076–93. doi: 10.1172/JCI121561
- van Gastel N, Stegen S, Eelen G, Schoors S, Carlier A, Daniels VW, et al. Lipid availability determines fate of skeletal progenitor cells Via Sox9. *Nature* (2020) 579(7797):111–7. doi: 10.1038/s41586-020-2050-1
- Peng Y, Wu S, Li Y, Crane JL. Type h blood vessels in bone modeling and remodeling. *Theranostics* (2020) 10(1):426–36. doi: 10.7150/thno.34126
- Pei YA, Chen S, Pei M. The essential anti-angiogenic strategies in cartilage engineering and osteoarthritic cartilage repair. *Cell Mol Life Sci* (2022) 79(1):71. doi: 10.1007/s00018-021-04105-0
- Rankin EB, Giaccia AJ, Schipani E. A central role for hypoxic signaling in cartilage, bone, and hematopoiesis. *Curr Osteoporos Rep* (2011) 9(2):46–52. doi: 10.1007/s11914-011-0047-2
- Jadaun PK, Zhang S, Koedam M, Demmers J, Chatterjee S, van Leeuwen JP, et al. Inhibition of hypoxia-induced mucin 1 alters the proteomic composition of human osteoblast-produced extracellular matrix, leading to reduced osteogenic and angiogenic potential. *J Cell Physiol* (2022) 237(2):1440–54. doi: 10.1002/jcp.30617
- Goldring SR, Goldring MB. Changes in the osteochondral unit during osteoarthritis: Structure, function and cartilage-bone crosstalk. *Nat Rev Rheumatol* (2016) 12(11):632–44. doi: 10.1038/nrrheum.2016.148
- Wang H, Flach H, Onizawa M, Wei L, McManus MT, Weiss A. Negative regulation of Hif1a expression and Th17 differentiation by the hypoxia-regulated microRNA mir-210. *Nat Immunol* (2014) 15(4):393–401. doi: 10.1038/ni.2846
- Huang X, Le QT, Giaccia AJ. Mir-210—micromanaging of the hypoxia pathway. *Trends Mol Med* (2010) 16(5):230–7. doi: 10.1016/j.molmed.2010.03.004
- Qin Q, Furong W, Baosheng L. Multiple functions of hypoxia-regulated mir-210 in cancer. *J Exp Clin Cancer Res* (2014) 33:50. doi: 10.1186/1756-9966-33-50
- Yuan HF, Christina VR, Guo CA, Chu YW, Liu RH, Yan ZQ. Involvement of microRNA-210 demethylation in steroid-associated osteonecrosis of the femoral head. *Sci Rep* (2016) 6:20046. doi: 10.1038/srep20046
- Yang Q, Wang P, Du X, Wang W, Zhang T, Chen Y. Direct repression of Igf2 is implicated in the anti-angiogenic function of microRNA-210 in human retinal endothelial cells. *Angiogenesis* (2018) 21(2):313–23. doi: 10.1007/s10456-018-9597-6
- Hayder H, Fu G, Nadeem L, O'Brien JA, Lye SJ, Peng C. Overexpression of mir-210-3p impairs extravillous trophoblast functions associated with uterine

Publisher's note

All claims expressed in this article are solely those of the authors and do not necessarily represent those of their affiliated organizations, or those of the publisher, the editors and the reviewers. Any product that may be evaluated in this article, or claim that may be made by its manufacturer, is not guaranteed or endorsed by the publisher.

Supplementary material

The Supplementary Material for this article can be found online at: <https://www.frontiersin.org/articles/10.3389/fimmu.2022.982278/full#supplementary-material>

spiral artery remodeling. *Int J Mol Sci* (2021) 22(8):3961. doi: 10.3390/ijms22083961

29. Coutu DL, Kokkalis KD, Kunz L, Schroeder T. Three-dimensional map of nonhematopoietic bone and bone-marrow cells and molecules. *Nat Biotechnol* (2017) 35(12):1202–10. doi: 10.1038/nbt.4006

30. Langen UH, Pitulescu ME, Kim JM, Enriquez-Gasca R, Sivaraj KK, Kusumbe AP, et al. Cell-matrix signals specify bone endothelial cells during developmental osteogenesis. *Nat Cell Biol* (2017) 19(3):189–201. doi: 10.1038/ncb3476

31. Dzumukova M, Brunner TM, Miotla-Zarebska J, Heinrich F, Brylka L, Mashreghi MF, et al. Mechanical forces couple bone matrix mineralization with inhibition of angiogenesis to limit adolescent bone growth. *Nat Commun* (2022) 13(1):3059. doi: 10.1038/s41467-022-30618-8

32. Henrotin Y, Pesses L, Sanchez C. Subchondral bone and osteoarthritis: Biological and cellular aspects. *Osteoporos Int* (2012) 23 Suppl 8:S47–51. doi: 10.1007/s00198-012-2162-z

33. Nakashima T, Hayashi M, Fukunaga T, Kurata K, Oh-Hora M, Feng JQ, et al. Evidence for osteocyte regulation of bone homeostasis through rankl expression. *Nat Med* (2011) 17(10):1231–4. doi: 10.1038/nm.2452

34. Jiang W, Jin Y, Zhang S, Ding Y, Huo K, Yang J, et al. Pge2 activates Ep4 in subchondral bone osteoclasts to regulate osteoarthritis. *Bone Res* (2022) 10(1):27. doi: 10.1038/s41413-022-00201-4

35. Xiong J, Onal M, Jilka RL, Weinstein RS, Manolagas SC, O'Brien CA. Matrix-embedded cells control osteoclast formation. *Nat Med* (2011) 17(10):1235–41. doi: 10.1038/nm.2448

36. Sanchez C, Gabay O, Salvat C, Henrotin YE, Berenbaum F. Mechanical loading highly increases il-6 production and decreases opg expression by osteoblasts. *Osteoarthritis Cartil* (2009) 17(4):473–81. doi: 10.1016/j.joca.2008.09.007

37. Su W, Liu G, Liu X, Zhou Y, Sun Q, Zhen G, et al. Angiogenesis stimulated by elevated pdgf-bb in subchondral bone contributes to osteoarthritis development. *JCI Insight* (2020) 5(8):e135446. doi: 10.1172/jci.insight.135446

38. Zhen G, Cao X. Targeting tgfbeta signaling in subchondral bone and articular cartilage homeostasis. *Trends Pharmacol Sci* (2014) 35(5):227–36. doi: 10.1016/j.tips.2014.03.005

39. Coutinho de Almeida R, Ramos YFM, Mahfouz A, den Hollander W, Lakenberg N, Houtman E, et al. RNA sequencing data integration reveals an mirna interactome of osteoarthritis cartilage. *Ann Rheum Dis* (2019) 78(2):270–7. doi: 10.1136/annrheumdis-2018-213882

40. Shen S, Wu Y, Chen J, Xie Z, Huang K, Wang G, et al. Circserpine2 protects against osteoarthritis by targeting mir-1271 and ets-related gene. *Ann Rheum Dis* (2019) 78(6):826–36. doi: 10.1136/annrheumdis-2018-214786

41. Kung LHW, Ravi V, Rowley L, Angelucci C, Fosang AJ, Bell KM, et al. Cartilage microRNA dysregulation during the onset and progression of mouse osteoarthritis is independent of aggrecanolytic and overlaps with candidates from end-stage human disease. *Arthritis Rheumatol* (2018) 70(3):383–95. doi: 10.1002/art.40378

42. Cao Y, Tang S, Nie X, Zhou Z, Ruan G, Han W, et al. Decreased mir-214-3p activates nf-kappab pathway and aggravates osteoarthritis progression. *EBioMedicine* (2021) 65:103283. doi: 10.1016/j.ebiom.2021.103283

43. Huang J, Zhao L, Fan Y, Liao L, Ma PX, Xiao G, et al. The microRNAs mir-204 and mir-211 maintain joint homeostasis and protect against osteoarthritis progression. *Nat Commun* (2019) 10(1):2876. doi: 10.1038/s41467-019-10753-5

44. Nakamura A, Rampersaud YR, Nakamura S, Sharma A, Zeng F, Rossomacha E, et al. MicroRNA-181a-5p antisense oligonucleotides attenuate osteoarthritis in facet and knee joints. *Ann Rheum Dis* (2019) 78(1):111–21. doi: 10.1136/annrheumdis-2018-213629

45. Woods S, Barter MJ, Elliott HR, McGillivray CM, Birch MA, Clark IM, et al. Mir-324-5p is up regulated in end-stage osteoarthritis and regulates Indian hedgehog signalling by differing mechanisms in human and mouse. *Matrix Biol* (2019) 77:87–100. doi: 10.1016/j.matbio.2018.08.009

46. Wang H, Zhang H, Sun Q, Wang Y, Yang J, Yang J, et al. Intra-articular delivery of antago-Mir-483-5p inhibits osteoarthritis by modulating matrilin 3 and tissue inhibitor of metalloproteinase 2. *Mol Ther* (2017) 25(3):715–27. doi: 10.1016/j.ymthe.2016.12.020

47. Lu J, Ji ML, Zhang XJ, Shi PL, Wu H, Wang C, et al. MicroRNA-218-5p as a potential target for the treatment of human osteoarthritis. *Mol Ther* (2017) 25(12):2676–88. doi: 10.1016/j.ymthe.2017.08.009

48. Zhang H, Wu J, Wu J, Fan Q, Zhou J, Wu J, et al. Exosome-mediated targeted delivery of mir-210 for angiogenic therapy after cerebral ischemia in mice. *J Nanobiotechnol* (2019) 17(1):29. doi: 10.1186/s12951-019-0461-7

49. Besnier M, Gasparino S, Vono R, Sangalli E, Facchetti A, Bollati V, et al. Mir-210 enhances the therapeutic potential of bone-Marrow-Derived circulating proangiogenic cells in the setting of limb ischemia. *Mol Ther* (2018) 26(7):1694–705. doi: 10.1016/j.ymthe.2018.06.003

50. Lin XJ, Fang JH, Yang XJ, Zhang C, Yuan Y, Zheng L, et al. Hepatocellular carcinoma cell-secreted exosomal microRNA-210 promotes angiogenesis in vitro and in vivo. *Mol Ther Nucleic Acids* (2018) 11:243–52. doi: 10.1016/j.omtn.2018.02.014

51. Zaccagnini G, Greco S, Longo M, Maimone B, Voellenkle C, Fuschi P, et al. Hypoxia-induced mir-210 modulates the inflammatory response and fibrosis upon acute ischemia. *Cell Death Dis* (2021) 12(5):435. doi: 10.1038/s41419-021-03713-9

52. Zhao J, Florentin J, Tai YY, Torrino S, Ohayon L, Brzoska T, et al. Long range endocrine delivery of circulating mir-210 to endothelium promotes pulmonary hypertension. *Circ Res* (2020) 127(5):677–92. doi: 10.1161/CIRCRESAHA.119.316398

53. White K, Lu Y, Annis S, Hale AE, Chau BN, Dahlman JE, et al. Genetic and hypoxic alterations of the microRNA-210-Iscu1/2 axis promote iron-sulfur deficiency and pulmonary hypertension. *EMBO Mol Med* (2015) 7(6):695–713. doi: 10.15252/emmm.201404511

54. Zolotukhin S, Vandenberghe LH. Aav capsid design: A goldilocks challenge. *Trends Mol Med* (2022) 28(3):183–93. doi: 10.1016/j.molmed.2022.01.003

55. Batty P, Mo A, Hurlbut D, Ishida J, Yates B, Brown C, et al. Long-term follow-up of liver-directed, adeno-associated vector-mediated gene therapy in the canine model of hemophilia a. *Blood* (2022). doi: 10.1182/blood.202104735

56. George LA, Monahan PE, Eyster ME, Sullivan SK, Ragni MV, Croteau SE, et al. Multiyear factor viii expression after aav gene transfer for hemophilia a. *N Engl J Med* (2021) 385(21):1961–73. doi: 10.1056/NEJMoa2104205

57. Rosen S, Tiefenbacher S, Robinson M, Huang M, Srimani J, Mackenzie D, et al. Activity of transgene-produced b-Domain-Deleted factor viii in human plasma following Aav5 gene therapy. *Blood* (2020) 136(22):2524–34. doi: 10.1182/blood.2020005683

58. Zhou C, Cui Y, Yang Y, Guo D, Zhang D, Fan Y, et al. Runx1 protects against the pathological progression of osteoarthritis. *Bone Res* (2021) 9(1):50. doi: 10.1038/s41413-021-00173-x

59. Miao Y, Chen Y, Xue F, Liu K, Zhu B, Gao J, et al. Contribution of ferroptosis and Gpx4's dual functions to osteoarthritis progression. *EBioMedicine* (2022) 76:103847. doi: 10.1016/j.ebiom.2022.103847

60. Wagner HJ, Weber W, Fussenegger M. Synthetic biology: Emerging concepts to design and advance adeno-associated viral vectors for gene therapy. *Adv Sci (Weinh)* (2021) 8(9):2004018. doi: 10.1002/adv.202004018

61. Yoon DS, Lee KM, Cho S, Ko EA, Kim J, Jung S, et al. Cellular and tissue selectivity of aav serotypes for gene delivery to chondrocytes and cartilage. *Int J Med Sci* (2021) 18(15):3353–60. doi: 10.1510/ijms.56760

62. Santangelo KS, Bertone AL. Effective reduction of the interleukin-1beta transcript in osteoarthritis-prone Guinea pig chondrocytes *Via* short hairpin rna mediated rna interference influences gene expression of mediators implicated in disease pathogenesis. *Osteoarthritis Cartil* (2011) 19(12):1449–57. doi: 10.1016/j.joca.2011.09.004

63. Askou AL, Alsing S, Benckendorff JNE, Holmgaard A, Mikkelsen JG, Aagaard L, et al. Suppression of choroidal neovascularization by aav-based dual-acting antiangiogenic gene therapy. *Mol Ther Nucleic Acids* (2019) 16:38–50. doi: 10.1016/j.omtn.2019.01.012

64. Vrouwe JPM, Meulenberg JJM, Klarenbeek NB, Navas-Canete A, Reijnierse M, Ruiterkamp G, et al. Administration of an adeno-associated viral vector expressing interferon-beta in patients with inflammatory hand arthritis, results of a phase I/II study. *Osteoarthritis Cartil* (2022) 30(1):52–60. doi: 10.1016/j.joca.2021.09.013

65. Yang YS, Xie J, Wang D, Kim JM, Tai PWL, Gravalles E, et al. Bone-targeting aav-mediated silencing of schnurri-3 prevents bone loss in osteoporosis. *Nat Commun* (2019) 10(1):2958. doi: 10.1038/s41467-019-10809-6

66. Gerber HP, Vu TH, Ryan AM, Kowalski J, Werb Z, Ferrara N. Vegf couples hypertrophic cartilage remodeling, ossification and angiogenesis during endochondral bone formation. *Nat Med* (1999) 5(6):623–8. doi: 10.1038/9467

67. Zhen G, Guo Q, Li Y, Wu C, Zhu S, Wang R, et al. Mechanical stress determines the configuration of tgfbeta activation in articular cartilage. *Nat Commun* (2021) 12(1):1706. doi: 10.1038/s41467-021-21948-0

68. Fontemaggi G, Dell'Orso S, Triscioglio D, Shay T, Melucci E, Fazi F, et al. The execution of the transcriptional axis mutant P53, E2f1 and Id4 promotes tumor neo-angiogenesis. *Nat Struct Mol Biol* (2009) 16(10):1086–93. doi: 10.1038/nsmb.1669



OPEN ACCESS

EDITED BY

Li-Long Pan,
Jiangnan University, China

REVIEWED BY

Susumu Ohya,
Nagoya City University, Japan
Hua Ren,
East China Normal University, China
Bian Yanqin,
Shanghai Guanghua Hospital of
Integrated Traditional Chinese and
Western Medicine, China

*CORRESPONDENCE

Wei Hu
huwei@ahmu.edu.cn
Ren-Peng Zhou
zhourenpeng@ahmu.edu.cn

[†]These authors have contributed
equally to this work and share
first authorship

SPECIALTY SECTION

This article was submitted to
Autoimmune and Autoinflammatory
Disorders: Autoimmune Disorders,
a section of the journal
Frontiers in Immunology

RECEIVED 19 July 2022

ACCEPTED 16 September 2022

PUBLISHED 05 October 2022

CITATION

Lin Y, Zhao Y-J, Zhang H-L, Hao W-J,
Zhu R-D, Wang Y, Hu W and Zhou R-P
(2022) Regulatory role of KCa3.1 in
immune cell function and its emerging
association with rheumatoid arthritis.
Front. Immunol. 13:997621.
doi: 10.3389/fimmu.2022.997621

COPYRIGHT

© 2022 Lin, Zhao, Zhang, Hao, Zhu,
Wang, Hu and Zhou. This is an open-
access article distributed under the
terms of the [Creative Commons
Attribution License \(CC BY\)](#). The use,
distribution or reproduction in other
forums is permitted, provided the
original author(s) and the copyright
owner(s) are credited and that the
original publication in this journal is
cited, in accordance with accepted
academic practice. No use,
distribution or reproduction is
permitted which does not comply with
these terms.

Regulatory role of KCa3.1 in immune cell function and its emerging association with rheumatoid arthritis

Yi Lin^{1,2†}, Ying-Jie Zhao^{1†}, Hai-Lin Zhang^{1,2}, Wen-Juan Hao^{1,2},
Ren-Di Zhu^{1,2}, Yan Wang^{1,2}, Wei Hu^{1,3*} and Ren-Peng Zhou^{1,3*}

¹Department of Clinical Pharmacology, The Second Hospital of Anhui Medical University, Hefei, China,

²Inflammation and Immune Mediated Diseases Laboratory of Anhui Province, Anhui Institute of Innovative Drugs, School of Pharmacy, Anhui Medical University, Hefei, China, ³The Key Laboratory of Anti-inflammatory and Immune Medicine, Ministry of Education, Anhui Medical University, Hefei, China

Rheumatoid arthritis (RA) is a common autoimmune disease characterized by chronic inflammation. Immune dysfunction is an essential mechanism in the pathogenesis of RA and directly linked to synovial inflammation and cartilage/bone destruction. Intermediate conductance Ca^{2+} -activated K^{+} channel (KCa3.1) is considered a significant regulator of proliferation, differentiation, and migration of immune cells by mediating Ca^{2+} signal transduction. Earlier studies have demonstrated abnormal activation of KCa3.1 in the peripheral blood and articular synovium of RA patients. Moreover, knockout of KCa3.1 reduced the severity of synovial inflammation and cartilage damage to a significant extent in a mouse collagen antibody-induced arthritis (CAIA) model. Accumulating evidence implicates KCa3.1 as a potential therapeutic target for RA. Here, we provide an overview of the KCa3.1 channel and its pharmacological properties, discuss the significance of KCa3.1 in immune cells and feasibility as a drug target for modulating the immune balance, and highlight its emerging role in pathological progression of RA.

KEYWORDS

KCa3.1, immune cells, joint inflammation, rheumatoid arthritis, synovitis

Introduction

Rheumatoid arthritis (RA) is an autoimmune disease that primarily affects the joints. The average global incidence is 0.5% to 1.0%, with genetic factors accounting for approximately 60% risk of RA (1). The primary goal of RA therapy is to restore the immune balance and reduce synovial inflammation and joint damage. The traditional drug of RA ranges from disease-modifying anti-rheumatic drugs (DMARDs) (eg, methotrexate and Janus kinase inhibitor tofacitinib) to biologic agents (eg, tumor

necrosis factor inhibitors) and some adjuvant therapy drugs like non-steroidal anti-inflammatory drugs (NSAIDs) and glucocorticoids (GC) (1). However, the currently available drugs provide limited long-term efficacy along with increased risk of severe side-effects. Therefore, management of RA remains a topic of considerable research focus. In this context, we propose potential novel strategies for the treatment of RA by searching for targets that restore the balance of immune function.

KCa3.1, a Ca^{2+} -activated intermediate conductance K^+ channel regulated by the Ca^{2+} -binding protein calmodulin (CaM), was first identified in erythrocytes by Gardos in 1958 (therefore also designated the Gardos channel) (2). The channel is encoded by the *KCNN4* gene and directly pre-associated with CaM in the absence of Ca^{2+} . When the intracellular free Ca^{2+} concentration is higher than 100 nM, the KCa3.1 channel is activated after Ca^{2+} binds to CaM (3). This results in increased K^+ efflux and change in membrane potential, providing a driving force for Ca^{2+} influx. Physiological and pharmacological studies have shown that the KCa3.1 channel modulates membrane potential and Ca^{2+} signaling in activated T and B cells, macrophages and fibroblasts (4). From a pathological perspective, the KCa3.1 channel is abnormally opened to maintain Ca^{2+} homeostasis, thereby regulating various cellular functions ranging from proliferation and differentiation to migration (5). Therefore, the KCa3.1 channel may serve as a potential therapeutic target for diseases associated with cell activation and hyperproliferation, such as diabetic nephropathy (6), ulcerative colitis (7), and RA (8).

The pathological process of RA involves interactions of multiple immune cells, synovial fibroblasts, cytokines, and proteases. Synovial tissue gradually develops chronic inflammation that progresses to cartilage damage and bone erosion, leading to joint damage and multiple clinical symptoms (1, 9). Several studies have provided evidence that KCa3.1 contributes substantially to immune imbalance in RA. Notably, obstruction of the KCa3.1 channel effectively inhibits disease progression by alleviating immune inflammation and joint damage, suggestive of its significant therapeutic value in RA. This article provides a summary of the current information on the immunoregulatory mechanisms related to KCa3.1, its functional roles in the development of RA, and potential as a pharmacological target for disease management.

Overview of KCa3.1

KCa3.1 is a multifunctional intermediate conduction channel also known as IKCa1, SK4, IK-1 or KCa4 (10, 11). This channel belongs to a gene family consisting of all Ca^{2+} -activated K^+ channels. The International Union of Pharmacology has now classified the gene family into three groups: KCa1.1 (BK, big-conductance K^+ channel), KCa2.1, KCa2.2, KCa2.3 (SK, small-conductance K^+ channel) and KCa3.1 (IK, intermediate-

conductance K^+ channel) (12). KCa3.1 is a membrane-spanning protein composed of four α -subunits (13). Each α -subunit has six transmembrane segments (S1-S6) with a pore motif between S5 and S6. The pore region is formed by the transmembrane helices S5 and S6 in the symmetrical center of the tetramer, generating a K^+ conduction pathway (14). In genetics, the coding gene *KCNN4* is located at the q13.2 locus of human chromosome 19 (15, 16). The encoded protein contains 427 amino acids with a short N-terminal domain and long C-terminal tail. The C-lobe of CaM constitutively binds to CAM-binding domain (CAMBD) 1 (positions 312-329) in a Ca^{2+} -independent manner at the C-terminus of KCa3.1, whereas the CaM N-lobe barely binds to the channel and its binding pocket remains closed. In the presence of high Ca^{2+} , the N-lobe of CaM binds with Ca^{2+} and rearranges into an open conformation. The N-lobe of CaM pulls the S45A (first helix of the S4-S5 linker) helix down, keeping the S45B (tightly coupled to the pore-lining S6 helix) away from the pore axis. This expands the S6 helical bundle and eventually opens the pore (17). The N-lobe of CaM binds to KCa3.1 at CAMBD2A (a nearby segment, positions 344-353) in the same subunit and CAMBD2B (a distal segment, positions 360-373) in an adjacent subunit (18). Furthermore, a pivotal role of channel tetramerization and trafficking of two leucine zipper (LZ) motifs in the N- and C-termini has been reported (19, 20). The structure of KCa3.1 is shown schematically in Figure 1.

Here we focus on the transcriptional regulation, spliceosome regulation and epigenetic regulation of KCa3.1 (21). At the transcriptional level, activation protein-1 (AP-1) in conjunction with transcription factor Ikaros-2, was demonstrated to enhance KCa3.1 channel expression, which promoted the mitogenesis of preactivated lymphocytes (22). Additionally, laminar shear stress upregulates endothelial KCa3.1 by binding of AP-1 and cAMP response element (CRE) to promoter in a CaMK/Akt/p300 pathway-dependent manner (23). Mutation of the AP-1 binding motif in T cells as well as the transfection of AP-1 decoy oligonucleotides into cardiac fibroblasts were shown to significantly downregulate the expression of KCa3.1 (22, 24). Furthermore, two NF- κ B binding sites were identified in the promoter region of KCa3.1, and the up-regulation of KCa3.1 in colon cancer cells was mediated in an NF- κ B-dependent manner (25). A functional repressor element 1-silencing transcription factor (REST or NRSF) was confirmed to be a negative regulator of KCa3.1 transcription (26). In a study on tumors, histone deacetylase 2 (HDAC2) and HDAC3 were found to downregulate KCa3.1 transcript levels in a REST-independent and insulin-like growth factor-binding protein 5 (IGFBP5)-independent manner in the breast cancer cell line, TMB-1 (27). Meanwhile, HDAC2 and HDAC3 were found to be involved in the epigenetic regulation of KCa3.1 in the KCa3.1-expressing human prostate cancer cell line, PC-3. Epigenetically, *KCNN4* is hypermethylated in memory B cells in common variable immunodeficiency (CVID) individuals relative to healthy individuals (28). However, in a genome-wide DNA methylation analysis, Bulk et al. found that the *KCNN4* promoter was

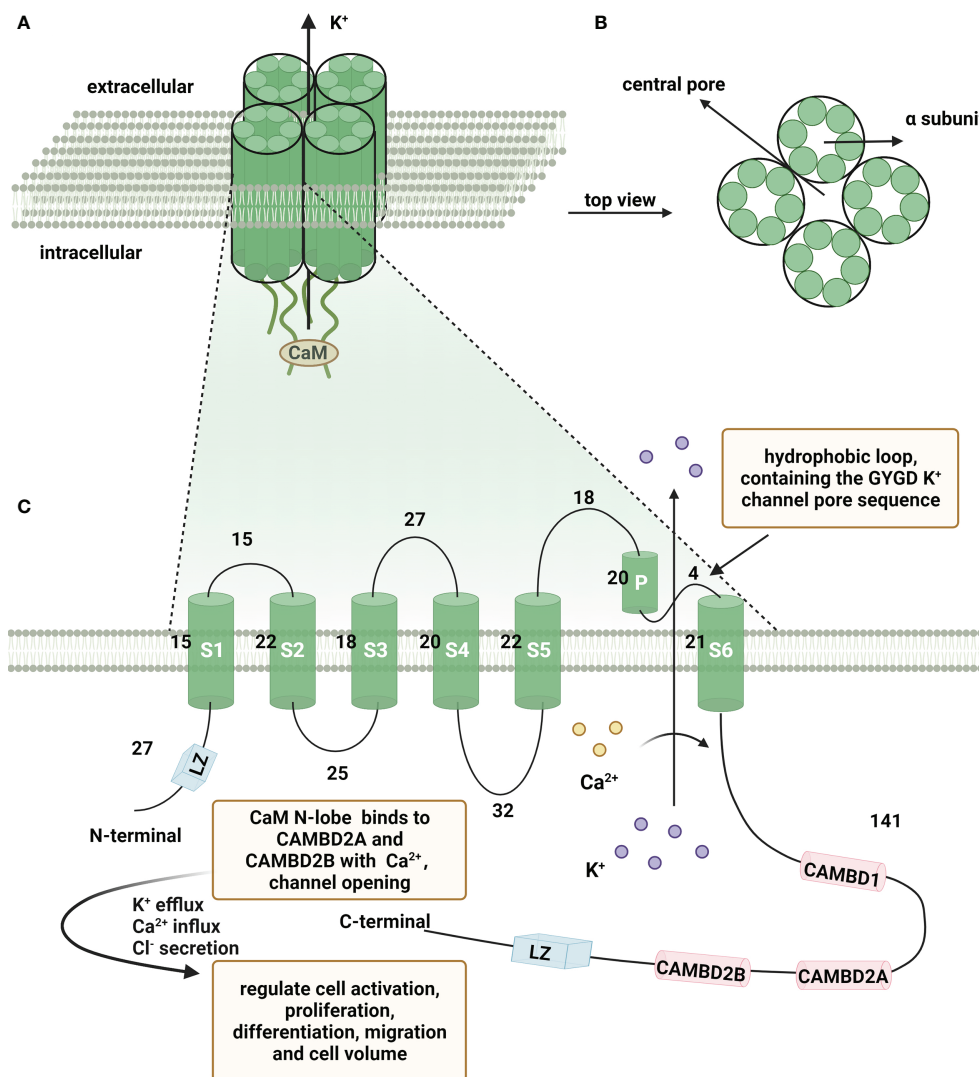


FIGURE 1

Schematic representation of the structure of KCa3.1. A functional Ca^{2+} -activated intermediate conductance K^+ channel (KCa3.1) comprises four α subunits organized around a central pore through which K^+ flows out of the cell. (A) KCa3.1 channel composed of four α subunits. (B) Top view of four α subunits around the central pore. (C) Schematic representation of a single KCa3.1 subunit, showing a total of 427 amino acids and consists of six transmembrane segments, named S1-S6. The K^+ ion conduction pore is located between the loop and S6, containing the GYGDK K^+ channel pore sequence. CaM N-lobe binds to CAMBD2A and CAMBD2B with Ca^{2+} , leading to channel opening. (Created with BioRender.com).

hypomethylated in lung cancer (29). Besides, Ohya et al. identified novel spliced variants of KCa3.1 (human(h) KCa3.1b) from the human thymus, which differs from hKCa3.1a for the lack of the N-terminal domains. The study suggests that the N-terminal domain of KCa3.1 is essential for channel trafficking to the plasma membrane (30). Moreover, Du et al. showed that *KCNN4* was regulated by several microRNAs, such as miR-204-5p studied in the research of pancreatic ductal adenocarcinoma (PDAC) (31).

KCa3.1 is located in the lung, distal colon, and immune-related tissues, such as thymus, bone marrow, and lymph nodes (32). In-depth studies have shown that KCa3.1 is almost expressed in non-

excitable cells, such as fibroblasts, lymphocytes, and other immune cells. At the cellular level, electrophysiological and pharmacological characterization studies have identified the presence of KCa3.1 in plasmalemma and mitochondrial membrane (33). KCa3.1 channels are additionally voltage-independent and unaffected by membrane potential, with Ca^{2+} -dependent and inwardly rectifying properties of intermediate conduction (34). Functionally, basolateral KCa3.1 provides the driving force for Cl^- secretion induced by activators such as Ca^{2+} in human and rat colon (35). KCa3.1 is also involved in regulation of cell volume in lymphocytes (36). Similarly, patch-clamp studies showed that the CFT1-LCFSN cell, a cystic fibrosis airway cell line, copes with hypotonic challenge *via* increasing the

KCa3.1 current (37). Moreover, the KCa3.1 channel is activated at elevated cytosolic Ca^{2+} concentrations of above 100 nM. Substantial activation of the KCa3.1 channel leads to K^+ efflux, thereby restoring and stabilizing the fully hyperpolarized membrane potential to maintain a continuous driving force of Ca^{2+} influx (38). While Ca^{2+} is indispensable for various physiological activities of the body, continuous influx is necessary for activation, proliferation and other physiological function of immune cells and cytokine production (39). Thus, the functions of KCa3.1 described above suggest the potential of targeting KCa3.1 in the treatment of diseases associated with immune imbalance.

Activators and inhibitors of KCa3.1

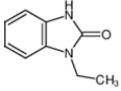
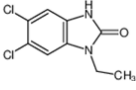
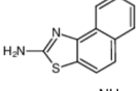
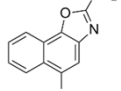
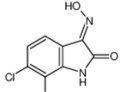
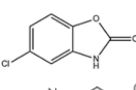
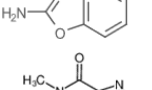
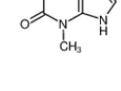
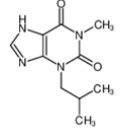
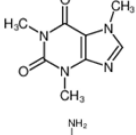
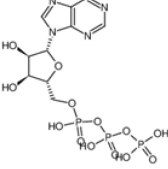
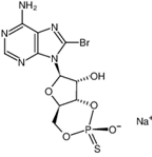
The pharmacological effects of the KCa3.1 channel have been widely explored and its activators and inhibitors analyzed in various diseases (Table 1). The majority examples of channel activators are documented in the literature related to cardiovascular diseases, neurological diseases and immune diseases. For instance, 1-ethyl-2-benzimidazolidinone (1-EBIO) serves as a direct and potent specific activator of KCa3.1 *via* increasing sensitivity of the channel to resting levels of Ca^{2+} (43). A dichloro analog of benzimidazolidinone, 5,6-dichloro-1-EBIO (DC-EBIO), is reported to be 30 times more potent than EBIO (44). Naphtho [1, 2-d] thiazole-2-ylamine (SKA-31) and its optimized product, 5-methylnaphtho [2,1-d] oxazole-2-amine (SKA-121), act in a similar manner to EBIO (45). Another preliminary study showed for the first time that 6,7-dichloro-1H-indole-2,3-dione-3-oxime (NS309) positively regulates KCa3.1 with higher potency and selectivity than 1-EBIO in the HEK-293 cells (human embryonic kidney cells). The above findings indicate that NS309 presents an excellent alternative to 1-EBIO as a pharmacological tool in KCa3.1 activation-related research (46). In addition, chlorzoxazone (CZ) and zoxazolamide (ZOX) are often used clinically as pharmacological activators of the KCa3.1 channel and have entered Phase IV and Phase II clinical trials, respectively (51). Classical methylxanthine compounds, including theophylline, 3-isobutyl-1-methylxanthine (IBMX) and caffeine, are reported to interact directly with channel proteins to activate KCa3.1 (47). Gerlach et al. demonstrated that ATP activates KCa3.1 in excised, inside-out patches in a protein kinase A inhibitor 5-24-dependent manner (52). In their experiments, ATP specifically activated chimera containing the KCa3.1 C-terminal amino acids His²⁹⁹-Lys⁴²⁷, but not other highly homologous Ca^{2+} -activated K^+ channels. In terms of indirect activation, the human single cAMP-dependent protein kinase (PKA) site (S334A) on the KCa3.1 α subunit is dependent on phosphorylation of PKA to reduce binding of CaM to the KCa3.1 channel. PKA signaling pathway inhibitors, such as PKI14-22, Rp-8-Br-cAMPS, and N-[2-(4-bromocinnamylamino) ethyl]-5-isoquinoline (H-89), significantly reversed downregulation of KCa3.1 channel, thereby restoring its function, while Sp-8-Br-cAMPS, a PKA activator, exerted the opposite effect (48, 53). Interestingly, PKA-mediated

phosphorylation was shown to have no regulatory effect on KCa3.1 channel in the above study (50). Moreover, a monoclonal blocking antibody against programmed death 1, pembrolizumab, has been identified that promotes KCa3.1 activity and concomitantly increases Ca^{2+} flux in cytotoxic T cells of patients immediately after treatment (54, 55). In conclusion, most KCa3.1 channel activators have low potency and poor selectivity and modulate other ion channels simultaneously.

KCa3.1 channel inhibitors are divided into two main categories: peptides and small molecule inhibitors. Peptide blockers bind to the outer vestibule of the channel and form multi-point contacts with channel residues whereas small-molecule blockers pass through the membrane and bind the cavity from the inside, blocking K^+ outflow (38). The majority of KCa3.1 channel peptide inhibitors are toxin polypeptides. The most common is the scorpion toxin Glu32-charybdotoxin, initially isolated from *Leiurus quinquestriatus*. Nevertheless, the scorpion toxin peptide has low selectivity for KCa3.1 and additionally shows activity against both KCa1.1 and Kv1.3 channel (a voltage-gated K^+ channel) (56, 57). Maurotoxin (MTX) (58) and urotoxin (α -KTx6) (59) display affinity for KCa3.1 but also affect the Kv1.2 channel (a voltage-gated K^+ channel). Accordingly, toxin polypeptide KCa3.1 channel blockers have limited experimental value for *in vivo* research on KCa3.1 due to their low specificity and are more commonly used to investigate the pharmacological properties of KCa3.1 *in vitro* (60).

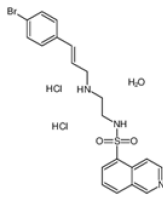
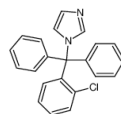
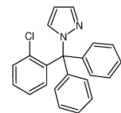
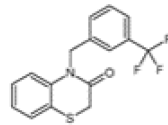
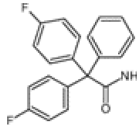
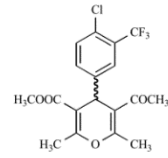
Small-molecule inhibitors of KCa3.1, primarily derived from the antibacterial drug clotrimazole, effectively block the channel and inhibit mitosis of activated prolymphocytes (22). However, clotrimazole inhibits cytochrome P450 enzymes *in vivo*, causing severe side-effects, which limits its pharmaceutical value (45). A derivative inhibitor of clotrimazole, 1-[(2-chlorophenyl) diphenylmethyl]-1H-pyrazole (TRAM-34), was further developed, which could avoid the adverse reactions of cytochrome P450 enzyme inhibition (61). TRAM-34 is the most commonly used KCa3.1 channel inhibitor in pharmacological experiments. Mechanistically, TRAM-34 binds threonine 250 and valine 275 in the pore cavity of the KCa3.1 channel, preventing penetration of ion (62). 4-[[3-(trifluoromethyl) phenyl] methyl]-2H-1, 4-benzothiazin-3 (4H)-one (NS6180) inhibits KCa3.1 channel activity using the same mechanism as TRAM-34 but has low bioavailability and is therefore only suitable for topical therapy. Senicapoc, also known as ICA-17043, is a potent and selective blocker of KCa3.1. Compared to other receptors, senicapoc displays higher selectivity for KCa3.1 and lower possibility of off-target effects (63, 64). A number of novel compounds have been synthesized using the L-type Ca^{2+} channel blocker nifedipine as the template, such as cyclohexadiene 4 (32) and the nano-affinity KCa3.1 channel inhibitor cyclohexadiene lactone composed of cyclohexadiene (4), and phenyl-4H-pyran. Due to the difficulty in synthesizing phenyl-4H-pyran and its short

TABLE 1 Inhibitors and Activators of KCa3.1.

Activators/ Inhibitors	Substances	Structure/ formula	IC ₅₀ /EC ₅₀	Experimental cells	Description	Clinical trial	References
Channel activators	1-EBIO		84 μM(EC ₅₀)	Xenopus oocytes	Increase channel open rate	\	(29, 32)
	DC-EBIO		Test at 100 μM	Capan-1 cells	Increase channel open rate	\	(40, 41)
	SKA-31		260 nM (EC ₅₀)	COS-7 cells	open channel	\	(30)
	SKA-121		110 nM (EC ₅₀)	COS-7 cells	open channel	\	(30)
	NS309		10 nM (EC ₅₀)	HEK-293 cell	open channel	\	(31)
	CZ		98 μM(EC ₅₀)	Xenopus oocytes	Increase channel open rate	Phase I-IV	(32)
	ZOX		Test at 300 μM	Xenopus oocytes	Increase channel open rate	Phase I-II	(32)
	theophylline		Test at 0~1500 μM	HEK-293 cell	Mandatory Ca ²⁺ -dependent, independent of phosphorylation	Phase I-IV;	(33)
Channel activators	IBMX		Only test at 1mM	HEK-293 cell	Mandatory calcium dependence	\	(33)
	Caffeine		Only test at 1mM	HEK-293 cell	Mandatory calcium dependence	Phase I-IV	(33)
	ATP		Only test at 100 μM	Human microglia	activate purinergic receptors, free [Ca ²⁺] _i ↑	Phase I-IV	(42)
	PKI14-22	C ₅₃ H ₁₀₀ N ₂₀ O ₁₂	Only test at 10M	MLS-9 microglia, primary rat microglia	Inhibit PKA, increase current	\	(35)
	Rp-8-Br-cAMPS		Test at 10M, 100μM	MLS-9 microglia, HEK-293 cell, post-SE neurons	Inhibit PKA, increase current	\	(35, 36)
	H-89		Test at 1μM, 10 μM		Inhibit PKA	\	(36)

(Continued)

TABLE 1 Continued

Activators/ Inhibitors	Substances	Structure/ formula	IC ₅₀ /EC ₅₀	Experimental cells	Description	Clinical trial	References
				Post-SE neurons, HEK-293 cell			
Peptide inhibitors	ChTX-Glu ³²	C ₁₇₅ H ₂₇₂ N ₅₆ O ₅₇ S ₇	250 nM (E _{max})	Human T-lymphocytes	Salt bridge anchors the outer vestibule	\	(43, 44)
	MTX	C ₁₄₅ H ₂₃₁ N ₄₅ O ₄₇ S ₈	1.4 nM (IC ₅₀)	CHO cells	Selective inhibitor	\	(45)
	α-KTx6	\	\	\	Inhibit KCa3.1 with nanomolar affinity	\	(46)
Small molecule inhibitors	clotrimazole		3±0.5 μM (EC ₅₀)	T cell	inhibit mitosis	Phase I-IV	(47)
	TRAM-34		5.5±0.5 μM (EC ₅₀)	T cell	inhibit mitosis	\	(47)
	NS6180		Human: 14 Nm; Mouse: 15 nM; Rat: 9 nM (IC ₅₀)	human, mice, and rat erythrocytes	binding amino acid	\	(48, 49)
	ICA-17043		11±2 nM (IC ₅₀)	Human erythrocytes	High selective	Phase I-III	(50)
	4-Phenyl-4H-pyran		8nM (IC ₅₀)	C6BU1 rat glioma cells	Inhibit ion conduction directly	\	(20, 48)

half-life after intravenous injection (62), the compound is not a suitable replacement for TRAM-34 as a KCa3.1 inhibitor. Clinically, the antihypertensive drug nitrendipine blocks KCa3.1 channel in a dose of 100 nM (65). Previous studies have shown that in the PI3K-PI(3)P signaling pathway, LY29400259 (a phosphatidylinositol 3-kinase inhibitor) (55) and ellagic acid (a nucleoside diphosphate kinase B kinase inhibitor) (66), prevent phosphorylation of specific group amino acid and inhibit activity of the KCa3.1 channel. Recently, Licochalcone A, a chalcone compound extracted from licorice, was shown to block KCa3.1 in a concentration-dependent manner, with anti-inflammatory effects (67). In general, the pharmacological effects of the KCa3.1 channel are relatively well characterized and meet the pharmacological needs in the relevant studies. However, the most rigorous obstacle to

clinical application of KCa3.1 modulators is almost associated with their low selectivity, so it is of great significance to explore highly specific drugs targeting KCa3.1 for conforming to clinical use.

Abnormal expression of KCa3.1 in rheumatoid arthritis

RA is an autoimmune disease characterized by inflammation of the synovium, with the essential site of inflammation identified as the synovial lining. In the process of lymphocyte activation and pathological function in rheumatoid arthritis, the increase of transient intracellular free calcium level plays a crucial role. A study have found that compared with healthy

people, RA patients have elevated basal cytoplasmic free calcium level ($[Ca^{2+}]_{cyt}$) and abnormal activation of KCa3.1 channel to maintain calcium influx in peripheral T lymphocytes (68). Additionally, Ca^{2+} -activated K^+ currents with the characteristics of KCa3.1 channel were detected in synovial fibroblasts from RA patients. TGF- β 1-induced KCa3.1 overexpression stimulates the proliferation and mediator secretion of synovial fibroblasts, which can be suppressed by KCa3.1 inhibitors. This result supports the theory that KCa3.1 is closely related to synovial inflammation (8). In addition, *KCNN4* is required for fusion of macrophages to form osteoclasts or multinucleated macrophages (MGCs) during the immune response to RA (69). KCa3.1 is expressed in both physiological and inflammatory osteoclast formation and is the only channel in the Ca^{2+} -activated K^+ channel family that is upregulated during the process of receptor activator of nuclear factor- κ B ligand (RANKL)-induced osteoclast formation. The collective results confirm an association of abnormal expression of KCa3.1 with pathogenesis of RA.

Experimental studies on animal models suggest that KCa3.1 is significantly associated with inflammation and pathogenesis of RA. In a collagen antibody-induced arthritis (CAIA) model, alleviated joint inflammation and tissue damage was observed in *KCNN4*^{-/-} mice compared to *KCNN4*^{+/+} mice (69). One extremely interesting phenomenon was that collagen-induced arthritis (CIA) *KCNN4*^{-/-} mice did not develop autoimmune arthritis (70). Specifically, following intradermal injection of chicken collagen type II into the base of the tail of *KCNN4*^{-/-} mice on days 0 and 21, no *KCNN4*^{-/-} mice developed clinical evidence or histological signs of arthritis, in contrast to wild-type mice. Notably, the CIA *KCNN4*^{-/-} model indicates a possible pro-inflammatory effect of KCa3.1 in RA. However, the specific mechanisms by which deficiency of *KCNN4* induces resistance against joint inflammation in CIA models remain unclear. These findings suggest that targeting KCa3.1 deficiency may alleviate joint inflammation and limit the development of persistent joint damage in experimental animal models, presenting a potential strategy for RA therapy.

Regulatory roles of KCa3.1 in immune cells

Role of KCa3.1 in T cells

The most prominent cell type in immune diseases is the T cell, which is responsible for recognizing antigens and generating immune responses. During pathogenesis of RA, autoantigens are presented to T cells by antigen-presenting cells. Following activation of pathogenic self-reactive T cells, various innate immunocytes are activated. Immediately afterwards, inflammatory signaling pathways are initiated, secreting various cytokines to trigger synovial tissue inflammation. KCa3.1 expressed in T cells initiates expression of genes that

promote T cell activation and proliferation (71). Notably, stimulated activated T cells express significantly higher levels of KCa3.1 than resting T cells (22).

CD4⁺ T cells are core cells of the immune system, coordinating the adaptive immune response and regulating immune and non-immune cell functions through cytokine production (72, 73). In CD4⁺ T cells, the KCa3.1 channel is activated mainly through the phosphatidylinositol 3 phosphate (PI(3)P) signaling pathway. After antigen presentation to T cell receptors, the class II phosphatidylinositol 3 kinase C2 β (PI3K-C2 β) is activated, which, in turn, promotes production of PI(3)P (74). Several studies indicate that KCa3.1 channel activation by PI(3)P is associated with NDPK-B. The inhibitory effect of the 14 amino acid region at CT of KCa3.1 is eliminated upon recruitment of nucleoside diphosphate kinase B (NDPK-B) to phosphorylate the histidine residue H358 in this region (75). Based on the above mechanism, existing studies have focused on inhibition of KCa3.1 channel opening through potential effects on three sites of activity. First, intracellular PI(3)P synthesis is restricted by the PI(3)P phosphatase myotubularin-related protein 6 (MTMR6). Consistently, the highly selective PI3K inhibitor wortmannin depletes intracellular PI(3)P that results in inhibition of KCa3.1 (75, 76). Second, phosphoglycerate mutase family 5 (PGAM5) induces dephosphorylation of NDPK-B and directly inhibits NDPK-B-mediated histidine phosphorylation, thereby blocking KCa3.1 channel activation (77). Third, the mammalian protein histidine phosphatase (PHPT-1) binds directly to phosphorylated H358, triggering its dephosphorylation to achieve inhibition of KCa3.1 channel activity (78). Moreover, intracellular copper deficiency is associated with elevated H358 phosphorylation, implying that the use of copper chelators may enhance the activity of KCa3.1 (79). In an established KCa3.1^{-/-} mouse model, it was observed that T helper (Th)-0, Th1, and Th2 cells isolated from KCa3.1^{-/-} mouse are defective in Ca^{2+} flux and cytokine production, while the Th17 and Treg subsets displayed normal function. The above phenomenon supports a key role of KCa3.1 in Th0, Th1, and Th2-mediated diseases, including RA, colitis, and several other immune inflammatory disorders (80). Consistently, pharmacological inhibition of KCa3.1 decreased inflammatory bowel disease mice symptoms *via* increasing IL-10 production in T_{reg} cells, suggests that KCa3.1 is responsible for the invalidation of anti-inflammatory efficiency of T_{reg} cells in chronic inflammatory disorders (81, 82).

CD8⁺ cells are cytotoxic T lymphocytes that infiltrate solid tumors to perform immune surveillance functions. Chimote et al. provided evidence of compartmental reduction of CaM levels at the plasma membrane of CD8⁺ T cells in head and neck squamous cell carcinoma (HNSCC) patients, leading to decreased activity and chemotaxis of KCa3.1 (83). Similarly, another recent study showed that targeted KCa3.1 activation could restore the chemotaxis ability of HNSCC CD8⁺ T cells in the presence of adenosine (84). Furthermore, KCa3.1 is reported to support the migration of

CD8⁺ T cells. Reduced K⁺ channel activity could be restored by cytokines, ultimately leading to functional recovery of impaired CD8⁺ T cells, facilitating clearance of pathogens or control of local tissue inflammation (85).

Role of KCa3.1 in B cells

The primary function of B cells is to differentiate into plasma cells that secrete antibodies to mediate humoral immune response under conditions of antigen stimulation and Th cell assistance. In RA condition, abnormal activation of B cells lead to autoantibodies secretion following autoantigen presentation by certain antigen presenting cells. In addition, B cells can regulate bone formation in RA by inhibiting differentiation of osteoblasts (86). Other than supporting T cell proliferation, KCa3.1 coordinates the proliferation and migration of B cells. KCa3.1 is reported to be expressed in B cells and activity of the channel is significantly elevated during differentiation of activated naive B cells into memory B cells (87, 88). As professional antigen-presenting cells, B cells play a significant role in the adaptive immune response. Mechanistically, B cells ingest, process, and present antigens by expressing the B cell receptor (BCR) and regulating the human leukocyte antigen HLA-DO (89). Non-competitive anti-N-methyl-D-aspartate-receptor (NMDAR) antagonists modulate BCR-induced B cell proliferation, migration, and production of the anti-inflammatory factor interleukin-10 (IL-10) through negative regulation of the KCa3.1 channel (88). *KCNN4* encoding KCa3.1 has been characterized as a tissue-specific transcriptional coactivator (OCA-B)-dependent gene involved in B cell proliferation and function that is required for antigen-dependent B cell differentiation.

In contrast to the above findings, KCa3.1 has been shown to be positively engaged in BCR-induced B cell proliferation but not required during the active phase of B cell differentiation (90). After TRAM-34 treatment, the ability of B lymphocytes to proliferate was weaker and expression of chemokine (C-C motif) ligand 7, a chemotactic-related factor that promotes B cell migration, significantly decreased (91). While the underlying mechanisms have not been established, it is reasonable to speculate that Ca²⁺-associated changes are significantly linked to inhibition of KCa3.1 channel in B cells. At the molecular level, activation of the extracellular signal-regulated kinase (ERK) upstream protein RAS affects the ERK signaling pathway, leading to reduced secretion of B cell chemokines and recruitment of inflammatory cells (92).

Role of KCa3.1 in macrophages

Macrophages play a fundamental role in the pathogenesis of RA disease, with significant infiltration at the inflamed synovium and cartilage junction, promoting inflammation by secreting

cytokines and chemokines (93). Studies demonstrated that macrophages may contribute to RA synovial inflammation through activation of Notch signaling, leading to M1 pro-inflammatory phenotype, or *via* c-Jun N-terminal kinase (JNK) signaling channels activating nuclear factor κ B and producing large amounts of tumor necrosis factor- α (TNF- α) (94). Earlier *in vitro* studies have demonstrated KCa3.1 expression in macrophages, with key roles in regulation of macrophage proliferation, migration, reactive oxygen species (ROS), and cytokine production (95, 96). In keeping with its role in T and B cells, KCa3.1 is reported to maintain Ca²⁺ influx and membrane hyperpolarization in macrophages (97). Upon blockage of the KCa3.1 channel in a study by Xu et al., the activity of signal transducer and activator of transcription 1 (STAT-1) protein was inhibited and phosphorylation levels reduced in macrophages (98). Moreover, the levels of pro-inflammatory cytokines and chemokines were significantly decreased in M1 macrophages whereas markers in M2 macrophages remained unchanged, suggesting that the KCa3.1 channel mainly regulates the function of M1 type macrophages and expression of pro-inflammatory genes. In chronic diseases, such as RA, multinucleation of macrophages is a critical step in the formation, differentiation and activation of osteoclasts, which lead to bone erosion and long-term inflammation (99, 100). In a microarray analysis of fused rat macrophages and human monocytes forming osteoclasts by Kang et al., the role of *KCNN4* as a potential modulator of multinucleation was validated (69). The main downstream effect of nuclear factor- κ B (NF- κ B) activation is upregulation of T cell dephosphorylation by nuclear translocation of nuclear factor cytoplasmic 1 (NFATc1), which stimulates Ca²⁺ signaling and activates Akt. Silencing or blockage of KCa3.1 suppressed NFATc1 expression and Akt activation, implying that *KCNN4* is also closely associated with cell death (69). Another study reported that TNF- α mediates the NF- κ B pathway through increased autocrine secretion. NF- κ B binds directly to the promoter region of *KCNN4* and enhances its activity to upregulate gene expression and promote cell proliferation (101). Furthermore, blockade of the KCa3.1 channel with TRAM-34 negatively regulates NF- κ B and STAT3 signaling and impairs the ability of macrophages to differentiate into the pro-inflammatory M1 phenotype, in parallel with reduced levels of inflammatory factors, such as interleukin-1 (IL-1), interleukin-6 (IL-6), TNF- α and monocyte chemoattractant protein-1 (MCP-1) (102). The majority of studies indicate that the role of KCa3.1 in macrophages is closely associated with NF- κ B and STAT signaling pathways.

Role of KCa3.1 in mast cells

Mast cells (MCs) recognize endogenous and exogenous mediators, which boost the release of various mediators from

other immune and non-immune cells, consequently regulating different physiological activities *in vivo* (103). During the process of RA, activated MCs produce an array of pro-inflammatory mediators that activate other immune system cells, initiating and maintaining the inflammatory response. TNF- α preformed by mast cells initiates an inflammatory cascade response promoting cytokine expression. Meanwhile, products of mast cells, in particular, histamine and TNF- α , promote proliferation and catabolic effects of articular chondrocytes and synovial stromal cells, leading to the development of RA (104). A number of previous studies have confirmed the presence of KCa3.1 in mast cells. Activation of the KCa3.1 channel maintains high concentrations of intracellular free Ca^{2+} in mast cells, promotes IgE-dependent histamine release, and regulates the secretory responses of mast cells (105). The Orai/CRACM1 ion channel provides the major Ca^{2+} influx pathway for mast cells to release mediators and activation of the KCa3.1 channel in mast cells is highly dependent on this process (106). Prostaglandin E2 (PGE2) suppresses the IgE-dependent cell activation pathway by inhibiting activation of EP2 receptors. Inactivation of EP2 receptors limits the influx of free cytoplasmic Ca^{2+} , leading to reduced chemokine production and subsequent closure of the KCa3.1 channel (107). Upon interference with channel gene expression *via* lentiviral targeting of KCa3.1, signaling pathways are disrupted and mast cell activity is reduced, followed by attenuation of the immune inflammatory response (108). In addition, E3 ubiquitin ligase (containing a tripartite motif of protein 27) negatively regulates high-affinity receptor for IgE (Fc ϵ RI) activation and downstream signaling of KCa3.1 through ubiquitination and inhibition of PI3K β in mast cells (109). The levels of chemokine CXC motif chemokine ligand 10, chemokine stem cell factor, and TNF- α in mast cells are reported to be significantly decreased by charybdotoxin and TRAM-34, along with diminished mast cell migration capacity (110).

Role of KCa3.1 in dendritic cells

Dendritic cells (DCs) participate in the presentation of autoantigens and production of pro-inflammatory factors, which contribute to ongoing inflammation in RA. In addition, DCs are in charge of maintenance and differentiation of autoimmune B and T cells which directly participated in RA pathogenesis (111). Studies show that the binding of lymphatic chemokines CCL19 and CCL21 to their receptor CCR7 induces mobilization of Ca^{2+} stored in mature DCs and subsequent opening of the KCa3.1 channel (112, 113). The migratory capacity of DCs is tightly regulated by the intracellular Ca^{2+} concentration and chemokine receptors are differentially expressed in DCs at two states of maturation. In the presence of TRAM-34, temporal coupling between KCa3.1 and Ca^{2+} inward flow was shown to be disrupted and subsequent CCR7-induced chemotaxis impaired (112). Paradoxically, KCa3.1 exhibited migratory capacity only in immature dendritic cells and

expression of its migration marker CCR5 was modified in the presence of TRAM-34 (114, 115). Data from the above study additionally confirmed that activation of T lymphocyte proliferation by dendritic cells is not affected by KCa3.1. *In vitro*, prevention of $[\text{Ca}^{2+}]_i$ elevation under conditions of KCa3.1 deficiency decreased the directed migration of lipopolysaccharide (LPS)-challenged DCs, supporting the involvement of KCa3.1 in LPS-induced DC migration (116).

Roles of KCa3.1 in other immune cells

In RA, neutrophils can activate other immune cells that perpetuate inflammation and lead to the destruction of cartilage and bone in affected joints. This pathogenic effect occurs primarily through mechanisms including increased cell survival and migration capacity, abnormal inflammatory activity, elevated oxidative stress, and exacerbated neutrophil extracellular trap formation (117). Recently, Henríquez et al. demonstrated the existence of KCa3.1 in mammalian neutrophils for the first time and showed a positive correlation between upregulation of the channel and neutrophil migration (118). Concomitantly, targeted KCa3.1 inhibition altered the capacity of cells to properly regulate cell volume and limited neutrophil migration *in vitro* with no effect on Ca^{2+} homeostasis. Likewise, the membrane potential of the *KCNN4*^{-/-} neutrophil subpopulation was balanced in a study by Grimes et al., resulting in a homogeneous lower-calcium (Ca^{10}) response (119). In addition, erythrocytes have a partial immune function although they are not conventional immune cells. The KCa3.1 channel present on erythrocytes regulates cellular volume by transporting K^+ across the membrane and its activity increases in response to high cytokine levels (120). The role of KCa3.1 in immune cells has been summarized in the Table 2.

Correlative regulation of KCa3.1 and immune-inflammatory cytokines

Synovial inflammation is a critical process in the pathogenesis of RA and directly associated with clinical symptoms, such as inflammatory pain, joint swelling and progressive destruction of multiple joints. Accumulating evidence suggests that the KCa3.1 channel is capable of cytokine regulation with potential significant implications in immune-inflammatory diseases (Figure 2). KCa3.1 has been shown to stimulate TGF- β 1 production. In experiments by C. Huang et al., treatment with TRAM-34 suppressed transcription of TGF- β 1 and TGF- β 1 type II receptor mRNA and negatively regulated phosphorylation of Smad2/3 (122). The above processes led to reduced production of inflammatory cytokines, PAI-1, and matrix proteins in the nucleus, with anti-inflammatory and anti-fibrotic effects. The

KCa3.1 channel is reported to mediate K^+ efflux, promote intracellular Ca^{2+} concentrations, and activate calmodulin kinase IV (CaMKIV), which facilitates CREB phosphorylation, contributing to upregulation of c-fos/AP-1 and NFATc1 expression, and ultimately leading to osteoclast formation (123). Moreover, NF- κ B and STAT3 signaling pathways are inactivated upon blockade of the KCa3.1 channel. Consequently, decreased secretion of pro-inflammatory factors, such as IL-1 β , IL-6, TNF- α , and MCP-1, limits the progression of inflammation (102). In regulatory T cells, suppression of KCa3.1 channel activity initiates phosphorylation of JNK and c-Jun, activation of JNK/c-Jun signaling, and E4BP4/Blimp1-mediated anti-inflammatory IL-10 cytokine secretion (81, 82). The above findings suggest that inhibition of KCa3.1 channel activity modulates immune-inflammatory factors and alleviates inflammation. Paradoxically, TRAM-34 is reported to activate two types of transcriptional regulators, KLF4 and/or TRIM33, and mediate upregulation of pro-inflammatory IL-17A (82). Another study disclosed no pro-inflammatory changes in T cell subsets and plasma cytokines or chemokines following administration of SKA-31, a KCa3.1 activator, in rats (124).

The KCa3.1 channel both regulates and is regulated by cytokines (Figure 3). TGF- β 1 has the capability to inhibit catalase activity and promote hydrogen peroxide levels, thereby inducing an increase in KCa3.1 expression. The p38MAPK signaling pathway plays a vital role in stress responses, such as inflammation and apoptosis. p38MAPK/AP-1/NF- κ B signaling activates the AP1 complex (composed of c-fos and c-Jun) and promotes transcription and translation of KCa3.1 (125). Upregulation of KCa3.1 stimulates the

expression and production of interferon- γ (IFN- γ), in turn, mediating the mobilization and accumulation of inflammatory T cells, which are involved in inflammation (126). In addition, IL-1 β stimulation is reported to activate NF- κ B signaling and upregulate the KCa3.1 channel in pancreatic islet cells. The drug modafinil suppresses progression of inflammation *via* elevation of adenosine 3', 5 cyclic monophosphate (cAMP) and inhibition of KCa3.1 channel activity (127). Furthermore, IL-4 specifically binds type I receptors and regulates JAK3 and RAS/MEK/ERK signaling pathways. In the above mechanisms, the transcription factor AP-1 is activated and upregulates KCa3.1 (128). However, in-depth studies revealed that IL-4 increases the current in the KCa3.1 channel only slightly, inducing no significant changes in channel density with increasing membrane area (40). Based on the available information, targeting the KCa3.1 channel is proposed as a means to effectively regulate immune-related molecules, such as cytokines and inflammatory factors, which play a crucial part in immune system-mediated disorders.

KCa3.1 as a potential drug target for RA

Targeting the inflammatory process of RA

The occurrence and continuous development of RA is manifested by failure of spontaneous regression of inflammation. Increasing evidence suggests that KCa3.1 promotes secretion of inflammatory factors by regulating

TABLE 2 Role of KCa3.1 in immune cell.

Cells	Experimental cells	Inhibition/activation of KCa3.1	Mechanism	References
T lymphocytes	CD4 ⁺ T cells	MTMR6/ Wortmannin	PI(3)P↓, KCa3.1↓, proliferation↓	(75, 76)
	CD4 ⁺ T cells	PGAM5	Dephosphorylation NDPK-B, Histidine phosphorylation↓, KCa3.1↑	(77)
	CD4 ⁺ T cells	PHPT-1	Bind p-H358, dephosphorylation p-H358, KCa3.1↓	(78)
	CD8 ⁺ T cells	1-EBIO	Chemotactic capacity↑	(84)
B lymphocytes	Splenic B cells	NMDAR antagonists	Inhibit BCR, KCa3.1↓, IgM, IgG↓, IL-10↑	(88)
	Splenic B cells	TRAM-34	KCa3.1↓, cells proliferation↓, CCL7↓, migration↓	(91)
Macrophages	THP-1 cells	TRAM-34	KCa3.1↓, STAT-1↓, type M1 polarization↓	(98)
	Human macrophages	KCNN4 deficiency	KCa3.1↓, RANKL↓, NF- κ B↓, NFATc1↓, Akt↑	(69)
Mast cells	HLMC	AH6809	EP2↓, KCa3.1↓, chemokine↓, migration↓	(107)
	P815 cells	LV-KCa3.1-shRNA	KCa3.1↓, AKT phosphorylation↓, IL-6, IL-8↓, mast cell activity↓	(108)
	BMMC	TRIM27 ^{-/-}	FcεR1↑, PI3KC2β↑, KCa3.1↑, mast cell activation↑	(121)
	HLMC	TRAM-34	KCa3.1↓, CXCL10, TNF- α ↓, migration↓	(110)
Dendritic cells	Lung dendritic cells	TRAM-34	CCR7 inhibition, KCa3.1↓, migration↓	(112)
	Immature dendritic cells	TRAM-34	CCR5 inhibition, KCa3.1↓, migration↓	(114)

The symbols ↑ and ↓ mean the up-regulation and down-regulation of KCa3.1 expression, respectively.

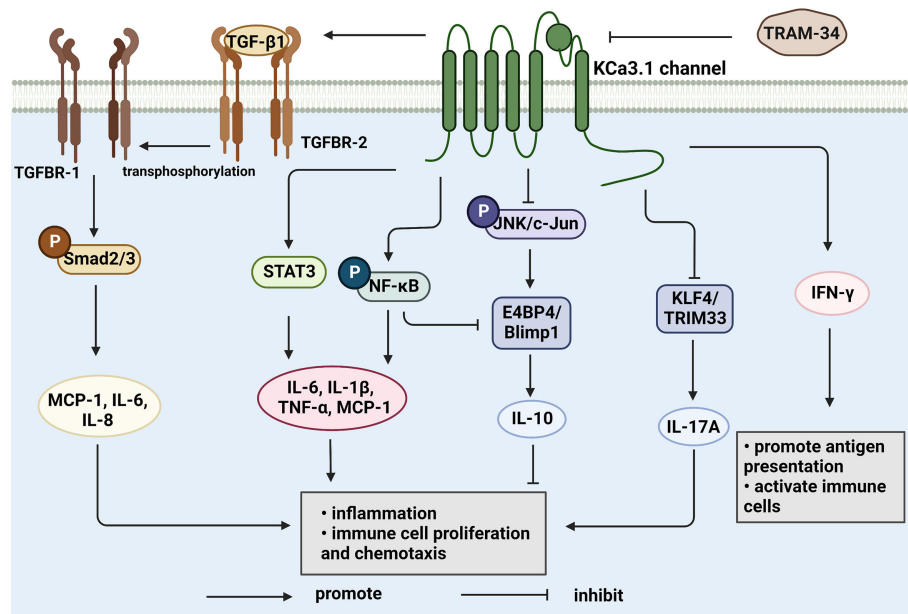


FIGURE 2

KCa3.1 regulates cytokine production and secretion. TGF- β 1 binds to type II receptors and transphosphorylates type I receptors, phosphorylates Smad2/3 and secretes many inflammatory factors. Activation of KCa3.1 also promotes the secretion of IL-1 β , IL-6, IL-8, TNF- α , and MCP-1 through the STAT3 and NF- κ B signaling pathways. IFN- γ is upregulated by KCa3.1 either. KCa3.1 restrains the production of IL-10 through the JNK/c-Jun and NF- κ B pathways. The blocked KCa3.1 channel by TRAM-34 inhibits these pathways. IL-17A is a pro-inflammatory cytokine that is upregulated by TRAM-34 through activation of KLF4 and/or TRIM33. (Created with BioRender.com).

immune-inflammatory cells in RA. In related reports, KCa3.1 is considered a pro-inflammatory ion channel that activates the function of inflammasome. Hydroxychloroquine is reported to impair the inflammasome and inhibit neutrophil recruitment in a dose-dependent manner through inhibition of Ca²⁺-activated K⁺ conductance in THP-1 macrophages (70). Interestingly, earlier findings indicate that TGF- β induces transcription and translation of KCa3.1 and, conversely, silencing or inhibition of KCa3.1 negatively regulates TGF- β (8). In addition, the pro-inflammatory and invasive behavior of synovial fibroblasts plays an essential role in RA. Another study showed that blockage of KCa3.1 with TRAM-34 or siRNA treatment could suppress proliferation of RA-SFs. Inactivation of the channel led to downregulation of the pro-inflammatory factors IL-6, interleukin-8 (IL-8), and MCP-1, as well as tissue-destructive protease MMP3 at both mRNA and protein levels. Notably, inhibition of the KCa3.1 channel also upregulated MMP1 mRNA and enhanced secretion of IL-1 β while decreasing that of IL-1-RA, resulting in inhibition of short-term activation of Th2 lymphocytes in RA and consequently, a shift in the inflammatory homeostasis of RA to a pro-inflammatory state (41). However, limited data on the specific role of KCa3.1 in inflammation of RA are available at present. Further studies are

required to elucidate the functions and mechanisms of action of KCa3.1 in the inflammatory process associated with RA.

Targeting of cartilage destruction and bone erosion

The pathogenesis of RA is synovial inflammation accompanied by cartilage damage and bone erosion. In addition to synovial tissue and immune cells that show critical immune-inflammatory activities, synovial fibroblasts and osteoclasts play a central role in cartilage and bone destruction and bone erosion in RA. Although no evidence of direct mediation of RA cartilage and osteogenic destruction by KCa3.1 has been obtained, its involvement in these processes *via* regulation of fibroblast (FLS) and osteoclast activation is a strong possibility.

Previous studies have shown that highly activated FLS can promote inflammation and tissue invasion and mediate tissue damage with tissue-infiltrating macrophages and immune cells, such as T cells and B cells (42). FLS are involved in the pathological process of synovitis, synovial lining hyperplasia, activation of a number of synovial cells, and destruction of

cartilage matrix through production of cytokines and chemokines. The p38 MAPK (mitogen-activated protein kinase) pathway is a crucial signal transduction step during chronic inflammation (49). Two isoforms of p38MAPK, α and γ , are expressed in FLS, which play key roles in the inflammatory process by activating the p38MAPK signaling pathway to produce inflammatory factors, such as TNF- α , IL-1 β and IL-6 (129). In addition, FLS regulate the proliferation and differentiation of immune cells through the p38 pathway. Transcriptional growth factor β 1 (TNF- β 1) is highly expressed in RA-SFs and can induce expression of pro-inflammatory and pro-destructive proteins (130). TNF- β 1 has been shown to induce *KCNN4* transcription and translation, activate the KCa3.1 channel, increase K⁺ current, provide continuous power for Ca²⁺ influx, and promote inflammatory processes (131). At present, studies on the mechanism of action of KCa3.1 in synovial fibroblasts are lacking and the pathways underlying KCa3.1 upregulation by TGF- β 1 remain to be established. Further clarification of whether KCa3.1 has functional activity in RA-SFs through signaling pathways, such as p38MAPK (132) and NF- κ B (133, 134), should further support its potential involvement in RA cartilage injury.

Osteoclasts and RANKL act together to promote the occurrence of bone erosion (124, 125). In a recent study, activation of endogenous fibroblast-like synoviocytes induced RANKL expression and stimulated osteoclast formation (135, 136). The KCa3.1 channel inhibitors, TRAM-34 and ICA-17043, have been shown to inhibit monocyte formation in osteoclasts in a dose-dependent manner but the precise molecular mechanisms remain to be established (69). It is speculated that the KCa3.1 channel is functionally active in the formation of osteoclasts. KCa3.1 can prevent the progression of bone erosion by inhibiting the differentiation and formation of osteoclasts, thereby relieving the clinical symptoms of RA patients, providing further support for its utility in management of RA.

Blockage of the KCa3.1 channel

In applications of KCa3.1 channel inhibitors, existing studies indicate that TRAM-34 exerts no notable side-effects when used at a high concentration (~120 mg/kg) and has no effect on blood biochemistry and hematology parameters (137). Senicapoc has passed Phase I-III clinical trials for clinical drug use in sickle cell disease, with a reported IC₅₀ value of 11 nm (138). Senicapoc may

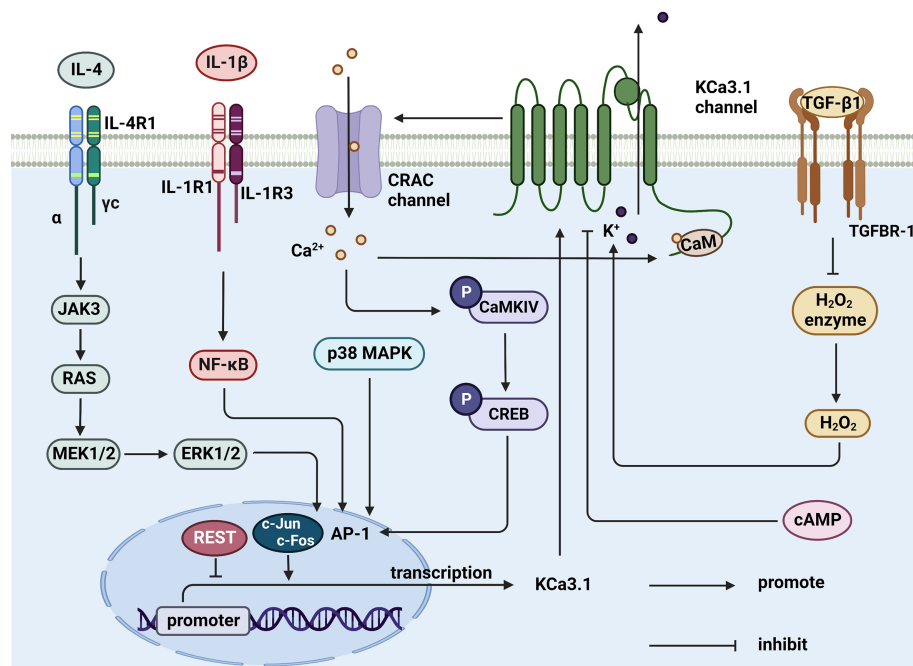


FIGURE 3

Cytokines regulate KCa3.1 expression and activity. TGF- β 1 inhibits catalase, thereby synthesizing hydrogen peroxide to activate KCa3.1. IL-4 and IL-1 β upregulates AP-1 through JAK3/RAS/MEK/ERK and NF- κ B signaling pathway, resulting in the initiation of KCa3.1 transcription. AP-1 can be upregulated by activated CaMKIV/CREB and p38 MAPK pathway, either. KCa3.1 activity is controlled by elevated cAMP in response to agents. (Created with BioRender.com).

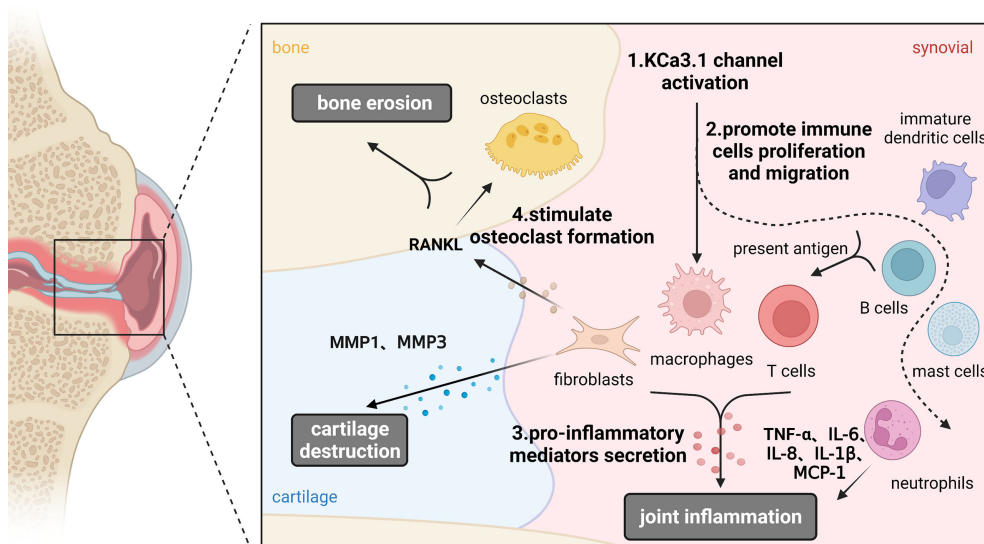


FIGURE 4

Functions of KCa3.1 channel in the pathological process of rheumatoid arthritis. KCa3.1 is involved in RA inflammation, cartilage and bone destruction by regulating the abnormal activation of immune cells, synoviocytes and osteoclasts. Dashed arrows indicate possible mechanisms in rheumatoid arthritis. (Created with [BioRender.com](https://www.biorender.com)).

cause diarrhea, nausea, and other adverse reactions in a dose-dependent manner, but overall drug safety is good. The KCa3.1 inhibitors TRAM-34 and Senicapoc have been used in RA-related *in vitro* studies (8, 69). Clotrimazole and nitrendipine have progressed to the clinical trial stage and are widely used to treat a number of diseases. According to the tissue distribution characteristics of the KCa3.1 channel, KCa3.1 generally not expressed in excitable tissues and reproductive organs, which indicates a low-risk, acute-toxicology profile of KCa3.1 channel blockade. The results obtained to date support the feasibility, efficacy, and safety of the KCa3.1 channel as a therapeutic target in RA. However, extensive research is required before introduction of KCa3.1 channel blockers in the clinic. Remarkably, related studies have shown that the KCa3.1 channel is the basis of slow afterhyperpolarization (SAHP) in neurons and may exert side-effects that affect sensory transmission (139).

Conclusions and outlook

KCa3.1 promotes inflammation, cartilage damage, and bone erosion in synovial fibroblasts and osteoclasts that are mechanistically involved in development of RA. Based on its ability to restore the immune balance by interfering with Ca^{2+} signaling, KCa3.1 presents a promising therapeutic target for RA. The possible functions of KCa3.1 in the pathological process

of RA is shown in [Figure 4](#). Despite interesting experimental findings to date, research in this field is still in its infancy. Considerable work remains to be done to elucidate the in-depth mechanisms underlying the involvement of KCa3.1 in RA. For example, the issue of whether KCa3.1 directly mediates cartilage and bone destruction in RA is yet to be resolved. Furthermore, no clinical trials have directly investigated the effects of KCa3.1-specific inhibitors and activators in RA as yet. In summary, KCa3.1 provides excellent research prospects for treatment of RA and further development of drugs targeting this channel may be of considerable benefit to patients.

Author contributions

RP-Z and WH conceived this project. LY and Y-JZ prepared the first draft. H-LZ, W-JH, R-DZ, YW and R-PZ revised the manuscript. All authors contributed to the article and approved the submitted version.

Funding

This work was supported by grants from the National Natural Science Foundation of China (82272450, 81902182, 82071591) and the Natural Science Foundation Incubation

Program of The Second Hospital of Anhui Medical University (2021GMFY06).

Conflict of interest

The authors declare that the research was conducted in the absence of any commercial or financial relationships that could be construed as a potential conflict of interest.

References

- Smolen JS, Aletaha D, Barton A, Burmester GR, Emery P, Firestein GS, et al. Rheumatoid arthritis. *Nat Rev Dis Primers* (2018) 4:18002. doi: 10.1038/nrdp.2018.2
- Maher AD, Kuchel PW. The gárdos channel: a review of the Ca²⁺-activated K⁺ channel in human erythrocytes. *Int J Biochem Cell Biol* (2003) 35(8):1182–97. doi: 10.1016/S1357-2725(02)00310-2
- Fanger CM, Ghanshani S, Logsdon NJ, Rauer H, Kalman K, Zhou J, et al. Calmodulin mediates calcium-dependent activation of the intermediate conductance K_{Ca} channel, IK_{Ca}1. *J Biol Chem* (1999) 274(9):5746–54. doi: 10.1074/jbc.274.9.5746
- Wulff H, Castle NA. Therapeutic potential of K_{Ca}3.1 blockers: recent advances and promising trends. *Expert Rev Clin Pharmacol* (2010) 3(3):385–96. doi: 10.1586/ecp.10.11
- Hara MR, Snyder SH. Cell signaling and neuronal death. *Annu Rev Pharmacol Toxicol* (2007) 47:117–41. doi: 10.1146/annurev.pharmtox.47.120505.105311
- Huang C, Pollock CA, Chen XM. Role of the potassium channel K_{Ca}3.1 in diabetic nephropathy. *Clin Sci (Lond)* (2014) 127(7):423–33. doi: 10.1042/CS20140075
- Koch Hansen L, Sevelsted-Møller L, Rabjerg M, Larsen D, Hansen TP, Klinge L, et al. Expression of T-cell KV1.3 potassium channel correlates with pro-inflammatory cytokines and disease activity in ulcerative colitis. *J Crohns Colitis* (2014) 8(11):1378–91. doi: 10.1016/j.crohns.2014.04.003
- Friebel K, Schonherr R, Kinne RW, Kunisch E. Functional role of the K_{Ca}3.1 potassium channel in synovial fibroblasts from rheumatoid arthritis patients. *J Cell Physiol* (2015) 230(7):1677–88. doi: 10.1002/jcp.24924
- Zhao J, Guo S, Schrodi SJ, He D. Molecular and cellular heterogeneity in rheumatoid arthritis: Mechanisms and clinical implications. *Front Immunol* (2021) 12:790122. doi: 10.3389/fimmu.2021.790122
- Chou C-C, Lunn CA, Murgolo NJ. K_{Ca}3.1: target and marker for cancer, autoimmune disorder and vascular inflammation? *Expert Rev Mol Diagn* (2008) 8(2):179–87. doi: 10.1586/14737159.8.2.179
- Wang J, Xiang M. Targeting potassium channels Kv1.3 and KCa 3.1: routes to selective immunomodulators in autoimmune disorder treatment? *Pharmacotherapy* (2013) 33(5):515–28. doi: 10.1002/phar.1236
- Wei AD, Gutman GA, Aldrich R, Chandy KG, Grissmer S, Wulff H. International union of pharmacology. LII. nomenclature and molecular relationships of calcium-activated potassium channels. *Pharmacol Rev* (2005) 57(4):463–72. doi: 10.1124/pr.57.4.9
- Jensen BS, Hertz M, Christophersen P, Madsen LS. The Ca²⁺-activated K⁺ channel of intermediate conductance: a possible target for immune suppression. *Expert Opin Ther Targets* (2002) 6(6):623–36. doi: 10.1517/14728222.6.6.623
- Vianna-Jorge R, Suarez-Kurtz G. Potassium channels in T lymphocytes: therapeutic targets for autoimmune disorders? *BioDrugs* (2004) 18(5):329–41. doi: 10.2165/00063030-200418050-00005
- Ghanshani S, Coleman M, Gustavsson P, Wu AC, Gargus JJ, Gutman GA, et al. Human calcium-activated potassium channel gene KCNN4 maps to chromosome 19q13.2 in the region deleted in diamond-blackfan anemia. *Genomics* (1998) 51(1):160–1. doi: 10.1006/geno.1998.5333
- Sforza L, Megaro A, Pessia M, Franciolini F, Catacuzzeno L. Structure, gating and basic functions of the Ca²⁺-activated K channel of intermediate conductance. *Curr Neuropharmacol* (2018) 16(5):608–17. doi: 10.2174/1570159X15666170830122402
- Lee CH, MacKinnon R. Activation mechanism of a human SK-calmodulin channel complex elucidated by cryo-EM structures. *Sci (New York NY)* (2018) 360(6388):508–13. doi: 10.1126/science.aas9466
- Morales P, Garneau L, Klein H, Lavoie MF, Parent L, Sauvé R. Contribution of the K_{Ca}3.1 channel-calmodulin interactions to the regulation of the K_{Ca}3.1 gating process. *J Gen Physiol* (2013) 142(1):37–60. doi: 10.1085/jgp.201210933
- Jones HM, Hamilton KL, Papworth GD, Syme CA, Watkins SC, Bradbury NA, et al. Role of the NH2 terminus in the assembly and trafficking of the intermediate conductance Ca²⁺-activated K⁺ channel hK1. *J Biol Chem* (2004) 279(15):15531–40. doi: 10.1074/jbc.M400069200
- Syme CA, Hamilton KL, Jones HM, Gerlach AC, Giltinan L, Papworth GD, et al. Trafficking of the Ca²⁺-activated K⁺ channel, hK1, is dependent upon a c-terminal leucine zipper. *J Biol Chem* (2003) 278(10):8476–86. doi: 10.1074/jbc.M210072200
- Ohya S, Kito H, Hatano N, Muraki K. Recent advances in therapeutic strategies that focus on the regulation of ion channel expression. *Pharmacol Ther* (2016) 160:11–43. doi: 10.1016/j.pharmthera.2016.02.001
- Ghanshani S, Wulff H, Miller MJ, Rohm H, Neben A, Gutman GA, et al. Up-regulation of the IK_{Ca}1 potassium channel during T-cell activation. *J Biol Chem* (2000) 275(47):37137–49. doi: 10.1074/jbc.M003941200
- Takai J, Santu A, Zheng H, Koh SD, Ohta M, Filimban LM, et al. Laminar shear stress upregulates endothelial Ca(2+)-activated k(+) channels KCa2.3 and K_{Ca}3.1 via a Ca(2+)-calmodulin-dependent protein kinase kinase/Akt/p300 cascade. *Am J Physiol Heart Circ Physiol* (2013) 305(4):H484–93. doi: 10.1152/ajpheart.00642.2012
- Wang LP, Wang Y, Zhao LM, Li GR, Deng XL. Angiotensin II upregulates K(Ca)3.1 channels and stimulates cell proliferation in rat cardiac fibroblasts. *Biochem Pharmacol* (2013) 85(10):1486–94. doi: 10.1016/j.bcp.2013.02.032
- Lai W, Chen S, Wu H, Guan Y, Liu L, Zeng Y, et al. PRL-3 promotes the proliferation of LoVo cells via the upregulation of KCNN4 channels. *Oncol Rep* (2011) 26(4):909–17. doi: 10.3892/or.2011.1366
- Cheong A, Bingham AJ, Li J, Kumar B, Sukumar P, Munsch C, et al. Downregulated REST transcription factor is a switch enabling critical potassium channel expression and cell proliferation. *Mol Cell* (2005) 20(1):45–52. doi: 10.1016/j.molcel.2005.08.030
- Ohya S, Kanatsuka S, Hatano N, Kito H, Matsui A, Fujimoto M, et al. Downregulation of the Ca(2+)-activated k(+) channel KCa 3.1 by histone deacetylase inhibition in human breast cancer cells. *Pharmacol Res Perspect* (2016) 4(2):e00228. doi: 10.1002/prp2.228
- Rodriguez-Cortez V, Del Pino-Molina L, Rodriguez-Ubrea J, Ciudad L, Gomez-Cabrero D, Company C, et al. Monozygotic twins discordant for common variable immunodeficiency reveal impaired DNA demethylation during naive-to-memory b-cell transition. *Nat Commun* (2015) 6:7335. doi: 10.1038/ncomms8335
- Bulk E, Ay AS, Hammadi M, Ouadid-Ahidouch H, Schelhaas S, Hascher A, et al. Epigenetic dysregulation of K_{Ca} 3.1 channels induces poor prognosis in lung cancer. *Int J Cancer* (2015) 137(6):1306–17. doi: 10.1002/ijc.29490
- Ohya S, Niwa S, Yanagi A, Fukuyo Y, Yamamura H, Imaizumi Y. Involvement of dominant-negative spliced variants of the intermediate conductance Ca²⁺-activated K⁺ channel, K(Ca)3.1, in immune function of lymphoid cells. *J Biol Chem* (2011) 286(19):16940–52. doi: 10.1074/jbc.M110.184192
- Du B, Su F, Wang H, Liang H, Song X, Shao Z, et al. Identification of potential core genes at single-cell level contributing to pathogenesis of pancreatic ductal adenocarcinoma through bioinformatics analysis. *Cancer Biomarkers* (2022) 34(1):1–12. doi: 10.3233/CBM-210271
- Wulff H, Kolski-Andreaco A, Sankaranarayanan A, Sabatier J-M, Shakkottai V. Modulators of small- and intermediate-conductance calcium-

Publisher's note

All claims expressed in this article are solely those of the authors and do not necessarily represent those of their affiliated organizations, or those of the publisher, the editors and the reviewers. Any product that may be evaluated in this article, or claim that may be made by its manufacturer, is not guaranteed or endorsed by the publisher.

activated potassium channels and their therapeutic indications. *Curr Med Chem* (2007) 14(13):1437–57. doi: 10.2174/092986707780831186

33. De Marchi U, Sassi N, Fioretti B, Catacuzzeno L, Cereghetti GM, Szabo I, et al. Intermediate conductance Ca^{2+} -activated potassium channel (KCa3.1) in the inner mitochondrial membrane of human colon cancer cells. *Cell Calcium* (2009) 45(5):509–16. doi: 10.1016/j.ceca.2009.03.014

34. Basalingappa KM, Rajendran VM, Wonderlin WF. Characteristics of Kcnn4 channels in the apical membranes of an intestinal epithelial cell line. *Am J Physiol Gastrointest Liver Physiol* (2011) 301(5):G905–11. doi: 10.1152/ajpgi.00558.2010

35. Greger R, Bleich M, Riedemann N, van Driessche W, Ecker D, Warth R. The role of k^{+} channels in colonic Cl^{-} secretion. *Comp Biochem Physiol Part A Physiol* (1997) 118(2):271–5. doi: 10.1016/S0300-9629(96)00304-0

36. Khanna R, Chang MC, Joiner WJ, Kaczmarek LK, Schlichter LC. hSK4/hIK1, a calmodulin-binding KCa channel in human T lymphocytes. roles in proliferation and volume regulation. *J Biol Chem* (1999) 274(21):14838–49. doi: 10.1074/jbc.274.21.14838

37. Vázquez E, Nobles M, Valverde MA. Defective regulatory volume decrease in human cystic fibrosis tracheal cells because of altered regulation of intermediate conductance Ca^{2+} -dependent potassium channels. *Proc Natl Acad Sci U States A* (2001) 98(9):5329–34. doi: 10.1073/pnas.091096498

38. Panyi G, Possani LD, Rodríguez de la Vega RC, Gáspár R, Varga Z. K^{+} channel blockers: novel tools to inhibit T cell activation leading to specific immunosuppression. *Curr Pharm Des* (2006) 12(18):2199–220. doi: 10.2174/13816120677585120

39. Feske S, Wulff H, Skolnik EY. Ion channels in innate and adaptive immunity. *Annu Rev Immunol* (2015) 33:291–353. doi: 10.1146/annurev-immunol-032414-112212

40. Blomster LV, Strobaek D, Hougaard C, Klein J, Pinborg LH, Mikkelsen JD, et al. Quantification of the functional expression of the Ca^{2+} -activated k^{+} channel KCa 3.1 on microglia from adult human neocortical tissue. *Glia* (2016) 64(12):2065–78. doi: 10.1002/glia.23040

41. Toldi G, Munoz L, Herrmann M, Schett G, Balog A. The effects of Kv1.3 and IKCa1 channel inhibition on cytokine production and calcium influx of T lymphocytes in rheumatoid arthritis and ankylosing spondylitis. *Immunol Res* (2016) 64(2):627–31. doi: 10.1007/s12026-015-8683-8

42. Weyand CM, Goronzy JJ. The immunology of rheumatoid arthritis. *Nat Immunol* (2021) 22(1):10–8. doi: 10.1038/s41590-020-00816-x

43. Devor DC, Singh AK, Frizzell RA, Bridges RJ. Modulation of Cl^{-} secretion by benzimidazolones. I. direct activation of a Ca^{2+} -dependent k^{+} channel. *Am J Physiol* (1996) 271(5 Pt 1):L775–L84. doi: 10.1152/ajplung.1996.271.5.L775

44. Manfroni G, Ragonese F, Monarca L, Astolfi A, Mancinelli L, Iannitti RG, et al. New insights on KCa3.1 channel modulation. *Curr Pharm Des* (2020) 26(18):2096–101. doi: 10.2174/1381612826666200316152645

45. Brown BM, Shim H, Zhang M, Yarov-Yarovoy V, Wulff H. Structural determinants for the selectivity of the positive KCa3.1 gating modulator 5-Methylanthro[2,1-d]oxazol-2-amine (SKA-121). *Mol Pharmacol* (2017) 92(4):469–80. doi: 10.1124/mol.117.109421

46. Strobaek D, Teuber L, Jorgensen TD, Ahring PK, Kjaer K, Hansen RS, et al. Activation of human IK and SK Ca^{2+} -activated k^{+} channels by NS309 (6,7-dichloro-1H-indole-2,3-dione 3-oxime). *Biochim Biophys Acta* (2004) 1665(1–2):1–5. doi: 10.1016/j.bbame.2004.07.006

47. Ehrlich BE, Kaftan E, Bezprozvannaya S, Bezprozvanny I. The pharmacology of intracellular Ca^{2+} -release channels. *Trends Pharmacol Sci* (1994) 15(5):145–9. doi: 10.1016/0165-6147(94)90074-4

48. Wong R, Schlichter LC. PKA reduces the rat and human KCa3.1 current, CaM binding, and Ca^{2+} signaling, which requires Ser332/334 in the CaM -binding c terminus. *J Neurosci* (2014) 34(40):13371–83. doi: 10.1523/JNEUROSCI.1008-14.2014

49. Liao CR, Wang SN, Zhu SY, Wang YQ, Li ZZ, Liu ZY, et al. Advanced oxidation protein products increase $\text{TNF-}\alpha$ and $\text{IL-1}\beta$ expression in chondrocytes via NADPH oxidase 4 and accelerate cartilage degeneration in osteoarthritis progression. *Redox Biol* (2020) 28:101306. doi: 10.1016/j.redox.2019.101306

50. Schroder RL, Jensen BS, Strobaek D, Olesen SP, Christophersen P. Activation of the human, intermediate-conductance, Ca^{2+} -activated k^{+} channel by methylxanthines. *Pflugers Arch* (2000) 440(6):809–18. doi: 10.1007/s004240000364

51. Syme CA, Gerlach AC, Singh AK, Devor DC. Pharmacological activation of cloned intermediate- and small-conductance Ca^{2+} -activated k^{+} channels. *Am J Physiol Cell Physiol* (2000) 278(3):C570–C81. doi: 10.1152/ajpcell.2000.278.3.C570

52. Gerlach AC, Syme CA, Giltinan L, Adelman JP, Devor DC. ATP-dependent activation of the intermediate conductance, Ca^{2+} -activated k^{+} channel, hIK1, is conferred by a c-terminal domain. *J Biol Chem* (2001) 276(14):10963–70. doi: 10.1074/jbc.M007716200

53. Tiwari MN, Mohan S, Biala Y, Yaari Y. Protein kinase a-mediated suppression of the slow afterhyperpolarizing KCa3.1 current in temporal lobe epilepsy. *J Neurosci* (2019) 39(50):9914–26. doi: 10.1523/JNEUROSCI.1603-19.2019

54. Newton HS, Gawali VS, Chimote AA, Lehn MA, Palackdharry SM, Hinrichs BH, et al. PD1 blockade enhances k^{+} channel activity, Ca^{2+} signaling, and migratory ability in cytotoxic T lymphocytes of patients with head and neck cancer. *J Immunother Cancer* (2020) 8(2):e000844. doi: 10.1136/jitc-2020-000844

55. Gawali VS, Chimote AA, Newton HS, Faria-Garzon MG, Chirra M, Janssen EM, et al. Immune checkpoint inhibitors regulate k^{+} channel activity in cytotoxic T lymphocytes of head and neck cancer patients. *Front Pharmacol* (2021) 12:742862. doi: 10.3389/fphar.2021.742862

56. Brown BM, Shim H, Christophersen P, Wulff H. Pharmacology of small- and intermediate-conductance calcium-activated potassium channels. *Annu Rev Pharmacol Toxicol* (2020) 60:219–40. doi: 10.1146/annurev-pharmtox-010919-023420

57. Rauer H, Lanigan MD, Pennington MW, Aiyar J, Ghanshani S, Cahalan MD, et al. Structure-guided transformation of charybdotoxin yields an analog that selectively targets Ca^{2+} -activated over voltage-gated k^{+} channels. *J Biol Chem* (2000) 275(2):1201–8. doi: 10.1074/jbc.275.2.1201

58. Castle NA, London DO, Creech C, Fajloun Z, Stocker JW, Sabatier JM. Maurotoxin: a potent inhibitor of intermediate conductance Ca^{2+} -activated potassium channels. *Mol Pharmacol* (2003) 63(2):409–18. doi: 10.1124/mol.63.2.409

59. Luna-Ramirez K, Csoti A, McArthur JR, Chin YKY, Anangi R, Najera RDC, et al. Structural basis of the potency and selectivity of urotoxin, a potent Kv1 blocker from scorpion venom. *Biochem Pharmacol* (2020) 174:113782. doi: 10.1016/j.bcp.2019.113782

60. Vigneault P, Parent S, Kanda P, Michie C, Davis DR, Nattel S. Electrophysiological engineering of heart-derived cells with calcium-dependent potassium channels improves cell therapy efficacy for cardioprotection. *Nat Commun* (2021) 12(1):4963. doi: 10.1038/s41467-021-25180-8

61. Cocozza G, di Castro MA, Carbonari L, Grimaldi A, Antonangeli F, Garofalo S, et al. Ca^{2+} -activated k^{+} channels modulate microglia affecting motor neuron survival in hSOD1(G93A) mice. *Brain Behav Immun* (2018) 73:584–95. doi: 10.1016/j.bbi.2018.07.002

62. Brown BM, Pressley B, Wulff H. KCa3.1 channel modulators as potential therapeutic compounds for glioblastoma. *Curr Neuropharmacol* (2018) 16(5):618–26. doi: 10.2174/1570159X15666170630164226

63. Petersen AG, Lind PC, Mogensen S, Jensen AB, Granfeldt A, Simonsen U. Treatment with senicapoc, a K^{+} channel blocker, alleviates hypoxaemia in a mouse model of acute respiratory distress syndrome. *Br J Pharmacol* (2022) 179(10):2175–92. doi: 10.1111/bph.15704

64. Brommel K, Maskri S, Maisuls I, Konken CP, Rieke M, Petho Z, et al. Synthesis of small-molecule fluorescent probes for the *In vitro* imaging of calcium-activated potassium channel KCa 3.1. *Angew Chem Int Ed Engl* (2020) 59(21):8277–84. doi: 10.1002/anie.202001201

65. Ellory JC, Culliford SJ, Smith PA, Wolowyk MW, Knaus EE. Specific inhibition of Ca^{2+} -activated K^{+} channels in red cells by selected dihydropyridine derivatives. *Br J Pharmacol* (1994) 111(3):903–5. doi: 10.1111/j.1476-5381.1994.tb14823.x

66. Ohya S. [Physiological role of k^{+} channels in the regulation of T cell function]. *Yakugaku Zasshi* (2016) 136(3):479–83. doi: 10.1248/yakushi.15-00246-4

67. Phan HTL, Kim HJ, Jo S, Kim WK, Namkung W, Nam JH. Anti-inflammatory effect of licochalcone A via regulation of ORAI1 and K^{+} channels in T-lymphocytes. *Int J Mol Sci* (2021) 22(19):10847. doi: 10.3390/ijms221910847

68. Toldi G, Bajnok A, Dobi D, Kaposi A, Kovacs L, Vasarhelyi B, et al. The effects of Kv1.3 and IKCa1 potassium channel inhibition on calcium influx of human peripheral T lymphocytes in rheumatoid arthritis. *Immunobiology* (2013) 218(3):311–6. doi: 10.1016/j.imbio.2012.05.013

69. Kang H, Kerloc'h A, Rotival M, Xu X, Zhang Q, D'Souza Z, et al. Kcnn4 is a regulator of macrophage multinucleation in bone homeostasis and inflammatory disease. *Cell Rep* (2014) 8(4):1210–24. doi: 10.1016/j.celrep.2014.07.032

70. Raychaudhuri SK, Wulff H, Raychaudhuri SP. KCa3.1(–/–) mice do not develop CIA: Regulatory role for KCa3.1 in autoimmune arthritis. *J Cell Physiol* (2016) 231(11):2313–4. doi: 10.1002/jcp.25356

71. Fernández-Orth J, Rolles L, Gola L, Bittner S, Andronic J, Sukhorukov VL, et al. A role for TASK2 channels in the human immunological synapse. *Eur J Immunol* (2021) 51(2):342–53. doi: 10.1002/eji.201948269

72. Dong C. Cytokine regulation and function in T cells. *Annu Rev Immunol* (2021) 39:51–76. doi: 10.1146/annurev-immunol-061020-053702

73. Zhu X, Zhu J. CD4 T helper cell subsets and related human immunological disorders. *Int J Mol Sci* (2020) 21(21):8011. doi: 10.3390/ijms21218011

74. Srivastava S, Di L, Zhdanova O, Li Z, Vardhana S, Wan Q, et al. The class II phosphatidylinositol 3 kinase C2beta is required for the activation of the k+ channel KCa3.1 and CD4 T-cells. *Mol Biol Cell* (2009) 20(17):3783–91. doi: 10.1091/mbc.09-05-0390
75. Srivastava S, Li Z, Ko K, Choudhury P, Albaum M, Johnson AK, et al. Histidine phosphorylation of the potassium channel KCa3.1 by nucleoside diphosphate kinase b is required for activation of KCa3.1 and CD4 T cells. *Mol Cell* (2006) 24(5):665–75. doi: 10.1016/j.molcel.2006.11.012
76. Srivastava S, Li Z, Lin L, Liu G, Ko K, Coetzee WA, et al. The phosphatidylinositol 3-phosphate phosphatase myotubularin-related protein 6 (MTMR6) is a negative regulator of the Ca2+-activated k+ channel KCa3.1. *Mol Cell Biol* (2005) 25(9):3630–8. doi: 10.1128/MCB.25.9.3630-3638.2005
77. Panda S, Srivastava S, Li Z, Vaeth M, Fuhs SR, Hunter T, et al. Identification of PGAM5 as a mammalian protein histidine phosphatase that plays a central role to negatively regulate CD4(+) T cells. *Mol Cell* (2016) 63(3):457–69. doi: 10.1016/j.molcel.2016.06.021
78. Srivastava S, Zhdanova O, Di L, Li Z, Albaum M, Wulff H, et al. Protein histidine phosphatase 1 negatively regulates CD4 T cells by inhibiting the k+ channel KCa3.1. *Proc Natl Acad Sci U States America* (2008) 105(38):14442–6. doi: 10.1073/pnas.0803678105
79. Srivastava S, Panda S, Li Z, Fuhs SR, Hunter T, Thiele DJ, et al. Histidine phosphorylation relieves copper inhibition in the mammalian potassium channel KCa3.1. *Elife* (2016) 5:e16093. doi: 10.7554/eLife.16093
80. Di L, Srivastava S, Zhdanova O, Ding Y, Li Z, Wulff H, et al. Inhibition of the k+ channel KCa3.1 ameliorates T cell-mediated colitis. *Proc Natl Acad Sci U States America* (2010) 107(4):1541–6. doi: 10.1073/pnas.0910133107
81. Ohya S, Matsui M, Kajikuri J, Endo K, Kito H. Increased interleukin-10 expression by the inhibition of Ca(2+)-activated k(+) channel KCa3.1 in CD4(+) CD25(+) regulatory T cells in the recovery phase in an inflammatory bowel disease mouse model. *J Pharmacol Exp Ther* (2021) 377(1):75–85. doi: 10.1124/jpet.120.000395
82. Matsui M, Kajikuri J, Endo K, Kito H, Ohya S. KCa3.1 inhibition-induced activation of the JNK/c-jun signaling pathway enhances IL-10 expression in peripherally-induced regulatory T cells. *J Pharmacol Sci* (2022) 148(1):1–5. doi: 10.1016/j.jphs.2021.09.007
83. Chimote AA, Gawali VS, Newton HS, Wise-Draper TM, Conforti L. A compartmentalized reduction in membrane-proximal calmodulin reduces the immune surveillance capabilities of CD8(+) T cells in head and neck cancer. *Front Pharmacol* (2020) 11:143. doi: 10.3389/fphar.2020.00143
84. Chimote AA, Balajthy A, Arnold MJ, Newton HS, Hajdu P, Qualtieri J, et al. A defect in KCa3.1 channel activity limits the ability of CD8(+) T cells from cancer patients to infiltrate an adenosine-rich microenvironment. *Sci Signaling* (2018) 11(527):eaq1616. doi: 10.1126/scisignal.aag1616
85. Sim JH, Kim KS, Park H, Kim KJ, Lin H, Kim TJ, et al. Differentially expressed potassium channels are associated with function of human effector memory CD8(+) T cells. *Front Immunol* (2017) 8:859. doi: 10.3389/fimmu.2017.00859
86. Sun W, Meednu N, Rosenberg A, Rangel-Moreno J, Wang V, Glanzman J, et al. B cells inhibit bone formation in rheumatoid arthritis by suppressing osteoblast differentiation. *Nat Commun* (2018) 9(1):5127. doi: 10.1038/s41467-018-07626-8
87. Wulff H, Knaus HG, Pennington M, Chandy KG. K+ channel expression during b cell differentiation: implications for immunomodulation and autoimmunity. *J Immunol* (2004) 173(2):776–86. doi: 10.4049/jimmunol.173.2.776
88. Simma N, Bose T, Kahlfuss S, Mankiewicz J, Lowin T, Lühder F, et al. NMDA-receptor antagonists block b-cell function but foster IL-10 production in BCR/CD40-activated b cells. *Cell Communication Signaling CCS* (2014) 12:75. doi: 10.1186/s12964-014-0075-5
89. Ghosh D, Jiang W, Mukhopadhyay D, Mellins ED. New insights into b cells as antigen presenting cells. *Curr Opin Immunol* (2021) 70:129–37. doi: 10.1016/j.coi.2021.06.003
90. Kim U, Siegel R, Ren X, Gunther CS, Gaasterland T, Roeder RG. Identification of transcription coactivator OCA-b-dependent genes involved in antigen-dependent b cell differentiation by cDNA array analyses. *Proc Natl Acad Sci U States A* (2003) 100(15):8868–73. doi: 10.1073/pnas.1033108100
91. Zhang S, Wang X, Ju C, Zhu L, Du Y, Gao C. Blockage of K(Ca)3.1 and Kv1.3 channels of the b lymphocyte decreases the inflammatory monocyte chemotaxis. *Int Immunopharmacol* (2016) 31:266–71. doi: 10.1016/j.intimp.2015.12.032
92. Edwards JC, Cambridge G. B-cell targeting in rheumatoid arthritis and other autoimmune diseases. *Nat Rev Immunol* (2006) 6(5):394–403. doi: 10.1038/nri1838
93. Castegna A, Gissi R, Menga A, Montopoli M, Favia M, Viola A, et al. Pharmacological targets of metabolism in disease: Opportunities from macrophages. *Pharmacol Ther* (2020) 210:107521. doi: 10.1016/j.pharmthera.2020.107521
94. Wang Y, Han CC, Cui D, Li Y, Ma Y, Wei W. Is macrophage polarization important in rheumatoid arthritis? *Int Immunopharmacol* (2017) 50:345–52. doi: 10.1016/j.intimp.2017.07.019
95. Toyama K, Wulff H, Chandy KG, Azam P, Raman G, Saito T, et al. The intermediate-conductance calcium-activated potassium channel KCa3.1 contributes to atherogenesis in mice and humans. *J Clin Invest* (2008) 118(9):3025–37. doi: 10.1172/JCI30836
96. Hanley PJ, Musset B, Renigunta V, Limberg SH, Dalpke AH, Sus R, et al. Extracellular ATP induces oscillations of intracellular Ca2+ and membrane potential and promotes transcription of IL-6 in macrophages. *Proc Natl Acad Sci U States A* (2004) 101(25):9479–84. doi: 10.1073/pnas.0400733101
97. Zhu Y-R, Jiang X-X, Zhang D-M. Critical regulation of atherosclerosis by the KCa3.1 channel and the retargeting of this therapeutic target in in-stent neointimal sclerosis. *J Mol Med (Berl)* (2019) 97(9):1219–29. doi: 10.1007/s00109-019-01814-9
98. Xu R, Li C, Wu Y, Shen L, Ma J, Qian J, et al. Role of KCa3.1 channels in macrophage polarization and its relevance in atherosclerotic plaque instability. *Arterioscler Thromb Vasc Biol* (2017) 37(2):226–36. doi: 10.1161/ATVBAHA.116.308461
99. Yagi M, Miyamoto T, Sawatani Y, Iwamoto K, Hosogane N, Fujita N, et al. DC-STAMP is essential for cell-cell fusion in osteoclasts and foreign body giant cells. *J Exp Med* (2005) 202(3):345–51. doi: 10.1084/jem.20050645
100. Zhu XW, Price NM, Gilman RH, Recarvarren S, Friedland JS. Multinucleate giant cells release functionally unopposed matrix metalloproteinase-9 in vitro and in vivo. *J Infect Dis* (2007) 196(7):1076–9. doi: 10.1086/521030
101. Xu H, Lai W, Zhang Y, Liu L, Luo X, Zeng Y, et al. Tumor-associated macrophage-derived IL-6 and IL-8 enhance invasive activity of LoVo cells induced by PRL-3 in a KCNN4 channel-dependent manner. *BMC Cancer* (2014) 14:330. doi: 10.1186/1471-2407-14-330
102. Zheng F, Tao Y, Liu J, Geng Z, Wang Y, Wang Y, et al. KCa3.1 inhibition of macrophages suppresses inflammatory response leading to endothelial damage in a cell model of Kawasaki disease. *J Inflammation Res* (2021) 14:719–35. doi: 10.2147/JIR.S297131
103. Dahlin JS, Maurer M, Metcalfe DD, Pejler G, Sagi-Eisenberg R, Nilsson G. The ingenious mast cell: Contemporary insights into mast cell behavior and function. *Allergy* (2022) 77(1):83–99. doi: 10.1111/all.14881
104. Woolley DE. The mast cell in inflammatory arthritis. *New Engl J Med* (2003) 348(17):1709–11. doi: 10.1056/NEJMcibr023206
105. Mark Duffy S, Berger P, Cruse G, Yang W, Bolton SJ, Bradding P. The k+ channel iKCA1 potentiates Ca2+ influx and degranulation in human lung mast cells. *J Allergy Clin Immunol* (2004) 114(1):66–72. doi: 10.1016/j.jaci.2004.04.005
106. Duffy SM, Ashmole I, Smallwood DT, Leyland ML, Bradding P, Orai/CRACM1 and KCa3.1 ion channels interact in the human lung mast cell plasma membrane. *Cell Communication Signaling CCS* (2015) 13:32. doi: 10.1186/s12964-015-0112-z
107. Duffy SM, Cruse G, Cockerill SL, Brightling CE, Bradding P. Engagement of the EP2 prostanoid receptor closes the k+ channel KCa3.1 in human lung mast cells and attenuates their migration. *Eur J Immunol* (2008) 38(9):2548–56. doi: 10.1002/eji.200738106
108. Lin H, Zheng C, Li J, Yang C, Hu L. Lentiviral shRNA against KCa3.1 inhibits allergic response in allergic rhinitis and suppresses mast cell activity via PI3K/AKT signaling pathway. *Sci Rep* (2015) 5:13127. doi: 10.1038/srep13127
109. Srivastava S, Cai X, Li Z, Sun Y, Skolnik EY. Phosphatidylinositol-3-kinase C2beta and TRIM27 function to positively and negatively regulate IgE receptor activation of mast cells. *Mol Cell Biol* (2012) 32(15):3132–9. doi: 10.1128/MCB.00019-12
110. Cruse G, Duffy SM, Brightling CE, Bradding P. Functional KCa3.1 k+ channels are required for human lung mast cell migration. *Thorax* (2006) 61(10):880–5. doi: 10.1136/thx.2006.060319
111. Khan S, Greenberg JD, Bhardwaj N. Dendritic cells as targets for therapy in rheumatoid arthritis. *Nat Rev Rheumatol* (2009) 5(10):566–71. doi: 10.1038/nrrheum.2009.185
112. Shao Z, Makinde TO, Agrawal DK. Calcium-activated potassium channel KCa3.1 in lung dendritic cell migration. *Am J Respir Cell Mol Biol* (2011) 45(5):962–8. doi: 10.1165/rcmb.2010-0514OC
113. Shao Z, Gaurav R, Agrawal DK. Intermediate-conductance calcium-activated potassium channel KCa3.1 and chloride channel modulate chemokine ligand (CCL19/CCL21)-induced migration of dendritic cells. *Transl Res* (2015) 166(1):89–102. doi: 10.1016/j.trsl.2014.11.010
114. Crottes D, Felix R, Meley D, Chadet S, Herr F, Audiger C, et al. Immature human dendritic cells enhance their migration through KCa3.1 channel activation. *Cell Calcium* (2016) 59(4):198–207. doi: 10.1016/j.cecc.2016.02.008
115. Vandier C, Velge-Roussel F. Regulation of human dendritic cell immune functions by ion channels. *Curr Opin Immunol* (2018) 52:27–31. doi: 10.1016/j.coi.2018.03.011

116. Grobner S, Lukowski R, Autenrieth IB, Ruth P. Lipopolysaccharide induces cell volume increase and migration of dendritic cells. *Microbiol Immunol* (2014) 58 (1):61–7. doi: 10.1111/1348-0421.12116
117. Cecchi I, Arias de la Rosa I, Menegatti E, Roccatello D, Collantes-Estevez E, Lopez-Pedraza C, et al. Neutrophils: Novel key players in rheumatoid arthritis. current and future therapeutic targets. *Autoimmun Rev* (2018) 17(11):1138–49. doi: 10.1016/j.autrev.2018.06.006
118. Henriquez C, Riquelme TT, Vera D, Julio-Kalajzic F, Ehrenfeld P, Melvin JE, et al. The calcium-activated potassium channel KCa3.1 plays a central role in the chemotactic response of mammalian neutrophils. *Acta Physiol (Oxf)* (2016) 216 (1):132–45. doi: 10.1111/apha.12548
119. Grimes D, Johnson R, Pashos M, Cummings C, Kang C, Sampedro GR, et al. ORAI1 and ORAI2 modulate murine neutrophil calcium signaling, cellular activation, and host defense. *Proc Natl Acad Sci U States A* (2020) 117(39):24403–14. doi: 10.1073/pnas.2008032117
120. Karsten E, Herbert BR. The emerging role of red blood cells in cytokine signalling and modulating immune cells. *Blood Rev* (2020) 41:100644. doi: 10.1016/j.blre.2019.100644
121. Srivastava S, Cai X, Li Z, Sun Y, Skolnik EY. Phosphatidylinositol-3-kinase C2 β and TRIM27 function to positively and negatively regulate IgE receptor activation of mast cells. *Mol Cell Biol* (2012) 32(15):3132–9. doi: 10.1128/MCB.00019-12
122. Huang C, Shen S, Ma Q, Chen J, Gill A, Pollock CA, et al. Blockade of KCa3.1 ameliorates renal fibrosis through the TGF- β 1/Smad pathway in diabetic mice. *Diabetes* (2013) 62(8):2923–34. doi: 10.2337/db13-0135
123. Grossinger EM, Kang M, Bouchareychas L, Sarin R, Haudenschild DR, Borodinsky LN, et al. Ca(2+)-dependent regulation of NFATc1 via KCa3.1 in inflammatory osteoclastogenesis. *J Immunol* (2018) 200(2):749–57. doi: 10.4049/jimmunol.1701170
124. John CM, Khaddaj Mallat R, Mishra RC, George G, Singh V, Turnbull JD, et al. SKA-31, an activator of Ca(2+)-activated k(+) channels, improves cardiovascular function in aging. *Pharmacol Res* (2020) 151:104539. doi: 10.1016/j.phrs.2019.104539
125. He S, Wang Y, Yao Y, Cao Z, Yin J, Zi L, et al. Inhibition of KCa3.1 channels suppresses atrial fibrillation via the attenuation of macrophage pro-inflammatory polarization in a canine model with prolonged rapid atrial pacing. *Front Cardiovasc Med* (2021) 8:656631. doi: 10.3389/fcvm.2021.656631
126. Matsui M, Terasawa K, Kajikuri J, Kito H, Endo K, Jaikhan P, et al. Histone deacetylases enhance Ca(2+)-activated k(+) channel KCa3.1 expression in murine inflammatory CD4(+) T cells. *Int J Mol Sci* (2018) 19(10):2942. doi: 10.3390/ijms19102942
127. Choi S, Kim JA, Li H, Jo SE, Lee H, Kim TH, et al. Anti-inflammatory and anti-fibrotic effects of modafinil in nonalcoholic liver disease. *BioMed Pharmacother* (2021) 144:112372. doi: 10.1016/j.biopha.2021.112372
128. Ferreira R, Lively S, Schlichter LC. IL-4 type 1 receptor signaling up-regulates KCNN4 expression, and increases the KCa3.1 current and its contribution to migration of alternative-activated microglia. *Front Cell Neurosci* (2014) 8:183. doi: 10.3389/fncel.2014.00183
129. Korb A, Tohidast-Akrad M, Cetin E, Axmann R, Smolen J, Schett G. Differential tissue expression and activation of p38 MAPK α , β , γ , and δ isoforms in rheumatoid arthritis. *Arthritis Rheumatol* (2006) 54(9):2745–56. doi: 10.1002/art.22080
130. Lefevre S, Schwarz M, Meier FMP, Zimmermann-Geller B, Tarner IH, Rickert M, et al. Disease-specific effects of matrix and growth factors on adhesion and migration of rheumatoid synovial fibroblasts. *J Immunol* (2017) 198(12):4588–95. doi: 10.4049/jimmunol.1600989
131. Chandy KG, Wulff H, Beeton C, Pennington M, Gutman GA, Cahalan MD. K+ channels as targets for specific immunomodulation. *Trends Pharmacol Sci* (2004) 25(5):280–9. doi: 10.1016/j.tips.2004.03.010
132. Kunisch E, Gandesiri M, Fuhrmann R, Roth A, Winter R, Kinne RW. Predominant activation of MAP kinases and pro-destructive/pro-inflammatory features by TNF α in early-passage synovial fibroblasts via TNF receptor-1: failure of p38 inhibition to suppress matrix metalloproteinase-1 in rheumatoid arthritis. *Ann Rheumatic Diseases* (2007) 66(8):1043–51. doi: 10.1136/ard.2006.062521
133. Xia ZB, Meng FR, Fang YX, Wu X, Zhang CW, Liu Y, et al. Inhibition of NF- κ B signaling pathway induces apoptosis and suppresses proliferation and angiogenesis of human fibroblast-like synovial cells in rheumatoid arthritis. *Medicine* (2018) 97(23):e10920. doi: 10.1097/MD.00000000000010920
134. Li G, Xia Z, Liu Y, Meng F, Wu X, Fang Y, et al. SIRT1 inhibits rheumatoid arthritis fibroblast-like synoviocyte aggressiveness and inflammatory response via suppressing NF- κ B pathway. *Biosci Rep* (2018) 38(3):BSR20180541. doi: 10.1042/BSR20180541
135. Chen Z, Bozec A, Ramming A, Schett G. Anti-inflammatory and immune-regulatory cytokines in rheumatoid arthritis. *Nat Rev Rheumatol* (2019) 15(1):9–17. doi: 10.1038/s41584-018-0109-2
136. Schett G, Gravallesse E. Bone erosion in rheumatoid arthritis: mechanisms, diagnosis and treatment. *Nat Rev Rheumatol* (2012) 8(11):656–64. doi: 10.1038/nrrheum.2012.153
137. Yu ZH, Xu JR, Wang YX, Xu GN, Xu ZP, Yang K, et al. Targeted inhibition of KCa3.1 channel attenuates airway inflammation and remodeling in allergic asthma. *Am J Respir Cell Mol Biol* (2013) 48(6):685–93. doi: 10.1165/rcmb.2012-0236OC
138. Hua X, Deuse T, Chen YJ, Wulff H, Stubbendorff M, Köhler R, et al. The potassium channel KCa3.1 as new therapeutic target for the prevention of obliterative airway disease. *Transplantation* (2013) 95(2):285–92. doi: 10.1097/TP.0b013e318275a2f4
139. King B, Rizwan AP, Asmara H, Heath NC, Engbers JD, Dykstra S, et al. IKCa channels are a critical determinant of the slow AHP in CA1 pyramidal neurons. *Cell Rep* (2015) 11(2):175–82. doi: 10.1016/j.celrep.2015.03.026

Glossary

1-EBIO	1-Ethyl-2-benzimidazolidinone
AP-1	activation protein-1
BCR	B cell receptor
BMMC	bone marrow-derived mast cells
CAIA	collagen antibody-induced arthritis
CaM	calmodulin
CAMBD	CAM-binding domain
CaMKIV	calmodulin kinase IV
cAMP	adenosine 3', 5 cyclic monophosphate
CHO cells	Chinese hamster ovary cells
CIA	collagen-induced arthritis
CRE	cAMP response element
CVID	common variable immunodeficiency
CZ	chlorzoxazone
DCs	dendritic cells
DC-EBIO	5, 6-dichloro-1-EBIO
DMARDs	disease-modifying anti-rheumatic drugs
EC ₅₀	effective concentration producing 50% of maximum response
FLS	fibroblast-like synoviocytes
GC	glucocorticoids
H-89	N-[2-(4-bromocinnamylamino) ethyl]-5-isoquinoline
HDAC	histone deacetylase
HEK-293 cells	human embryonic kidney cells
HNSCC	head and neck squamous cell carcinoma
IBMX	3-isobutyl-1-methylxanthine
IC ₅₀	inhibitory concentration (e.g. 50% inhibition of maximum)
IFN- γ	interferon- γ
IGFBP5	insulin-like growth factor-binding protein 5
IL	interleukin
JNK	c-Jun N-terminal kinase
KCa3.1	intermediate conductance Ca ²⁺ -activated K ⁺ channel
LPS	lipopolysaccharide
LZ	leucine zipper
MAPK	mitogen-activated protein kinase
MCP-1	monocyte chemoattractant protein-1
MCs	mast cells
MGCs	multinucleated macrophages
MTMR6	myotubularin-related protein 6
MTX	Maurotoxin
NDPK-B	nucleoside diphosphate kinase B
NFATc1	nuclear translocation of nuclear factor cytoplasmic 1
NF- κ B	nuclear factor- κ B
NMDAR	anti-N-methyl-D-aspartate-receptor
NS309	6, 7-dichloro-1H-indole-2, 3-dione-3-oxime
NS6180	4-[[3-(trifluoromethyl) phenyl] methyl]-2H-1, 4-benzothiazin-3 (4H)-one
NSAIDs	non-steroidal anti-inflammatory drugs

(Continued)

Continued

PGAM5	phosphoglycerate mutase family 5
PGE2	prostaglandin E2
PHPT-1	protein histidine phosphatase
PI3K	phosphatidylinositol 3-kinase
PI3K-C2 β	the class II phosphatidylinositol 3 kinase C2 β
PI(3)P	phosphatidylinositol 3 phosphate
PKA	cAMP-dependent protein kinase
RA	rheumatoid arthritis
RANKL	receptor activator of nuclear factor- κ B ligand
REST	repressor element 1-silencing transcription
SKA-121	5-methylnaphtho [2, 1-d] oxazol-2-amine
SKA-31	Naphtho [1, 2-d] thiazole-2-ylamine
STAT-1	signal transducer and activator of transcription 1
TNF- α	tumor necrosis factor- α
TNF- β 1	transcriptional growth factor β 1
TRAM-34	1-[(2-chlorophenyl) diphenylmethyl]-1H-pyrazole
TRIM27	tripartite motif containing protein 27
ZOX	zoxazolamide



OPEN ACCESS

EDITED BY

Shanshan Hu,
Anhui Medical University, China

REVIEWED BY

Jin Lin,
Zhejiang University, China
Yolande Ramos,
Leiden University Medical Center
(LUMC), Netherlands

*CORRESPONDENCE

Wayne Yuk Wai Lee
waynelee@cuhk.edu.hk

SPECIALTY SECTION

This article was submitted to
Autoimmune and
Autoinflammatory Disorders,
a section of the journal
Frontiers in Immunology

RECEIVED 30 June 2022

ACCEPTED 08 September 2022

PUBLISHED 11 October 2022

CITATION

Wang R, Shiu HT and Lee WYW (2022)
Emerging role of lncRNAs in
osteoarthritis: An updated review.
Front. Immunol. 13:982773.
doi: 10.3389/fimmu.2022.982773

COPYRIGHT

© 2022 Wang, Shiu and Lee. This is an
open-access article distributed under
the terms of the [Creative Commons
Attribution License \(CC BY\)](#). The use,
distribution or reproduction in other
forums is permitted, provided the
original author(s) and the copyright
owner(s) are credited and that the
original publication in this journal is
cited, in accordance with accepted
academic practice. No use,
distribution or reproduction is
permitted which does not comply with
these terms.

Emerging role of lncRNAs in osteoarthritis: An updated review

Rongliang Wang^{1,2,3}, Hoi Ting Shiu^{1,2}
and Wayne Yuk Wai Lee^{1,2,3*}

¹Department of Orthopaedics and Traumatology, Faculty of Medicine, Prince of Wales Hospital, The Chinese University of Hong Kong, Hong Kong, China, ²Li Ka Shing Institute of Health Sciences, The Chinese University of Hong Kong, Hong Kong, China, ³SH Ho Scoliosis Research Laboratory, Joint Scoliosis Research Center of the Chinese University of Hong Kong and Nanjing University, The Chinese University of Hong Kong, Hong Kong, China

Osteoarthritis (OA) is a prevalent joint disease, which is associated with progressive articular cartilage loss, synovial inflammation, subchondral sclerosis and meniscus injury. The molecular mechanism underlying OA pathogenesis is multifactorial. Long non-coding RNAs (lncRNAs) are non-protein coding RNAs with length more than 200 nucleotides. They have various functions such as modulating transcription and protein activity, as well as forming endogenous small interfering RNAs (siRNAs) and microRNA (miRNA) sponges. Emerging evidence suggests that lncRNAs might be involved in the pathogenesis of OA which opens up a new avenue for the development of new biomarkers and therapeutic strategies. The purpose of this review is to summarize the current clinical and basic experiments related to lncRNAs and OA with a focus on the extensively studied H19, GAS5, MALAT1, XIST and HOTAIR. The potential translational value of these lncRNAs as therapeutic targets for OA is also discussed.

KEYWORDS

long non-coding RNA, osteoarthritis, pathogenesis, biomarkers, therapeutic strategies

Introduction

Osteoarthritis (OA) is a prevalent joint disease in aging and obese populations, resulting in joint pain, stiffness, and movement limitation (1). It has been estimated that OA affects more than 240 million people all over the world which is projected to double in the next 20 years (2). OA is regarded as one of the leading causes of major health and socioeconomic burdens in many countries (3). OA was once considered as a disease of articular cartilage alone. However, it is now generally believed that OA pathogenesis is associated with pathological changes of other joint tissues, such as synovial inflammation, subchondral bone remodeling and meniscal degeneration (4, 5). Risk factors, such as aging,

obesity, trauma, genetic predisposition, and bone density, have been implicated in the onset and development of OA (6). Despite these well documented factors and other routinely used clinical parameters such as patient history and radiographic examination, there is still a lack of sensitive approach to detect OA at its reversible stage (7, 8). In the clinics, multiple conservative treatments are available at the early stage of OA, such as physical measures or pharmacological anti-inflammatory and analgesic drugs (6). Surgical interventions, such as osteotomies and total replacement surgeries are served as the ultimate therapeutic options to rehabilitate the persistent pain and functional limitations of patients suffering from severe OA (9, 10). Obviously, these approaches are not able to halt or the progressive degeneration in the joints. Collectively, a better understanding of the molecular mechanism underlying this complex pathogenesis will provide an insight into the development of more specific and sensitive biomarkers as well as disease-modifying drugs for OA prevention and treatment (11).

In human genome, approximately 2% of genome is made up of protein-coding genes. The remaining 98% genome was thought to be nonfunctional evolutionary leftovers. It is now evidenced that these widely distributed non-coding genomes can be classified into two groups, namely short (< 200 nucleotides) and lncRNAs (> 200 nucleotides) which have diverse biological functions in various human diseases (12). In general, lncRNAs modulate the expression of target genes or the activity of downstream pathways by direct binding to DNA, RNA and proteins (13). Increasing evidence reveals that there are differential expressions of lncRNAs at cellular and tissue levels in human OA condition (14), suggesting the undefined roles of lncRNAs in OA development and progression (15), and potentially a new class of biomarkers for OA (16).

To supplement our current understanding as summarized in previous reviews and to update the landscape of lncRNAs research in OA (17, 18), this review takes a more comprehensive approach to critically review the current findings about the role of lncRNAs in OA pathobiology and diagnosis with emphasis on those extensively studied lncRNAs, including lncRNA H19, GAS5, MALAT1, XIST and HOTAIR and their effects on various joint tissues, and to propose novel treatment strategies *via* targeting lncRNAs.

This review on clinical and basic studies was conducted to provide a current understanding about the lncRNAs research on multiple joint tissues of OA pathogenesis through searching published articles on the PubMed, Google Scholar, and ScienceDirect databases from February 2003 to August 2022. The searching keywords include (“long non-coding RNA” OR “lncRNA”) AND (“osteoarthritis” OR “arthritis” OR “osteoarthritis treatment”) AND (“plasma” OR “synovial fluid” OR “body fluid” OR “cartilage” OR “synovium” OR “subchondral bone” OR “meniscus” OR “chondrocyte” OR “synoviocyte” OR “osteoblast” OR “exosome” OR “nanoparticle” OR “siRNA” OR “Gene-editing”).

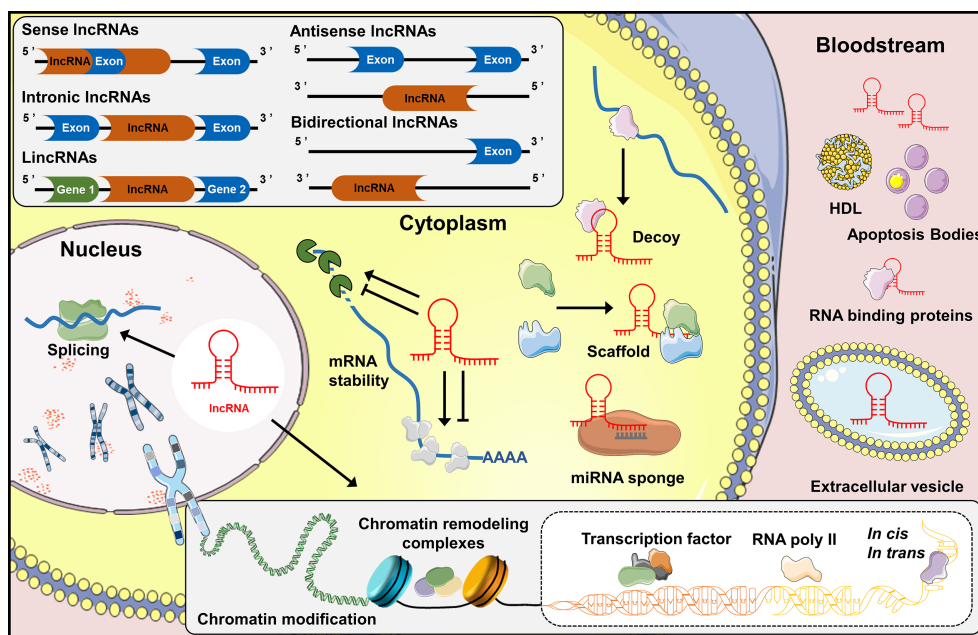
Classification and function of lncRNAs

One common classification of lncRNAs is based on their positions to protein-coding genes: (i) Sense lncRNAs and (ii) antisense lncRNAs are those overlap with the same and opposite strand of coding genes, respectively; (iii) Intronic lncRNAs are those locate in the same intronic region of protein-coding genes. While (iv) bidirectional lncRNAs are transcribed from the same promoter as the protein-coding genes, but in the opposite direction and (v) long intergenic noncoding RNAs (lincRNAs) locate in the genomic interval between two genes (19) (Figure 1). In addition, lncRNAs can be further classified by their interactions with targets, including decoy lncRNAs, guide lncRNAs, scaffold lncRNAs, stabilizing lncRNAs and competitive endogenous-lncRNAs. Decoy lncRNAs sequester DNA-binding proteins to limit their bindings to DNA recognition elements. Guide lncRNAs recruit chromatin remodeling agents to impart specificity to genomic locations through either DNA-protein or RNA-DNA recognition. While scaffold lncRNAs join several proteins together in a complex, and stabilizing lncRNAs bind to target mRNA transcripts, stabilize and promote their translations. Competitive endogenous-lncRNAs (ceRNAs) or ‘RNA sponges’ compete with miRNAs to limit their effects on protein-coding mRNA targets (20).

Extensive research over the past decade has deciphered various biological functions of lncRNAs (21). In general, lncRNAs regulate gene expression *via* chromatin modification, transcription and post-transcriptional processes (22). During chromatin modification, lncRNAs recruit chromatin remodeling complexes to specific chromatin loci (23). Transcriptional regulation is the core role of lncRNAs in which they serve as pervasive enhancers or promoters of transcription. In addition, lncRNAs also behave as RNA binding proteins, transcription factors and RNA polymerase (RNAP) II in regulating the initiation of transcription (21). During post-transcriptional regulation, lncRNAs mediate mRNA dynamics in both cis- and trans-targets (24). Overall, lncRNAs serve as master regulators of gene expression, and it is not surprising that the value of lncRNAs in key aspects of OA progression has attracted considerable attention.

Overview of lncRNAs in OA pathogenesis

Currently, most of the studies focused on the lncRNAs functions in OA cartilage/chondrocyte. Given that OA is a disease of the whole joint (25), it is of clinical value to provide an overview regarding the lncRNAs expression in different joint tissues. The section summarizes some recent key findings about



Biogenesis and function of lncRNAs. Classification of lncRNAs into five classes: sense lncRNAs, intronic lncRNAs, lincRNAs, antisense lncRNAs and bidirectional lncRNAs, based upon their genomic locations and transcription. lncRNAs regulate the expression of genes in the cytoplasm by interacting directly with microRNAs (miRNAs) or proteins, and stabilizing mRNA transcripts. Noncoding transcripts in the nucleus are known to regulate gene expression at the level of chromatin modification, transcription and post-transcriptional processing. In addition, lncRNAs are considered as biomarkers or participant in tissue crosstalk by entering the bloodstream directly, or bound to carrier proteins, even incorporated into extracellular vesicles which can be further released into bloodstream.

lncRNAs in Cartilage

chondrocyte function (127, 128). Liu and colleagues are one of the pioneer groups to profile lncRNA in human OA cartilage tissues, providing a new insight into the mechanism of cartilage injury and the progression of ECM degradation (52). Similarly, Hoolwerff and colleagues reported the differential expression of lncRNAs with OA pathophysiology in cartilage, and they discussed the potential of antisense lncRNA P3H2-AS1 on collagen chain assembly in lesioned OA cartilage *via* the regulation of P3H2 expression (129). On the other hand, Pearson et al. identified 125 lncRNAs were differentially expressed upon IL-1 β stimulation in primary human OA chondrocytes. Amongst, two novel lncRNAs, namely ClLinc01 and ClLinc02, were found to mediate the secretion of proinflammatory cytokines in IL-1 stimulated human chondrocytes, suggesting that some lncRNAs might mediate the response of chondrocytes to inflammation and inflammation-driven cartilage degeneration within the OA joint (92). Of note, different types of cellular model, such as cartilage derived primary cell culture or immortalized cell line with or without prior stimulation, were used in previous studies to delineate the effects of various lncRNAs on chondrocytes (130). Whether these effects are associated with or even causative factors in OA development or

TABLE 1 The dysregulated lncRNA in clinical OA samples.

LncRNA	Human tissue/ cells	Expression in OA	Potential targets	Cellular process	Proposed molecular mechanism	References
<i>H19</i>	OA Cartilage	Upregulated	COL2A1, COL9A1, COL10A1, CILP, and HTRA1	ECM anabolism	miR675 host	(26)
	OA chondrocyte	Upregulated	PCNA, CyclinD1, and cleaved Caspase 3	Cell proliferation	Interaction with miR106-5p	(27)
	OA Cartilage	Upregulated	IL-38	Inflammatory response	Interaction with p53	(28)
	OA Cartilage	Upregulated	Bax and Bcl2	Cell apoptosis	Interaction with miR140-5p	(29)
			COL2A1, MMP1, and MMP13 ALP, OCN, and BSP	ECM degradation Ossification		
<i>GAS5</i>	OA synovium	Upregulated	–	–	–	(30)
	OA chondrocyte	Upregulated	MMP2, MMP3, MMP9, MMP13, and ADAMTS4	ECM degradation	Interaction with miR21 in autophagy	(31)
	OA chondrocyte	Upregulated	Bax and Bcl2	Cell apoptosis	Interaction with miR34a	(32)
	OA Cartilage	Upregulated	Caspase 3, Bax, and Bcl 2	Cell apoptosis	Interaction with miR137	(33)
	OA synovium	Downregulated	Caspase 3, and Bax	Cell apoptosis	–	(34)
<i>MALAT1</i>	OA chondrocyte	Upregulated	ADAMTS5, COL2A1, ACAN, and COMP	ECM degradation	Interaction with miR145	(35)
	OA Cartilage	Upregulated	OPN	Cell proliferation	Regulated PI3K/Akt pathway by interacting with miR127-5p	(36)
	OA synoviocytes	Upregulated	IL-6 and CXCL8	Inflammatory response	–	(37)
	OA Subchondral bone	Upregulated	PGE2	Inflammatory response	–	(38)
	OA Cartilage	Upregulated	Cleaved caspase3 and Bcl2	Cell apoptosis	Regulated DNMT3A by interacting with miR149-5p	(39)
			COL2 and aggrecan	ECM degradation		
	OA Cartilage	Upregulated	Cleaved caspase3 and Bcl2	Cell apoptosis	Regulated GNG5 by interacting with miR675-3p	(40)
			COL2A1 and MMP13	ECM degradation		
			IL-6 and IL-8	Inflammatory response		
	OA Cartilage	Upregulated	CXCR4	Cell proliferation	Regulated MAPK signaling by interacting with miR211	(41)
<i>HOTAIR</i>	OA synovium (Macrophagy)	Upregulated	IL-4, IL-6, IL-10, IL-1 β , and TNF- α ICAM1, MMP3, MMP9, and MRP8 OPN, ACAN, and COL2 in chondrocyte	Inflammatory response Migration Crosstalk	Interaction with miR376	(42)
	OA Cartilage	Upregulated	Bcl2, cleave caspase3, p62 and LC3B	Cell apoptosis	Regulated ADAM10 by interacting with miR222-3p	(43)
			COL2, COL10, SOX9, and MMP13,	ECM degradation		
			IL-6, IL-10 and TNF- α	Inflammatory response		
	OA Cartilage	Upregulated	Cleaved caspase3, Survivin, Bcl2 and Bax	Cell apoptosis	Regulated BCL2L13 by interacting with miR130a-3p	(44)
	OA Cartilage	Upregulated	IL-1 β and TNF- α	Inflammatory response	Regulated STGB by interacting with miR1277-5p	(45)
			Aggrecan and COL2	ECM degradation		
	OA Cartilage	Upregulated	Aggrecan, COL2, MMP13 and MMP9	ECM degradation	Regulated CXCL12 by interacting with miR107	(46)
			–	Cell apoptosis		

(Continued)

TABLE 1 Continued

LncRNA	Human tissue/ cells	Expression in OA	Potential targets	Cellular process	Proposed molecular mechanism	References
	OA chondrocyte	Upregulated	ADAMTS5 MMP13, ADAMTS5, COL2, and ACAN	ECM degradation	Interaction with promotor	(47)
	OA Cartilage	Upregulated	Cleaved caspase3, cleaved caspase9 and Bax	ECM degradation Cell apoptosis	Regulated FUT2/WNT aixe by interacting with miR17-5p	(48)
<i>HOTTIP</i>	OA Cartilage	Upregulated	COL2, MMP9, MMP13, TIMP3, ACAN and ADAMTS5	ECM degradation	Regulated WIF1/WNT pathway	(49)
	OA chondrocyte	Upregulated	HoxA cluster	–	Epigenetic regulation	(50)
	OA Cartilage	Upregulated	–	Cell proliferation	Regulated FRK by interacting with miR 663a	(51)
<i>CIR</i>	OA Cartilage	Upregulated	MMP13, ADAMTS5, COL2, COL1, and ACAN	ECM degradation	Vimentin inhibition	(52)
	OA chondrocyte	Upregulated	MMP13	ECM degradation	Interaction with miR27	(53)
	OA Cartilage	Upregulated	COL2A1, and MMP13	ECM degradation	Activating autophagy	(54)
<i>MSR</i>	OA Cartilage	Upregulated	COL2A1, ACAN, MMP13, and ADAMTS5	ECM degradation	Regulated TMSB4 by interacting with miR152	(55)
<i>PVT1</i>	OA Cartilage	Upregulated	COL2, ACAN, MMP3, MMP9 and MMP13	ECM degradation	Interaction with miR149	(56)
			PGE2, NO, IL-6, IL-8, and TNF- α	Inflammatory response		
	OA Cartilage	Upregulated	Cleaved caspase3 and autophagy	Cell apoptosis	Regulated TRAF3 by interacting with miR27b-3p	(57)
	OA synovium	Upregulated	Caspase 3, and Bax	Cell apoptosis	–	(34)
<i>Nespas</i>	OA chondrocyte	Upregulated	COL2, COL1, MMP2 and MMP13	ECM degradation	Interaction with miRNAs	(58)
<i>UCA1</i>	OA Cartilage	Upregulated	COL2, COL4, and MMP13	ECM degradation	Interaction with miR204-5p	(59)
			–	Cell proliferation		
			Caspase3 and Bcl2	Cell apoptosis	Regulated SphK2 by competing with miR577	(60)
<i>DANCR</i>	OA Cartilage	Upregulated	IL-6 and IL-8	Inflammatory response	Regulated JAK2/STAT3 signaling by interacting with miR216a-5p	(61)
	OA Cartilage	Upregulated	IL-1, IL-6, IL-8, and TNF- α	Inflammatory response	Regulated DANCR by interacting with miR19a	(62)
			–	Cell apoptosis		
<i>LncHIFCAR</i>	OA Cartilage	Upregulated	MMP1, MMP3 and MMP13	ECM degradation	Regulated HIF-1 α , HIF-1 α target genes, and PI3K/AKT/mTOR pathway	(63)
			TNF- α and IL-6	Inflammatory response		
			Bcl2, Bax, and Cytochrome C	Cell proliferation		
<i>FAS-AS1</i>	OA Cartilage	Upregulated	COL2, MMP1 and MMP13	ECM degradation	–	(64)
			–	Cell proliferation	–	
			CCND1	Cell proliferation	Interaction with miR206	(65)
<i>FOXD2-AS1</i>	OA Cartilage	Upregulated	Bcl2, and Bax	Cell apoptosis	Interaction with miR451	(66)
<i>p21</i>	OA chondrocyte	Upregulated	MMP13	ECM degradation	Regulated TGF- β signaling by interacting with miR22	(67)
<i>TM1P3</i>	OA chondrocyte	Upregulated	IL-6 and IL-8	Inflammatory response	Regulated FGFR1 by interacting with miR376-3p	(68)
<i>TNFSF10</i>	OA chondrocyte	Upregulated	–	Cell proliferation		

(Continued)

TABLE 1 Continued

LncRNA	Human tissue/ cells	Expression in OA	Potential targets	Cellular process	Proposed molecular mechanism	References
<i>LINC01534</i>	OA Cartilage	Upregulated	–	Cell apoptosis		
			MMP3, MMP9, MMP13, COL2 and aggrecan	ECM degradation	Interaction with miR140-5p	(69)
			NO, PGE2, TNF- α , IL-6, and IL-8	Inflammatory response		
<i>NKILA</i>	OA Cartilage	Upregulated	Bcl2, Bax, and cleaved caspase3	Cell apoptosis	Regulated SP1/NF- κ B axis by interacting with miR145	(70)
<i>LINC00461</i>	OA Cartilage	Upregulated	IL-6, IL-10	Inflammatory response	Interaction with miR30a-5p	(71)
			COL2, MMP2, MMP3 and MMP13	ECM degradation		
			–	Cell proliferation		
<i>LOXL1-AS1</i>	OA Cartilage	Upregulated	Cleaved Caspase 3, Cleaved Caspase 9, and Bax	Cell apoptosis	Regulated KDM5C by interacting with miR423-5p	(72)
			IL-6, IL-8	Inflammatory response		
<i>PCAT-1</i>	OA chondrocyte	Upregulated	Cleaved Caspase3, Bcl2, and Bax	Cell apoptosis	Interaction with miR27b-3p	(73)
<i>ARFRP1</i>	OA Cartilage	Upregulated	CCND1, Bcl2, and Bax	Cell apoptosis	Regulated TLR4/NF- κ B axis by interacting with miR15a-5p	(74)
			TNF- α , IL-6, and IL-1 β	Inflammatory response		
<i>TUG1</i>	OA Cartilage	Upregulated	MMP13, COL2 and aggrecan	ECM degradation	Regulated FUT1 by interacting with miR17-5p	(75)
			–	Cell apoptosis		
<i>LINC00671</i>	OA Cartilage	Upregulated	Col2A1, Aggrecan, MMP3, MMP13, ADAMTS4, and ADAMTS5	ECM degradation	Regulated ONECUT2/Smurf2/GSK-3 β axis	(76)
<i>RMRP</i>	OA Cartilage	Upregulated	–	Cell proliferation	Regulated CDK9 by interacting with miR206	(77)
<i>KCNQ1OT1</i>	OA Cartilage	Upregulated	IL-1 β , TNF- α and IL-6	Inflammatory response	Regulated TCF4 by interacting with miR211-5p	(78)
			COL2, COL10, and MMP13	ECM degradation		
	OA Cartilage	Downregulated	COL2, and MMP13	ECM degradation	Regulated TRPS1 by interacting with miR126-5p	(79)
			–	Cell proliferation		
<i>RP11-364P22.2</i>	OA Cartilage	Upregulated	Col2A1, Aggrecan, and MMP13	ECM degradation	Regulated ATF3	(80)
			Caspase3, and NF- κ B	Cell apoptosis		
<i>Cox2</i>	OA Cartilage	Upregulated	Ki67 and PCNA	Cell proliferation	Regulated Wnt/ β -catenin pathway by interacting with miR150	(81)
			Caspase3, Caspase9, and Bax	Cell apoptosis		
<i>CASC19</i>	OA Cartilage	Upregulated	IL-6, IL-8, and TNF- α	Inflammatory response	Regulated DDX6 by interacting with miR152-3p	(82)
			–	Cell apoptosis		
<i>MIR22HG</i>	OA Cartilage	Upregulated	COL2A1, ACAN, MMP13, ADAMTS5	ECM degradation	Interaction with miR9-3p	(83)
			–	Cell apoptosis		
<i>LINC01385</i>	OA Cartilage	Upregulated	IL-6, TNF- α , PGE ₂	Inflammatory response	Interaction with miR 140-3p/TLR4 axis	(84)
<i>LINC00707</i>	OA Cartilage	Upregulated	–	Cell apoptosis	Interaction with miR199-3p	(85)
	OA Cartilage	Upregulated	–	Cell apoptosis	Regulated FSHR by interacting with miR330-5p	(86)
			COL2, ACAN, MMP13, MMP3	ECM degradation		
			IL-6, TNF- α	Inflammatory response		

(Continued)

TABLE 1 Continued

LncRNA	Human tissue/ cells	Expression in OA	Potential targets	Cellular process	Proposed molecular mechanism	References
<i>LINC00680</i>	OA Cartilage	Upregulated	–	Cell proliferation	Regulated SIRT1 by interacting with IGF2BP2	(87)
<i>PILA</i>	OA Cartilage	Upregulated	COL2, ACAN, MMP13, MMP13, MMP3, ADAMTS4	ECM degradation	Regulated TAK1/NF- κ B axis by interacting with PRMT1	(88)
<i>DLEU1</i>	OA Cartilage	Upregulated	–	Cell apoptosis		
			COL2, ACAN, ADAMTS5 and MMP3	ECM degradation	Interaction with miR671-5p	(89)
			IL-1, IL-6, and TNF- α	Inflammatory response		
<i>MEG3</i>	OA Cartilage	Downregulated	VEGF	Angiogenesis	–	(90)
	OA chondrocyte	Downregulated	Ki67 and PCNA	Cell proliferation	Regulated FOXO1 by interacting with miR361-5p	(91)
			Bcl2 and Bax	Cell apoptosis		
			MMP13, ADAMTS5, COL2, ACAN	ECM degradation		
<i>CILinc01</i>	OA chondrocyte	Downregulated	IL-6	Inflammatory response	–	(92)
<i>CILinc02</i>	OA Cartilage	Upregulated	IL-1, IL-6, and IL-17	Inflammatory response	–	(93)
			TIMP1, MMP1 and MMP13	ECM degradation	–	
			–	Cell apoptosis	–	
<i>UFC1</i>	OA Cartilage	Downregulated	–	Cell proliferation	Interaction with miR34a	(94)
<i>SNHG5</i>	OA Cartilage	Downregulated	SOX2	Cell proliferation	Interaction with miR26a	(95)
	OA Cartilage	Downregulated	MMP13, ADAMTS5, COL3 and ACAN	ECM degradation	Regulated autophagy by interacting with miR141-3p	(96)
			Cleaved caspase3	Cell apoptosis		
	OA Cartilage	Downregulated	Cleaved caspase3, and cleaved caspase9	Cell apoptosis	Regulated H3F3B by interacting with miR10a-5p	(97)
			COL2, and ADAMTS5	ECM degradation		
	OA Cartilage	Upregulated	MMP13 and ADAMTS5	ECM degradation		
					Regulated TGFB3 by interacting with miR181a-5p	(98)
Caspase3	Cell apoptosis					
<i>HOTAIRM1-1</i>	OA Cartilage	Downregulated	–	Chondrogenic differentiation	Regulated BMPR2/MAPK axis by interacting with miR125b	(99)
			Cleaved caspase3, cleaved caspase9, Bcl2 and Bax	Cell apoptosis		
			COL2, COL10, and aggrecan	ECM degradation		
<i>LINC00341</i>	OA Cartilage	Downregulated	Bcl2, and Bax	Cell apoptosis	Regulated YAF2 by interacting with miR141	(100)
<i>DNM3OS</i>	OA Cartilage	Downregulated	Cleaved caspase3, Bcl2, and Bax	Cell proliferation	Regulated IGF1 by interacting with miR126	(101)
<i>PART1</i>	OA Cartilage	Downregulated	Cleaved caspase3, cleaved caspase9 and Bax	Cell apoptosis	Regulated TGFB2/Smad3 axis by interacting with miR590-3p	(102)
	OA Cartilage	Downregulated	MMP13, COL2, and ACAN	ECM degradation	Regulated SOX4 by interacting with miR373-3p	(103)
			Bcl2, Bax and cleaved caspase3	Cell apoptosis		
<i>NEAT1</i>	OA Cartilage	Downregulated	ACAN, Col2a1, MMP3, MMP13, and ADAMTS5	ECM degradation	Regulated SOX5 by interacting with miR373-3p	(104)
			IL-1, TNF- α , IL-6, and IL-8	Inflammatory response		

(Continued)

TABLE 1 Continued

LncRNA	Human tissue/ cells	Expression in OA	Potential targets	Cellular process	Proposed molecular mechanism	References
	OA Cartilage	Upregulated	–	Cell apoptosis		
			MMP3, MMP9, and MMP13	ECM degradation	Regulated PLA2G4A by interacting with miR543	(105)
			IL-6, and IL-8	Inflammatory response		
			p-Akt1 and Bcl2	Cell proliferation		
<i>LINC00662</i>	OA chondrocyte	Downregulated	TNF- α , IL-6, and IL-8	Inflammatory response	Regulated GPR120 by interacting with miR15b-5p	(106)
			Cleaved caspase3, cleaved caspase9 and Bax	Cell apoptosis		
<i>OIP5-AS1</i>	OA Cartilage	Downregulated	IL-6, IL-8, and TNF- α	Inflammatory response	Regulated PGRN by interacting with miR29b-3p	(107)
			Bax	Cell apoptosis		
<i>LINC00623</i>	OA Cartilage	Downregulated	MMP13, and COL2	ECM degradation	Regulated HRAS/MAPK axis by interacting with miR101	(108)
			Cleaved caspase3, and cleaved caspase7	Cell apoptosis		
<i>SNHG7</i>	OA Cartilage	Downregulated	Cleaved Caspase3, Cleaved Caspase7	Cell apoptosis	Regulated SNHG7/PPAR γ axis by interacting with miR214-5p	(109)
			IL-1 β , TNF- α and IL-6	Inflammatory response		
<i>ROR</i>	OA Cartilage	Downregulated	COL2, ACAN, MMP13 and COL10	Chondrogenesis	Regulated SOX9 by interacting with miR138 and miR145	(110)
<i>OIP5-AS1</i>	OA Cartilage	Downregulated	Caspase 3, Caspase 9, Bax, and Bcl2	Cell apoptosis	Interaction with miR30a-5p	(111)
			IL-6, IL-8, and TNF- α	Inflammatory response		
<i>FGD5-AS1</i>	OA Cartilage	Downregulated	–	Cell apoptosis	Regulated TGFBR2 by interacting with miR302d-3p	(112)
<i>MCM3AP-AS1</i>	OA Cartilage	Downregulated	–	Cell apoptosis	Regulated SIRT1 by interacting with miR138-5p	(113)
<i>MEG8</i>	OA Cartilage	Downregulated	Caspase3	Cell apoptosis	Regulated PI3K/AKT signaling	(114)
			IL-6 and TNF- α	Inflammatory response		
<i>ZFAS1</i>	OA Cartilage	Downregulated	ROS, SOD, and Catalase	Oxidative stress	Regulated NRF2 by interacting with miR1323	(115)
			IL-1 β , TNF- α and IL-6	Inflammatory response		
			–	Cell apoptosis		
<i>GACAT3</i>	OA synoviocytes	Upregulated	Caspase3	Cell proliferation	Regulated STAT3	(116)
<i>ANRIL</i>	OA synoviocytes	Upregulated	Cleaved caspase3, Bax, and Bcl2	Cell proliferation	Regulated DUSP4 by interacting with miR122-5p	(117)
<i>PCGEM1</i>	OA synoviocytes	Upregulated	PARP and caspase9	Cell proliferation	Interaction with miR770	(118)
	OA synoviocytes	Upregulated	Chondrocyte apoptosis and cartilage matrix degradation	Crosstalk	Interaction with miR142-5p	(119)
<i>AK094629</i>	OA synovium	Upregulated	IL-6	Inflammatory response	Regulated MAP3K4	(120)
<i>IGHCγ1</i>	PBMCs	Upregulated	IL-6 and TNF- α	Inflammatory response	Regulated TLR4/NF- κ B axis by interacting with miR6891-3p	(121)
<i>AC005165.1</i>	OA Subchondral bone	Downregulated	–	–	Regulated FRZB/WNT signaling	(122)
<i>LOC107986251</i>	OA Menisci	Upregulated	–	–	Regulated SESN3 by interacting with miR212-5p	(123)

COL, Collagen; CILP, Cartilage intermediate layer protein; ECM, Extracellular matrix; PCNA, Proliferating cell nuclear antigen; MMPs, Matrix metalloproteinases; ALP, Alkaline phosphatase; OCN, Osteocalcin; BSP, Bone sialoprotein; ACAN, Aggrecan; ADAMTS, A disintegrin and metalloproteinase with thrombospondin motifs; COMP, Cartilage oligomeric matrix protein; PGE2, Prostaglandin E2; OPN, Osteopontin; TIMPs, Tissue inhibitor of metalloproteinases; CXCL, C-X-C Motif Chemokine Ligand; CXCR, C-X-C chemokine receptor; MRP, Multidrug resistance-associated protein; CCND1, Cyclin D1; VEGF, Vascular endothelial growth factor; ROS, Reactive oxygen species; SOD, Superoxide Dismutase; PBMCs, Peripheral Blood Mononuclear Cells.

progression requires further investigation with appropriate transgenic animal models.

lncRNAs in Synovium

Synovium is a specialized connective membrane lining the inner surface of synovial joint capsules, and almost 75% of cells in the synovium are fibroblast-like synoviocytes (FLS) (131). Increasing evidence shows that FLS secretes proinflammatory cytokines which mediate the degradation of cartilage during OA progression (132), which has been speculated to be associated with disease progression (133). Till now, the effects of lncRNAs on OA synovium remains elusive. Early work by Xiang and colleagues identified the differential expressions of 17 lncRNAs in OA synovium of aged patients undergoing total knee replacement surgery, in which some of these lncRNAs were found to be related to immune response. The recruitment of younger control subjects requiring arthroscopic meniscectomy in this case-control study is ethically sound but not ideal to exclude the influences of the acute injury of meniscus on the lncRNAs in the synovial microenvironment (134). Li and colleagues focused on a hepatocellular carcinoma associated lncRNA (ANRIL) and found a higher level of ANRIL in the OA cartilage tissue when compared with that of normal cartilage tissue obtained from subjects requiring traumatic emergency amputation without OA or rheumatic arthritis. Then primary chondrocytes isolated from the collected cartilage tissues, and commercially available normal and OA synoviocytes were used to show differentially upregulated ANRIL expression in OA synoviocytes but not in OA chondrocytes. It appears that ANRIL dysregulation in OA is cell-type specific, affecting the proliferation of synoviocytes *via* binding to miR-122-5p (117). However, it should be noted that the information of the subjects where those chondrocytes and synoviocytes derived from (such as age and sex) were not provided, which should be taken into consideration.

lncRNAs in Subchondral bone

Impaired mineralization is a pathological feature of osteoarthritic subchondral bone. Such distinct microstructural alterations, including sclerotic changes and osteophyte formation, are both believed to arise from elevated bone turnover with an increase in osteoblastic over osteoclastic activities (135). In addition, the subchondral bone is also considered as a major site of OA pain, likely due to the innervation with sensory neurons and vascular channels (136). From bone remodeling perspective, it is evidenced that several lncRNAs could regulate osteoblast and osteoclast activities, and

there are attempts to modulate lncRNAs expression *in vivo via* various strategies (137). Therefore, it is of interest to ask whether aberrant subchondral bone remodeling in OA is associated with lncRNAs dysregulation. By comparing subchondral bone samples collected from hip and knee, Tuerlings and colleagues identified 21 lncRNAs differentially expressed between preserved and lesioned OA subchondral bone significantly. It is interesting to note that a further stratified analysis identified 15 lncRNAs were differentially expressed in knee samples but none in hip samples (122). These findings prompt to further research questions. 1) Whether lncRNAs differential expression in OA subchondral bone is site-specific and associated with aberrant mechanical loading? 2) What are the biological functions of these lncRNAs in OA subchondral bone remodeling? Further investigation on the effects of lncRNAs on osteoblasts, osteoclasts and osteocytes functions related to subchondral bone mineralization and remodeling is warranted to develop a more comprehensive understanding of the lncRNAs and their roles and therapeutic values in OA.

lncRNAs in Meniscus

Meniscus is a crucial tissue for supporting the structure, stability, and biomechanical function of the knee joint (138). During OA progression, it undergoes various histopathological changes, including tears, calcification, and atypical cell arrangement (139). Till now, there is limited studies exploring the mechanism of meniscal pathogenesis in OA, and only two studies were found to investigate the expression level of lncRNAs in OA meniscus tissues. The work by Brophy and colleagues depicted the transcriptome profile in the meniscus between end stage OA patients and patients undergoing arthroscopic partial meniscectomy with no evidence of OA. The subjects in the OA group were older and had higher BMI. Twenty-six and 10 lncRNAs were found up- and down-regulated in the OA group, respectively. lnc-RPL19-1 and lnc-ICOSLG-5 were highlighted because of their correlations with some cartilage disease related genes. qPCR was performed to validate the microarray results (140). Recently, Jiang and colleagues performed a whole-transcriptome profile of lncRNAs dysregulation using isolated meniscus cells from OA patients with and without IL-1 β , suggesting a potential crosslink between menisci and cartilage during OA. Of note, LCN2 and RAB27B were consistently upregulated in both OA meniscus and IL-1 β treated primary meniscus cells derived from three OA meniscus samples, and appears to be associated with OA severity (123). Although different samples were used in the analysis, these two works both illustrated the potential link between inflammatory phenotype in meniscus and lncRNAs, which is subjected to further investigation to confirm the molecular mechanisms and biological functions of these lncRNAs in OA meniscus injury.

Clinical biomarkers of lncRNAs for OA diagnosis

In general, the secretion and transport of lncRNAs into extracellular environment are mediated by three manners (1): Direct release of extracellular RNAs by joint tissues and cells (2). Encapsulated in high density lipoprotein (HDL) or apoptosis bodies or associated with protein complexes (3). Packed in membrane vesicles, such as exosomes and micro-vesicles (141). In clinical research, serum and synovial fluid are often the preferred biological fluid samples for OA biomarker discovery (142). Recent detections of the extracellular lncRNAs in these biological fluids of OA subjects implicate that they might serve as alternative indicators for OA onset and progression (Table 2).

Circulation

Previous studies have shown that there is a relationship between the blood level of lncRNAs and OA progression

(Table 2). For instance, lncRNA DILC (145), and lncRNA FER1L4 (146) were also found to be closely associated with OA inflammatory condition in plasma. As ANCR is known to regulate TGF- β signaling, Li and colleagues proposed that the plasma levels of TGF- β 1 and ANCR could differentiate OA patients from healthy control subjects. They found a higher TGF- β 1 and a lower ANCR level in OA plasma (N=62) when compared with that of healthy controls (N=46), which was inversely correlated. The mean area under curve (AUC) for OA plasma TGF- β 1 and ANCR were 0.8929 and 0.8845, respectively (147). However, it is not shown if combination of plasma TGF- β 1 and ANCR could enhance the sensitivity and specificity. Zhou et al. indicated that the expression of lncRNA H19 was negatively correlated with bone metabolic index of OA patients, such as Procollagen I N-Terminal Propeptide (PINP), N-MID-Osteocalcin, bone Gla protein (BGP), and bone alkaline phosphatase (BALP). Particularly, lncRNA H19 is highly correlated with K-L grading, VAS, WOMAC and Lysholm scores, suggesting H19 was associated with disease severity in OA patients (144). These two biomarkers discovery studies show encouraging AUC value, however, discussion on confounding factors and validation with separate cohort were missing.

TABLE 2 lncRNAs as biomarkers for OA diagnosis.

lncRNA	Human Samples	Expression in OA	Sample size(Health vs OA)	AUC	Correlation	References
<i>ATB</i>	Serum	Downregulated	76 vs 98	0.8902	No significant association with the clinical data	(143)
<i>H19</i>	Peripheral Blood	Upregulated	100 vs 103	0.891	K-L grading, and Bone metabolism indexes	(144)
<i>DILC</i>	Plasma	Downregulated	52 vs 87	0.9321	IL-6	(145)
	Synovial Fluid	Downregulated	14 vs 22	–	–	
<i>FER1L4</i>	Plasma	Downregulated	49 vs 81	0.9221	IL-6	(146)
	Synovial Fluid	Downregulated	16 vs 19	–	–	
<i>ANCR</i>	Plasma	Downregulated	62 vs 46	0.8845	TGF- β 1	(147)
<i>MIR4435-2HG</i>	Plasma	Downregulated	58 vs 78	–	–	(148)
	Synovial Fluid	Downregulated		0.96		
<i>LUADT1</i>	Synovial Fluid	Downregulated	60 vs 60	–	–	(149)
<i>CAIF</i>	Synovial Fluid	Downregulated	60 vs 60	0.89	miR1246 and IL-6	(150)
<i>PMS2L2</i>	Synovial Fluid	Downregulated	62 vs 62	–	OA stages	(151)
<i>HOTAIR</i>	Synovial Fluid	Upregulated	13 vs 21	–	–	(152)
<i>CASC2</i>	Synovial Fluid	Upregulated	60 vs 60	–	miR93-5p	(153)
<i>CTBP1-AS2</i>	Synovial Fluid	Upregulated	62 vs 62	–	miR130a	(154)
<i>GASS</i>	Synovial Fluid	Downregulated	45 vs 45	–	–	(155)
	Synovial Fluid	Downregulated	62 vs 62	–	–	(34)
	Peripheral Blood Mononuclear Cells	Downregulated	60 vs 67	–	–	(156)
<i>LINC00167</i>	Peripheral Blood Leukocytes	Downregulated	60 vs 60	0.879	No significant association with the clinical data	(157)
<i>PVT1</i>	Serum/Serum Exosomes	Upregulated	30 vs 30	–	miR93-5p	(158)
	Synovial Fluid	Upregulated	62 vs 62	–	–	(34)
<i>PCGEM1</i>	Synovial Fluid Exosomes	Upregulated	20 vs 42	0.879	OA Stages, and WOMAC Index	(159)

Synovial fluid

Based on current findings, it is reasonable to speculate that the expression of lncRNAs is cell and tissue specific in OA joint. Therefore, the information from research on synovial fluid is likely to provide additional clues on the clinical values of lncRNAs as OA biomarkers. Qi and colleagues showed lower levels of CAIF in the synovial fluid collected from the hip and knee of OA patients, and CAIF was inversely and significantly correlated with IL-6 expression level (150). Meanwhile, Xiao and colleagues reported lower levels of lncRNA MIR4436-2HG in both plasma and synovial fluid of OA patients. The mean AUC for CAIF and MIR-4435-2HG were found to be 0.89 and 0.96, respectively. It is interesting to note that 1 or 3 months treatment including exercise, prescription of non-steroidal anti-inflammatory drugs (NSAIDs) and joint burden reduction seems to increase the plasma level of MIR-4435-2HG (148). Although the study design, the details of these treatment and the compliance were not mentioned, this preliminary result suggests that lncRNAs level in circulation could be modulated. In these studies, healthy volunteers were recruited as control group for the collection of synovial fluid. If the collections of synovial fluid from mild to moderate stages are also ethically feasible, it will be of clinical interest to determine the correlations between lncRNAs level in synovial fluid and OA severity and progression in order to explore the prognostic value of those selected lncRNAs.

Others

lncRNAs in cells/extracellular carriers within the blood and synovial fluid are another sources of biomarker candidates (160). The expression profile of lncRNAs in peripheral blood leukocytes of OA patients showed that LINC00167 may serve as a potential early diagnosis marker for OA in clinical practice (157). In addition, lncRNA GAS5 in the peripheral blood mononuclear cells isolated from the knee of OA patients was also lower than that of healthy subjects, indicating a novel marker for occurrence and progression of OA (156). The first study of lncRNA profiles in human OA synovial exosomes by Wu et al. found that exosomal lncRNA PCGEM1 is a potential indicator to distinguish the early stage of OA from the late-stage. Moreover, the expression of lncRNA PCGEM1 in synovial exosome rather than that in plasma was found to be closely associated with the WOMAC Index (159).

Biological functions of lncRNAs in OA pathogenesis

lncRNA H19

H19 lncRNA is located on chromosome 11p15.5, and its transcription product, H19 RNA, primarily resides in cytoplasm

(161). It is the first reported mammalian lncRNA (162), which is highly expressed during fetal stage but markedly down-regulated after birth. H19 was found to be upregulated in OA cartilage, and appears to be associated with the disease progression (26, 163, 164). In primary human chondrocytes, H19 and H19-derived miR675 increased the matrix production of differentiated chondrocytes *via* activating COL2 transcription (165). Furthermore, H19 could regulate the proliferation and apoptosis of chondrocytes treated by IL-1b *via* sponging miR106a-5p (27). Meanwhile, lncRNA H19 upregulated IL-38, which is bound to IL-36R and brought about suppression of knee joint inflammation in mouse chondrocytes (28). Inconsistent outcomes were observed in different *in vitro* models and upon different stimulations. Knockdown of lncRNA H19 could alleviate apoptosis and inflammatory response *via* sponging miR130a in LPS-stimulated human C28/I2 chondrocytes (166). Furthermore, the effect of H19 silencing suppressed the expression of matrix metalloproteinases (MMPs) family (MMP1 and MMP3) *via* targeting miR-140-5p in human HC-A chondrocyte cells, suggesting a protective role of H19 on the degradation of the chondrocyte extracellular matrix (29). Besides OA chondrocyte, H19 RNA level in OA synovial tissue was also found to be significantly higher than those in synovium of normal and trauma joint (30). However, there is a lack of strong evidence supporting that H19 RNA upregulation is a sign of inflammation of synovial FLSs nor polarization of synovial macrophages (167). Notably, rats FLS-derived exosomal lncRNA H19 was found to promote chondrocyte viability and migration, as well as inhibit ECM degradation in IL-1 β -induced chondrocytes by targeting miR106b-5p expression (168). Altogether, these studies suggest that lncRNA H19 may play an essential role in the crosstalk between synovium and cartilage during OA progression, and H19-targeted therapy is expected to open new perspectives for OA management.

lncRNA GAS5

The growth arrest-specific 5 (GAS5) lncRNA is located on chromosome 1q25.1 and consists of 12 exons with a short open reading frame (ORF) (169). Its name reflects its nature and predominant expression in growth-arrested cells (170). As such, GAS5 is mainly responsible for suppressing multiple anti-apoptotic genes, thereby enhancing the vulnerability of cells to pro-apoptotic signals (171). In OA cartilage, GAS5 was found to be upregulated with positive correlation pattern to the disease stages (172, 173). Overexpression of GAS5 was reported to increase the activity level of chondrocyte catabolism (several MMPs), and apoptosis (31). Meanwhile, GAS5 can serve as negative regulators for miR21 (31), miR34a (32), miR137 (33), miR144 (173) and miR27a (174). It is also evidenced that GAS5 could directly target KLF2 to alleviate LPS-induced inflammatory damage in murine chondrocytic ATDC5 cell

line (175). On the contrary, the expression levels of GAS5 in synovial fluid and tissues were significantly lower in OA (34, 155), which possibly implicate different functions of GAS5 in OA synovium. Considering the small sample size (N=45) and a lack of *in vivo* functional analysis, future study is required to evaluate the function of GAS5 in OA synovium by including a clinical study with a larger sample size and experiments with appropriate animal models.

lncRNA MALAT1

Metastasis-associated lung adenocarcinoma transcript 1 (MALAT1), also known as NEAT2 for nuclear-enriched abundant transcript 2, is transcribed by RNA polymerase II at human chromosome 11q13 (176). It is a highly abundant nuclear transcript localized to the nuclear speckles and have a longer half-life (9–12 h) than other lncRNAs owing to bipartite triple helix structure (177, 178). MALAT1 is upregulated in human OA cartilage and IL-1 β -induced chondrocyte cells (35). Overexpression of MALAT1 in human chondrocytes inhibited cells viability and promoted cartilage ECM degradation through targeting miR145 (35). Also, lncRNA MALAT1 overexpression in human C28/I2 chondrocyte cells was proved to promote chondrocyte migration, inflammation suppression, and ECM degradation (179). Besides, MALAT1 could act as sponges for other miRNAs, like miR127-5p (36), miR150-5p (180) and miR146a (181), thus likely to play some regulatory roles in OA cartilage. It should be noted that lower level of MALAT1 was also reported in IL-1b stimulated rat chondrocytes, which enhanced cell proliferation and type II collagen (Col II) expression by blocking JNK signaling activation (182). In synovium, the synovial fibroblasts isolated from OA patients had a higher expression of MALAT1 compared with that of normal subjects, which could be owing to proinflammatory challenge in synoviocytes especially to IL-6 and CXCL-8 (37). It is worth mentioning that MALAT1 is the first lncRNA to be investigated in OA subchondral bone. Higher expression level of MALAT1 was reported in both knee and hip subchondral bone of patients with OA, and its expression in the osteoblasts appears to be associated with the production of inflammatory prostacyclins. Since the subchondral bone is considered to be an important site of OA pain, MALAT1 may play an important role in the development of OA bone pain and inflammation (38). Based on current evidence, it appears that MALAT1 plays more pro-inflammatory role in OA synovial and subchondral bone, which represents a potential candidate for research on OA pathogenesis and therapeutic target.

lncRNA XIST

X-inactive specific transcript (XIST) encodes a 17-kb lncRNA which, despite being capped, spliced and polyadenylated, it is retained in the nucleus (183). lncRNA XIST and its associated chromatin modifying complex play vital roles in the regulation of the X-chromosome inactivation process (184). Emerging evidence indicates that it is correlated with the modification of ECM component of OA (185). XIST was upregulated in OA cartilage and promoted MMP-13 and ADAMTS-5 expression in human chondrocytes, indicating its role in ECM degradation through functioning as a ceRNA of miR1277-5p (186). Notably, the consistency results could be seen in the studies of XIST in terms of repressing the development of OA as indicated by different models. For instance, in IL-1b induced human C28/I2 chondrocyte cells, the knockdown of XIST expression suppressed the production of IL-6, TNF- α , PGE2 and NO through the interaction with miR130a (187). XIST regulated IL-1 β -induced chondrocyte growth, apoptosis and ECM synthesis through sponging with miR-142-5p in human chondrosarcoma cell line SW1353 (188). Moreover, the silencing of XIST could promote cell viability but inhibit cell apoptosis through acting as a sponge for miR149-5p in human CHON-001 chondrocyte cell line (39). In addition, XIST expression was significantly upregulated in the OA synovium compared with that in normal synovium. More importantly, XIST/miR376c-5p/OPN axis has been proven to modulate the inflammatory microenvironment in OA synovial macrophage, subsequently affecting chondrocyte apoptosis and ECM degradation (42).

lncRNA HOTAIR

HOX transcript antisense RNA (HOTAIR) resides within the intergenic region in HOXC cluster on chromosome 12, and acts as a crucial modulator of chromatin re-modeling and transcriptional silencing (189). As an epigenetic agent, HOTAIR can interact with various factors, leading to genomic stability, proliferation, survival, invasion, migration, metastasis, and drug resistance (190). In OA cartilage, HOTAIR was upregulated than that of normal samples (164). HOTAIR was reported as a promising promoter for ADAMTS-5 expression and ECM degradation in human OA articular chondrocytes (47). HOTAIR silencing reduced cartilage tissue damage in OA mice, and promoted the expression of collagen II and aggrecan in cartilage tissue, while inhibited the expression of MMP-13 and ADAMTS-5 by targeting miR-20b/PTEN axis in mouse

primary chondrocytes (191). Interestingly, cumulative evidence shows that Wnt/ β -catenin pathway might play a certain role in the pathogenesis of cartilage damage, and lncRNA HOTAIR could directly bind to miR17-5p and indirectly regulate FUT2/ β -catenin axis in connection with OA progression, such as ECM degradation and cell apoptosis (48). Wnt inhibitory factor 1 (WIF-1), a key inhibitor of the Wnt/ β -catenin pathway, could be directly modulated by HOTAIR and interfered with the activation of downstream pathway and relative genes expression on cartilage degradation in human chondrosarcoma cell line SW1353 (49). Overexpression of HOTAIR in human CHON-001 chondrocyte cell line could aggravate LPS-induced cell apoptosis and inflammatory cytokines influx, including IL-1 β , IL-6, IL-8 and TNF- α . While blocking HOTAIR could suppress cleavage of caspase-3 and p62 proteins and elevated secretion of IL-6 and TNF- α *via* suppression of miR222-3p (43). Meanwhile, HOTAIR inhibited chondrocytes proliferation *via* sponging with other miRNAs, including miR130a-3p (44), miR1277-5p (45), miR107 (46), and miR221 (192). Therefore, all HOTAIR-related factors form a comprehensive regulatory network, suggesting the central role of HOTAIR in the physiology of chondrocytes during OA (130).

Collectively, the identification of disease-specific lncRNAs for OA pathophysiology, including H19, GAS5, MALAT1, XIST,

HOTAIR and future identified lncRNAs, emphasized the general consistency of lncRNAs functions in various tissues, which might be further developed as lncRNAs-targeted therapies for OA treatment in the future.

Targeting lncRNAs: A novel treatment strategy for OA?

Based on current evidence, it is worthwhile to explore if targeting lncRNAs could be a novel strategy for preventing and/or treating OA. Till now, according to clinical trials registries (clinicaltrials.gov), there is only one registered clinical trial studying the role of lncRNAs as biomarkers for OA articular microenvironment. Without relevant clinical studies can be included for discussion, we attempted to propose strategies developed for lncRNA delivery and targeting with reference to published animal studies (Figure 2).

Extracellular vesicles hold some promise to be a vehicle for selective delivery of target genes into tissues of interest (193). In animal study, intra-articular injection of exosomes with overexpressed lncRNA H19 is found to promote cartilage repair and restore OA joint homeostasis (194). Liu and colleagues highlighted the possible mechanism for OA therapy

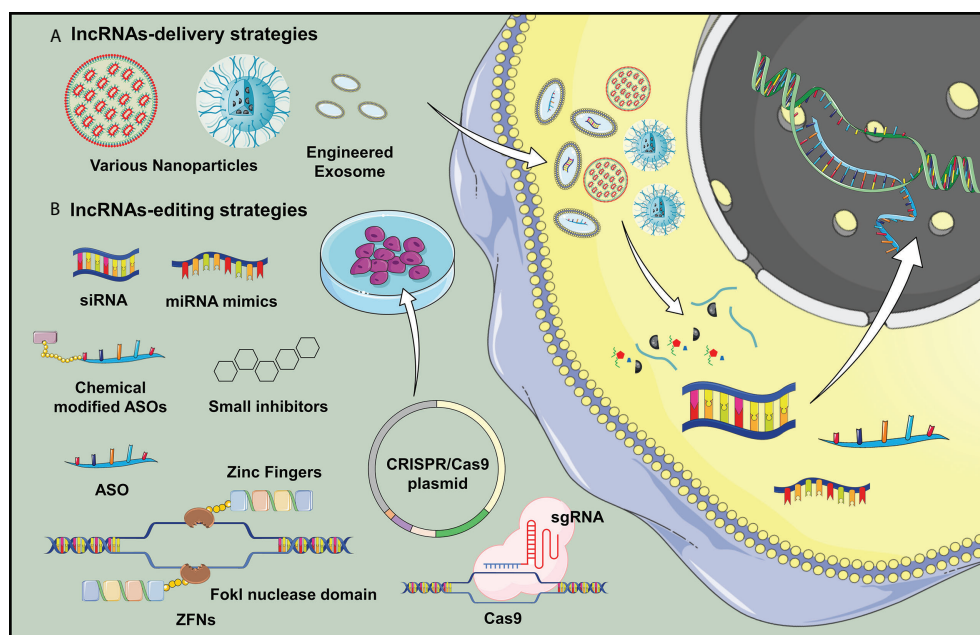


FIGURE 2

Potential delivery strategies for lncRNA H19 is proposed in OA treatment. (A) Nanotechnology and lncRNA-loaded exosomes could overcome the low efficiency of *in vivo* transgene lncRNA transfection, which would be applicable for widespread clinical application of gene therapy targeting lncRNAs. (B) Various transgene technologies may benefit lncRNA overexpression or downregulations *in vivo* studies, which opened a new door in studying the delivery of genetic material for OA treatment.

by cellular delivery of exosomal lncRNA KLF3-AS1, which could facilitate cartilage repair by promoting chondrocyte proliferation and migration and inhibiting apoptosis (195). Zhang and colleagues also reported that targeting lncRNA NEAT1 through artificial exosomes could be one of the options to elevate chondrocyte proliferation for OA treatment (196). Pan and colleagues confirmed the effect of MALAT1 on chondrocytes, which exhibited a slight cartilage damage and a smooth surface after intra-articular injection of LAMAT1 extracellular vesicles in OA animal model (179). In addition, the use of nanoparticles as an effective delivery vehicle for targeting lncRNAs provides a new therapeutic strategy owing to improved stability, biocompatibility, and high-dose therapeutic payloads (197). Recent advancement in lipid nanoparticles, polymeric nanocarrier and metal-based delivery system provides novel approaches for delivering of nucleic acids and lncRNAs-based therapeutic agents (198–200). At the time of writing, although nanoparticle delivery strategies for targeting lncRNAs in OA field has not been reported, therapeutic carriers, exosomes and nanomaterials pose enormous potential as vehicles loading gene-editing systems for OA treatment.

Considering upregulation of lncRNAs in OA pathogenesis appears to be the most common aberrant change, it is reasonable to propose approaches which can inhibit their expression or activity. Short interfering RNAs (siRNAs) is currently one of the *in vivo* feasible methods that has been shown to alleviate joint inflammation and decrease the expression of pro-inflammatory mediators by targeting lncRNA PVT1 in OA mice (201). Other *in vivo* approaches to regulate lncRNAs expression, such as locked nucleic acids (LNA) and ASOs have been shown to be effective to inhibit cancer progression (202, 203), which is pending for testing in OA animal models. Gene-editing enzymatic systems, such as zinc finger nucleases (ZFNs) and clustered regularly interspaced short palindromic repeats (CRISPR), are known far superior to RNAi technique for lncRNAs knockdown (204). Recently, some small molecule inhibitors are identified to systematically target lncRNA expression by masking the binding sites or disrupting the RNA structure (205).

Conclusions and future direction

Increasing evidence indicates that lncRNAs are playing certain important roles associated with the pathological changes of OA joints through diverse actions on various joint components, which is exemplified by lncRNAs H19, GAS5, MALAT1, XIST and HOTAIR in this review.

The roles of lncRNAs have been mainly investigated with OA cartilage tissues and chondrocytes, and found to participate

in the regulation of cartilage metabolism and chondrocyte function as a miRNA sponge regulating target genes expression. However, this kind of action and post-transcriptional regulation on target genes/proteins might not represent the whole picture of lncRNAs function in the context of OA. In addition, it should be admitted that the diverse methods employed in previous studies for lncRNA expression and functional analyses, such as the source of the testing cells, experimental procedures and even stimulation approaches, might lead to inconsistent findings.

In addition, the following questions remain elusive (1): the cause of lncRNAs dysregulation in the onset, development and progression of OA is still unclear. Whether the inflammation, hypoxia (26) or mechanical stress (206) are the major upstream factors leading to the aberrant expression of lncRNAs (2). Numerous miRNAs or proteins are reported to be downstream targets of lncRNAs, but their roles in line with lncRNAs dysfunction in OA pathogenesis remains largely unclear (3). In view of the diverse biological functions of lncRNAs, it is uncertain whether the effect of lncRNAs on the development and progression of OA is tissue- and/or cell-specific.

In view of the association with OA phenotypes, the clinical value of lncRNAs as biomarkers for disease severity and prognostication also draws much attention. However, it should be admitted that this kind of preliminary findings need to be validated further. It will be desired to (1) develop a standardized lncRNAs testing system, including sample preparation, extraction, selection of appropriate endogenous controls (2); other statistical approaches such as predictive value, likelihood ratio, odd ratio and so on subjecting to the purpose of the biomarkers under investigation (3); conduct a multi-center study with a larger sample size to eliminate discrepancy such as ethnicity and sampling bias (4); perform a longitudinal study to validate lncRNAs as biomarkers for OA.

It appears that the modulation of the expression and activity of lncRNAs might be a novel strategy for OA management. Despite therapeutic nucleic acids have been reported in OA treatment, several technical concerns including mechanism of action and an effective and specific delivery approach are not fully understood nor developed for OA application. Furthermore, the clinical application of lncRNAs-based therapy requires more stringent and robust investigation particularly safety issues including immunogenicity, cytotoxicity and long-term safety profile (207). In addition, the specificity of targeting lncRNAs is very important, and further studies are needed to avoid off-target side effects. Last but not least, a suitable target lncRNAs would lead to a more effective approach for OA treatment, and the focus of disease-specific lncRNAs described herein might draw some attention collaterally as the fields of gene-delivery and editing therapy develop.

Author contributions

RL prepared the draft of the manuscript, which was revised by HS and WL. All authors have read and approved the final version of the manuscript.

Funding

This work was partly supported by the General Research Fund (Ref. No. 24121622), Area of Excellence (Ref. No. AoE/M-402/20) and Research Matching Grant Scheme, University Grants Committee, Hong Kong; Start-up Fund, The Chinese University of Hong Kong, Hong Kong; Innovation and Technology Fund (Ref. No. PRP/090/20FX), Hong Kong; 2020 Rising Star Award provided by American Society for Bone and Mineral Research.

References

- Katz JN, Arant KR, Loeser RF. Diagnosis and treatment of hip and knee osteoarthritis: A review. *JAMA* (2021) 325(6):568–78. doi: 10.1001/jama.2020.22171
- Hunter DJ, Bierma-Zeinstra S. Osteoarthritis. *Lancet* (2019) 393(10182):1745–59. doi: 10.1016/S0140-6736(19)30417-9
- Hunter DJ, Schofield D, Callander E. The individual and socioeconomic impact of osteoarthritis. *Nat Rev Rheumatol* (2014) 10(7):437–41. doi: 10.1038/nrrheum.2014.44
- Hu Y, Chen X, Wang S, Jing Y, Su J. Subchondral bone microenvironment in osteoarthritis and pain. *Bone Res* (2021) 9(1):20. doi: 10.1038/s41413-021-00147-z
- Mobasheri A, Rayman MP, Gualillo O, Sellam J, van der Kraan P, Fearon U. The Role of Metabolism in the Pathogenesis of Osteoarthritis. *Nat Rev Rheumatol* (2017) 13(5):302–11. doi: 10.1038/nrrheum.2017.50
- Zhang Y, Liu T, Yang H, He F, Zhu X. Melatonin: A novel candidate for the treatment of osteoarthritis. *Ageing Res Rev* (2022) 78:101635. doi: 10.1016/j.arr.2022.101635
- Okuyan HM, Begon MA. LncRNAs in osteoarthritis. *Clin Chim Acta* (2022) 532:145–63. doi: 10.1016/j.cca.2022.05.030
- Budd E, Nalesso G, Mobasheri A. Extracellular genomic biomarkers of osteoarthritis. *Expert Rev Mol Diagn* (2018) 18(1):55–74. doi: 10.1080/14737159.2018.1415757
- Chen T, Weng W, Liu Y, Aspera-Werz RH, Nussler AK, Xu J. Update on novel non-operative treatment for osteoarthritis: Current status and future trends. *Front Pharmacol* (2021) 12:755230. doi: 10.3389/fphar.2021.755230
- Madry H. Surgical therapy in osteoarthritis. *Osteoarthritis Cartilage* (2022) 30(8):1019–34. doi: 10.1016/j.joca.2022.01.012
- Zhu X, Chen F, Lu K, Wei A, Jiang Q, Cao W. PPARgamma preservation via promoter demethylation alleviates osteoarthritis in mice. *Ann Rheum Dis* (2019) 78(10):1420–9. doi: 10.1136/annrheumdis-2018-214940
- Kapranov P, Cheng J, Dike S, Nix DA, Duttagupta R, Willingham AT, et al. RNA Maps reveal new RNA classes and a possible function for pervasive transcription. *Science* (2007) 316(5830):1484–8. doi: 10.1126/science.1138341
- Bartel DP. MicroRNAs: target recognition and regulatory functions. *Cell* (2009) 136(2):215–33. doi: 10.1016/j.cell.2009.01.002
- Abbasifard M, Kamiab Z, Bagheri-Hosseiniabadi Z, Sadeghi I. The role and function of long non-coding RNAs in osteoarthritis. *Exp Mol Pathol* (2020) 114:104407. doi: 10.1016/j.yexmp.2020.104407
- Ali SA, Peffers MJ, Ormseth MJ, Jurisica I, Kapoor M. The non-coding RNA interactome in joint health and disease. *Nat Rev Rheumatol* (2021) 17(11):692–705. doi: 10.1038/s41584-021-00687-y
- Xie F, Liu YL, Chen XY, Li Q, Zhong J, Dai BY, et al. Role of MicroRNA, LncRNA, and exosomes in the progression of osteoarthritis: A review of recent literature. *Orthop Surg* (2020) 12(3):708–16. doi: 10.1111/os.12690
- Wang J, Sun Y, Liu J, Yang B, Wang T, Zhang Z, et al. Roles of long noncoding RNA in osteoarthritis (Review). *Int J Mol Med* (2021) 48(1):133–40. doi: 10.3892/ijmm.2021.4966
- Ghafouri-Fard S, Poulet C, Malaise M, Abak A, Mahmud Hussien B, Taheriazam A, et al. The emerging role of non-coding RNAs in osteoarthritis. *Front Immunol* (2021) 12:773171. doi: 10.3389/fimmu.2021.773171
- McCabe EM, Rasmussen TP. LncRNA involvement in cancer stem cell function and epithelial-mesenchymal transitions. *Semin Cancer Biol* (2020) 75:38–48. doi: 10.1016/j.semcancer.2020.12.012
- Thomson DW, Dinger ME. Endogenous microRNA sponges: Evidence and controversy. *Nat Rev Genet* (2016) 17(5):272–83. doi: 10.1038/nrg.2016.20
- Long Y, Wang X, Youmans DT, Cech TR. How do lncRNAs regulate transcription? *Sci Adv* (2017) 3(9):eaao2110. doi: 10.1126/sciadv.aao2110
- Mercer TR, Dinger ME, Mattick JS. Long non-coding RNAs: Insights into functions. *Nat Rev Genet* (2009) 10(3):155–9. doi: 10.1038/nrg2521
- Qian X, Yang J, Qiu Q, Li X, Jiang C, Li J, et al. LCAT3, a novel m6A-regulated long non-coding RNA, plays an oncogenic role in lung cancer via binding with FUBP1 to activate c-MYC. *J Hematol Oncol* (2021) 14(1):112. doi: 10.1186/s13045-021-01123-0
- Chen LL. Linking long noncoding RNA localization and function. *Trends Biochem Sci* (2016) 41(9):761–72. doi: 10.1016/j.tibs.2016.07.003
- Kraus VB, Blanco FJ, Englund M, Karsdal MA, Lohmander LS. Call for standardized definitions of osteoarthritis and risk stratification for clinical trials and clinical use. *Osteoarthritis Cartilage* (2015) 23(8):1233–41. doi: 10.1016/j.joca.2015.03.036
- Steck E, Boeuf S, Gabler J, Werth N, Schnatzer P, Diederichs S, et al. Regulation of H19 and its encoded microRNA-675 in osteoarthritis and under anabolic and catabolic *in vitro* conditions. *J Mol Med (Berl)* (2012) 90(10):1185–95. doi: 10.1007/s00109-012-0895-y
- Zhang X, Liu X, Ni X, Feng P, Wang YU. Long non-coding RNA H19 modulates proliferation and apoptosis in osteoarthritis via regulating miR-106a-5p. *J Biosci* (2019) 44(6):128–37. doi: 10.1007/s12038-019-9943-x
- Zhou Y, Li J, Xu F, Ji E, Wang C, Pan Z. Long noncoding RNA H19 alleviates inflammation in osteoarthritis through interactions between TP53, IL-38, and IL-36 receptor. *Bone Joint Res* (2022) 11(8):594–607. doi: 10.1302/2046-3758.118.BJR-2021-0188.R1
- Yang B, Xu L, Wang S. Regulation of lncRNA-H19/miR-140-5p in cartilage matrix degradation and calcification in osteoarthritis. *Ann Palliat Med* (2020) 9(4):1896–904. doi: 10.21037/apm-20-929
- Stuhlmüller B, Kunisch E, Franz J, Martinez-Gamboa L, Hernandez MM, Pruss A, et al. Detection of oncofetal h19 RNA in rheumatoid arthritis synovial tissue. *Am J Pathol* (2003) 163(3):901–11. doi: 10.1016/S0002-9440(10)63450-5
- Song J, Ahn C, Chun CH, Jin EJ. A long non-coding RNA, GAS5, plays a critical role in the regulation of miR-21 during osteoarthritis. *J Orthop Res* (2014) 32(12):1628–35. doi: 10.1002/jor.22718
- Ji Q, Qiao X, Liu Y, Wang D, Yan J. Silencing of longchain noncoding RNA GAS5 in osteoarthritic chondrocytes is mediated by targeting the miR34a/Bcl2 axis. *Mol Med Rep* (2020) 21(3):1310–9. doi: 10.3892/mmr.2019.10900. doi: 10.26355/currev_202011_23582.

Conflict of interest

The authors declare that the research was conducted in the absence of any commercial or financial relationships that could be construed as a potential conflict of interest.

Publisher's note

All claims expressed in this article are solely those of the authors and do not necessarily represent those of their affiliated organizations, or those of the publisher, the editors and the reviewers. Any product that may be evaluated in this article, or claim that may be made by its manufacturer, is not guaranteed or endorsed by the publisher.

33. Gao ST, Yu YM, Wan LP, Liu ZM, Lin JX. LncRNA GAS5 induces chondrocyte apoptosis by down-regulating miR-137. *Eur Rev Med Pharmacol Sci* (2020) 24(21):10984–91. doi: 10.26355/eurrev_202011_23582
34. Cai L, Huang N, Zhang X, Wu S, Wang L, Ke Q. Long non-coding RNA plasmacytoma variant translocation 1 and growth arrest specific 5 regulate each other in osteoarthritis to regulate the apoptosis of chondrocytes. *Bioengineered* (2022) 13(5):13680–8. doi: 10.1080/21655979.2022.2063653
35. Liu C, Ren S, Zhao S, Wang Y. LncRNA MALAT1/miR-145 adjusts IL-1 β -induced chondrocytes viability and cartilage matrix degradation by regulating ADAMTS5 in human osteoarthritis. *Yonsei Med J* (2019) 60(11):1081–92. doi: 10.3349/ymj.2019.60.11.1081
36. Liang J, Xu L, Zhou F, Liu AM, Ge HX, Chen YY, et al. MALAT1/miR-127-5p regulates osteopontin (OPN)-mediated proliferation of human chondrocytes through PI3K/Akt pathway. *J Cell Biochem* (2018) 119(1):431–9. doi: 10.1002/jcb.26200
37. Nanus DE, Wijesinghe SN, Pearson MJ, Hadjicharalambous MR, Rosser A, Davis ET, et al. Regulation of the inflammatory synovial fibroblast phenotype by metastasis-associated lung adenocarcinoma transcript 1 long noncoding RNA in obese patients with osteoarthritis. *Arthritis Rheumatol* (2020) 72(4):609–19. doi: 10.1002/art.41158
38. Alnajjar FA, Sharma-Oates A, Wijesinghe SN, Farah H, Nanus DE, Nicholson T, et al. The expression and function of metastases associated lung adenocarcinoma transcript-1 long non-coding RNA in subchondral bone and osteoblasts from patients with osteoarthritis. *Cells* (2021) 10(4):786–92. doi: 10.3390/cells10040786
39. Liu Y, Liu K, Tang C, Shi Z, Jing K, Zheng J. Long non-coding RNA XIST contributes to osteoarthritis progression via miR-149-5p/DNMT3A axis. *BioMed Pharmacother* (2020) 128:110349. doi: 10.1016/j.biopha.2020.110349
40. Shen XF, Cheng Y, Dong QR, Zheng MQ. MicroRNA-675-3p regulates IL-1 β -stimulated human chondrocyte apoptosis and cartilage degradation by targeting GNG5. *Biochem Biophys Res Commun* (2020) 527(2):458–65. doi: 10.1016/j.bbrc.2020.04.044
41. Li L, Lv G, Wang B, Kuang L. The role of lncRNA XIST/miR-211 axis in modulating the proliferation and apoptosis of osteoarthritis chondrocytes through CXCR4 and MAPK signaling. *Biochem Biophys Res Commun* (2018) 503(4):2555–62. doi: 10.1016/j.bbrc.2018.07.015
42. Li L, Lv G, Wang B, Kuang L. XIST/miR-376c-5p/OPN axis modulates the influence of proinflammatory M1 macrophages on osteoarthritis chondrocyte apoptosis. *J Cell Physiol* (2020) 235(1):281–93. doi: 10.1002/jcp.28968
43. Wang J, Luo X, Cai S, Sun J, Wang S, Wei X. Blocking HOTAIR protects human chondrocytes against IL-1 β -induced cell apoptosis, ECM degradation, inflammatory response and oxidative stress via regulating miR-222-3p/ADAM10 axis. *Int Immunopharmacol* (2021) 98:107903. doi: 10.1016/j.intimp.2021.107903
44. He B, Jiang D. HOTAIR-induced apoptosis is mediated by sponging miR-130a-3p to repress chondrocyte autophagy in knee osteoarthritis. *Cell Biol Int* (2020) 44(2):524–35. doi: 10.1002/cbin.11253
45. Wang B, Sun Y, Liu N, Liu H. LncRNA HOTAIR modulates chondrocyte apoptosis and inflammation in osteoarthritis via regulating miR-1277-5p/SGTB axis. *Wound Repair Regen* (2021) 29(3):495–504. doi: 10.1111/wrr.12908
46. Lu J, Wu Z, Xiong Y. Knockdown of long noncoding RNA HOTAIR inhibits osteoarthritis chondrocyte injury by miR-107/CXCL12 axis. *J Orthop Surg Res* (2021) 16(1):410. doi: 10.1186/s13018-021-02547-7
47. Dou P, Hu R, Zhu W, Tang Q, Li D, Li H, et al. Long non-coding RNA HOTAIR promotes expression of ADAMTS-5 in human osteoarthritic articular chondrocytes. *Pharmazie* (2017) 72(2):113–7. doi: 10.1691/ph.2017.6649
48. Hu J, Wang Z, Shan Y, Pan Y, Ma J, Jia L. Long non-coding RNA HOTAIR promotes osteoarthritis progression via miR-17-5p/FUT2/ β -catenin axis. *Cell Death Dis* (2018) 9(7):711. doi: 10.1038/s41419-018-0746-z
49. Yang Y, Xing D, Wang Y, Jia H, Li B, Li JJ. A long non-coding RNA, HOTAIR, promotes cartilage degradation in osteoarthritis by inhibiting WIF-1 expression and activating wnt pathway. *BMC Mol Cell Biol* (2020) 21(1):53. doi: 10.1186/s12860-020-00299-6
50. Kim D, Song J, Han J, Kim Y, Chun CH, Jin EJ. Two non-coding RNAs, MicroRNA-101 and HOTTIP contribute cartilage integrity by epigenetic and homeotic regulation of integrin- α 1. *Cell Signal* (2013) 25(12):2878–87. doi: 10.1016/j.cellsig.2013.08.034
51. He X, Gao K, Lu S, Wu R. LncRNA HOTTIP leads to osteoarthritis progression via regulating miR-663a/Fyn-related kinase axis. *BMC Musculoskelet Disord* (2021) 22(1):67. doi: 10.1186/s12891-020-03861-7
52. Liu Q, Zhang X, Dai L, Hu X, Zhu J, Li L, et al. Long noncoding RNA related to cartilage injury promotes chondrocyte extracellular matrix degradation in osteoarthritis. *Arthritis Rheumatol* (2014) 66(4):969–78. doi: 10.1002/art.38309
53. Li YF, Li SH, Liu Y, Luo YT. Long noncoding RNA CIR promotes chondrocyte extracellular matrix degradation in osteoarthritis by acting as a sponge for mir-27b. *Cell Physiol Biochem* (2017) 43(2):602–10. doi: 10.1159/000480532
54. Wang CL, Peng JP, Chen XD. LncRNA-CIR promotes articular cartilage degeneration in osteoarthritis by regulating autophagy. *Biochem Biophys Res Commun* (2018) 505(3):692–8. doi: 10.1016/j.bbrc.2018.09.163
55. Liu Q, Hu X, Zhang X, Dai L, Duan X, Zhou C, et al. The TMSB4 pseudogene lncRNA functions as a competing endogenous RNA to promote cartilage degradation in human osteoarthritis. *Mol Ther* (2016) 24(10):1726–33. doi: 10.1038/mt.2016.151
56. Zhao Y, Zhao J, Guo X, She J, Liu Y. Long non-coding RNA PVT1, a molecular sponge for miR-149, contributes aberrant metabolic dysfunction and inflammation in IL-1 β -simulated osteoarthritic chondrocytes. *Biosci Rep* (2018) 38(5):1–11. doi: 10.1042/BSR20180576
57. Lu X, Yu Y, Yin F, Yang C, Li B, Lin J, et al. Knockdown of PVT1 inhibits IL-1 β -induced injury in chondrocytes by regulating miR-27b-3p/TRAFA3 axis. *Int Immunopharmacol* (2020) 79:106052. doi: 10.1016/j.intimp.2019.106052
58. Park S, Lee M, Chun CH, Jin EJ. The lncRNA, nespas, is associated with osteoarthritis progression and serves as a potential new prognostic biomarker. *Cartilage* (2019) 10(2):148–56. doi: 10.1177/1947603517725566
59. Wang G, Bu X, Zhang Y, Zhao X, Kong Y, Ma L, et al. LncRNA-UCA1 enhances MMP-13 expression by inhibiting miR-204-5p in human chondrocytes. *Oncotarget* (2017) 8(53):91281–90. doi: 10.18632/oncotarget.20108
60. Fan X, Yuan J, Xie J, Pan Z, Yao X, Sun X, et al. Long non-protein coding RNA DANCER functions as a competing endogenous RNA to regulate osteoarthritis progression via miR-577/SphK2 axis. *Biochem Biophys Res Commun* (2018) 500(3):658–64. doi: 10.1016/j.bbrc.2018.04.130
61. Zhang L, Zhang P, Sun X, Zhou L, Zhao J. Long non-coding RNA DANCER regulates proliferation and apoptosis of chondrocytes in osteoarthritis via miR-216a-5p/JAK2-STAT3 axis. *Biosci Rep* (2018) 38(6):1–11. doi: 10.1042/BSR20181228
62. Li XP, Wei X, Wang SQ, Sun G, Zhao YC, Yin H, et al. Differentiation antagonizing non-protein coding RNA knockdown alleviates lipopolysaccharide-induced inflammatory injury and apoptosis in human chondrocyte primary chondrocyte cells through upregulating miRNA-19a-3p. *Orthop Surg* (2021) 13(1):276–84. doi: 10.1111/os.12845
63. Sun J, Song X, Su L, Cao S. Long non-coding RNA LncHIFCAR promotes osteoarthritis development via positively regulating HIF-1 α and activating the PI3K/AKT/mTOR pathway. *Int J Clin Exp Pathol* (2018) 11(6):3000–9.
64. Zhu JK, He TD, Wei ZX, Wang YM. LncRNA FAS-AS1 promotes the degradation of extracellular matrix of cartilage in osteoarthritis. *Eur Rev Med Pharmacol Sci* (2018) 22(10):2966–72. doi: 10.26355/eurrev_201805_15051
65. Cao L, Wang Y, Wang Q, Huang J. LncRNA FOXD2-AS1 regulates chondrocyte proliferation in osteoarthritis by acting as a sponge of miR-206 to modulate CCND1 expression. *BioMed Pharmacother* (2018) 106:1220–6. doi: 10.1016/j.biopha.2018.07.048
66. Tang L, Ding J, Zhou G, Liu Z. LncRNAp21 promotes chondrocyte apoptosis in osteoarthritis by acting as a sponge for miR451. *Mol Med Rep* (2018) 18(6):5295–301. doi: 10.3892/mmr.2018.9506
67. Li Y, Li Z, Li C, Zeng Y, Liu Y. Long noncoding RNA TM1P3 is involved in osteoarthritis by mediating chondrocyte extracellular matrix degradation. *J Cell Biochem* (2019) 120(8):12702–12. doi: 10.1002/jcb.28539
68. Huang B, Yu H, Li Y, Zhang W, Liu X. Upregulation of long noncoding TNFSF10 contributes to osteoarthritis progression through the miR-376-3p/FGFR1 axis. *J Cell Biochem* (2019) 120(12):19610–20. doi: 10.1002/jcb.29267
69. Wei W, He S, Wang Z, Dong J, Xiang D, Li Y, et al. LINC01534 promotes the aberrant metabolic dysfunction and inflammation in IL-1 β -simulated osteoarthritic chondrocytes by targeting miR-140-5p. *Cartilage* (2021) 13(2_suppl):898S–907S. doi: 10.1177/1947603519888787
70. Xue H, Yu P, Wang WZ, Niu YY, Li X. The reduced lncRNA NKILA inhibited proliferation and promoted apoptosis of chondrocytes via miR-145/SP1/NF- κ B signaling in human osteoarthritis. *Eur Rev Med Pharmacol Sci* (2020) 24(2):535–48. doi: 10.26355/eurrev_202001_20030
71. Zhang Y, Ma L, Wang C, Wang L, Guo Y, Wang G. Long noncoding RNA LINC00461 induced osteoarthritis progression by inhibiting miR-30a-5p. *Aging (Albany NY)* (2020) 12(5):4111–23. doi: 10.18632/aging.102839
72. Chen K, Fang H, Xu N. LncRNA LOXL1-AS1 is transcriptionally activated by JUND and contributes to osteoarthritis progression via targeting the miR-423-5p/KDM5C axis. *Life Sci* (2020) 258:118095. doi: 10.1016/j.lfs.2020.118095
73. Zhou L, Gu M, Ma X, Wen L, Zhang B, Lin Y, et al. Long non-coding RNA PCAT-1 regulates apoptosis of chondrocytes in osteoarthritis by sponging miR-27b-3p. *J Bone Miner Metab* (2021) 39(2):139–47. doi: 10.1007/s00774-020-01128-8
74. Zhang G, Zhang Q, Zhu J, Tang J, Nie M. LncRNA ARFRP1 knockdown inhibits LPS-induced the injury of chondrocytes by regulation of NF- κ B pathway through modulating miR-15a-5p/TLR4 axis. *Life Sci* (2020) 261:118429. doi: 10.1016/j.lfs.2020.118429

75. Li Z, Wang J, Yang J. TUG1 knockdown promoted viability and inhibited apoptosis and cartilage ECM degradation in chondrocytes via the miR-17-5p/FUT1 pathway in osteoarthritis. *Exp Ther Med* (2020) 20(6):154. doi: 10.3892/etm.2020.9283
76. Chen C, Xu Y. Long noncoding RNA LINC00671 exacerbates osteoarthritis by promoting ONECUT2-mediated Smurf2 expression and extracellular matrix degradation. *Int Immunopharmacol* (2021) 90:106846. doi: 10.1016/j.intimp.2020.106846
77. Lu JF, Qi LG, Zhu XB, Shen YX. LncRNA RMRP knockdown promotes proliferation and inhibits apoptosis in osteoarthritis chondrocytes by miR-206/CDK9 axis. *Pharmazie* (2020) 75(10):500–4. doi: 10.1691/ph.2020.0591
78. Aili D, Wu T, Gu Y, Chen Z, Wang W. Knockdown of long non-coding RNA KCNQ1OT1 suppresses the progression of osteoarthritis by mediating the miR-211-5p/TCF4 axis *in vitro*. *Exp Ther Med* (2021) 21(5):455. doi: 10.3892/etm.2021.9886
79. Wang B, Liu X. Long non-coding RNA KCNQ1OT1 promotes cell viability and migration as well as inhibiting degradation of CHON-001 cells by regulating miR-126-5p/TRPS1 axis. *Adv Rheumatol* (2021) 61(1):31. doi: 10.1186/s42358-021-00187-3
80. Li X, Li Y, Yang X, Liao R, Chen L, Guo Q, et al. PR11-364P22.2/ATF3 protein interaction mediates IL-1 β -induced catabolic effects in cartilage tissue and chondrocytes. *J Cell Mol Med* (2021) 25(13):6188–202. doi: 10.1111/jcmm.16561
81. Jiang M, Xu K, Ren H, Wang M, Hou X, Cao J. Role of lincRNA-Cox2 targeting miR-150 in regulating the viability of chondrocytes in osteoarthritis. *Exp Ther Med* (2021) 22(2):800. doi: 10.3892/etm.2021.10232
82. Zhou C, He T, Chen L. LncRNA CASC19 accelerates chondrocytes apoptosis and proinflammatory cytokine production to exacerbate osteoarthritis progression through regulating the miR-152-3p/DDX6 axis. *J Orthop Surg Res* (2021) 16(1):399. doi: 10.1186/s13018-021-02543-x
83. Long H, Li Q, Xiao Z, Yang B. LncRNA MIR22HG promotes osteoarthritis progression via regulating miR-9-3p/ADAMTS5 pathway. *Bioengineered* (2021) 12(1):3148–58. doi: 10.1080/21655979.2021.1945362
84. Wang Z, Huang C, Zhao C, Zhang H, Zhen Z, Xu D. Knockdown of LINC01385 inhibits osteoarthritis progression by modulating the microRNA-140-3p/TLR4 axis. *Exp Ther Med* (2021) 22(5):1244. doi: 10.3892/etm.2021.10679
85. Xu Y, Duan L, Liu S, Yang Y, Qiao Z, Shi L. Long intergenic non-protein coding RNA 00707 regulates chondrocyte apoptosis and proliferation in osteoarthritis by serving as a sponge for microRNA-199-3p. *Bioengineered* (2022) 13(4):11137–45. doi: 10.1080/21655979.2022.2061287
86. Qian M, Shi Y, Lu W. LINC00707 knockdown inhibits IL-1 β -induced apoptosis and extracellular matrix degradation of osteoarthritis chondrocytes by the miR-330-5p/FSHR axis. *Immunopharmacol Immunotoxicol* (2022) 44(4):1–11. doi: 10.1080/08923973.2022.2076241
87. Ren J, Li Y, Wuermanbieke S, Hu S, Huang G. N(6)-methyladenosine (m(6)A) methyltransferase METTL3-mediated LINC00680 accelerates osteoarthritis through m(6)A/SIRT1 manner. *Cell Death Discovery* (2022) 8(1):240. doi: 10.1038/s41420-022-00890-0
88. Tang S, Cao Y, Cai Z, Nie X, Ruan J, Zhou Z, et al. The lncRNA PILA promotes NF- κ B signaling in osteoarthritis by stimulating the activity of the protein arginine methyltransferase PRMT1. *Sci Signal* (2022) 15(735):eabm6265. doi: 10.1126/scisignal.abm6265
89. Wu X, Yin S, Yan L, Liu Y, Shang L, Liu J. LncRNA DLEU1 modulates proliferation, inflammation, and extracellular matrix degradation of chondrocytes through regulating miR-671-5p. *J Immunol Res* (2022) 2022:1816217. doi: 10.1155/2022/1816217
90. Su W, Xie W, Shang Q, Su B. The long noncoding RNA MEG3 is downregulated and inversely associated with VEGF levels in osteoarthritis. *BioMed Res Int* (2015) 2015:356893. doi: 10.1155/2015/356893
91. Wang A, Hu N, Zhang Y, Chen Y, Su C, Lv Y, et al. MEG3 promotes proliferation and inhibits apoptosis in osteoarthritis chondrocytes by miR-361-5p/FOXO1 axis. *BMC Med Genomics* (2019) 12(1):201. doi: 10.1186/s12920-019-0649-6
92. Pearson MJ, Philp AM, Heward JA, Roux BT, Walsh DA, Davis ET, et al. Long intergenic noncoding RNAs mediate the human chondrocyte inflammatory response and are differentially expressed in osteoarthritis cartilage. *Arthritis Rheumatol* (2016) 68(4):845–56. doi: 10.1002/art.39520
93. Zheng J, Li Q. Methylene blue regulates inflammatory response in osteoarthritis by noncoding long chain RNA CILINC02. *J Cell Biochem* (2019) 120(3):3331–8. doi: 10.1002/jcb.27602
94. Zhang G, Wu Y, Xu D, Yan X. Long noncoding RNA UFC1 promotes proliferation of chondrocyte in osteoarthritis by acting as a sponge for miR-34a. *DNA Cell Biol* (2016) 35(11):691–5. doi: 10.1089/dna.2016.3397
95. Shen H, Wang Y, Shi W, Sun G, Hong L, Zhang Y. LncRNA SNHG5/miR-26a/SOX2 signal axis enhances proliferation of chondrocyte in osteoarthritis. *Acta Biochim Biophys Sin (Shanghai)* (2018) 50(2):191–8. doi: 10.1093/abbs/gmx141
96. Zhang X, Huang CR, Pan S, Pang Y, Chen YS, Zha GC, et al. Long non-coding RNA SNHG15 is a competing endogenous RNA of miR-141-3p that prevents osteoarthritis progression by upregulating BCL2L13 expression. *Int Immunopharmacol* (2020) 83:106425. doi: 10.1016/j.intimp.2020.106425
97. Jiang H, Pang H, Wu P, Cao Z, Li Z, Yang X. LncRNA SNHG5 promotes chondrocyte proliferation and inhibits apoptosis in osteoarthritis by regulating miR-10a-5p/H3F3B axis. *Connect Tissue Res* (2021) 62(6):605–14. doi: 10.1080/03008207.2020.1825701
98. Yue Y, Zhibo S, Feng L, Yuanzhang B, Fei W. SNHG5 protects chondrocytes in interleukin-1 β -stimulated osteoarthritis via regulating miR-181a-5p/TGFB3 axis. *J Biochem Mol Toxicol* (2021) 35(10):e22866. doi: 10.1002/jbt.22866
99. Xiao Y, Yan X, Yang Y, Ma X. Downregulation of long noncoding RNA HOTAIRM1 variant 1 contributes to osteoarthritis via regulating miR-125b/BMP2 axis and activating JNK/MAPK/ERK pathway. *BioMed Pharmacother* (2019) 109:1569–77. doi: 10.1016/j.biopha.2018.10.181
100. Yang Q, Li X, Zhou Y, Fu W, Wang J, Wei Q. A LINC00341-mediated regulatory pathway supports chondrocyte survival and may prevent osteoarthritis progression. *J Cell Biochem* (2019) 120(6):10812–20. doi: 10.1002/jcb.28372
101. Ai D, Yu F. LncRNA DNMT3OS promotes proliferation and inhibits apoptosis through modulating IGF1 expression by sponging MiR-126 in CHON-001 cells. *Diagn Pathol* (2019) 14(1):106. doi: 10.1186/s13000-019-0877-2
102. Lu C, Li Z, Hu S, Cai Y, Peng K. LncRNA PART-1 targets TGFBR2/Smad3 to regulate cell viability and apoptosis of chondrocytes via acting as miR-590-3p sponge in osteoarthritis. *J Cell Mol Med* (2019) 23(12):8196–205. doi: 10.1111/jcmm.14690
103. Zhu YJ, Jiang DM. LncRNA PART1 modulates chondrocyte proliferation, apoptosis, and extracellular matrix degradation in osteoarthritis via regulating miR-373-3p/SOX4 axis. *Eur Rev Med Pharmacol Sci* (2019) 23(19):8175–85. doi: 10.26355/eurrev_201910_19124
104. Liu F, Liu X, Yang Y, Sun Z, Deng S, Jiang Z, et al. NEAT1/miR-193a-3p/SOX5 axis regulates cartilage matrix degradation in human osteoarthritis. *Cell Biol Int* (2020) 44(4):947–57. doi: 10.1002/cbin.11291
105. Xiao P, Zhu X, Sun J, Zhang Y, Qiu W, Li J, et al. LncRNA NEAT1 regulates chondrocyte proliferation and apoptosis via targeting miR-543/PLA2G4A axis. *Hum Cell* (2021) 34(1):60–75. doi: 10.1007/s13577-020-00433-8
106. Lu M, Zhou E. Long noncoding RNA LINC00662-miR-15b-5p mediated GPR120 dysregulation contributes to osteoarthritis. *Pathol Int* (2020) 70(3):155–65. doi: 10.1111/pin.12875
107. Zhi L, Zhao J, Zhao H, Qing Z, Liu H, Ma J. Downregulation of LncRNA OIP5-AS1 induced by IL-1 β aggravates osteoarthritis via regulating miR-29b-3p/PGRN. *Cartilage* (2021) 13(2_suppl):1345S–55S. doi: 10.1177/1947603519900801
108. Lu G, Li L, Wang B, Kuang L. LINC00623/miR-101/HRAS axis modulates IL-1 β -mediated ECM degradation, apoptosis and senescence of osteoarthritis chondrocytes. *Aging (Albany NY)* (2020) 12(4):3218–37. doi: 10.18632/aging.102801
109. Xu J, Pei Y, Lu J, Liang X, Li Y, Wang J, et al. LncRNA SNHG7 alleviates IL-1 β -induced osteoarthritis by inhibiting miR-214-5p-mediated PPARGC1B signaling pathways. *Int Immunopharmacol* (2021) 90:107150. doi: 10.1016/j.intimp.2020.107150
110. Feng L, Yang ZM, Li YC, Wang HX, Lo JHT, Zhang XT, et al. Linc-ROR promotes mesenchymal stem cells chondrogenesis and cartilage formation via regulating SOX9 expression. *Osteoarthritis Cartilage* (2021) 29(4):568–78. doi: 10.1016/j.joca.2020.12.020
111. Qin GH, Yang WC, Yao JN, Zhao Y, Wu XJ. LncRNA OIP5-AS1 affects the biological behaviors of chondrocytes of patients with osteoarthritis by regulating micro-30a-5p. *Eur Rev Med Pharmacol Sci* (2021) 25(3):1215–24. doi: 10.26355/eurrev_202102_24825
112. Yang Y, Sun Z, Liu F, Bai Y, Wu F. FGD5-AS1 inhibits osteoarthritis development by modulating miR-302d-3p/TGFB2 axis. *Cartilage* (2021) 13(2_suppl):1412S–20S. doi: 10.1177/19476035211003324
113. Shi J, Cao F, Chang Y, Xin C, Jiang X, Xu J, et al. Long non-coding RNA MCM3AP-AS1 protects chondrocytes ATDC5 and CHON-001 from IL-1 β -induced inflammation via regulating miR-138-5p/SIRT1. *Bioengineered* (2021) 12(1):1445–56. doi: 10.1080/21655979.2021.1905247
114. Xie W, Jiang L, Huang X, Shang H, Gao M, You W, et al. LncRNA MEG8 is downregulated in osteoarthritis and regulates chondrocyte cell proliferation, apoptosis and inflammation. *Exp Ther Med* (2021) 22(4):1153. doi: 10.3892/etm.2021.10587
115. Gu Y, Wang G, Xu H. Long non-coding RNA ZNF1 antisense 1 (ZFAS1) suppresses anti-oxidative stress in chondrocytes during osteoarthritis by sponging microRNA-1323. *Bioengineered* (2022) 13(5):13188–200. doi: 10.1080/21655979.2022.2074770
116. Li X, Ren W, Xiao ZY, Wu LF, Wang H, Guo PY. GACAT3 promoted proliferation of osteoarthritis synovocytes by IL-6/STAT3 signaling pathway. *Eur*

Rev Med Pharmacol Sci (2018) 22(16):5114–20. doi: 10.26355/eurrev_201808_15705

117. Li X, Huang TL, Zhang GD, Jiang JT, Guo PY. LncRNA ANRIL impacts the progress of osteoarthritis via regulating proliferation and apoptosis of osteoarthritis synoviocytes. *Eur Rev Med Pharmacol Sci* (2019) 23(22):9729–37. doi: 10.26355/eurrev_201911_19535

118. Kang Y, Song J, Kim D, Ahn C, Park S, Chun CH, et al. PCGEM1 stimulates proliferation of osteoarthritic synoviocytes by acting as a sponge for miR-770. *J Orthop Res* (2016) 34(3):412–8. doi: 10.1002/jor.23046

119. Zeng G, Deng G, Xiao S, Li F. Fibroblast-like synoviocytes-derived exosomal PCGEM1 accelerates IL-1 β -induced apoptosis and cartilage matrix degradation by miR-142-5p/RUNX2 in chondrocytes. *Immunol Invest* (2022) 51(5):1284–301. doi: 10.1080/08820139.2021.1936010

120. Jia J, Sun J, Liao W, Qin L, Su K, He Y, et al. Knockdown of long noncoding RNA AK094629 attenuates the interleukin1 β induced expression of interleukin6 in synoviumderived mesenchymal stem cells from the temporomandibular joint. *Mol Med Rep* (2020) 22(2):1195–204. doi: 10.3892/mmr.2020.11193

121. Zhang P, Sun J, Liang C, Gu B, Xu Y, Lu H, et al. LncRNA IGHGcgamma1 acts as a ceRNA to regulate macrophage inflammation via the miR-6891-3p/TLR4 axis in osteoarthritis. *Mediators Inflamm* (2020) 2020:9743037. doi: 10.1155/2020/9743037

122. Tuerlings M, van Hoolwerff M, van Bokkum JM, Suchiman HED, Lakenberg N, Broekhuijs D, et al. Long non-coding RNA expression profiling of subchondral bone reveals AC005165.1 modifying FRZB expression during osteoarthritis. *Rheumatol (Oxford)* (2021) 61(7):3023–32. doi: 10.1093/rheumatology/keab826

123. Jiang Z, Du X, Wen X, Li H, Zeng A, Sun H, et al. Whole-transcriptome sequence of degenerative meniscus cells unveiling diagnostic markers and therapeutic targets for osteoarthritis. *Front Genet* (2021) 12:754421. doi: 10.3389/fgene.2021.754421

124. Chen S, Fu P, Wu H, Pei M. Meniscus, articular cartilage and nucleus pulposus: a comparative review of cartilage-like tissues in anatomy, development and function. *Cell Tissue Res* (2017) 370(1):53–70. doi: 10.1007/s00441-017-2613-0

125. Goldring MB, Marcu KB. Cartilage homeostasis in health and rheumatic diseases. *Arthritis Res Ther* (2009) 11(3):224. doi: 10.1186/ar2592

126. Hodgkinson T, Kelly DC, Curtin CM, O'Brien FJ. Mechanosignalling in cartilage: An emerging target for the treatment of osteoarthritis. *Nat Rev Rheumatol* (2021) 18:67–84. doi: 10.1038/s41584-021-00724-w

127. Fu M, Huang G, Zhang Z, Liu J, Zhang Z, Huang Z, et al. Expression profile of long noncoding RNAs in cartilage from knee osteoarthritis patients. *Osteoarthritis Cartilage* (2015) 23(3):423–32. doi: 10.1016/j.joca.2014.12.001

128. Li X, Liao Z, Deng Z, Chen N, Zhao L. Combining bulk and single-cell RNA-sequencing data to reveal gene expression pattern of chondrocytes in the osteoarthritic knee. *Bioengineered* (2021) 12(1):997–1007. doi: 10.1080/21655979.2021.1903207

129. van Hoolwerff M, Metselaar PI, Tuerlings M, Suchiman HED, Lakenberg N, Ramos YFM, et al. Elucidating epigenetic regulation by identifying functional cis-acting long noncoding RNAs and their targets in osteoarthritic articular cartilage. *Arthritis Rheumatol* (2020) 72(11):1845–54. doi: 10.1002/art.41396

130. Tu J, Huang W, Zhang W, Mei J, Zhu C. The emerging role of lncRNAs in chondrocytes from osteoarthritis patients. *BioMed Pharmacother* (2020) 131:110642. doi: 10.1016/j.biopha.2020.110642

131. Firestein GS, McInnes IB. Immunopathogenesis of rheumatoid arthritis. *Immunity* (2017) 46(2):183–96. doi: 10.1016/j.immuni.2017.02.006

132. Doherty M. Synovial inflammation and osteoarthritis progression: effects of nonsteroidal antiinflammatory drugs. *Osteoarthritis Cartilage* (1999) 7(3):319–20. doi: 10.1053/joca.1998.0179

133. Wenham CY, Conaghan PG. The role of synovitis in osteoarthritis. *Ther Adv Musculoskelet Dis* (2010) 2(6):349–59. doi: 10.1177/1759720X10378373

134. Xiang S, Li Z, Bian Y, Weng X. Identification of changed expression of mRNAs and lncRNAs in osteoarthritic synovium by RNA-sequencing. *Gene* (2019) 685:55–61. doi: 10.1016/j.gene.2018.10.076

135. Dai G, Xiao H, Liao J, Zhou N, Zhao C, Xu W, et al. Osteocyte TGF β 1/Smad2/3 is positively associated with bone turnover parameters in subchondral bone of advanced osteoarthritis. *Int J Mol Med* (2020) 46(1):167–78. doi: 10.3892/ijmm.2020.4576

136. Suri S, Gill SE, Massena de Camin S, Wilson D, McWilliams DF, Walsh DA. Neurovascular invasion at the osteochondral junction and in osteophytes in osteoarthritis. *Ann Rheum Dis* (2007) 66(11):1423–8. doi: 10.1136/ard.2006.063354

137. Silva AM, Moura SR, Teixeira JH, Barbosa MA, Santos SG, Almeida MI. Long noncoding RNAs: a missing link in osteoporosis. *Bone Res* (2019) 7:10. doi: 10.1038/s41413-019-0048-9

138. Makris EA, Hadidi P, Athanasiou KA. The knee meniscus: structure-function, pathophysiology, current repair techniques, and prospects for regeneration. *Biomaterials* (2011) 32(30):7411–31. doi: 10.1016/j.biomaterials.2011.06.037

139. Murphy CA, Garg AK, Silva-Correia J, Reis RL, Oliveira JM, Collins MN. The meniscus in normal and osteoarthritic tissues: Facing the structure property challenges and current treatment trends. *Annu Rev BioMed Eng* (2019) 21:495–521. doi: 10.1146/annurev-bioeng-060418-052547

140. Brophy RH, Zhang B, Cai L, Wright RW, Sandell LJ, Rai MF. Transcriptome comparison of meniscus from patients with and without osteoarthritis. *Osteoarthritis Cartilage* (2018) 26(3):422–32. doi: 10.1016/j.joca.2017.12.004

141. Shi T, Gao G, Cao Y. Long noncoding RNAs as novel biomarkers have a promising future in cancer diagnostics. *Dis Markers* (2016) 2016:9085195. doi: 10.1155/2016/9085195

142. De Ceuninck F, Sabatini M, Pastoureaux P. Recent progress toward biomarker identification in osteoarthritis. *Drug Discovery Today* (2011) 16(9–10):443–9. doi: 10.1016/j.drudis.2011.01.004

143. Dang X, Lian L, Wu D. The diagnostic value and pathogenetic role of lncRNA-ATB in patients with osteoarthritis. *Cell Mol Biol Lett* (2018) 23:55. doi: 10.1186/s11658-018-0118-9

144. Zhou L, Wan Y, Cheng Q, Shi B, Zhang L, Chen S. The expression and diagnostic value of LncRNA H19 in the blood of patients with osteoarthritis. *Iran J Public Health* (2020) 49(8):1494–501. doi: 10.18502/ijph.v49i8.3893

145. Huang J, Liu L, Yang J, Ding J, Xu X. LncRNA DILC is downregulated in osteoarthritis and regulates IL-6 expression in chondrocytes. *J Cell Biochem* (2019) 120(9):16019–24. doi: 10.1002/jcb.28880

146. He J, Wang L, Ding Y, Liu H, Zou G. LncRNA FER1L4 is dysregulated in osteoarthritis and regulates IL-6 expression in human chondrocyte cells. *Sci Rep* (2021) 11(1):13032. doi: 10.1038/s41598-021-92474-8

147. Li Q, Zhang Z, Guo S, Tang G, Lu W, Qi X. LncRNA ANCR is positively correlated with transforming growth factor- β 1 in patients with osteoarthritis. *J Cell Biochem* (2019) 120(9):14226–32. doi: 10.1002/jcb.28881

148. Xiao Y, Bao Y, Tang L, Wang L. LncRNA MIR4435-2HG is downregulated in osteoarthritis and regulates chondrocyte cell proliferation and apoptosis. *J Orthop Surg Res* (2019) 14(1):247. doi: 10.1186/s13018-019-1278-7

149. Ni S, Xu C, Zhuang C, Zhao G, Li C, Wang Y, et al. LncRNA LUADT1 regulates miR-34a/SIRT1 to participate in chondrocyte apoptosis. *J Cell Biochem* (2020) 122(9):1003–8. doi: 10.1002/jcb.29637

150. Qi K, Lin R, Xue C, Liu T, Wang Y, Zhang Y, et al. Long non-coding RNA (LncRNA) CAIF is downregulated in osteoarthritis and inhibits LPS-induced interleukin 6 (IL-6) upregulation by downregulation of MiR-1246. *Med Sci Monit* (2019) 25:8019–24. doi: 10.12659/MSM.917135

151. Yang F, Zhao M, Sang Q, Yan C, Wang Z. Long non-coding RNA PMS2L2 is down-regulated in osteoarthritis and inhibits chondrocyte proliferation by up-regulating miR-34a. *J Immunotoxicol* (2022) 19(1):74–80. doi: 10.1080/1547691X.2022.2049664

152. Zhang C, Wang P, Jiang P, Lv Y, Dong C, Dai X, et al. Upregulation of lncRNA HOTAIR contributes to IL-1 β -induced MMP overexpression and chondrocytes apoptosis in temporomandibular joint osteoarthritis. *Gene* (2016) 586(2):248–53. doi: 10.1016/j.gene.2016.04.016

153. Sun Y, Kang S, Pei S, Sang C, Huang Y, et al. Mir93-5p Inhibits Chondrocyte Apoptosis in Osteoarthritis by Targeting Lncrna Casc2. *BMC Musculoskelet Disord* (2020) 21(1):26–32. doi: 10.1186/s12891-019-3025-y

154. Zhang H, Li J, Shao W, Shen N. LncRNA CTBP1-AS2 is upregulated in osteoarthritis and increases the methylation of miR-130a gene to inhibit chondrocyte proliferation. *Clin Rheumatol* (2020) 39(11):3473–8. doi: 10.1007/s10067-020-05113-4

155. Zhang D, Qiu S. LncRNA GAS5 upregulates Smad4 to suppress the apoptosis of chondrocytes induced by lipopolysaccharide. *Arch Gerontol Geriatr* (2021) 97:104478. doi: 10.1016/j.archger.2021.104478

156. Zhang H, Wu Y, Li W, Chen H. Clinical significance and mechanism of LncRNA GAS-5 in osteoarthritis. *Am J Transl Res* (2021) 13(7):8465–70.

157. Jiang L, Zhou Y, Shen J, Chen Y, Ma Z, Yu Y, et al. RNA Sequencing reveals LINC00167 as a potential diagnosis biomarker for primary osteoarthritis: A multi-stage study. *Front Genet* (2020) 11:539489. doi: 10.3389/fgene.2020.539489

158. Meng Y, Qiu S, Sun L, Zuo J. Knockdown of exosomemediated lncPVT1 alleviates lipopolysaccharideinduced osteoarthritis progression by mediating the HMGB1/TLR4/NF κ B pathway via miR935p. *Mol Med Rep* (2020) 22(6):5313–25. doi: 10.3892/mmr.2020.11594

159. Zhao Y, Xu J. Synovial fluid-derived exosomal lncRNA PCGEM1 as biomarker for the different stages of osteoarthritis. *Int Orthop* (2018) 42(12):2865–72. doi: 10.1007/s00264-018-4093-6

160. Wu X, Bian B, Lin Z, Wu C, Sun Y, Pan Y, et al. Identification of exosomal mRNA, lncRNA and circRNA signatures in an osteoarthritis synovial fluid-exosomal study. *Exp Cell Res* (2022) 410(1):112881. doi: 10.1016/j.yexcr.2021.112881
161. Wang J, Sun J, Yang F. The role of long non-coding RNA H19 in breast cancer. *Oncol Lett* (2020) 19(1):7–16. doi: 10.3892/ol.2019.11093
162. Pachnis V, Belayew A, Tilghman SM. Locus unlinked to alpha-fetoprotein under the control of the murine raf and rif genes. *Proc Natl Acad Sci U S A* (1984) 81(17):5523–7. doi: 10.1073/pnas.81.17.5523
163. Zhou X, Cao H, Wang M, Zou J, Wu W. Moderate-intensity treadmill running relieves motion-induced post-traumatic osteoarthritis mice by up-regulating the expression of lncRNA H19. *BioMed Eng Online* (2021) 20(1):111. doi: 10.1186/s12938-021-00949-6
164. Xing D, Liang JQ, Li Y, Lu J, Jia HB, Xu LY, et al. Identification of long noncoding RNA associated with osteoarthritis in humans. *Orthop Surg* (2014) 6(4):288–93. doi: 10.1111/os.12147
165. Dudek KA, Lafont JE, Martinez-Sanchez A, Murphy CL. Type II collagen expression is regulated by tissue-specific miR-675 in human articular chondrocytes. *J Biol Chem* (2010) 285(32):24381–7. doi: 10.1074/jbc.M110.111328
166. Hu Y, Li S, Zou Y. Knockdown of lncRNA H19 relieves LPS-induced damage by modulating miR-130a in osteoarthritis. *Yonsei Med J* (2019) 60(4):381–8. doi: 10.3349/ymj.2019.60.4.381
167. Wang Y, Yu D, Liu Z, Zhou F, Dai J, Wu B, et al. Exosomes from embryonic mesenchymal stem cells alleviate osteoarthritis through balancing synthesis and degradation of cartilage extracellular matrix. *Stem Cell Res Ther* (2017) 8(1):189. doi: 10.1186/s13287-017-0632-0
168. Tan F, Wang D, Yuan Z. The fibroblast-like synoviocyte derived exosomal long non-coding RNA H19 alleviates osteoarthritis progression through the miR-106b-5p/TIMP2 axis. *Inflammation* (2020) 43(4):1498–509. doi: 10.1007/s10753-020-01227-8
169. Smith CM, Steitz JA. Classification of gas5 as a multi-small-nucleolar-RNA (snoRNA) host gene and a member of the 5'-terminal oligopyrimidine gene family reveals common features of snoRNA host genes. *Mol Cell Biol* (1998) 18(12):6897–909. doi: 10.1128/MCB.18.12.6897
170. Filippova EA, Fridman MV, Burdennyy AM, Loginov VI, Pronina IV, Lukina SS, et al. Long noncoding RNA GAS5 in breast cancer: Epigenetic mechanisms and biological functions. *Int J Mol Sci* (2021) 22(13):6810–26. doi: 10.3390/ijms22136810
171. Zhou Z, Chen J, Huang Y, Liu D, Chen S, Qin S. Long noncoding RNA GAS5: A new factor involved in bone diseases. *Front Cell Dev Biol* (2021) 9:807419. doi: 10.3389/fcell.2021.807419
172. Xiao K, Yang Y, Bian Y, Feng B, Li Z, Wu Z, et al. Identification of differentially expressed long noncoding RNAs in human knee osteoarthritis. *J Cell Biochem* (2019) 120(3):4620–33. doi: 10.1002/jcb.27750
173. Ji Q, Qiao X, Liu Y, Wang D. Expression of long-chain noncoding RNA GAS5 in osteoarthritis and its effect on apoptosis and autophagy of osteoarthritis chondrocytes. *Histol Histopathol* (2021) 36(4):475–84. doi: 10.14670/HH-18-312
174. Zheng T, Zhou Q, Huang J, Lai J, Ji G, Kong D. Xanthohumol inhibited mechanical stimulation-induced articular ECM degradation by mediating lncRNA GAS5/miR-27a axis. *Front Pharmacol* (2021) 12:737552. doi: 10.3389/fphar.2021.737552
175. Li F, Sun J, Huang S, Su G, Pi G. LncRNA GAS5 overexpression reverses LPS-induced inflammatory injury and apoptosis through up-regulating KLF2 expression in ATDC5 chondrocytes. *Cell Physiol Biochem* (2018) 45(3):1241–51. doi: 10.1159/000487455
176. Muller-Tidow C, Diederichs S, Thomas M, Serve H. Genome-wide screening for prognosis-predicting genes in early-stage non-small-cell lung cancer. *Lung Cancer* (2004) 45(Suppl 2):S145–50. doi: 10.1016/j.lungcan.2004.07.979
177. Yoshimoto R, Mayeda A, Yoshida M, Nakagawa S. MALAT1 long non-coding RNA in cancer. *Biochim Biophys Acta* (2016) 1859(1):192–9. doi: 10.1016/j.bbagr.2015.09.012
178. Brown JA, Bulkley D, Wang J, Valenstein ML, Yario TA, Steitz TA, et al. Structural insights into the stabilization of MALAT1 noncoding RNA by a bipartite triple helix. *Nat Struct Mol Biol* (2014) 21(7):633–40. doi: 10.1038/nsmb.2844
179. Pan C, Huang W, Chen Q, Xu J, Yao G, Li B, et al. LncRNA malat-1 from MSCs-derived extracellular vesicles suppresses inflammation and cartilage degradation in osteoarthritis. *Front Bioeng Biotechnol* (2021) 9:772002. doi: 10.3389/fbioe.2021.772002
180. Zhang Y, Wang F, Chen G, He R, Yang L. LncRNA MALAT1 promotes osteoarthritis by modulating miR-150-5p/AKT3 axis. *Cell Biosci* (2019) 9:54. doi: 10.1186/s13578-019-0302-2
181. Li H, Xie S, Li H, Zhang R, Zhang H. LncRNA MALAT1 mediates proliferation of LPS treated-articular chondrocytes by targeting the miR-146a-P13K/Akt/mTOR axis. *Life Sci* (2020) 254:116801. doi: 10.1016/j.lfs.2019.116801
182. Gao GC, Cheng XG, Wei QQ, Chen WC, Huang WZ. Long noncoding RNA MALAT-1 inhibits apoptosis and matrix metabolism disorder in interleukin-1beta-induced inflammation in articular chondrocytes via the JNK signaling pathway. *J Cell Biochem* (2019) 120(10):17167–79. doi: 10.1002/jcb.28977
183. Cerase A, Pintacuda G, Tattermusch A, Avner P. Xist localization and function: new insights from multiple levels. *Genome Biol* (2015) 16:166. doi: 10.1186/s13059-015-0733-y
184. da Rocha ST, Heard E. Novel players in X inactivation: insights into xist-mediated gene silencing and chromosome conformation. *Nat Struct Mol Biol* (2017) 24(3):197–204. doi: 10.1038/nsmb.3370
185. Akbari Dilmaghani N, Shoori H, Sharifi G, Mohaqiq M, Majidpoor J, Dinger ME, et al. Non-coding RNAs modulate function of extracellular matrix proteins. *BioMed Pharmacother* (2021) 136:111240. doi: 10.1016/j.biopha.2021.111240
186. Wang T, Liu Y, Wang Y, Huang X, Zhao W, Zhao Z. Long non-coding RNA XIST promotes extracellular matrix degradation by functioning as a competing endogenous RNA of miR-1277-5p in osteoarthritis. *Int J Mol Med* (2019) 44(2):630–42. doi: 10.3892/ijmm.2019.4240
187. Xiao Y, Liu L, Zheng Y, Liu W, Xu Y. Kaempferol attenuates the effects of XIST/miR-130a/STAT3 on inflammation and extracellular matrix degradation in osteoarthritis. *Future Med Chem* (2021) 13(17):1451–64. doi: 10.4155/fmc-2021-0127
188. Sun P, Wu Y, Li X, Jia Y. miR-142-5p protects against osteoarthritis through competing with lncRNA XIST. *J Gene Med* (2020) 22(4):e3158. doi: 10.1002/jgm.3158
189. Rinn JL, Kertesz M, Wang JK, Squazzo SL, Xu X, Bruggmann SA, et al. Functional demarcation of active and silent chromatin domains in human HOX loci by noncoding RNAs. *Cell* (2007) 129(7):1311–23. doi: 10.1016/j.cell.2007.05.022
190. Kong W, Yin G, Zheng S, Liu X, Zhu A, Yu P, et al. Long noncoding RNA (lncRNA) HOTAIR: Pathogenic roles and therapeutic opportunities in gastric cancer. *Genes Dis* (2022) 9(5):1269–80. doi: 10.1016/j.gendis.2021.07.006
191. Chen Y, Zhang L, Li E, Zhang G, Hou Y, Yuan W, et al. Long-chain non-coding RNA HOTAIR promotes the progression of osteoarthritis via sponging miR-20b/PTEN axis. *Life Sci* (2020) 253:117685. doi: 10.1016/j.lfs.2020.117685
192. Zheng T, Huang J, Lai J, Zhou Q, Liu T, Xu Q, et al. Long non-coding RNA HOTAIR increased mechanical stimulation-induced apoptosis by regulating microRNA-221/BBC3 axis in C28/I2 cells. *Bioengineered* (2021) 12(2):10734–44. doi: 10.1080/21655979.2021.2003129
193. Herrmann IK, Wood MJA, Fuhrmann G. Extracellular vesicles as a next-generation drug delivery platform. *Nat Nanotechnol* (2021) 16(7):748–59. doi: 10.1038/s41565-021-00931-2
194. Yan L, Liu G, Wu X, et al. The Umbilical Cord Mesenchymal Stem Cell-Derived Exosomal lncRNA H19 Improves Osteochondral Activity through Mir-29b-3p/Foxo3 Axis. *Clin Transl Med* (2021) 11(1):e255–70. doi: 10.1002/ctm.255
195. Liu Y, Zou R, Wang Z, Wen C, Zhang F, Lin F. Exosomal KLF3-AS1 from hMSCs promoted cartilage repair and chondrocyte proliferation in osteoarthritis. *Biochem J* (2018) 475(22):3629–38. doi: 10.1042/BCJ20180675
196. Zhang S, Jin Z. Bone mesenchymal stem cell-derived extracellular vesicles containing long noncoding RNA NEAT1 relieve osteoarthritis. *Oxid Med Cell Longev* (2022) 2022:5517648. doi: 10.1155/2022/5517648
197. Pi YN, Qi WC, Xia BR, Lou G, Jin WL. Long non-coding RNAs in the tumor immune microenvironment: Biological properties and therapeutic potential. *Front Immunol* (2021) 12:697083. doi: 10.3389/fimmu.2021.697083
198. Vaidya AM, Sun Z, Ayat N, Schilb A, Liu X, Jiang H, et al. Systemic delivery of tumor-targeting siRNA nanoparticles against an oncogenic lncRNA facilitates effective triple-negative breast cancer therapy. *Bioconjug Chem* (2019) 30(3):907–19. doi: 10.1021/acs.bioconjchem.9b00028
199. Watanabe S, Hayashi K, Toh K, Kim HJ, Liu X, Chaya H, et al. In vivo rendezvous of small nucleic acid drugs with charge-matched block cationomers to target cancers. *Nat Commun* (2019) 10(1):1894. doi: 10.1038/s41467-019-09856-w
200. Lin B, Lu L, Wang Y, Zhang Q, Wang Z, Cheng G, et al. Nanomedicine directs neuronal differentiation of neural stem cells via silencing long noncoding RNA for stroke therapy. *Nano Lett* (2021) 21(1):806–15. doi: 10.1021/acs.nanolett.0c04560
201. Wang YZ, Yao L, Liang SK, Ding LB, Feng L, Guan J, et al. lncPVT1 promotes cartilage degradation in diabetic OA mice by downregulating miR-146a

and activating TGF-beta/SMAD4 signaling. *J Bone Miner Metab* (2021) 39(4):534–46. doi: 10.1007/s00774-020-01199-7

202. Sherman Lim YW, Xiang X, Garg M, Le MT, Li-Ann Wong A, Wang L, et al. The double-edged sword of H19 lncRNA: Insights into cancer therapy. *Cancer Lett* (2021) 500:253–62. doi: 10.1016/j.canlet.2020.11.006

203. Liu SJ, Dang HX, Lim DA, Feng FY, Maher CA. Long noncoding RNAs in cancer metastasis. *Nat Rev Cancer* (2021) 21(7):446–60. doi: 10.1038/s41568-021-00353-1

204. Gutschner T, Baas M, Diederichs S. Noncoding RNA gene silencing through genomic integration of RNA destabilizing elements using zinc finger nucleases. *Genome Res* (2011) 21(11):1944–54. doi: 10.1101/gr.122358.111

205. Aguilar R, Spencer KB, Kesner B, Rizvi NF, Badmalia MD, Mrozowich T, et al. Targeting xist with compounds that disrupt RNA structure and X inactivation. *Nature* (2022) 604:160–6. doi: 10.1038/s41586-022-04537-z

206. Wang CL, Zuo B, Li, Zhu JF, Xiao F, Zhang XL, et al. The long noncoding RNA H19 attenuates force-driven cartilage degeneration via miR-483-5p/Dusp5. *Biochem Biophys Res Commun* (2020) 529(2):210–7. doi: 10.1016/j.bbrc.2020.05.180

207. Yin B, Ni J, Witherel CE, Yang M, Burdick JA, Wen C, et al. Harnessing tissue-derived extracellular vesicles for osteoarthritis theranostics. *Theranostics* (2022) 12(1):207–31. doi: 10.7150/thno.62708



OPEN ACCESS

EDITED BY

Yan Chang,
Anhui Medical University, China

REVIEWED BY

Anna Scanu,
University of Padua, Italy
Richard Wilson,
University of Tasmania, Australia

*CORRESPONDENCE

Wei Huang,
zgkdhwei@ustc.edu.cn
Hui Zhang,
zhanghui@ahmu.edu.cn
Zongsheng Yin,
yinzongsheng@sina.com

[†]These authors have contributed equally to this work and share first authorship

SPECIALTY SECTION

This article was submitted to
Inflammation Pharmacology,
a section of the journal
Frontiers in Pharmacology

RECEIVED 21 July 2022

ACCEPTED 10 October 2022

PUBLISHED 10 November 2022

CITATION

Tang H, Qin K, Wang A, Li S, Fang S,
Gao W, Lu M, Huang W, Zhang H and
Yin Z (2022), 3,3'-diindolylmethane
inhibits LPS-induced human
chondrocytes apoptosis and
extracellular matrix degradation by
activating PI3K-Akt-mTOR-
mediated autophagy.
Front. Pharmacol. 13:999851.
doi: 10.3389/fphar.2022.999851

COPYRIGHT

© 2022 Tang, Qin, Wang, Li, Fang, Gao,
Lu, Huang, Zhang and Yin. This is an
open-access article distributed under
the terms of the [Creative Commons
Attribution License \(CC BY\)](https://creativecommons.org/licenses/by/4.0/). The use,
distribution or reproduction in other
forums is permitted, provided the
original author(s) and the copyright
owner(s) are credited and that the
original publication in this journal is
cited, in accordance with accepted
academic practice. No use, distribution
or reproduction is permitted which does
not comply with these terms.

3,3'-diindolylmethane inhibits LPS-induced human chondrocytes apoptosis and extracellular matrix degradation by activating PI3K-Akt-mTOR-mediated autophagy

Hao Tang^{1,2†}, Kunpeng Qin^{1†}, Anquan Wang¹, Shuang Li¹,
Sheng Fang³, Weilu Gao¹, Ming Lu¹, Wei Huang^{4*}, Hui Zhang^{1*}
and Zongsheng Yin^{1*}

¹Department of Orthopedics, The First Affiliated Hospital of Anhui Medical University, Hefei, China,

²The Key Laboratory of Microbiology and Parasitology of Anhui Province, The Key Laboratory of Zoonoses of High Institutions in Anhui, Anhui Medical University, Hefei, China, ³Department of Orthopedics, The Second People's Hospital of Hefei, Hefei, China, ⁴Department of Orthopedics, The First Affiliated Hospital of USTC, Division of Life Sciences and Medicine, University of Science and Technology of China, Hefei, China

Osteoarthritis (OA) is a chronic degenerative joint disease characterized by articular cartilage destruction. The pathological mechanisms are complex; in particular, inflammation, autophagy, and apoptosis are often involved. 3,3'-Diindolylmethane (DIM), a phytoconstituent extracted from cruciferous vegetables, has various effects such as anti-inflammatory, antioxidant and anti-apoptotic. However, the effects of DIM on osteoarthritic chondrocytes remain undetermined. In this study, we simulated a lipopolysaccharide (LPS)-induced osteoarthritis model in human primary chondrocytes. We found that LPS stimulation significantly inhibited autophagy, induced chondrocyte apoptosis and extracellular matrix (ECM) degradation, which could be ameliorated by DIM. DIM inhibited the expression of a disintegrin and metalloproteinase with thrombospondin motif 5 (ADAMTS-5), matrix metalloproteinase 13 (MMP13), cleaved caspase-3, Bax, and p62, and increased the expression level of collagen II, aggrecan, Bcl-2, light chain 3 II (LC3 II), and beclin-1. Mechanistic studies showed that DIM increased chondrocyte autophagy levels by inhibiting the activation of PI3K/AKT/mTOR pathway. In mice destabilization of the medial meniscus (DMM) model, immunohistochemical analysis showed that DIM inhibited the expression of p-PI3K and cleaved caspase-3, increased the expression of LC3 II. Furthermore, DIM relieved joint cartilage degeneration. In conclusion, our findings demonstrate for the first time that DIM inhibits LPS-induced chondrocyte apoptosis and ECM degradation by regulating the PI3K/AKT/mTOR-autophagy axis and delays OA progression *in vivo*.

KEYWORDS

3, 3'-diindolylmethane, osteoarthritis, apoptosis, autophagy, chondrocyte

Introduction

Osteoarthritis (OA) is a degenerative joint disease that affects older people worldwide, characterized by progressive destruction and inflammation of articular cartilage (Glyn-Jones et al., 2015). The incidence of OA is reported to be increasing year by year, and the condition is a major cause of disability in older adults. Contemporary treatment mainly improves symptoms, and there is no effective treatment to prevent the progression of OA (Maudens et al., 2018). Therefore, it is clinically important to develop more convenient and effective interventions to slow down progression of the disease (Goldring, 2006). Degenerative changes of articular cartilage are the most important pathological changes in OA, and articular cartilage consists of only chondrocytes and extracellular matrix (ECM). The main matrix components of the ECM are collagen II and aggrecan, and the main ECM catabolic enzymes are matrix metalloproteinases (MMPs) and a disintegrin and metalloproteinase with thrombospondin motifs (ADAMTS) (Cucchiari et al., 2016). Under normal physiological conditions, chondrocytes maintain the balance of ECM synthesis and catabolism to ensure the structural and functional integrity of cartilage (Musumeci et al., 2011a).

Recently, an increasing number of studies have shown that OA has diverse causative factors and a complex pathogenesis and determined that the release of inflammatory mediators causes inhibition of cellular autophagy, resulting in increased apoptosis, which ultimately leads to an imbalance in ECM metabolism and accelerates OA development (Li et al., 2019). Previous study has reported that apoptosis is positively correlated with the severity of cartilage destruction and matrix depletion in human OA tissue specimens (Musumeci et al., 2015). Chondrocytes freshly isolated from human OA cartilage displayed morphological evidence of apoptosis, while those from normal donors did not have any apoptotic cell signatures. These findings suggest that OA chondrocytes exhibit distinct apoptotic propensities (Musumeci et al., 2011a; Musumeci et al., 2011b). In addition, when chondrocyte homeostasis is unbalanced, the release of inflammatory mediators and catabolic enzymes is accelerated, the destruction of ECM speeds up, and OA progression occurs (Zhao et al., 2020).

Autophagy is a mechanism and a dynamic cellular process whereby damaged cellular components (such as organelles and proteins) are wrapped by membrane structures to form autophagic vesicles, which then fuse with lysosomes, and whose contents are degraded and recycled to maintain normal cellular metabolism (He and Klionsky, 2009; Ravikumar et al., 2010; Polewska, 2012; Li et al., 2016). It has been reported that normal cartilage tissue expresses abundant LC3 II, Beclin1 and

other important autophagy-related proteins, suggesting that autophagy may be involved in maintaining the normal physiological function and structural integrity of cartilage tissue (Sasaki et al., 2012; Zhang et al., 2015; Qin et al., 2017). In contrast, the expression of autophagy-related proteins is reduced in human OA chondrocytes (Loeser, 2011; Lian et al., 2018). Activation of autophagy increases the expression levels of both collagen II and aggrecan while reducing those of ADAMTS-5 and MMP-13 in chondrocytes and ameliorating arthritis progression (Qin et al., 2017; Huang et al., 2020; Lin et al., 2021). Furthermore, inhibition of autophagy in mice chondrocytes exacerbated arthritis progression (Bouderlique et al., 2016), while intra-articular injection of rapamycin to activate autophagy in a mice destabilization of the medial meniscus (DMM) model improved cartilage degeneration (Takayama et al., 2014).

3,3-diindolylmethane (DIM) is a natural product found in cruciferous edible plants, such as cauliflower, cabbage, and broccoli. Previous studies have reported that DIM has several preventive effects, especially displaying anti-tumor, anti-inflammatory, antioxidant and free radical scavenging roles (Luo et al., 2018; Ye et al., 2021). Recent studies have determined that DIM also protects against kidney, heart, and liver damage. It has been reported that DIM attenuated carbon tetrachloride-induced acute liver injury in mice by inhibiting inflammatory responses and apoptosis and by modulating oxidative stress (Munakarmi et al., 2020). DIM has been reported to attenuate oxidative stress-induced apoptosis in hippocampal neurons (Lee et al., 2019) and protect neuronal cells from inflammation and brain tissue ischemia (Rzemieniec et al., 2016; Lee et al., 2019). In addition, DIM attenuates lipopolysaccharide (LPS)-induced inflammatory responses and apoptosis in cardiomyopathy (Luo et al., 2018) and induces protective autophagy in prostate cancer (Draz et al., 2017). In a rat model of rheumatoid arthritis, DIM was observed to block osteoclast formation (Dong et al., 2010) and, through inhibition of the MAPK and AKT/mTOR pathways, inhibit synovial fibroblast proliferation, migration, invasion, and inflammatory factor release and attenuate experimental arthritis progression (Du et al., 2019).

Although previous studies have extensively investigated the function of DIM, the potential role of DIM in osteoarthritis and its effects on chondrocytes remain undetermined. In the present study, we observed the effects of DIM on LPS stimulation-induced chondrocyte autophagy, apoptosis, and ECM metabolism *in vitro* and explored the possible molecular mechanisms. The potential therapeutic function of DIM was also evaluated in a DMM mice model of OA.

Materials and methods

Experimental design

DIM was purchased from MCE (HY-15758, Monmouth Junction, NJ, United States) (purity >99%). LPS is currently the main pro-inflammatory inducer (Mayeux, 1997), which is commonly used to induce arthritis models in chondrocytes (Yoshino et al., 2000; Lorenz et al., 2013; Ding et al., 2019; Li et al., 2020; Zeng et al., 2021). So, we used LPS (10 µg/ml, Sigma-Aldrich) to treat human primary chondrocytes to simulate OA models. Six groups were established. The control group contained chondrocytes without any treatment. The negative control group contained chondrocytes to which only DIM (40 µM) was added. The LPS group contained chondrocytes only treated with LPS (10 µg/ml). The LPS + DIM group contained the chondrocytes treated with different concentrations of DIM (10, 20, 40 µM) for 2 h, and then LPS was added in the medium to stimulate chondrocytes for 24 h (without replacing the medium). We used 40 µM of DIM for the detection of immunofluorescence, flow cytometry, monodansylcadaverine (MDC) staining, transmission electron microscopy (TEM) and glycosaminoglycan (GAG) experiments.

In vivo, mice were randomly divided into a sham-operated group, an OA group (DMM), and a DIM-treated OA group (DMM + DIM) ($n = 10$ in each group). Mice DMM model creation took place in the OA group, and the DIM-treated OA group received a 50 mg/kg/day dose of DIM (*via* daily intraperitoneal injection for 8 weeks). Mice in the Sham and DMM groups received equal amounts of saline. All animals were executed 8 weeks after surgery, and cartilage samples were collected for immunological and histological analysis.

Isolation and culture of primary chondrocytes

The collection of cartilage tissue involving human OA was approved by the Medical Ethics Committee of the First Affiliated Hospital of Anhui Medical University (ethics no. PJ2022-04-55), and all participants signed an informed consent form. Articular cartilage was obtained from patients who had undergone total knee arthroplasty at the First Affiliated Hospital of Anhui Medical University. The specimens were rapidly transferred to the operating table and washed 3–5 times with phosphate-buffered saline (PBS) in a sterile environment, and the cartilage tissue was then cut into bone pieces of 1 mm³ in size and then digested with 0.25% trypsin (Beyotime, Shanghai, China) for 30 min, followed by 0.2% collagenase II (Sigma-Aldrich) in a 37°C incubator overnight. The digested chondrocytes were then resuspended and inoculated in culture flasks containing Dulbecco's modified Eagle medium/nutrient mixture F-12, 10% fetal bovine serum, and 1% penicillin/streptomycin antibiotics; when 80%–90% fusion was

achieved, the cells were then digested using 0.25% trypsin solution, centrifuged, resuspended, and passaged. The complete medium was changed every 2 days, and only cells of the first or second generation were used for the experiments to avoid phenotypic changes.

Toluidine blue staining of chondrocytes

Chondrocytes were inoculated in 24-well plates and cultured for 24 h, then washed three times with PBS solution for 5 min/time and subsequently fixed in 4% paraformaldehyde solution for 20 min. After being washed with PBS, they were treated with 1% toluidine blue solution (Solarbio, Beijing, China) for 1 h at room temperature, washed with PBS again, dried and placed on slides, and then sealed with neutral gum. All chondrocytes were observed under a microscope (Tissue FAXS Plus S; Tissue Gnostics, Vienna, Austria) and photographed.

Cell viability assay

The cytotoxicity of DIM on human chondrocytes was assayed with a cell counting kit 8 (CCK-8) (Beyotime). First, human chondrocytes were cultured in 96-well plates (5×10³ cells/well) for 24 h with different concentrations of DIM (0, 1, 5, 10, 20, 40, or 80 µM) for 24 or 48 h. After each well washed with PBS, 100 µL new medium containing 10% CCK8 was added to each well, incubated at 37°C for 2 h. The absorbance was then detected at 450 nm using a microplate reader (Leica Microsystems, Wetzlar, Germany).

RNA extraction and quantitative real-time polymerase chain reaction (qRT-PCR)

The treated cells were washed with enzyme-free water, and total cellular RNA was subsequently extracted with TRIzol reagent (Invitrogen, Carlsbad, CA, United States), RNA purity was assessed according to a 260-/280-nm ratio using a NanoDrop One device (Thermo Fisher Scientific, Waltham, MA, United States), and RNA concentrations were measured using a reverse transcription kit (Takara Bio, Kusatsu, Japan). A 10-µL reaction system was set up to reverse-transcribe the extracted RNA to complementary DNA. Subsequently, qRT-PCR of the target genes was performed according to the SYBR® Premix Ex Taq™ II kit (Takara Bio), and data analysis was performed with the Light Cycler 96 software (Roche, Alameda, CA, United States). The target gene messenger RNA levels were normalized to GAPDH levels, and the data obtained were analyzed using the 2^{−ΔΔCT} method. All experiments were repeated three times. The primer sequences were provided by Sangon (Shanghai, China) and are listed in Supplementary Table S1.

Protein extraction and western blotting

A western blot technique was used to detect the expressions of related proteins. The treated cells were collected, radioimmunoprecipitation assay (RIPA) lysis buffer (Beyotime) and phenylmethylsulfonyl fluoride (PMSF) (Beyotime) were added, and the mixture was placed on ice for 30 min to lyse. Then, the supernatant was centrifuged and subsequently protein concentration was measured by BCA method (Beyotime) and added to 5 × sodium dodecyl sulfate–polyacrylamide gel electrophoresis (SDS-PAGE) protein loading buffer (Beyotime) and boiled for 10 min to obtain the total protein. Each well was loaded with 20 µg protein, and then under the same GAPDH condition, the loading volume of each sample was calculated according to the required loading amount of protein and the sample protein concentration. The protein was subsequently separated by SDS-PAGE, then transferred to a polyvinylidene fluoride membrane (Millipore, Burlington, MA, United States) in constant flow. The membranes were subsequently closed with 5% skim milk for 2 h at room temperature, washed with tris-buffered saline and polysorbate 20 and incubated with the specific primary antibody overnight at 4°C, then washed and incubated with the corresponding specific secondary antibody for 2 h at room temperature, respectively. Finally, all band signals were detected using ECL ultrasensitive chemiluminescence reagents (Thermo Fisher Scientific, Waltham, MA, United States) and detected using the ImageJ version 1.53c software (U.S. National Institutes of Health, Bethesda, MD, United States) for quantitative analysis. The following antibodies were used in the western blot analysis: anti–collagen II antibody (1:1000, 28459-1-AP, Proteintech Group, Rosemont, IL, United States), anti–aggrecan antibody (1:1000, 13880-1-AP, Proteintech Group), anti–ADAMTS-5 antibody (1:1000, Ab41037, Abcam, Cambridge, United Kingdom), anti–MMP-13 antibody (1:1000, 18165-1-AP, Proteintech Group), anti–LC3 A/B antibody (1:1000, 12741, CST, Danvers, MA, United States), anti-p62 antibody (1:10000, Ab109012, Abcam), anti–beclin-1 antibody (1:1000, Ab62557, Abcam), anti–cleaved caspase-3 antibody (1:1000, 5A1E, CST), anti-Bax antibody (1:5000, Ab32503, Abcam), anti–Bcl-2 antibody (1:1000, Ab32124, Abcam), anti–p-PI3K antibody (1:1000, ab151549, Abcam), anti–PI3K antibody (1:1000, 3358, CST), anti-AKT antibody (1:1000, 4691, CST), anti–phospho-AKT antibody (1:2000, 4060, CST), anti-mTOR antibody (1:5000, Ab32028, Abcam), anti–phospho-mTOR antibody (1:5000, Ab109268, Abcam), and anti-GAPDH antibody (1:10000, 60004-1-Ig, Proteintech Group).

Immunofluorescence staining

The treated cells were washed with PBS, then underwent 4% paraformaldehyde fixation for 20 min, were washed with PBS three more times, and underwent 0.3% Triton X-100 permeabilized for 15 min at room temperature. The cells were

then closed with 10% bovine serum albumin (BSA) (goat serum blocking solution, Beyotime) for 1 h, then were washed with PBS and incubated overnight at 4°C in a wet box with the appropriate specific primary antibody, as follows: anti–collagen II antibody (1:300, 28459-1-AP, Proteintech Group), anti–MMP-13 antibody (1:300, 18165-1-AP, Proteintech Group), anti–LC3 A/B antibody (1:200, 12741, CST), anti–cleaved caspase-3 antibody (1:400, 5A1E, CST), or anti–p-PI3K antibody (1:300, Ab151549, Abcam). After three washes, the cells were incubated with fluorescein isothiocyanate (FITC) or rhodamine-labeled secondary antibody (1:100ZF-0311/ZF-0316, ZSGB-BIO, Beijing, China) for 1 h at room temperature and protected from light. Subsequently, 4',6-diamidino-2-phenylindole (DAPI) staining solution (Beyotime) was added to label cell nuclei for 5 min, and finally anti-fluorescence quenching mounting solution was added dropwise. Images were observed and obtained under an automatic positive fluorescence microscope (DM6B; Leica, Wetzlar, Germany) and were quantified using ImageJ version 1.53c (U.S. National Institutes of Health, Bethesda).

MDC staining

MDC is one of the most used fluorescent probes for cellular autophagy detection. It can specifically label autophagosomes through ion capture and specific binding to membrane lipids (Biederbick et al., 1995; Niemann et al., 2000; Niemann et al., 2001; Vázquez and Colombo, 2009). During our study, treated chondrocyte crawls were fixed in 4% paraformaldehyde for 20 min, washed three times with PBS, and incubated with MDC staining solution (Beyotime) for 60 min at 37°C in an incubator protected from light. Then, we washed them three times with assay buffer. Green fluorescence was observed under an automatic positive fluorescence microscope (DM6B; Leica).

Transmission electron microscopy (TEM)

The treated cells were collected, then the samples were fixed with 2.5% glutaraldehyde in 0.1 M phosphate buffer (P885738, Macklin, Shanghai, China) at 4°C overnight. After washing with phosphate buffer, the samples were fixed in phosphate buffer with 1% OsO₄ at 4°C for 2 h and rinsed thoroughly with ddH₂O. The 2% aqueous uranyl acetate was used for *en bloc* staining for 2 h and then the samples were serially dehydrated with 50%, 70%, 90% and 100% alcohol and 100% acetone and embedded in epoxy resin for making the blocks of samples. Silver sections were cut with an ultramicrotome (EM UC7, Leica; thickness 70–90 nm), stained with lead citrate and uranyl acetate, and observed with an electron microscope (Talos L120C G2, Thermo Scientific, MA, United States).

Cellular safranin O staining

Safranin O is a cationic dye that binds polyanions and binds to GAGs in chondrocytes to give them a red color, with the intensity of the red color being directly proportional to the GAG content. It is used to assess the content of GAGs in chondrocytes and can reflect the ability of chondrocytes to perform anabolic and catabolic activities. We washed the treated chondrocytes with PBS and fixed them with 4% paraformaldehyde for 20 min, then washed them with PBS and incubated them with safranin O staining solution (Solarbio, Beijing, China) for 30 min at room temperature. The cells were then washed with PBS and observed by microscopy (Tissue FAXS Plus S; Tissue Gnostics), and photographs were taken.

Apoptosis analysis

The treated chondrocytes were collected in flow tubes, washed twice with cold PBS, and resuspended with 400 μ L of $1 \times$ annexin V conjugate using the annexin V-FITC/propidium iodide double-stained apoptosis assay kit (BestBio, Shanghai, China), followed by the addition of 5 μ L of annexin V-FITC staining solution and incubation for 15 min at 4°C under light-proof conditions. Finally, 5 μ L of propidium iodide (PI) staining solution was added and incubated for 3 min at 4°C under light-proof conditions, followed by flow cytometry (BD Celesta, San Jose, CA, United States). Flow analysis was performed with FlowJo version 10.6.0 (FlowJo LLC, Ashland, OR, United States).

Animal model

Thirty 10-week-old C57BL/6 male wild-type mice were obtained from the Animal Center of Anhui Medical University. All surgical interventions, treatments, and postoperative animal care procedures were administered in accordance with the Guide for the Care and Use of Laboratory Animals of the National Institutes of Health and were performed in strict accordance with the requirements of the Animal Ethics Committee of Anhui Medical University (ethics no. LISC20190738). All the mice in the experiment were housed in standard experimental cages with a 12-h light/dark cycle and were freely access to water and standard food. Mice OA models were created by DMM surgery. Anesthesia was performed by intraperitoneal injection of an appropriate amount of 2% pentobarbital, followed by exposure of the joint capsule medial to the patellar tendon of the right knee and dissection of the medial meniscus tibial ligament with microsurgical scissors. In the sham group, only the joint capsule was incised, and the medial meniscal tibial ligament was not treated.

Immunohistochemical assay

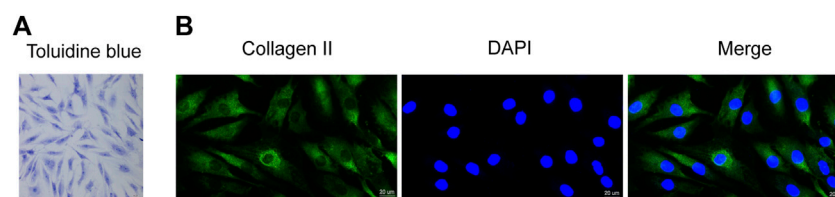
The obtained knee joints were fixed in 4% paraformaldehyde for 24 h, then decalcified, paraffin-embedded, cut into 5- μ m sections, dewaxed, and rehydrated. Antigen repair was performed using the E enzyme method (DIG-3008; MXB, Fuzhou China), and appropriate amounts of rabbit- or mouse-derived endogenous peroxidase blocker (PV-6001/PV-6002, ZSGB-BIO) were added and incubated at room temperature for 10 min. After rinsing with PBS, an appropriate amount of primary antibody was added dropwise and incubated at 37°C for 60 min, using the appropriate specific primary antibody, as follows: anti-LC3 A/B antibody (1:300, 12741, CST), anti-cleaved caspase-3 antibody (1:1000, 5A1E, CST), anti-p-PI3K antibody (1:100, Ab151549, Abcam), anti-collagen II antibody (1:800, 28459-1-AP, Proteintech Group), anti-aggrecan antibody (1:200, 13880-1-AP, Proteintech Group), anti-ADAMTS-5 antibody (1: 200, DF13268, Affinity), anti-MMP-13 antibody (1:200, 18165-1-AP, Proteintech Group). This was followed by the addition of the corresponding enzyme-labeled goat anti-rabbit or mouse immunoglobulin G polymer (PV-6001/PV-6002, ZSGB-BIO) dropwise to the section, then incubation at room temperature for 20 min; the addition of DAB (ZLI-9018, ZSGB-BIO) color development solution. Finally, re-staining, dehydration, transparency, and sealing of the section. The staining results were observed and interpreted by a qualified pathologist under a light microscope.

Histopathological analysis

The obtained mice knee sections were dewaxed, hydrated, and stained with hematoxylin and eosin (H and E) staining as well as safranin O/fast green staining (Servicebio, Wuhan, China) to assess cartilage destruction. The extent of cartilage degeneration in the stained sections was assessed using the Osteoarthritis Research Society International (OARSI) scoring system (Glasson et al., 2010). The extent of synovial tissue changes in the stained sections was assessed using the Krenn Synovitis Score Criteria (Krenn et al., 2002; Krenn et al., 2006).

X-ray imaging method

Eight weeks after DMM, mice were placed on a digital X-ray machine (Labscope, Glenbrook Technologies Inc, Randolph, NJ, United States) to undergo X-ray frontal and lateral imaging of all knee joints to assess the joint space, cartilage surface sclerosis, and bone formation. X-ray machine settings were 25 kV and 0.1 mA.

**FIGURE 1**

Identification of human primary chondrocytes and the effect of DIM on human OA chondrocyte viability (A) Proteoglycans in human primary chondrocytes were stained purple by toluidine blue (scale bar, 50 μ m) (B) Collagen II immunofluorescence staining showed that the collagen II was stained green, while cell nuclei were stained blue by DAPI (scale bar, 20 μ m).

Statistical analysis

All experiments were performed at least three times, and data are presented as mean \pm standard deviation (SD) values. Statistical analysis was performed using the Prism version 9.0 software (GraphPad Software, San Diego, CA, United States). Statistically significant differences between the two groups were analyzed by *t* test, one-way ANOVA was used to compare multiple data groups. $p < 0.05$ was statistically significant.

Results

Identification of human chondrocytes

First, we used toluidine blue staining and immunofluorescence staining to identify the isolated primary chondrocytes. Toluidine blue staining showed that the proteoglycans in the chondrocytes stained blue-purple, and the chondrocytes were spindle-shaped (Figure 1A). In addition, immunofluorescence staining showed greenish collagen II in the cytoplasm of chondrocytes and no positive staining in cell nuclei (Figure 1B). These two staining methods confirmed that the primary cells extracted from articular cartilage were chondrocytes.

Effects of DIM on human chondrocyte viability

The chemical structure of DIM is illustrated in Figure 2A. To clarify the cytotoxic effect of DIM on human chondrocytes, we assayed the cell viability by CCK-8 assay. Different concentrations of DIM (0, 1, 5, 10, 20, 40, and 80 μ M) were incubated with chondrocytes for 24 and 48 h. After DIM treatment of chondrocytes for 24 and 48 h, there was no significant cytotoxic effect on primary chondrocytes at concentrations of 0–40 μ M, but the high concentration of

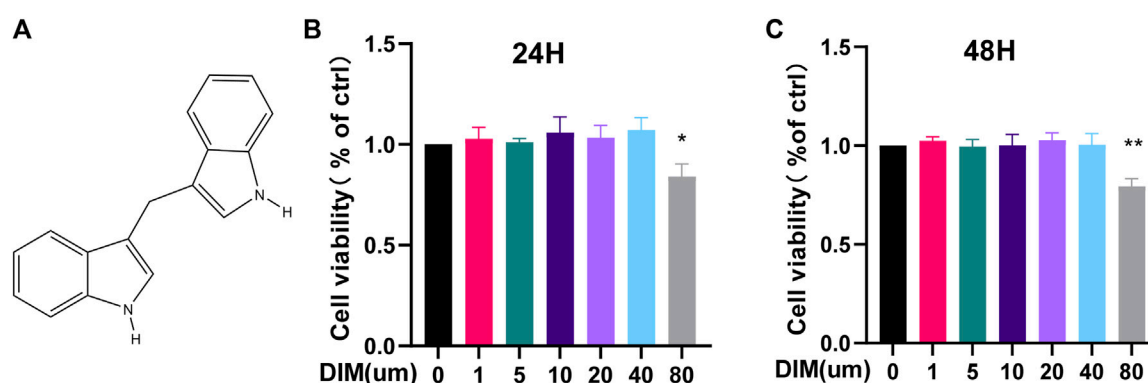
80 μ M reflected significant cytotoxicity and affected cell viability (Figures 2B,C). Therefore, the safe concentrations of 0, 10, 20, or 40 μ M of DIM were used in subsequent related experiments.

DIM alleviates LPS-induced ECM degradation in human chondrocytes

We used western blot analysis (Figures 3A,B) and qRT-PCR (Figure 3C) to detect the expression of the following anabolic and catabolic indicators in cartilage: collagen II, aggrecan, ADAMTS-5, and MMP-13. Collagen II and aggrecan were significantly reduced in the LPS group, while ADAMTS-5 and MMP-13 were significantly increased. Pre-treatment with DIM reversed the downregulation of collagen II and aggrecan and the upregulation of ADAMTS-5 and MMP-13 induced by LPS stimulation in a dose-dependent relationship. We further examined the deposition of GAGs in human chondrocytes using safranin O staining, and GAG expression appeared significantly reduced in LPS-treated chondrocytes compared to controls, whereas DIM treatment ameliorated the LPS-induced loss of GAGs (Figure 3D, Supplementary Figure S2). In addition, we detected the expressions of collagen II and MMP-13 by immunofluorescence, and the results of fluorescence analysis were consistent with the western blot results (Figures 3E,F). Overall, the results showed that DIM ameliorated LPS-induced human primary chondrocytes anabolic and catabolic imbalance, which in turn reflected that DIM improved LPS-induced ECM degradation.

DIM attenuates LPS-induced apoptosis in human chondrocytes

We detected the expressions of Bax, Bcl-2, and cleaved caspase-3 by western blot analysis and further detected the expression of cleaved caspase-3 by immunofluorescence staining. Compared to the control group, LPS stimulation

**FIGURE 2**

(A) Chemical structure of DIM (B,C) The cytotoxicity of DIM on chondrocytes was examined at various concentrations of DIM (0, 1, 5, 10, 20, 40, and 80 μ M) for 24 and 48 h by using the CCK-8 assay. The data are presented as mean \pm SD values from 3 independent experiments. Using one-way ANOVA, * $p < 0.05$, ** $p < 0.01$ vs. the control.

upregulated Bax and cleaved caspase-3 expression, while Bcl-2 expression was significantly down-regulated. In contrast, the expressions of Bax and cleaved caspase-3 were significantly down-regulated in the LPS group with the addition of DIM pre-treatment, while Bcl-2 expression was significantly increased (Figures 4A,B). Similarly, immunofluorescence staining for labeled cleaved caspase-3 results showed that DIM treatment decreased the intensity of cleaved caspase-3 (Figures 4C,D). In addition, apoptotic cells were examined by flow cytometry, and LPS caused an increase in chondrocyte apoptosis compared to the control group. However, the percentage of LPS-induced apoptosis was significantly reduced following pre-treatment with 40 μ M of DIM (Figures 4E,F). These data suggest that DIM has an anti-apoptotic effect in human chondrocytes.

DIM relieves the LPS-induced inhibition of autophagy and enhances autophagic flux in chondrocytes

Autophagy is a common mechanism for the removal of redundant or damaged organelles during development and aging. Moreover, autophagy plays a key role in regulating energy cycling and cellular homeostasis in chondrocytes (Mizushima and Levine, 2020). To investigate whether DIM activates autophagy in chondrocytes, we performed western blot analysis to assess changes in beclin-1, LC3 II, and p62 protein levels in human chondrocytes under different treatment conditions, which play a key role in the onset of autophagy (Glick et al., 2010; Boya et al., 2013). In LPS-treated primary human chondrocytes, a significant increase in LC3 II and beclin-1 levels and a significant decrease in p62 levels were observed in cells pre-treated with increased DIM (Figures 5A,B). Then, immunofluorescence staining results showed that

DIM pre-treatment significantly increased the expression of LC3 II in LPS-stimulated chondrocytes (Figures 5C,D). In addition, MDC is an eosinophilic fluorescent dye that is specific for autophagosome formation. we assessed autophagic flux by MDC staining and transmission electron microscopy to observe the effect of DIM as well as that of LPS on the number of autophagosomes in chondrocytes; the intensity of MDC staining was diminished and the number of autophagosomes was reduced in LPS-treated chondrocytes compared to the blank control group. The intensity of MDC staining and the number of autophagosomes were significantly increased in primary human chondrocytes in the LPS + DIM group compared to the LPS group (Figures 5E,F). Based on these results, DIM could ameliorate the LPS-induced inhibition of autophagy and restore chondrocyte autophagy levels.

DIM inhibits activation of the PI3K/AKT/mTOR signaling pathway

It is well known that the PI3K/AKT/mTOR signaling pathway is a key regulatory pathway for autophagy, and activation of the PI3K/AKT/mTOR pathway in OA is associated with autophagy inhibition (Xue et al., 2017). To confirm whether the mechanism of enhanced autophagy by DIM is related to the PI3K/AKT/mTOR signaling pathway, p-PI3K, p-AKT, and p-mTOR were detected by western blot analysis. The results showed that LPS treatment activated the PI3K/AKT/mTOR pathway compared to the control group, and the expressions of p-PI3K, p-AKT, and p-mTOR were significantly increased; meanwhile, the addition of DIM pre-treatment to the LPS group dose-dependently down-regulated the expressions of p-PI3K, p-AKT, and p-mTOR but did not affect the expressions of total PI3K, total AKT, or total mTOR

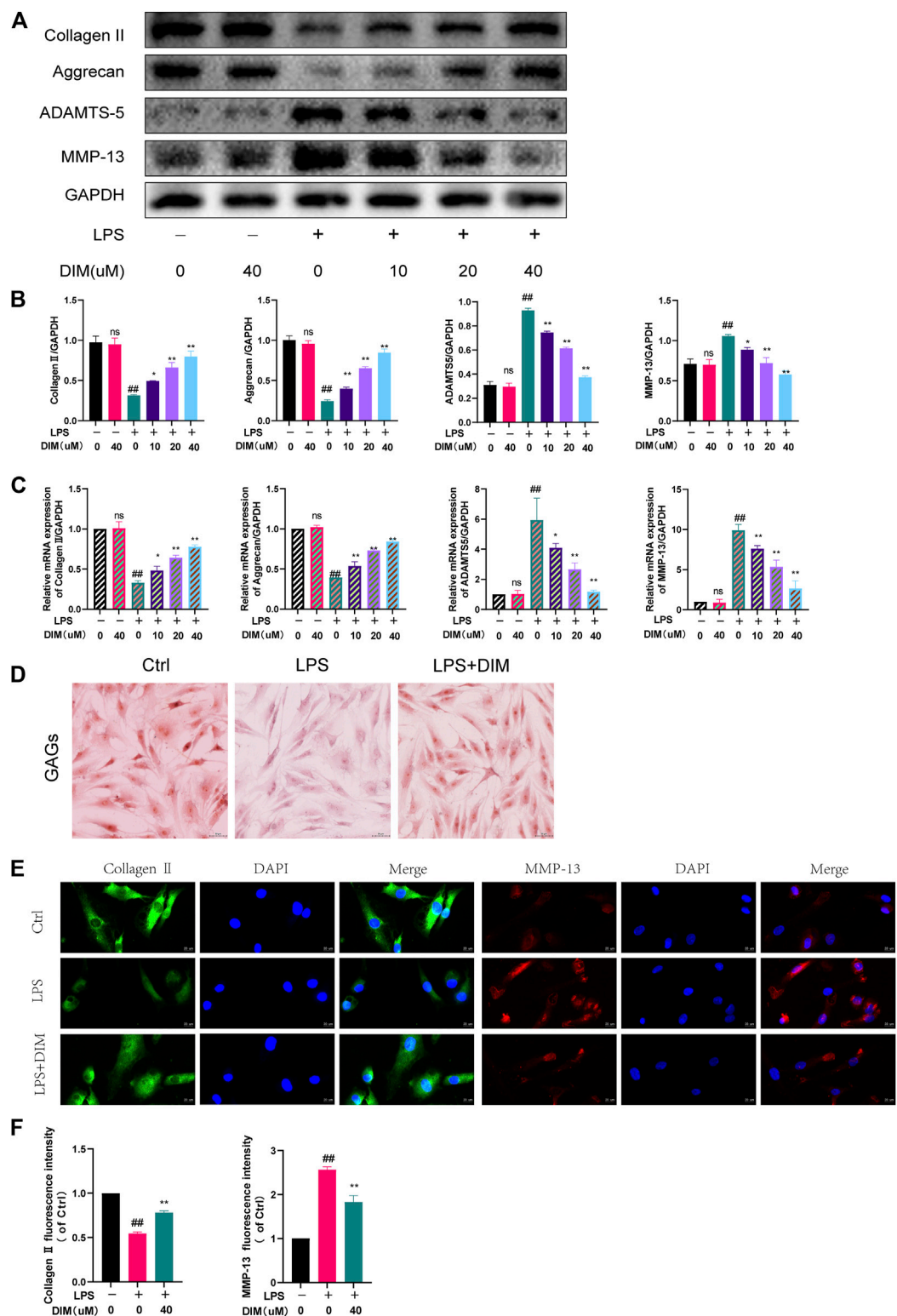


FIGURE 3 DIM alleviates LPS-induced ECM degradation in human chondrocytes (A,B) Effects of DIM on the protein expression levels of collagen II, aggrecan, ADAMTS-5, and MMP-13 in human chondrocytes treated as above were measured by western blotting and quantitation (C) Effects of DIM on the messenger RNA expression levels of collagen II, aggrecan, ADAMTS-5, and MMP-13 in human chondrocytes treated as above were measured by qRT-PCR (D) Safranin O staining of GAGs in human primary chondrocytes in each group (scale bar, 50 μ m) (E) After treatment, (Continued)

FIGURE 3 (Continued)

immunofluorescence staining showed the changes in the fluorescence intensity of collagen II and MMP-13 in each group (scale bar, 20 μ m) (F). The fluorescence intensity was measured with the ImageJ software (U.S. National Institutes of Health, Bethesda). The data are presented as mean \pm SD values from three independent experiments. Using one-way ANOVA, NS, no statistical difference. # $p < 0.05$ vs. the control; ## $p < 0.01$ vs. the control; * $p < 0.05$ vs. the LPS group; ** $p < 0.01$ vs. the LPS group.

(Figure 6A). The western blotting quantification analysis were based on the ratio of phosphorylated proteins (p-PI3K, p-AKT and p-mTOR) to total proteins (PI3K, AKT and mTOR) (Figure 6B). Immunofluorescence staining showed that DIM pre-treatment significantly inhibited p-PI3K activation (Figures 6C,D). These data suggest that the DIM can inhibit activation of the PI3K/AKT/mTOR pathway in human chondrocytes.

DIM enhances autophagy levels via the PI3K/AKT/mTOR signaling pathway

To determine whether DIM-enhanced autophagy was mediated by the PI3K/AKT/mTOR pathway, the pathway activator 740Y-P (HY-P0175, MCE, Monmouth Junction, NJ, United States) and inhibitor LY294002 (HY-10108, MCE, Monmouth Junction, NJ, United States) were used for functional reversion experiments (Figures 7A,B). DIM increased LC3 II and beclin-1 expression levels and decreased p62 levels in the LPS group, but the increase in autophagy triggered by DIM was eliminated with 740Y-P, while the increase in autophagy triggered by DIM was enhanced with LY294002. Similar results were obtained for immunofluorescence labeling of LC3 II. Compared to the LPS + DIM group, the green fluorescence intensity of LC3 II decreased after 740Y-P use and increased after LY294002 use (Figures 7C,D). In addition, we observed the number of autophagosomes by MDC staining and transmission electron microscopy in chondrocytes. Compared to the LPS + DIM group, The intensity of MDC staining and the number of autophagosomes were significantly decreased after 740Y-P used and increased after LY294002 used (Figures 7E,F). These data suggested that the regulatory effect of DIM on autophagy was mediated *via* the PI3K/AKT/mTOR pathway.

DIM attenuates LPS-induced apoptosis in chondrocytes *via* autophagy

We used chloroquine (CQ), an autophagy inhibitor (HY-17589A, MCE), and rapamycin (Rapa), an autophagy activator (HY-10219, MCE), to determine whether autophagy was involved in the inhibitive effects of DIM on apoptosis. Compared to the LPS + DIM group, CQ effectively abolished the effects of DIM on reducing cleaved caspase-3 and Bax

expression levels as well as increasing Bcl-2 expression levels. Compared to the LPS + DIM group, Rapa further reduced cleaved caspase-3 and Bax expression levels as well as increased Bcl-2 expression levels (Figures 8A,B). Additionally, we also detected the expression level of cleaved caspase-3 by immunofluorescence staining (Figures 8C,D) and the apoptosis of chondrocytes by flow cytometry (Figures 8E,F). Compared to the LPS + DIM group, the fluorescence intensity of cleaved caspase-3 and the chondrocyte apoptosis were significantly increased after CQ treatment. In contrast, both the fluorescence intensity of cleaved caspase-3 and chondrocyte apoptosis were reduced after Rapa treatment. These data suggested that inhibition of chondrocyte apoptosis by DIM in LPS-treated chondrocytes is mediated by autophagy.

DIM alleviates OA cartilage degeneration in the surgical DMM mice model

We evaluated the therapeutic effect of DIM using a mice DMM model. The morphological and histological changes of the model mice were observed by H and E staining, safranin O/fast green staining, and X-ray analysis. X-ray (Figure 9A) and Hematoxylin and eosin staining (Figure 9B) results revealed that, compared to the Sham group, the joint space of the mice in the DMM group was significantly narrowed; the cartilage surface was hardened, rough, and uneven; and osteophyte counts were increased. However, DIM treatment alleviated this pathological manifestation. In addition, safranin O/fast green staining showed that, compared to the Sham group, the DMM group had significant loss of proteoglycan in the articular cartilage and aggravated cartilage erosion; however, these changes were improved after DIM treatment (Figure 9C). The OARSI scores and Synovitis Scores were consistent with the above pathological results, indicating that the DMM mice model treated with DIM were significantly different from the OA group, and the OARSI scores and Synovitis Scores of the DMM + DIM group were significantly lower than those of the OA group (Figure 9D, Supplementary Figure S3). Immunohistochemical results showed that the average optical densities (AODs) of p-PI3K and cleaved caspase-3 in the DMM group were significantly higher than those in the sham group, while the AOD of LC3 II was lower than that in the sham group. Compared to the DMM group, the AOD of LC3 II was significantly increased after DIM treatment, while the AODs of p-PI3K and cleaved caspase-3 were significantly decreased (Figures

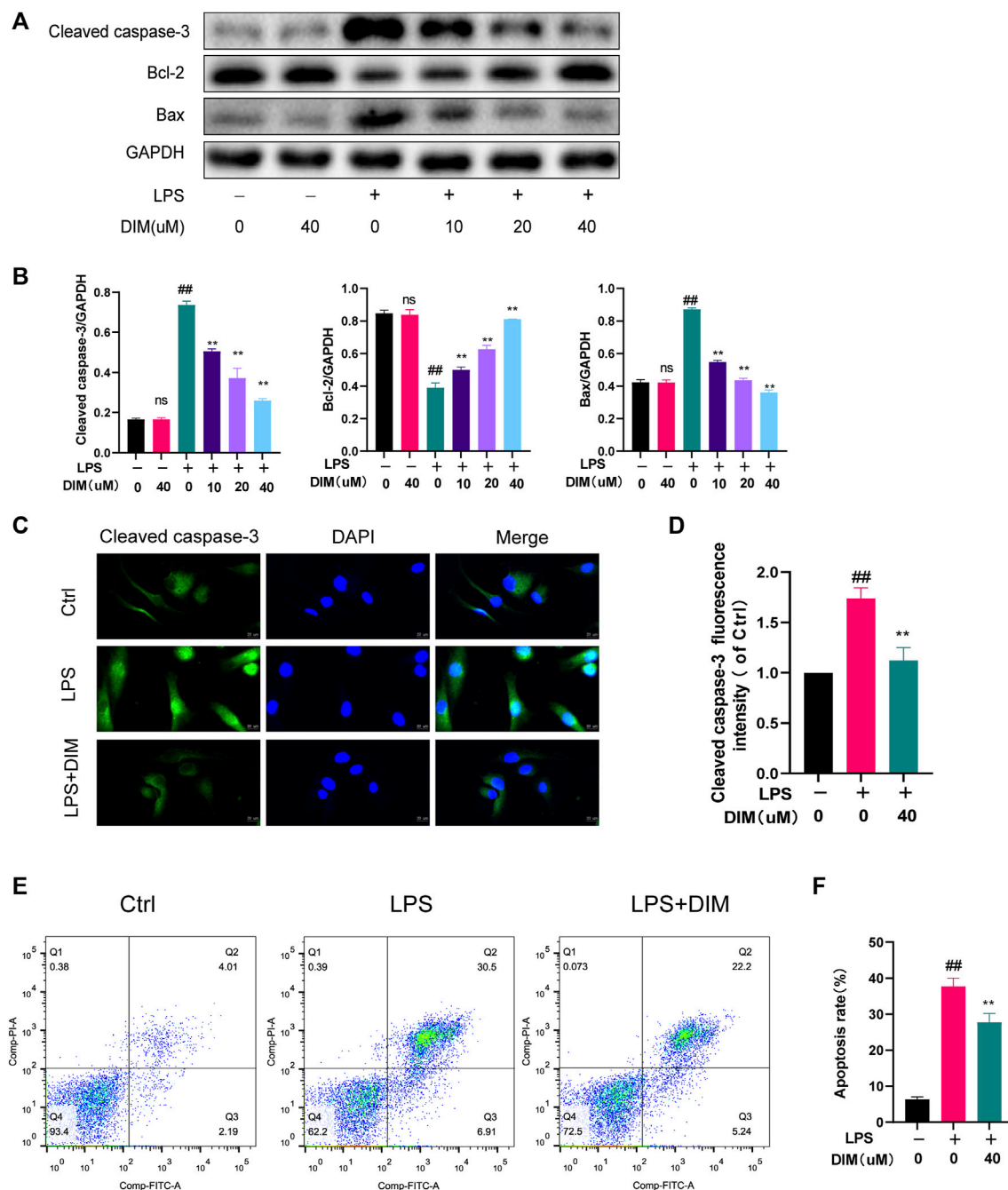


FIGURE 4

DIM attenuates LPS-induced apoptosis in human chondrocytes (A,B) Effects of DIM on the protein expression levels of cleaved caspase-3, Bcl-2, and Bax in human chondrocytes treated as above were measured by western blotting and quantitation (C) After treatment, immunofluorescence staining showed the changes in the fluorescence intensity of cleaved caspase-3 in each group (scale bar, 20 μ m) (D) The fluorescence intensity was measured with the ImageJ software (U.S. National Institutes of Health, Bethesda) (E,F) After treatment, the results of flow cytometry detection of apoptotic cells in each group and quantitation. The data are presented as mean \pm SD values from three independent experiments. Using one-way ANOVA, NS, no statistical difference. # $p < 0.05$ vs. the control; ## $p < 0.01$ vs. the control; * $p < 0.05$ vs. the LPS group; ** $p < 0.01$ vs. the LPS group.

9E,F). The AODs of MMP-13 and ADAMTS-5 in the DMM group were significantly higher than those in the sham group. Compared to the DMM group, the AODs of MMP-13

and ADAMTS-5 were significantly decreased after DIM treatment (Supplementary Figure S4). In addition, immunohistochemical staining analysis of Collagen II and

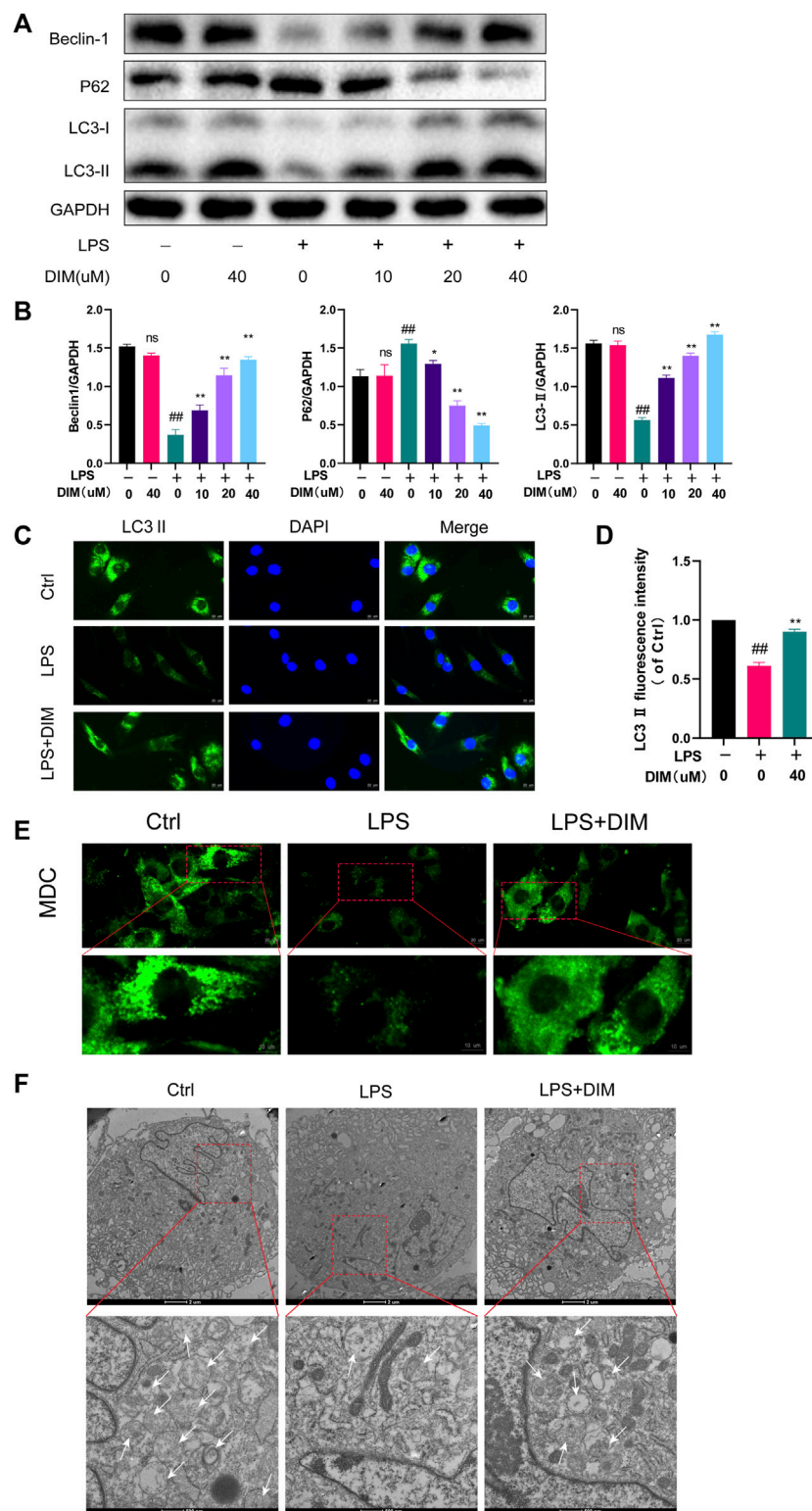


FIGURE 5
DIM relieves the LPS-induced inhibition of autophagy (A,B) Effects of DIM on the protein expression levels of beclin-1, LC3 II, and p62 in human chondrocytes treated as above were measured by western blotting and quantitation (C) After treatment, immunofluorescence staining showed the changes in the fluorescence intensity of LC3 II in each group (scale bar, 20 μ m) (D) The fluorescence intensity was measured with the ImageJ software (U.S. National Institutes of Health, Bethesda) (E) After treatment, the effects of DIM and LPS on the number of chondrocytes (Continued)

FIGURE 5 (Continued)

autophagosomes were observed by MDC staining (punctate green staining represents autophagosomes; scale bar, 20 μ m; partially enlarged image scale bar, 10 μ m) (F) Microstructural detection of autophagosomes by transmission electron microscopy (White arrows indicate the formation of autophagosomes. Scale bar = 2 μ m; partially enlarged image scale bar, 500 nm). The data are presented as mean \pm SD values from three independent experiments. NS, no statistical difference; # p < 0.05 vs. the control; ## p < 0.01 vs. the control; * p < 0.05 vs. the LPS group; ** p < 0.01 vs. the LPS group.

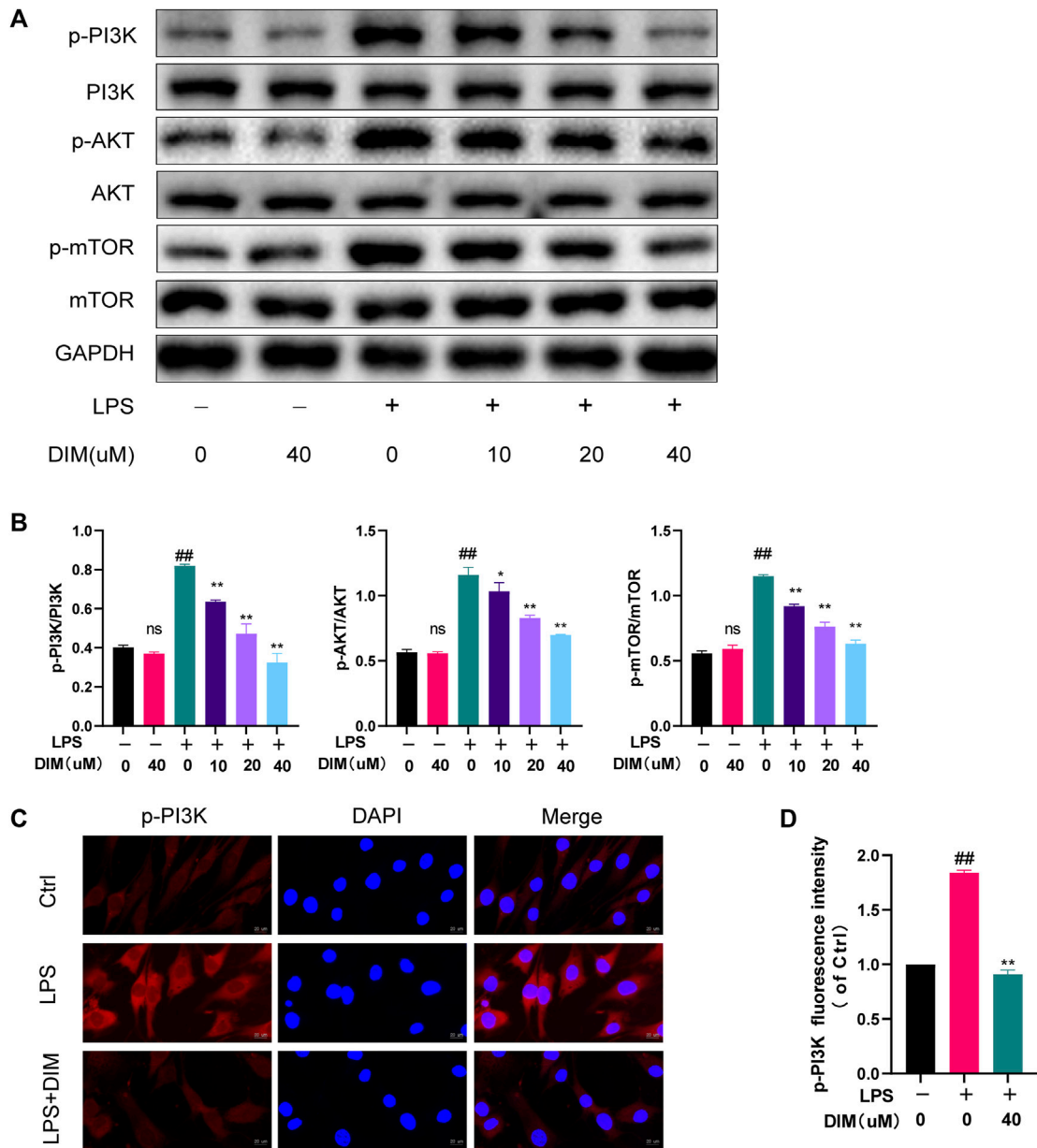
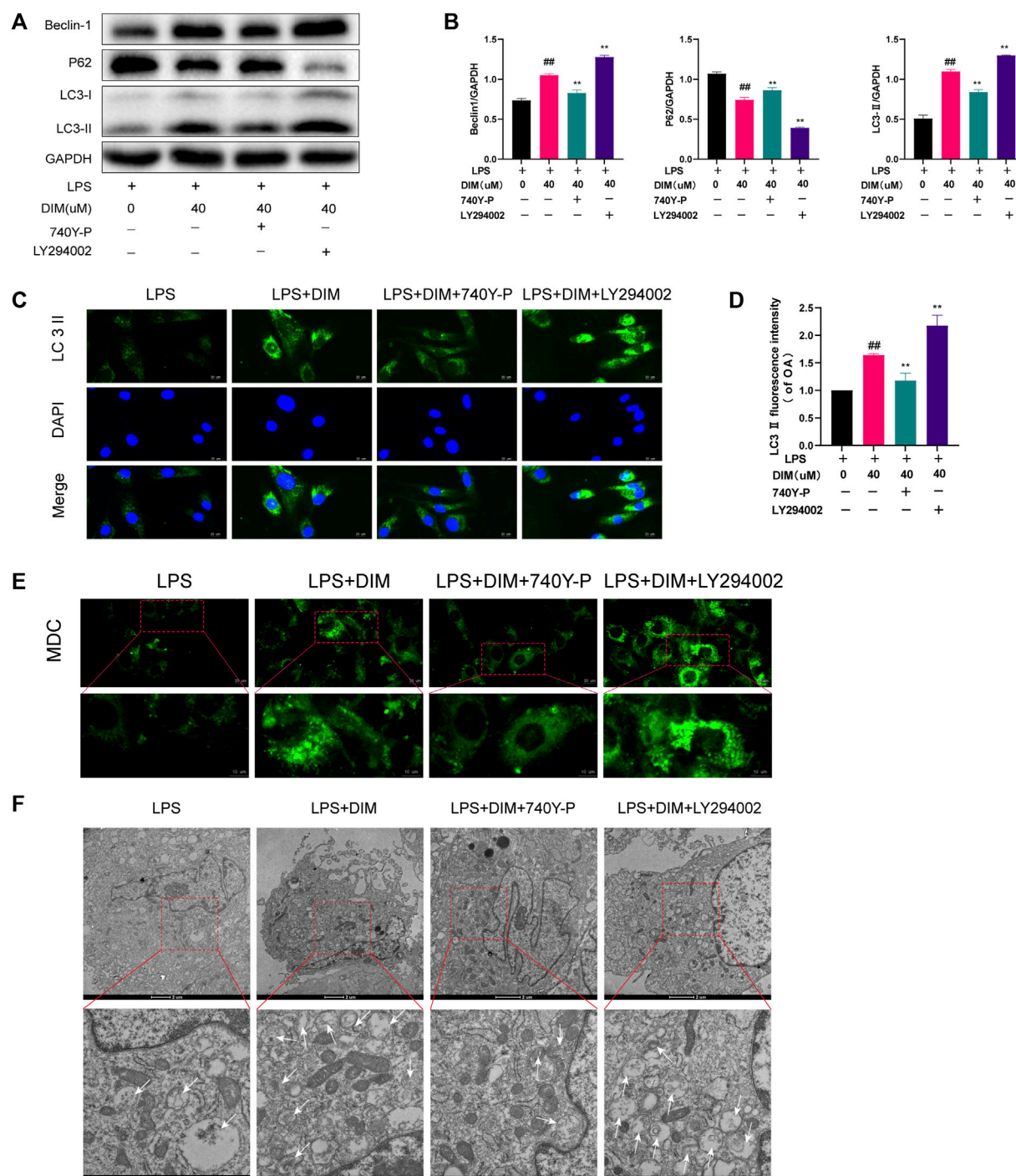


FIGURE 6

DIM inhibits the activation of the PI3K/AKT/mTOR signaling pathway (A,B) Effects of DIM on the protein expression levels of p-PI3K, total PI3K, p-AKT, total AKT, p-mTOR, and total mTOR in human chondrocytes treated as above were measured by western blotting and quantitation (C) After treatment, immunofluorescence staining showed the changes in the fluorescence intensity of p-PI3K in each group (scale bar, 20 μ m) (D) The fluorescence intensity was measured with the ImageJ software (U.S. National Institutes of Health, Bethesda). The data are presented as mean \pm SD values from three independent experiments. Using one-way ANOVA, NS, no statistical difference; # p < 0.05 vs. the control; ## p < 0.01 vs. the control; * p < 0.05 vs. the LPS group; ** p < 0.01 vs. the LPS group.

**FIGURE 7**

DIM enhances autophagy levels by modulating the PI3K/AKT/mTOR signaling pathway (A,B) Compared to the LPS + DIM group, the addition of PI3K activator (740Y-P) after treatment triggered a reduction in the level of autophagy, while the addition of PI3K inhibitor LY294002 increased the level of autophagy. Levels of autophagic marker proteins (beclin-1, p62, and LC3 II) were measured by western blotting and quantitation (C) The fluorescence intensity of LC3 II was detected by immunofluorescence staining (scale bar, 20 μ m) (D) The fluorescence intensity was measured with the ImageJ software (U.S. National Institutes of Health, Bethesda) (E) The number of chondrocytes autophagosomes was observed by MDC staining (punctate green staining represents autophagosomes; scale bar, 20 μ m; partially enlarged image scale bar, 10 μ m) (F) Microstructural detection of autophagosomes by transmission electron microscopy (White arrows indicate the formation of autophagosomes. Scale bar = 2 μ m; partially enlarged image scale bar, 500 nm). The data are presented as mean \pm SD values from three independent experiments. Using one-way ANOVA, NS, no statistical difference; # p < 0.05 vs. the LPS group; ## p < 0.01 vs. the LPS group; * p < 0.05 vs. the LPS + DIM group; ** p < 0.01 vs. the LPS + DIM group.

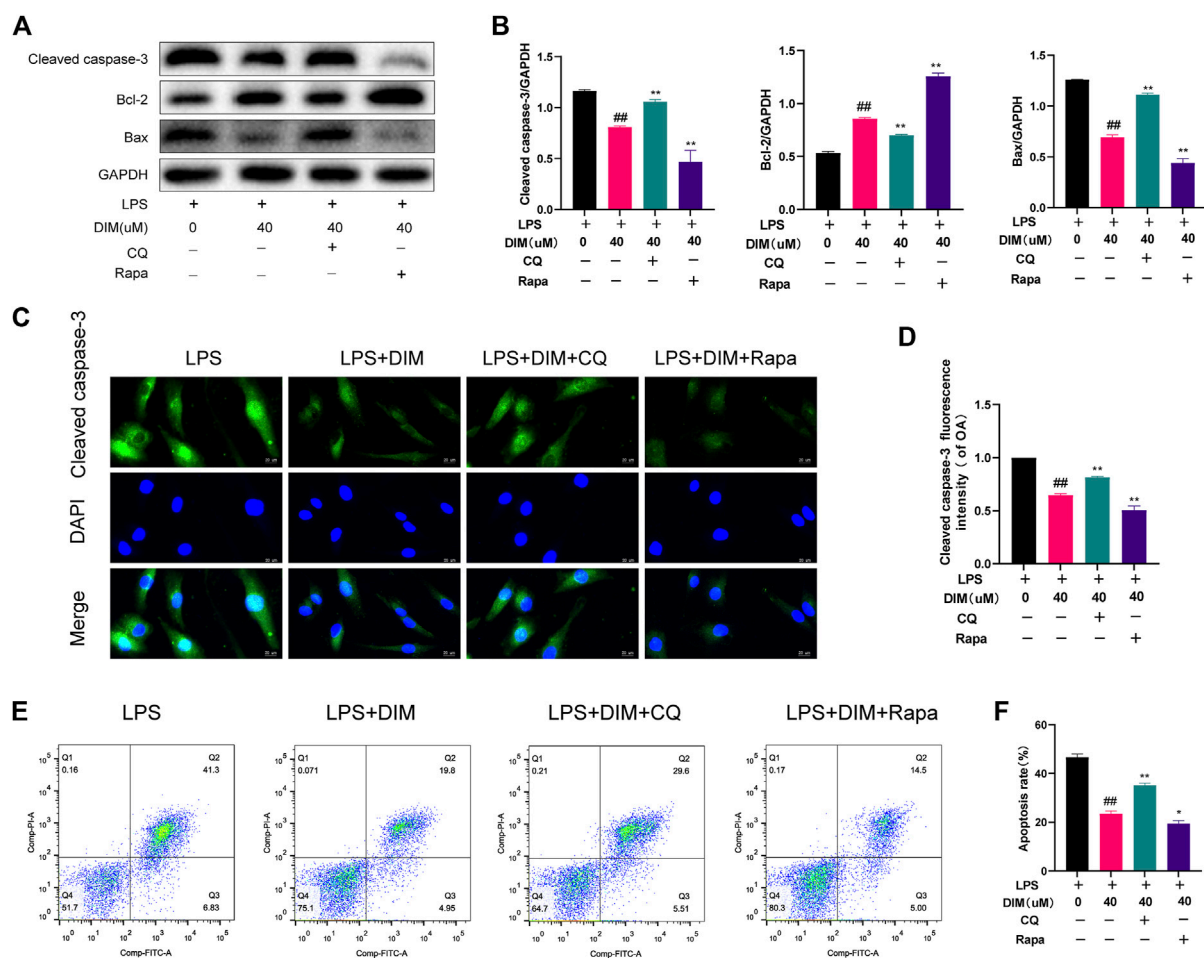


FIGURE 8

Activation of autophagy by DIM ameliorates LPS-induced chondrocyte apoptosis (A,B) Compared to the LPS + DIM group, the addition of an autophagy inhibitor (CQ) after treatment increased chondrocyte apoptosis, while the addition of an autophagy activator (Rapa) reduced chondrocyte apoptosis. Apoptosis marker proteins (cleaved caspase-3, Bcl-2, and Bax) were measured by western blotting and quantitation (C) The fluorescence intensity of cleaved caspase-3 was detected by immunofluorescence staining (scale bar, 20 μ m) (D) the fluorescence intensity was measured with the ImageJ software (U.S. National Institutes of Health, Bethesda) (E,F) The apoptosis rate of chondrocytes was detected by flow cytometry and quantitation. The data are presented as mean \pm SD values from three independent experiments. Using one-way ANOVA, NS, no statistical difference; # $p < 0.05$ vs. the LPS group; ## $p < 0.01$ vs. the LPS group; * $p < 0.05$ vs. the LPS + DIM group; ** $p < 0.01$ vs. the LPS + DIM group.

Aggrecan showed that the AODs of Collagen II and Aggrecan in articular cartilage were lower in the DMM group than those in the sham group. Compared to the DMM group, the AODs of Collagen II and Aggrecan were significantly increased after DIM treatment (Supplementary Figure S5), consistent with the *in vitro* results.

Discussion

OA is the most common joint disease and the leading cause of disability worldwide. It can limit the patient's daily activities, such as walking and running and other dependent behaviors, and severely affecting their quality of life, causing a significant social burden, with

a high prevalence in the elderly population. Recent epidemiological findings show that the prevalence of OA is 9.6% in elder men and 18% in elder women (Woolf and Pfleger, 2003; Verlaan et al., 2018). The most affected site of OA is the knee joint (Fransen et al., 2011). OA is caused by a variety of factors and is an extremely complex pathogenic process that involves several different pathophysiological mechanisms, including increased inflammatory stimulation, an imbalance in chondrocyte metabolism, increased apoptosis, and degradation of the cartilage matrix (Li et al., 2019). Current treatments are limited to oral medications, which can relieve joint swelling and pain but cannot completely cure the development of OA, and joint replacement surgery is still required in the long term, so there is still a need to develop safer and more effective drugs to treat OA (Vaishya et al., 2016).

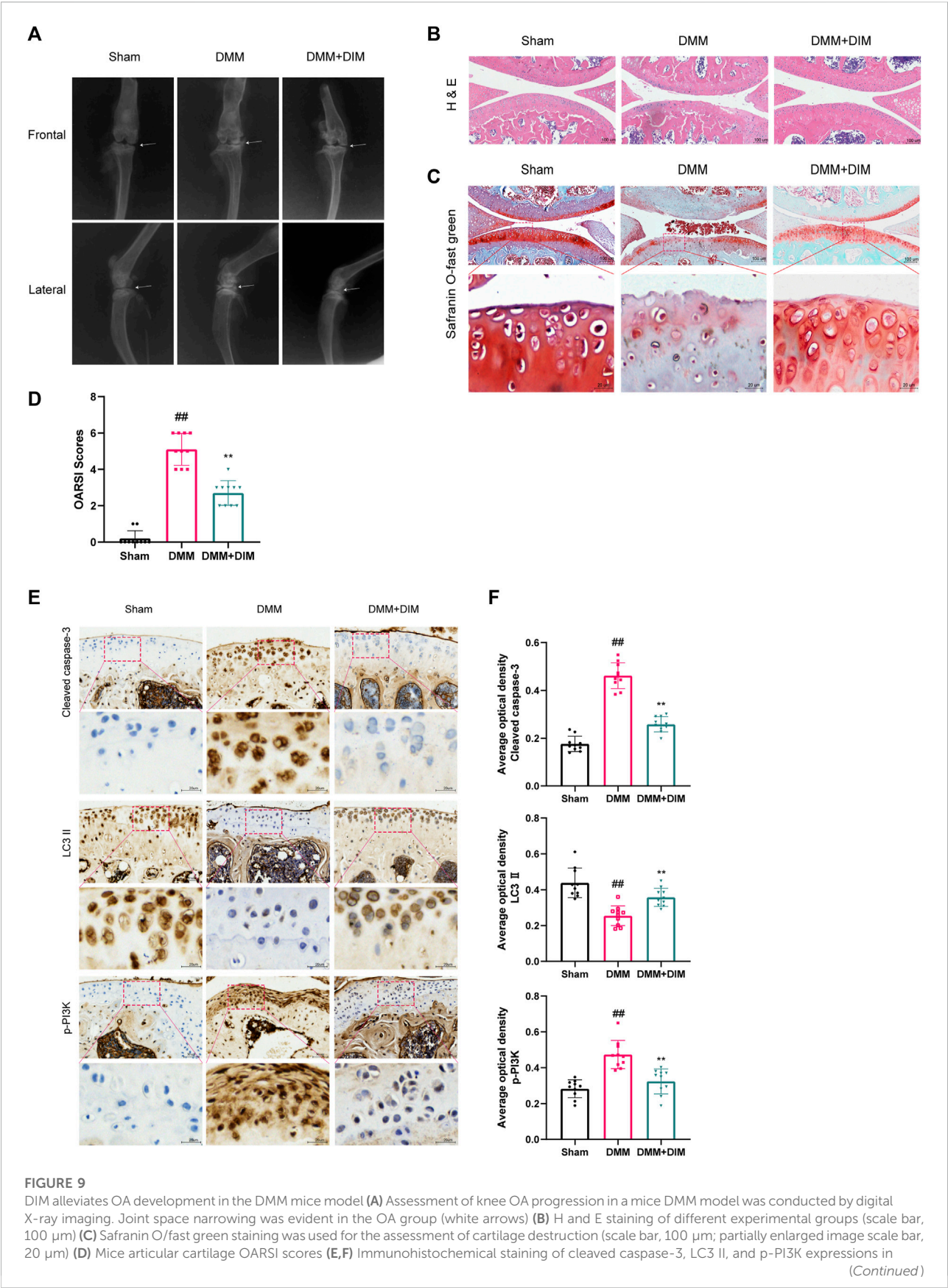


FIGURE 9 (Continued)

cartilage samples of different experimental groups (scale bar, 50 μm ; partially enlarged image scale bar, 20 μm) and AODs were analyzed by the ImageJ software (U.S. National Institutes of Health, Bethesda). The data are presented as mean \pm SD values from three independent experiments ($n = 10$ in each group). Using one-way ANOVA, NS, no statistical difference; # $p < 0.05$ vs. the Sham group; ## $p < 0.01$, vs. the Sham group, * $p < 0.05$ vs. the DMM group; ** $p < 0.01$ vs. the DMM group.

DIM is a natural Fat-soluble small molecule compound harvested from cruciferous vegetables which belongs to the class of indole glucosinolate (Maruthanila et al., 2014; Shi et al., 2017). Due to its lipophilic nature, DIM can directly cross the cell membrane into the cytoplasm to exert biological activity (Jellinck et al., 1993; Carpenter et al., 2016; Khan et al., 2019; Ong and Amstad, 2019; Martinotti et al., 2020). DIM can intracellularly regulate a variety of signaling pathways as well as signaling enzymes (Laiakis et al., 2020). For example, DIM can block PI3K/Akt/MTOR/NF- κ B signaling (Ahmad et al., 2013), activate AMP-activated protein kinases (Chen et al., 2012), inhibit nuclear factor kappa B (Cho et al., 2008; Weng et al., 2012), inhibit cell cycle protein-dependent kinases (Kim et al., 2012), and reduce androgen receptor levels (Palomera-Sanchez et al., 2017). In recent years, an increasing number of studies have explored the chondroprotective effects of plant components (Sukhikh et al., 2021). DIM has been found to have various health-promoting benefits. However, it remains unclear whether DIM has any effect on OA chondrocytes, which is explored in depth in this paper. We investigated the role and mechanism of DIM in arthritis both *in vivo* and *in vitro*.

It has been reported that chondrocytes are the only cell type that constitutes articular cartilage and are responsible for the synthesis and secretion of cartilage ECM macromolecules, such as collagen II and aggrecan (Goldring and Marcu, 2009; Musumeci et al., 2015; Guilak et al., 2018). In addition, chondrocytes also can synthesize matrix degrading enzymes, such as MMP-13 and ADAMTS-5 (Vincenti and Brinckerhoff, 2002; Rowan et al., 2008; Takahata et al., 2019; Meng et al., 2020). Currently, the synthesis and degradation status of cartilage matrix is mainly reflected indirectly by detecting anabolic and catabolic marker proteins as well as proteoglycan moieties in chondrocytes (Chang et al., 2019; Huang et al., 2020; Lin et al., 2021). Under normal physiological conditions, chondrocytes maintain a balance between the synthesis and degradation of ECM components to ensure the structural and functional integrity of cartilage (Musumeci et al., 2011a). However, in the pathogenesis of OA, chondrocytes produce excess matrix-degrading enzymes to damage the extracellular matrix, particularly MMP-13 and ADAMTS-5 (Kapoor et al., 2011). MMP-13 is a subclass of collagenase with the function of cleaving ECM collagen II (Bramono et al., 2004), while ADAMTS-5 is a zinc protein hydrolase that destroys aggrecan (Gendron et al., 2007). The decrease in matrix component synthesis and the increase in chondrocyte matrix breakdown by catabolic proteins

resulted in loss of cartilage matrix components and increased cartilage destruction. It has been reported that therapeutic substances targeting MMP-13 and ADAMTS-5 may be ideal agents for the treatment of OA (Burrage et al., 2006; Mead and Apte, 2018). In the present study, we found that DIM acts against LPS-induced chondrocyte matrix degradation with a protective effect, and DIM significantly inhibited the expression of catabolic indicators MMP-13 and ADAMTS-5 and increased the expression of anabolic indicators collagen II and aggrecan in cartilage ECM.

Increased apoptosis is another major cause of matrix degradation. Apoptosis is a form of programmed cell death that can be activated through several different pathways, including death receptor-mediated and mitochondria-dependent apoptosis (Musumeci et al., 2011a; Zamli and Sharif, 2011). Among the biomarkers of OA, inflammatory mediators play a clear role in chondrocyte apoptosis. The synthesis of pro-inflammatory cytokines, which contribute to increased apoptosis, is involved in the degeneration of the cartilage ECM (Wu et al., 2007; Musumeci et al., 2011b). Indeed, in human OA tissue specimens, dissolution and calcification of the descending ECM correlate with apoptosis, and the rate of apoptosis is positively correlated with the severity of OA (Musumeci et al., 2011a). Abnormal mechanical stress on normal cartilage can lead to chondrocyte apoptosis and result in cartilage degeneration and loss (Kim et al., 2002). In addition, the literature reports that DIM exerts neuroprotective effects through the production of brain-derived neurotrophic factor and antioxidant enzymes in oxidative stress-induced apoptosis in hippocampal neurons (Lee et al., 2019). We found that chondrocyte apoptosis was significantly increased after LPS stimulation, while pre-treatment with the addition of DIM reversed LPS-induced chondrocyte apoptosis and revealed an increase in anti-apoptotic protein levels (Bcl-2) and a decrease in pro-apoptotic protein levels (Bax and cleaved caspase-3). This indicates that DIM can also play an anti-apoptotic role in chondrocytes.

Our previous studies have demonstrated that ECM degradation can be improved by activating autophagy in OA chondrocytes (Huang et al., 2020; Wang et al., 2022). Next, we conducted an in-depth study of the mechanism by which DIM inhibits LPS-induced chondrocyte apoptosis *in vitro*. Previously, it was reported that, in human prostate cancer cells, DIM induced cytoprotective autophagy through the induction of AMPK activation by AEG-1 (Draz et al., 2017). DIM inhibited the

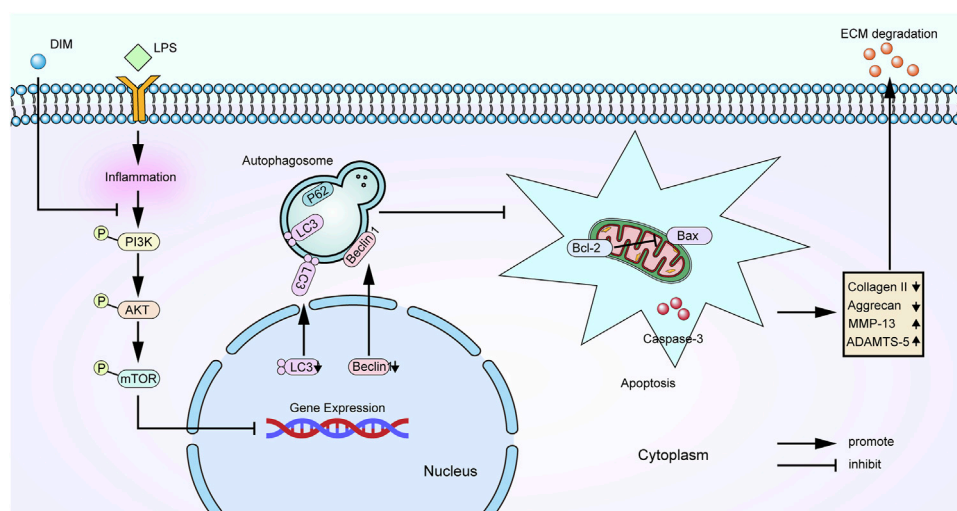


FIGURE 10
Schematic representation of the role of DIM in OA chondrocytes.

proliferation of gastric cancer cells through the miR-30e/ATG5 pathway involved in autophagy control (Ye et al., 2016). Therefore, we hypothesized that the molecular mechanism by which DIM exerts its protective effect may be related to restoring the level of chondrocyte autophagy. Cellular autophagy is an important protective mechanism for cells to maintain homeostasis and survival in the internal environment (Mizushima, 2007; He and Klionsky, 2009; Ryter et al., 2013), and changes in inflammation, starvation, pathogen infection, and endoplasmic reticulum stress can cause alterations in autophagy. In addition, autophagy is known to regulate a variety of cellular processes, such as apoptosis, pathogen removal, antigen presentation, and inflammation and is associated with many human diseases (Levine and Kroemer, 2008; Doria et al., 2013). Autophagy has been widely reported to be associated with the development of OA, and autophagic flux has been suggested as a possible therapeutic target for OA (He and Cheng, 2018; Huang et al., 2020; Xu et al., 2021). *In vitro*, we found that autophagy in chondrocytes after LPS stimulation was significantly decreased and LC3 II and beclin-1 protein expression levels were decreased, p62 protein expression was increased, the number of autophagic vesicles was decreased, and autophagic flux was blocked, but these phenomena were significantly reversed after the application of DIM treatment. We employed CQ and Rapa, as a specific inhibitor and activators of autophagy, to determine whether DIM regulates apoptosis through autophagy. We found that DIM ameliorated LPS-induced apoptosis, but CQ reversed this phenomenon; while activation of autophagy by Rapa further inhibited apoptosis, acting synergistically with DIM. Our results indicate that DIM inhibits LPS-induced chondrocyte apoptosis by restoring the level of chondrocyte autophagy.

The literature reports that the PI3K/AKT/mTOR signaling pathway regulates a variety of cellular processes, including cellular autophagy, metabolism, inflammation, metabolism, angiogenesis, and the cell cycle (Malemud, 2015). It is also an important regulator of chondrocyte autophagic flux, and inhibition of PI3K/AKT/mTOR signaling pathway activation to promote increased autophagy is an effective strategy to improve OA symptoms (Xue et al., 2017; He and Cheng, 2018; Han et al., 2021). In our study, we found that the PI3K/AKT/mTOR signaling pathway was activated after LPS stimulation of chondrocytes compared to the normal group, and the expressions of p-PI3K, p-AKT, and p-mTOR were increased, while DIM treatment significantly inhibited LPS-induced activation of this pathway. Moreover, we employed the PI3K agonist 740Y-P and PI3K inhibitor LY294002 to determine whether DIM regulates autophagy through PI3K/AKT/mTOR signal pathway. We found that activation of the PI3K/AKT/mTOR pathway by 740Y-P reversed DIM-induced autophagy recovery, while LY294002 inhibited the activation of the PI3K/AKT/mTOR pathway and further enhanced autophagy in chondrocytes, synergizing with DIM. The results showed that DIM enhanced the autophagy level of chondrocytes by inhibiting the PI3K/AKT/mTOR signaling pathway.

In vivo, we used the DMM method to establish a C57BL/6 mice OA model, which was assessed by hematoxylin and eosin staining, X-ray, safranin O/fast green staining, and immunohistochemistry. We found that, compared to mice in the sham group, the model mice in the DMM group showed severe cartilage destruction in the knee joint with rough surfaces, massive proteoglycan loss, reduced autophagy protein levels, increased apoptotic protein levels, and activated pathway proteins, while DIM treatment improved these

symptoms, reversed chondrocyte apoptosis and ECM degradation, and reduced the OARSI score in DMM mice. The results of *in vivo* and *in vitro* were generally consistent. Taken together, the present study showed that DIM, as an easily accessible botanical component, not only improved the degeneration of articular cartilage in mice, but also had a significant protective effect on inflammation-induced chondrocyte destruction. Therefore, it is of great value to further investigate the potential applications of DIM in the treatment of osteoarthritis.

Conclusion

We found that DIM can act as a protective agent for chondrocytes. More importantly, our results reveal the mechanism by which DIM exerts its chondroprotective effects (Figure 10). DIM can reduce inflammation-induced chondrocytes apoptosis and extracellular matrix degradation by activating PI3K/AKT/mTOR-mediated autophagy. This study provides new guiding directions for DIM as a promising drug for the treatment of OA.

Data availability statement

The original contributions presented in the study are included in the article/Supplementary Material, further inquiries can be directed to the corresponding authors.

Ethics statement

The study was conducted in accordance with the Declaration of Helsinki and approved by the Medical Ethics Committee of the First Affiliated Hospital of Anhui Medical University (protocol code PJ2022-04-55) for studies involving humans. The animal study protocol was approved by the Animal Ethics Committee of Anhui Medical University (protocol code LISC20190738).

Author contributions

HT and KQ: Conceptualization, Validation, Data curation and Writing—original draft. AW: Methodology. SL: Formal

analysis. SF: Software. WG: Resources. ML: Investigation. WH, HZ, and ZY: Writing—review and editing, Funding acquisition, Supervision, Visualization.

Funding

This study was supported by the Provincial Natural Science Foundation of Anhui (2008085MH247) and Provincial University Natural Science Foundation of Anhui (KJ 2021A0299).

Acknowledgments

We thank WS, YK, RZ, JW, YR, and MW for their technical guidance during the experiments. We also thank the Center for Scientific Research of Anhui Medical University for providing valuable experimental facilities.

Conflict of interest

The authors declare that the research was conducted in the absence of any commercial or financial relationships that could be construed as a potential conflict of interest.

The handling editor YC declared a shared parent affiliation with the author(s) at the time of review.

Publisher's note

All claims expressed in this article are solely those of the authors and do not necessarily represent those of their affiliated organizations, or those of the publisher, the editors and the reviewers. Any product that may be evaluated in this article, or claim that may be made by its manufacturer, is not guaranteed or endorsed by the publisher.

Supplementary material

The Supplementary Material for this article can be found online at: <https://www.frontiersin.org/articles/10.3389/fphar.2022.999851/full#supplementary-material>

References

- Ahmad, A., Biersack, B., Li, Y., Kong, D., Bao, B., Schobert, R., et al. (2013). Targeted regulation of PI3K/Akt/mTOR/NF- κ B signaling by indole compounds and their derivatives: Mechanistic details and biological implications for cancer therapy. *Anticancer. Agents Med. Chem.* 13 (7), 1002–1013. doi:10.2174/18715206113139990078
- Biederick, A., Kern, H. F., and Elsässer, H. P. (1995). Monodansylcadaverine (MDC) is a specific *in vivo* marker for autophagic vacuoles. *Eur. J. Cell Biol.* 66 (1), 3–14.
- Bouderlique, T., Vuppalapati, K. K., Newton, P. T., Li, L., Barenus, B., and Chagin, A. S. (2016). Targeted deletion of Atg5 in chondrocytes promotes age-related osteoarthritis. *Ann. Rheum. Dis.* 75 (3), 627–631. doi:10.1136/annrheumdis-2015-207742
- Boya, P., Reggiori, F., and Codogno, P. (2013). Emerging regulation and functions of autophagy. *Nat. Cell Biol.* 15 (7), 713–720. doi:10.1038/ncb2788

- Bramono, D. S., Richmond, J. C., Weitzel, P. P., Kaplan, D. L., and Altman, G. H. (2004). Matrix metalloproteinases and their clinical applications in orthopaedics. *Clin. Orthop. Relat. Res.* 428, 272–285. doi:10.1097/01.blo.0000144166.66737.3a
- Burrage, P. S., Mix, K. S., and Brinckerhoff, C. E. (2006). Matrix metalloproteinases: Role in arthritis. *Front. Biosci.* 11, 529–543. doi:10.2741/1817
- Carpenter, T. S., Parkin, J., and Khalid, S. (2016). The free energy of small solute permeation through the *Escherichia coli* outer membrane has a distinctly asymmetric profile. *J. Phys. Chem. Lett.* 7 (17), 3446–3451. doi:10.1021/acs.jpclett.6b01399
- Chang, S. H., Mori, D., Kobayashi, H., Mori, Y., Nakamoto, H., Okada, K., et al. (2019). Excessive mechanical loading promotes osteoarthritis through the gremlin-1-NF- κ B pathway. *Nat. Commun.* 10 (1), 1442. doi:10.1038/s41467-019-09491-5
- Chen, D., Banerjee, S., Cui, Q. C., Kong, D., Sarkar, F. H., and Dou, Q. P. (2012). Activation of AMP-activated protein kinase by 3, 3'-Diindolylmethane (DIM) is associated with human prostate cancer cell death *in vitro* and *in vivo*. *PLoS One* 7 (10), e47186. doi:10.1371/journal.pone.0047186
- Cho, H. J., Seon, M. R., Lee, Y. M., Kim, J., Kim, J. K., Kim, S. G., et al. (2008). 3, 3'-Diindolylmethane suppresses the inflammatory response to lipopolysaccharide in murine macrophages. *J. Nutr.* 138 (1), 17–23. doi:10.1093/jn/138.1.17
- Cucchiari, M., de Girolamo, L., Filardo, G., Oliveira, J. M., Orth, P., Pape, D., et al. (2016). Basic science of osteoarthritis. *J. Exp. Orthop.* 3 (1), 22. doi:10.1186/s40634-016-0060-6
- Ding, Y., Wang, L., Zhao, Q., Wu, Z., and Kong, L. (2019). MicroRNA-93 inhibits chondrocyte apoptosis and inflammation in osteoarthritis by targeting the TLR4/NF- κ B signaling pathway. *Int. J. Mol. Med.* 43 (2), 779–790. doi:10.3892/ijmm.2018.4033
- Dong, L., Xia, S., Gao, F., Zhang, D., Chen, J., and Zhang, J. (2010). 3, 3'-Diindolylmethane attenuates experimental arthritis and osteoclastogenesis. *Biochem. Pharmacol.* 79 (5), 715–721. doi:10.1016/j.bcp.2009.10.010
- Doria, A., Gatto, M., and Punzi, L. (2013). Autophagy in human health and disease. *N. Engl. J. Med.* 368 (19), 1845–1846. doi:10.1056/NEJMc1303158
- Draz, H., Goldberg, A. A., Titorenko, V. I., Tomlinson, G. S., Safe, S. H., and Sanderson, J. T. (2017). Diindolylmethane and its halogenated derivatives induce protective autophagy in human prostate cancer cells via induction of the oncogenic protein AEG-1 and activation of AMP-activated protein kinase (AMPK). *Cell. Signal.* 40, 172–182. doi:10.1016/j.cellsig.2017.09.006
- Du, H., Zhang, X., Zeng, Y., Huang, X., Chen, H., Wang, S., et al. (2019). A novel phytochemical, DIM, inhibits proliferation, migration, invasion and TNF- α induced inflammatory cytokine production of synovial fibroblasts from rheumatoid arthritis patients by targeting MAPK and AKT/mTOR signal pathway. *Front. Immunol.* 10, 1620. doi:10.3389/fimmu.2019.01620
- Fransen, M., Bridgett, L., March, L., Hoy, D., Penserga, E., and Brooks, P. (2011). The epidemiology of osteoarthritis in Asia. *Int. J. Rheum. Dis.* 14 (2), 113–121. doi:10.1111/j.1756-185X.2011.01608.x
- Gendron, C., Kashiwagi, M., Lim, N. H., Enghild, J. J., Thøgersen, I. B., Hughes, C., et al. (2007). Proteolytic activities of human ADAMTS-5: Comparative studies with ADAMTS-4. *J. Biol. Chem.* 282 (25), 18294–18306. doi:10.1074/jbc.M701523200
- Glasson, S. S., Chambers, M. G., Van Den Berg, W. B., and Little, C. B. (2010). The OARSI histopathology initiative - recommendations for histological assessments of osteoarthritis in the mouse. *Osteoarthr. Cartil.* 18 (3), S17–S23. doi:10.1016/j.joca.2010.05.025
- Glick, D., Barth, S., and Macleod, K. F. (2010). Autophagy: Cellular and molecular mechanisms. *J. Pathol.* 221 (1), 3–12. doi:10.1002/path.2697
- Glyn-Jones, S., Palmer, A. J. R., Agricola, R., Price, A. J., Vincent, T. L., Weinans, H., et al. (2015). Osteoarthritis. *Lancet* 386 (9991), 376–387. doi:10.1016/s0140-6736(14)60802-3
- Goldring, M. B., and Marcu, K. B. (2009). Cartilage homeostasis in health and rheumatic diseases. *Arthritis Res. Ther.* 11 (3), 224. doi:10.1186/ar2592
- Goldring, M. B. (2006). Update on the biology of the chondrocyte and new approaches to treating cartilage diseases. *Best. Pract. Res. Clin. Rheumatol.* 20 (5), 1003–1025. doi:10.1016/j.berh.2006.06.003
- Guilak, F., Nims, R. J., Dicks, A., Wu, C. L., and Meulenbelt, I. (2018). Osteoarthritis as a disease of the cartilage pericellular matrix. *Matrix Biol.* 71–72, 40–50. doi:10.1016/j.matbio.2018.05.008
- Han, G., Zhang, Y., and Li, H. (2021). The combination treatment of curcumin and probucol protects chondrocytes from TNF- α induced inflammation by enhancing autophagy and reducing apoptosis via the PI3K-Akt-mTOR pathway. *Oxid. Med. Cell. Longev.* 2021, 5558066. doi:10.1155/2021/5558066
- He, C., and Klionsky, D. J. (2009). Regulation mechanisms and signaling pathways of autophagy. *Annu. Rev. Genet.* 43, 67–93. doi:10.1146/annurev-genet-102808-114910
- He, W., and Cheng, Y. (2018). Inhibition of miR-20 promotes proliferation and autophagy in articular chondrocytes by PI3K/AKT/mTOR signaling pathway. *Biomed. Pharmacother.* 97, 607–615. doi:10.1016/j.biopha.2017.10.152
- Huang, W., Cheng, C., Shan, W. S., Ding, Z. F., Liu, F. E., Lu, W., et al. (2020). Knockdown of SGK1 alleviates the IL-1 β -induced chondrocyte anabolic and catabolic imbalance by activating FoxO1-mediated autophagy in human chondrocytes. *FEBS J.* 287 (1), 94–107. doi:10.1111/febs.15009
- Jellinck, P. H., Makin, H. L., Sepkovic, D. W., and Bradlow, H. L. (1993). Influence of indole carbinols and growth hormone on the metabolism of 4-androstenedione by rat liver microsomes. *J. Steroid Biochem. Mol. Biol.* 46 (6), 791–798. doi:10.1016/0960-0760(93)90320-v
- Kapoor, M., Martel-Pelletier, J., Lajeunesse, D., Pelletier, J. P., and Fahmi, H. (2011). Role of proinflammatory cytokines in the pathophysiology of osteoarthritis. *Nat. Rev. Rheumatol.* 7 (1), 33–42. doi:10.1038/nrrheum.2010.196
- Khan, A., Wang, C., Sun, X., Killpatrick, A., and Guo, M. (2019). Physicochemical and microstructural properties of polymerized whey protein encapsulated 3, 3'-diindolylmethane nanoparticles. *Molecules* 24 (4), E702. doi:10.3390/molecules24040702
- Kim, H. T., Lo, M. Y., and Pillarisetty, R. (2002). Chondrocyte apoptosis following intraarticular fracture in humans. *Osteoarthr. Cartil.* 10 (9), 747–749. doi:10.1053/joca.2002.0828
- Kim, S. J., Lee, J. S., and Kim, S. M. (2012). 3, 3'-Diindolylmethane suppresses growth of human esophageal squamous cancer cells by G1 cell cycle arrest. *Oncol. Rep.* 27 (5), 1669–1673. doi:10.3892/or.2012.1662
- Krenn, V., Morawietz, L., Burmester, G. R., Kinne, R. W., Mueller-Ladner, U., Muller, B., et al. (2006). Synovitis score: Discrimination between chronic low-grade and high-grade synovitis. *Histopathology* 49 (4), 358–364. doi:10.1111/j.1365-2559.2006.02508.x
- Krenn, V., Morawietz, L., Häupl, T., Neidel, J., Petersen, I., König, A., et al. (2002). Grading of chronic synovitis—a histopathological grading system for molecular and diagnostic pathology. *Pathol. Res. Pract.* 198 (5), 317–325. doi:10.1078/0344-0338-5710261
- Laiakis, E. C., McCart, E. A., Deziel, A., Rittase, W. B., Bouten, R. M., Jha, J., et al. (2020). Effect of 3, 3'-diindolylmethane on pulmonary injury following thoracic irradiation in CBA mice. *Health Phys.* 119 (6), 746–757. doi:10.1097/hp.0000000000001257
- Lee, B. D., Yoo, J. M., Baek, S. Y., Li, F. Y., Sok, D. E., and Kim, M. R. (2019). 3, 3'-diindolylmethane promotes BDNF and antioxidant enzyme formation via TrkB/akt pathway activation for neuroprotection against oxidative stress-induced apoptosis in hippocampal neuronal cells. *Antioxidants (Basel)* 9 (1), E3. doi:10.3390/antiox9010003
- Levine, B., and Kroemer, G. (2008). Autophagy in the pathogenesis of disease. *Cell* 132 (1), 27–42. doi:10.1016/j.cell.2007.12.018
- Li, H., Xie, S., Li, H., Zhang, R., and Zhang, H. (2020). LncRNA MALAT1 mediates proliferation of LPS treated-articular chondrocytes by targeting the miR-146a-PI3K/Akt/mTOR axis. *Life Sci.* 254, 116801. doi:10.1016/j.lfs.2019.116801
- Li, Y. S., Zhang, F. J., Zeng, C., Luo, W., Xiao, W. F., Gao, S. G., et al. (2016). Autophagy in osteoarthritis. *Jt. Bone Spine* 83 (2), 143–148. doi:10.1016/j.jbspin.2015.06.009
- Li, Y., Wu, Y., Jiang, K., Han, W., Zhang, J., Xie, L., et al. (2019). Mangiferin prevents TBHP-induced apoptosis and ECM degradation in mouse osteoarthritic chondrocytes via restoring autophagy and ameliorates murine osteoarthritis. *Oxid. Med. Cell. Longev.* 2019, 8783197. doi:10.1155/2019/8783197
- Lian, W. S., Ko, J. Y., Wu, R. W., Sun, Y. C., Chen, Y. S., Wu, S. L., et al. (2018). MicroRNA-128a represses chondrocyte autophagy and exacerbates knee osteoarthritis by disrupting Atg12. *Cell Death Dis.* 9 (9), 919. doi:10.1038/s41419-018-0994-y
- Lin, Z., Miao, J., Zhang, T., He, M., Wang, Z., Feng, X., et al. (2021). JUNB-FBXO21-ERK axis promotes cartilage degeneration in osteoarthritis by inhibiting autophagy. *Aging Cell* 20 (2), e13306. doi:10.1111/acel.13306
- Loeser, R. F. (2011). Aging and osteoarthritis. *Curr. Opin. Rheumatol.* 23 (5), 492–496. doi:10.1097/BOR.0b013e3283494005
- Lorenz, W., Buhrmann, C., Mobasheri, A., Lueders, C., and Shakibaei, M. (2013). Bacterial lipopolysaccharides form procollagen-endotoxin complexes that trigger cartilage inflammation and degeneration: Implications for the development of rheumatoid arthritis. *Arthritis Res. Ther.* 15 (5), R111. doi:10.1186/ar4291
- Luo, Q., Yang, A., Cao, Q., and Guan, H. (2018). 3, 3'-Diindolylmethane protects cardiomyocytes from LPS-induced inflammatory response and apoptosis. *BMC Pharmacol. Toxicol.* 19 (1), 71. doi:10.1186/s40360-018-0262-x
- Malemud, C. J. (2015). The PI3K/akt/PTEN/mTOR pathway: A fruitful target for inducing cell death in rheumatoid arthritis? *Future Med. Chem.* 7 (9), 1137–1147. doi:10.4155/fmc.15.55
- Martinotti, C., Ruiz-Perez, L., Deplazes, E., and Mancera, R. L. (2020). Molecular dynamics simulation of small molecules interacting with biological membranes. *Chemphyschem* 21 (14), 1486–1514. doi:10.1002/cphc.202000219

- Maruthanila, V. L., Poornima, J., and Mirunalini, S. (2014). Attenuation of carcinogenesis and the mechanism underlying by the influence of indole-3-carbinol and its metabolite 3, 3'-diindolylmethane: A therapeutic marvel. *Adv. Pharmacol. Sci.* 2014, 832161. doi:10.1155/2014/832161
- Maudens, P., Jordan, O., and Allémann, E. (2018). Recent advances in intra-articular drug delivery systems for osteoarthritis therapy. *Drug Discov. Today* 23 (10), 1761–1775. doi:10.1016/j.drudis.2018.05.023
- Mayeux, P. R. (1997). Pathobiology of lipopolysaccharide. *J. Toxicol. Environ. Health* 51 (5), 415–435. doi:10.1080/00984109708984034
- Mead, T. J., and Apte, S. S. (2018). ADAMTS proteins in human disorders. *Matrix Biol.* 71–72, 225–239. doi:10.1016/j.matbio.2018.06.002
- Meng, P., Zhang, F., Zhang, Y., Wei, H., Tan, S., Guo, X., et al. (2020). ADAMTS4 and ADAMTS5 may be considered as new molecular therapeutic targets for cartilage damages with Kashin-Beck Disease. *Med. Hypotheses* 135, 109440. doi:10.1016/j.mehy.2019.109440
- Mizushima, N. (2007). Autophagy: Process and function. *Genes Dev.* 21, 2861–2873. doi:10.1101/gad.1599207
- Mizushima, N., and Levine, B. (2020). Autophagy in human diseases. *N. Engl. J. Med.* 383 (16), 1564–1576. doi:10.1056/NEJMr2022774
- Munakarmi, S., Chand, L., Shin, H. B., Jang, K. Y., and Jeong, Y. J. (2020). Indole-3-Carbinol derivative DIM mitigates carbon tetrachloride-induced acute liver injury in mice by inhibiting inflammatory response, apoptosis and regulating oxidative stress. *Int. J. Mol. Sci.* 21 (6), E2048. doi:10.3390/ijms21062048
- Musumeci, G., Aiello, F. C., Szyclinska, M. A., Di Rosa, M., Castrogiovanni, P., and Mobasher, A. (2015). Osteoarthritis in the XXIst century: Risk factors and behaviours that influence disease onset and progression. *Int. J. Mol. Sci.* 16 (3), 6093–6112. doi:10.3390/ijms16036093
- Musumeci, G., Loreto, C., Carnazza, M. L., and Martinez, G. (2011a). Characterization of apoptosis in articular cartilage derived from the knee joints of patients with osteoarthritis. *Knee Surg. Sports Traumatol. Arthrosc.* 19 (2), 307–313. doi:10.1007/s00167-010-1215-0
- Musumeci, G., Loreto, C., Carnazza, M. L., Strehin, I., and Elisseeff, J. (2011b). OA cartilage derived chondrocytes encapsulated in poly(ethylene glycol) diacrylate (PEGDA) for the evaluation of cartilage restoration and apoptosis in an *in vitro* model. *Histol. Histopathol.* 26 (10), 1265–1278. doi:10.14670/hh-26.1265
- Niemann, A., Baltes, J., and Elsässer, H. P. (2001). Fluorescence properties and staining behavior of monodansylpentane, a structural homologue of the lysosomotropic agent monodansylcadaverine. *J. Histochem. Cytochem.* 49 (2), 177–185. doi:10.1177/002215540104900205
- Niemann, A., Takatsuki, A., and Elsässer, H. P. (2000). The lysosomotropic agent monodansylcadaverine also acts as a solvent polarity probe. *J. Histochem. Cytochem.* 48 (2), 251–258. doi:10.1177/002215540004800210
- Ong, I. L. H., and Amstad, E. (2019). Selectively permeable double emulsions. *Small* 15 (44), e1903054. doi:10.1002/smll.201903054
- Palomera-Sanchez, Z., Watson, G. W., Wong, C. P., Beaver, L. M., Williams, D. E., Dashwood, R. H., et al. (2017). The phytochemical 3, 3'-diindolylmethane decreases expression of AR-controlled DNA damage repair genes through repressive chromatin modifications and is associated with DNA damage in prostate cancer cells. *J. Nutr. Biochem.* 47, 113–119. doi:10.1016/j.jnutbio.2017.05.005
- Polewska, J. (2012). Autophagy--molecular mechanism, apoptosis and cancer. *Postepy Hig. Med. Dosw.* 66, 921–936. doi:10.5604/17322693.1021109
- Qin, N., Wei, L., Li, W., Yang, W., Cai, L., Qian, Z., et al. (2017). Local intra-articular injection of resveratrol delays cartilage degeneration in C57BL/6 mice by inducing autophagy via AMPK/mTOR pathway. *J. Pharmacol. Sci.* 134 (3), 166–174. doi:10.1016/j.jphs.2017.06.002
- Ravikumar, B., Sarkar, S., Davies, J. E., Futter, M., Garcia-Arencibia, M., Green-Thompson, Z. W., et al. (2010). Regulation of mammalian autophagy in physiology and pathophysiology. *Physiol. Rev.* 90 (4), 1383–1435. doi:10.1152/physrev.00030.2009
- Rowan, A. D., Litherland, G. J., Hui, W., and Milner, J. M. (2008). Metalloproteases as potential therapeutic targets in arthritis treatment. *Expert Opin. Ther. Targets* 12 (1), 1–18. doi:10.1517/14728222.12.1.1
- Ryter, S. W., CloonanSuzanne, M., Choi and Augustine, M. K. (2013). Autophagy: A critical regulator of cellular metabolism and homeostasis. *Mol. Cells* 36 (1), 7–16. doi:10.1007/s10059-013-0140-8
- Rzemieniec, J., Litwa, E., Wnuk, A., Lason, W., Krzeptowski, W., and Kajta, M. (2016). Selective aryl hydrocarbon receptor modulator 3, 3'-diindolylmethane impairs AhR and ARNT signaling and protects mouse neuronal cells against hypoxia. *Mol. Neurobiol.* 53 (8), 5591–5606. doi:10.1007/s12035-015-9471-0
- Sasaki, H., Takayama, K., Matsushita, T., Ishida, K., Kubo, S., Matsumoto, T., et al. (2012). Autophagy modulates osteoarthritis-related gene expression in human chondrocytes. *Arthritis Rheum.* 64 (6), 1920–1928. doi:10.1002/art.34323
- Shi, H., Xu, X., Zhang, B., Xu, J., Pan, Z., Gong, A., et al. (2017). 3, 3'-Diindolylmethane stimulates exosomal Wnt11 autocrine signaling in human umbilical cord mesenchymal stem cells to enhance wound healing. *Theranostics* 7 (6), 1674–1688. doi:10.7150/thno.18082
- Sukhikh, S., Noskova, S., Ivanova, S., Ulrikh, E., Izgaryshev, A., and Babich, O. (2021). Chondroprotection and molecular mechanism of action of phytonutraceuticals on osteoarthritis. *Molecules* 26 (8), 2391. doi:10.3390/molecules26082391
- Takahata, Y., Nakamura, E., Hata, K., Wakabayashi, M., Murakami, T., Wakamori, K., et al. (2019). Sox4 is involved in osteoarthritic cartilage deterioration through induction of ADAMTS4 and ADAMTS5. *Faseb J.* 33 (1), 619–630. doi:10.1096/fj.201800259R
- Takayama, K., Kawakami, Y., Kobayashi, M., Greco, N., Cummins, J. H., Matsushita, T., et al. (2014). Local intra-articular injection of rapamycin delays articular cartilage degeneration in a murine model of osteoarthritis. *Arthritis Res. Ther.* 16 (6), 482. doi:10.1186/s13075-014-0482-4
- Vaishya, R., Pariyo, G. B., Agarwal, A. K., and Vijay, V. (2016). Non-operative management of osteoarthritis of the knee joint. *J. Clin. Orthop. Trauma* 7 (3), 170–176. doi:10.1016/j.jcot.2016.05.005
- Vázquez, C. L., and Colombo, M. I. (2009). Assays to assess autophagy induction and fusion of autophagic vacuoles with a degradative compartment, using monodansylcadaverine (MDC) and DQ-BSA. *Methods Enzymol.* 452, 85–95. doi:10.1016/s0076-6879(08)03606-9
- Verlaan, L., Boeckesteijn, R. J., Oomen, P. W., Liu, W. Y., Peters, M. J. M., Witlox, M. A., et al. (2018). Biomechanical alterations during sit-to-stand transfer are caused by a synergy between knee osteoarthritis and obesity. *Biomed. Res. Int.* 2018, 3519498. doi:10.1155/2018/3519498
- Vincenti, M. P., and Brinckerhoff, C. E. (2002). Transcriptional regulation of collagenase (MMP-1, MMP-13) genes in arthritis: Integration of complex signaling pathways for the recruitment of gene-specific transcription factors. *Arthritis Res.* 4 (3), 157–164. doi:10.1186/ar401
- Wang, A., Fang, S., Zhong, L., Lu, M., Zhou, H., Huang, W., et al. (2022). Shikonin, a promising therapeutic drug for osteoarthritis that acts via autophagy activation. *Int. Immunopharmacol.* 106, 108563. doi:10.1016/j.intimp.2022.108563
- Weng, J. R., Bai, L. Y., Chiu, C. F., Wang, Y. C., and Tsai, M. H. (2012). The dietary phytochemical 3, 3'-diindolylmethane induces G2/M arrest and apoptosis in oral squamous cell carcinoma by modulating Akt-NF-κB, MAPK, and p53 signaling. *Chem. Biol. Interact.* 195 (3), 224–230. doi:10.1016/j.cbi.2012.01.003
- Woolf, A. D., and Pfleger, B. (2003). Burden of major musculoskeletal conditions. *Bull. World Health Organ.* 81 (9), 646–656. doi:10.1590/S0042-96862003000900007
- Wu, G. J., Chen, T. G., Chang, H. C., Chiu, W. T., Chang, C. C., and Chen, R. M. (2007). Nitric oxide from both exogenous and endogenous sources activates mitochondria-dependent events and induces insults to human chondrocytes. *J. Cell. Biochem.* 101 (6), 1520–1531. doi:10.1002/jcb.21268
- Xu, K., He, Y., Moqbel, S. A. A., Zhou, X., Wu, L., and Bao, J. (2021). SIRT3 ameliorates osteoarthritis via regulating chondrocyte autophagy and apoptosis through the PI3K/Akt/mTOR pathway. *Int. J. Biol. Macromol.* 175, 351–360. doi:10.1016/j.ijbiomac.2021.02.029
- Xue, J. F., Shi, Z. M., Zou, J., and Li, X. L. (2017). Inhibition of PI3K/AKT/mTOR signaling pathway promotes autophagy of articular chondrocytes and attenuates inflammatory response in rats with osteoarthritis. *Biomed. Pharmacother.* 89, 1252–1261. doi:10.1016/j.biopha.2017.01.130
- Ye, Y., Fang, Y., Xu, W., Wang, Q., Zhou, J., and Lu, R. (2016). 3, 3'-Diindolylmethane induces anti-human gastric cancer cells by the miR-30e-ATG5 modulating autophagy. *Biochem. Pharmacol.* 115, 77–84. doi:10.1016/j.bcp.2016.06.018
- Ye, Y., Li, X., Wang, Z., Ye, F., Xu, W., Lu, R., et al. (2021). 3, 3'-Diindolylmethane induces gastric cancer cells death via STIM1 mediated store-operated calcium entry. *Int. J. Biol. Sci.* 17 (5), 1217–1233. doi:10.7150/ijbs.56833
- Yoshino, S., Sasatomi, E., and Ohsawa, M. (2000). Bacterial lipopolysaccharide acts as an adjuvant to induce autoimmune arthritis in mice. *Immunology* 99 (4), 607–614. doi:10.1046/j.1365-2567.2000.00015.x
- Zamli, Z., and Sharif, M. (2011). Chondrocyte apoptosis: A cause or consequence of osteoarthritis? *Int. J. Rheum. Dis.* 14 (2), 159–166. doi:10.1111/j.1756-185X.2011.01618.x
- Zeng, R., Lu, X., Lin, J., Ron, Z., Fang, J., Liu, Z., et al. (2021). FOXM1 activates JAK1/STAT3 pathway in human osteoarthritis cartilage cell inflammatory reaction. *Exp. Biol. Med.* 246 (6), 644–653. doi:10.1177/1535370220974933
- Zhang, Y., Vasheghani, F., Li, Y. H., Blati, M., Simeone, K., Fahmi, H., et al. (2015). Cartilage-specific deletion of mTOR upregulates autophagy and protects mice from osteoarthritis. *Ann. Rheum. Dis.* 74 (7), 1432–1440. doi:10.1136/annrheumdis-2013-204599
- Zhao, Z., Li, Y., Wang, M., Zhao, S., Zhao, Z., and Fang, J. (2020). Mechanotransduction pathways in the regulation of cartilage chondrocyte homeostasis. *J. Cell. Mol. Med.* 24 (10), 5408–5419. doi:10.1111/jcmm.15204

Frontiers in Immunology

Explores novel approaches and diagnoses to treat immune disorders.

The official journal of the International Union of Immunological Societies (IUIS) and the most cited in its field, leading the way for research across basic, translational and clinical immunology.

Discover the latest Research Topics

[See more →](#)

Frontiers

Avenue du Tribunal-Fédéral 34
1005 Lausanne, Switzerland
frontiersin.org

Contact us

+41 (0)21 510 17 00
frontiersin.org/about/contact

